Elucidating the Vulnerability of Glioblastoma Stem-like Cells to Lysosomal Dysfunctions

Clément Maghe

COLLEGE DOCTORAL PAYS DE LA LOIRE ED BIOLOGIE SANTE

Nantes Université

THESE DE DOCTORAT

NANTES UNIVERSITE

ECOLE DOCTORALE N° 605
Biologie-Santé
Spécialité : « *Biologie Cellulaire, Biologie du Développement* »

Par
Clément MAGHE

« Elucidating the Vulnerability of Glioblastoma Stem-like Cells to Lysosomal Dysfunctions »

Thèse présentée et soutenue à Nantes, le 15 décembre 2023.
Unité de recherche : CRCI^{2}NA - INSERM U1307, CNRS UMR6075

Rapporteurs avant soutenance :

Pr. Pirjo Laakkonen	Professeur d'Université, Université d'Helsinki
Dr. Viktor Korolchuk	Enseignant-Chercheur, Université de Newcastle

Composition du Jury :

Président :	Dr. Graça Raposo	Directrice de Recherche, Institut Curie
Examinateurs :	Dr. Graça Raposo	Directrice de Recherche, Institut Curie
	Dr. Thierry Galli	Directeur de Recherche, Université Paris Descartes
	Pr. Daniel Krappmann	Professeur d'Université, German Research Center for Environmental Health
Directrice de thèse : Dr. Julie Gavard		Directrice de Recherche, Nantes Université

Acknowledgements

I would like to thank the jury members Pr. Pirjo Laakkonen, Dr. Viktor Korolchuk, Dr. Graça Raposo, Dr. Thierry Galli, and Pr. Daniel Krappmann, for evaluating this work and participating to my thesis defense.

I would like to thank and express my sincere gratitude to my PhD supervisor Dr. Julie Gavard. Since my first steps in the lab six years ago, you have been able to share your passion for sciences, which today has shaped my personal scientific interests, and pushed me to continue this adventure on the other side of the Atlantic. Your unfailing support allowed me to experience much more than what I was expecting, ranging from insightful corridor discussions to international congresses presentations, as well as enriching debates with top-leading scientists. Your constant help kept me on track to complete this thesis and affirmed my desire to continue along this path. Your positivity and perpetual desire to see everyone improve have created such a pleasant and dynamic working environment, that I truly hope to be able to find again one day. Thank you for everything.

I am also grateful to Dr. Nicolas Bidère for the invaluable scientific inputs and discussions throughout the last six years. Your availability and support were key in the completion of this work and have greatly participated in my professional development.

I am thankful to La Ligue Contre le Cancer that financed my PhD, to all collaborators and platforms for their contributions, and to Marc Grégoire and Philippe Juin, directors of the CRCI2NA, for welcoming me in the research unit.

To all past and current SOAP lab members: Laëtitia, Gwennan, Kilian, Sara, Jane, Laïs, Quentin, Clotilde, Mathilde K, Mathilde R, Yanis, Laura, Margaux, Rosalie, Kathryn, Carolina, An, Tiphaine, Isabelle, Fiorella, this adventure would not have been the same without your everyday happiness and constant support. Thank you, my friends.

To my friends and family, you were there the moments I needed, and for this, thank you.

Juliette, I hope these few words can convey all my gratitude for your constant support and encouragement. I'm extremely proud to have you by my side, to accompany me on our new adventures. Thank you so much.

Table of contents

List of figures

List of tables

Abbreviations

4EBP: eIF4E Binding Protein
AbTAC: Antibody-based PROTAC
ADP: Adenosine Diphosphate
ALR: Autophagic Lysosome Reformation
AML: Acute Myeloid Leukemia
AMP: Adenosine Monophosphate
AMPK: AMP-activated Protein Kinase
ASM: Acid Sphingomyelinase
ATCC: American Type Culture Collection
ATG: Autophagy related Gene
ATP: Adenosine triphosphate
ATTEC: Autophagosome Tethering Compound
AUTAC: Autophagy-Targeting Chimeras
BBB: Blood Brain Barrier
BCL10: B-Cell Lymphoma/leukemia 10
BCR: B-Cell antigen Receptor
BIRC3/API2: Baculoviral IAP Repeat-Containing Protein 3
BORC: BLOC1-Related Complex
BRD4: Bromodomain-containing protein 4
BTIC: Brain Tumor Initiating Cell
BTK: Bruton's Tyrosine Kinase
CAD: Cationic Amphiphilic Drug
CARM1: Co-activator-associated Arginine Methyltransferase 1
CARMA/CARD: Caspase Recruitment domain-containing protein
CBM: CARMA-BCL10-MALT1
CD-M6PR: Cation-Dependent of 300kDa Mannose-6-Phosphate Receptor
CHMP: Chromatin-Modifying Protein/Charged Multivesicular body Protein
CI-M6PR: Cation-Independent of 46kDa Mannose-6-Phosphate Receptor
CK1α : Casein Kinase 1 isoform alpha
CLEAR: Coordinated Lysosomal Expression And Regulation
CMA: Chaperone-Mediated Autophagy
CNS: Central Nervous System
CORVET: class C core Vacuole/Endosome Tethering complex
CRISPR: Clustered Regularly Interspaced Short Palindromic Repeats
CSC: Cancer Stem Cell
CTS: Cathepsin
CYLD: Cylindromatosis
DAG: Diacylglycerol
DAMP: Damage-Associated Molecular Pattern
DD: Death Domain
DDR: DNA Damage Response
DLBCL: Diffuse Large B-Cell Lymphoma
DNA: deoxyribonucleic acid
DUB: Deubiquitinase
EAE: Experimental Autoimmune Encephalomyelitis
EC: Endothelial Cell
ECM: Extracellular Matrix
EE: Early Endosomes
EGF: Epithelial Growth Factor
EGFR: Epithelial Growth Factor Receptor
EL: Endo-Lysosome
EMT: Epithelial to Mesenchymal Transition
ER: Endoplasmic Reticulum
ERK1/2: Extracellular signal-Regulated Kinase 1/2
ERT: Enzyme Replacement Therapy
ESCRT: Endosomal Sorting Complexes Required for Transport
FGF: Fibroblast Growth Factor
FGFR: Fibroblast Growth Factor Receptor
FIP200: FAK family kinase-Interacting Protein of 200 kDa
FKBP12: 12-kDa FK506-Binding Protein
FLCN: Folliculin
FRB: FKBP12-Rapamycin-Binding domain
Gal: Galectin
GAP: Guanosine triphosphatase Activating Protein
GATOR: GAP Activity Toward Rags complex
GB: Glioblastoma
GDP: Guanosine Diphosphate

GEF: Guanine nucleotide Exchange Factor
GEMMs: Genetic Engineered Mouse Models
GFAP: Glial Fibrillary Acidic Protein
GlcChol: Glucosyl-β-D-Cholesterol
GPCR: G-Protein Coupled Receptor
GSC: Glioblastoma Stem-like Cell
GSEA: Gene Set Enrichment Analysis
GSK3β: Glycogen Synthase Kinase 3 beta
GTP: Guanosine Triphosphate
Gy: Grays
HOPS: Homotypic fusion and Protein Sorting
HPβCD: 2-Hydroxypropyl-Beta-Cyclodextrin
HSP: Heat Shock Protein
IDH: Isocitrate dehydrogenase
Ig: Immunoglobulin
IGF: Insulin-like Growth Factor
IKK: Inhibitor of nuclear factor Kappa-B Kinase
IL: Interleukin
ILV: Intralumenal Vesicle
IP: Immunoprecipitation
iPSC: induced Pluripotent Stem Cell
ITAM: Immunoreceptor Tyrosine-based Activation Motif
JNK: c-Jun N-terminal Kinase
KO: Knock-Out
LAL: Lysosomal Acid Lipase
LAMP: Lysosome-Associated Membrane Protein
LAP: Lysosome Associated Protein
LBPA: Lysobisphosphatidic Acid
LC-MS/MS: Liquid Chromatography coupled to tandem Mass Spectrometry
LC3B: microtubule-associated proteins 1A/1B Light Chain 3B
LCD: Lysosomal Cell Death
LDL: Low-Density Lipoprotein
LDLR: Low-Density Lipoprotein Receptor
LE: Late Endosome
LIMA1: LIM domain and actin-binding protein 1
LIMP: Lysosomal Integral Membrane Protein
LIR: LC3-Interaction Region
LLOMe: L-Leucyl-L-Leucine Methyl ester
LMP: Lysosomal Membrane Permeabilization
LPS: Lipopolysaccharide
LSD: Lysosomal Storage Disease
LUBAC: Linear Ubiquitin chain Assembly Complex
LXR: Liver X Receptor
LYCHOS: Lysosomal Cholesterol Sensing protein
LYTAC: Lysosome-Targeting Chimera
M6P: Mannose-6-Phosphate
M6PR: Mannose-6-Phosphate Receptor
MAGUK: Membrane-Associated Guanylate Kinase
MALT: Mucosa-Associated Lymphoid Tissue
MALT1: Mucosa-Associated Lymphoid Tissue lymphoma translocation 1
MC: Monocyte
mESC: mouse Embryonic Stem Cell
MGMT: methylguanine methyltransferase
MHC: Major Histocompatibility Complex
MRI: Magnetic Resonance Imaging
MTOC: Microtubule-Organizing Center
mTOR: mechanistic Target Of Rapamycin
mTORC1/2: mechanistic Target Of Rapamycin Complex 1/2
MVB: Multivesicular Body
MΦ: Macrophage
NEMO: NF-kappa-B Essential Modulator
NF-κB: Nuclear Factor-Kappa B
NGS: Next Generation Sequencing
NIK: NF-κB Inducing Kinase
NK: Natural Killer
NOD-SCID: Non-Obese Diabetic Severe Combined Immunodeficiency
NPC: Neural Progenitor Cell
NPC: Niemann-Pick type C
NRP1: Neuropilin-1
NSC: Neural Stem Cell
NUFIP1: Nuclear Fragile X mental retardation-Interacting Protein 1
OPC: Oligodendrocyte Progenitor Cell

OPTN: Optineurin
ORP: Oxysterol-binding protein-Related Protein
ORP1L: Oxysterol binding protein Related Protein 1L
OSBP: Oxysterol-Binding Protein
P/I: PMA/Ionomycin
PAMP: Pathogen-Associated Molecular Pattern
PCR: Polymerase Chain Reaction
PD-L1: Programmed Death-Ligand 1
PD: Protease-Dead
PDGF: Platelet-Derived Growth Factor
PDGFR: Platelet-Derived Growth Factor Receptor
PE: Phosphatidylethanolamine
PI3K: Phosphoinositide 3-Kinase
PI3P: Phosphoinositide 3-Phosphate
PKC: Protein Kinase C
PLC: Phospholipase C
PLEKHM1: Pleckstrin Homology domain containing protein family Member 1
POI: Protein Of Interest
PROTAC: Proteolysis Targeting Chimera
PRR: Pattern Recognition Receptor
QKI: Quaking
RILP: Rab-Interacting Lysosomal Protein
RNA: Ribonucleic Acid
RNAseq: Ribonucleic acid sequencing
RNF: RING Finger
ROS: Reactive Oxygen Species
RTK: Receptor Tyrosine Kinase
S6K: p70S6 Kinase 1
SAR: Selective Autophagy Receptor
scRNAseq: single-cell Ribonucleic Acid sequencing
sEV: small Extracellular Vesicle
SILAC: Stable Isotope Labelling by Amino Acids in cell culture
SK1: Sphingosine Kinase-1
SMAC: Second Mitochondria-derived Activator of caspases
SNAP: Synaptosomal-Associated Protein
SNARE: N-ethylmaleimide-sensitive factor-attachment protein receptor
SQSTM1/P62: Sequestosome-1
SREBP1/2: Sterol Regulatory Element-Binding Protein 1/2
STX: Syntaxin
SVZ: Sub-Ventricular Zone
TAB: TGF-beta-activated kinase 1 and MAP3K7-binding protein
TAK1: Transforming growth factor-β Activated Kinase 1
TAX1BP1: Tax1-Binding Protein 1
TBK1: TANK-binding kinase 1
TCGA: The Cancer Genome Atlas
TCR: T-Cell antigen Receptor
TFE3: Transcription Factor binding to IGHM Enhancer 3
TFEB: Transcription Factor EB
TGN: Trans-Golgi Network
TM: Transmembrane
TMZ: Temozolomide
TNFR: Tumor Necrosis Factor Receptor
TNFα: Tumor Necrosis Factor α
TPD: Targeted Protein Degradation
TRAF: TNF Receptor-Associated Factor
TRPML1: Transient Receptor Potential channel Mucolipin 1
TSC: Tuberous Sclerosis Complex
ULK: Unc-51-Like Kinase
UPS: Ubiquitin Proteasome System
V-ATPase: Vacuolar-ATPase
VAMP: Vesicle-Associated Membrane Protein
VAP: VAMP-Associated Protein
VEGF: Vascular Endothelial Growth Factor
VEGFR: Vascular Endothelial Growth Factor Receptor
Vps: Vacuolar protein sorting-associated protein
WCL: Whole Cell Lysate
WHO: World Health Organization
WT: Wild-Type
βGC: Beta-Glucocerebrosidase

Abstract

Glioblastoma (GB) is the deadliest and most prevalent primary tumor of the central nervous system (CNS) in adults. Despite invasive treatments of surgical resection followed by radio- and chemotherapy, the median survival of patients hardly reaches 15 months. This aggressiveness is thought to be in part linked to the presence of a subset of cancer stem cells termed glioblastoma stem-like cells (GSCs) within the tumor mass. Involved in the initiation, growth, and recurrence of GB tumors, these cells therefore represent a promising target.

In this context, lysosomes are critical for the maintenance of GSCs homeostasis. These organelles, standing at the crossroad between anabolism and catabolism, permit the survival of GSCs in unfavorable conditions. Their destabilization culminates in the specific cell death of GSCs, defining lysosomes as a checkpoint for life-and-death decisions in this cellular context.

The MALT1 paracaspase was recently defined as a crucial mediator of lysosomal homeostasis in GSCs. This protease, initially involved in immune responses, restrains the lysosomal compartment, its inhibition resulting in lysosomal-dependent cell death of GSCs through a mechanism involving the RNA binding protein Quaking. However, the events resulting in the lysosomal destabilization and cell death of GSCs remained unclear.

In this context, my thesis work allowed the cartography of cellular and organellar events leading to GSC cell death upon MALT1 inhibition and silencing. Notably, by combining the proteomic definition of GSCs and of the purified lysosomal compartment upon inhibition of MALT1, we uncovered the lysosomal-cholesterol transport machinery as central in GSCs survival. The Niemann-Pick type C1 (NPC1) protein, major lysosomal cholesterol exporter, was dispersed from the degradative organelle, resulting in the sequestration of cholesterol in lysosomes of MALT1-inhibited GSCs. Autophagy blockade, transcriptional upregulation of the cholesterol synthesis pathway as well as cell death induced by loss of NPC1 lysosomal localization were rescued by addition of exogenous cholesterol, placing this lipid at the intersection between lysosomal homeostasis and GSCs fate. Consecutively, the direct inhibition of NPC1 activity resulted in the specific elimination of GSCs, emphasizing the functions of the lysosomal cholesterol handling machinery in GSCs' life and death decisions.

Résumé

Le glioblastome (GB) est le cancer du système nerveux central de l'adulte le plus commun et le plus meurtrier. Malgré un traitement invasif de résection chirurgicale suivi de séances de radio- et de chimiothérapies, la survie des patients atteints difficilement les 15 mois. Cette agressivité est considérée comme liée notamment à la présence de cellules souches cancéreuses appelées cellules de type souche de glioblastome, ou GSCs. Ces cellules, impliquées dans l'initiation, la croissance, et la récurrence du GB, sont considérées comme des cibles préférentielles.

Les lysosomes jouent un rôle critique dans le maintien de l'homéostasie des GSCs. Ces organelles, agissant à la croisée des mécanismes d'anabolisme et de catabolisme, permettent la survie des GSCs hors de leur niche protectrice. Dans les GSCs, leur déstabilisation culmine en une mort spécifique, définissant ainsi les lysosomes comme un point de contrôle des décisions vie-et-mort dans ce contexte cellulaire.

La paracaspase MALT1 a récemment été définie comme un médiateur crucial de l'homéostasie des lysosomes dans les GSCs. Cette protéase, initialement décrite comme impliquée dans les réponses immunitaires, restreint le compartiment lysosomal, son inhibition aboutissant en une mort lysosome-dépendante des GSCs, via un mécanisme impliquant la protéine de liaison à l'ARNm Quaking. Cependant, les événements engendrant la déstabilisation lysosomale ainsi que la mort des GSCs restaient incertains.

Ainsi, mon travail de thèse a permis la cartographie des événements participant à la déstabilisation lysosomale suivant le ciblage de la paracaspase MALT1. Notamment, par combinaison de la définition protéomique des GSCs et de leur compartiment lysosomal suite à l'inhibition de MALT1, nous avons mis en évidence le rôle central du transport lysosomal du cholestérol dans la survie des GSCs. La protéine Niemann-Pick type C1 (NPC1), principal transporteur du cholestérol lysosomal, est dispersée hors de cette organelle, entrainant la séquestration du cholestérol dans les lysosomes. De manière intéressante, le blocage de l'autophagie, l'augmentation transcriptionnelle de la voie de synthèse du cholestérol ainsi que la mort cellulaire induite par la perte de la localisation lysosomale de NPC1, sont normalisés après ajout de cholestérol exogène, plaçant ce lipide à l'intersection entre l'homéostasie lysosomale et le destin des GSCs. En parallèle, l'inhibition directe de l'activité de NPC1 entraine l'élimination spécifique des GSCs, soulignant ainsi les fonctions primordiales de la machinerie d'export lysosomal du cholestérol dans la survie des GSCs.

Introduction

A- The plurality of glioblastoma

A-I- An overview

A-I-1- World Health Organization (WHO) classification and definition

As stated in the fifth edition of the World Health Organization (WHO) classification of Tumors of the Central Nervous System (CNS) published in 2021, glioblastoma (GB) is considered a CNS grade 4 tumor[1,2]. As compared to the previous edition, histological, but also genetic and molecular parameters are now taking into account, allowing a more accurate categorization of adult diffuse gliomas[1,3]. As GB is concerned, the moderate use of the Not Otherwise Specified (NOS) and Not Elsewhere Classified (NEC) diagnoses, as well as the consideration of the wildtype status of the isocitrate dehydrogenase 1 and 2 (IDH-wildtype) as a genetic criterion, now allow to distinctly separate GB from astrocytoma and oligodendroglioma. In this regard, GB is now classified in the setting of an IDH-wildtype diffuse and astrocytic glioma in adults presenting necrosis or microvascular proliferation, and, in the absence of these histological settings, on the highlight of at least one of the three following genetic alterations: TERT promoter mutation, +7/-10 chromosome copy number changes, or EGFR gene amplification[2].

A-I-2- Epidemiology

According to the *CBTRUS (central brain tumor registry of the United States) statistical report* that analyzed the incidence of CNS tumors in the United States between 2015-2019 (classified according to the *2016 WHO classification*), GB is the most common primary malignant CNS tumor (50.1% of all malignant tumors, 3.26 per 100,000 U.S. population), affecting primarily older adults (median age of 65 at diagnosis) and with a more frequent occurrence in males than females (1.6 times more common)[4]. Still according to this U.S. database, the survival of glioblastoma patients reached only 42.7% one year after diagnosis and 6.9% five years after diagnosis, making it the most aggressive primary CNS tumor in adults[4]. It is noteworthy that the 2021 WHO GB classification now only includes the most common and aggressive form of GB (IDH-wildtype, 76.8% of all glioblastomas as per the 2016 WHO classification), making the numbers listed above probably low estimates of actual figures[1,2].

A-I-3- Clinical presentation

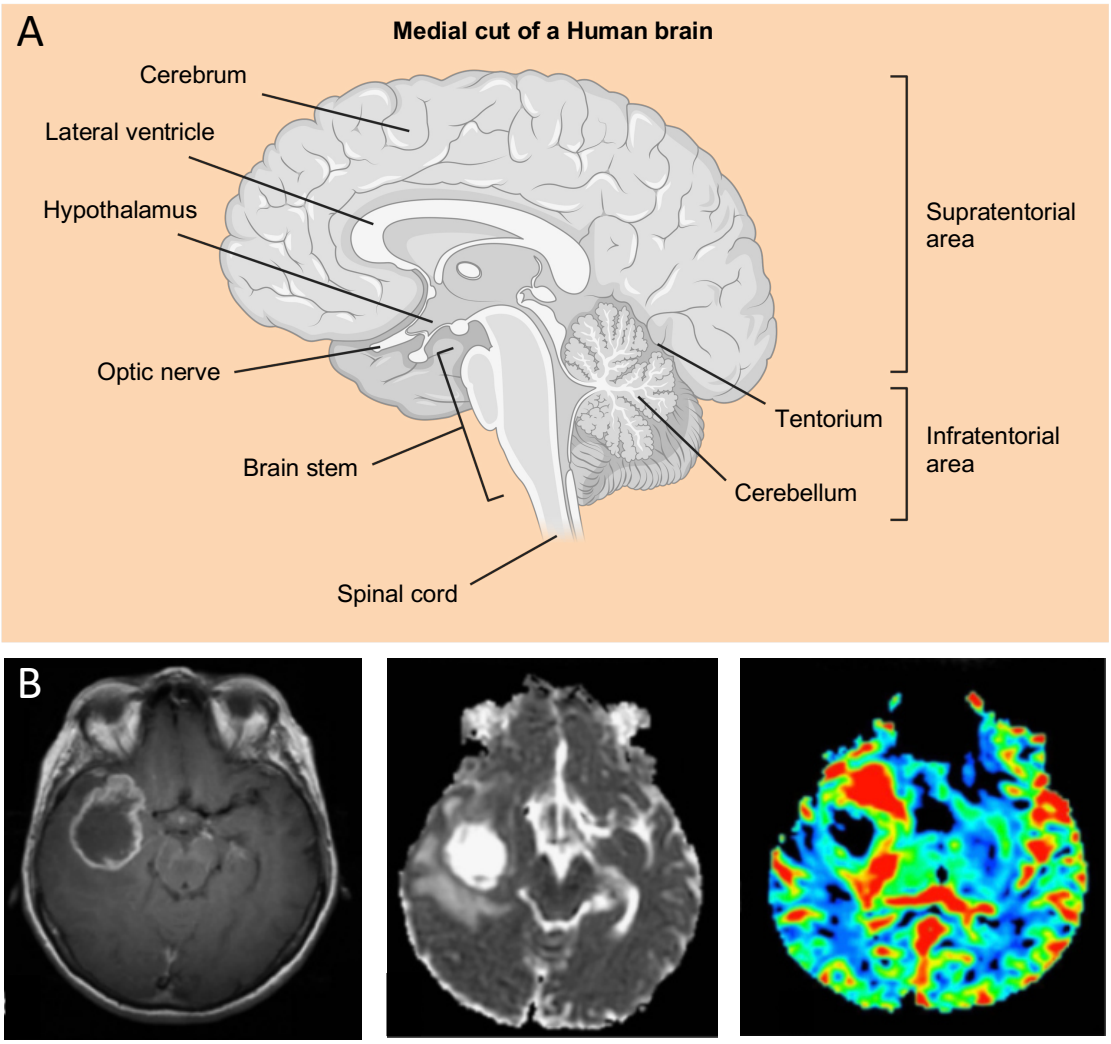

Figure 1: A) Schematic representation of a human medial brain cut with major areas annotated. The supratentorial area, where 95% of GB develop, is indicated. B) Magnetic resonance imaging (MRI) of a human GB. Different methods of imaging were used to assess brain lesions of tumor perfusion. From left to right: T1-weighted post contrast image; Apparent diffusion coefficient image; Standardization of cerebral blood volume
GB pictures from: Svolos, P. et al., Cancer Imaging (2014)

GB may arise from different regions of the brain, but ninety-five percent of GB tumors develop in the supratentorial region[5]. The five percent remaining are found in the brainstem, spinal cord, or cerebellum (Fig. 1A).

While the precise causes for GB development are still debated, few risk factors are associated with an increased occurrence of the disease. Beside age and gender[4], the only confirmed external risk factor is the exposure to high dose ionizing radiation. Several studies demonstrated a link between radiotherapy and GB occurrence in

both adults and children[6–9]. Of note, routine exposure to diagnostic doses of radiation does not increase the risk of developing GB in these two populations[6].

GB is an aggressive brain cancer, developing rapidly, and therefore affecting several primary functions. The location of the tumor in the brain is an important factor that leads to the development of different symptoms. Cognitive impairment, neural deficit, hearing and visual problems are classically associated with a temporal lobe tumor, whereas personality change is a sign of frontal lobe localization[9]. The intracranial pressure also increases in response to the tumoral mass resulting in unilaterally localized headaches with progressive severity and seizures[9].

A-I-4- Standard-of-care therapies

Imaging is an important step to guide patient care, to localize the tumor, formulate treatment plans, and for post-treatment management. Computed tomography as well as magnetic resonance imaging (MRI), are routinely used for these purposes. Technological advances in MRI techniques now allow not only to visualize the tumor mass, but also to assess important parameters, such as blood perfusion or brain activation during task completion[10] (Fig. 1B).

GB treatment is a complicated challenge owing to its heterogenous and complex biology, as well as its location. Surgical resection, when possible, is the most effective treatment for GB. A more extensive resection is notably correlated with a sixty-one percent increase in survival at one year compared to subtotal resection. At two years, this number drops to nineteen percent, still proving efficacy. In parallel, the progression-free survival is increased by fifty-one percent upon total debulking, demonstrating the importance of the surgical resection step during GB treatment[11]. The use of fluorescent dyes, such as 5-aminolevulinic acid, to guide neurosurgeons during tumor removal, increases the rate of complete tumor removal from thirty-six percent to sixty-five percent, and improves significantly the progression-free survival rate[12].

Based on the pioneered clinical trials of Roger Stupp, the administration of the alkylating agent temozolomide (TMZ, aka Temodal) concomitant to radiotherapy became the standard-of-care therapy for newly diagnosed GB (Stupp protocol). This 20-years old treatment consists in focal irradiation of two Grays (Gy) five days per week for six weeks (60 Gy total) plus daily administration of TMZ at 75mg per square meter of body surface. These six weeks of treatment are followed by six cycles of

adjuvant TMZ administration (150-200mg per square meter of body surface) for five days every twenty-eight days[13,14] (Fig. 2). More recently, the use of tumor-treating fields in complement to the adjuvant TMZ have gained interest and received approvals for its use in GB. It was notably demonstrated that the continuous use of this portable and non-invasive device increased the median progression-free survival of chemoradiation-treated patients by 3 months, therefore almost doubling the initial value. Likewise, the median overall survival increased from sixteen months in the TMZ-alone group to twenty and a half months in the tumor-treating fields plus TMZ group[15].

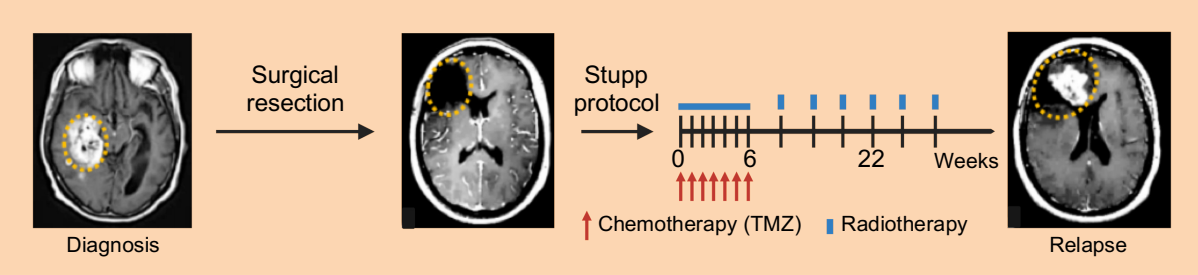

Figure 2: The Stupp protocol. Patients diagnosed with GB undergo maximum surgical resection followed by concomitant radio- and chemotherapy with TMZ. Adjuvant TMZ is then administered for 6 weeks. Despite this invasive protocol, relapses remain inevitable.

Of note, the MGMT (methylguanine methyltransferase) status of the patient is an important parameter to consider when administrating TMZ. Indeed, this enzyme, by removing methylation marks on DNA, counteracts TMZ mode of action[16]. TMZ is an alkylating agent belonging to the class of imidazotetrazines able to cross the BBB (blood brain barrier) due to its relatively small size. Upon reaching neutral or basic pH, TMZ is converted into the metabolite MTIC, itself rapidly converted in the active methyldiazonium ion. This ion is responsible for the methylation of guanine residues in DNA. O^6- and N^7-methylguanines generated upon TMZ administration lead to apoptotic pathway activation, as well as cell cycle arrest[17].

Besides the Stupp protocol, many clinical trials were conducted in an attempt to improve survival of GB patients. Anti-angiogenic therapies were promising, as GB tumors importantly rely on the aberrant neo-vascularization for their growth, and feature microvascular proliferation. Angiogenesis is the process by which new blood vessels grow from preexisting ones, increasing the perfusion of nutrient and oxygen

to cells. Therefore, this process is often hijacked in tumors and notably in GB. VEGF (vascular endothelial growth factor) is a pro-angiogenic factor, promoting angiogenesis via binding to its receptor (VEGFR) on endothelial cells (ECs), inducing their growth and migration[18]. To counteract this process, the VEGF-blocking antibody Bevacizumab was developed by Genentech[19] and commercialized under the name Avastin. Based on *in vitro* assays and mice models, Bevacizumab demonstrated promising preliminary results, effectively blocking angiogenesis and tumor growth[20,21]. However, clinical trials on recurrent or newly diagnosed GB failed to demonstrate results on the overall survival of patients[22–24]. The best benefit observed was the reduction of edema, allowing patients to reduce or stop the use of corticosteroids, improving patient-quality of life[25]. In contrast, the rate of adverse events was higher in patients treated with Bevacizumab, as compared to the placebo group[22–24]. Bevacizumab remains nonetheless still commonly administrated in recurrent GB as a compassionate treatment.

Aside from the major development of the Stupp protocol for the treatment of newly diagnosed GB in 2005, new strategies to fight this tumor clearly lack. The localization as well as the important heterogeneity and invasive properties of this cancer makes its treatment a complicated challenge.

A-I-5- Glioblastoma models

A-I-5-1- Conventional cell lines

Several GB cell lines are commercially available on the ATCC (American type culture collection) or from biological research companies. The most widely used are U87MG (isolated from a 44-year-old male patient with a malignant glioma, likely GB), T98G (isolated from a 61-year-old male patient with GB), LN229 (isolated from a 60-year-old female patient with GB), and U251MG (isolated from a 75-year-old male patient with GB). These cells represent the easiest and fastest way to obtain *in vitro* results, as their culture is relatively easy using media containing serum[26]. In contrast, and as it is the case for most immortalized cancer cell models, these cells fail to recapitulate the initial tumor and its microenvironment[26]. Of note, they grow in adherent conditions, but low-adhesion culture plates can be employed to maintain them in floating spheres, and to isolate cancer stem cells (CSCs) present in the original population of these commercial cell lines[27]. Even though these cell lines contain a subpopulation of CSCs, the use of serum in the media induces their neuronal and

astrocytic differentiation, rendering complicated the study of this important population[27,28]. Moreover, a 2016 study made a striking discovery showing that the widely used U87MG cell line was genetically and transcriptomically different when compared to the cells of origin. The ATCC-available cells were demonstrated as originating from a human GB, but from unknown origin, raising important questions regarding the many studies using this commercially available cell line[29].

A-I-5-2- Patient-derived cell lines

The development of techniques to culture mouse and rat neural stem cells *in vitro* unleashed the potential of using patient-derived neural stem cells in laboratories. It was indeed proven that a precise mixture of serum-free media containing growth factors including EGF (epithelial growth factor), FGF (fibroblast growth factor), and insulin, was able to maintain the stemness properties of freshly isolated mammalian neural stem cells[30,31]. Of interest, the same growth-factors-enriched media can be used to culture glioblastoma stem-like cells (GSCs)[32–34]. In these conditions, GSCs grow in suspension in sphere-like structures defined as neurospheres, maintain the transcriptional status of the parental tumor, and can recapitulate the tumor of origin when transplanted in mice[33,35](Fig. 3). As such, they represent a more suitable model than classical GB cellular models. However, even though the heterogeneity of patient-derived samples is a clear advantage to understand the disease and to explore new therapeutic opportunities *in vitro*, this heterogeneity is lost upon serial passages. Indeed, quiescent GSCs, owing to their low proliferation rate, are counter selected. In parallel, subclone populations can emerge as a result of proliferative advantage[36]. Still, the use of these patient-derived cells provides meaningful information as they mimic more closely the tumor of origin.

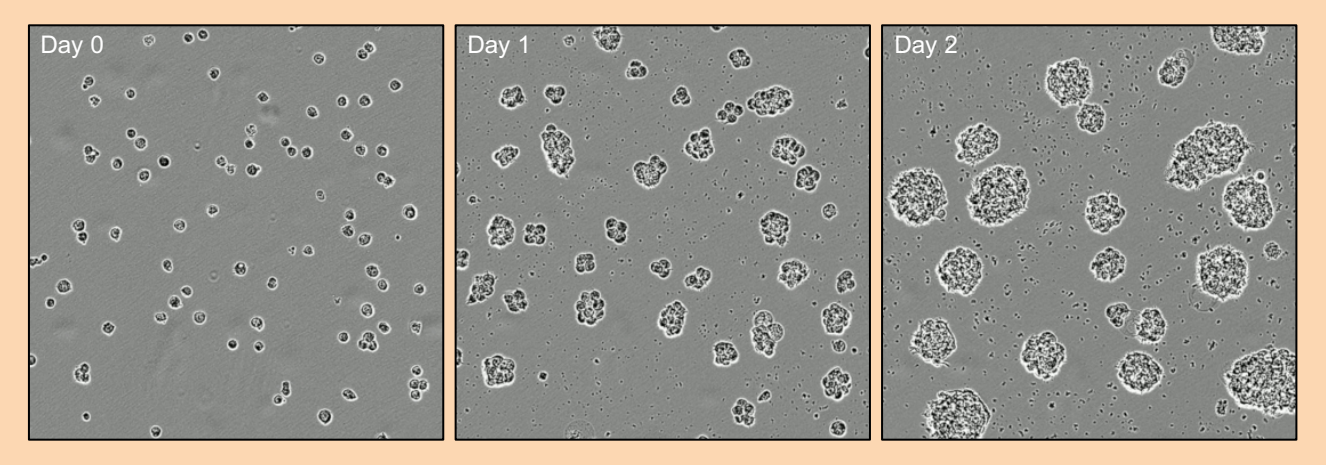

Figure 3: Time-lapse imaging of patient-derived GSCs culture. Dissociated single GSCs have the ability to form neurospheres with time when cultured in an appropriate media containing growth factors and deprived of serum.

A-I-5-3- 3D models and organoids

Because of the relatively simple culture conditions and of their properties, GB cell lines and patient-derived cells are widely used in laboratories working on this cancer and can provide valuable results when looking at new therapeutic opportunities. However, this *in vitro* system does not fully recapitulate the tumor microenvironment. To achieve this goal, several models were developed. For example, the interaction between GB cells and extracellular matrix (ECM) components such as laminin or collagen can be studied in a 2D model system by coating culture plates with these proteins. Matrigel or hydrogels with various protein concentrations, composition, and mechanical properties, can also be employed[37].

While better recapitulating the structural organization, 2D culture systems do not completely copy 3D conditions, such as nutrient diffusion or hypoxia. With the need of culture models resembling as much as possible the tumor of origin, 3 dimensions GB cell culture methods were developed. Once again, Matrigel or hydrogels can be used to culture neurospheres and monitor their invasive properties or response to treatments[37,38] (Fig. 4A).

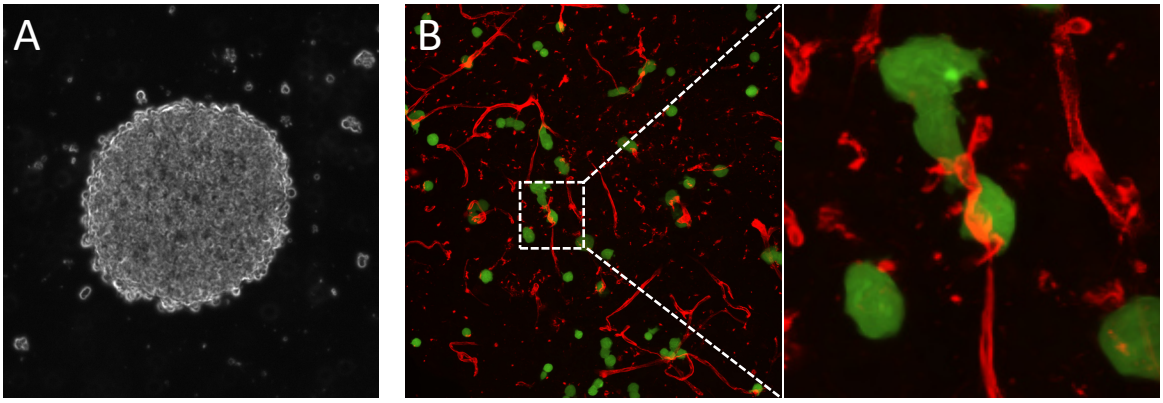

Figure 4: 3D models employed to study GB. A) Confocal microscopy imaging of a spheroid formed using patient-derived GSCs. B) Confocal imaging of an organotypic brain slice culture system between a mouse brain and patient-derived GSCs (green). Isolectin (red) was used to stain blood vessels.

Organotypic slice co-culture is also a valuable tool to study GB cell interactions within a healthy microenvironment. This technique consists in the *ex vivo* engraftment of mouse or human GSCs on freshly cut adult mouse brain slices that can remain alive in serum-free media for several weeks. Using immunostaining, GSC implantation and behavior can be monitored, therefore providing informative results concerning the *ex vivo* functions of GSCs[39] (Fig. 4B).

In 2013, Madeline Lancaster and colleagues developed a cerebral organoid model[40]. Starting from iPSCs (induced pluripotent stem cells) or Matrigel cultured-embryoid bodies (aggregates of pluripotent stem cells derived from the blastocyst), cerebral organoids can be formed in two to four weeks and survive at least ten months. Of note, these organoids form brain regions reminiscent of the cerebral cortex, the choroid plexus, the retina and the meninges, showing the spatial organization of this model. However, and due to the lack of vascular system, nutrients and oxygen availability is not ensured in the core of the organoid, promoting cell death. Still, this ingenious tool provides the most developed and closely related brain model to study GB development and response to treatments. In line with this, the group of Jeremy Rich was able to use patient-derived GB tissue to generate organoids. By injecting 6-months-old GB organoid cells into the brain of mice, they demonstrated the ability of these cells to maintain their proliferative and tumorigenic potential as one hundred percent of the mice died with a brain tumor. Using this model, a gradual organization of GSCs within the organoid was uncovered, with quiescent cells residing in the hypoxic core, whereas proliferative ones accumulated at the surface. Of note, this

enable to maintain quiescent cells in culture, a complicated challenge otherwise, as proliferative cells often take the lead in classical culture conditions[41].

Brain organoids, rather than generated from tumor samples, can also be transduced. For example, the electroporation of plasmids encoding the oncogenic $HRas^{GV12}$ and a single-guide RNA against the TP53 locus into the organoid can lead to tumor development. Of note, GSC markers were increased as compared to control organoids, showing that this model permits the maintenance of this cell subpopulation. As a proof of concept, these transduced GB organoid models were shown to be serially transplantable *in vivo*[42]*.* In parallel, Fadi Jacob demonstrated the potential of using fresh surgically resected GB samples from patients to establish organoids. Concomitantly to their biobanking, organoids were tested for their biological properties, and demonstrated impressive abilities in recapitulating the tumor of origin. Of interest, the inter- and intra-tumor heterogeneity was maintained, allowing for personalized drug testing[43].

Finally, a recent study highlighted the potential of using brain organoids to understand GSC implantation and infiltration. Indeed, one hundred percent of brain organoids are infiltrated by GSCs when co-cultured for twenty four hours, and the tumors formed preserve key genetic and signaling alterations of the parental tumor[44].

Overall, advanced 3D culture systems using brain organoids allow the *in vitro* study of cancer growth in conditions similar to what can be observed *in vivo*. Notably, these systems present important GB features such as hypoxia or necrosis, that are hardly mimicked using classical culture conditions. However, the time consumption is important, and again, the lack of vascularization does not allow the system to fully reiterate *in vivo* tumor organization.

A-I-5-4- *In vivo* models

Animal study is a prerequisite before clinical investigations of potential new effective therapeutics. Beside rodents, several animal models have been employed to study GB, such as drosophila or zebrafish. Drosophila can be an interesting model to screen for genetic alterations responsible for GB growth, as tissue-specific genetic manipulation is relatively unchallenging in this model. Moreover, the CNS in flies and humans share similarities[45]. Zebrafishes, for their part, represent an attractive model to study GB as their immune system is not fully developed during embryogenesis, allowing for xenotransplantation experiment. In addition, and as for drosophila,

genetic manipulation is relatively easy, and their complete transparency allow for cellular tracking without sacrificing the animal. As an important point for drug testing, zebrafishes possess a BBB resembling the one of humans[46].

Canine models are also interesting for the study of GB. Indeed, some dogs spontaneously develop tumors similar to human gliomas. For example, infiltration, expression of immunohistochemical markers, as well as microscopical characteristics, are found similar[26]. Furthermore, the presence of highly proliferative progenitor cells was demonstrated within canine tumors, further shown to be GSCs as per the expression of specific markers and their ability to grow as neurospheres[47–49]. However, the detection of canine gliomas is complicated, and ethical rules need to be respected for animal welfare.

Mice are the most accessible model to study GB and their use is widely developed. Mice can be manipulated as host for allo- or xenograft transplantation either orthotopically, or subcutaneously. Allografts allow the study of GB growth in an immuno-competent model. Most of these studies employ the GL261 cell line that was initially generated by glioma induction in a mouse by intracranial injection of methylcholanthrene followed by serial transplantation of tumor in the brain. This was accompanied by the establishment of the cell line in the mid-1990s[50]. However, this model is often neglected, as not perfectly reflecting the histology of human GB.

Oppositely, xenograft models take advantage of immuno-deficient mice, such as NOD-SCID (non-obese diabetic severe combined immunodeficiency) or nude mice to study human GB *in vivo*. Commercially available cell lines such as U87 can be used, but as previously enunciated, the use of patient-derived cells is more efficient in recapitulating the initial tumor[26]. In any case, cells can be transplanted either ectopically in the flank of the animal, or orthotopically in the brain. The first option allows for an easier manipulation and visualization of the tumor, but does not recapitulate the CNS microenvironment. Moreover, the absence of the BBB may result in incorrect pharmacological studies as some molecules cannot cross this barrier[26]. As such, orthotopic investigation of GB biology in response to specific inputs should be implemented alongside ectopic studies.

Genetic engineered mouse models (GEMMs) can be generated to understand the mechanisms responsible for GB development and growth. Restrictive viral transduction of specific genes leads to the development of GB in mice. For example, adenoviral transduction of the mutant form of the EGFR (EGFRvIII) in mice harboring

RAS activating mutation recapitulate GB development[51]. These systems allow for the growth of complex tumors without surgical intervention in an immuno-competent animal. Several conventional mutations observed in patients can recapitulate tumor growth in mice. These include: expression of the v-src kinase under the control of the GFAP (glial fibrillary acidic protein) promoter[52]; aberrant activation of the p21-RAS signaling pathway[53]; overexpression of an active form of IDH in the SVZ (sub-ventricular zone) of adult mice[54]; combination of Trp53 knockout and Nf1 inactivating mutation[55], overexpression of c-Myc[56,57]. Of note, combining the use of these different models recapitulating the distinct subtypes of human GB can provide important insights into GB biology. For example, the group of Simona Parrinello demonstrated that regardless of the driver mutation, tumor cells converge on the same neural-like state. Moreover, it was shown that the tumor bulk shelters neural progenitor-like cells, oppositely to the margin, where cells differentiate toward an astrocyte-like phenotype, responsible for the high infiltration of the tumor[58]. In line with this, Takashi Shingu demonstrated the preponderant function of the RNA binding protein Quaking (QKI) in the maintenance of stem properties by premalignant neural stem cells (NSCs). In a $Trp53^{-/-}$ $Pten^{-/-}$ background, NSCs were shown to proliferate within the protective and nutritive SVZ niche, but failed to survive without, and no gliomas were formed. However, deleting QKI in this genetic background potently increases the formation of tumors, rising to a penetrance of ninety-two percent. Mechanistically, QKI deletion downregulated the lysosomal compartment, responsible for the degradation of plasma membrane signaling receptors. As such, signaling was maintained even in harsh conditions, outside the protective niche[59].

Finally, a recent study highlighted that epigenetic lesions in specific DNA regions enhance GB development in mice. Hypermethylation-mediated inhibition of CDKN2A in combination with PDGFRA methylation-induced expression mediate oligodendrocyte progenitor cells (OPCs) proliferation and gliomagenesis[60]. As such, not only the manipulation of genes, but also their expression via modification of the DNA methylation status can be used in mice to study GB biology.

GB model	Advantages	Disadvantages
Conventional cell lines	- Easy culture system - Isolation of CSCs possible	- Do not recapitulate the tumor of origin - Cultured in serum-containing media
Patient-derived cell lines	- Maintain the transcriptional status of the original tumor - Replicate the original tumor in mice models - Heterogeneity	- Loss of heterogeneity with passages - No micro-environment
3D culture	- Nutrient diffusion and hypoxia	- Precise culture conditions
Organotypic slice co-culture	- *Ex vivo* with viable mammalian brain - Interaction GB cells/micro-environment	- Fresh brain slices - Expert culture conditions
Cerebral organoid	- *In vitro* "mini brain" - Closely mirror brain organization	- Complicated process - Time consuming
Drosophila	- Screening for genetic alterations - CNS organization and development conserved with humans	- Short lifetime - Distant from Human
Zebrafish	- Functional BBB - Immature immune system - Transparent	- Distant from Human - Few materials developed for analysis (antibodies)
Mice	- Spontaneous, allograft, or xenograft models - Ectopic or orthotopic transplantation - Different genetic backgrounds	- High cost - Hardly scalable to high throughput

Table 1: Different *in vitro* and *in vivo* GB models. Advantages and disadvantages of the different models are indicated.

A-II- Glioblastoma stem-like cells (GSCs)

A-II-1- Discovery and definition

Cancer stem cells (CSCs) were first identified in acute myeloid leukemia (AML) in 1994, after injection of human AML cells into SCID mice, leading to the discovery of the leukemia initiating cells[61]. Later, their stem properties resembling these of normal hematopoietic stem cells were described, notably their capacity to proliferate, self-renew, and differentiate[62]. In line with this discovery, the CSC hypothesis was proposed, changing the way to think about therapeutic approaches. Indeed, this hypothesis suggests that tumor heterogeneity is linked to the stem properties of CSCs, and that treatments bypassing this cell subpopulation cannot be used as a cure, as CSCs ultimately repopulate the tumor mass[63,64]. Concomitantly, CSCs were

associated with development and recurrence of several other solid cancers such as breast and colorectal cancers[65].

The identification of brain stem cells able to repopulate the neuronal, glial, and astrocytic populations in the adult brain led to the hypothesis that CSCs may also exist in brain cancers[31,66,67]. Pivotal findings by Sheila Singh from the group of Peter Dirks highlighted that brain tumors are composed by a portion of cells positive for the cell surface marker CD133 (prominin-1), able to self-renew and to initiate tumors in immuno-deficient mice models[33,34]. These cells were termed glioblastoma stem-like cells or GSCs, in reference to their stem properties. This discovery was further confirmed by another independent group that also demonstrated the same properties for these tumor initiating cells[32]. GSCs were later defined for their capacity to self-renew, to proliferate indefinitely, to initiate tumor, to differentiate along multiple lineages, and to express specific surface markers, such as CD133, CD15, or CD44[68]. Interestingly, CD133, originally described as a marker of GSC, today appears as non-sufficient to define the whole cancer stem cell population within GB tumors[68,69]. Other markers serve the definition and identification of this cell subpopulation, mostly shared with normal neural stem cells such as SOX2[70], OLIG2[71], NANOG[72], or NESTIN[73]. The expression profile of specific markers therefore does not allow to fully identify the GSC population. They are rather defined with their stem properties, such as self-renewal, neurosphere formation, differentiation, resistance to treatment, and tumor initiation potential[68].

A-II-2- Properties

Many terms are found in the literature to name GSCs, such as BTIC (brain tumor initiating cells) or brain tumor stem cells. While the term ‘’stem’’ is often used to describe this cell population, the hypothesis that GSCs solely derive from neural stem cells is still debated. Indeed, before the discovery of adult NSCs, astrocytes, through a dedifferentiation mechanism, were believed to be the cell of origin for GSCs[74]. However, as NSCs display self-renewal and multipotency abilities, they were suspected to give rise to the GSC population upon transformation. Astrocyte-like NSCs contained within the SVZ in GB patients harbored driver mutations, such as in EGFR, PTEN, or TP53, are able to migrate in distant brain regions to initiate tumor development[75]. Together, while the origin of GSCs still remains uncertain, they can be defined with their stem abilities, such as multipotency and self-renewal (Fig. 5).

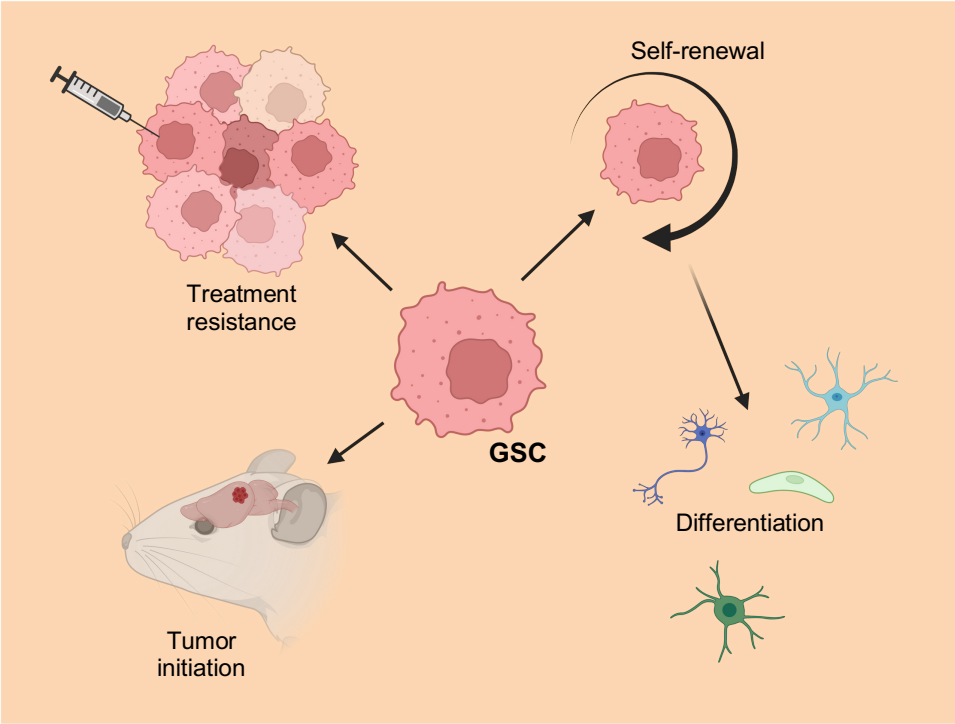

Figure 5: GSC properties. GSCs have a high self-renewal and differentiation capacity. They were shown to differentiate into astrocytes, neurons, oligodendrocytes, endothelial cells, or pericytes. GSCs are also highly resistant to current standard-of-care treatments. Finally, GSCs are able to recapitulate the tumor of origin when implanted in the brain of mice model, demonstrating their plasticity and tumor initiation potential.

Another major hallmark of GSCs is their ability to repopulate the tumor mass after treatment or upon transplantation. Indeed, and as previously stated (see section A-II-1), CD133-positive GSCs were demonstrated as capable of inducing a tumor phenocopying the tumor of origin, even when injected at a very low concentration[33]. GSCs also play a crucial role in the aberrations that distinguish tumor angiogenesis. Indeed, alongside pro-angiogenic effectors, GSCs can secrete VEGF, therefore promoting EC migration and tube formation[20]. Moreover, it was proposed that GSCs can transdifferentiate into EC, promoting aberrant vascularization, fueling the tumor mass[76,77]. It was demonstrated the appearance of human ECs carrying the same genomic alterations as the cells of origin in the brain of mice that received human GSCs, pointing toward a differentiation mechanism[77]. Interestingly, another group demonstrated the potential transdifferentiation of GSCs toward pericytes, assisting the constitution of new blood vessels in the tumor[78]. In parallel, TGF-β and Notch pathway activation were proposed as drivers of GSCs differentiation toward pericytes[79,80]. However, this phenomenon is still importantly debated.

An important trait of GSCs is their ability to resist to current standard-of-care treatments. The first line treatment for GB is surgical resection, proving efficacy for patient survival based on the extent of debulking[11] (please see section A-I-4). However, GSCs are also highly invasive and engaged in tight interaction with healthy brain cells, rendering their complete elimination by surgery almost impossible[68]. GSCs are therefore thought to play major functions in GB relapses.

In line with this, several studies using *in vivo* models defined the migratory and invasive capacities of GSCs. For example, orthotopic implantation of transformed NSCs demonstrated a remarkable invasive profile, weeks before the development of the tumor. Notably, GB cells migrated along blood vessels, as well as fiber tracts[81]. Using *in vivo* live cell tracking, Frank Winkler showed the interactions between blood vessels and glioma cells, and demonstrated that these interactions favor the tumor cell migration[82]. Of note, GSCs were shown to be more invasive than their non-stem counterparts, and depending on the GSC model used, the mode of migration was also different, ranging from single cell migration, to collective migration in ''finger-like'' projections[83]. This is notably believed to be due to the expression of pro-invasive genes, such as metalloproteinases[84,85]. All these characteristics make GSCs highly migratory and infiltrative.

On top of this ability to evade surgical resection, GSCs were shown to resist to chemo- and radiotherapy. Indeed, a small population of human GB cells can survive when treated to lethal doses using the chemotherapeutic agent BCNU (1,3-bis(2-chloroethyl)-1-nitrosourea). Interestingly, these resistant cells were shown to be enriched in CD133-positive GSCs, able to reproduce a tumor when injected in mice models[33]. Furthermore, GSCs display increased expression of anti-apoptotic genes, as well as DNA repair effectors, such as MGMT, counteracting TMZ[86] (please see section A-I-4). Of note, MGMT promoter methylation status, that correlates with its expression level, was linked to GB patients' probability of survival, with a low activity of MGMT associated to a better probability of survival of the patients[87].

Moreover, Luis Parada's group, using genetically engineered mice models, demonstrated the high recurrency potential of GSCs upon TMZ treatment. Indeed, administration of TMZ stopped the tumor growth, but inevitable re-growth originated from a Nestin-positive population of quiescent GSCs. Of interest, eradicating this subpopulation of cells completely abrogated tumor re-growth[88]. In line with this result, GSCs were shown to be quiescent, slowly dividing cells, therefore not targeted by

chemotherapeutic agents, such as TMZ, killing highly proliferative cells[89]. Therefore, it was proposed that the quiescent pool of GSCs, resistant to chemotherapy, give rise to the actively proliferating GSC subpopulation, able to regenerate the tumor mass[88,90].Radiotherapy has also proved difficulties to eradicate the GSC population from tumors. A pivotal study by the group of Jeremy Rich identified the important activation of the DDR (DNA damage response) in GSCs in response to radiation[91]. Notably, GSCs isolated from primary human tumors resist to ionizing radiation in increased proportions compared to non-GSCs tumor cells. This was mechanistically explained by the preferential activation of DNA repair mechanism. Indeed, checkpoint kinases for DDR and repair were significantly more active in GSCs after radiation, demonstrating their radio-resistance capacities[91].

Overall, this demonstrates the ability of GSCs to evade and resist to current standard-of-care treatments and provide evidence for their ability to repopulate the tumor mass albeit surgery, radio-, and chemotherapy efficiently eradicate a major fraction of the tumor mass. Therefore, targeted therapies are urgently needed to specifically eradicate this resistant initiating and recurrent cell subpopulation.

A-III- Heterogeneity of glioblastoma

A-III-1- Definition of tumor niches

GB is molecularly, cellularly (Fig. 6), and histologically highly heterogenous. This feature differentiates GB from lower grade gliomas, as per the presentation of pseudopalisading necrosis and vascular proliferation. Overall, GB can be dissected into specific niches, modulating immune surveillance, metabolic needs, invasion, and GSC maintenance. Three main niches coexist within GB tumors: perivascular, hypoxic, and invasive[92] (Fig. 7).

The perivascular niche provides a protective and nutritive environment for GSCs[21]. In turn, GSCs can produce pro-angiogenic factors such as VEGF, leading to aberrant angiogenesis, therefore sustaining tumor growth[20]. Moreover, GSCs are capable of transdifferentiation into ECs or pericytes, therefore directly implicated in vasculature organization within the tumor[76,77]. However, this mechanism is still debated as several groups obtained discordant results[92,93].

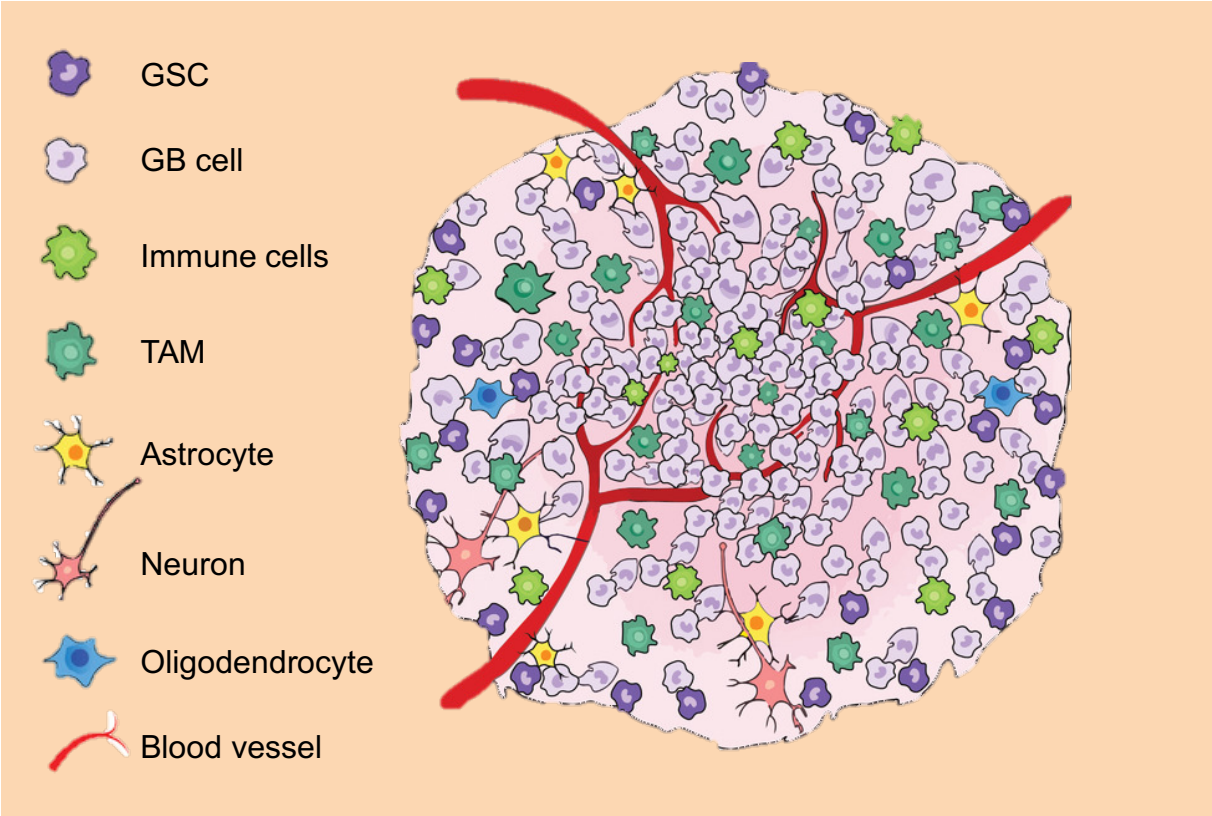

Figure 6: GB tumor cellular composition. GB tumors are a heterogenous mixture of malignant cells, GSC, immunes cells (microglia, lymphocytes, DC), blood vessels, as well as healthy tumor associated brain cells such as astrocytes and oligodendrocytes.
TAM: Tumor-associated macrophage, DC: Dendritic cell
Adapted from: Tang, M. et al., Advanced materials (2021)

GSCs were shown to rely on EC secretome to survive and proliferate. While Eric Holland's group identified that aberrant mTOR (mechanistic Target Of Rapamycin) signaling is necessary for GSC maintenance[94], our group demonstrated that the activation of the pathway relies on factors secreted by ECs, among which is apelin[95]. Indeed, the use of selective competitive antagonists of the apelin receptor abrogated GSC expansion *in vitro* and *in vivo*[96]. This result was further corroborated by an independent group, highlighting that GSCs-mediated secretion of apelin can promote tumor angiogenesis[97]. Moreover, the protein GP130 governs the plasma membrane availability of the apelin receptor, therefore acting as a switch for the endothelial secretome-mediated GSCs growth[98,99]. Interestingly, GP130 was also linked to GSC plasticity and chemoresistance through STAT3 activation[100].

Deregulated vascular functions are a hallmark of GB. Notably, inconsistent tumor-induced vascularization together with exponential tumor proliferation generate local regions of hypoxia. When vascular defects are too important, pseudopalisading

necrosis areas develop. This morphological feature of GB is formed by aligned tumor cells around the necrotic centre[101]. Of note, these areas showing increased cell death and decreased oxygen perfusion are of particular importance for tumor progression and aggressiveness. Indeed, several studies demonstrated that hypoxic niches promote stemness and protect cells from chemotherapeutic agents, therefore maintaining GSCs in conditions allowing GB expansion[102–104].

GB is a highly infiltrative tumor and migrating GB cells therefore form the invasive niche. GB cells were shown to migrate along white matter tracts as well as blood vessels allowing the invasion of the normal brain parenchyma[105]. Vessel co-option, the mechanism by which cancer cells utilizes pre-existing blood vessels to sustain their growth and infiltration, is a common mechanism they developed. Of note, migratory GB cells were shown to displace healthy astrocytes along their invasive route, disrupting the BBB, and taking control of the vascular tone for their growth[106].

Rather appearing as independent, these niches are however highly dynamic and interconnected. Indeed, as GB cells migrate toward healthy tissues, the tumor mass engulf the preceding invasive niche, transitioning toward hypoxic and perivascular niches, generating a sequence favoring GB growth and resistance to treatment.

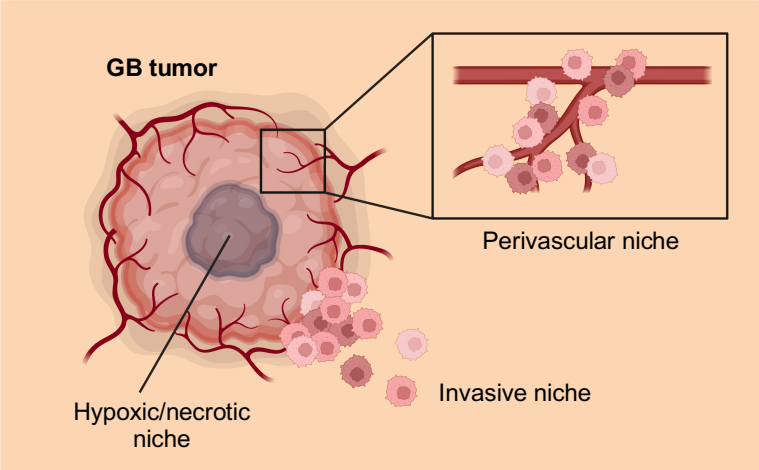

Figure 7: Different niches coexist within GB tumors. The hypoxic niche is often found at the center of the tumor, excluded from the perfusion by blood vessels. Oppositely, the perivascular niche is a nutritive environment for GB cells. Cells that migrate along white matter tract or blood vessels and invade the healthy brain are part of the invasive niche.

A-III-2- Molecular subtypes and plasticity in the GSC population

A-III-2-1- Molecular subtypes

Roel Verhaak and colleagues published in 2010 a pioneering study concerning the molecular classification of GB tumors[107]. Using *in silico* integration of TCGA (the cancer genome atlas) GB data and independent GB datasets, the group defined four distinct molecular subtypes named as proneural, neural, classical, and mesenchymal. The following section will provide information relative to the functional annotation of the different subtypes and their evolution[107].

Proneural: associated with higher frequencies of PDGFRA alteration, IDH1, TP53, and PIK3CA/R1 mutations, higher expression of oligodendrocytic markers, such as OLIG2, lower expression of the tumor suppressor p21, Increased level of proneural development genes such as ASCL1 and TCF4. Of note, the gene-ontology annotation of this subtype revealed signatures associated with proliferation and cell cycle processes.

Subtype	Proneural	Classical	Mesenchymal
Frequency	29%	39%	29%
Mutations	PDGFRA IDH1 TP53 PIK3CA/R1	EGFRvIII CDKN2A	NF1 PTEN
Mean survival (months)	17.0	14.7	11.5

Table 2: Molecular characterization of GB. Frequency, mean survival, and common mutations observed in the three different GB molecular subtypes.

Classical: characterized by chromosome 7 amplification and chromosome 10 loss, EGFR amplification and mutation (EGFRvIII), homozygous deletion of CDKN2A, high expression of the stem cell marker NES (Nestin) and of the components of the Notch and Sonic hedgehog signaling pathways.

Mesenchymal: defined by the deletion and reduced expression of the NF1 tumor suppressor gene, PTEN mutations, high expression of mesenchymal and astrocytic markers such as CHI3L1 and MERTK, respectively, increased expression of the NF-κB (Nuclear Factor-Kappa B) pathway members RELB and TRADD.

Neural: Expression of neural markers such as NEFL, SYT1, and SLC12A5, and associated *in silico* with the neuron projection, axon and synaptic transmission signatures. Interestingly, this molecular subtype was closely related to the healthy brain tissue samples analyzed, as these samples felt in this category during the

TCGA analysis. However, and as stated in the study, the pathology slides from the proneural tumors contained few normal cells[107]. Seven years later, and taking advantage of technological advances, the group of Roel Verhaak performed scRNAseq analysis on one-hundred thirty-three GB cells extracted from three distinct tumors[108]. This analysis, coupled to the one performed by Anoop Patel[109], determined that the neural subtype might indeed be healthy neural cells from the margin of the tumor, and therefore, was removed from the molecular subtype classification. In any case, the inter-tumor heterogeneity represented by the three distinct molecular subtypes was confirmed[108] (Table 2). In parallel, the study uncovered the high intra-tumor heterogeneity of GB, a phenomenon already described by Patel and colleagues three years before[108,109]. Indeed, GB tumors were shown to present a mixture of cells belonging to the different subtypes, with variable transcriptional programs, an important spectrum of stemness and differentiation states, and irregular proliferative capacities[109] (Fig. 8). Overall, this study had a remarkable impact on the understanding of GB biology as a heterogenous entity.

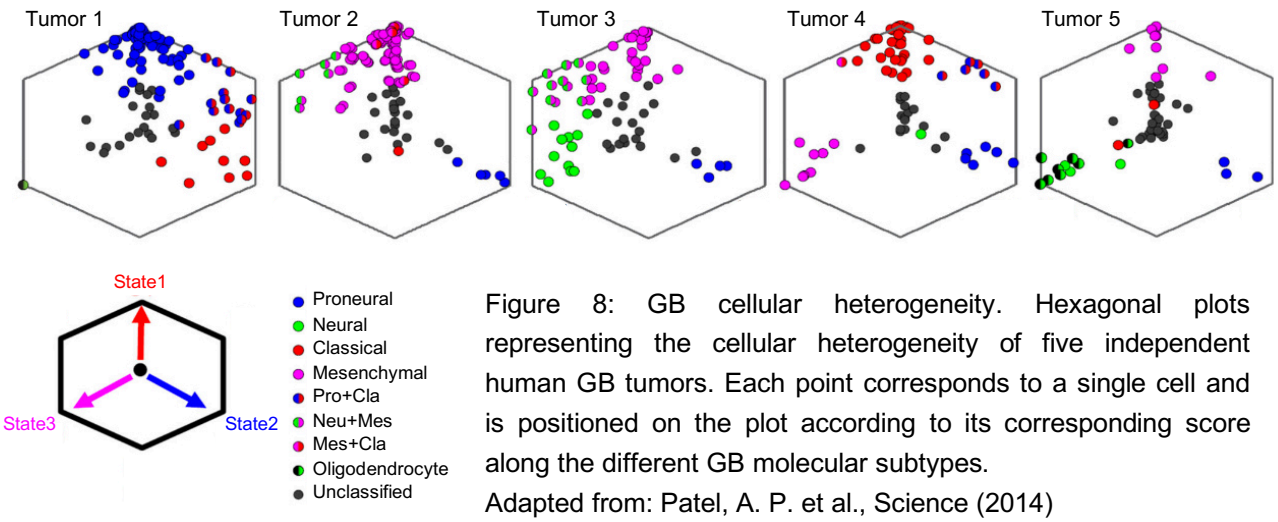

Figure 8: GB cellular heterogeneity. Hexagonal plots representing the cellular heterogeneity of five independent human GB tumors. Each point corresponds to a single cell and is positioned on the plot according to its corresponding score along the different GB molecular subtypes.
Adapted from: Patel, A. P. et al., Science (2014)

Other studies gained interest in the differentiation between the core and the margin of GB tumors. Indeed, the margins are often left behind during surgery as compared to the tumor core. Therefore, characterizing the tumor margins possibly responsible for GB relapses was of paramount importance. Combining radiographically localized biopsies to RNAseq, Brian Gill and colleagues deciphered the molecular characteristics of GB margins. They were notably able to explain that the important infiltration of microglia within the margin of mesenchymal GB tumors was linked to

the high expression level of inflammatory genes[110]. In line with these results, another group developed *ex vivo* culture of spatially distinct tumor tissues. Of interest, the cultured samples recapitulated the original tumor, and tissues from the leading edge appeared molecularly distinct from the core. Notably, cells from GB margins retained their highly invasive properties, whether cells extracted from the core of the tumor were strongly resistant to therapies. Mechanistically, it was demonstrated that the secretome of core cells promoted aggressiveness of their edge counterparts[111].

In conclusion, GB is defined as a highly heterogenous tumor, from the classical inter-patient heterogeneity to the intra-tumor one, either in term of spatial organization of the tumor, or with the important mixture of the tumoral cell status. Understanding this plurality of GB tumors is a complex but important challenge starting to be elucidated thanks to technological advances. For example, freely available databases such as Gliovis or Ivy Glioblastoma Atlas, allow researchers to explore GB RNAseq datasets for the expression and correlation with the probability of survival of patients clustered based on the expression of their genes of interest[112,113].

A-III-2-2- Cellular plasticity

Cellular plasticity is a major driver of intra-tumoral heterogeneity and is defined as the ability for cells to modify their phenotypes without intervention of any genetic alterations, but rather in response to environmental cues[114]. In this context, GB appears as highly plastic. This is notably believed to be due to the important contribution of GSCs in GB development. In the normal brain, the development process is pyramidal, with NSCs giving rise to various progenitors, themselves creating fully differentiated and effector cells. In GB, this pyramidal hierarchy is not maintained, with the heterogenous mixture of malignant cells existing in a gradient of transcriptional states, and differences between GSCs and differentiated-like cells being relatively small[115] (Fig. 9). Therefore, identifying effective therapies appears challenging, as these cells exist in multiple different states, not responding similarly to treatments, and presenting the ability to remodel their transcriptional status to cope with deleterious therapies.

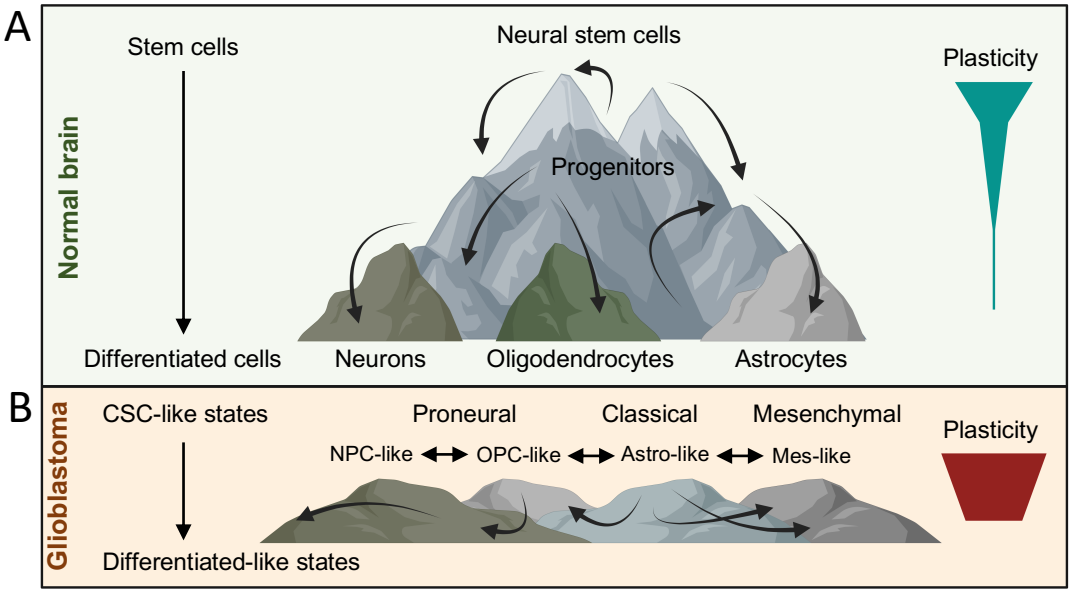

Figure 9: The GB cell heterogeneity and plasticity concept. A) In the normal brain, stem cells give rise to defined progenitors, themselves giving rise to differentiated cells. Along the maturation route, the plasticity of NSCs is lost, and specialized differentiated cells cannot go back to the stem state. B) In GB, this hierarchical organization is lost, with GSCs able to give rise to malignant differentiated cells, and vice versa. The different molecular and cellular states also coexist within a tumor, and was shown to be highly plastic, making GB a highly heterogenous tumor.
Adapted from: Yabo, Y. A. et al., Neuro-oncology (2022)

Using scRNAseq analysis of twenty-eight tumors concomitantly to lineage tracing experiments, a seminal study by Cyril Neftel and colleagues unraveled that malignant GB cells exist in four distinct cellular states[116]. Interestingly, they demonstrated that these four cellular states recapitulate the distinct neural cell types, namely OPC (oligodendrocyte progenitor), NPC (neural progenitor), astrocyte, and mesenchymal, that coexist within one tumor. Notably, genetic alterations are linked to the increased proportion of one given state, with CDK4 alteration being associated with the NPC-like state, EGFR with astrocyte-like, PDGFRA with the OPC-like, and NF1 with the mesenchymal-like. Finally, by deploying *in vivo* single cell lineage tracing experiments, it was shown that the induction of a tumor with cells belonging to a given cellular state was able to give rise to a tumor composed of the four identified states previously described. The extracted tumor was even showing similarities to the initial tumor in term of cellular states proportion, demonstrating the high plasticity of GB malignant cells, able to transition among states[116].

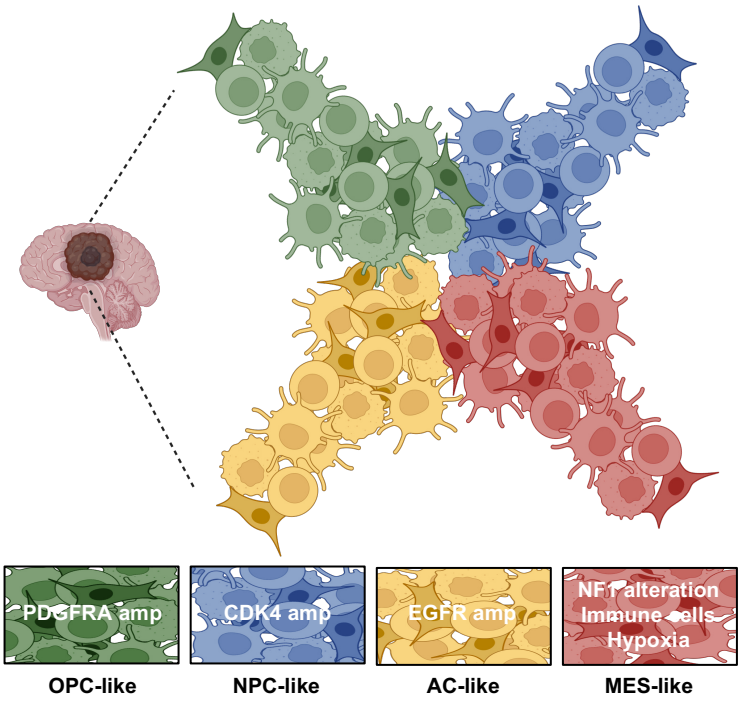

Figure 10: Distinct GB cellular states coexist within GB tumors. Four cellular states drive GB heterogeneity and are influenced by genetic and micro-environmental conditions. GB cells are characterized by an important plasticity, with one single cell able to give rise to the four different cellular states.
Adapted from: Neftel, C. et al., Cell (2019)

In the last decades, GSCs appeared as major drivers of GB development and recurrence. As such, several studies attempted to decipher their behavior and transcriptional status.

For example, the YAP/TAZ transcriptional coactivators were implemented as regulators of GSC plasticity, regardless of the subtype. Indeed, the inhibition of YAP/TAZ blocked GSC properties, differentiation, and further initiation potential and recurrence. The plasticity of differentiated GB cells was also abrogated, placing YAP/TAZ as important regulators of GB heterogeneity and adaptation to environmental cues[117]. YAP/TAZ activity was also linked to GB recurrence in response to radiation[118]. Indeed, radiation induces expression of the CD109 protein in proneural GB cells localized at the invading edges of the tumor. This protein is linked to the mesenchymal subtype of GB, and associates with a worse prognosis for patients, showing the adaptative ability of GB cells. Finally, CD109 expression correlates with a higher activity of the YAP/TAZ pathway, itself responsible for the aggressivity of the transformed cells[118].

In conjunction with these results showing plasticity and adaptation of GB cells to treatment, the group of Paul Rabadan highlighted the clonal evolution of GB under therapy[119]. Using longitudinal genomic and transcriptomic analyses of one hundred fourteen patients' tumor, the group identified that upon recurrence, more than sixty percent of patients experience a subtype change. It was also highlighted, using a mathematical model, that cells responsible for recurrence were present in the tumor

years before diagnosis, and that these cells presented hypermutated highly expressed genes[119]. This demonstrates the high adaptability of GB cells in response to treatment, and how these cells can reproduce a tumor after surgery, radiotherapy, and chemotherapy.

A-III-3- Weaknesses and opportunities

Because of their primordial implication in GB development and recurrence, and of their apparent resistance to current standard-of-care treatments, GSCs have attracted important scientific attention. The eradication of GSCs indeed appears as the starting point to better treat GB. In this context, many research groups have identified several weaknesses and opportunities for their targeting.

As it will be discussed later (see section B-II), lysosomes are major metabolic, signaling, and degradative hubs of cells[120]. In the context of GSCs, lysosomes act in the maintenance of their stemness properties, as well as their survival[59,121,122]. As such, our group and others have linked lysosomal destabilization to the specific eradication of GSCs, opening new therapeutic opportunities, notably via the use of repurposed pharmaceutical compounds (see section B-III-3)[121–127].

In line with this, the mTOR pathway, major regulator of cellular catabolism and anabolism acting at the surface of lysosomes[128] was demonstrated as a pillar of GSCs survival and growth. EGFR amplification and PTEN loss are commonly observed in GB tumors and correlate with a stronger basal activity of the PI3K/Akt/mTOR pathway[107,129]. Because mTOR controls cellular growth and proliferation, its inhibition appeared attractive for GB treatment. However, classical mTOR inhibitors such as rapalogs failed to prove efficacy in clinical trials[130–133]. This is notably believed to be due to the inability of rapalogs to efficiently inhibit mTORC2, therefore allowing the reactivation of the pathway[134], but also to the incapacity of these inhibitors to block specific functions of mTORC1 such as repression of autophagy[135]. As such, new dual inhibitors of mTORC1 and mTORC2 are under development and phase I clinical trials for GB[136]. This is an interesting option as GSCs are addicted to the mTOR pathway[95,137]. mTOR, via the regulation of translation and transcription, modulates the sensitivity of cancer cells to radiotherapy, notably GSCs. In this context, it has been proven that the dual blockade of mTORC1 and mTORC2 using AZD2014 enhances GSC radiosensitivity. Moreover, orthotopic

xenotransplanted mice survived significantly longer when treated with the mTOR inhibitor and irradiated, as compared to the irradiation-alone condition[138].

In line with the hypothesis that lysosomes and mTOR represent weaknesses of GSCs, autophagy, standing at the crossroad, therefore also modulates GB biology and GSCs behavior. However, the precise implication of autophagy is still controversial. As it will be discussed later, the autophagic degradative pathway is repressed by mTOR (see section B-II-3) and requires a functional lysosomal compartment to fulfil its functions (see section B-II-1). In healthy cells, autophagy is viewed as a tumor-suppressive function, maintaining cellular homeostasis. In GB, it however appears as a double-edged sword, regulating cell fitness, but also strongly implicated in cell death mechanisms[139]. As an example, the activation of the Notch pathway induces protective autophagy, allowing GSC resistance to chemotherapy[140]. Indeed, autophagy activation under metabolic stress might allow GSCs to survive by switching their metabolic input[139]. Conversely, autophagy activation was demonstrated as implicated in several GSC characteristics such as migration, proliferation, treatment resistance, and stem properties[141–145].

Altogether, this demonstrates the potential of targeting these three interconnected pathways (lysosomes-mTOR-autophagy) for the eradication of GSCs. However, as their implication in GB biology is still controversial, further work needs to be established and validated to pursue the use of mTOR or autophagy inhibitors in clinic.

Alternatively, therapies targeting lipid synthesis and storage have emerged as potential opportunities for GB treatment. Indeed, GSCs have an altered lipid metabolism when compared to their non-stem counterparts. Of interest, this was demonstrated to be linked to the modified expression of key fatty acid synthesis enzymes such as FADS1/2. As stated by the authors, this may be linked not only to an adaptation to the microenvironment, but also to a specific cellular state, demonstrating the possibility to target lipid synthesis pathways to eradicate GSCs[146].

In this context, the group of Deliang Guo analyzed the influence of fatty acid accumulation. They notably discovered that GB cells accumulate high amount of triglycerides within lipid droplets. Inhibiting DGAT1 (triglyceride-synthesizing enzyme diacylglycerol acyltransferase-1), a critical enzyme for lipid droplet formation, resulted in GB cell death[147]. In parallel, they discovered that lipid droplets are hydrolyzed by autophagy in nutrient-poor conditions, favoring energy production when in

unpropitious conditions. Therefore, inhibiting autophagy resulted in lipid droplet accumulation and loss of energy production in the mitochondria, culminating in GB cell death[148].

Recently, the group of Pirjo Laakkonen identified a weakness of GB cells linked to lysosomal fitness and lipid homeostasis. They identified MDGI (fatty acid binding protein 3; FABP3), a linoleic acid importer, as upregulated by mesenchymal GB tumors and linked it to the poor probability of survival of patients. This protein was further shown to mediate lysosomal membrane composition, and its silencing induced lysosomal membrane permeabilization and further lysosomal-dependent cell death of GB cells[149].

Cholesterol, a major signaling lipid and critical for membrane constitution is also strongly implicated in GB biology and expansion. This is of particular interest as almost twenty percent of the whole-body cholesterol is located in the brain, and as its homeostasis is finely regulated to maintain neural and cognitive functions[150]. Astrocytes and oligodendrocytes are the main sources of brain cholesterol, as this lipid can hardly cross the BBB. In parallel, its excretion by specialized transporters beforehand requests its transformation in hydroxylated cholesterol to cross the BBB and reach the liver to be eliminated. In this context, Mingzhi Han identified CYP46A1, an enzyme necessary for the transformation of cholesterol into 24(S)-hydroxycholesterol, as strongly downregulated in GB samples as compared to healthy tissues. The low expression of this enzyme correlates with poor survival of GB patients, while its re-expression induced a strong cell death of patient-derived GB cells. Mechanistically, 24(S)-hydroxycholesterol generated by this enzyme was shown to reduce the overall cholesterol content of GB cells by activating cholesterol efflux pathways, and inhibiting cholesterol synthesis pathways, ultimately leading to their death. Of interest, a chemical compound, Efavirenz, a known activator of CYP46A1 and able to cross the BBB, reduces GB tumor growth in mice models[151].

Linked to this result, the group of Paul Mischel, that previously demonstrated that GB cells upregulate the expression of the cholesterol importer LDLR (low-density lipoprotein receptor) for their survival[152], showed the dependency of this cancer toward a finely regulated cholesterol homeostasis[153]. They first identified that the rate limiting enzymes for cholesterol synthesis were strongly downregulated as compared to normal brain, indicative of a probable external uptake of this lipid. As such, these cells were resistant to inhibitors of cholesterol synthesis, statins, oppositely to

astrocytes, that synthetize an important amount of this lipid. In contrast, GB cells were highly sensitive to 24(S)-hydroxycholesterol, known activation of the transcription factor LXR (liver X receptor). Mechanistically, LXR activation induces the expression of enzymes necessary for cholesterol export, therefore depleting GB cells of cholesterol, and significantly impairing their viability. Notably, the use of LXR-623, an LXR agonist already used in clinical trials, demonstrated promising results in mice models for the treatment of GB[153].

Oppositely, a study demonstrated that inhibiting the cholesterol uptake and synthesis in GB cells could be an interesting option. They notably investigated the activity of the sterol regulatory element-binding protein (SREBP) transcription factors in GB cells. This family of transcription factor controls the synthesis and uptake of fatty acids and cholesterol in response to nutrient availability[154]. SREBPs were found activated in low-nutrients conditions, favoring GB growth. Therefore, their inhibition resulted in the arrest of GB cell growth in hypoxic conditions[155]. However, other data argue in favor of a downregulation of the SREBP2 transcription factor in GB samples, hypothesizing that cholesterol synthesis and uptake is decreased in this cancer[156]. The role of SREBP activity in GB growth and survival therefore remains to be clearly elucidated.

It however appears clear that this tumor, as others, is sensitive to fluctuations in lipid homeostasis. Cholesterol, important modulator of brain functions, emerges as central in GB sustenance, and modulation of its synthesis, traffic, or elimination, could improve GB treatment strategies.

B- The catabolic and anabolic lysosome in brain homeostasis

B-I- Allegory of a degradative organelle

B-I-1- Historical overview

The year 1949 marked the premises of the discovery of lysosomes. Christian de Duve and colleagues, while working on the activity of the glucose-6-phosphatase in livers, identified a specific subset of this enzyme[157] and therefore started in 1951 the "Tissue Fractionation Studies" series in rat livers, studying the roles and localization of this enzyme[158]. Firstly identified as linked to mitochondria[158,159], it quickly appeared that the acid phosphatase enzyme was in fact localized in specialized but heterogenous membrane-bounded cytoplasmic granules[160,161]. In 1954, four additional acid hydrolases, including cathepsin, were added to the list of these cytoplasmic granules components[160,162]. One year later, the 18th February 1955, the term lysosome (*lúsis sóma*, "digestive body" in Greek) was introduced for the first time by Christian de Duve and colleagues in the article entitled: 6. intracellular distribution patterns of enzymes in rat-liver tissue, from the series "Tissue Fractionation Studies", in reference of their enrichment in hydrolytic enzymes[163]. In a collaborative work published in 1956, Alex Novikoff, Christian de Duve, and colleagues where the first to image lysosomes by electron microscopy, defining these entities as electron-dense bodies, a feature still widely used today to identify lysosomes[164] (Fig. 11). The definitive identification of lysosomes was set in 1965 with the imaging of highly purified lysosomes from rat livers[165], irrevocably opening the path to decades of research on the major, but still incompletely understood, catabolic and anabolic organelle. This pioneer discovery, as well as the incredible technological development of cellular fractionation and electronic microscopy, led Christian de Duve, Albert Claude, and George E. Palade, to jointly obtain the Nobel Prize in Physiology or Medicine in 1974 for their definition of "the structural and functional organization of the cell"[166].

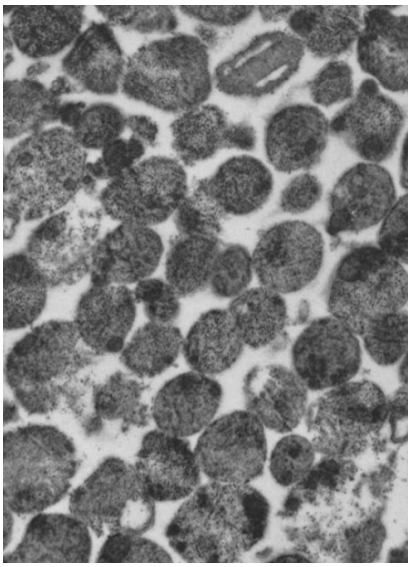

Figure 11: First electron microscopy imaging of highly purified lysosomes, referred as dense bodies.
From Baudhuin, P. et al., JCB (1965)

B-I-2- Lysosome biogenesis and composition

B-I-2-1- Biogenesis

Vesicular trafficking

The lysosomes are defined and characterized as specific entities, with an acidic lumen containing hydrolases, and able to degrade imported compounds[167]. Even though lysosomes are specialized organelles, they are part of a complex continuum of vesicles, the endosomal system / endocytic pathway, that needs to be taken into account when defining their biogenesis[168–170] (Fig. 12).

Endocytic vesicles bud intracellularly from the plasma membrane via active mechanisms involving modifications in membrane tension and activity of coating proteins, such as clathrin and caveolin[171]. The resulting vesicles can fuse together to form early-endosomes (EE), or to a pre-existing EE[168]. EEs are themselves nested in a complex entanglement of vesicles oscillating between recycling and degradation[168,170,172]. Recycling can occur within minutes after endocytosis, and allows to bring back to the plasma membrane, both receptors and membranes that were incorporated into EEs during the process[168,172]. If not recycled back to the plasma membrane, EEs undergo a maturation process that consists in the stamping of the vesicles with specific effector proteins and lipids allowing them to accept proteins from the trans-golgi network (TGN) and to form intra-luminal vesicles (ILVs), ultimately evolving in late-endosomes (LEs) / multivesicular bodies (MVBs)[168,170,173–175]. Rab-GTPases play a prominent function in this process, together with the phosphoinositide composition of the endosomal membranes (Fig. 12). Rab5, for example, is predominantly found on EEs, and, via the recruitment of class II or class III phosphoinositide 3-kinases (PI3K), such as the Vps34 complex II, allows the synthesis of phosphoinositide 3-phosphate (PI3P) at the EE membrane. The recruitment of phosphatases also permits the conversion of $PI(3,4)P_2$ into PI(3)P, a major determinant of EE fate[168,173,174]. The maturation of EEs to LEs is marked by the conversion from Rab5 to Rab7, controlling the recruitment of different effectors at the endosomal membrane[168,174,176]. The EE pool of PI(3)P enables the recruitment of the PIKFYVE kinase, able to generate $PI(3,5)P_2$ from this original reservoir of phosphoinositide[168]. PIKFYVE activity was notably linked to lysosome reformation form endo-lysosomes. Indeed, the inhibition of the kinase and further down-regulation of the level of $PI(3,5)P_2$ on endo-lysosomes lead to enlargement of LAMP1-positive vesicles, less able to generate tubules, reducing the overall number

of terminal storage lysosomes[177]. Altogether, Rab7 and PI(3,5)P_2, among a plethora of effectors, are involved in the generation of ILVs and the acidification of the endocytic vacuole, and therefore in EE-LE transition, as well as the regeneration of the compartment[168,173–175,178].

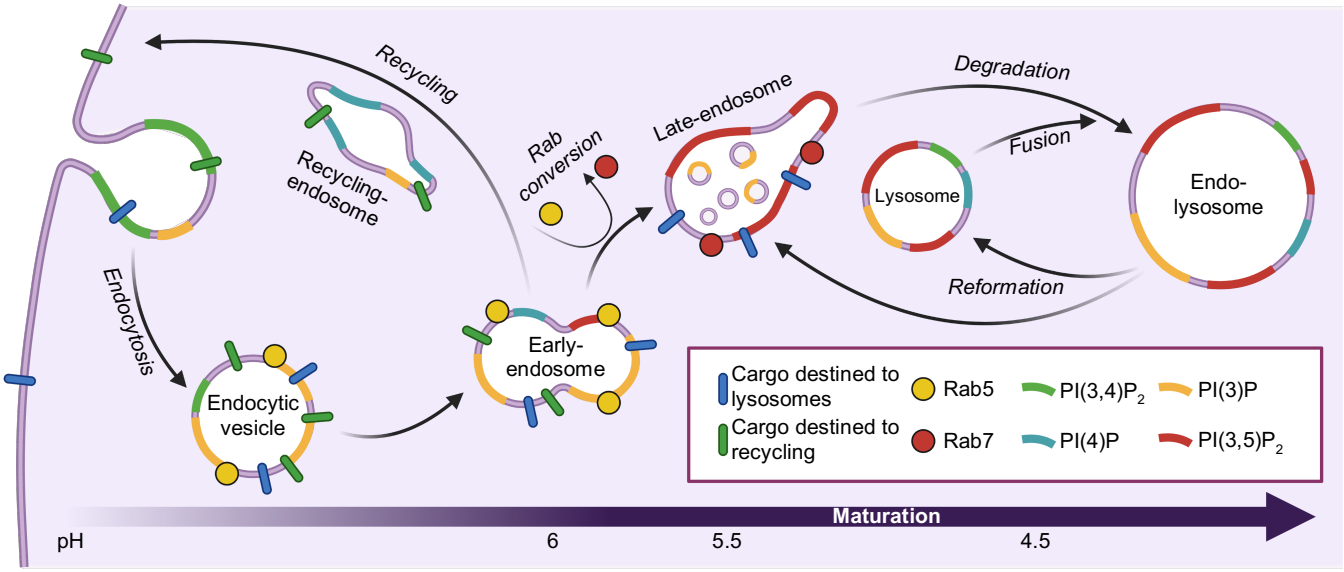

Figure 12: Endosome maturation. Endocytosis generates endocytic vesicles that can fuse together or with pre-existing EEs. Recycling occurs rapidly after endocytosis thourgh recycling endosomes. Otherwise, EEs undergo several maturation processes involving conversion of Rab-GTPases and PIs. Degradation occurs upon fusion of LEs with lysosomes. Lysosomes can regenerate via fission from ELs or being synthesized from the TGN. The pH of endodomes greatly varies, ranging from 6 for EEs to 4.5 for lysosomes and ELs as a result of V-ATPase activity, and strongly influence endosomes functions.
EE: Early-endosomes, PI: Phosphoinositide, TGN: Trans-Golgi network

LEs/MVBs, although committed to the dead-end of the degradative pathway, are still able to fuse with the plasma membrane in order to operate the secretion of small extracellular vesicles (sEVs)[179]. Along the maturation route, endosomes also acquire an acidic pH, ranging from pH:6 for EEs to pH:4.5 for lysosomes, allowing the activation of hydrolases to ensure an appropriate degradative capacity[168,180]. The pH of the endosomal compartment is tightly controlled by the activity of a proton (H+) pump, the vacuolar-ATPase (V-ATPase / H+-ATPase), found inserted in the membranes of all type of endosomes[181]. The V-ATPase activity is dependent on the assembly of two multimeric subunits V1 (cytoplasmic) and V0 (inserted in the vacuolar membrane), that itself depends on the cellular need for increased degradation burden sensed by nutrient availability[178,181–184]. Studies demonstrated that the phosphoinositide composition of endosomal membranes tunes V-ATPase activity, reinforcing the idea that the evolution of endosomes throughout the

maturation process unleashes their recycling or degradative ability[185]. Along the maturation process, and for their acidification, hydrolases stability and macromolecules degradation, endosomes also acquire a precise ionic balance[169,175,180,186,187] (see section B-I-2-3).

The endo-lysosomes (ELs), the main degradative organelles, represent the last step of the endocytic pathway[168,170]. ELs are generated by direct maturation of LEs or their fusion with pre-existing lysosomes. Therefore, lysosomes, even though shown as dynamic and heterogenous, co-exist as a separate, unique entity, characterized by an extremely acidic pH (pH:4.5), the abundance of acid hydrolases, and the presence of specific membrane-associated proteins heavily glycosylated[167,170,187–189] (see sections B-I-2-2 and B-I-2-3). The incorporation of dedicated acid hydrolases and membrane proteins is one of the main steps in the process of lysosomal biogenesis and maturation.

Important fusion processes occur within the endocytic pathway for endosome maturation. As such, dedicated machineries are at play to ensure homotypic and heterotypic fusion of the vesicles comprised in the endosomal compartment. In this context, the CORVET (class C core vacuole/endosome tethering complex) and HOPS (homotypic fusion and protein sorting) complexes play major functions. The two complexes share most of their components (Vps11, -16, -18, and -33) but differ on two, with CORVET assembling with Vps3 and -8, and HOPS with Vps39 and -41[190,191]. Even though structurally similar and able to interconvert, the two complexes play different functions. The CORVET complex is recruited to EEs in a Rab5-GTP dependent fashion and allows the homotypic tethering and fusion of early endosomes[192,193], whereas HOPS is recruited to Rab7-GTP late-endosomes / lysosomes for their homo- or heterotypic fusion[190,194]. Accordingly, a recent study by the group of Juan Bonifacino demonstrated that inhibiting the ability of intracellular vesicles destined for degradation to fuse with the lysosomes resulted in an increase in the fusion of these vesicles with the plasma membrane. Consequently, extracellular vesicles contained in MVBs where found secreted in higher concentration in Vps39 knock-out cells.[195].

Autophagy, the process by which cells engulf and digest cytoplasmic materials, is governed by the generation of double-membraned vesicles termed autophagosomes, and relies on the degradative activity of lysosomes for the recycling of their content[196]. Autophagosomes gravitate around the endocytic pathway and their direct

fusion with lysosomes generates autolysosomes, defined by the presence of lysosomal markers together with autophagic components, such as the ATG8 protein microtubule-associated proteins 1A/1B light chain 3B (MAP1LC3B/LC3B)[197]. Similarly, autophagosomes can fuse with LEs/MVBs, generating an intermediate organelle termed as amphisome, maturing in autolysosome upon fusion with a lysosome[198]. The acidic pH of autolysosomes, provided by the lysosome, supports the optimal activation of lysosomal hydrolases required for the degradation of the autophagosome content. At the peak of autophagy, most of the lysosomes can be consumed to form autolysosomes. Autophagic lysosome reformation (ALR) is the mechanism by which the pool of lysosomes is regenerated[199]. The activity of the mechanistic target of rapamycin (mTOR) kinase, in response to nutrient replenishment, have been shown to be primordial in this context, by first inhibiting the autophagic process, and secondly by generating tubules on autolysosomes that extrude and mature into fully functional lysosomes[200]. Notably, the generation of a cluster of $PI(4,5)P_2$ allows the recruitment of clathrin adaptors together with the protein kinesin family member 5B (KIF5B) motor protein, pulling on tubules[201]. A recent study by the group of Ivan Đikić however demonstrated a primordial function of the TBC1 domain family member 15 (TBC1D15) protein in the ALR process independtly of the mTOR and TFEB pathways. Upon lysosomal damage, TBC1D15 interacts with the lysosomal integral membrane protein type 2 (LIMP2), acting as a lysophagy receptor in this context, and bridging the ALR machinery (clathrin, dynamin, kinesin) to lysosomes for their reformation[202].

Protein sorting

Several specialized trafficking roads orchestrate the sorting of proteins destined to the lysosomal compartment[203–210]. Many hydrolases, synthesized as pro-enzymes in the endoplasmic reticulum (ER), traffic through the TGN before reaching maturing endosomes[206–208]. This marks lysosomal hydrolases with a mannose-6-phosphate (M6P) modification on N-linked glycan chains achieved via the consecutive actions of GlcNAc-1-phosphotransferase (GNPT) and M6P-uncovering enzyme (UCE)[206,208]. The transmembrane protein TMEM251 (LYSET) was recently shown to be necessary for GNPT enzyme activity by maintaining its Golgi localization. LYSET was therefore defined as an integral actor of the M6P pathway for lysosomal enzyme trafficking[211,212]. M6P tagged lysosomal proteins are then recognized by two distinct type of M6P-receptors (M6PR) in the luminal part of the Golgi apparatus[206–208]. The

cation-independent of 46kDa (CI-M6PR / M6PR46) and cation-dependant of 300kDa (CD-M6PR / M6PR300), although structurally different, operate similar functions (Fig. 13). Several studies indicated a complementary role of the two receptors in the trafficking of lysosomal enzymes toward their final destination[206–208,213]. M6PR genetic loss or loss-of-functions mutations lead to massive mistargeting of lysosomal enzymes, rewired extracellularly by the secretory pathway. This phenocopies the defects observed in cells from patients carrying mutations in the enzymes responsible for the M6P modification[211–215]. Depending on the cell type, recapture of extracellularly targeted lysosomal enzymes can however minimize the intralysosomal defects in hydrolases[215]. Other lysosomal enzymes-sorting pathways complement the M6PR road. LIMP2 was demonstrated to be the main sorting receptor for the (βGC) protein via the binding of the soluble enzyme to a luminal coiled-coil domain[205]. Likewise, Sortilin is a transmembrane protein presenting a dileucine-based sorting signal (DXXLL, with X being any amino acid) necessary for its recognition by clathrin adaptor proteins and further shuttling from the TGN to the endo-lysosomes[210]. Sortilin is notably involved in the sorting of cathepsins D and H, prosaposins, and acid sphingomyelinase (ASM)[203,204,209,210].

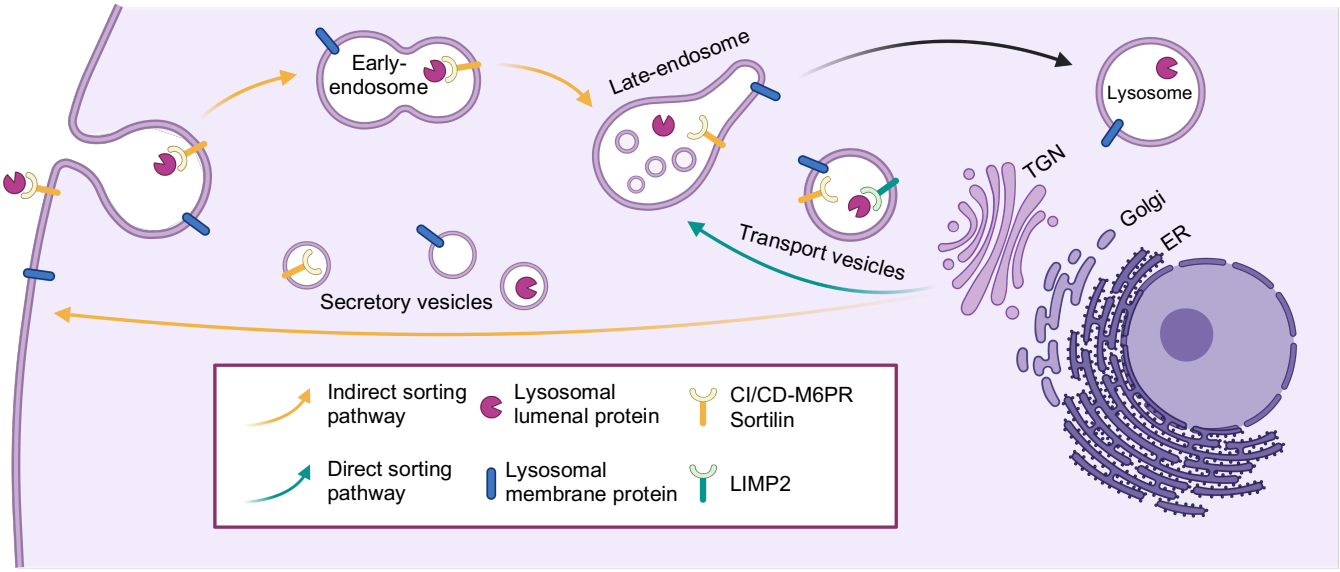

Figure 13: Major pathways deployed by cells for lysosomal protein sorting. Lysosomal proteins are synthesized in the ER and transit through the Golgi where some acquire a M6P tag. Specialized receptors are involved in the direct sorting of lysosomal proteins from the TGN to LEs via transport vesicles. Lysosomal proteins can be secreted into secretory vesicles and be re-internalized via active mechanisms involving recognition by specialized receptors and endocytosis, therefore ending up in their final destination, LEs, via the indirect sorting pathway.
LE: Late-endosomes, ER: Endoplasmic reticulum, TGN: Trans-Golgi network, M6P: Mannose-6-phosphate, CI-M6PR: Clathrin independent mannose-6-phosphate receptor, CD-M6PR: Clathrin dependent mannose-6-phosphate receptor

Lysosomal transmembrane proteins, such as lysosome associated transmembrane proteins (LAMPs), also express the specific dileucine-based or tyrosine-based (YXXØ, with Ø being an hydrophobic residue) sorting signal, allowing their recognition by clathrin adaptors and direct transfer to endosomes[210,216]. In parallel, the transport of these lysosomal transmembrane proteins from the TGN to the plasma membrane and further internalization through the endocytic pathway represents the indirect sorting pathway[208,210].

Transcriptional regulation

The transcriptional regulation of lysosomal genes is tightly regulated in regard to environmental conditions or tissue type. To this end, most of the known lysosomal genes possess a coordinated lysosomal expression and regulation (CLEAR; GTCACGTGAC) consensus sequence in the promoter region. This palindromic 10-base pair motif is recognized by basic helix-loop-helix (bHLH) transcription factors[217]. Among them, transcription factor EB (TFEB) and transcription factor binding to IGHM enhancer 3 (TFE3) are recognized as master regulators of lysosomal biogenesis[218]. The autophagic degradative process, that depends on lysosome activity, was also shown to be transcriptionally regulated by TFEB and TFE3[219]. As major switches between anabolism and catabolism, lysosomes and autophagy are strictly regulated in starvation and nutrient-rich conditions. As such, phosphorylation events sensitive to nutrients articulate TFEB localization and activity. Notably, when nutrients are abundant, the TFEB phosphorylation juxtaposed to its nuclear export signal induces its shuttling to the cytosol[220]. Further phosphorylation at several serine residues by extracellular signal-regulated kinase 2 (ERK2), glycogen synthase kinase 3 beta (GSK3β) or mechanistic target of rapamycin complex 1 (mTORC1) provokes binding to 14-3-3, abolishing its ability to shuttle to the nucleus[219–224]. Conversely, starvation, reactive oxygen species (ROS) production, and lysosomal stress, induce both the inhibition of TFEB phosphorylation, and activates the calcineurin phosphatase (ie TFEB dephosphorylation), inducing its nuclear localization, and ultimately the transcription of lysosomal and autophagic genes[224–226]. Additional actors play important roles in autophagy/lysosomes transcriptional regulation. The co-activator-associated arginine methyltransferase 1 (CARM1) protein was shown, in response to nutrient cues, to bind to TFEB and regulate histone H3 arginine 17 dimethylation and subsequent TFEB transcriptional activity[227]. Bromodomain-containing protein 4

(BRD4), a protein known to bind to acetylated histones and to recruit transcriptional regulators[228], was reported to inhibit an autophagic and lysosomal transcriptional program independent of TFEB. Via binding to acetylated histones, BRD4 recruits the lysine methyltransferase G9a and blocks the transcription of major lysosomal genes, such as lysosomal associated membrane protein 2 (LAMP2), acid sphingomyelinase (ASM), and cathepsins B and D (CTSB, CTSD). Removal of BRD4 increases lysosomal activity even in TFEB/TFE3 silenced cells[229]. At another level of regulation, the Quaking (QKI) STAR RNA-binding protein is a regulator of the endo-lysosome compartment. Indeed, QKI was shown to bind and regulate the stability / splicing / translation of endo-lysosomes-encoding RNAs, still in a TFEB-independent fashion[230].

B-I-2-2- Limiting membrane

Delineating the composition of different cellular compartments or specific organelles is of upmost importance. Indeed, the high complexity of the cellular organization into several compartments allows to discriminate their functions and capacities. Lysosomes, since their discovery, have attracted a lot of effort for their characterization. Back in 1949, Christian de Duve and collaborators were already deploying cellular fractionation to purify lysosomes[157]. This notably allowed the characterization of the hydrolases rich lumen, enclosing notably cathepsins[162]. Combining this purification method to high resolution microscopy allowed to further define the lysosome morphology[165]. The collective effort in lysosome research and the technological advances have considerably pushed our knowledge of this complex organelle (Fig. 14).

Lysosomes are heterogenous in terms of composition and morphology, with a size comprised between 0.1 and 0.5µm in diameter[231]. The lysosomal limiting membrane consists in a 7 to 10nm thick single phospholipid bilayer appearing of low electron density by electron-microscopy[232]. As lysosomes do not possess the machinery for lipid biosynthesis, they rely on their import from the plasma membrane via the endocytic pathway or via active exchanges with close organelles. The lysosomal limiting membrane is rich in sphingomyelin while the internal lysosomal membranes can be selectively identified by the presence of a specific lipid called lysobisphosphatidic acid (LBPA/BMP)[233]. As previously described, phosphoinositides are major signaling lipids stamping the endocytic route and evolving together with the

maturation of endosomes. Plethora of kinases and phosphatases are involved in the regulation of the phosphoinositide code to dictate intracellular vesicle functions, such as lysosomal positioning or recruitment of signaling complexes[173]. Moreover, as lysosomes acquire membranes from other organelles via membrane contact sites or vesicle-mediated transport, the phosphoinositide composition remains highly versatile as compared to maturing endosomes[173]. However, a dysregulated balance of phosphoinositides at the surface of lysosomes have notably been associated with the development of human diseases, such as Parkinson's or Charcot-Marie-Tooth[173]. Cholesterol, typically inserted in cellular membranes, is found in a limited concentration in the lysosomal membrane. Conversely, this lipid is found enriched in recycling endosomes and MVBs[233]. Even at low concentration, cholesterol is thought to play major roles in the organization of the lysosomal limiting membrane, notably via high-order microdomains or lipid rafts enriched with the marker flotillin-1. This process, relying on the concentration of cholesterol, was notably shown to promote clusterization of the lysosomal membrane protein LAMP2 and further proteolytic processing, therefore modulating the process of chaperone-mediated autophagy (CMA)[234]. More recently, senescence-associated lysosomal-cholesterol accumulation was demonstrated as important for mTORC1 activation through the increase of microdomains structures at the lysosomal membrane[235].

Alongside their atypic lipidic composition, the lysosomal membrane also exposes a specific set of proteins, with LAMP1, LAMP2, LIMP2 and the tetraspanin CD63 being the most representated lysosomal membrane proteins. Of note, these lysosomal membrane proteins are heavily glycosylated in the Golgi apparatus en route for their final destination[232,236]. This process is of particular interest in the case of LAMP1 and LAMP2, as defects in their glycosylation lead to their degradation by intralysosomal hydrolases[232,237]. Robin Kundra and Stuart Kornfeld demonstrated that this defect was however not affecting the general organization of lysosomes, but rather their capacity to fuse with autophagosomes[237]. Linked to that, the generation of mice lacking LAMP2 allowed the *in vivo* demonstration of the role of this protein in autophagy termination. Indeed, mice recapitulated Danon's disease, a syndrome characterized by autophagosome accumulation leading to cardiomyopathy and mental retardation[238,239]. The lysosomal distribution of cholesterol also appeared modified upon deficiency of both LAMPs in mouse fibroblasts, allowing Paul Saftig's group to demonstrate the primordial function of LAMP2 in lysosomal cholesterol

transport[240]. Conversely, LAMP1-specific deficient mice only showed an increased expression in LAMP2, probably by a compensatory mechanism, without any major effect on the lysosomal compartment, except mild alterations in the brain (increased and altered pattern of expression of cathepsin D and astrogliosis)[241]. The authors stated that since LAMP2 is almost not detectable in the brain of mice, LAMP1 deficiency could not be compensated in this organ[241]. More recently, Paul Saftig's group demonstrated the role of LIMP2 in lysosomal cholesterol transport. Using *in silico* structural description as well as cell biology and biochemistry assays, the channel structure of LIMP2 was shown to export cholesterol from the endo-lysosomal compartment toward lipid droplets or the plasma membrane[242].

In the last decade, the considerable technological advances of organelle isolation, combined with the increased sensibility and specificity of proteomic analysis allowed to extend the list of proteins found in each organelle, notably lysosomes. In 2009, lysosomes were thought to contain approximately twenty-five membrane proteins[170,243], but several studies were already demonstrating that it might be way more important[244–246]. In addition to the "structural core proteins" LAMPs and LIMPs, lysosomes harbor numerous ion transporters involved in the maintenance of the acidity of the lumen, as well as exporters able to transfer the recycled materials[170]. Linked to their dynamic interactions with various organelles and their high motility, proteomic studies of lysosomes often highlight this phenomenon. Whether proteins transiently interacting with the organelle needs to be classified as lysosomal proteins is still under debate. It is notably the case for mTORC1, a cytosolic complex found at the surface of lysosomes upon activation[247,248]. However, the generation of lysosomal proteomic datasets helps researchers defining the precise composition of the lysosomal membrane. This was notably useful for the group of Roberto Zoncu via the generation of a "lysosome master list" of proteins. Applying different criteria such as the specific localization in the lysosomal membrane and the predicted structure of the protein, the protein GPR155 of unknown function was reported for its role in the cholesterol-dependent activation of mTORC1 on lysosomes[249]. The composition of the lysosomal membrane is far from being solved and informatics tools as well as multi-cell line analysis of the lysosomal proteome might assist the characterization of unknown lysosomal proteins[250].

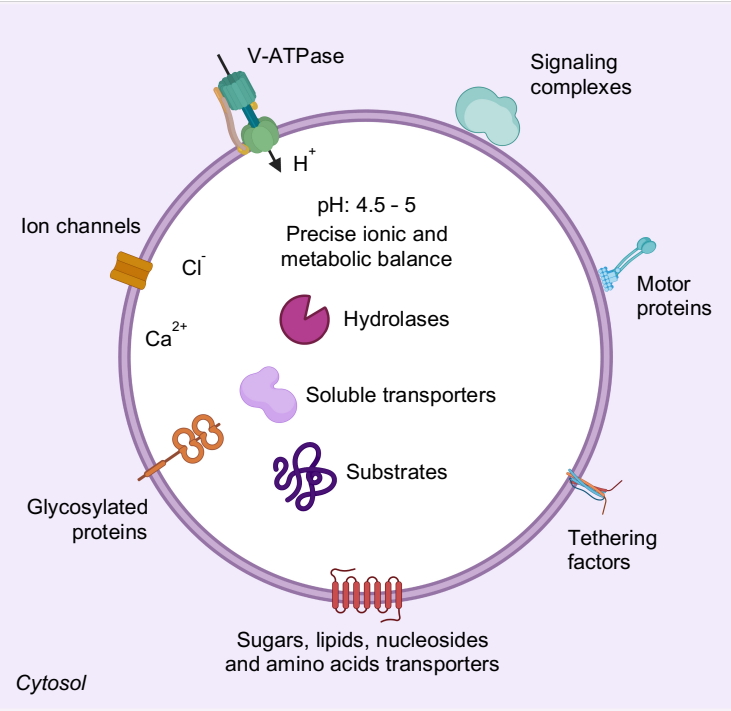

Figure 14: Lysosomes are composed of specific membrane and lumenal proteins. Glycosylated proteins protect the lipidic membrane from the acidic environment and hydrolases. Specialized transporters and channels transport basic building blocks as well as ions for maintenance of the lysosomal functions. Motor proteins and tethering factors ensure lysosomal positioning and fusion to other compartments. Lysosomes are also an important platform for the setting of signaling pathways. The activity of the V-ATPase promotes acidification of the lumen of lysosomes for proper degradation of substrates sent to them for degradation and recycling.
Adapted from: Ballabio, A. & Bonifacino J. S., Nat. Rev. Mol. Cell. Biol. (2020)

B-I-2-3- Lumen

Comparably to the description of the lysosomal limiting membrane, the technological innovations developed in the recent years (Fig. 15) have allowed to lengthen the list of intra-lysosomal proteins and metabolites (Fig. 14). Lysosomes enclose more than sixty acid hydrolases with cathepsins being the most predominant. Fifteen cathepsins have been described, falling into three distinct protease families that are as follow: serine proteases (CTSA and G), aspartic proteases (CTSD and E), and cysteine proteases (CTSB, C, F, H, K, L, O, S, V, X and W)[251]. Cathepsins are essential for protein processing in the lumen of lysosomes. As such, cathepsin inactivation leads to the development of broad variety of pathologies, such as Alzheimer's and Parkinson's, as well as auto-immune diseases[251]. Cathepsins are all synthesized in the ER as preprocathepsins. A co-translational cleavage occurs in the lumen of the ER generating procathepsins, able to transit through the Golgi apparatus where they acquire a M6P tag for their subsequent transfer to the endo-lysosomal compartment[206,251]. When reaching the acidic lumen of lysosomes, cathepsins are further processed by other proteases or autonomously[251]. This lysosomal processing has been demonstrated to be dependent on the acidic pH of lysosomes, comprised between 4.5 and 5, and maintained by the activity of the V-ATPase[183,251]. It should be noted that lysosomes are heterogenous in term of pH and hydrolase activity. Indeed, the fusion of storage lysosomes with late-endosomes into endo-lysosomes was shown to promotes the acidification and further activation of hydrolases. The pH was

further demonstrated to increase upon processing of the engulfed substrates and during the cycle of lysosome maturation and reformation, regenerating deacidified storage lysosomes[188]. Accordingly, the perinuclear localization of lysosomes favors the activity of the V-ATPase through a Rab7-dependent recruitment of the V1G1 subunit of the proton pump, generating a gradient of acidity in between peripheral and perinuclear lysosomes[252].

In parallel, chloride (Cl^-) concentration is essential for optimal activation of a subset of lysosomal hydrolases. Notably, two recent studies showed that depleting the lysosomal Cl^-/H^+ exchanger ClC-7 led to defects in autophagosome processing in the lysosomes, due to CTSC, lysozyme, and DNase II reduced activity. These studies also demonstrated that the H^+ gradient generated by the activity of the V-ATPase was necessary for Cl^- entry in the lysosomes, and further optimal activation of hydrolases[253,254]. In parallel, James Osei-Owusu highlighted that Cl^-, as the counterion of H^+, could be exported from lysosomes by the proton-activated Cl^- (PAC) channel in a pH dependent manner, therefore regulating H^+ influx and subsequently the lysosomal pH. The study notably showed that overexpression of PAC induced a large export of lysosomal Cl^- and deacidified lysosomes[186]. Calcium (Ca^{2+}) signaling is also key for lysosomal functions such as fusion events[120]. As for Cl^-, lysosomal Ca^{2+} concentration appears dependent on lysosomal pH. Indeed, alkalinization of lysosomes correlates with Ca^{2+} efflux into the cytosol[255], probably through a mechanism involving the P2X4 channel[256]. TRPML1 is a major lysosomal Ca^{2+} exporter[120]. The gene encoding the TRPML1 transporter was identified in 2000 in patients presenting the mucolipidosis type IV lysosome storage disease[257,258]. This disease is characterized by defective lysosomal exocytosis, lysosomal cholesterol retention, and accumulation of undigested autophagosomes, demonstrating the primordial role of calcium in lysosomal activity[259,260]. In keeping with this idea, most of the phenotypes presented by lysosomal storage diseases-patient fibroblasts can be rescued by chemically activating the lysosomal Ca^{2+} channel TPC2[261].

The development of the lysoIP technique by David Sabatini's group allowed the absolute quantification of intra-lysosomal metabolites. Notably the lysosomal concentration of specific metabolites showed a discrepancy with the one defined in the whole-cell samples, demonstrating that lysosomes might deploy specific transport machinery. This was notably true for proline, glutamate or alanine, found less concentrated in lysosomes than in whole-cell samples. This study also enabled the

description of mTOR and proton gradient-dependent mechanisms for amino acid transport across the lysosomal membrane[262]. In a parallel study, lysosomal arginine concentration was found correlated with the ability of lysosomes to export most of the essential amino acids they contain in an SLC38A9 dependent fashion[263]. This was in link with previous studies reporting that SLC38A9 regulates mTORC1 in an amino acid dependent mechanism[264–266].

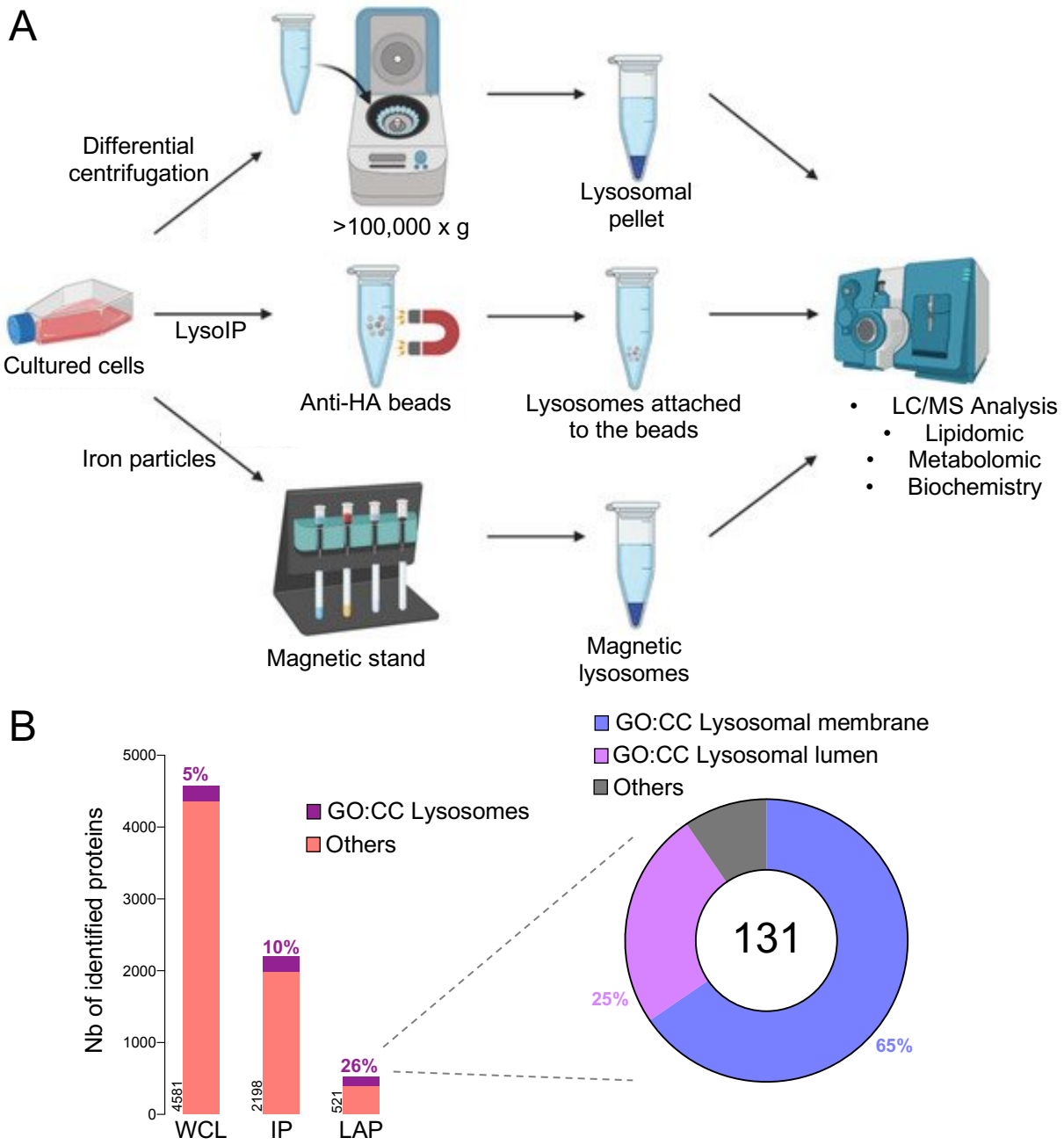

Figure 15: Lysosomes enrichment techniques. (A) Three main protocols allow efficient lysosomes purification and enrichment from cultured cells: i) differential centrifugation, ii) LysoIP, iii) iron partciles loading. Purified lysosomes can then be analyzed by mass-spectrometry or biochemically. B) Graph represents the number of proteins identified in the GSCs whole cell lysate (WCL), in the immunopurified lysosome fraction after LysoIP (IP), and in the lysosomes associated proteins fraction (LAP, proteins significantly enriched in the IP) of GSCs. The percentage of GO:CC lysosomes proteins identified *in silico* is indicated in purple. The donut graphic represents the percentage of membranous (blue) and lumenal (pink) lysosomal proteins identified in a lysoIP proteomic analysis of GSCs. The percentage of other type of proteins is indicated in grey. For each graphic, the number of proteins is reported.
Adapted from: Chen, C. et al., Biomolecules (2022)

As endo-lysosomes are the digestive organ of cells, many various and miscellaneous proteins abound in its lumen. It is therefore important to discriminate lysosomal-resident proteins, from the ones sent for degradation. The identification of the nuclear fragile X mental retardation-interacting protein 1 (NUFIP1) as a bridge for autophagic degradation of ribosomes is a good example[267]. Using the lysoIP technique, eight hundred twenty-eight unique proteins were identified in HEK293T purified lysosomes, among which the regulatory network of mTOR. Interestingly, upon mTOR inhibition using Torin1 or nutrient starvation, the lysosomal proteome was modulated and NUFIP1 was found enriched in the degradative compartment. Using biochemical assays, NUFIP1 was further shown to act as a specific autophagy receptor, bridging LC3B to ribosomes, inducing mTORC1 dependent ribophagy and regulation of protein translation[267].

Similar to proteins, many lipids are transported to the lysosomal lumen in an endocytic and autophagic dependent fashion. The selective autophagic degradation of lipid droplets, termed lipophagy, is an important process for intracellular lipid metabolism[268]. The endocytosis of low-density lipoproteins (LDL) from the extracellular milieu and digestion into lysosomes also contribute to the maintenance of lipid homeostasis[269]. In this context, the activity of the lysosomal acid lipase (LAL) enzyme is primordial. Triglycerides and cholesteryl ester, the respective storage forms of fatty acids and cholesterol are indeed digested by the LAL in the acidic environment of the lysosomes[269–271]. The free fatty acids generated can then freely diffuse in the cytosol to be used for ATP generation. As such, LAL deficiency causes Wolman disease, a severe form of lysosomal storage disease characterized by liver and brain accumulation of lipids[272]. For cholesterol, its water insoluble biophysical property makes it necessary to rapidly engage specific handling in lysosomes, such as incorporation into pre-existing membranes, association to specific transporters, or modification into a more water-soluble form[269]. The glucosylation of free cholesterol by β-glucocerebrosidase was shown to promote formation of glucosyl-β-D-cholesterol (GlcChol), a form of cholesterol more suited for transport[273]. In parallel, protein-dependent transport of cholesterol out of the lysosomes is crucial. This mechanism is thought to be regulated by the Niemann-Pick disease type C2 (NPC2) protein. NPC2 is a small 132-amino-acids lysosomal soluble protein harboring a cholesterol binding pocket, allowing transfer of lysosomal-soluble free cholesterol toward the lysosomal membrane-anchored cholesterol transporter Niemann-Pick type C1 (NPC1) protein

for cholesterol egress in a pH dependent fashion[274]. As already mentioned, LAMP2 and LIMP2 lysosomal membrane proteins were also ascribed a function in lysosomal cholesterol exit[240,242,275]. As for fatty acids, lysosomal handling of cholesterol is necessary for lysosomal functions and further maintenance of cellular homeostasis. Mutations in NPC1 or NPC2 engender Niemann-Pick disease, a rare metabolic lysosomal storage disease characterized by cholesterol retention in lysosomes of several organs[276].

Recently, the group of Roberto Zoncu demonstrated the important function of intra-lysosomal cholesterol concentration and of its regulatory proteins in mTORC1 activity. NPC1 was shown, via its cholesterol transport activity, to couple lysosomal cholesterol concentration to mTOR recruitment and activation on lysosomes[249,277,278]. Indeed, loss of function mutations of NPC1 led to the constitutive activity of mTOR, deregulating mitochondria homeostasis, a phenotype observed in patients carrying NPC1 mutations[277]. Linked to that, LYCHOS (lysosomal cholesterol sensing protein) was shown to directly sense intra-lysosomal cholesterol via its amino-terminal permease-like region and to positively regulates mTORC1 through the cytosolic sequestration of the mTORC1-inhibitory complex GATOR1 (GAP Activity Toward Rags complex 1)[249] (see section B-II-3). Oppositely, mTORC1 activity was described as a regulator of intra-lysosomal turnover of lipids. By performing lysosomes purification and targeted lipidomic analysis, Aaron Hosios described that upon mTOR inhibition, the endocytic delivery of plasma membrane phospholipids to the lysosomes is favored, increasing the release of free fatty acids necessary for triglycerides synthesis and storage into lipid droplets. *A contrario*, mTOR activation switched this pathway toward phospholipid synthesis, demonstrating the important role of mTOR in lysosomal lipid turnover and more globally in cellular lipid handling and energy production[279].

B-II- A multifaceted organelle

B-II-1- Degradative ability

Autophagy

Active destruction of cellular biomass is necessary for removal of damaged or toxic components as well as nutrient cycling during fasting. In this context, both the autophagic pathway and the lysosomes play considerable functions[167]. The activity of lysosomes, as previously stated, relies on acidic hydrolases and acidic pH via the activity of the V-ATPase. Autophagy, for its part, can be classified into three main types, namely chaperone-mediated autophagy, micro-autophagy, and macro-autophagy, depending on the nature of the substrate or the delivery route to lysosomes[196]. Micro-autophagy, unlike the two other types of autophagy, is directly mediated by lysosomal action. Either by protrusion or invagination of the lysosomal membrane, non-specific cargoes are directly catched by lysosomes to be degraded[280]. Rather appearing as a nonspecific and random mechanism, increasing evidence also demonstrated the existence of selective micro-autophagy. As an example, micro-lysophagy, the process by which lysosomal membrane is internalized into the lysosomal lumen for recycling, was shown to play a prominent role in lysosome turnover under stress. Mechanistically, Lee C. and colleagues demonstrated that under glucose starvation or lysosomal osmotic stress induced by the use of the chemical compound L-Leucyl-L-Leucine methyl ester (LLOMe), lysosomes are decorated by the lipidated form of LC3B, inducing the formation of intraluminal vesicles, maintaining lysosomal fitness[281]. The authors also highlighted that depending on the stress input, the micro-autophagy observed was either globally affecting lysosomes, or specific of certain substrates. Indeed, LLOMe treatment induced the recycling of most of lysosomal proteins, whereas glucose starvation affected the internalization of a specific pool of lysosomal ion channels[281].

Macro-autophagy, referred to as autophagy, is the most studied form of autophagy. Long seen as a non-specific degradative pathway, macro-autophagy is however tightly modulated under distinct environmental or stress conditions and can be highly specific of the substrate[282]. Macro-autophagy is a complex mechanism involving cargo recognition, encapsulation of the cargo in a double-membraned autophagosome, and fusion with a LE or lysosome for degradation.

Selective autophagy allows to maintain the integrity and number of organelles as well as the clearance of toxic protein aggregates and pathogens. Upon cellular stress, cargoes are stamped with signaling molecules such as ubiquitin, sugars, or lipids[283]. These marks are then recognized by selective autophagy receptors (SAR). An extensive number of studies allowed the description and classification of SARs (Table 3)[284]. Among them, the proteins sequestosome-1 (SQSTM1/P62), next to BRCA1 gene 1 protein (NBR1) or tax1-binding protein 1 (TAX1BP1), are involved in the recognition of different cargoes[284]. By presentation of a LC3-interaction region (LIR), SAR and their bound cargo are recruited to ATG8s decorated nascent phagophores for their engulfment, a process explained later in the paragraph[285]. Lysosome permeabilization (see section B-II-4) can lead to cell death if the machinery for repair or turnover of the organelle is not efficient. The integrity of lysosomes is therefore strictly regulated. Several SAR have been shown to recognize damaged lysosomes for their autophagic recycling, among which P62, TAX1BP1 and NDP52[283,286]. Upon lysosomal membrane permeabilization (LMP), intra-lysosomal glycans directly recruit the ubiquitin ligases UBE2QL1 or FBXO27, that ubiquitinate lysosomal membrane proteins and lead to the recognition of damaged lysosomes by P62 or TAX1BP1 SAR[287–289]. NDP52 does not recognize ubiquitin modifications, but rather lectins bound to exposed lysosomal glycans, notably galectin-8[290]. Other galectins, such as galectin-3, were also shown to play important functions in lysosomal repair and autophagic clearance by directing mTOR activity as well as recruiting autophagic effectors[291–293] (see section B-II-4). Once tagged with SAR, damaged lysosomes are engulfed in a phagophore to be sent for degradation in another lysosome.

Type of selective autophagy	SARs
Aggrephagy	P62, NBR1, OPTN, TOLLIP, TAX1BP1
Lipophagy	P62
Lysophagy	P62, TAX1BP1, NDP52, TRIM16
Mitophagy	P62, NDP52, TAX1BP1, OPTN, TOLLIP, BNIP3
Ribophagy	NUFIP1
Pexophagy	P62, NBR1
Xenophagy	P62, NDP52, OPTN, TAX1BP1

Table 3: Major types of selective autophagy and associated selective autophagy receptors (SARs).
SAR: Specific autophagy receptor.
Adapted from: Gubas, A. & Dikic, I., FEBS J. (2022)

Five core autophagy complexes are involved in the processes of membrane nucleation, elongation, and closure of the autophagosome[294] (Table 4, Fig. 16). Nutrient availability is an important determinant of autophagosome biogenesis, with mTORC1 and AMPK (AMP-activated protein kinase) being upstream negative regulators of the ULK (Unc-51-like kinase) and PIK3C3-C1 complexes under nutrient-rich conditions[295]. Upon activation, the ULK complex is recruited to the endoplasmic reticulum membrane in a PI(4)P dependent manner, where it can stabilize the PIK3C3-C1 complex, generating PI(3)P-rich domains termed omegasomes[296,297]. The phagophore elongation process further relies on several lipids transport pathways, such as vesicle-mediated delivery, extrusion from pre-existing organelles or protein-mediated transport[294]. Notably, ATG9-containing vesicles emanating from the Golgi apparatus, the ER, or endosomes, were shown to feed the nascent autophagosome[298,299]. Recently, using purified proteins and biochemical reconstitution of the autophagic initiation complexes, Ahn Nguyen and colleagues uncovered the predominant function of ATG13 and ATG101, two components of the ULK complex, in the assembly of the supercomplex necessary for phagophore generation on the endoplasmic reticulum. They notably show that the conformational changes, that they defined as metamorphosis, in a tripartite complex (ATG13, ATG101, ATG9), provide a time-dependent regulatory mechanism for lipid transfer to the nascent phagophore via the classical lipid transfer protein ATG2[300].

ATG8s (LC3s/GABARAPs) proteins are also major determinant of phagophore elongation and substrate recognition. Through the activity of a lipidation complex, ATG8s are cleaved and subsequently conjugated to phosphatidylethanolamine (PE) for their anchorage to the phagophore[301]. As previously discussed, lipidated ATG8s are able to recognize SAR decorated-cargoes destined for specific macro-autophagy[285]. Lipidated ATG8s were also shown to play an important function in phagophore curvature, elongation, and closure. Indeed, the expression of an inactive mutant form of ATG4B, one of the component of the lipidation machinery of ATG8s, was shown to induce accumulation of unclosed phagophores[302]. Another study demonstrated, in a cell-free system, that LC3 itself, via the presentation of charged amino acids in its N terminus, could trigger membrane tethering and fusion[303].

The ESCRT machinery (see section B-II-4) is strongly implicated in the phagophore closure. ESCRT-I binding to the site of closure is followed by the recruitment of the ESCRT-III components CHMP2A and -4B, further polymerazing and closely

appositioning the two adjacent membranes, inducing their fission and phagophore closure[304,305]. Recent studies demonstrated other sites of phagophore formation. Indeed, the FAK family kinase-interacting protein of 200 kDa (FIP200) protein, component of the ULK complex, was demonstrated to interact directly with SAR decorated cargoes. Notably, NDP52 was shown to promote this interaction through its activation by the TANK-binding kinase 1 (TBK1)[306,307]. The PIK3C3-C1 complex, recruited together with the ULK complex, induces PI(3)P production on the nascent phagophore, enabling the recruitment of ATG8 and its lipidation machinery, inducing phagophore elongation and closure, as discussed previously[294]. This is notably true for mitophagy in which ubiquitin-decorated mitochondria are recognized by NDP52 for their subsequent engulfment. In parallel, an unconventional mechanism for mitophagy was recently described. Optineurin (OPTN), another SAR recognizing ubiquitin chains, directly recruits TBK1 at the surface of mitochondria for PIK3C3-C1 activation, PI3P production, and subsequent generation of the phagophore around the cargo, bypassing the activity of the ULK complex[308]

Complex	Components	Functions
ULK complex	ULK1/2, ATG13, FIP200, ATG101	Recruitment and stabilization of the core autophagic-biogenesis machinery
PIK3C3-C1	VPS34, BECN1, p150, ATG14L, NRFB2	Generation of PI(3)P-rich domains, omegasomes, necessary for nucleation
ATG12	ATG5, ATG7, ATG10, ATG12, ATG16L1	Cleavage and lipidation of ATG8s proteins. Also involved in the delipidation process for recycling of ATG8s
ATG8	ATG3, ATG4A-D, ATG7, ATG12-ATG5, ATG16L1, ATG8s	Ubiquitin-like proteins anchored to membrane through PE conjugation. Involved in phagophore expansion, transport to lysosomes and capture of cargoes
ATG2	ATG2A/B, ATG9, WIPI1-4	Tethering of the autophagosome to the ER for lipid transfer

Table 4: List of core autophagy complexes composition and functions.
ATG8s: LC3A-C, GABARAP, GABARAPL1/2, ATG: Autophagy-related genes, ULK: Unc51-like kinase, PIK3C3-C1: Class III phosphatidylinositol 3-kinase complex I, PI(3)P: Phosphatidylinositol 3-phosphate, PE: Phosphatidylethanolamine, ER: Endoplasmic reticulum. Adapted from: Melia, T. J. et al., JCB (2020)

The last step of autophagy involves the fusion between the degradative lysosomes and autophagosomes for their destruction. The precise molecular mechanism started to be elucidated by Eisuke Itakura in 2012[309]. Syntaxin-17 (STX17), a classical SNARE (N-ethylmaleimide-sensitive factor-attachment protein receptor) was described to specifically associate with completed autophagosomes in their membrane and to mediate lysosome-autophagosome fusion events. Via its interaction with SNAP29 (synaptosomal-associated protein 29) on the autophagosomal membrane, and its link with VAMP8 (vesicle-associated membrane protein 8) on the lysosomal membrane, STX17 induces the formation of a trans-SNARE complex driving membrane apposition and fusion. It was notably demonstrated that the independent removal of each of these components are impairing lysosome-autophagosome fusion, leading to autophagosome accumulation[309]. This discovery opened the path for a more precise description of the machinery involved in this fusion process. The HOPS tethering complex, previously described as necessary for lysosome homotypic fusion[310], promotes autophagosome-lysosome fusion through interaction with STX17 and its fusion partners. As such, removal of the main components within the complex, such as VPS33A, VPS16, or VPS39 blocked the autophagic flux[311]. A later study by the group of Ivan Đikić demonstrated the role of PLEKHM1 (pleckstrin homology domain containing protein family member 1) in bridging ATG8 positive autophagosomes together with Rab7 and the HOPS complex for lysosome-autophagosome fusion[312]. As previously discussed, Rab7 is an important determinant of LE/lysosome fate. It also appears as an important effector of autophagosome-lysosome fusion via recruitment of specific effectors such as PLEKHM1[312]. Among others, the proteins FYCO1 (FYVE and coiled-coil containing 1) and RILP (rab-interacting lysosomal protein) were shown to promote fusion between lysosomes and autophagosomes via interaction with GTP-loaded Rab7 and further regulation of the traffic and localization of lysosomes and autophagosomes[313,314] (see section B-II-2). The technological advances operated during the last twenty years allowed to physically resolve the structure of SNARE complexes[315,316]. Today, with the development of optimized cryo-electron microscopy, as well as *in silico* structural prediction, entire fusion complexes and their function are deciphered, as it was recently published for the HOPS complex[317], allowing a more complex and precise description of fusion events and their subsequent regulation.

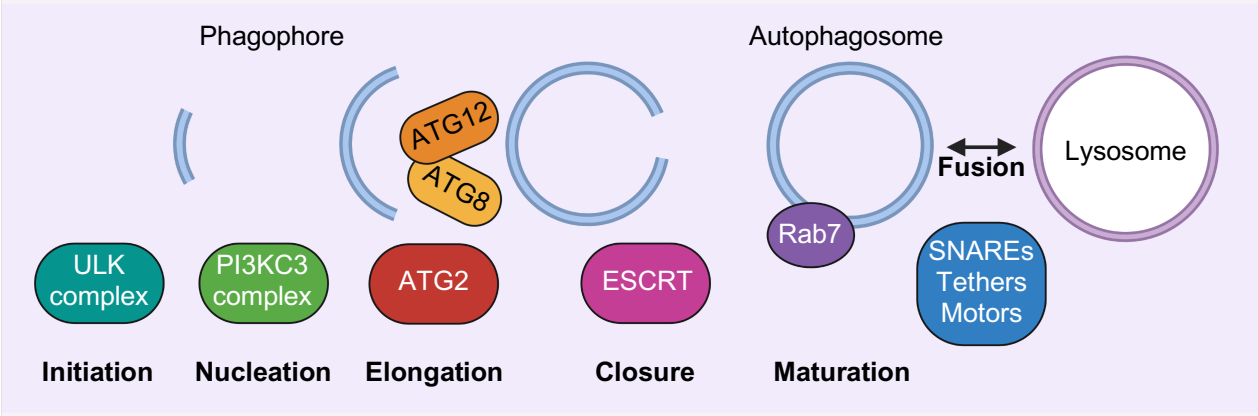

Figure 16: Autophagosome biogenesis. Key effector complexes and molecules are linked to the different steps of autophagosome biogenesis. See table 4 for complete composition and function of the different complexes.
ULK: Unc-51 like autophagy activating kinase, PI3KC3: Class III phosphatidylinositol 3-kinase, ATG: Autophagy related genes, ESCRT: Endosomal sorting complexes required for transport, SNARE: Soluble N-ethylmaleimide-sensitive-factor attachment protein receptor.
Adapted from: Reggiori, F. et al., Glycoconj J. (2021)

Lysosomal-degradative ability subversion

In recent years, the development of targeted protein degradation (TPD) has considerably improved the arsenal of approaches used to deplete specific proteins. TPD takes advantage of the cells' own degradation machinery, namely the ubiquitin proteasome system (UPS) and the autophagy-lysosome pathway[319]. In 2001, the first proteolysis targeting chimera (PROTAC) molecule was developed in order to target the protein methionine aminopeptidase-2 (MetAP-2) to a specific ubiquitin ligase complex and further proteasome dependent degradation[320]. This first demonstration of molecular-based TPD led to the generation of several classes of technologies classified according to the use of the UPS, the endo-lysosome system, or the autophagy-lysosome system, for the final degradation of the targeted product[319]. Lysosome-based TPD have the potential to target numerous compounds, such as intra- or extra-cellular proteins, either cytoplasmic or anchored in membranes, protein aggregates and entire organelles, making them much more attractive than proteasome-based TPD, that can only target certain intracellular proteins[319]. The first lysosome-based TPD technology was developed in 2014, taking advantage of the chaperone-mediated autophagy process, provoked by the recognition of a KFERQ sequence on the target protein by the heat shock cognate 71 kDa protein (HSPA8)[321]. Thus, a synthetic peptide harboring a cell penetrating domain, the KFERQ sequence, and a protein of interest (POI) binding sequence, can effectively send the cytoplasmic target to the surface of lysosomes, where the interaction with

the LAMP2 protein allows its internalization inside the lumen of lysosomes for degradation[322]. Following this innovation, other groups demonstrated the potential of using the autophagic machinery for the degradation of intracellular components. The autophagosome tethering compound (ATTEC) and autophagy-targeting chimeras (AUTOTAC and AUTAC) systems indeed target the protein of interest to nascent autophagosomes for their subsequent degradation in the autolysosomes[323–325]. As compared to the CMA-based TPD, autophagy-based TPD can lead to the degradation of protein aggregates and entire organelles[323–325]. Since 2020, several technologies subverting the endo-lysosomal pathway for TPD were engineered. The antibody-based PROTAC (AbTAC) utilizes bispecific antibodies that recognizes on one hand an extracellular or transmembrane POI, and on the other hand, the transmembrane E3 ligase RNF43, leading to the complexation of the two targets and further internalization and degradation in the lysosomal compartment[326]. This technique has notably proven efficient for the degradation of the transmembrane protein programmed death-ligand 1 (PD-L1), a known suppressor of T-cell response, overexpressed in numerous cancers[326]. Such as AbTAC, the lysosome-targeting chimera (LYTAC) system was also developed in order to degrade transmembrane or extracellular proteins. The later benefits from the presence at the plasma membrane of residual CI-M6PR. By fusing poly-M6P (CI-M6PR-targeting ligand) on molecules or antibodies directed against specific proteins, the targeted substrate is then recognized by the lysosomal-targeting receptor for further internalization and delivery to the lysosomes[327] (Fig. 17). Although effective in removing proteins or entire organelles, these nascent lysosome-based TPD systems need further investigations to decipher the impact of this hijacking on the lysosomal system.

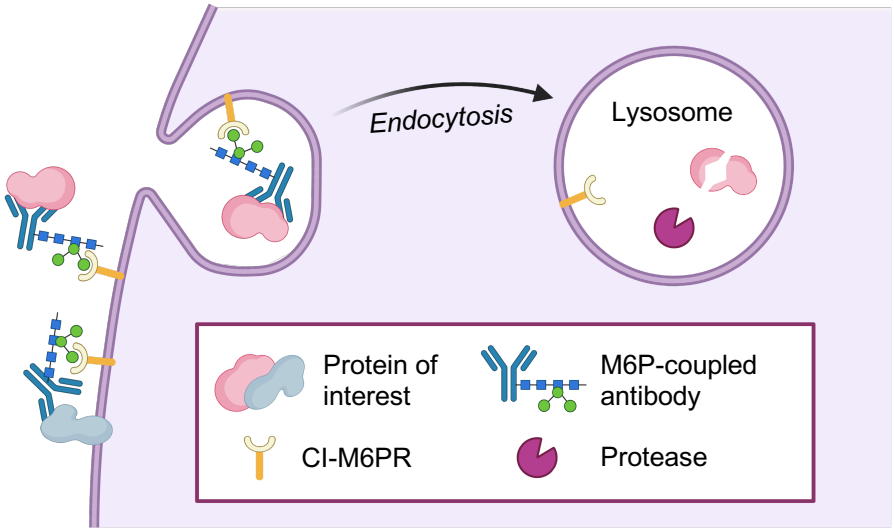

Figure 17: LYTAC system. M6P-coupled molecules or antibodies target the soluble or membrane bounded protein of interest. Once recognized, the M6P tag binds CI-M6PR present at the plasma membrane, and engulfed in the endocytic pathway. The protein is degraded in the lysosomes by proteases.
M6P: Mannose-6-phosphate, CI-M6PR: Clathrin independent mannose-6-phosphate receptor.
Adapted from: Zhao, L. et al, Signal transd. and targeted therapy (2022)

B-II-2- Intracellular trafficking / Lysosomal positioning

Lysosomes are dynamic organelles and their distribution throughout the cytosol have been shown to correlate with their degradative and signaling abilities. Because of their implication in catabolism and anabolism, their position therefore contributes to many cellular functions. Two main pools of lysosomes exist within cells: a peripheral, moving one, and a perinuclear, relatively immobile[328,329]. As such, lysosomes associate with active directional effectors moving along microtubules (Fig. 18A-C). For the minus-end transport of lysosomes (toward the microtubule-organizing center; MTOC; perinuclear), Rab7 stamped LEs/lysosomes recruits RILP, itself recruiting p150(Glued), further interacting with dynein and dynactin, important motor machinery for lysosome transport[330,331]. Interestingly, lysosomal cholesterol level was shown to promote this process via the cholesterol-sensing ability of ORP1L (oxysterol binding protein related protein 1L). Under low lysosomal-cholesterol level, ORP1L induces ER-lysosomes contacts. These contacts allow the ER protein VAP (VAMP-associated protein) to untie the interaction of motor proteins with Rab7, unleashing lysosomes toward the periphery. Oppositely, lysosomal cholesterol accumulation, as in Niemann-Pick type C disease, leads to lysosomal clustering in the perinuclear cloud[332].

Even though Rab7 is a major actor of lysosomal positioning, the GTP-binding protein SEPT9 (Septin-9) was recently shown to induce dynein-dynactin-retrograde transport of lysosomes in a Rab7-independent fashion. In contrast to Rab7, SEPT9 preferentially binds to GDP-bound dynein, favoring this mode of transport during oxidative stress or allowing another regulatory layer of movement at steady state[333].

Other signals enable lysosomal transport next to the nucleus. Ca^{2+} and phosphoinositides were linked to lysosomal movement. During the maturation process, PI(3)P is converted into $PI(3,5)P_2$ (see section B-I-2-1), upstream regulator of the lysosomal calcium channel TRPML1[334]. Ca^{2+} release from lysosomes recruits ALG-2 (Apoptosis-linked gene 2), a known interactor of dynein for minus-end transport[335]. Of note, nutrient starvation was shown, via mTORC1 activation and TFEB nuclear translocation, to increase TRPML1 activity, therefore inducing lysosomal perinuclear localization[336].

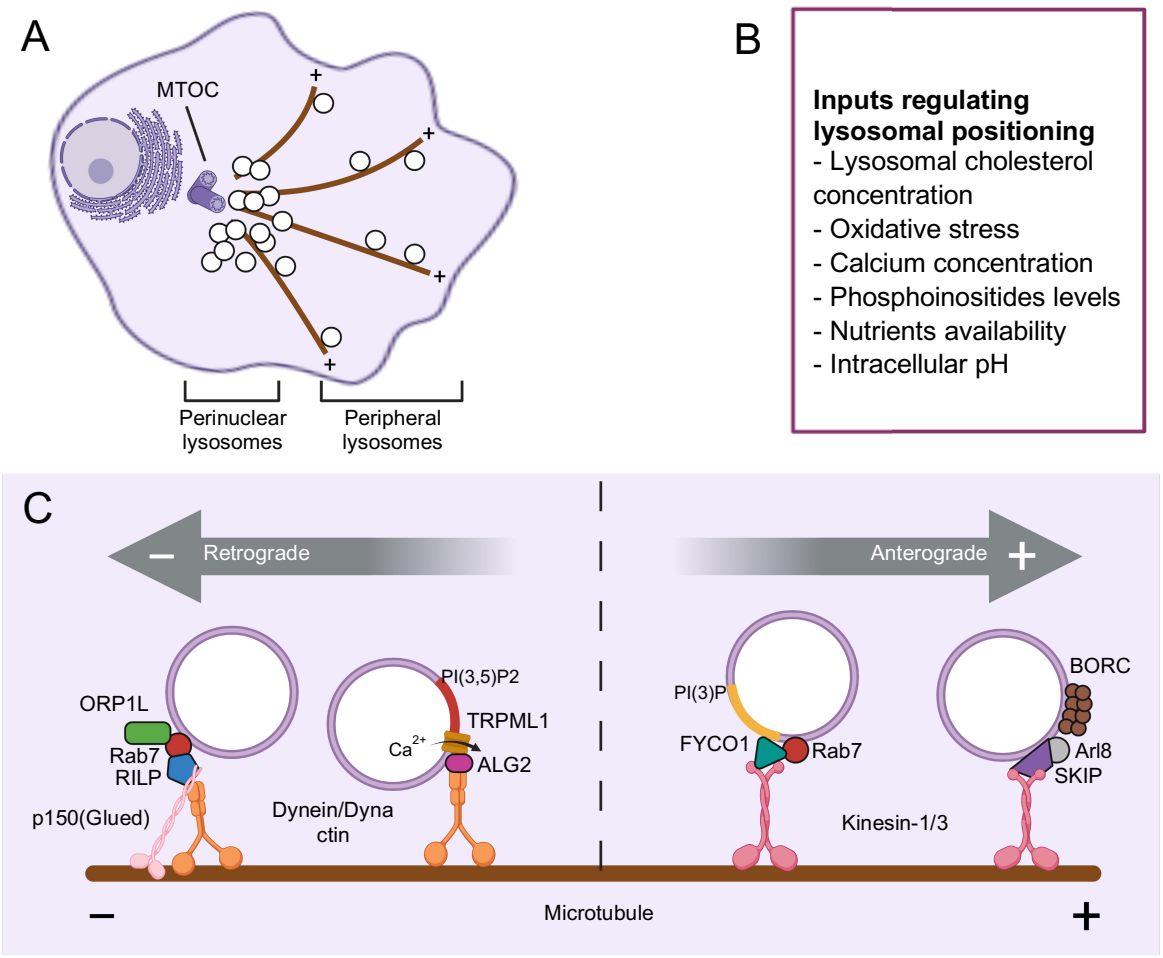

Figure 18: Mechanisms of lysosomal positioning. (A) Main lysosomal localizations in cells. Lysosomes can transit from a perinuclear cloud to the cell periphery along microtubules. (B) Major inputs regulating lysosomal positioning. (C) Main molecular actors of lysosomes positioning. Adapted from: Cabukusta, B. & Neefjes, J., Traffic (2018)

TFEB activity was found linked to lysosomes positioning via the upregulation of TMEM55B, a lysosomal interactor of JIP4 (JNK-interacting protein 4), connecting dynein to their surface[337]. Moreover, oxidative stress induced by H_2O_2 treatment promotes TRPML1-dependent Ca^{2+} release, ALG-2 recruitment to lysosomes and JIP4 phosphorylation, leading to nuclear clusterization of lysosomes for increased autophagic degradation as a defence mechanism[338].

Plus-end transport of lysosomes toward the cell periphery requires the activity of kinesins. PI(3)P level on the lysosomal membrane, in combination with the activity of Rab7, recruits FYCO1, bridging lysosomes and autophagosomes to kinesin-1 motor protein[313]. As mediated by phosphoinositide level, this process is highly dependent on ER-lysosomes contacts. Indeed, when such contacts happen, kinesin-1 is transferred from ER-localized protrudin to FYCO1-stamped lysosomes[339]. This is

notably true in fed cells in which PI(3)P is generated at the surface of lysosomes[173]. Alternatively, the BORC (BLOC1-related complex; composed of BLOS-1 and -2, Snapin, KXD1, myrlysin, lyspersin, diaskedin, and MEF2BNB) recruits SKIP via activation of Arl8b. SKIP can then bind to kinesin-1 (KIF5B) or kinesin-3 (KIF3B and KIF1A) for anterograde transport of lysosomes[340–342]. Starvation triggers dynein-mediated anterograde transport of lysosomes toward the nuclear cloud, while inhibits kinesin-mediated transport toward the periphery[329]. Indeed, amino acids removal induces folliculin recruitment to RILP, tethering lysosomes at Golgi contact sites through interaction with Rab34[343]. Concomitantly, Arl8b, via the BORC complex, is recruited to the Ragulator complex on lysosomes through the C-terminal domain of lyspersin, blocking its ability to bind kinesin-1[344,345]. Altogether, this demonstrates that lysosomes are dynamically responding to different cellular inputs, such as stress or nutrients. Subsequently, lysosomal positioning regulates the ability of lysosomes to fuse with membranes, degrade their substrates, and activate the mTOR kinase.

Lysosome positioning is of particular importance for the optimal regulation of mTORC1. Pioneering work performed by Viktor Korolchuk demonstrated that lysosomal positioning modulates mTORC1 in response to nutrients availability. Peripherally localized mTORC1 is indeed closer to its upstream regulators, resulting in a faster response to nutrient input. Oppositely, in response to starvation, lysosomes are clustered perinuclearly, resulting in a slowest response of mTORC1 upon amino acids replenishment[346]. Mechanistically, the intracellular pH, which modulates lysosome positioning[347], was shown to increase in response to starvation. This affected the ability of Arl8b and KIF2A to bind to lysosomes, resulting in the perinuclear clustering of lysosomes[346]. Even though the mechanism by which lysosome positioning controls mTORC1 activity appears complex, studies tend to demonstrate that peripheral dispersion of this organelle indeed converge on mTOR activation. PI(3)P production upon amino acid stimulation was indeed shown to promote lysosomal peripheral positioning in a Protrudin-FYCO1 dependent fashion and to allow mTORC1 activation[348]. Starvation induces mTOR inhibition, as well as increased autophagic flux. In accordance, lysosomal positioning also matches with their ability to fuse with autophagosomes and to degrade them[349]. Under starvation conditions, when cellular need for recycling is increased, newly generated autophagosomes are rapidly transported to the perinuclear cloud of lysosomes in an LC3-dynein dependent fashion[350]. This is thought to increase the probability of

encounter of the two vesicles[346,350]. Lysosome position correlates with the level of Rab7 at their surface, with peripheral lysosomes harboring less of the GTPase. Concomitantly, this results in less recruitment of the Rab7-interacting protein RILP, a known recruitment factor of the V1G1 V-ATPase subunit. As a consequence, peripheral lysosomes are found less acidic than perinuclear ones, less able to degrade autophagic cargoes[252]. This study was in accordance with the concept that lysosomes, within a cell, are highly heterogenous in their composition and functions[188].

Exocytosis of lysosomes is an important process in several pathological conditions. The peripheral localization and apposition of lysosomes next-to the plasma membrane are important determinant of this process[351]. The fusion process, that involves SNARE interaction and Ca^{2+} signaling, mediates plasma membrane repair and remodelling. LAMP1 indeed accumulates at sites of plasma membrane damage in a Ca^{2+} and fusion machinery-dependent fashion[352]. Lately, extracellularly released cathepsins B and L were shown to promote extracellular matrix remodelling allowing sphingomyelinase activity at the site of wound for repair. Cathepsin D in turn degrade the sphingomyelinase enzyme to terminate the process[353]. Lysosome exocytosis plays a major function in cellular detoxification. TRPML1 dependent Ca^{2+} release from lysosomes is an important process for lipid extrusion from lysosomes to the extracellular milieu. It is notably the case in lysosome storage diseases such as mucolipidosis type IV or Niemann-Pick disease in which TFEB is inhibited by constitutive mTORC1 signaling, downregulating TRPML1 and further lysosomal exocytosis. Lipid accumulation was also shown to directly inhibit TRPML1 function[354–357]. Even though appearing as essential for detoxification, lysosomal exocytosis can also be hijacked. β-coronaviruses uses this uncommon secretory pathway for their egress. This was shown to rely on a Arl8b and Rab7-dependent lysosomal positioning pathway[358]. More recently, SARS-CoV-2 protein ORF3a was shown to recruit the HOPS complex component VPS39 to the lysosomal surface, further implicated in the assembly of a BORC-VAMP7-STX4 complex, enforcing peripheral positioning of lysosomes and exocytosis of newly generated viruses[359].

B-II-3- The lysosome as a signaling platform

Lysosomes, via their degradative capacity, act as major regulators of catabolism. In parallel, through recycling of substrates into basic building blocks and via the regulation of the mTORC1 signaling complex, are primordial effectors of cellular anabolism[189]. As previously stated, the lysosomal lumen is a complex cluster of I) hydrolases dividing proteins, sugars, and lipids into their precursors units, II) transporters, allowing the exit of these components toward other organelles, and III) sensors, transmitting the concentration of amino acids, fatty acids, and cholesterol to dedicated signaling pathways[167,189]. In this context, the mechanistic target of rapamycin (mTOR) serine/threonine kinase is central to coordinate the nutrient concentrations to anabolism and catabolism. mTOR assembles into two distinct complexes known as mTOR complex 1 (mTORC1) and mTOR complex 2 (mTORC2)[128]. mTORC1 is composed of three core components: mTOR, Raptor and mLST8, with the two latest regulating mTOR localization and substrate binding to the kinase, and stabilization of the kinase domain of mTOR for optimal activation, respectively[360–364]. In addition, DEPTOR and PRAS40, two negative regulators of mTOR activity, were described as part of the complex[365–368].

The complete description of the pathway started in 1994 with the description of mTOR as the direct target of the rapamycin-FKBP12 complex, previously shown to block cell growth and proliferation[369,370]. This inhibitory complex binds mTOR to the subsequently named FKBP12-rapamycin-binding (FRB) domain, blocking the interaction between the kinase domain of mTOR and its substrates[371]. Because of its functions on proliferation and growth, mTOR received incredible consideration in order to decipher its upstream regulators.

Growth factors

The response to growth factors of mTORC1 was the first one to be described. Indeed, as far as the discovery of the effect of the rapamycin-FKBP12 complex in 1992, serum was shown to promote the growth effect of mTOR[372]. EGF, VEGF, IGF, and insulin, are among the many growth factors positively regulating mTORC1[373]. Upon binding to their respective receptors, growth factor-associated tyrosine kinase receptors converge on the activation of the ERK or AKT pathways, central regulators of cell survival and growth[374]. ERK and AKT regulate mTORC1 activity through the inhibition of the inhibitory tuberous sclerosis complex (TSC). The TSC is composed of TSC1, TSC2, and TBC1D7, and negatively regulates the small GTPase Rheb.

Upon growth factor stimulation, lysosome-bound TSC, via the G3BP tethers, therefore dissociates from the lysosomal surface, enabling Rheb GTP loading and further mTORC1 activation by conformational reorganization of the kinase[375–379].

Cellular stress response

ATP, oxygen levels, as well as DNA damage, were shown to modulate the activity of mTORC1. AMPK appears as a central regulator of the stress regulation of mTOR[128]. A decreased level of glucose and oxygen correlates with a reduced production of ATP within mitochondria, activating AMPK, itself inhibiting mTORC1 via activation of TSC[380,381]. In parallel, oxygen can promote REDD1 (regulated in development DNA damages responses 1) activity that acts in parallel of AMPK to activate TSC, thereby negatively regulating mTORC1 activity[382]. Notably, AMPK was shown to directly phosphorylate Raptor to block the activity of mTOR[383]. Lysosomal damage sensed by the GALTOR system also converge in the activation of AMPK and inhibition of mTORC1[292,384] (see section B-II-4). DNA damage, via a transcriptional regulatory network induced by p53 increases TSC activity[385].

Amino acids

As a sensor of nutrient availability, it is not surprising that mTORC1 responds to amino-acid level. The upstream regulation of mTOR by amino-acids is complex and involves several cytoplasmic sensors, as well as lysosomal transporters and tethers for mTORC1 anchorage to the lysosomal surface[128,167,189,373] (Fig. 19). Three main complexes transmit the cytosolic level of amino acids toward the Ragulator-RagGTPases for mTORC1 recruitment to the surface of lysosomes. GATOR2 (Mios, WDR24, WDR59, Seh1L and Sec13) negatively regulates GATOR1 (DEPDC5, Nprl2 and Nprl3)[386], itself tethered to the lysosomal membrane by KICSTOR (Kaptin, ITFG2, C12ORF66 and SZT2)[248,387]. The Ragulator complex (MP1, P14, p18, HBXIP and C7ORF59, also known as Lamtor1-5) bridges the Rags to the lysosomal surface for mTORC1 activation[388,389]. One important determinant of mTORC1 activity is the nucleotide-bound state of the Rags. Rags are heterodimers comprised of RagA or RagB bound to RagC or RagD. The GAP activity of GATOR1 toward RagA negatively regulates the ability of Rags to recruit mTOR-bound RAPTOR to the lysosomes to further complete the activation by Rheb-GTPase[388,389]. In parallel, the FLCN/FNIP complex acts as a GAP for RagC/D, helping mTORC1 recruitment and activation upon high nutrient configuration[390–393]. However, as recently published, the Rag dimer code regulation of mTORC1 appears more sophisticated than the one

previously described. Indeed, the expression of RagC/D correlated with the mTORC1-substrate specificity, whereas RagA/B expression was linked to mTORC1 recruitment to lysosomes, with RagB expressing cells maintaining the lysosomal localization of mTORC1 even upon starvation[394]. Interestingly, the expression of the different Rags varies between cell types, depending on the feeding state, and seems altered in certain cancers, opening new regulatory modes in disease-associated states[394]. Several sensors of amino acids transmit the feeding state of cells to the GATOR1 complex for further mTORC1 activation. CASTOR1, Sestrin2, and SAMTOR, senses respectively arginine, leucine, and methionine. SAMTOR indirectly transmits methionine availability via S-adenosylmethione (SAM), a metabolite generated depending on methionine concentration[395].

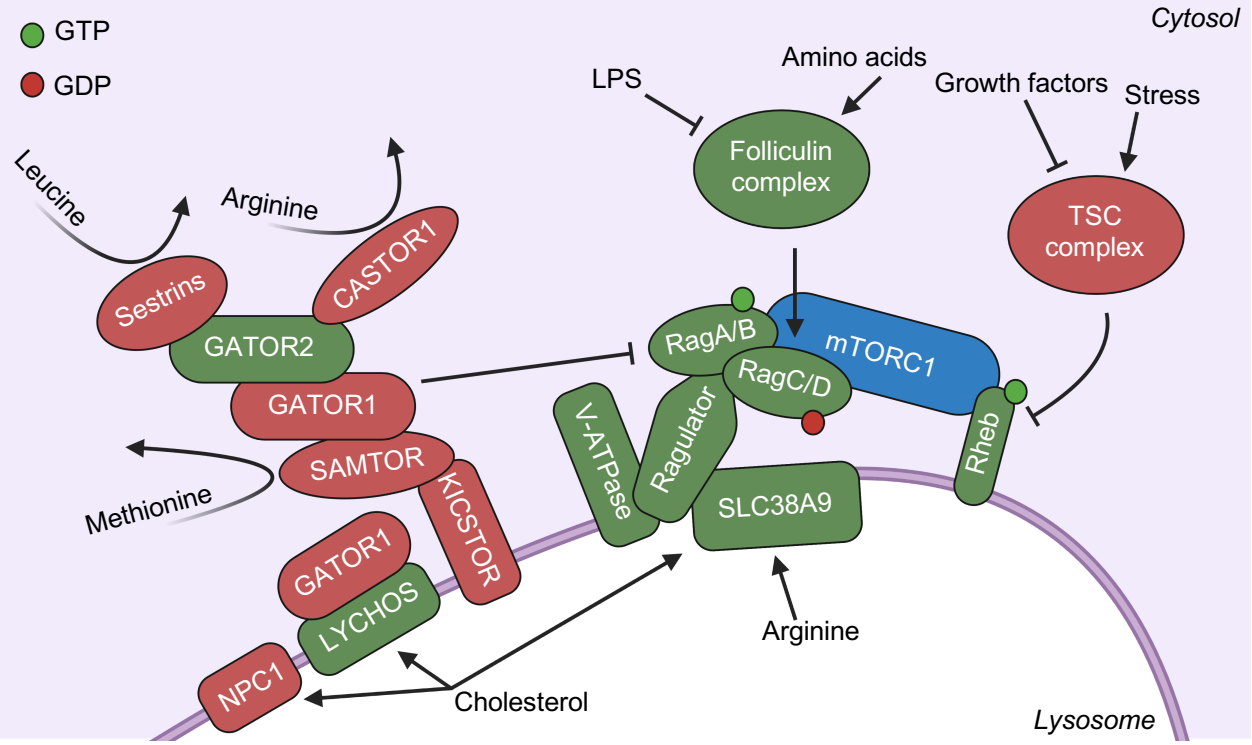

Figure 19: mTORC1 signaling pathway. An important signaling platform is present at the surface of lysosomes to regulate mTORC1 lysosomal recruitment and activation. The TSC complex integrates growth factors and stress signals. When activated, negatively regulates the small GTPase Rheb, an essential activator of mTORC1 when in a GTP bound form. On the other side, several cytoplasmic proteins and complexes sense amino acids concentration and transmit it the GATOR complexes. For optimal activation of mTORC1, GATOR1 needs to be inactivated. LYCHOS and GATOR2 acts as negative regulators of GATOR1 in response to amino acids or cholesterol concentration, respectively. The amino acids and cholesterol sensing machineries converge on the RagGTPases. The GTP bound form of RagA/B in complex with the GDP bound form of RagC/D regulates substrates recruitment and bridges mTORC1 to the surface of lysosomes through interaction with the lysosomal bound Ragulator complex.
Positive regulators are depicted in green, negative regulators in red.
GTP: Guanosine triphosphate, GDP: Guanosine diphosphate, LPS: Lipopolysaccharide, TSC: Tuberous sclerosis complex, mTORC1: mammalian target of rapamycin complex 1.
Adapted from: Kim, J. & Guan, K-L., Nat. Cell Biol. (2019)

Upon sensing, these proteins are inhibited, releasing the pressure put on GATOR2 thereby inhibiting GATOR1, leading to RagA/B GTP loading and further mTORC1 recruitment[395–400]. Recently, SAR1B was demonstrated to act in parallel of Sestrin2 for leucine sensing, GATOR2 inhibition, and further Rags activation[401]. Interestingly, the lysosomal level of arginine can be sensed by the amino-acid permease SLC38A9. When the lysosomal-arginine level is high, SLC38A9 regulates leucine export for its cytosolic sensing and activation of mTORC1[262–266].

The V-ATPase is also importantly implicated in the process via binding to the Ragulator and SLC38A9[262,389,402]. Of note, mTORC1 also appears essential for optimal V-ATPase assembly and activity, proposing a regulatory loop mechanism[183]. Therefore, the combined regulation of mTORC1 localization by the cytosolic and lysosomal amino sensing machinery and Rags recruitment, coupled to the growth factors regulation of Rheb activity through TSC, contributes to the lysosomal activation of mTORC1.

Cholesterol

The description of cholesterol as an input signal for mTORC1 started with the discovery that obese and high fat diet-fed rat presents high mTORC1 activity[403]. Ten years later, the group of Roberto Zoncu officially identified cholesterol as a nutrient input regulating mTORC1 recruitment at the lysosomes and activation. Intra-lysosomal cholesterol recognition by SLC38A9 as well as the cholesterol export function of NPC1 were shown essential in this process. In the following years, many aspects of the NPC1-mTORC1 axis were deciphered, notably how NPC1 deficient cells sustain a constitutive activity of mTOR. Membrane contact sites between the ER and lysosomes indeed induce the translocation of cholesterol from its synthesis site toward its sensing platform, lysosomes. The OSBP cholesterol transporter was shown essential, as its removal restores mTORC1 activity in an NPC model[404]. Furthermore, lysosomal targeted proteomic uncovered the degradative defects induced by cholesterol build-up in NPC1-deficient cells. This study revealed that autophagic cargo accumulation in lysosomes as well as the increased propensity for lysosomal membrane permeabilization upon NPC1 inhibition resulted from the constitutive activity of mTORC1, as its inhibition using Torin1 restored these phenotypes. Interestingly, cholesterol accumulation was not restored, indicative of a mechanism consistent with classical mTOR regulated processes such as protein synthesis or autophagy inhibition[277]. Lastly, LYCHOS, a multidomain lysosomal

transmembrane protein, was identified as the lysosomal cholesterol sensor and Rags activator. Upon intra-lysosomal cholesterol sensing, LYCHOS sequesters the GATOR1 complex, thereby allowing Rags dependent recruitment of mTORC1 to its activating platform[249]. Of note, and as for the Rags, LYCHOS and NPC1 protein levels are correlated with the feeding state of cells. High nutrients availability indeed increases transcription of LYCHOS and decreases the one of NPC1, fuelling the mTORC1 activating machinery[249].

As a pleiotropic kinase regulated by the feeding state, activated mTOR regulates major anabolic and catabolic processes. When nutrients are abundant, mTOR activity allows cell growth and proliferation while negatively regulates the lysosomal-autophagic catabolic process (Fig. 20).

Anabolism

The activating phosphorylation of p70S6 kinase 1 (S6K) and the parallel inhibitory phosphorylation of eIF4E binding protein (4EBP) by mTORC1 favors protein translation[405–407]. S6K phosphorylation by mTORC1 was also shown to activate a lipid and pyrimidine synthesis pathway through the activation of sterol responsive element binding protein 1 (SREBP1) and carbamoyl-phosphate synthetase (CAD), respectively[408–410]. Moreover, mTORC1 indirectly increases the expression of MTHFD2, a key enzyme in purine synthesis[411]. mTORC1 also phosphorylates Lipin1, known negative regulator of SREBP1, a key transcription factor involved in lipid synthesis[412,413]. Finally, STAT3 phosphorylation by mTORC1 was shown to promote HIF1α transcription, further increasingly translated because of S6K and 4EBP regulation, regulating glucose production[409,414]. Altogether, this demonstrates the preponderant role of mTORC1 in regulation of proliferation and cell growth by modulating lipid and protein synthesis.

Catabolism

mTORC1 activation negatively correlates with the main cellular catabolic process, the autophagic/lysosome degradative pathway. mTORC1 directly phosphorylates and inhibits ULK1, ATG13, UVRAG, and ATG14L, regulators of autophagosome biogenesis and maturation[295,415,416]. TFEB, the master transcriptional regulator of lysosomes and autophagy is also directly controlled by mTORC1. Indeed, TFEB phosphorylation by mTOR at the serines S122, S138, S142, and S211, induces its shuttling from the nucleus to the cytosol and retention by the 14-3-3 proteins, blocking its transcriptional activity[220–224]. TFEB retention results in a global decrease

of the autophagic flux as a consequence of reduced autophagosome and lysosomes biogenesis. In parallel of the regulation of autophagy, mTORC1 inhibits ERK5, blocking proteasome assembly and downregulating its ability to degrade ubiquitin-tagged proteins. General protein ubiquitylation was also globally increased upon mTORC1 activation[417,418]. Of note, several studies demonstrated a RagC/D dependent recruitment of TFEB to mTORC1 for its phosphorylation, suggesting an amino acid-exclusive regulation of TFEB[222,394]. This is of particular interest in Birt-Hogg-Dubé syndrome, in which the upstream regulator of Rags, FLCN, is mutated. A study by the group of Andrea Ballabio showed that mutated FLCN blocks RagC/D in their GTP form, enabling TFEB dephosphorylation and shuttling to the nucleus. Of note, TFEB upregulates the transcription of RagC/D, increasing their activity. Therefore, the mechanistic understanding of this syndrome allowed the description of the specific roles of the Rags and of their GTP-GDP bound state for mTORC1 activity[419].

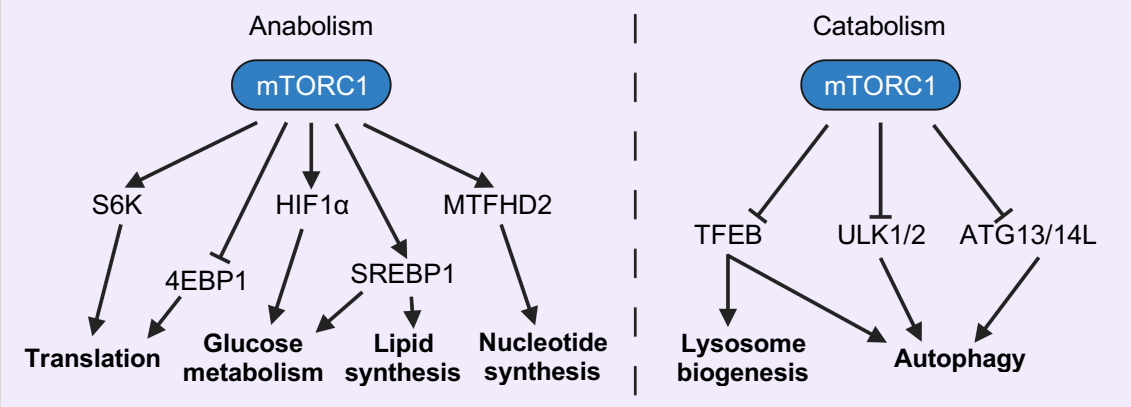

Figure 20: mTORC1 at the crossroad between anabolism and catabolism. Once activated, mTORC1 positively regulates protein, lipid, nucleotide, and glucose synthesis. Oppositely, it counteracts lysosome biogenesis and autophagy initiation. Numerous mTORC1 substrates have been described, some of them are annotated here.
Adapted from: Saxton R. A. & Sabatini, D. M., Cell (2017)

B-II-4- Implications in cell death

Lysosomal cell death

When firstly classified, cell death pathways were categorized according to morphological changes. Because of the difficulty to observe changes in lysosomal morphology depending on the cell death pathway engaged, lysosomal cell death (LCD) was only recently brought up to date, even though lysosomes, when described, were already nicknamed as "suicide bags". LCD occurs upon lysosomal membrane permeabilization and release in the cytosol of the lysosomal content[420,421],

a process not overtly affecting their shape and overall morphology[422]. The cell death pathway further engaged upon LMP depends on the extent of lysosomal leakage, ranging from apoptosis when LMP is limited, to necrosis when the lysosomal membrane is importantly compromised[423]. The work of Kagedal and colleagues twenty years ago nicely demonstrated that the addition of sphingosine, a detergent lipid accumulating in acidic compartment, led to LMP. Using increasing concentrations of this lipid, they described that the extent of LMP was indeed linked to different outcomes for cells, with the most important concentrations leading to the complete rupture of lysosomes and uncontrolled necrosis[423]. However, pharmacological or genetic inhibition of cathepsins B and D was shown to promote a significant protection against limited LMP[420,423]. Further demonstrating the role of cathepsins in cell death induced upon LMP, microinjection of CTSB[424] or CTSD[425] promoted mitochondrial permeabilization and further apoptosis.

Several pathways and inductors converge on lysosomal membrane permeabilization, leading to lysosomal cell death[420,421] (Fig. 21). The recent gain of interest in LCD allowed to distinguish between post-death alterations of lysosomes and LMP-induced cell death. Indeed, several actors of the classical cell death pathway apoptosis were described to induce LMP. TNFα (tumor necrosis factor alpha) was for example shown to induce caspases -8 and -9 activation and further LCD[426,427]. The work of the group of Marja Jäätelä demonstrated that TNFα can trigger apoptosis and LMP in parallel via the activation of caspases -8 and -9, and that the separate inhibition of the two pathways was only modestly delaying cell death, while the combination effectively rescued cell death[426]. Interestingly, some evidence also points toward a global modification in the sphingosine level in lysosomes upon TNFα stimulation that could trigger LMP. TNFα stimulation is associated with the activation of the protein factor associated with neutral sphingomyelinase activation (FAN)[428], leading to sphingomyelinase activation and further conversion of ceramide in sphingosine, its level correlating with the extent of LMP[423,427,429]. In line with this, CTSB release upon LMP promotes sphingosine kinase-1 (SK1) cleavage and reduction in the conversion of sphingosine into sphingosine-1-phosphate, contributing to LMP amplification[430].

Lysosomes, as the terminal compartment of autophagy, accept iron-containing proteins and are therefore enriched with this element[431]. In presence of hydrogen peroxide (H_2O_2) and when cells lack anti-oxidative activity, iron catalyses Fenton reactions, generating highly toxic hydroxyl radicals, leading to lipid peroxidation and

damaging lysosomal membrane proteins ending up in LMP[420,432]. The group of Raphaël Rodriguez notably identified that salinomycin and its derivative ironomycin, two agents previously identified as specifically eradicating breast cancer stem cells by unknown mechanisms, induces lysosomal iron accumulation and LCD[433]. Linked to that, several chemical compounds known to accumulate in lysosomes and therefore termed lysosomotropic agents, were shown to induce LMP. Siramesine represents the prototype of lysosomotropic compound, inducing a dramatic rise in lysosomal pH, ROS accumulation, cathepsins leakage and accumulation of autophagosomes due to lysosomes dysfunctions[434–436].

Besides sphingosine as a major driver of LMP, cholesterol also appears as an important lipid in the regulation of lysosomal integrity. However, whether lysosomal cholesterol accumulation protects or weakens the lysosomal membrane is still unclear and might depend on the trigger used to produce LMP. Hanna Appelqvist, as well as John Reiners, demonstrated the protective effect of lysosomal cholesterol accumulation. Upon use of U18666A, an inhibitor of the lysosomal cholesterol exporter NPC1 and inductor of lysosomal cholesterol accumulation, cells were less sensitive to photoirradiation or detergent-induced LMP[437–439].

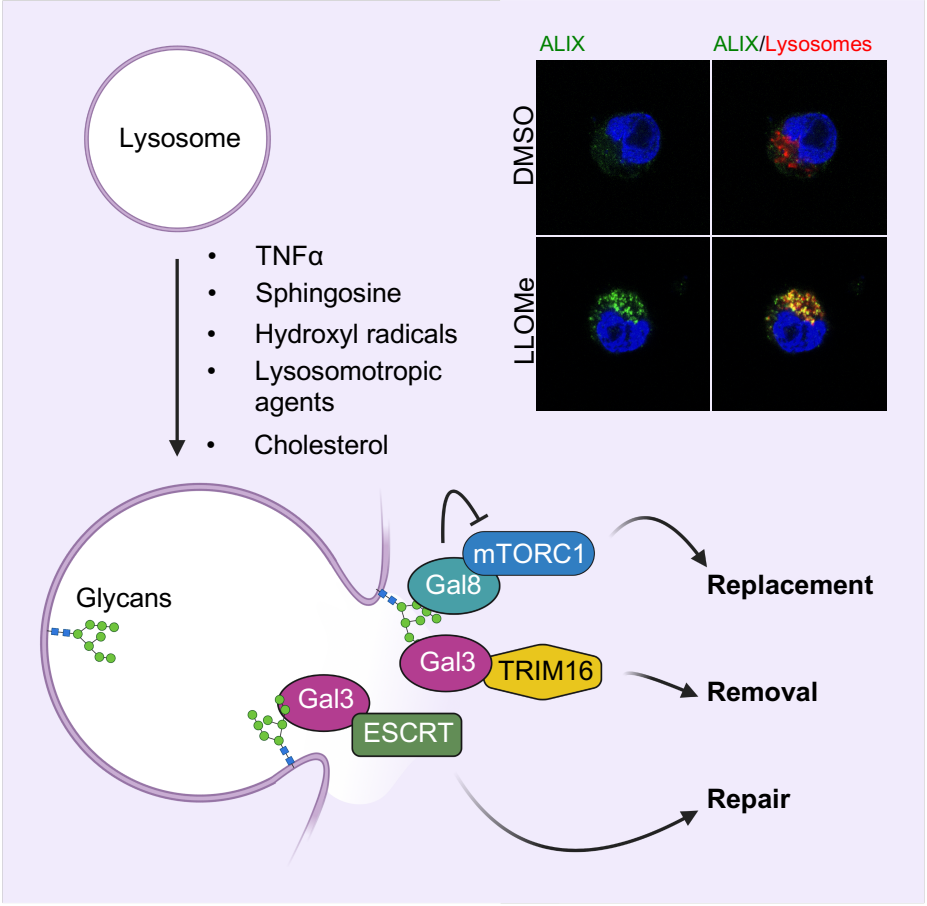

Figure 21: Lysosomal repair, removal, and replacement. Lysosomal membrane permeabilization (LMP) can occur in response to several inputs such as hydroxyl radicals production or lysosomotropic agents. Upon permeabilization, the galectin system recognizes cytosolic-exposed glycans and coordinates the recruitment of the ESCRT machinery for lysosomal repair, TRIM16 for autophagic removal, and the RagGTPases for mTORC1 inhibition.
In the top right corner, GSCs were treated with the lysosomotropic compound LLOMe and the integrity of lysosomes (red) was assessed with the recruitment of ALIX (green).
Gal: Galectin, TNFα: Tumor necrosis factor, ESCRT: Endosomal sorting complexes required for transport, LLOMe: L-leucyl-L-leucine methyl ester, GSC: Glioblastoma stem-like cell.
Adapted from: Jia, J. et al., Dev. Cell (2020)

More recently, the work of Oliver Davis revealed a contradictory effect of cholesterol accumulation on lysosome stability. In a model of human embryonic kidney cells, the knock-out of NPC1 or the use of U18666A increased the lysosomal propensity for damage induced by the membrane destabilizing agent LLOMe[277]. Whether the mechanism by which cholesterol modulates lysosome stability is cell type or input dependent remains of debate.

Lysosomal repair and removal

One major determinant of LCD is the ability for cells to sense and cope with LMP. Sonja Aits from the Marja Jäätelä group firstly described a sensitive assay to follow LMP. Given the fact that galectins bind to β-galactosides, they hypothesized that galectins would recognize lysosomal membrane rupture. In accordance with a previous report demonstrating galectin-8 recruitment to bacterial loaded and damaged vesicles, they indeed demonstrated that galectins -1, -3, -8, and -9, were able to aggregate on damaged lysosomes[290,440]. Following the description of this sensitive assay for LMP detection, the group of Vojo Deretic extensively ascribed molecular functions to galectins-recognition of damaged lysosomes. Several galectins were showed to bind to tripartite motif (TRIM) proteins, classical autophagy receptors. Notably, lysosomal galectin-3 binds to TRIM16, inducing the recruitment of the autophagic machinery for lysosomal removal and cell protection[291]. Following this discovery, the GALTOR system was uncovered. Co-IP experiments as well as a proximity biotinylation assays revealed that galectin-8 is dynamically associated with mTOR itself, as well as its close regulators. Jingyue Jia described that upon LMP, galectin-8 associates with the amino acid transporter SLC38A9 at the surface of lysosomes in a glycan-binding dependent fashion, sequestrating the Rag machinery and releasing mTOR out of this complex, inhibiting in turn its activity. In parallel, galectin-9 resides in complex with TAK1 (transforming growth factor-β activated kinase 1) and AMPK, activating the latest, further enforcing mTOR inhibition and activation of the autophagic pathway for lysosomal removal and replacement[292]. Following the description of galectins as important actors of lysosomal removal by autophagy, the group of Vojo Deretic further highlighted the function of galectin-3 in lysosomal repair, an event preceding autophagic replacement of lysosomes. By performing proximity biotinylation assay, they demonstrated that galectin-3 interacts with the ESCRT machinery, a complex necessary for membrane sealing, and already

described as necessary for lysosomal repair[441,442]. Notably, galectin-3 was demonstrated as necessary for the early recruitment of ALIX and CHMP4, two ESCRT components, at the surface of damaged lysosomes. At later time points, when the repair fails, galectin-3 induces autophagic removal of lysosomes[291–293] (Fig. 21). As previously described, autophagic lysosome reformation (ALR) might also play an important role in lysosomal regeneration. The recruitment of the ALR machinery by the TBC1D15 protein on ATG8-bound LIMP2 upon LMP for lysosome reformation is a recent example of this phenomenon[202]. As previously annotated, ESCRT recruitment to the site of damage is a primordial process for lysosomal repair. The ESCRT machinery is convoluted and composed of several complexes separately involved in different steps of membrane dynamic[305]. In the process of lysosomal repair, TSG101 and ALIX, two components of the ESCRT-I complex, were demonstrated as essential for the recruitment of the ESCRT-III complex, mostly represented by the protein CHMP4B, involved in membrane constriction together with the ATPase VPS4[441,442]. Mechanistically, LMP-induced Ca^{2+} release promotes the recruitment of the protein ALG-2 to their surface, further recruiting the ESCRT-I complex, engaging the ESCRT-dependent membrane repair mechanism[442,443].

The transfer of lipids between the ER and lysosomes have also emerged as a rapid way for cells to resolve the damage to the latest organelle independently of ESCRT recruitment. Indeed, recent studies highlighted that upon damage, the phosphatidylinositol-4 kinase type 2α is rapidly recruited to the lysosomal membrane to generate PI(4)P, mobilizing oxysterol-binding protein-related protein (ORP) family members, such as ORP9, -10, -11, OSBP, and ORP1L. In turn, via the interaction with the ER resident proteins VAPA/B, lysosomal ORP proteins induce membrane contact sites, allowing the transfer of cholesterol and phosphatidylserine from the ER to the damaged lysosomes in exchange of PI(4)P[444,445]. Finally, in response to the increased amount of phosphatidylserine in the lysosomal membrane, the ATG2 protein is recruited and activated, acting as a direct channel for lipid transfer from the ER to the lysosomes, allowing rapid lysosome repair[444]. Altogether, all the processes chronologically set up by cells to overcome lysosome damage demonstrate the importance of a tightly regulated lysosomal homeostasis for the maintenance of the cellular fitness.

B-III- Patho-physiological implications in the brain

B-III-1- Lysosomal storage diseases (LSDs)

Lysosomal storage diseases are a group of inherited metabolic disorders defined by lysosomal perturbations. Approximately seventy diseases compose this group of disorders and even if individually they do not affect many births, collectively, 1/5000 birth is subjected to the development of LSD[446]. Because lysosomes yield incredible importance in anabolic and catabolic processes, their dysfunctions consequently affect several organs and induce plethora of clinical manifestations such as visceral, skeletal, and neurological disabilities[447]. LSDs are classified according to the type of substrate found to accumulate within lysosomes or depending on the enzyme or protein found mutated[447] (Table 5). There is an important discrepancy in terms of survival when looking at specific LSDs, ranging from seventy years of life expectancy for Fabry's disease when symptoms are mild, to less than one year for the untreated infantile-onset Pompe's disease[448,449]. Since most of the phenotypes induced by LSDs are not apparent at birth and that this class of diseases induces multi-organ failure, the diagnosis is complicated and firstly attributed at the onset of symptoms[450]. Diagnostic methods for LSDs mostly consist at first in enzymatic and molecular assays. Other methods such as DNA sequencing, PCR, or more recently next generation sequencing (NGS), are also widely used to characterize mutations of lysosomal proteins[450].

Despite the apparent lack of early diagnosis, this one must be made as early as possible as some treatments can improve the quality of life of patients[447]. There is no cure for LSDs, only supportive cares and treatments, but the important work performed in the last few years to better understand lysosomes and the subsequent associated diseases raise reasonable hopes for the development of innovative therapies[451,452]. Enzyme replacement therapy (ERT) is an interesting approach to compensate deficits in enzymes affected by mutations. Intravenously injected enzymes, by using the physiological M6PR pathway, can be taken up extracellularly and incorporated into lysosomes. However, some tissues such as the brain, which is often affected by LSDs, are hardly reachable for the infused enzymes[452].

As its name implies, the substrate reduction approach consists in the inhibition of enzymes responsible for production of accumulating substrates. As compared to ERT, these treatments can cross the BBB allowing reduction in brain phenotypes,

and are not responsible for immune reactions, as it can be observed upon ERT[452]. Miglustat for example, is used in the treatment of Gaucher's and Niemann-Pick type C diseases. Through inhibition of the glucosylceramide synthase enzyme, it reduces the production of glycosphingolipids, and therefore acts on the neurodegenerative phenotypes in patients, increasing lifespan[453,454].

Heat shock protein 70 (HSP70) is a known stabilizer of the lysosomal membrane through interaction with the lipid LBPA and stabilization of the acid sphingomyelinase close to its substrate, sphingomyelin. LSDs are often characterized by lysosomal membrane destabilization, and as such, induction of HSP70 expression was thought to reduce lysosomal defects in LSDs[455,456]. This was notably shown in NPC1 deficient mice treated with the HSP70 co-inducer arimoclomol. Treated mice showed strong recovery of the respiratory and neurologic defects induced by loss of NPC1[457].

β-cyclodextrins are molecular cages known to solubilize cholesterol in their hydrophobic core[458]. Therefore, several studies demonstrated the opportunity of using this molecular compound to rescue NPC-induced phenotypes[459–461]. 2-hydroxypropyl-beta-cyclodextrin (HPβCD) have notably reached late-stage clinical trials for the treatment of NPC. Due to potential toxicity upon high-dose treatment, complementary molecules are already under study. As an example, distearyl-phosphatidylethanolamine-polyethylene-glycol could promote accumulation of HPβCD in cholesterol-rich endosomes, favoring and potentiating the lysosomal-cholesterol efflux-effect of HPβCD[462].

Disease	Mutated product	Symptoms
Fabry's disease	α-galactosidase A	Gastroenteritis, nephropathy, cardiomyopathy, cerebrovascular disease
Pompe's disease	Lysosomal α-glucosidase	Cardiomegaly, muscle atrophy, hypotonia
Danon's disease	LAMP2	Cardiomyopathy, arrhythmia, intellectual disability
Gaucher's disease	β-glucocerebrosidase	Hepatosplenomegaly, arthritis, epilepsy, limited psychomotor development
Niemann-Pick disease type C1/2	NPC1/2	Dystonia, ataxia, splenomegaly, intellectual decline
Niemann-Pick disease type A/B	SMPD1 (ASM)	hepatosplenomegaly, pulmonary infections, psychomotor regression

Table 5: List of few known LSDs, the mutated protein responsible for the development of the disease, and the described phenotypes.
LSD: Lysosomal storage disease, ASM: Acid sphingomyelinase

Niemann-Pick disease

Niemann-Pick diseases is a subgroup of LSDs that can be classified into four main types, namely Niemann-Pick type A (NPA), type B (NPB), type C1, and type C2 (NPC)[463]. Overall, Niemann-Pick diseases are defined according to the inability of lysosomes to traffic lipids, mostly cholesterol, further leading to autophagic dysfunctions and lysosomal destabilization. NPA and NPB are associated with mutations in the SMPD1 gene encoding for the ASM enzyme, whereas NPCs affect the lysosomal cholesterol transporters NPC1 or NPC2[464–466]. Niemann-Pick type C1 is the most common of the Niemann-Pick diseases, with a prevalence of around 1 per 100,000 births, but that greatly varies according to the country[463,467]. As such, an important effort was deployed to better characterize this disease and allowed major discoveries such as cholesterol as a nutrient input for mTORC1 signaling[277,278,404]. NPC1 is a thirteen transmembrane domains protein of 1278-amino-acids with three intra-lysosomal loops involved in cholesterol and NPC2 binding[468,469] (Fig. 22)[475]. Through NPC2 binding and cholesterol sensing, NPC1, when targeted to the late-endocytic compartment, allows the export of cholesterol from this compartment[466]. Many mutations have been identified within the NPC1 gene. As such, the different genotypes lead to variable phenotypes, such as mislocalization of the protein or defective cholesterol sensing, binding, or transit[470]. In the brain, NPC1 mutations lead to important defects in neurons, oligodendrocytes, as well as microglia. Many mice studies allowed the description of cell type specific effect of NPC rescue. Min Zhang notably showed that astrocyte-specific re-expression of NPC1 rescued the myelination defects, neuronal cholesterol accumulation, and tripled the life span of mice[471]. In parallel, two other studies demonstrated the importance of NPC1 expression in oligodendrocytes, as the re-expression of the protein rescued the myelination defects observed in patients and in mice models[472,473]. Finally, and demonstrating the complexity of the disease, specific re-expression of NPC1 in the neurons of deficient mice is sufficient to mitigate the disease by allowing oligodendrocyte maturation, myelin production, and reducing the inflammatory response[473,474]. Molecularly, the study of Daniel Mitroi demonstrated that the D1005G mutation of NPC1 that induces its premature degradation, alters neuronal synapse formation by blocking the membrane delivery of two important actors of synapse functions, CYP46A1 and GluA1[475]. Altogether, this demonstrates the extensive interplay between lysosomal cholesterol transport, notably by NPC1 and NPC2, and

CNS functions. It also however demonstrates the need for multi-cellular studies of NPC1 functions, as brain phenotypes are appearing dependant on the concomitant modulation of the different cell types functions upon loss of function of the transporters. It also overall demonstrates the dependency of neurons and other brain cell types toward fully functional lysosomes, as single mutations lead to the development of LSDs. One interesting parallel can be made with the process of aging in which neurodegeneration often occur due to impaired lysosomes functions and proteostasis.

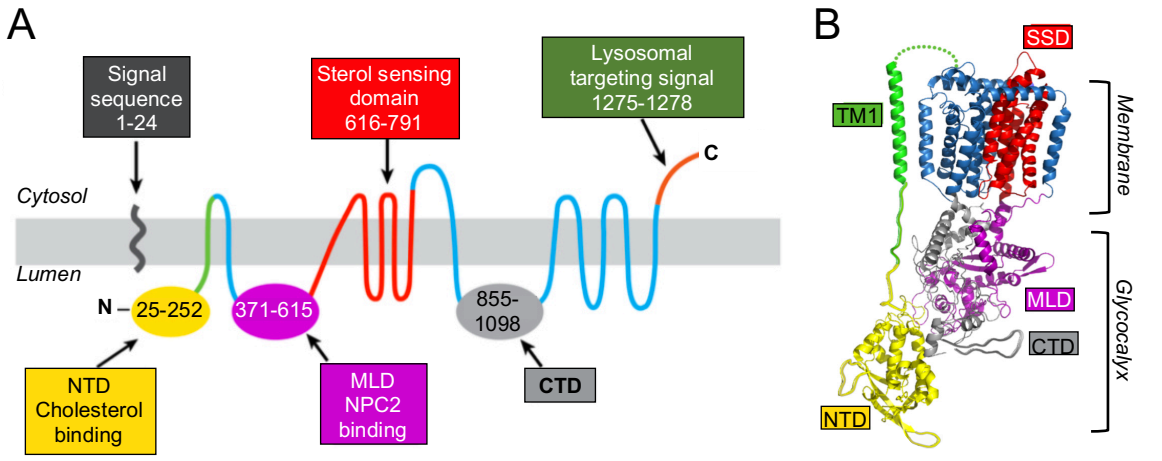

Figure 22: (A) Predicted topology of the human NPC1 protein. NPC1 possesses thirteen transmembrane helices playing a role of cholesterol channel when assembled in the lysosomal membrane. The C-terminal lysosomal targeting signal is necessary for NPC1 traffic to the lysosomes. The NPC2 binding domain allows the interaction between NPC1 and NPC2, favoring cholesterol transfer from NPC2 toward the cholesterol binding domain of NPC1. Once transfered, cholesterol is embedded in the glycocalyx and binds to the sterol sensing domain of NPC1 for its transfer across the lysosomal membrane. (B) Cryo-electron microscopic structure of NPC1. The thirteen transmembrane helices span the lysosomal membrane and exposes the cholesterol and NPC2 binding domains in the lumen of lysosomes.
NPC: Niemann-Pick type C, NTD: N-terminal domain, MLD: Middle lumenal domain, CTD: D-terminal domain, TM: Transmembrane, SSD: Sterol sensing domain.
Adapted from: Trinh, M. N. et al., Elife (2018)

B-III-2- Age-related reorganization

Aging often correlates with neurodegeneration, with notably the appearance of aging-related disorders, such as Parkinson's and Alzheimer's diseases. Of note, these diseases are characterized by defective autophagy, dysfunctional lysosomes, and aberrant mTOR signaling[476,477]. NSCs allow the generation of astrocytes, oligodendrocytes, and neurons during development, and contribute to neurogenesis in adults, their decline correlating with aging[478]. Several works unravelled an important remodelling of the lysosomal compartment for stem cells and particularly NSCs maintenance and activation during aging. Indeed, Florian Villegas identified that mouse embryonic stem cells (mESCs) inhibit Tfe3, master transcriptional

regulator of autophagy and lysosomes, to induce a differentiation program[218,479]. A genome-wide CRISPR/Cas9 screen revealed that removal of upstream regulators of mTORC1 (such as Ragulator or FLCN) induced the expected nuclear translocation of Tfe3, followed by impaired differentiation of mESCs. It was further demonstrated that lysosomal catabolism is a major driver of mESCs differentiation as the use of classical lysosomal inhibitors such as bafilomycin A1, chloroquine, or vacuolin-1, impaired the exit from their self-renewal state. This effect was linked to RagC/D inability to recruit Tfe3 for its inhibition at the surface of lysosomes. As a proof of concept, disease-associated mutants of Tfe3, which produce a constitutively active form of the transcription factor, induce a developmental disorder affecting muscles and the nervous system[479]. Therefore, lysosomal functions and regulation appear intimately linked to stem cell fate. In line with this result, Anne Brunet's group identified that lysosomal functions are necessary for NSCs activation during aging[480]. NSCs exist in two distinct pools, one quiescent (qNSCs), giving rise to the active one (aNSCs), itself responsible for the generation of new neurons, astrocytes, and oligodendrocytes. Of note, the adult brain mostly contain qNSCs, and their activation decline with age, supporting the observed degeneration[481]. The mechanism relied on the ability of qNSCs to engulf protein aggregates in large and numerous lysosomes, as compared to aNSCs, relying on the proteasome-ubiquitin system to clear proteins. However, the study demonstrated that old qNSCs display lysosome defects, notably reduced abundance of the organelle, as well as defective autophagic degradation, leading to protein aggregates accumulation, hallmark of neurodegeneration. Of note, TFEB overexpression or mTOR inhibition counteracted the phenotypes induced during aging, demonstrating the primordial function of lysosomes in the activation of NSCs[480].

Autophagy and mTOR are two major regulators of cellular health and rely on functional lysosomes to complete their missions[476]. Compelling evidences showed aberrant accumulation of autophagosomes as well as hyperactive mTOR in *post-mortem* Alzheimer's patient's brains[482,483]. Accordingly, autophagy blockade by the mean of Atg5 deletion in mice neural cells induces the accumulation of inclusion bodies and deficits in motor functions[484]. Mostly described as the effector of neurodegeneration, autophagic dysfunction is thought to be linked to mTOR hyperactivity. As such, inhibition of mTOR was described to extend lifespan in several organisms[485–488]. However, how is mTOR regulated in the onset of aging, as

well as the downstream effects are still not fully understood. As mTOR positively controls protein synthesis and negatively correlates with lysosomal and autophagic degradation, the resulting increased protein burden may account for the higher propensity of neurodegeneration linked to protein aggregate accumulation. Of note, administration of everolimus, a derivative of rapamycin, to heart transplant recipients, demonstrated favorable psychiatric outcomes including memory and concentration scores[489]. Cholesterol metabolism represents an interesting link between lysosomes, mTOR, and neurodegeneration. The E4 variant of the APOE gene (APOE4) is the main identified genetic driver of Alzheimer's disease[490,491]. The role of APOE is to transport cholesterol between neural cells, and the expression of the E4 variant was also linked to modified cholesterol homeostasis in these cells, as well as reduced degradation of amyloid beta, the main constituent of senile plaque[492–494]. As lysosomes act as central hubs for cholesterol and that mTOR was recently shown to respond to the lysosomal concentration of cholesterol[249,269,277,278], it is therefore tempting to speculate that lysosomal-cholesterol homeostasis is of particular importance in the development of neurodegenerative disorders, notably Alzheimer's disease. Lysosomes therefore appear as important drivers of aging, their malfunction culminating in neurodegeneration. In this context, glioblastoma, that primarily occurs in older patients, have been shown to present altered lysosomes[495]. This is notably true in glioblastoma stem-like cells (GSCs)[496,497], a subset of cells harboring stem properties and believed to be responsible for the initiation and recurrence of glioblastoma, raising the idea that lysosomes, regulating NSC maintenance and activation, could also be involved in oncogenic processes.

B-III-3- Impact in cancer

Cancer cells display an increased biosynthetic and bioenergetic demand to proliferate and survive. As such, lysosome functions and homeostasis are central for cancer growth and most of cancer hallmarks phenotypes can be linked to lysosomal functions[498]. Drug resistance and escape is a leading cause of cancer-related mortality and treatment failure. Hydrophobic weak-base chemotherapeutic compounds can freely diffuse across membranes and become protonated in the acidic H^+ rich lumen of lysosomes, disabling their diffusing properties, reducing the probability of encounter with their target[499,500]. Of note, weak-base

chemotherapeutics induce lysosomal biogenesis by lysosomal stress-induced TFEB activation, further enabling compound sequestration[501–503].

The increased turnover of proteins and organelles within cancer cells implies a well-orchestrated catabolism program. As such, the expression of cathepsins is increased in several cancers[504–506]. Cathepsin D expression was notably shown to correlate with breast cancer severity and proposed as a prognostic marker[507,508]. Notably, inhibition of cathepsin D induces sensitization of several carcinomas to TRAIL-induced apoptosis[509]. Other known mechanisms for cathepsins mediated cancer growth are the extracellular matrix remodeling and angiogenesis induction. Indeed, lysosomal exocytosis is promoted during cancer progression by relocalization of lysosomes close to the plasma membrane, allowing efficient cathepsin secretion in the extracellular space[510,511]. This is notably thought to be mediated by the global acidification of cancer cells, promoting LAMP2 presentation at the plasma membrane[512].

Lysosomal modifications occurring during cancer development are of particular interest for dissemination and growth. However, some of them can also be seen as anti-tumorigenic operators via lysosomal destabilization[513]. Cathepsins overexpression, via the cleavage of LAMP1 and LAMP2, leads to destabilization of lysosomes, found more prone to LMP[514,515]. Acid sphingomyelinase level is downregulated in several cancers to ensure a reduction in the production of ceramide, a well characterized apoptosis inducer[516]. However, at the level of lysosomes, this modification induces destabilization of the membrane, sensitizing cells to LMP[513]. Even in these conditions, cancer cells deploy an arsenal of molecular pathways to circumvent lysosome stability. A striking example is the retargeting of the Myoferlin protein to the surface of lysosomes in pancreatic cancer. The group of Rushika Perera demonstrated that this protein, already known to regulate plasma membrane repair, was uniquely present at the surface of lysosomes of several pancreatic ductal adenocarcinomas (PDAC), as compared to lysosomes isolated from healthy pancreatic epithelial cells. As PDAC upregulates their lysosomal mass to ensure stress resistance and bioenergetic supply, the lysosomal localization of Myoferlin therefore promotes their stabilization and allows lysosomal-dependent cancer growth[517].

Glioblastoma

A pivotal study by Takashi Shingu and colleagues demonstrated the important function of the STAR-RNA binding protein Quaking (QKI) in maintenance of the lysosomal compartment in GSCs[496]. This work highlighted that the downregulation of the endo-lysosomal compartment by QKI deletion enhances the ability of GSCs to maintain their stemness outside the protective perivascular niche. Molecularly, via direct regulation of RNA stability and translation, QKI increases the endo-lysosomal compartment, and its loss restrains the degradative compartment. Consequently, various receptors involved in stemness maintenance, such as EGFR, Frizzled, FGFR, are recycled back to the plasma membrane rather than degraded by lysosomes, leading to sustained signaling even in low-ligands concentration conditions. Of note, QKI is frequently found downregulated in GB samples, emphasizing the role of this protein in GB development[518]. More recently, the paracaspase mucosa-associated lymphoid tissue lymphoma translocation 1 (MALT1) was shown to regulate lysosomal homeostasis in GSCs through a mechanism involving QKI (Fig. 23).

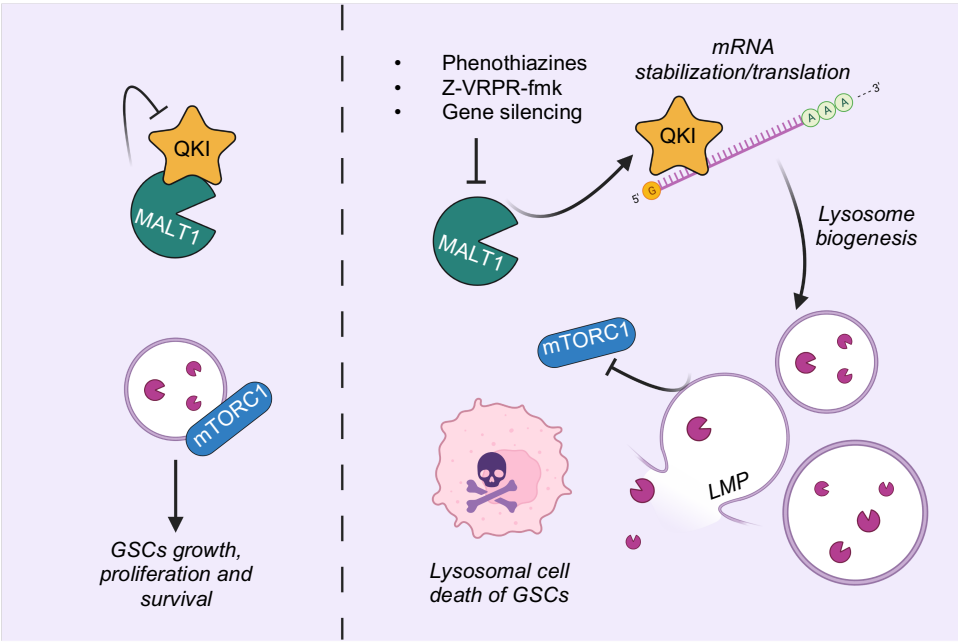

Figure 23: MALT1 negatively regulates lysosomes homeostasis in GSCs. (A) MALT1 constitutive activity retains QKI inactive, reducing the amount of lysosomes in GSCs. Upon MALT1 inhibition, QKI is unleashed, enabling lysosomal proteins encoding-mRNA translation. The consecutive aberrant lysosomal biogenesis is followed by LMP and mTORC1 release from its lysosomal hub. The combined phenotypes are responsible for lysosomal dependent cell death of GSCs.
GSC: Glioblastoma stem-like cell, QKI: Quaking, LMP: Lysosome membrane permeabilization

The constitutive activity of MALT1 could retain QKI, therefore inhibiting its activity. Blocking MALT1 activity resulted in the release of QKI, unleashing lysosomal biogenesis ultimately leading to LMP and lysosomal dependent cell death. mTOR activity was also demonstrated affected by the dramatic modification of the lysosomal compartment in a still unidentified mechanism, involving either lysosomal stress or control by the protease activity of MALT1. Of note, the phenotypes induced upon MALT1 inhibition were strongly specific to patient-derived GSCs, as healthy astrocytes or brain endothelial cells were not affected. As a confirmation, the *in vivo* injection of mepazine, a known inhibitor of the paracaspase previously used in clinic to treat psychiatric disorders, impaired GSCs growth in a flank-xenografted mice model, opening a new therapeutic avenue for GSCs eradication and demonstrating the important fragility of lysosomes in GB[519].

Linked to that, several other compounds were shown to target the lysosomal compartment of glioblastoma cells[495]. In a study by Vadim Le Joncour, the mammary-derived growth inhibitor (MDGI/FABP3) protein was demonstrated as crucial for the lysosomal lipidic-membrane composition. Indeed, its downregulation correlates with better prognosis in GB patients, and *in vitro*, resulted in mistrafficking of polyunsaturated fatty acids engendering lysosomal cell death of patients-derived GSCs through modification of the lysosomal membrane composition. Consequently, the use clemastine, a cationic amphiphilic antihistamine provoking LMP specifically eradicate GSCs in an *in vivo* model of brain-xenografted mice[149].

In accordance with the ability of this lysosomal targeting compound to disrupt GSCs viability, the widely used cationic amphiphile drug siramesine showed promising *in vitro* results in conventional GB cell lines as well as in patient-derived cells. However, the study failed to show *in vivo* efficacy as a mice xenograft model as well as an organotypic three dimensional spheroid brain slice culture model were not affected by siramesine administration[520].

Lys05, another lysosomotropic compound, allowed the demonstration that coupling lysosome destabilization to standard-of-care therapy such as radiation could be a promising opportunity[521]. Thus, cationic amphiphilic drugs showed promising *in vitro* results for the eradication of GB cells, but failed to clearly prove their efficacy *in vivo*, therefore raising the need of further evaluation of these interesting compounds.

Another innovative strategy developed by Jeffrey Wojton consisted in the generation of nanovesicles of dioleoylphosphatidylserine (DOPS) coupled to saposin C (SapC),

a known activator of sphingosine production and further LMP. This treatment showed *in vitro* and *in vivo* efficacy, demonstrating the possibility of altering lipid homeostasis for lysosomal destabilization and GSCs cell death[522]. Accordingly, treating GB cell lines with a combination of TNFα, lipopolysaccharide and interferon gamma (TLI) altered sphingosine production, resulting in lysosomal accumulation of ceramide, culminating in LMP and cell death of the malignant cells. Concomitantly, inhibition of the sphingosine kinase enzyme using SKI-II strongly impaired GB cell expansion[523].
Finally, Stefanie Enzenmüller, using GDC-0941, a PI3K inhibitor inducing TFEB nuclear translocation and activation of the transcription of lysosomal genes, in combination with B10, a derivative of betulinic acid, effectively triggered cell death in glioblastoma cells. B10 effectively destabilized the numerous lysosomes generated upon TFEB activation[524]. Altogether, these studies demonstrated the important fragility of lysosomes in GB cells, notably in the subset of GSCs, responsible for glioblastoma initiation and recurrence. This supports the idea that targeting the lysosomal compartment is an interesting strategy for the treatment of this deadly cancer.

Treatments	Targets
Phenothiazine	MALT1
Clemastine	CAD
Siramesine	CAD
Lys05	CAD
SapC-DOPS	sphingosine metabolism
TLI	sphingosine metabolism
GDC-0941 / B10	PI3K / CAD

Table 6: List of the compounds and respective targets reported to induce lysosomal cell death of glioblastoma cells. CAD: Cationic amphiphilic drug, TLI: TNFα-lipopolysaccharide-interferon gamma, SapC: Saposin C, DOPS: dioleoylphosphatidylserine, PI3K: phosphoinositide 3-kinase

C- MALT1 paracaspase: a versatile protein in pathogenic conditions

C-I- Prelude

Mucosa, or mucous membranes, are epithelial membranes covering digestive, respiratory, and reproductive organs, and via the secretion of a ‘’gel-like’’ mucus, protects the body from pathogens or internal acidity, as it is the case in the digestive tract[525]. Another layer of protection rises from the high infiltration of immune cells in mucosa. Indeed, mucosa comprise specialized lymphoid tissues, termed mucosa-associated lymphoid tissues (MALT), able to collect antigens directly from the site in which they are found[525]. As important sites of B-cell collection, MALT are the location of non-Hodgkin marginal zone lymphoma development[526,527]. MALT lymphoma can develop in numerous body sites, such as lungs, eyes, thyroid, but mostly occurs in the stomach. As such, MALT lymphomas are classified into the gastric- and non-gastric subtypes[528]. Rather indolent and considered as low-grade lymphomas, MALT lymphomas can however progress into aggressive forms of diffuse large B-cell lymphomas (DLBCL)[529,530]. Chromosomal translocations are major drivers of MALT lymphomagenesis. Four main translocations have been associated with development of MALT lymphomas: t(3;14)(p14.1;q32), t(1;14)(p22;q32), t(14;18)(q32;q21), and t(11;18)(q21;q21)[527]. Notably, the description of the t(11;18)(q21;q21) translocation allowed the characterization of the MALT1 gene in 1999[531,532]. Previously termed MLT (MALT1 lymphoma-associated translocation), this gene was shown to fuse with BIRC3/API2 (baculoviral IAP repeat-containing protein 3), generating the API2-MLT fusion protein, suggested to act as an oncogenic driver for MALT lymphomas[531,532]. One year later, seminal work by the group of Vishva Dixit deepened the knowledge on the C-terminal part of the fusion protein[533]. Performing alignment between the sequences of traditional human caspases (1, 2, 3, 8, and 9) and the novel human caspase-like MALT1, Dixit’s group demonstrated the presence of a caspase-like domain in the C-terminal part of the protein, characterized by the universally conserved catalytic cysteine and histidine dyad required for catalysis. However, 3D model analysis of the catalytic site demonstrated dissimilarities between caspases and MALT1, showing potential differences in substrate specificity. Notably, caspases are known to cleave acidic residues in the P1 position, *a contrario* to MALT1 that was predicted to cleave at uncharged residues. Moreover, as MALT1, unlike caspases,

possesses a death domain (DD) and three immunoglobulin (Ig) domains, was therefore classified as a paracaspase[533]. On top of this major discovery, the study uncovers the direct binding of MALT1 to BCL10 (B-cell lymphoma/leukemia 10), a protein previously shown to be involved in the t(1;14)(p22;q32) translocation of rare cases of MALT lymphomas[533,534]. Finally, the product of the t(11;18)(q21;q21) translocation (API2-MALT1 fusion protein) was demonstrated to activate the NF-κB pathway, and the catalytic activity of the paracaspase was shown to be partially responsible for this phenotype. As NF-κB is an important regulator of lymphocyte development, this finding had an extensive impact in the understanding of the pathway and opened new therapeutic opportunities for MALT lymphomas treatment. Overall, MALT1 was shown to control the NF-κB pathway when hyperactivated and a dual scaffold-protease mechanism was already hypothesized, dissecting the molecular pathways affected during MALT lymphomagenesis[533]. In 2003, three independent groups implemented MALT1 alongside CARMA1 (caspase recruitment domain-containing protein 1) and BCL10 in the regulation of the NF-κB pathway upon lymphocyte activation[535–537]. This complex is now referred to as the CBM (CARMA1-BCL10-MALT1) signalosome.

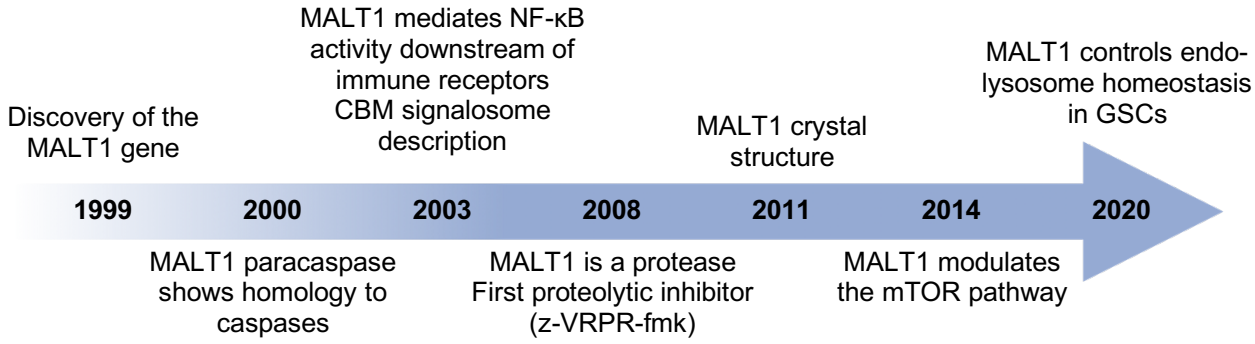

Figure 24: MALT1 and important related discoveries.
Adapted from: Hachmann, J. & Salvesen, G. S., Biochimie (2017)

Despite the definition of MALT1 as a protease in 2000, eight years were necessary to discover the first two substrates of the paracaspase. The groups of Rudi Beyaert and Margot Thome identified A20 and BCL10, respectively, as processed by MALT1 upon lymphocyte activation[538–540]. As such, the hypothetic MALT1 catalytic site was defined. The substitution of the cysteine C464 of the paracaspase was shown to abolish its proteolytic activity. Moreover, it further emphasizes the importance of

MALT1 in the ‘’fine tuning’’ of T cell antigen receptor (TCR) signaling[539,540]. Following this breakthrough, several groups were able to identify other MALT1 substrates (see section C-III), enlarging the list to up to fourteen substrates until recently, with most of them involved in direct control of the NF-κB pathway or mRNA stability[541,542]. Using a high throughput bioinformatic screening strategy, the group of Christopher Overall classified several potential MALT1 substrates according to their sequence and functions. Seven new substrates were validated *in vitro* using an overexpression system, suggesting the potential of this strategy to identify novel MALT1 substrates[542].

C-II- The CBM signalosome

C-II-1- Assembly of the CBM

Due to its homology with classical caspases, its paramount role in lymphomagenesis, and the necessity of the development of specific inhibitors[533,543,544], the first crystal structure description of MALT1 was an important step in the understanding of the paracaspase. Two teams simultaneously published the first crystal structure of MALT1[545,546]. Either in a ligand-free conformation or bound to a peptide inhibitor, the crystal structures unravelled the primordial role of the symmetric dimerization of MALT1 for its catalytic activity. Notably, the paracaspase domain of MALT1 was shown to closely resembles the catalytic domain of classical caspases, composed of a central β-sheet of six β-strands surrounded by two α-helices on a side and three on the other side, with the β6 strand of the β-sheet essential for the dimerization[545,546] (Fig. 25). Of note, a single point mutation in the β6-strand (R551E) abolished the catalytic activity of MALT1 *in vitro*[545]. Interestingly, it was hypothesized that MALT1 might exist as a monomer in solution, as the addition of a peptide inhibitor, z-VRPR-fmk, led to the assembly MALT1 dimers[546]. However, it was also showed that MALT1 could crystalize in dimers even in the absence of peptide binding, but in an inactive conformation. In this state, the C-terminal Ig3 domain interacts and locks the adjacent protease domain inactive[545]. As such, neither the dimerization of MALT1 nor the binding of specific peptides were necessary for its activation.

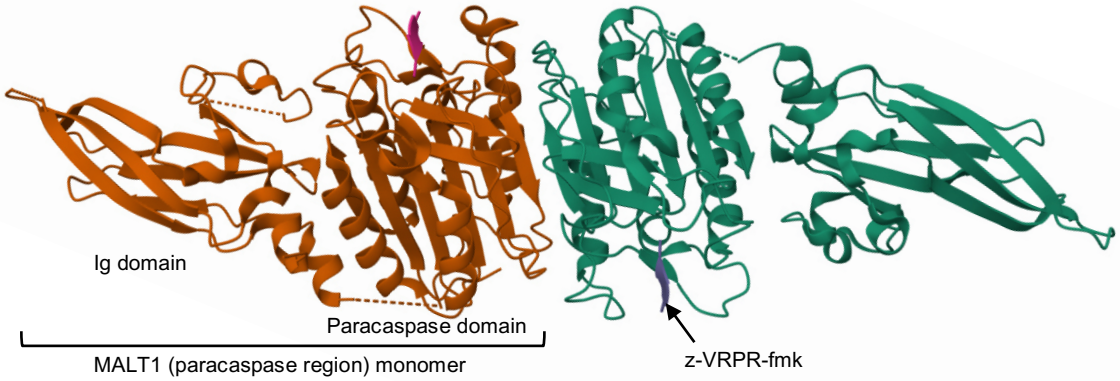

Figure 25: Ribbon representation of the C-terminal part of MALT1 in its homodimer form. The inhibitory peptide z-VRPR-fmk is shown by an arrow.
Adapted from: Yu, J. W. et al., PNAS (2011); PDB DOI: https://doi.org/10.2210/pdb3UOA/pdb

The assembly of the signalosome itself is necessary for signal amplification and optimal response to upstream activators. Notably, crystallographic studies as well as electron microscopy analysis of the CBM revealed the mechanism by which it polymerizes (Fig. 26). CARMA1 was shown to nucleate at one end of BCL10 filaments, providing a platform for MALT1 dimerization and activation. As a proof of concept, mutations of residues in BCL10 necessary for its polymerization (R36, D39, R42, E50, E53, R62, K63) significantly impaired MALT1 and NF-κB activation[547–549]. This filamentous organization of the CBM is thought to resemble the one hypothesized as necessary for other proteases complexes activation, such as the apoptosome, the pyddosome, and the inflammasome[550]. Of note, BCL10 is recruited to CARMA through a CARD/CARD interaction[551–553] and constantly associates with MALT1 via its C-terminal serine/threonine rich domain that binds to the N-terminal Ig domains of the paracaspase[533].

In this context, CARMA/CARD (caspase recruitment domain-containing protein) protein adaptor are major determinants of CBM assembly and activity[554]. Various signaling receptors converge on the CBM assembly and MALT1 activation (see section C-II-2). Depending on the cell type and the upstream signal, different CARMA proteins are engaged for CBM assembly[554–556]. As an example, CARD9 was linked to CBM assembly and NF-κB pathway in response to fungal infection in myeloid cells upon Dectin-1 receptor activation. Notably, CARD9 was shown to be dispensable for TCR-mediated CBM assembly[551,557]. Conversely, CARMA1, induces CBM assembly in T- and B-cells in response to antigen receptor engagement[535,552,558]. CARMA2 expression appears importantly restricted to dermal cells, with a major implication in keratinocytes and in the development of skin associated diseases such as

psoriasis[552,559–561]. Finally, CARMA3 was shown to be engaged downstream of G-protein coupled receptors (GPCRs) and receptor tyrosine kinase (RTK) signaling in non-immune cells[562–566] (Fig. 27).

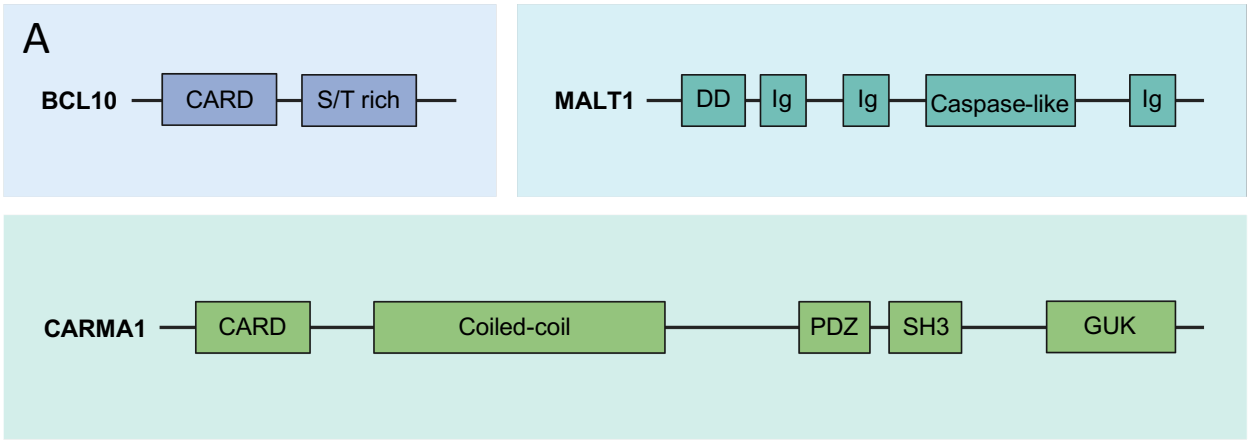

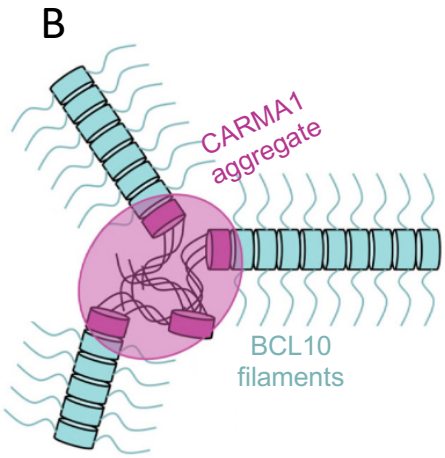

Figure 26: A) General structures of the CBM components BCL10, MALT1, and CARMA1. B) Schematic representation of CARMA1/BCL10 filaments. Upon activation, CARMA1 nucleates, offering a platform for BCL10 oligomerization of filaments generation.
CARD: caspase recruitment domain, S/T: serine/threonine, IKK: inhibitor of nuclear factor kappa-B kinase, CAMKII: Ca^{2+}-calmodulin-dependent kinase II, DD: death domain, Ig: immunoglobulin, CK1α: casein kinase 1 alpha, PDZ: postsynaptic density-95 (PSD-95) discs-large zona occludens 1 (ZO-1), SH3: SRC homology 3 domain, GUK: guanylate kinase-like.
Adapted from: Qiao, Q. et al., Mol. Cell (2013)

Although CARMA proteins appear to have different pattern of expression, the mechanism by which they assemble the CBM signalosome is similar. Indeed, the residues necessary for BCL10 nucleation are conserved throughout the four CARMA proteins[547]. The mode of activation of CARMA proteins is also shared, as the phosphorylation in the linker region comprised between the coiled coil and MAGUK (membrane-associated guanylate kinase) domains of the proteins by PKC family members induces a conformational rearrangement necessary for BCL10 recruitment and polymerization[552,567–571]. On the other hand, specific phosphatases counteracts CARMA1 phosphorylation, limiting the CBM assembly and NF-κB activation upon T-cell activation[572] (see section C-II-3).

C-II-2- Upstream modulators

C-II-2-1- Immune receptors

Lymphoid cells

The CBM complex is rendered active under various stimulus[554] (Fig. 27). A prototypical example is the engagement of the TCR on T-cells by MHC (major histocompatibility complex) class I or II presenting antigens on the antigen presenting cell. Lymphoid cells express receptors necessary for the recognition of extracellular non-self features, such as the BCR and the TCR in B- and T-lymphocytes, respectively, and for the induction of immune responses. A general attribute of these receptors is the presentation of ITAMs (immunoreceptor tyrosine-based activation motif) on specific chains of the receptors[573–575]. Of note, the ITAM is a major prerequisite for CBM assembly. Once the TCR is activated, the Src-family kinase LCK that is associated with the cytoplasmic tail of the CD4/8 co-receptor phosphorylates tyrosine residues in the ITAMs[576]. This molecular event triggers the recruitment of the Syk-family kinase ZAP70 (zeta-chain-associated protein of 70kDa), and its activation[573,577]. In turn, ZAP70 was shown to phosphorylate the adapter protein LAT (linker for activation of T cells), generating anchorage sites for signaling molecules, ending up in the formation of an intricate signalosome[578]. One major effector of this downstream signaling is the PLCγ1 (1-phosphatidylinositol 4,5-bisphosphate phosphodiesterase gamma-1), hydrolysing plasma membrane $PI(4,5)P_2$ (phosphatidylinositol 4,5-bisphophate) in $I(1,4,5)P_3$ (inositol 1, 4, 5-triphosphate) and DAG (diacylglycerol)[579,580]. $I(1,4,5)P_3$ induces the liberation in the cytosol of Ca^{2+} from the ER, as well as influx from plasma membrane-located CRAC (Ca^{2+}-release-activated Ca^{2+}) channel. The increased cytosolic concentration of Ca^{2+} activates several downstream effectors such as the NFAT (nuclear factor of activated T-cells) transcription factor, itself responsible for interleukin production and T-cell activation[581,582]. DAG, for its part, can activate the RAS-MAPK-ERK pathway, culminating in the nuclear activation of the AP-1 transcription factor, regulator of interleukin production and T-cell activation[573,583]. In parallel, the DAG liberated upon $PI(4,5)P_2$ hydrolysis is a known activator of the PKCθ (protein kinase C θ), major signaling event in CBM activation[554,584]. Indeed, PKCθ is a direct kinase for CARMA1 at serines S552 and S645, allowing its conformational activation for recruitment of BCL10 and induction of the CBM signalosome[547,552,567,568]. Of note, TCR activation

modulates the splicing of the MALT1 gene. Two MALT1 isoforms co-exist, MALT1A and MALT1B, with MALT1A including the 33-base-pairs exon 7, encoding for the amino acids 309–319 positioned between the Ig2- and caspase-like domains of human MALT1. MALT1A expression is induced by TCR stimulation, therefore increasing MALT1 scaffold activity and downstream signaling, but not affecting its proteolytic activity[585].

The BCR is composed of an immunoglobulin, acting as the receptor for the antigen, and of a heterodimer of CD79A and B chains[586]. Such as for the TCR, the Ig domain of the BCR, which serves as the recognition molecule, does not transmit the information intracellularly *per se*. The CD79 chains possessing one ITAM each, therefore act as the platform for the downstream intracellular signaling. Upon BCR engagement, CD79 ITAMs are phosphorylated by the Src family kinase LYN, inducing the recruitment of the SYK kinase, itself activator of BLNK (B-cell linker protein). Activated BLNK scaffolds for BTK (Bruton's tyrosine kinase) and PLCγ2 recruitment, where BTK may phosphorylate and activate PLCγ2[587]. PLCγ2 operates the same way as PLCγ1, generating $I(1,4,5)P_3$ and DAG from $PI(4,5)P_2$ hydrolysis serving further for PKCβ activation[588], CARMA1 phosphorylation, CBM assembly, and NF-κB activation.

Myeloid and mast cells

The CBM assembly is triggered by signaling events relying on the presence of ITAM on the upstream receptors or to associated chains. As such, the Fc$R\gamma$ chain containing ITAM, associating with the NK (natural killer) cell receptors NK1.1, Ly49D, Ly49H, or NKG2D, may transmit activating signals toward CARMA1 and the CBM complex upon binding to specific sets of ligands[589,590] (Fig. 27). Myeloid and mast cells, such as macrophages, monocytes, or dendritic cells, also express an important panel of ITAM containing-cell surface receptors. The dectin family of receptors (dectin-1, -2, and -3), FcεRI, FcγRIII, OSCAR (osteoclast-associated immunoglobulin-like receptor), CLEC4E (C-type lectin domain family 4 member E), and TREM-1 (triggering receptor expressed on myeloid cells 1) receptors are part of this arsenal[557,571,591–595]. Most of these receptors serve as PRRs (pattern recognition receptors), recognizing DAMPs (damage-associated molecular patterns) presented by PAMPs (pathogen-associated molecular patterns), and are therefore fully involved in the innate immune system. Via the presence of ITAMs in their structure, these

receptors, upon recognition of DAMPs, engage the Src, Syk, PLCγ, PKC pathway for CBM assembly and NF-κB activation. Of note, this does not trigger the phosphorylation of CARMA1 as in B- and T-cells, but rather of CARD9, generating a specific CBM signalosome (Fig. 27).

C-II-2-2- Non-immune receptors

Several non-lymphoid cell receptors can trigger the formation of the CBM. Notably, GPCRs and RTKs were shown to activate NF-κB. Seven transmembrane domains GPCRs such as CXCR2 and 4, PAR-1, AT1R, or LPA1-6, were demonstrated to induce the formation of the CBM via G-protein mediated activation of PLCβ, generation of DAG, and PKC mediated CARMA3 phosphorylation[562,564–566,596–598]. The same is true for RTKs such as EGFR (epithelial growth factor receptor) or HER2 (human epidermal growth factor receptor-2) in response to their respective ligand binding[563,599,600]. In parallel of the PLC/PKC pathway involved in the phosphorylation of CARMA and assembly of the CBM, the PI3K/Akt pathway regulates the CBM activity in response to activation of the previously enunciated receptors. Indeed, TCR, BCR, or PRR activation-mediated ITAM phosphorylation, mediate the recruitment of PI3K, enabling $PI(4,5)P_2$ phosphorylation and generation of $PI(3,4,5)P_3$ (phosphatidylinositol 3,4,5-triphophate). Of note, GPCR and RTK also regulate PI3K activity[601]. Plasma membrane generated $PI(3,4,5)P_3$ in turn engages Akt, therefore available for PDK1 (pyruvate dehydrogenase kinase 1) phosphorylation. Active Akt can enhance CARMA activity via S645 phosphorylation[602] (see section C-II-3). Overall, this highlights the variety of receptors and therefore of stimuli implicated in the CBM assembly and NF-κB activation. ITAMs in immune receptors as well as GPCRs and RTKs may control the assembly of this major signalosome. Importantly, although the signaling pathways converge on different CARMA protein phosphorylation depending on the cell type and the receptor engaged, the different CBM complexes generated ultimately control NF-κB activation in a similar manner, as well as MALT1 scaffold and proteolytic activity.

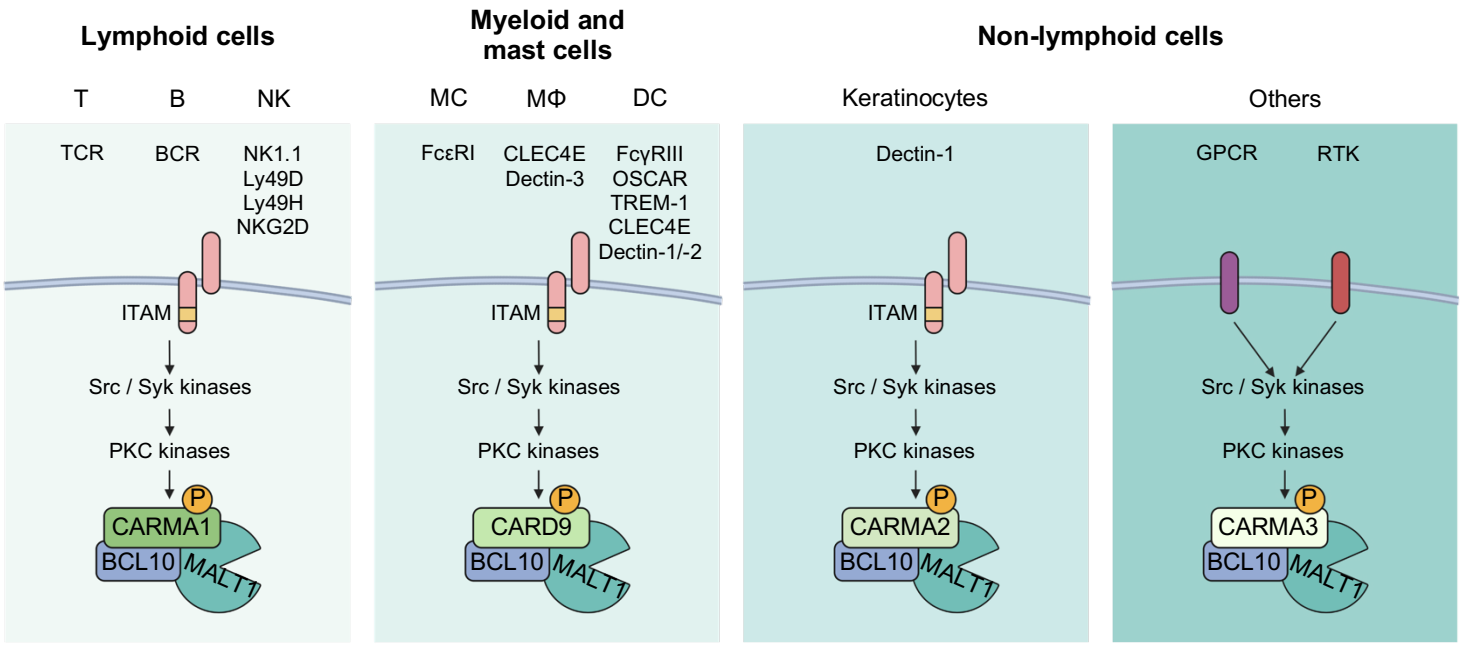

Figure 27: The CBM can signal in several cell types and in response to various upstream stimuli. ITAM-containing receptors in immune cells and keratinocytes, as well as GPCR and RTK in non-immune cells, mediate a signalisation cascade ending up in the assembly of the CBM. Different CARMA proteins modulate this assembly depending on the cell type and the upstream signal.
T: T-lymphocyte, B: B-lymphocyte, NK: Natural killer, MC: myeloid cell, MΦ: macrophage, DC: dendritic cell, TCR: T-cell receptor, BCR: B-cell receptor, GPCR: G-protein-coupled receptors, RTK: receptor tyrosine kinases, PKC: protein kinase C.
Adapted from: Juilland, M. & Thome, M., Front. Immunol. (2018)

C-II-3- Post-translational modifications in the CBM

C-II-3-1- Mucosa-associated lymphoid tissue lymphoma translocation protein 1 (MALT1)

The groups of Margot Thome and Daniel Krappmann performed extensive work to unravel post-translational modifications that modulate MALT1 activity (Fig. 29). The glutamine 549 (E549), localized in the protease domain of MALT1 at the dimerization interface, was shown to be necessary for MALT1 dimerization, ubiquitination, and for MALT1 activation. Indeed, the expression of the E549A mutant form of MALT1 could not rescue the survival of ABC-DLBCL cell lines in which MALT1 was silenced[603]. In the same line, the lysine 644 (K644) of MALT1 was identified as being mono-ubiquitinated in response to activating stimuli. K644-mono-ubiquitination was required and sufficient for MALT1 dimerization and further protease activity. Of note, ABC-DLBCL cell lines express a constitutively mono-ubiquitinated form of MALT1, and the re-expression of the mono-ubiquitination deficient MALT1 (K644R) in silenced cells could not rescue their viability, demonstrating the importance of this modification for MALT1 activity. This effect was also true in the context of T-cells, being unable to

activate NF-κB upon TCR engagement[604]. It is only recently that the mechanism by which the K644 mono-ubiquitination of MALT1 can lead to its activation was unmasked. The negatively charged residues E696 and D697 of the Ig3 domain of MALT1 recruited positively charged ubiquitin, probably through a mechanism involving undiscovered E2 and E3 ubiquitin ligases. Once mono-ubiquitinated, the K644 residue induces a conformational change of the paracaspase, unleashing the interactions between the Y657 at the surface of the Ig3 domain and the Y357 and L506 residues at the surface of the protease domain, leading to the adoption of a catalytically active conformation of MALT1[605].

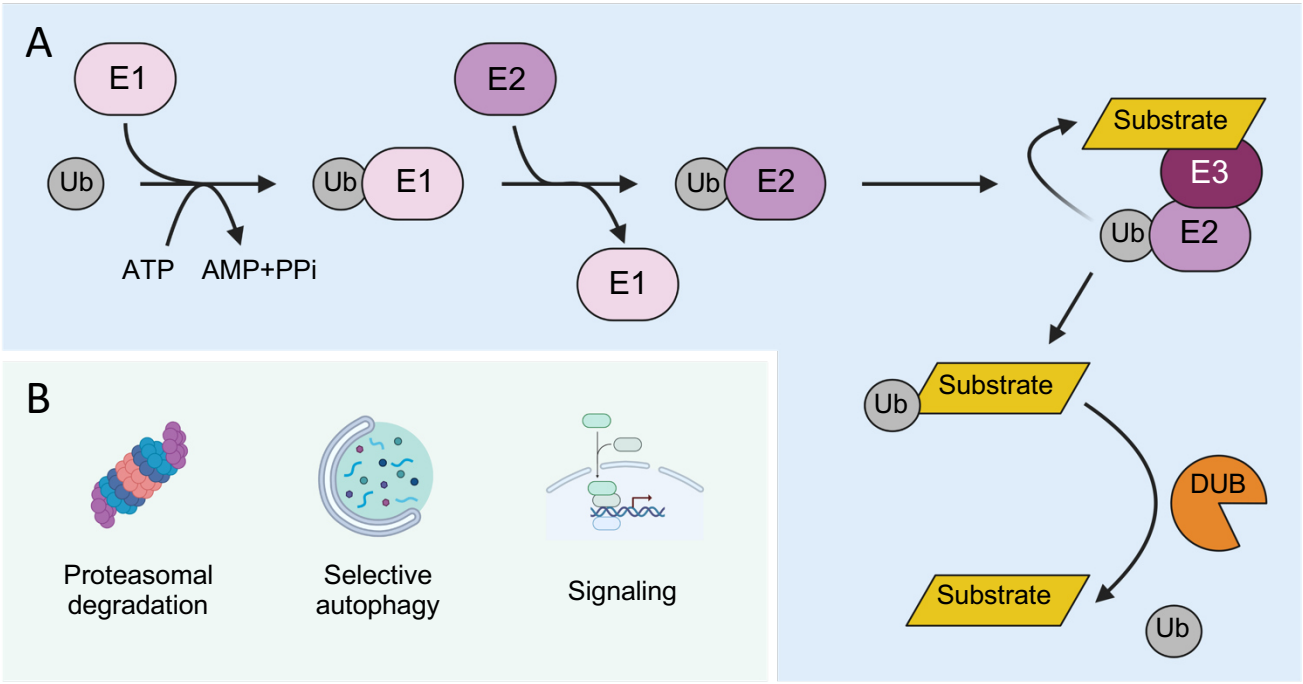

Figure 28: A) Schematic representation of ubiquitination and deubiquitination reactions. Ubiquitin is attached to an E1 ubiquitin-activating enzyme in an ATP-dependent manner. Ubiquitin is then transferred to an E2 ubiquitin-conjugating enzyme. An E3 ubiquitin ligase then allows the transfer of ubiquitin from the E2 to a lysine residue on the substrate. Deubiquitination is performed by DUBs that trims the post-translational modification from the substrate. B) Example of important cellular functions mediated by ubiquitination.
Ub: ubiquitin, DUB: deubiquitinase, E1: Ubiquitin-activating enzyme, E2: ubiquitin-conjugating enzyme, E3: ubiquitin ligase.
Adapted from: Damgaard, R. B., Cell Death & Diff. (2021)

Parallel work demonstrated the requirement of other type of ubiquitination of MALT1 for its activation, as well as the importance of the scaffold function of the paracaspase. Indeed, preliminary work published in 2004 highlighted the role of the assembly of the CBM for the recruitment of the E3 ubiquitin ligase TRAF6 (TNF receptor-associated factor 6) by MALT1. Notably, MALT1-mediated mobilization of

TRAF6 was shown to promote its oligomerization and subsequent K63 poly-ubiquitination, resulting in NF-κB activation[606]. Further work performed by the group of Daniel Krappmann demonstrated a direct poly-ubiquitination of MALT1 by TRAF6. The multiple poly-ubiquitination sites encompassed the amino acids 612 and 683. They also uncovered the significance of this post-translational modification in an *in vitro* assay using mice-purified MALT1-deficient CD4+ T-cells rescued with either the wild-type (WT) form of MALT1 or MALT1 deficient for the C-terminal poly-ubiquitinated lysines. As demonstrated, the re-expression of WT MALT1 strikingly rescued the activation of the NF-κB pathway, as compared to the MALT1 poly-ubiquitination deficient mutant. It was therefore enunciated that the poly-ubiquitination of MALT1 serves as a platform for the recruitment of downstream NF-κB effectors for the complete activation of the pathway[607].

Of note, MALT1 activation within the CBM may occur even in the absence of TRAF6. Oppositely, TRAF6, when overexpressed in T-cells lacking CARMA1 and BCL10, is able to induce MALT1 dimers activation[608]. More recently, an unsuspected function for TRAF6 on MALT1 activity was identified. Indeed, TRAF6, already described as a signaling accelerator for CBM-dependant NF-κB activation, appeared as a molecular brake for MALT1 activity in resting T-cells. Mice harboring MALT1 TRAF6 binding mutant (TBM; E325A, E803A and 3814A) indeed developed an early and fatal inflammatory pathological condition. The destruction of the MALT1-TRAF6 interaction led to a hyperactivation of effector T-cells and further autoimmunity. Notably, TRAF6 deficient or TBM mice-T-cells showed defective NF-κB activity as well as constitutive MALT1 protease activity. This was also true in non-stimulated resting T-cells, leading to the fatal autoimmune disorder. Consecutively, the use of the MALT1 inhibitors MLT-943 and -985 efficiently rescued the phenotypes observed upon loss of TRAF6, providing evidence that MALT1 constitutive protease activity through loss of TRAF6 interaction drives fatal autoimmune inflammation[609].

Likewise, the HECTD3 (E6-associated protein carboxyl terminus domain containing 3) E3 ubiquitin ligase protein promotes MALT1 poly-ubiquitination. HECTD3 interacts with the N-terminal death-domain (DD) of MALT1 and induces its non-degradative poly-ubiquitination. This was notably true in two cancer cell lines (MCF7 and HeLa) that showed destabilization of MALT1 in response to HECTD3 depletion, demonstrating that the yet undiscovered type of ubiquitin linkage induced by

HECTD3 stabilizes MALT1. Interestingly, this effect might be important for cancer cell survival in response to the chemotherapeutic agent cisplatin[610]. It is only recently that Jonathan Cho proved that HECTD3 promotes K27 and K29-linked poly-ubiquitination of MALT1 at the K648 residue, stabilizing the protein and engendering the production of a distinct subtype of CD4+ T-cells responsible for the severity of the autoimmune phenotype observed in experimental autoimmune encephalomyelitis (EAE)[611].

As a major post-translational modification regulating MALT1 activity and CBM assembly, the ubiquitination of the paracaspase is tightly controlled by a set of deubiquitinating enzymes (DUBs). A20 (TNFAIP3), already known to negatively control the strength of NF-κB activation in response to TCR engagement[612], was shown to remove MALT1 K63-linked ubiquitin chains[613]. A20 controls the ability of ubiquitinated MALT1 to recruit the signaling machinery necessary for NF-κB activation. Interestingly, in response to MALT1 activation, A20 is inhibited by direct cleavage by MALT1 (see section C-III-2)[540], unleashing the ability of the CBM to activate NF-κB[613].

The transforming growth factor beta-activated kinase 1 (TAK1) emerged also as a critical regulator of MALT1 ubiquitination. TAK1 is recruited to the CBM in a TRAF6-poly-ubiquitination dependent mechanism and phosphorylate downstream effectors involved in NF-κB pathway[606], and finely regulates MALT1 activity, as its removal increases the assembly of the CBM, MALT1 ubiquitination, and proteolytic activity. This study allowed to uncover the important function of TAK1 in CBM assembly on top of its already described function in activating NF-κB[614]. However, the precise mechanism by which this occurs remains to be elucidated.

In 2019, the group of Daniel Krappmann continued the investigation of MALT1 post-translational modifications and discovered MALT1 phosphorylation as a process necessary for T-cell activation and survival of ABC-DLBCL[615]. Using liquid chromatography coupled to tandem mass spectrometry (LC-MS/MS) to detect phospho-peptides before and after T-cell stimulation, Torben Gehring identified six putative C-terminal phosphorylation sites (S559, S562, S645, S649, S803, S805). Monoclonal antibodies recognizing the S562, S649, and S803, were generated and allowed to identify that no more than twenty minutes are necessary for MALT1 phosphorylation at these three residues in response to PMA/ionomycin (P/I; activation of protein kinase C (PKC), bypassing TCR engagement). Interestingly,

CK1α (casein kinase 1 isoform alpha), a pleiotropic kinase already known to interact and modulate the CBM[616], directly phosphorylates MALT1 at the serine S562. This effect was necessary for CBM assembly downstream of TCR activation, as CK1α knock-out Jurkat T-cells or rescued with a kinase dead mutant of CK1α (D136N), were unable to induce CARMA1 recruitment to preassembled BCL10-MALT1 complexes. Moreover, the expression of a phospho-mutant version of MALT1 (lacking the six phosphorylated serines) in Jurkat and CD4+ T-cells led to the inability of TCR engagement to activate the NF-κB pathway. Therefore, CK1α-mediated phosphorylation of MALT1 is important for the activation of NF-κB in response to P/I or TCR engagement. Finally, MALT1 S562 is constitutively phosphorylated in ABC-DLBCL, but the specific removal of this modification was not overtly affecting cell survival. Oppositely, the S803/805A mutation, as well as the mutation of all of the six serines, led to a dramatic reduction in ABC-DLBCL survival. Overall, phosphorylation of MALT1 in its C-terminal region promotes CBM assembly and downstream NF-κB signaling. The kinase CK1α notably promotes this modification and positively regulates MALT1 activity.

C-II-3-2- Caspase recruitment domain-containing protein (CARMA/CARD)

Several kinases regulate CARMA1 phosphorylation[617] (Fig. 29). Notably, Akt at the S645[602], CaMKII (Ca^{2+}-calmodulin dependent kinase II) at the S109[618], IKKβ (inhibitor of nuclear factor kappa-B kinase subunit beta) at the S578[619], HPK1 (hematopoietic progenitor kinase 1) at the S551[620], and CK1α at the S608[616]. As previously mentioned (see section C-II-2-1) PKCθ is a direct kinase for CARMA1 at S552 and S645, and regulates the recruitment of BCL10[547,552,567,568]. Conversely, the serine/threonine protein phosphatase PP2A was demonstrated to be constitutively bound to CARMA1, therefore counteracting the S645-PKC dependent phosphorylation, limiting the CBM assembly and NF-κB activation upon T-cell activation[572]. Of note, all these phosphorylation marks were shown to enhance CARMA1 activity, excepted for the phospho S608 mediated by CK1α. Indeed, this modification might enhance the degradation of CARMA1, therefore terminating NF-κB activity after TCR engagement[616]. As for this negative regulation of CARMA1 by CK1α-mediated phosphorylation, K48 poly-ubiquitination of the GUK domain of the protein induces its proteasomal-dependent degradation. Substitutions of the probable

29 poly-ubiquitinated lysines in this domain triggered constitutive activity of NF-κB, as well as enhanced TCR mediated activation of the pathway in response to accumulated activated CARMA1[621].

C-II-3-3- B-cell lymphoma/leukemia 10 (BCL10)

BCL10, as MALT1 and CARMA, was shown to undergo post-translational modifications involved in the subsequent organization of the signalosome and NF-κB pathway (Fig. 29). A mixture of ubiquitination linkages decorate BCL10[617]. In 2009, the group of Daniel Krappmann identified the COP9 signalosome (CSN) as an important regulator of BCL10 stability. Indeed, CBM-bound CSN reduces the degradative ubiquitination of BCL10 in response to TCR stimulation, and knockdown of CSN2 or -5, two major components of the COP9 signalosome, showed faster ubiquitination and degradation of BCL10[622]. Even though the precise mechanism by which BCL10 ubiquitination is mediated by CSN is not fully uncovered, this provides evidence that degradative ubiquitination of BCL10 is a major determinant for CBM activity.

As an example, the E3 ligase RING finger protein RNF181 was demonstrated as a negative regulator of NF-κB downstream of CARMA1 by BCL10 ubiquitination leading to its degradation, at least in *in vitro* assays[623].

The cellular inhibitor of apoptosis protein 2 (cIAP2) is also an E3 ubiquitin ligase for BCL10. The loss of its function in the t(11;18)(q21;q21) translocation observed in some cases of MALT lymphomas therefore reduces BCL10 ubiquitination and degradation, increasing the activity of the NF-κB pathway necessary for lymphoma survival[624]. Notably, cIAP2 was shown to deposit K63-linked poly-ubiquitin chains in the context of ABC-DLBCL, favoring NF-κB activity. Inhibition by degradation of cIAP2 using SMAC (second mitochondria-derived activator of caspases) mimetics strongly impaired the growth of ABC-DLBCL lymphoma cell lines[625]. In addition, the E3 ubiquitin ligase β-TrCP can ubiquitinate BCL10 for sending it to proteasomal degradation in response to TCR activation[626]. However, these findings remain controversial and will need further investigation to fully understand the role of BCL10 degradation and its upstream regulators.

Finally, NEDD4 (E3 ubiquitin-protein ligase NEDD4) and Itch (E3 ubiquitin-protein ligase Itchy homolog), two E3 ubiquitin-protein ligases, induce the ubiquitination of

the CARD domain of BCL10 and subsequent lysosomal targeting for degradation. How are these two E3 ligases activated and targeting BCL10 for lysosomal degradation upon TCR stimulation however remains elusive[627].

In parallel of the negative regulation of BCL10 by ubiquitination, several publications showed the important function of BCL10 ubiquitination for downstream NF-κB activation[617]. Chuan-Jin Wu and Jonathan Ashwell demonstrated that BCL10 undergoes K63-linked poly-ubiquitination on lysines K31 and K63 in response to TCR activation. Mutations in these two residues resulted in the abrogation of TCR-induced activation of NF-κB as a result of the inability of NEMO (NF-kappa-B essential modulator) to recognize the non-ubiquitinated form of BCL10. Of note, the CBM assembly was not overtly affected, implying a major function of BCL10 ubiquitination in NF-κB activation downstream of MALT1 activity[628]. BCL10 K63 poly-ubiquitination induced its recruitment to the cytosolic leaflet of the ER via binding to the ER resident protein metadherin (MTDH), allowing optimal NF-κB activation in response to various stimuli[629].

The LUBAC (linear ubiquitin chain assembly complex) is also a major determinant of BCL10 and NEMO ubiquitination and NF-κB activation[629–631]. Notably, TRAF6-dependent K63 poly-ubiquitination of BCL10 was shown to mediate its Met1-linear ubiquitination via the LUBAC upon TCR and BCR engagement. Mechanistically, linear ubiquitination of BCL10 is necessary for NEMO recruitment to the CBM and further NF-κB signaling. Consequently, the spontaneous linear ubiquitination of BCL10 in ABC-DLBCL harboring oncogenic CARMA1 mutations is associated with constitutive NF-κB activity[632,633].

Finally, the deubiquitinase activity of USP9X (probable ubiquitin carboxyl-terminal hydrolase FAF-X), direct interactor of BCL10 and the CBM complex under stimulated conditions, specifically trim K48 poly-ubiquitin chains from BCL10, allowing proper CBM assembly[634].

Such as for CARMA1, BCL10 is a known phospho-protein. The two proteins share several regulating kinases, such as CaMKII, IKKβ, or Akt[617]. CaMKII phosphorylates BCL10 on S138 upon TCR engagement and disrupts its interaction with MALT1 to shut down the NF-κB pathway[635]. This model supports a sequential involvement of CaMKII in regulating CBM assembly and activity through first, CARMA phosphorylation (see section C-II-3-2), and secondly, via BCL10 phosphorylation, to

tightly control NF-κB response[618,635]. In parallel, it was demonstrated that the S138 phosphorylation of BCL10 regulates its ubiquitination and degradation, potentially explaining the diminished interaction with MALT1 observed in another study[636]. The serine S48 and threonine T91 are also phosphorylated by CaMKII in response to TCR activation. However, as compared to the S138 phosphorylation, mutating these sites into non-phosphorylable residues only modestly, but positively affected NF-κB activation[637]. As such, CaMKII appears to regulate BCL10 both negatively, via its degradation, and positively, by modulating its K63 poly-ubiquitination and subsequent NF-κB activation.

IKKβ likewise, operates a dual function of positive regulator of CBM assembly and negative regulator of BCL10 activity. Upon CBM signalosome assembly, IKKβ stabilizes the complex by a mechanism that remains to be elucidated, leading to the full activation of the pathway. After stimulation, IKKβ phosphorylates BCL10 in its C-terminal MALT1-interaction domain, abrogating the interaction between the two partners, attenuating the pathway[638]. Furthermore, T81 and S85 phosphorylation by IKKβ on BCL10 promotes its ubiquitination by the E3 ligase β-TrCP and its subsequent proteasomal degradation[626].

Finally, GSK3β (glycogen synthase kinase-3 beta), an important regulator of β-catenin protein level, was shown to interact with the CBM through CARMA1 in ABC-DLBCL cell lines. This effect was demonstrated as essential for lymphoma cell survival and establishment of an immunosuppressive microenvironment in the context of oncogenic CARMA1 mutations via the stabilization of the β-catenin protein[639]. Lately, a direct involvement of GSK3β for BCL10 phosphorylation and stabilization was proposed. GSK3β inhibition reduced the protease activity of MALT1 and downstream NF-κB signaling as a result of reduced CBM assembly. Interestingly, the sites phosphorylated by GSK3β are thought to be the same than the ones phosphorylated by IKKβ[640].

Another layer of regulation comes from the Ser/Thr phosphatase calcineurin, which positively regulates CBM assembly via its dephosphorylation activity toward BCL10 S138. Notably, TCR engagement and subsequent PLCγ activation induce an influx of Ca^{2+} activating the phosphatase, favoring the binding between CARMA1 and the BCL10-MALT1 dimer[641,642].

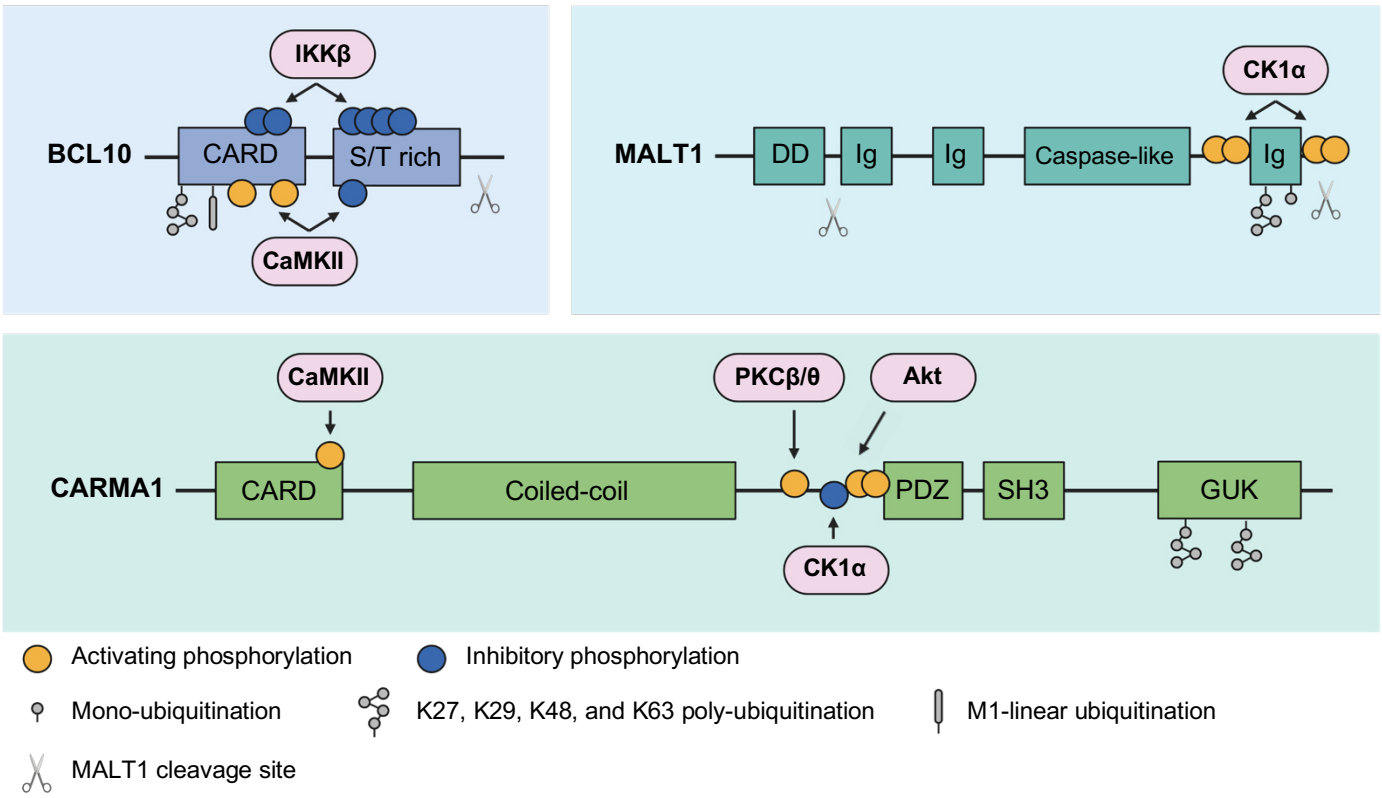

Figure 29: Structures and post-translational modifications of the CBM components BCL10, MALT1, and CARMA1. Phosphorylation is an important event for CBM assembly and activation. Several kinases (pink) modulate positively or negatively each of the CBM components. Ubiquitination (grey) also influence the CBM activity. For example, the mono-ubiquitination on the K644 of MALT1 is required and sufficient for MALT1 dimerization and activation. Finally, MALT1 itself and BCL10 were shown to be cleaved by MALT1 (scissors), therefore modulating their activity.
CARD: caspase recruitment domain, S/T: serine/threonine, IKK: inhibitor of nuclear factor kappa-B kinase, CAMKII: Ca^{2+}-calmodulin-dependent kinase II, DD: death domain, Ig: immunoglobulin, CK1α: casein kinase 1 alpha, PDZ: postsynaptic density-95 (PSD-95) discs-large zona occludens 1 (ZO-1), SH3: SRC homology 3 domain, GUK: guanylate kinase-like.
Adapted from: Ruland, J. & Hartjes, L., Nat. Rev. Immunol. (2019)

Altogether, the extensive work performed to characterize and understand the CBM signalosome allowed the precise definition of each of the three main components of the complex (CARMA, BCL10, MALT1) as well as their post-translational regulation through protein folding, complexation, phosphorylation, or ubiquitination. Identifying these modes of regulation allowed major breakthroughs in terms of treatment options for diseases relying on MALT1 activity for their expansion, such as lymphomas, inflammatory diseases, and certain cases of solid cancers.

C-III- MALT1 activation outcomes

C-III-1- NF-κB signaling cascade

The NF-κB (nuclear factor-kappa B) transcription factor regulates major cellular processes such as survival, proliferation, inflammation, and angiogenesis. Some of the known target genes of NF-κB are adhesion molecules, chemokines, cytokines, and cell cycle regulators[643]. Several upstream inputs are known regulators of the NF-κB pathway, but the CBM-mediated activation of the pathway will be the focus of this section.

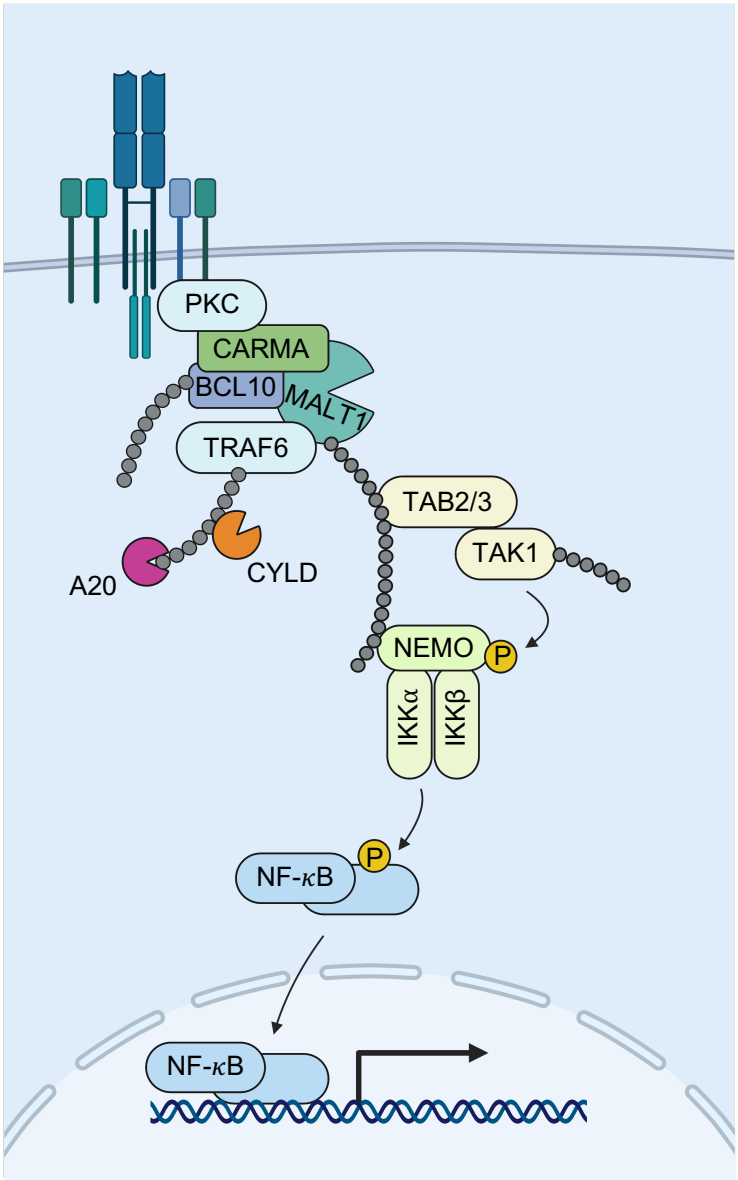

Figure 30: The CBM is crucial in the activation of the canonical NF-κB pathway. ITAM-containing receptors, GPCRs, or RTKs signaling engages the CBM through the PKC mediated activation of CARMA proteins. TRAF6 is recruited to the complex and mediates poly-ubiquitination of MALT1, BCL10, or itself, allowing TAK1 recruitment via TAB2/3. TAK1 phosphorylates IKKs, themselves phosphorylating the inhibitory subunit of NF-κB, leading to their degradation. The NF-κB transcription factor is then free to enter the nucleus and to regulate the transcription of genes involved in inflammation, survival, proliferation, and immune responses.

The abovementioned (see section C-II-2) signals converge on the assembly of the CBM signalosome, major determinant of NF-κB activation. Once the CBM is assembled (see section C-II-1), TRAF6 can auto-ubiquitinate and ubiquitinate BCL10 as well as MALT1[606,607], generating a platform allowing the recruitment of TAK1 via the adaptor proteins TAB1/2/3 (TGF-beta-activated kinase 1 and MAP3K7-binding protein 1/2/3), shown to bind to K63 poly-ubiquitinated TRAF6 and MALT1 through a

highly conserved zinc finger (ZnF) domain[606,644]. Of note, TAB1 is constitutively bound to TAK1, while TAB2/3 are recruited to the C-terminal part of the protein upon stimulation[645–648].

As part of the IKK complex with IKKα and IKKβ, NEMO can recognize and bind to K63 poly-ubiquitin chains formed on the CBM complex to ensure the close proximity between this complex and TAK1, favoring the TAK1-dependent phosphorylation of IKKβ at serine S177 and S181[649,650]. In turn, activated IKKs phosphorylate IκBα (nuclear factor of kappa light polypeptide gene enhancer in B-cells inhibitor, alpha) that retains inactive in the cytosol the two subunits of the NF-κB transcription factor, P65 and P50. The phosphorylation on serines S32 and S36 of IκBα allows its recognition by the SCF βTrCP (SKP1-CUL1-F-box ligase containing the F-box protein βTrCP) E3 ligase complex and its ubiquitin-mediated proteasomal degradation[649,651]. The NF-κB transcription factor is therefore free to enter the nucleus and induces the transcription of its target genes[652].

C-III-2- MALT1 proteolytic regulation of NF-κB and lymphocytes development

MALT1 has a preponderant function in immunoreceptor-induced events. Mice lacking MALT1 are immunodeficient and do not respond to viral infection or immunization as a consequence of impaired B- and T-cell responses[536,537]. NK and mast cells, possessing immune receptors responsible for CBM assembly upon engagement (see section C-II-2-1), also present defects in response to immunization in mice lacking the paracaspase[536,537,557,589,591]. Finally, mice lacking MALT1 were shown to have defects in the development of specific subsets of B- and T- lymphocytes[592,653–656]. Of note, uncoupling the scaffold and protease activities of MALT1 led to differential lymphocyte activation. Indeed, the group of Jürgen Ruland demonstrated that the protease activity of MALT1 was dispensable for lymphocyte activation, but necessary for regulatory T-cell and innate-like B-cell development *in vivo*[655]. Interestingly, patients harboring defects in MALT1 expression or protein stability are also immunodeficient, by showing failure to activate NF-κB in response to infection rather than affecting the overall number of immune cells[657–659].

As previously stated, the scaffolding function of MALT1 is preponderant for the assembly of the CBM and the consecutive activation of the NF-κB pathway and therefore for immune responses. In parallel, MALT1 arginine protease activity is

involved in optimal NF-κB activation (Table 7). The ubiquitin-editing enzyme A20 and the subunit of the CBM complex BCL10 were the first identified substrates of MALT1[538–540]. The two studies demonstrated that TCR stimulation induces the MALT1-dependent cleavage of A20 and BCL10 at arginine R439 and R228, respectively, resulting in their inactivation. A20 is a known negative regulator of the NF-κB pathway both as a result of the deubiquitination of TRAF6, MALT1, and NEMO[613,660,661], and ubiquitination for proteasomal degradation of E2 ubiquitin conjugating enzymes necessary for TRAF6 activity[662]. Expression of a non-cleavable mutant of A20 (R439A) resulted in the rapid inhibition of NF-κB upon TCR stimulation, as compared to the WT form of A20, not able to control NF-κB activity upon MALT1 processing[540]. Indeed, the recruitment of A20 to the CBM after TCR stimulation leads to the trimming of K63-linked ubiquitin on MALT1, blocking downstream signaling. Interestingly, it was recently demonstrated that A20 cooperates with ABIN-1 (A20-binding inhibitor of NF-kappa-B activation 1), a partner of the CBM, to negatively control MALT1 protease activation[663]. Of note, A20 is cleaved *in vivo* and promotes T-cell activation[664].

In parallel, the cleavage of BCL10 at R228 was identified by the group of Margot Thome. Interestingly, BCL10 cleavage by MALT1 in response to TCR engagement does not result in modification of downstream signaling pathways, such as NF-κB. However, BCL10 processing was shown to be essential for optimal lymphocyte adhesion to fibronectin, a mechanism thought to regulate lymphocyte priming and extravasation[539].

CYLD (cylindromatosis), another deubiquinating enzyme, has been shown to be cleaved by MALT1. As for A20, the tumor suppressor CYLD negatively regulates NF-κB as a result of its deubiquitinating activity toward TRAF2, TRAF6, and NEMO[665]. However, CYLD processing by MALT1 at R324 does not influence NF-κB activity, but rather the JNK signaling pathway. Indeed, the expression of a non-cleavable form of CYLD (R324A) reduces TCR-induced JNK phosphorylation[666]. As for A20, CYLD processing was also demonstrated *in vivo*, but its function on the JNK pathway remains mysterious, as a MALT1-deficient mice model had no effect on the phosphorylation of JNK upon B- and T-cell stimulation[537,664].

RelB, another negative regulator of the canonical NF-κB pathway, was shown to be cleaved at argigine R85 by MALT1[667]. RelB overexpression counteracts TCR-

mediated NF-κB activity in T-cells and reduces the viability of ABC-DLBCL cell lines, defining it as negative regulator of the pathway. Consequently, MALT1-dependent cleavage of RelB is accompanied by increased NF-κB activity[667].

MALT1 auto-processing at arginine R149 is also a determinant of the NF-κB activation downstream of TCR[668]. This auto-processing occurs between the N-terminal death-domain (DD) and the first Ig-domain of the paracaspase and results in the dissociation between MALT1 and BCL10. Rather appearing as a negative input for NF-κB signaling, this processing increases the transcriptional activity of NF-κB downstream of its nuclear accumulation[668]. Of note, MALT1 auto-proteolysis was visualized *in vivo* and demonstrated as essential for T-reg (regulatory T-cells) homeostasis downstream of IL2 production by activated CD4+ T-cells[669]. More recently, another MALT1 auto-processing site at its C-terminal part was identified. Oppositely to the R149 self-cleavage, the R781/R770 (depending on the isoform of the paracaspase) cleavage abrogates NF-κB signaling by inhibiting the R149 cleavage of MALT1 and reducing the interaction with TRAF6, revealing a sequential regulation of MALT1 by auto-processing[670].

The final layer of NF-κB regulation by the proteolytic activity of MALT1 comes from the processing of the LUBAC subunit HOIL1 (RanBP-type and C3H4-type zinc finger-containing protein 1, RBCK1), that three laboratories, including ours, have concomitantly identified. Indeed, Met1-linear ubiquitination of BCL10 and NEMO by the LUBAC are important determinant of NF-κB activation downstream of the CBM[631–633]. By cleaving HOIL1 at arginine R165 during the NF-κB activation cycle, MALT1 dampens NF-κB activity as a consequence of the reduced linear ubiquitination of NEMO and BCL10[671,672]. Notably, a study highlighted an intriguing function of the C-terminal fragment of HOIL1 generated upon cleavage. This proteolytically produced C-terminal fragment was shown to inhibit LUBAC activity and further NF-κB signaling[671]. In contrast to the other studies, our group demonstrated that MALT1-dependent cleavage of HOIL1 results in increased NF-κB activity. Indeed, the overexpression of a MALT1-insensitive version of HOIL1 mitigates TCR mediated activation of the pathway[673]. Therefore, the function of MALT1-mediated cleavage of HOIL1 is still debated and will need further investigations.

C-III-3- MALT1 proteolytic regulation of mRNA stability

In parallel to the regulation of the NF-κB pathway by its proteolytic activity, MALT1 was shown to modulate mRNA stability (Table 7). The proteins Regnase-1 (ZC3H12A), Roquin-1 (RC3H1), and Roquin-2 (RC3H2) were demonstrated to be proteolytically processed by the paracaspase at arginines R111, R579, and R509 respectively[674,675]. Of note, Regnase-1, Roquin-1, and Roquin-2, are importantly involved in auto-inflammation via the degradation of mRNA encoding interleukins or immune effectors[676]. Notably, mice deficient for these proteins develop severe auto-immune syndromes as a consequence of constitutive T-effector cell activation. This therefore demonstrates once again that MALT1 proteolytic activity is of major importance for the activation of lymphocytes in response to TCR engagement[674,675].

More recently, the RNase NEDD4-binding protein 1 (N4BP1), a potent inhibitor of HIV-1 (immunodeficiency virus type-1) replication, was shown to be cleaved by MALT1 at arginine R509. Mechanistically, N4BP1 inhibits HIV-1 replication by binding to viral RNA species and inducing their degradation. However, following CD4+ T-cell activation, MALT1 proteolytically inactivates the protein, promoting the reactivation of latent HIV-1 proviruses[677].

C-III-4- MALT1 proteolytic activity in the context of the t(11;18)(q21;q21) translocation (API2-MALT1 fusion protein)

The t(11;18)(q21;q21) translocation identified in MALT lymphoma patients leads to the generation of the API2-MALT1 fusion protein[531,532]. This chimeric protein was shown to auto-oligomerize and constitutively associate with TRAF2. As a result, the oncogenic fusion protein displays constitutive MALT1 proteolytic activity and constantly activates the NF-κB pathway[678] (Table 7). Notably, this fusion protein is often used in *in vitro* studies to characterize the proteolytic activity of MALT1 on its canonical substrates[666,668,672]. Moreover, the API2-MALT1 protein is a known regulator of the non-canonical NF-κB pathway, as compared to the classical canonical NF-κB pathway regulation downstream of the CBM assembly. This is notably thought to be the result of the cleavage of specific MALT1 substrates in this context of fusion protein[679].

Indeed, NIK (NF-κB inducing kinase) is the counterpart of the TAK1 kinase in the non-canonical NF-κB pathway. Upon TNFR (tumor necrosis factor receptor)

dependent activation, NIK phosphorylates IKKα, triggering the phosphorylation of the p100 subunit of NF-κB, inducing the nuclear translocation of the RelB/p52 heterodimer[680]. MALT1-mediated NIK cleavage at R325 releases a C-terminal fragment that retains its kinase activity and is resistant to proteasomal degradation, therefore mediating the constitutive activation of NF-κB though the non-canonical pathway[679]. Interestingly, the API2 moiety of the fusion protein was shown to mediate the recruitment of NIK to the paracaspase.

The same is true for LIMA1 (LIM domain and actin-binding protein 1), a known tumor suppressor, identified through unbiased tandem mass spectrometry-based analysis of API2-MALT1-binding partners. Of note, LIMA1 is cleaved at R206, but also surprisingly at an uncommon lysine residue (K289). This dual processing of LIMA1 by MALT1 was shown to generate a LIM domain-only (LMO)-containing fragment harboring the oncogenic properties of the protein. Indeed, the expression of the LMO fragment in a Hodgkin lymphoma cell line induced B-cell lymphomagenesis. Finally, the expression of a non-cleavable form of LIMA1 in a nude mice model reduced the ability of the API2-MALT1 fusion protein to promote lymphomagenesis[681].

C-III-5- Identification of new MALT1 substrates

Besides these well admitted substrates of MALT1, an important work is still performed to identify putative new substrates of the paracaspase. Using SILAC (stable isotope labelling by amino acids in cell culture)-based mass spectrometry analysis of the protein content of an ABC-DLBCL cell line with a constitutive MALT1 activity versus their MALT1-inhibited counterparts, Tensin-3 was recently proposed as a MALT1 substrate. Tensin-3 is a linker protein allowing the linkage of the actin cytoskeleton with the cytoplasmic tail of certain β-integrins, therefore regulating cellular adhesion, as does BCL10. Notably, Tensin-3 is cleaved at R614 upon BCR stimulation, therefore negatively modulating the adhesion of B-cells. The effect of Tensin-3 cleavage on B-cell activation was further confirmed *in vivo*, and shown to regulate the spreading of tumor cells[682].

Substrate	Cleaved sequence	Function
BCL10	LRSR$_{228}$TVS	T-cell adhesion
Tensin-3	LVSR$_{614}$CPA	Inhibition of B-cell adhesion
A20	GASR$_{439}$GEA	Positive regulation of NF-κB
RelB	LVSR$_{85}$GAA	Positive regulation of NF-κB
MALT1	LCCR$_{149}$ATG	Positive regulation of NF-κB
MALT1	HCSR$_{781}$TPD (isoform A) HCSR$_{770}$TPD (isoform B)	Negative regulation of NF-κB
CARMA3	LLAR$_{587}$GCG	Negative regulation of NF-κB
HOIL1	LQPR$_{165}$GPL	Regulation of NF-κB
CYLD	FMSR$_{324}$GVG	Positive regulation of JNK
Regnase-1	LVPR$_{111}$GGG	mRNA stability
Roquin-1	MVPR$_{579}$GSQ	mRNA stability
Roquin-2	LISR$_{509}$STD	mRNA stability
N4BP1	FVSR$_{509}$GAS	HIV-1 mRNA stabilization
NIK	CLSR$_{325}$GAH	Constitutive NF-κB activation
LIMA1	PDSR$_{206}$ASS	B-cell lymphomagenesis
LIMA1	FKSK$_{289}$GNY	B-cell lymphomagenesis

Table 7: List of all known MALT1 substrates, their respective cleavage site, and the function associated with their processing. NIK and LIMA1 are exclusive substrates of the fusion protein API2-MALT1.

As already mentioned, bio-informatic tool development now allows the prediction of important crosstalk between protein functions and subsequent signaling pathways modulation. This is notably the case for the identification of MALT1 substrates. A study by the group of Christopher Overall allowed the identification of seven new putative MALT1 substrates, most of them involved in the NF-κB pathway, such as TAB3 (TAK1 binding protein 3), TANK (TRAF family member Associated NF-κB activator), ZC3HD12D and -B (Zinc finger CCCH domain-containing protein 12D and -B), and CASP10 (Caspase 10). In parallel, the cilia-regulating protein CILK1 (ciliogenesis associated kinase 1), unrelated to the NF-κB pathway, also featured a strong cleavage by MALT1 in an overexpression system, showing the potential of using this predictive tool to identify new MALT1 substrates, related or not, to the classical functions of the CBM[542].

C-III-6- CBM-dependent regulation of the JNK and mTOR pathways

The JNK (c-Jun N-terminal kinase) pathway is a known output of TCR engagement in T-cells and regulates cytokine production as well as cell death effectors[683]. However, how is this kinase and the subsequent pathway regulated during TCR signaling remained mysterious for several years. Two separate studies demonstrated contradictory results concerning the activation of the pathway in MALT1-deficient mice in response to TCR stimulation[536,537]. The differences in mice models as well as the ability of the CBM to differentially regulate JNK1 and JNK2 isoforms might explain this discrepancy[684]. Later, a study by the group of Rudi Beyaert demonstrated that MALT1 is indeed a positive regulator of the JNK pathway via the cleavage of CYLD at R324[666]. However, MALT1 deficient mice do not present a deficit in JNK activation, raising questions regarding the roles of MALT1 and CYLD on the control of this signaling pathway[537].

Two consecutive publications demonstrated the role of the CBM signalosome and of MALT1 activity on the mTOR pathway downstream of TCR activation. Of note, the PI3K/Akt/mTOR pathway, was already associated with T-cell trafficking and activation[601,685]. The study by Kristia Hamilton and colleagues nicely demonstrated the essential role of CARMA1 activity downstream of TCR engagement for mTOR activation, as visualized by the phosphorylation of its known substrate ribosomal protein S6. Secondly, the study uncovers that MALT1, but not BCL10, is required for mTOR activation. Interestingly, inhibiting the proteolytic activity of MALT1 with the peptide z-VRPR-fmk resulted in a decreased phosphorylation of S6 in response to CD3/CD28 stimulation of primary mouse CD4+ T-cells, and therefore in a reduced proliferation. However, the precise molecular mechanism linking MALT1 proteolytic activity and mTOR remains unclear, but might potentially involve a MALT1 substrate[686]. The study by Mako Nakaya provided a deeper molecular mechanism to explain the regulatory function of MALT1 on the mTOR pathway. Indeed, the CBM complex subunit CARMA1 can bind to the glutamine importer ASCT2 (neutral amino acid transporter B(0)), also known as SLC1A5). In parallel, CARMA1 was shown to be important for the TCR-mediated increase in ASCT2 mRNA level. Consequently, depletion of CARMA1, MALT1, or BCL10 in CD4+ mice T-cells, resulted in a significant decrease in glutamine uptake upon CD3/CD28 stimulation, as well as a decrease in the mTOR-dependent phosphorylation of S6. Of note, the leucine uptake was also negatively affected as a result of the decreased glutamine gradient

generated, also affecting mTOR activation. Interestingly, z-VRPR-fmk treatment decreased the glutamine uptake upon TCR stimulation, once again providing evidence that the mTOR pathway might be regulated by a yet-unidentified MALT1 substrate. In conclusion, the MALT1-dependent glutamine and leucine uptake in response to TCR stimulation was shown to induce T-cell activation and differentiation into effector T-cells, such as Th17 or Th1[687]. Even though these two studies provide strong evidence for a MALT1-dependent regulation of mTORC1 through amino acid uptake, the precise and direct involvement of the protease function of MALT1 on the mTOR pathway remains to be elucidated.

Furthermore, our group identified Quaking (QKI), a RNA-binding protein, as a constituent of the pre-assembled CBM identified in GSCs[497]. We demonstrated that QKI is bound to BCL10/MALT1 dimers and provided evidence that the activity of MALT1 negatively regulates QKI function. As previously described (see section B-III-3), QKI positively regulates the endo-lysosome compartment[496], and its inhibition through binding to the CBM strongly impairs the abundance of these degradative organelles in GSCs. Interestingly, QKI activity correlates with the extent of mTORC1 activity. Indeed, inhibiting MALT1 resulted in a strong impairment of the mTOR pathway, as seen by the reduced phosphorylation of S6, and of the lysosomal dissociation of mTOR. This could be rescued by the silencing of QKI. This implies that QKI activity negatively regulates mTOR in response to MALT1 blockade. Whether this effect is direct or through the modulation of the lysosomal compartment is still unclear and will need further investigation[497].

C-IV- MALT1 targeting and implication in diseases

C-IV-1- MALT1 inhibitors

MALT1 is the unique member of the paracaspase family of cysteine proteases in mammals. Its proteolytic activity is of particular importance in lymphocytes and NF-κB activation, as well as lymphomagenesis and solid cancer cell expansion. Thus, the development of potent and selective MALT1 inhibitors has created a stir (Table 8). The first MALT1 inhibitor designed, z-VRPR-fmk, is a tetrapeptide (Val-Arg-Pro-Arg-fluoromethyl ketone) based on the optimal cleaved sequence of AtmC9, an *Arabidopsis thaliana* metacaspase substrate. Upon development, it proved efficacy in inhibiting BCL10 cleavage by MALT1 and NF-κB activation upon TCR engagement[539]. As previously stated, MALT1 activity is pivotal in DLBCL survival via

NF-κB sustenance. The direct targeting of the aberrant activity of MALT1 was therefore hypothesized as a better approach than inhibition of the pleiotropic NF-κB transcription factor. In this context, two groups discovered the important sensitivity of the ABC-DLBCL (activated B cell diffuse large B cell lymphoma) subtype toward a z-VRPR-fmk treatment. Indeed, MALT1 catalytic blockade led to the shutdown of the NF-κB pathway, major determinant of this subtype of lymphoid malignancy[543,544]. Unfortunately, it was already known that the fluoromethyl ketone (fmk) moiety of the compound, important factor for cysteine protease inhibition, was metabolized into the highly toxic metabolite fluoroacetate (FAC) *in vivo*, thus preventing its use in animals and humans[688].

In the quest for selective, potent, and non-toxic MALT1 inhibitors, the group of Ari Melnick developed MI-2, an irreversible inhibitor of the paracaspase[689]. Extensive characterization of the compound demonstrated its preferential binding in the catalytic site, as well as the necessity of a chloromethyl amide group to irreversibly inhibit MALT1. Biochemical analysis of ABC-DLBCL cell lines treated by MI-2 showed a strong reduction in MALT1 substrates cleavage, NF-κB activation, and reduced cell viability. Importantly, MI-2 was non-toxic in mice models, and potently suppresses the growth of xenografted ABC-DLBCL, demonstrating the potential of this compound for the treatment of human ABC-DLBCL[689].

The same year, two independent groups identified phenothiazines as potent and selective inhibitors of MALT1[690,691]. Notably, using a high throughput screening of approximately 18,000 compounds and assessing the activity of purified MALT1 on the fluorescent synthetic peptide Ac-LRSR-AMC (Fig. 31), fifteen hits, with three of them being part of the family of phenothiazines (Mepazine, Thioridazine, and Promazine) were identified.

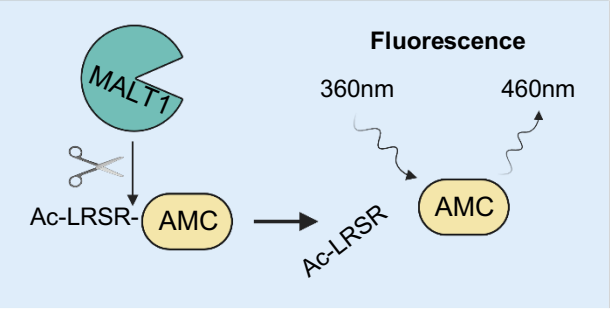

Figure 31: The peptide Ac-LRSR-AMC is recognized and cleaved by the MALT1 paracaspase *in vitro*. The resulting AMC fragment can be excited by a 360nm light source, and in turn emits 460nm fluorescence. The intensity of fluorescence generated reflects MALT1 proteolytic activity.
LRSR: Leu-Arg-Ser-Arg, AMC: 7-amino-4-methylcoumarin
Adapted from: May, M. J., Methods in Molecular Biology (2015)

As for the other MALT1 inhibitors, phenothiazines showed a strong inhibition of MALT1 catalytic activity as well as NF-κB pathway in activated T cells and impaired ABC-DLBCL growth[690]. Rather importantly demonstrating the potency of the compounds, the chemical mechanism of action was only hypothesized. In this context, the structural analysis of phenothiazines in complex with MALT1 was performed[691]. The glutamic acid E397 of MALT1 was identified as the binding site for phenothiazine. Therefore, these compounds operate as non-competitive allosteric inhibitors. The E397 is indeed located at the interface between the paracaspase and Ig3 domains, and binding of phenothiazines to this residue blocks MALT1 in an inactive conformation by displacing the tryptophan W580, flipping the helix $\alpha 1_{Ig3}$, resulting in increased flexibility of the Ig3 domain[691]. Of interest, phenothiazines were used in clinic as antipsychotic or sedative drugs, and all safety studies were already performed and available at the time they were identified as MALT1 inhibitors. This is notably true for Mepazine, commercially available under the name of Pacatal and previously used for the treatment of anxiety, depression, and schizophrenia[692–694]. It is however noteworthy that some patients developed side effects such as dry mouth and throat, reduced ability to accommodate to close vision, and a decrease in intestinal peristalsis[693]. That did not stop the research use of mepazine as a potential anticancer agent. Notably, the (S)-enantiomere of mepazine, which possesses an increased activity against MALT1 proteolytic activity[691], showed promising results in *in vivo* studies of several murine cancer types and in patient-derived organotypic tumor spheroids. Indeed, syngeneic transplanted tumors and *in vitro* organoids were affected by mepazine administration[691,695]. This antitumor effect was also demonstrated in GB by our group. MALT1 targeting by phenothiazines, notably mepazine, engendered a lysosomal dependent cell death of GSCs *in vitro*, as well as in a xenograft model of patient-derived GSCs[497] (see section B-III-3). Overall, the previous use in clinic of phenothiazines and their potent and selective ability to inhibit MALT1 make them promising therapeutic options for the treatment of diseases relying on MALT1 activity.

More recently, new MALT1 reversible allosteric inhibitors named MLT-747 and -748 were identified[696]. These two compounds mimic the ability of the tryptophan 580 (W580) of MALT1 to bind an allosteric pocket, therefore locking the paracaspase in an inactive conformation, abolishing its protease activity. Interestingly, the compounds were able to rescue the MALT1 W580S mutant functions. Indeed, this

mutation was demonstrated to reduce MALT1 stability, resulting in immunodeficiency for the patients harboring this defect, while MLT-747 and -748 treatments stabilize the protein, partially rescuing the scaffold and protease activity of MALT1. As stated by the authors, the ability of these chemical compounds to both inhibit the wild-type protein and to replace a mutated amino-acid to restore the protein function is a sole example. This therefore opens new opportunities for MALT1 inhibition or stabilization[696].

Finally, JNJ-67856633, a potent allosteric and reversible inhibitor synthesized upon high-throughput screening and several steps of optimization, proved efficacy against MALT1 activity via binding to the classical allosteric site of the paracaspase[697]. Several clinical trials were launched using this compound, notably in the treatment of non-Hodgkin lymphomas.

Overall, no more than twenty-five years were necessary to unveil the MALT1 paracaspase gene, its protease activity, its implication in major signaling pathways such as NF-κB, the critical role of MALT1 and its interactors in lymphomagenesis and inflammatory diseases, as well as to develop potent and selective inhibitors used in clinic. Acting as a critical regulator of NF-κB, MALT1 still concentrates efforts to elucidate its implications in solid tumors such as glioblastoma, and important works are needed to complete the list of rare MALT1 substrates.

Inhibitor	Mode of action	Limitations
z-VRPR-fmk	Proteolytic inhibition through binding in the catalytic pocket	*In vivo* toxicity of the fmk moiety
MI-2	Proteolytic inhibition through binding in the catalytic pocket	
Phenothiazines	Allosteric inhibitors. Block MALT1 in an inactive conformation by binding to the E397	Side effects in patients. Reversible inhibitors
MLT-748	Allosteric inhibitor. Blocks MALT1 in an inactive conformation by binding to the E397	Reversible inhibitor
JNJ-67856633	Allosteric inhibitor. Blocks MALT1 in an inactive conformation by binding to the E397	Reversible inhibitor

Table 8: Name, mode of action, and limitations of the most studied MALT1 inhibitors.

C-IV-2- Lymphomas

As already discussed in the introductive paragraph, the genetic description of MALT lymphomas allowed to identify recurrent chromosomal translocations associated with the development of this disease. Of note, the most common chromosomal translocations observed are associated with enhanced transcription or activity of CBM components. The t(1;14)(p22;q32) and t(14;18)(q32;q21) translocations, present in 1-2% and 15-20% of MALT lymphomas respectively, are associated with BCL10 or MALT1 translocation in the IgH (immunoglobulin heavy chain) enhancer region on the chromosome 14, increasing their transcription. Lastly, the t(11;18)(q21;q21) translocation induces the generation of the API2-MALT1 fusion protein, responsible for constitutive MALT1 activity[527]. Consequently, MALT lymphomas are defined by constitutive NF-κB activity due to hyperactive MALT1, as seen by the cleavage of the specific substrates of the fusion protein LIMA1 and NIK, themselves involved in the pathogenesis of the disease[679,681].

Diffuse large B-cell lymphomas (DLBCL) are the most common form of non-Hodgkin lymphomas and the most common lymphoid malignancy in adults worldwide. This cancer arises from pre-existing low-grade lymphomas such as MALT lymphoma, or through oncogenic mutations in B-lymphocytes[529,530]. DLBCL are divided into two main subtypes depending on the cell of origin: germinal center B-like (GCB) and activated B-cell (ABC). The ABC subtype, rather less common than its GCB counterparts (35% versus 50% of total DLBCL diagnosed, respectively), is nevertheless associated with a worser outcome for the patients. Of interest, the ABC subtype of DLBCL is characterized by a chronic activation of the NF-κB pathway[698]. Several mutations are described along the pathway leading to this constitutive NF-κB activation. These include activating mutations in the ITAM of the CD79A/B chains of the BCR (20% of cases) and of CARMA1 (10% of cases), as well as inactivating mutations in the NF-κB negative regulator A20 (20% of cases)[699]. A mutation of the first tyrosine in the CD79 ITAM leads to the inability of the Lyn kinase to mediate the internalization of the receptor as a feedback mechanism. As such, the BCR signaling is maintained and continuously ignites NF-κB activation[700].

Activating CARMA1 mutations are found contiguous or directly in the coiled-coil domain of the protein, allowing the constitutive assembly of the CBM, leading to increased NF-κB and JNK activity. Of note, the introduction of the L225I mutation in

CARMA1 is sufficient to drive *in vivo* lethal lymphoproliferation, but can be rescued by deletion of MALT1 or BCL10, as well as inhibition of NF-κB or JNK pathways[701,702].

In the case of A20, inactivating mutations induces constitutive NF-κB signaling. Therefore, it was shown that reconstituting A20 deficient DLBCL cell lines leads to cell growth arrest and apoptosis via inhibition of the NF-κB pathway[703]. Interestingly, inactivating mutations in the MALT1 substrate A20 are also identified in mantle cell lymphomas, another aggressive subtype of non-Hodgkin lymphoma[704,705].

In parallel, another study demonstrated the chronic activation of the CBM complex in several subtypes of mantle cell lymphomas as seen by the cleavage of the known substrate of MALT1 RelB. Moreover, BIRC3 (API2) was shown mutated in nearly 10% of the 165 patients analyzed, leading to its inability to inhibit the NIK-dependent activation of the non-canonical NF-κB pathway[706].

Finally, the LUBAC subunit HOIL1 was also demonstrated as crucial for NF-κB activation in ABC-DLBCL. Indeed, rare polymorphism in RNF31 (E3 ubiquitin-protein ligase RNF31) leads to its association with HOIL1, therefore increasing LUBAC enzymatic activity and NF-κB engagement[707]. In line with these results, our group denoted that removal of the LUBAC was toxic to ABC-DLBCL lymphoma cell lines[631].

Because MALT1 is central in the control of the NF-κB pathway in the context of lymphoma, several studies agreed on the interesting possibility to inhibit the paracaspase activity as a treatment to reduce the influence of the NF-κB pathway (see section C-IV-1).

C-IV-3- Autoimmune and inflammatory diseases

The NF-κB pathway is primordial in the regulation of adaptative and immune responses, and as such, deregulation of this pro-inflammatory pathway contributes to the pathogenesis of autoimmune and inflammatory diseases[708]. Multiple sclerosis (MS) is an auto-immune disease defined by chronic inflammatory affection of the CNS[709]. Experimental autoimmune encephalomyelitis (EAE) animal model is generally employed to study *in vivo* effects of MS because of the pathological similarities between the two diseases[710]. Notably, EAE is characterized by the differentiation of CD4+ T-cells into Th17 effector cells, producing important levels of pro-inflammatory IL17 in the CNS, recapitulating the development of the disease.

Interestingly, the CBM and more particularly MALT1, were shown to be necessary for the pathogenicity of Th17 cell. Indeed, MALT1-KO Th17 cells normally infiltrated the CNS but were non-pathogenic, producing reduced level of IL17 as a result of downregulated NF-κB signaling[656]. Of note, the adoptive transfer of MALT1 deficient splenocytes blocked the development of EAE, demonstrating the preponderant function of the paracaspase in the onset of the disease[664]. In parallel, the use of the MALT1 inhibitor mepazine demonstrated efficiency in reducing EAE pathology in mice[711].

In line with these results, MALT1 protease activity also appears of paramount importance in the regulation of autoimmune diseases. Indeed, the MALT1 substrate Regnase-1 (ZC3H12A), that mediates the decay of pro-inflammatory encoding mRNAs, is strongly involved in the development of immune disorders[676]. The loss of this protein promotes T-cell activation[674], but its chronic deletion induced Th17 T-cell differentiation and autoimmunity[675]. Of interest, MALT1-KO mice do not exhibit the same phenotypes as MALT1-protease-dead mice (MALT1-PD). Indeed, MALT1 deficient animals show strong defects in lymphocyte activation and are protected against autoimmune diseases development. In addition to these features, MALT1-PD animals also intriguingly developed autoimmune gastritis and multiorgan inflammation, as a consequence of the elevated number of activated T-cells and the reduced number of T-reg cells[653,654]. In line with these phenotypes, constitutive MALT1 activation in response to loss of TRAF6 induces fatal inflammation in mice models[609]. This discrepancy in the phenotypes observed between the two animal models argue in favor of specific functions of the two separate scaffold and protease activities of MALT1[655]. Of note, MALT1 deficient patients display important immunodeficiency caused by the inability of lymphocytes to activate NF-κB in response to infectious conditions[657–659].

The upstream modulator of MALT1, CARMA, was also extensively studied for its implication in inflammatory diseases. Benjamin Medoff notably identified the fundamental role of CARMA1 in allergic asthma. CARMA1 deleted mice did not develop asthma, showing that the CBM scaffold is an important actor in the instauration of inflammatory phenotypes[712]. In a following study, the group visualized that CARMA1 deletion could also restore the allergic inflammation already setup in the mice model, opening avenues for the treatment of this disease[713]. Finally, CARMA3 expressed by airway epithelial cells favors the development of the

inflammation by acting on the production of pro-asthmatic mediators in response to asthma-linked GPCR ligands such as house dust mite or lysophosphatidic acid[714]. As CARMA proteins are obligatory regulators of MALT1 activity, the paracaspase might therefore be implicated in this context.

Psoriasis is a chronic inflammatory skin disease defined by hyperproliferative keratinocytes and infiltrative immune cells. Although the origin of psoriasis is not well defined, some genetic lesions are commonly observed in patients[715]. One of these lesions was defined as positively affecting the CARMA2 (CARD14) gene, resulting in NF-κB-dependent CCL20 (C-C motif chemokine 20) and IL8 (interleukin-8) secretion by keratinocytes, favoring the development of inflammation[560,716]. Endothelial cells were also shown to express CARD14, therefore playing an important role in parallel of keratinocytes in the development of psoriasis[559]. The group of Rudi Beyaert took advantage of the knowledge that CARD14 gain-of-function mutations associate with psoriasis development to link the entire CBM activity to the disease. It was demonstrated that the inducible expression of mutated CARD14 (E138A) specifically in keratinocytes led to the development of psoriasis, and that deletion of MALT1 as well as oral administration of MLT-827, a specific inhibitor of MALT1 proteolytic activity, rescued psoriatic skin disease[561,717]. In a later study, the same group demonstrated the physical interaction between CARD14 and MALT1 and further showed that MALT1 is required for psoriasis-induced phenotypes downstream of CARD14 mutation[718]. The discovery of the cardinal function of MALT1 proteolytic activity in psoriasis, as well as in other inflammatory and autoimmune disorders, favored the development of MALT1 inhibitors, enriching the therapeutic arsenal directed against this protein[691,696,697,719–721].

C-IV-4- Solid cancers

The CBM complex is importantly involved in immune responses and regulation of the T-reg population downstream of the TCR signaling. This observation led several groups to investigate the function of the CBM in anti-tumor immune responses. Indeed, T-regs, dependent on MALT1 for their activation, are negative regulators of this phenomenon in order to maintain immune homeostasis[722]. The group of Jürgen Ruland demonstrated that MALT1 proteolytic activity mediates the suppressive function of T-regs. The deletion of BCL10 or MALT1 strongly impairs the expression of CTLA4 (cytotoxic T-lymphocyte protein 4), a suppressive marker of T-regs. Of

note, MALT1 inhibition in mice models had similar effect on the suppressive function of T-regs. This was further linked to immune suppression in melanoma, with mice models treated with mepazine or manipulated to have BCL10-deleted T-reg, presenting a better immune response and decreased tumor volume. Overall, this provided evidence for the tumor immunosuppressive function of MALT1 through T-reg response[723]. In parallel, tumor infiltrating T-regs deleted for CARMA1 or treated using mepazine were shown to produce important level of IFNγ, leading to reduced tumor growth in mice models of melanoma. However, tumor cells presented increased level of PD-L1 (programmed cell death protein 1), a known marker of adaptive immune resistance. Therefore, combining MALT1 inhibition with immune checkpoint therapy was proposed as a promising option to treat solid cancers characterized by high infiltration of immunosuppressive T-regs[724].

MALT1 and the CBM complex expression and activity were also highlighted as important for the proliferation, growth, and survival, of cancer cells of solid tumors. Several lines of evidence linked MALT1 and breast cancer aggressiveness. The HER2/Neu (receptor tyrosine-protein kinase erbB-2) protein tyrosine kinase is overexpressed in a large subset of breast cancers and correlates with bad prognosis, probably via a NF-κB -dependent mechanism. A study uncovers the crucial role of CARMA3 in this HER2/NF-κB axis. CARMA3 was shown involved in NF-κB activation downstream of HER2, and to promotes proliferation, survival, as well as metastasis through the upregulation of metalloproteinases. Of note, MALT1-KO mice models crossed with a mice model developing spontaneous HER2-overexpressing breast cancers delayed the progression of the disease[725]. The same activation of the CARMA3-BCL10-MALT1 complex was observed in AGTR1 (type-1 angiotensin II receptor) overexpressing breast cancer cells. This receptor for angiotensin-II was linked to NF-κB via the CBM in a ligand-dependent and ligand-independent manner, as the knockdown of either of the three components of the complex reduced proliferation of breast cancer cellular models *in vitro*[562]. In parallel, MALT1 activation induced epithelial to mesenchymal transition (EMT) in AGTR1 overexpressing breast cancer cells. As such, inhibiting MALT1 activity through its depletion or using mepazine effectively counteracted EMT induction and reduced the progression of breast cancer in xenograft mice models[726]. Finally, the thrombin GPCR PAR1 (protease-activated receptor 1) was shown to signal to NF-κB through the CBM.

PAR1-mediated activation of MALT1 activity led to expression of pro-metastatic genes such as IL8 and metalloproteinases in breast cancer and osteosarcoma models. Of interest, inhibiting MALT1 proteolytic activity using MI-2 or z-VRPR-fmk strongly impaired the expression of these genes *in vitro*, and MALT1 knockout significantly impaired metastasis development *in vivo*[727].

Ovarian cancer cells also depend on the CBM for their survival. A study uncovered that MALT1 is rendered active downstream of the lysophosphatidic acid receptor LPAR1 (lysophosphatidic acid receptor 1) and regulates invasion and migration of ovarian cancer cell models[728]. Similarly, EGFR stimulation mediates the activation of the CBM in lung cancer HCC827 cellular model. MALT1 scaffold activity, but not protease, was shown as important for NF-κB-dependent IL6 production and further STAT3 activation. Overall, this was necessary for lung cancer cells proliferation and survival[600]. Oppositely, another study demonstrated a role for MALT1 protease activity in IL6 production and survival of lung adenocarcinoma. Indeed, the cleavage of CARMA3 at R587 by the paracaspase reduces cancer cell survival. A point mutation in CARMA3 abolishing its cleavage further enhances tumor growth in mice model. Of note, inhibiting MALT1 in these mutated cells did not affect the downstream phenotypes, showing the specific effect of CARMA3 cleavage on lung cancer cell proliferation and survival[729].

MALT1 inhibition has been proposed as a strategy to treat pancreatic cancer. Indeed, MALT1 was shown frequently overexpressed in pancreatic cancer tissues as compared to healthy one, where its expression cannot be detected. Consequently, the use of mepazine induced cell death of pancreatic cancer cells as a result of the reduced NF-κB activity[730]. This observation was similar to the one made in hepatocellular carcinoma, in which MI-2 treatment strongly impaired the growth of SNU449 and Mahlavu hepatocellular carcinoma cell lines[731].

GB, the most aggressive form of brain tumor in adults, also relies on MALT1 expression and activity for its growth. Using U87 and U251 human GB cell lines, a study demonstrated the activation of NF-κB downstream of the CBM upon EGFR stimulation. As NF-κB is crucial in GB tumorigenesis, the MI-2-mediated inhibition of MALT1 or its deletion resulted in *in vitro* and *in vivo* cell death[732]. The same year, our group unravelled the dependency of GSCs toward the activity of MALT1. *In silico* analysis of GB samples from TCGA (the cancer genome atlas) demonstrated the

strong correlation between MALT1 expression and GB patients' survival. Moreover, MALT1 expression was significantly upregulated in GB samples as compared to healthy tissues. On top of this increased expression, GSCs presented a constitutive activity of the paracaspase, as seen by the cleavage of several known substrates such as CYLD and Roquin-1 and -2. However, how is MALT1 activated in this context remains unclear and will need further investigation. Mechanistically, far from its function in the NF-κB pathway, MALT1 protease activity was shown essential for GSC survival, and its effect on survival relied on its binding to the RNA-binding protein QKI, known modulator of lysosomal homeostasis. MALT1 inhibition resulted in QKI unleashing, promoting the generation of aberrant and dysfunctional lysosomes, further promoting mTOR inhibition and lysosomal dependent cell death (see section B-III-3). Finally, MALT1 inhibition using the compound mepazine significantly impaired the growth of GSCs *in vivo*[497].

As such, the dependency toward the activity of MALT1 was defined as a non-oncogene addiction, a mechanism by which non-mutated genes nor involved in the initiation of tumorigenesis are essential for the propagation of the disease[733]. This overall placed MALT1 as an interesting druggable target for cancers relying on MALT1 activity for survival.

Results

1) Jacobs KA et al., Paracaspase MALT1 regulates glioma cell survival by controlling endo-lysosome homeostasis. The EMBO Journal, 2020.

2) Maghe C et al., The paracaspase MALT1 controls cholesterol homeostasis in glioblastoma stem-like cells through lysosome proteome shaping. Cell Reports, in revision, 2023.

Project goals

Glioblastoma (GB) is the most common and aggressive primary brain tumor in adults with a median survival of around 15 months after diagnosis. Despite invasive treatments of surgical resection followed by radiotherapy and chemotherapy, GB is a fatal cancer, with relapses being almost inevitable.

Glioblastoma stem-like cells (GSCs), a subset of GB cells with stem properties, were described as able to repopulate the tumor mass after treatments. In parallel, GSCs were shown as capable of initiating GB tumors owing to their multipotency and self-renewing abilities. As such, GSCs eradication appears of preponderant importance for the treatment of GB, as new therapies are urgently needed.

The lysosomal compartment, acting at the crossroad between anabolism and catabolism, recently emerged as a regulator of GSCs fate. Lysosomal destabilization indeed proved efficacy in eradicating the GSC subpopulation and reducing GB tumor growth *in vitro* and *in vivo*. Notably, the constitutive activity of the MALT1 paracaspase was linked to the downregulation of the lysosomal compartment and to the promotion of GSCs stem properties, with MALT1 inhibition inducing lysosomal membrane permeabilization and further lysosomal cell death. However, the precise alterations occurring in lysosomes of MALT1-inhibited GSCs remained to be determined.

In this context, we hypothesized that the inhibition of the MALT1 paracaspase results in a profound remodeling of the lysosomes proteome, altering their degradative and recycling properties, resulting in the demise of GSCs. The precise characterization of this degradative compartment could therefore help the description of the events leading to GSCs death upon MALT1 inhibition, and to highlight weaknesses of this cell subpopulation.

Therefore, the main goals of this project were to:

1- Refine our current understanding on the functions of the paracaspase on the sustenance of GSCs
2- Identify new potential therapeutic windows for GSCs eradication.
3- Elucidate the reshaping of the lysosomal compartment upon MALT1 inhibition in GSCs

1) Jacobs KA et al., Paracaspase MALT1 regulates glioma cell survival by controlling endo-lysosome homeostasis. The EMBO Journal, 2020.

As the third author, I participated in the acquisition, analysis, and interpretation of the generated data.

In this study, I contributed to the investigation of the role of the MALT1 paracaspase in endo-lysosomes homeostasis and GSCs cell fitness. By performing immunofluorescent staining and confocal analysis, I visualized the massive accumulation of lysosomes and their redistribution upon MALT1 inhibition. I also explored the lysosomal localization of mTOR as well as its downstream signaling pathway. Moreover, by deploying flow-cytometric and biochemical-based cell viability assays, I demonstrated that the blockage of MALT1 induces a lysosomal-dependent cell death of GSCs.

Article

SOURCE DATA | TRANSPARENT PROCESS

THE EMBO JOURNAL

Paracaspase MALT1 regulates glioma cell survival by controlling endo-lysosome homeostasis

Kathryn A Jacobs[1], Gwennan André-Grégoire[1,2], Clément Maghe[1], An Thys[1], Ying Li[3], Elizabeth Harford-Wright[1], Kilian Trillet[1], Tiphaine Douanne[1], Carolina Alves Nicolau[1], Jean-Sébastien Frénel[2], Nicolas Bidère[1] & Julie Gavard[1,2,*]

Abstract

Glioblastoma is one of the most lethal forms of adult cancer with a median survival of around 15 months. A potential treatment strategy involves targeting glioblastoma stem-like cells (GSC), which constitute a cell autonomous reservoir of aberrant cells able to initiate, maintain, and repopulate the tumor mass. Here, we report that the expression of the paracaspase mucosa-associated lymphoid tissue l (MALT1), a protease previously linked to antigen receptor-mediated NF-κB activation and B-cell lymphoma survival, inversely correlates with patient probability of survival. The knockdown of MALT1 largely impaired the expansion of patient-derived stem-like cells *in vitro*, and this could be recapitulated with pharmacological inhibitors, *in vitro* and *in vivo*. Blocking MALT1 protease activity increases the endo-lysosome abundance, impairs autophagic flux, and culminates in lysosomal-mediated cell death, concomitantly with mTOR inactivation and dispersion from endo-lysosomes. These findings place MALT1 as a new druggable target involved in glioblastoma and unveil ways to modulate the homeostasis of endo-lysosomes.

Keywords glioma; lysosome; MALT1; mTOR; protease
Subject Categories Cancer; Autophagy & Cell Death; Membranes & Trafficking
DOI 10.15252/embj.2019102030 | Received 18 March 2019 | Revised 16 October 2019 | Accepted 25 October 2019 | Published online 27 November 2019
The EMBO Journal (2020) 39: e102030

Introduction

Glioblastoma multiforme (GBM) represents the most lethal adult primary brain tumors, with a median survival time of 15 months following diagnosis (Stupp *et al*, 2009, 2015). The current standard-of-care for the treatment of GBM includes a surgical resection of the tumor followed by treatment with alkylating agent temozolomide and radiation. While these standardized strategies have proved beneficial, they remain essentially palliative (Stupp *et al*, 2009; Chinot *et al*, 2014; Brown *et al*, 2016). Within these highly heterogeneous tumors exists a subpopulation of tumor cells named glioblastoma stem-like cells (GSCs). Although the molecular and functional definition of GSCs is still a matter of debate, there is compelling evidence that these cells can promote resistance to conventional therapies, invasion into normal brain, and angiogenesis (Singh *et al*, 2004; Bao *et al*, 2006; Chen *et al*, 2012; Yan *et al*, 2013; Lathia *et al*, 2015). As such, they are suspected to play a role in tumor initiation and progression, as well as recurrence and therapeutic resistance. Owing to their quiescent nature, GSCs resist to both chemotherapy and radiation, which target highly proliferative cancer cells (Bao *et al*, 2006; Chen *et al*, 2012). Hence, there is a clear need to identify novel therapeutic targets, designed to eradicate GSCs, in order to improve patient outcome.

GSCs constantly integrate external maintenance cues from their microenvironment and as such represent the most adaptive and resilient proportion of cells within the tumor mass (Lathia *et al*, 2015). Niches provide exclusive habitat where stem cells propagate continuously in an undifferentiated state through self-renewal (Lathia *et al*, 2015). GSCs are dispersed within tumors and methodically enriched in perivascular and hypoxic zones (Calabrese *et al*, 2007; Jin *et al*, 2017; Man *et al*, 2017). GSCs essentially received positive signals from endothelial cells and pericytes, such as ligand/receptor triggers of stemness pathways and adhesion components of the extracellular matrix (Calabrese *et al*, 2007; Galan-Moya *et al*, 2011; Pietras *et al*, 2014; Harford-Wright *et al*, 2017; Jacobs *et al*, 2017). GSCs are also protected in rather unfavorable conditions where they resist hypoxic stress, acidification, and nutrient deprivation (Shingu *et al*, 2016; Jin *et al*, 2017; Man *et al*, 2017). Recently, it has been suggested that this latter capacity is linked to the function of the RNA-binding protein Quaking (QKI), in the down-regulation of endocytosis, receptor trafficking, and endo-lysosome-mediated degradation. GSCs therefore down-regulate lysosomes as one adaptive mechanism to cope with the hostile tumor environment (Shingu *et al*, 2016).

Lysosomes operate as central hubs for macromolecule trafficking, degradation, and metabolism (Aits & Jaattela, 2013). Cancer cells usually show significant changes in lysosome morphology and composition, with reported enhancement in volume, protease activity, and membrane leakiness (Fennelly & Amaravadi, 2017). These

1 Team SOAP, CRCINA, Inserm, CNRS, Université de Nantes, Université d'Angers, Nantes, France
2 Integrated Center for Oncology, ICO, St. Herblain, France
3 Tsinghua University-Peking University Joint Center for Life Sciences, Technology Center for Protein Sciences, School of Life Sciences, Tsinghua University, Beijing, China
*Corresponding author. Tel: +33 2808 0327; E-mail: julie.gavard@inserm.fr

modifications can paradoxically serve tumor progression and drug resistance, while providing an opportunity for cancer therapies. The destabilization of the integrity of these organelles might indeed ignite a less common form of cell death, known as lysosomal membrane permeabilization (LMP). LMP occurs when lysosomal proteases leak into the cytosol and induce features of necrosis or apoptosis, depending on the degree of permeabilization (Aits & Jaattela, 2013). Recent reports also highlighted that lysosomal homeostasis is essential in cancer stem cell survival (Shingu *et al*, 2016; Mai *et al*, 2017; Le Joncour *et al*, 2019). Additionally, it has been shown that targeting the autophagic machinery is an effective treatment against apoptosis-resistant GBM (Shchors *et al*, 2015; Zielke *et al*, 2018). The autophagic flux inhibitor chloroquine can decrease cell viability and acts as an adjuvant for TMZ treatment in GBM. However, this treatment might cause neural degeneration at the high doses required for GBM treatment (Weyerhäuser *et al*, 2018). Therefore, it is preferable to find alternative drugs that elicit anti-tumor responses without harmful effects on healthy brain cells.

A growing body of literature supports the concept of non-oncogene addiction (NOA) in cancer. Although neither mutated nor involved in the initiation of tumorigenesis, NOA genes are essential for the propagation of the transformed phenotype (Luo *et al*, 2009). Because NOA gene products are pirated for the benefit of tumor cells' own survival, their targeting therefore constitutes an Achilles' heel. Among reported NOA genes and pathways (Staudt, 2010), the paracaspase mucosa-associated lymphoid tissue l (MALT1) might be of particular interest in GBM (please see Fig 1). This arginine-specific protease plays a key role in NF-κB signaling upon antigen receptor engagement in lymphocytes, via the assembly of the CARMA-BCL10-MALT1 (CBM) complex. In addition to this scaffold role in NF-κB activation, MALT1 regulates NF-κB activation, cell adhesion, mRNA stability, and mTOR signaling through its proteolytic activity (Rebeaud *et al*, 2008; Staal *et al*, 2011; Uehata *et al*, 2013; Hamilton *et al*, 2014; Jeltsch *et al*, 2014; Nakaya *et al*, 2014). MALT1 has been shown to be constitutively active in activated B-cell-like diffuse large B-cell lymphoma (ABC DLBCL), and its inhibition is lethal (Ngo *et al*, 2006; Hailfinger *et al*, 2009; Nagel *et al*, 2012). MALT1 was also recently reported to exert pro-metastatic effects in solid tumors (McAuley *et al*, 2019). However, the role of MALT1 in solid tumors has not been extensively investigated.

Here, we provide evidence of the role of MALT1 in disrupting GSC lysosomal homeostasis, which is associated with autophagic features. We found that targeting MALT1, notably through the phenothiazine family of drugs, including mepazine (MPZ), is lethal to GBM cells. We further established that MALT1 sequesters QKI and maintains low levels of lysosomes, while its inhibition unleashes QKI and hazardously increases endo-lysosomes, which subsequently impairs autophagic flux. This leads to cell death concomitant with mTOR inhibition and dispersion from lysosomes. Disrupting lysosomal homeostasis therefore represents an interesting therapeutic strategy against GSCs.

Results

MALT1 expression sustains glioblastoma cell growth

Glioblastoma stem-like cells (GSCs) are suspected to be able to survive outside the protective vascular niche, in non-favorable environments, under limited access to growth factors and nutrients (Calabrese *et al*, 2007; Shingu *et al*, 2016; Jin *et al*, 2017). While many signaling pathways can influence this process, the transcription factor NF-κB has been demonstrated to be instrumental in many cancers as it centralizes the paracrine action of cytokines, in addition to playing a major role in cell proliferation and survival of tumor cells and surrounding cells (Bargou *et al*, 1996; Davis *et al*, 2001; Karin & Greten, 2005; Li *et al*, 2009; McAuley *et al*, 2019). Because of this dual influence on both tumor cells and their microenvironment, we revisited The Cancer Genome Atlas (TCGA) for known mediators of the NF-κB pathway (Fig 1A). We found that *MALT1* expression was more significantly correlated with survival than other tested genes of the pathway (Fig 1B). This arginine-specific protease is crucial for antigen receptor-mediated NF-κB activation and B-cell lymphoma survival (Ngo *et al*, 2006). In addition, when GBM patients were grouped between low and high *MALT1* expression levels, there was a significant survival advantage for patients with lower *MALT1* expression (Fig 1C). Moreover, levels of *MALT1* mRNA are elevated in GBM (Grade IV) when compared with lower grade brain tumors (grades II and III) or non-tumor samples (Fig 1D and E).

Although this increased *MALT1* expression may be due to tumor-infiltrating immune cells, we first explored whether MALT1 was engaged in patient-derived GSCs, as these cells recapitulated *ex vivo* features of the tumor of origin (Lathia *et al*, 2015). The functional impact of MALT1 knockdown was thus evaluated by their viability and expansion *in vitro* (Fig 1F–J). Two individual short hairpin RNA sequences targeting MALT1 (sh*MALT1*) cloned in a lentiviral bi-cistronic GFP-expressing plasmid were delivered into GSC#1 (mesenchymal) and GSC#9 (classical) cells. We observed a reduced fraction of GFP-positive cells over time, while cells expressing non-silencing RNA plasmids (shc) maintained a steady proportion of GFP-positive cells, indicating that *MALT1* silencing was detrimental to GSCs (Fig 1F). Likewise, cells transfected with si*MALT1* had a lower percentage of EdU-positive cells as compared to non-silenced control cells (Fig 1G) and a higher incorporation of propidium iodide (PI) (Fig 1H). Additionally, GSCs either expressing sh*MALT1* or transfected with si*MALT1* had less stem traits, as evaluated by limited dilution assay and tumorsphere formation (Fig 1I and J). Taken together, these results indicate that MALT1 expression may be important for glioblastoma cell *ex vivo* expansion.

Pharmacological inhibition of MALT1 is lethal to glioblastoma cells

Next, to evaluate the potential of targeting MALT1 pharmacologically, we treated GSC #1 (mesenchymal), #4 (mesenchymal), #9 (classical), and #12 (neural) with the MALT1 allosteric inhibitor mepazine (MPZ) at a dose of 20 μM, as initially described (Nagel *et al*, 2012). All four GSCs showed a significant reduction in stemness by both limited dilution and tumorsphere assays (Fig 2A–C). Additionally, the competitive inhibitor Z-VRPR-FMK induced similar decrease in tumorsphere formation (Fig 2C). This was accompanied by a marked reduction in the abundance of SOX2 and NESTIN stemness markers (Fig 2D). Alongside the *in vitro* self-renewal impairment, GSC viability was largely annihilated by MPZ treatment, including reduction in EdU staining and increase in PI incorporation (Fig 2E–G). In contrast, MPZ had no significant effect on viability of

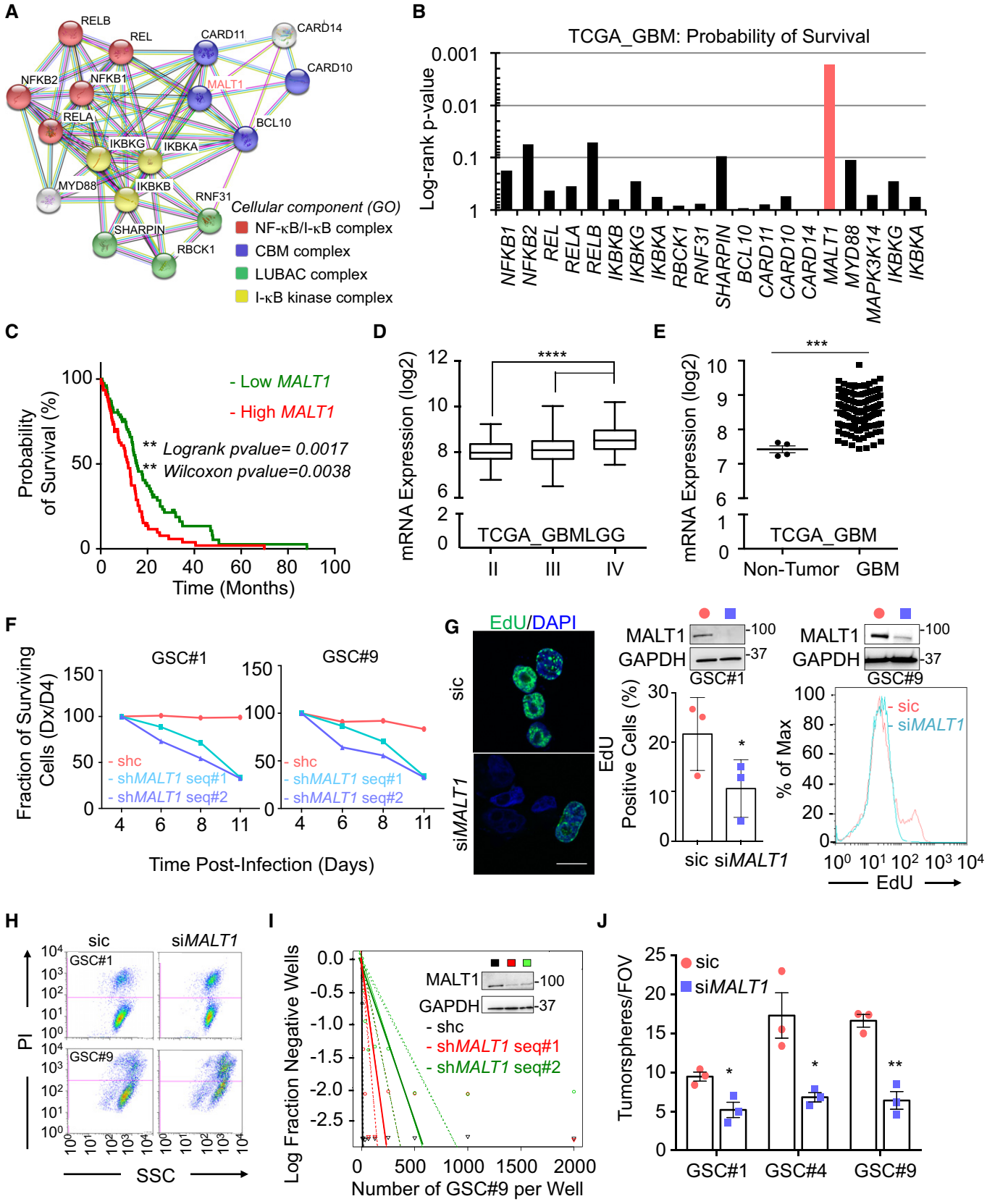

Figure 1.

Figure 1. MALT1 expression sustains glioblastoma cell growth.

A STRING diagram representation of the network of proteins involved in NF-κB pathway.

B The Cancer Genome Atlas (TCGA RNAseq dataset) was used on the GlioVis platform (Bowman *et al*, 2007) to analyze the probability of survival (log-rank *P*-value) of 155 GBM patients, for each gene encoding for the mediators of the NF-κB pathway.

C Kaplan–Meier curve of the probability of survival for 155 GBM patients with low or high *MALT1* RNA level, using median cutoff, based on the TCGA RNAseq dataset.

D, E Box and whisker plot of *MALT1* mRNA expression in low-grade glioma (LGG, grades II and III) or in GBM (grade IV) (TCGA GBMLGG, RNAseq dataset) (D). Horizontal line marks the median, box limits are the upper and lower quartiles, and error bars show the highest and lowest values. Alternatively, *MALT1* mRNA expression was plotted in non-tumor samples versus GBM samples (TCGA RNAseq dataset) (E). Each dot represents one clinical sample.

F Fraction of surviving cells over time in GSC#1 and GSC#9, transduced with control (shc) or bi-cistronic GFP plasmids using two different short hairpin RNA (sh*MALT1* sequences, seq #1 and #2). Data are plotted as the percentage of GFP-positive cells at the day of the analysis (Dx), normalized to the starting point (day 4 post-infection, D4).

G EdU incorporation (green, 2 h) was visualized by confocal imagery in GSC#1 or by FACS in GSC#9 transfected with sic or si*MALT1*. In GSC#1, the percentage of EdU-positive cells was quantified. Nuclei (DAPI) are shown in blue. $n > 240$ cells per replicate. Scale bar: 10 μm. Data are presented as the mean ± SEM on three independent experiments.

H FACS analysis of propidium iodide (PI) incorporation in GSC #1 and #9 transfected with non-silencing duplexes (sic) or *MALT1* siRNA duplexes (si*MALT1*) and analyzed 72 h later.

I Linear regression plot of *in vitro* limiting dilution assay (LDA) for control (shc) or sh*MALT1* seq#1 and seq#2 transduced GSC#9. Data are representative of $n = 2$. Knockdown efficiency was verified at day 3 by Western blot using anti-MALT1 antibodies. GAPDH served as a loading control.

J Tumorspheres per field of view (fov) were manually counted in sic or si*MALT1* transfected GSC#1, #4, and #9. Data are presented as the mean ± SEM on three independent experiments.

Data information: All data are representative of $n = 3$, unless specified. Statistics were performed using pairwise comparisons (Tukey's honest significant difference (HSD) with a 95% confidence interval for panels C–E), and a two-tailed *t*-test with a 95% confidence interval for panels (G and J), $*P < 0.05$, $**P < 0.01$, $***P < 0.001$, and $****P < 0.0001$.

Source data are available online for this figure.

brain-originated human cells (endothelial cells, astrocytes, and neurons), ruling out a non-selectively toxic effect (Fig 2E). Differentiated sister GSCs (DGCs) also showed reduced viability in response to MPZ, indicating that targeting MALT1 may have a pervasive effect on differentiated GBM tumor cells (Fig 2H).

MPZ is a drug, belonging to the phenothiazine family, and was formerly used in the treatment of schizophrenia (Lomas, 1957). Several anti-psychotic phenothiazines have been shown to potentially reduce glioma growth (Tan *et al*, 2018). We therefore evaluated whether clinically relevant phenothiazines could affect GSC viability (Fig EV1A–E). The effect on MALT1 inhibition was reflected in cell viability, with chlorpromazine (Oliva *et al*, 2017) and fluphenazine having robust effects on cell viability (Fig 2I). In addition to its effect on MALT1 protease activity (Fig EV1B and C) (Nagel *et al*, 2012; Schlauderer *et al*, 2013), MPZ may also exert off-target biological effects (Meloni *et al*, 2018). We took advantage of the well-characterized MPZ-resistant E397A MALT1 mutant (Schlauderer *et al*, 2013) to challenge the toxic action of phenothiazines in GSCs (Fig EV1F). E397A MALT1 expression in GSCs partially restored cell viability in phenothiazine-treated cells, suggesting that the main target of phenothiazine-mediated death involves MALT1 inhibition (Fig EV1F). Because MPZ has been shown to efficiently and safely obliterate MALT1 activity in experimental models (Nagel *et al*, 2012; McGuire *et al*, 2014; Kip *et al*, 2018; Di Pilato *et al*, 2019; Rosenbaum *et al*, 2019), ectopically implanted GSC#9 mice were challenged with MPZ. Daily MPZ administration reduced tumor volume in established xenografts, as well as NESTIN-positive staining (Fig 2J and K). This effect was prolonged for the week of measurement following treatment withdrawal (Fig 2J). Together, these data demonstrate that targeting MALT1 pharmacologically is toxic to GBM cells *in vitro* and *in vivo*.

GSCs maintain basal protease activity of MALT1

In addition to its scaffold function in the modulation of the NF-κB pathway, MALT1 also acts as a protease for a limited number of substrates (Juilland & Thome, 2018; Thys *et al*, 2018). No hallmarks of NF-κB activation such as phosphorylation and degradation of IκBα, or p65 and cREL nuclear translocation were observed, unless GSCs were treated with TNFα (Fig 3A and B). Nevertheless, the deubiquitinating enzyme CYLD (Staal *et al*, 2011) and the RNA-binding proteins ROQUIN 1 and 2 (Jeltsch *et al*, 2014), two known MALT1 substrates, were constitutively cleaved in GSCs (Fig 3C–F). This was, however, not the case of the MALT1 target HOIL1 (Douanne *et al*, 2016), suggesting that only a subset of MALT1 substrates is cleaved in GSCs (Fig 3C). Of note, CYLD proteolysis was not further increased upon stimulation with PMA plus ionomycin, in contrast to Jurkat lymphocytes, most likely due to a failure to co-opt this signaling route in GSCs (Fig 3C). However, CYLD processing was reduced in cells treated with MPZ or upon siRNA-mediated *MALT1* knockdown (Fig 3D and E). The same was true when MALT1 competitive inhibitor Z-VRPR-FMK was used (Fig 3F). Further supporting a role for MALT1 enzyme in GSCs, the expression of a protease-dead version of MALT1 (C464A) weakened CYLD trimming (Fig 3G and H). Interestingly, we found that refreshing medium also reduced CYLD cleavage, suggesting that MALT1 basal activity may rely on outside-in signals rather than cell autonomous misactivation (Fig 3I).

The activation of MALT1 habitually occurs within the microenvironment of the CBM complex (Thys *et al*, 2018). Accordingly, the knocking down of the CBM components *BCL10* or *CARD10* (i.e., CARMA3) also decreased CYLD processing (Fig 3J and K). In keeping with this, *BCL10*-silenced GSC#9 cells showed a reduction in cell viability (Fig 3K), therefore recapitulating the effect of knocking down MALT1. These data reinforce the hypothesis that a fraction of MALT1 is most likely active in growing GSCs, outside its canonical role in antigen receptor signaling and immune cancer cells.

MALT1 inhibition alters endo-lysosome homeostasis

To evaluate cell death modality triggered by MALT1 inhibition, transmission electron microscopy (TEM) was deployed to visualize

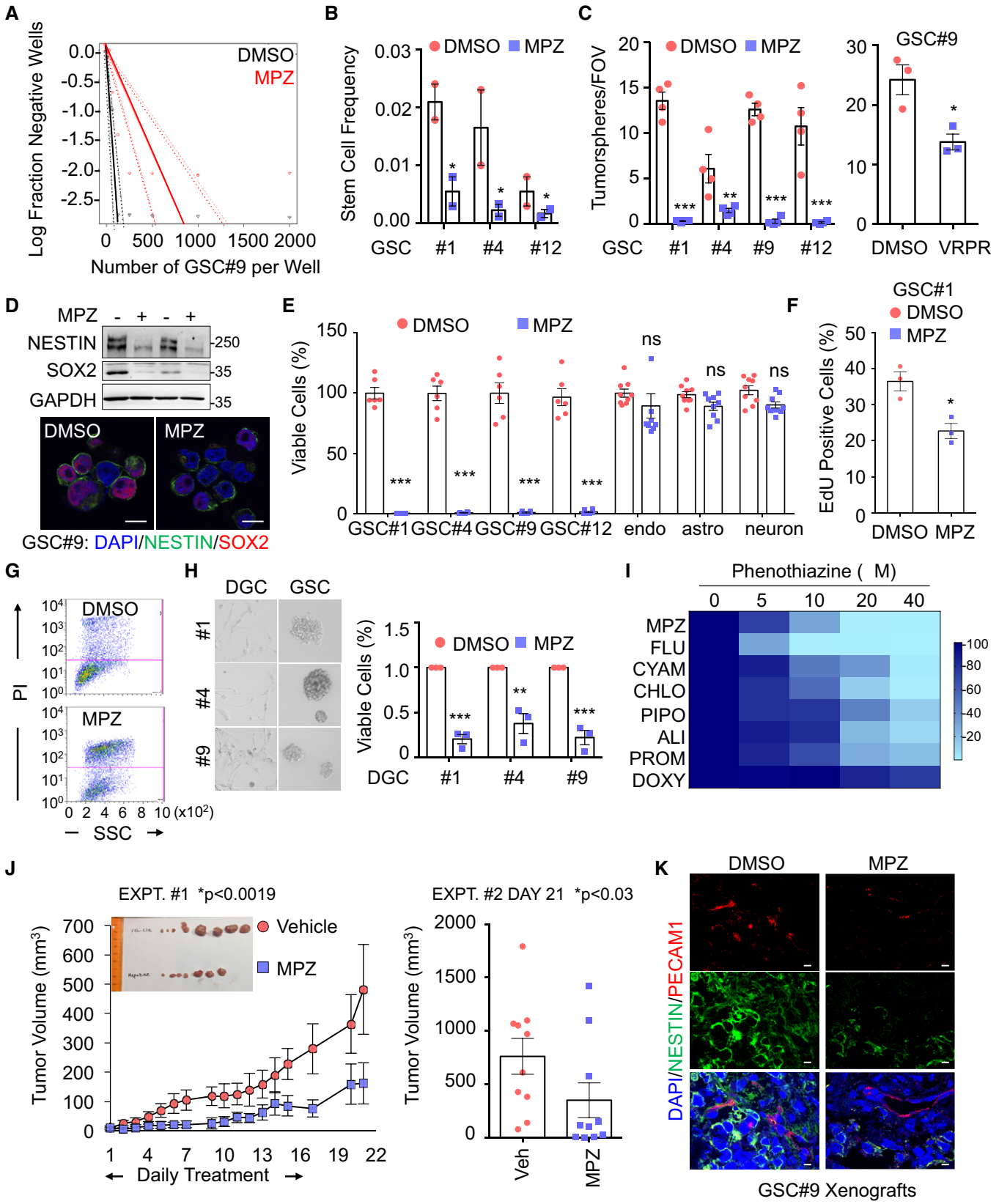

Figure 2.

Figure 2. MALT1 pharmacological inhibition is lethal to glioblastoma cells.

A Linear regression plot of *in vitro* limiting dilution assay (LDA) for GSC#9 treated with MALT1 inhibitor, mepazine (MPZ, 20 μM, 14 days). DMSO vehicle was used as a control. Data are representative of $n = 2$.

B Stem cell frequency was calculated from LDA in GSCs #1, #4, and #12 treated with MPZ treatment (20 μM, 14 days). Data are presented as the mean ± SEM on two independent experiments.

C Tumorspheres per field of view (fov) were manually counted in GSCs #1, #4, #9, and #12 in response to MPZ (20 μM) and vehicle (DMSO), and in GSC#9 treated with Z-VRPR-FMK (75 μM) and vehicle (H_2O) for 4 days. Data are presented as the mean ± SEM on 4 independent experiments for MPZ and three independent experiments for Z-VRPR-FMK.

D The expression of the stemness markers SOX2 and NESTIN was evaluated by Western blot and immunofluorescence (SOX2 in red NESTIN in green) in MPZ (+, 20 μM, 16 h) and vehicle (−, DMSO, 16 h) treated GSC#9. GAPDH served as a loading control. Scale bar: 10 μm.

E Cell viability was measured using Cell TiterGlo luminescent assay in GSCs #1, #4, #9, and #12, human brain endothelial cells (endo), human astrocytes (astro), and human neuron-like cells (neuron) treated for 48 h with DMSO or MPZ (20 μM). Data were normalized to their respective DMSO-treated controls and are presented as the mean ± SEM of three independent experiments in triplicate.

F FACS analysis of EdU staining was performed on GSC#1 treated overnight with MPZ (10 μM). Data are presented as the mean ± SEM on three independent experiments.

G FACS analysis of propidium iodide (PI) incorporation in GSC#9 treated for 48 h with vehicle (DMSO) or MPZ (20 μM).

H Cell viability was measured using Cell TiterGlo luminescent assay in differentiated GSC#1 #4, and #9 (DGCs) treated for 48 h with vehicle (DMSO) or MPZ (20 μM). Data were normalized to their respective DMSO-treated controls and are presented as the mean ± SEM of three independent experiments. Morphology of GSCs #1, #4, #9, and DGCs #1, #4, #9 was shown using brightfield images.

I Heatmap of cell viability of GSC#9 using increasing doses (0, 5, 10, 20, 40 μM) of phenothiazines: mepazine (MPZ), fluphenazine (FLU), cyamemazine (CYAM), chlorpromazine (CHLO), pipotiazine (PIPO), alimemazine (ALI), promethazine (PRO), and doxylamine (DOXY). Data were normalized to their respective DMSO-treated controls.

J Nude mice were implanted with GSC#9 (10^6 cells) in each flank, and randomized cages were treated with either vehicle (DMSO) or MPZ (8 mg/kg) daily i.p., for 14 consecutive days, once tumors were palpable. Tumor volume was measured from the start of treatment until 1 week after treatment was removed. Graph of tumor volume on day 21 post-treatment is presented. Data are presented as the mean ± SEM $n = 10$/group.

K Cryosections from GSC-xenografted tumors were stained for the endothelial marker PECAM1 (red) and tumor marker NESTIN (green). Nuclei (DAPI) are shown in blue. Scale bar: 20 μm.

Data information: All data are representative of $n = 3$, unless specified. Statistics were performed using a two-tailed *t*-test with a 95% confidence interval for panels (B, C, E, F, H), a two-way ANOVA with Bonferroni post-test at 95% confidence interval for panel (J), a Wilcoxon–Mann–Whitney test for Expt #2 with *P*-values stated for panel (J). $*P < 0.05$ $**P < 0.01$, $***P < 0.001$.

Source data are available online for this figure.

morphological changes upon MPZ treatment. TEM images showed increased vacuoles and lysosomes compared to control cells (Fig 4A). The augmentation was also visible in si*MALT1*-transfected cells (Fig EV2A). In fact, the abundance of the endo-lysosome protein LAMP2 was amplified upon MALT1 inhibition with MPZ, in a time-dependent manner (Figs 4B and EV2B). Additionally, treatment with the MALT1 competitive inhibitor Z-VRPR-FMK, other phenothiazines, or *MALT1* knockdown resulted in similar LAMP2 increase (Figs 4C–E and EV1D), therefore militating against putative drug-related action or deleterious accumulation in lysosomes. Moreover, the ectopic expression of a protease-dead MALT1 mutant (C464A) mimicked MPZ effect on lysosome staining, using the lysotracker probe (Fig 4D). In addition, CTSD and Rab7 endo-lysosomal protein levels were up-regulated as well upon MALT1 blockade (Figs 4C and EV2C). Conversely, other cellular organelles (early endosomes, mitochondria, Golgi, and peroxisomes) remained unchanged upon MPZ treatment (Fig EV2B and D). Furthermore, ectopic tumors, excised from mice challenged with a MPZ 2-week regime, showed a marked gain in LAMP2 staining intensity and protein amount, as compared to vehicle-treated tumors (Fig 4F). Finally, the treatment with MPZ of the ABC DLBCL lymphoma cell line HBL1, which displays constitutive MALT1 activity, also led to an increase in LAMP2 protein amount (Fig EV2E), indicating that MALT1's effect on lysosomal homeostasis might not be limited to GSCs.

The newly formed endo-lysosomes in GSCs appeared to be at least partially functional, as evidenced by pH-based Lysotracker staining, DQ-ovalbumin, and transferrin uptake (Figs 4G and EV2F). Of note, at a later time point (16 h) in MPZ-treated cells, DQ-ovalbumin staining was dimmer as compared to early time points (4 h), which might signify lysosomal membrane permeabilization (Fig EV2F). Our data demonstrated that MALT1 knockdown and pharmacological inhibition provoke a meaningful endo-lysosomal increase.

MALT1 inhibition induces autophagic features in GBM cells

Because autophagy is fueled by endo-lysosomal activity, the impact of MALT1 inhibition on autophagy in GSCs was explored and estimated by LC3B modifications. The turnover of LC3B and the degradation of the autophagy substrate P62 also reflect autophagic flux (Loos *et al*, 2014). Treatment with MPZ led to a significant increase in LC3B puncta at later time points (16 h), subsequent to lysosomal increase (4 h) (Fig 5A, left panel). Super-resolution microscopy using structured illumination microscopy (SIM) further revealed that these LC3 structures were covered with LAMP2-positive staining (Fig 5A, right panel). Upon MPZ treatment, there was also an accumulation of lipidated LC3B (LC3B-II) and P62 protein amount over time, suggesting impaired autophagic flux (Fig 5B). Likewise, there was an increase in lipidated LC3B protein amount in cells that received phenothiazines or were knocked down for MALT1 (Figs EV1D and 5C). Of note, chloroquine treatment did not further augment LC3 lipidation (Fig 5C and D). The effect of MPZ was concomitant with a reduced LC3B turnover, as evaluated via luciferase assay (Fig 5E), and P62 puncta accumulation in cells treated with MPZ and Z-VRPR-FMK, or knocked down for MALT1 (Fig 5F). Taken together, this suggests that MALT1 inhibition impairs autophagic flux in GSCs.

Lysosomes are the cornerstone of MPZ-induced cell death

To evaluate precisely the mechanism of cell death by MPZ, caspases were simultaneously blocked with Q-VD-OPh (QVD) (Fig 5G and H). However, this did not thwart MPZ-mediated cell death, suggesting another mechanism than apoptosis. Meanwhile, chloroquine treatment did not impact GSC#9 viability (Fig EV3A). Further, cells, in which autophagy was inhibited via knockdown of *BECN1* (*i.e.*,

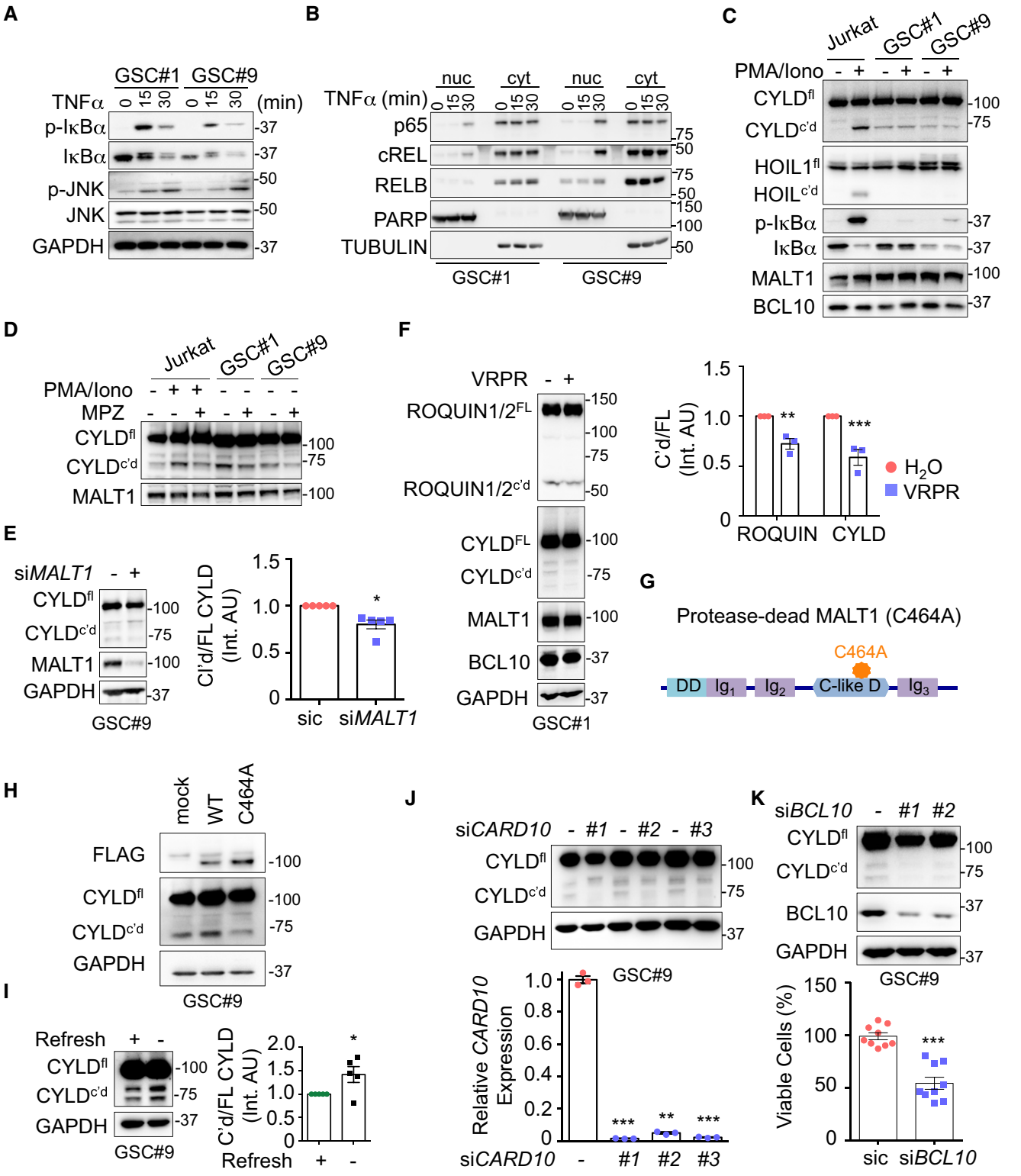

Figure 3.

Figure 3. MALT1 is active in GSCs.

A Total protein lysates from GSCs #1 and #9 challenged with TNFα (10 ng/ml, for the indicated times) were analyzed by Western blot for p-IκBα, IκBα, and p-JNK. Total JNK and GAPDH served as loading controls.

B Western blot analysis of p65, cREL, and RELB in cytosolic (cyt) and nuclear (nuc) cell fractionation from GSC#1 and GSC#9 stimulated with TNFα (10 ng/ml, for the indicated times). TUBULIN and PARP served as controls for each fraction.

C Jurkat T cells, GSC#1, and GSC#9 were stimulated with PMA (20 ng/ml) and ionomycin (Iono, 300 ng/ml) for 30 min. Total protein lysates were analyzed by Western blot for CYLD (full length, FL, and cleaved, c'd), HOIL1 (full length, FL, and cleaved, c'd), p-IκBα and IκBα. MALT1 and BCL10 served as loading controls.

D Jurkat T cells, GSC#1, and GSC#9 were treated with vehicle (DMSO) and mepazine (MPZ, 20 μM) for 4 h. PMA/ionomycin mixture was also administered to Jurkat cells for the last 30 min. Total protein lysates were analyzed by Western blot for CYLD (full length, FL, and cleaved, c'd). MALT1 served as a loading control.

E Western blot analysis of CYLD (full length, FL, and cleaved, c'd) and MALT1 in total protein lysates from GSC#9 transfected with non-silencing RNA duplexes (sic) or *MALT1* targeting duplexes (si*MALT1*). GAPDH served as a loading control. Densitometric analysis of c'd CYLD/FL CYLD was performed (right). Data are presented as the mean ± SEM on five independent experiments.

F (Left) Western blot analysis of CYLD, ROQUIN1/2, MALT1, and BCL10 in total protein lysates from GSC#9 treated for 4 h with vehicle (H_2O) or Z-VRPR-FMK (75 μM). GAPDH served as a loading control. (Right) Densitometric analysis of c'd/FL was performed for ROQUIN1/2 and CYLD. Data are presented as the mean ± SEM on three independent experiments.

G Schematic drawing of MALT1 structures highlighting the C464A substitution in the protease-dead version. DD: death domain, C-like D: caspase-like domain, Ig: immunoglobulin domain.

H Western blot analysis of CYLD and FLAG in total protein lysates from GSC#9 transfected with WT or C464A MALT1-FLAG. GAPDH served as a loading control.

I Western blot of CYLD (full length, FL, and cleaved, c'd) in total protein lysates from GSC#9 after refreshing the medium (+), as compared to 3-day-old culture (−). GAPDH served as a loading control. Densitometric analysis of c'd/FL CYLD was performed. Data are presented as the mean ± SEM on five independent experiments.

J Western blot analysis of CYLD (full length, FL, and cleaved, c'd) in total protein lysates from GSC#9 transfected with non-silencing RNA duplexes (sic) or *CARD10* targeting duplexes (si*CARD10 seq#1*, *seq#2*, and *seq#3*). GAPDH served as a loading control. qPCR analysis confirmed the knockdown of *CARD10* in GSC#9. Data are presented as the mean ± SEM on three independent experiments.

K Western blot analysis of CYLD and BCL10 in total protein lysates from GSC#9 transfected with non-silencing RNA duplexes (sic) or *BCL10* targeting duplexes (si*BCL10*, *seq#1*, and *seq#3*). GAPDH served as a loading control. Cell viability was measured using Cell TiterGlo luminescent assay in sic and seq#1 si*BCL10*-transfected cells. Data were normalized to their respective sic-treated controls and are presented as the mean ± SEM of three independent experiments, in triplicate.

Data information: All data are representative of $n = 3$, unless specified. Statistics were performed using a two-tailed *t*-test with a 95% confidence interval. $*P < 0.05$, $**P < 0.01$, $***P < 0.001$.

Source data are available online for this figure.

BECLIN1), were not protected either, suggesting that autophagy might be secondary to MPZ-induced cell death (Fig EV3B). Nonetheless, there was increased CTSD release by GSCs treated with MPZ or silenced for *MALT1*, which could signify either lysosomal membrane permeabilization or increased secretion of lysosomal enzymes (Fig 5I). Accordingly, treatment with lysosomal enzyme inhibitors partially rescued cells from MPZ-induced cell death (Fig 5J). Thus, lysosomes participate in MPZ-induced cell death, while MALT1 appears to be required to maintain innocuous level of endo-lysosomes in GSCs.

MALT1 modulates the lysosomal mTOR signaling pathway

In order to further characterize the mode of action of MALT1 inhibition in GSCs, we performed RNA-sequencing analysis on GSCs treated with MPZ for 4 h, prior to any functional sign of death. Our results identified 7474 differentially expressed genes, among which 9/10 randomly chosen top candidates were validated in both MPZ-treated and MALT1-silenced cells (Figs 6A and EV3C, Table EV1). No obvious endo-lysosomal protein encoding genes were found, which was further confirmed by qPCR (Fig 6A–E, Table EV1). Of note, VGF, recently shown to promote GSC/DGC survival, was down-regulated upon MPZ treatment (Wang *et al*, 2018a) (Figs 6E and EV3C, Table EV1). In line with a non-transcriptional regulation of lysosome biogenesis, knockdown of the master regulator of lysosomal transcription TFEB (Sardiello *et al*, 2009) failed to reduce autophagy signature and CTSD protein up-regulation upon MPZ treatment (Fig 6F). We thus hypothesized that the observed endo-lysosomal increase was due to modulation in their translation and/or RNA metabolism. When translation was blocked with cycloheximide, MPZ failed to increase endo-lysosomal protein amounts (Fig EV3D). Likewise, RNAseq analysis unveiled putative changes in translation (peptide chain elongation, ribosome, co-translational protein targeting, 3′-UTR mediated translational regulation), RNA biology (influenza viral RNA, nonsense mediated decay), metabolism (respiratory electron transport, ATP synthesis, oxidative phosphorylation, respiratory electron transport), and an mTOR signature (referred as Bilanges serum and rapamycin-sensitive genes) (Fig 6C and D). Because mTOR sustains GSC expansion and its activation is linked to lysosomal biogenesis (Yu *et al*, 2010; Galan-Moya *et al*, 2011; Settembre *et al*, 2012), we further explored this possibility. Notably, MALT1 activity has been shown to participate in mTOR activation upon antigen receptor engagement, although the mechanism of action remains poorly understood (Hamilton *et al*, 2014; Nakaya *et al*, 2014). In fact, MPZ and phenothiazine pharmacological challenge, as well as *MALT1* siRNA blunted mTOR activation in GSCs, as evaluated through the phosphorylation of AKT, p70S6K, and S6 ribosomal protein (Figs 6G–I and EV3E). MPZ treatment also reduced inhibitory phosphorylation of autophagy regulator ULK1 at serine 757 (Fig 6G), which may partially account for increased autophagic features upon MPZ treatment. In addition, the enforced expression of protease-dead MALT1 (C464A) reduced S6 phosphorylation levels, reiterating the importance of MALT1 catalytic activity in the observed phenotype (Fig 6J). Furthermore, as phosphorylation of 4EBP1 increases protein translation by releasing it from EIF4E (Gingras *et al*, 1998), and as it can be resistant to mTOR inhibition (Qin *et al*, 2016), we evaluated 4EBP1 phosphorylation levels over time in response to MPZ (Fig EV3F). Although reduced shortly upon MPZ addition, phosphorylation returned at later time points, which may allow for the observed translational effect despite mTOR inhibition. As mTOR signaling is intimately linked to lysosomes (Korolchuk *et al*,

2011), we explored the impact of MPZ treatment on mTOR positioning. Confocal microscopy analysis revealed that mTOR staining no longer colocalized with LAMP2-positive structures upon treatment with MPZ (Figs 6K and EV3G). Interestingly, TFEB silencing did not influence mTOR recruitment at endo-lysosomes (Fig EV3H). Conversely, mTOR staining appears dispersed from LAMP2 puncta upon Z-VRPR-FMK, phenothiazines treatment, or knockdown of MALT1 (Fig 6K). These results suggest that MALT1 affects lysosomal homeostasis post-transcriptionally, and that the increase in endo-lysosomes coincides with weakening of the mTOR signaling, which may be due to displacement of mTOR from its lysosomal signaling hub.

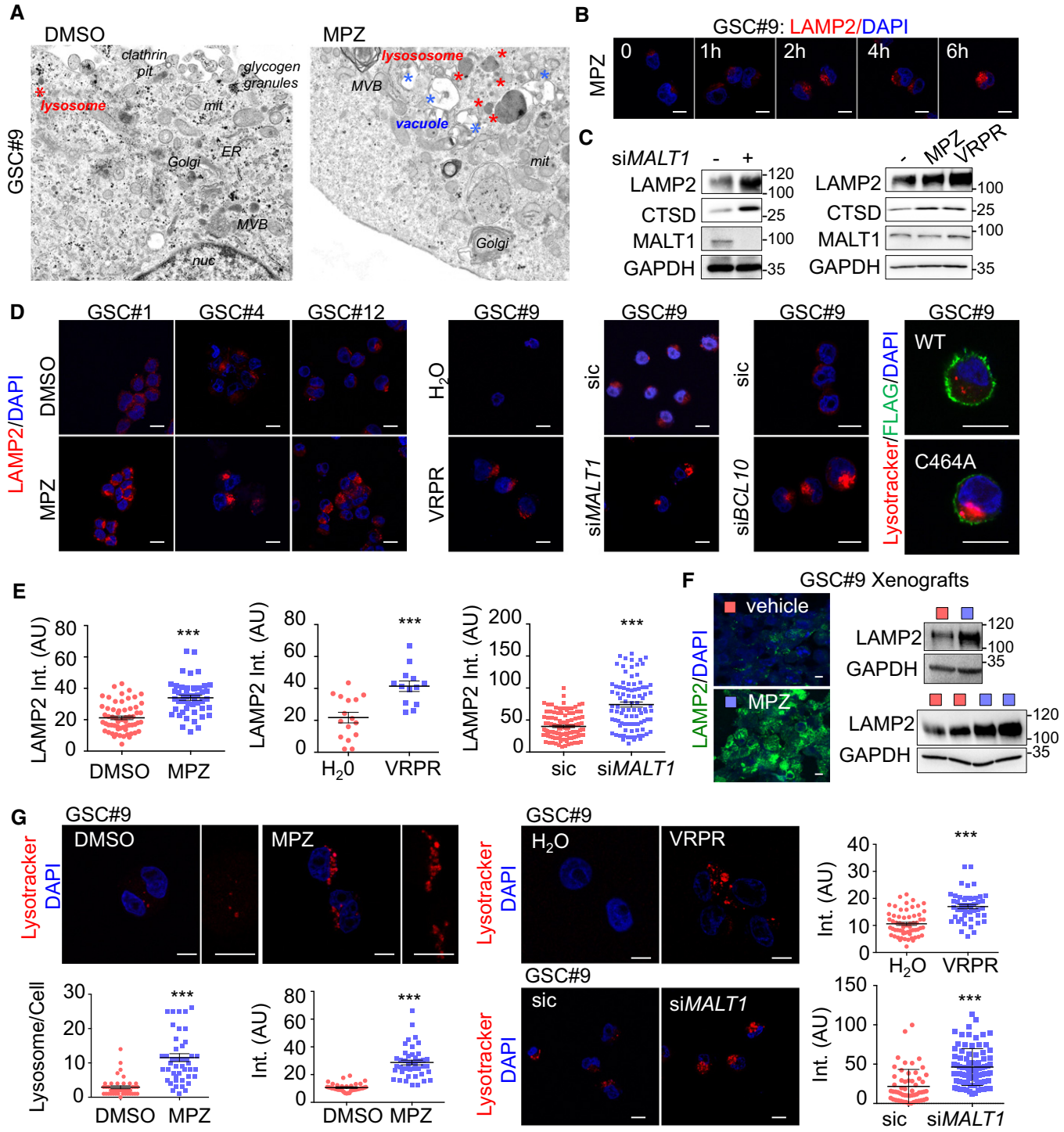

Figure 4.

Figure 4. MALT1 pharmacological inhibition alters endo-lysosome homeostasis.

A Transmission electron microscopy of GSC#9 treated with vehicle (DMSO) or MPZ (20 μM) for 16 h. ER: endoplasmic reticulum; MVB: multivesicular bodies; lys: lysosome; mit: mitochondria; nuc: nucleus. Red stars denote lysosomes; blue stars vacuoles.

B Confocal analysis of LAMP2 staining (red) at 0, 1, 2, 4, and 6 h post-MPZ (20 μM) treatment. Nuclei (DAPI) are shown in blue. Scale bar: 10 μm.

C Western blot analysis was performed in total protein lysates from GSC#9 transfected with non-silencing duplexes (sic) or *MALT1* targeting siRNA duplexes (si*MALT1*). Alternatively, Western blot analysis of LAMP2, CTSD, and MALT1 was done in total protein lysates from GSC#9 treated for 16 h with MPZ (20 μM) or Z-VRPR-FMK (75 μM). DMSO was used as vehicle. GAPDH served as a loading control.

D Confocal analysis of LAMP2 staining (red) in GSCs #1, #4, #12 treated for 16 h with vehicle (DMSO) or MPZ (20 μM). Alternatively, GSC#9 were either treated for 16 h with H_2O or Z-VRPR-FMK (75 μM). Additionally, cells were transfected with non-silencing duplexes (sic) or MALT1 and BCL10 targeting siRNA duplexes (si*MALT1* and si*BCL10*). Alternatively, lysotracker staining (red) was used to track for lysosomes in either GSC#9 expressing either wild-type (WT) or C464A FLAG-MALT1 (green). Scale bar: 10 μm.

E Quantification of LAMP2 staining pixel intensity on GSC#9 treated as described in panel (D). Data are presented as the mean ± SEM on three independent experiments. Each dot represents one cell. $n > 30$.

F Cryosections from GSC#9-xenografted tumors in vehicle and MPZ-challenged animals (as described in Fig 2J) and assessed for LAMP2 staining (green). Nuclei (DAPI) are shown in blue. Scale bar: 10 μm. Western blot analysis of LAMP2 was performed in tumor lysates. GAPDH served as a loading control.

G Confocal analysis of lysotracker staining (red) in GSC#9 treated for 16 h with vehicle (DMSO) or MPZ (20 μM). Alternatively, GSC#9 were either treated for 16 h with H_2O or Z-VRPR-FMK (75 μM) (upper panel) or transfected with sic and si*MALT1* (bottom panel). As indicated, number of lysotracker-positive puncta and lysotracker pixel intensity (arbitrary unit, AU) were quantified per cell. Data are presented as the mean ± SEM on three independent experiments. Each dot represents one cell. $n > 30$. Nuclei (DAPI) are shown in blue. Scale bars: 10 μm.

Data information: All data are representative of $n = 3$, unless specified. Statistics were performed using a two-tailed *t*-test with a 95% confidence interval. ***$P < 0.001$.

Source data are available online for this figure.

MALT1 is negatively linked to the endo-lysosomal regulator QKI

Shinghu *et al* recently demonstrated that the RNA-binding protein Quaking (QKI) regulates endo-lysosomal levels in GBM. They showed that GBM-initiating cells maintain low levels of endo-lysosomal trafficking in order to reduce receptor recycling (Shingu *et al*, 2016). QKI was suggested to regulate RNA homeostasis of endo-lysosome elements, independently of the TFEB-driven endo-lysosome biogenesis. TCGA analysis confirmed the prognosis value of QKI expression in GBM, as patients with higher expression of QKI had a slight survival advantage (Fig 7A). As our data suggest a counterbalancing role of MALT1 in lysosomal biogenesis, we revisited the TCGA and compared the expression of *MALT1* with that of *QKI* in GBM patients. Interestingly, there was a negative correlation between the levels of expression of the two genes (Fig 7A). In addition, *QKI* and *MALT1* were both linked to the expression of 7 common lysosomal lumen genes (Fig 7A). This prompted us to examine QKI pattern in GBM. First, QKI was indeed expressed in a panel of GSCs, as well as in ectopic xenografts (Fig EV4A). Similarly, human GBM samples from two patients showed pervasive QKI staining (Fig EV4B). As expected (Wu *et al*, 1999), QKI displayed cytosolic and nuclear forms, as evidenced by cellular fractionation and immunofluorescence (Fig EV4C and D). Given these findings, we decided to explore the possible link between MALT1 and QKI in GSCs. Co-immunoprecipitation experiments were thus deployed using QKI and the MALT1 binding partner BCL10 as baits. This showed that MALT1 was pulled down with QKI in GSC#1 and GSC#9, and *vice versa* (Fig 7B). Because MALT1 appeared excluded from nuclear fractions, the QKI/MALT1 interaction most likely occurs in the cytosol (Fig EV4C). Binding was, however, reduced in cells exposed to MPZ or Z-VRPR-FMK (Fig 7C). This suggests that active MALT1 tethered QKI in GSCs, while blocking MALT1 unleashed a fraction of QKI from the BCL10/MALT1 complex. Of note, QKI and MALT1 readily interacted in HBL1 ABC DLBCL lymphoma cells with constitutive MALT1 activation (Fig EV4E).

To next challenge the function of this putative neutralizing interaction of MALT1 and QKI, QKI expression was manipulated to alter QKI/MALT1 stoichiometry in GSCs. Strikingly, transient overexpression of QKI phenocopied the effect of MALT1 inhibition on endo-lysosomes. Reinforcing pioneer findings of QKI action on endo-lysosome components in transformed neural progenitors (Shingu *et al*, 2016), ectopically expressed QKI was sufficient to increase Lysotracker staining, LAMP2 protein amount and lipidated LC3B (Fig 7D–F). Accordingly, the augmented endo-lysosome staining synchronized with mTOR dispersion from a focalized organization, together with a decrease in the level of S6 phosphorylation (Fig 7G and H). Corroborating the surge of endo-lysosomes, the fraction of cells overexpressing QKI was drastically reduced over time, while the fraction of cells expressing an empty vector remained stable, suggesting that exacerbated QKI expression hampered cell viability (Fig 7I). Conversely, cells knocked down for *QKI* did not show the same MPZ-driven increase in LAMP2, CTSD, and lipidated LC3B (LC3B-II), suggesting that *QKI* knockdown can partially rescue cells from endo-lysosomal increase (Fig 7J and K). Reinforcing this idea, the dissipation of mTOR staining from endo-lysosomes and the reduction of S6 protein phosphorylation both provoked upon MPZ treatment were no longer observed without QKI (Fig 7K and L). Finally, double knockdown of QKI and MALT1 rescued cells from decreased proliferation and increased cell death triggered by MALT1 depletion (Figs 7M and N, and EV4F). Thus, *QKI* silencing rescued phenotype upon MALT1 inhibition or knockdown, further indicating that MALT1 is negatively linked to the endo-lysosomal regulator QKI.

Discussion

Here, we provide evidence that the activity of the paracaspase MALT1 is decisive for growth and survival of GBM cells. Our data indicate that MALT1 inhibition causes indiscipline of endo-lysosomal and autophagic proteins, which appears to occur in conjunction with a deficit in mTOR signaling. In addition to the known MALT1 inhibitor mepazine (Nagel *et al*, 2012), we show that several other clinically relevant phenothiazines can potently suppress MALT1 enzymatic activity and have similar effects to MPZ on endo-lysosomes and cell death in GSCs. Our data with MALT1

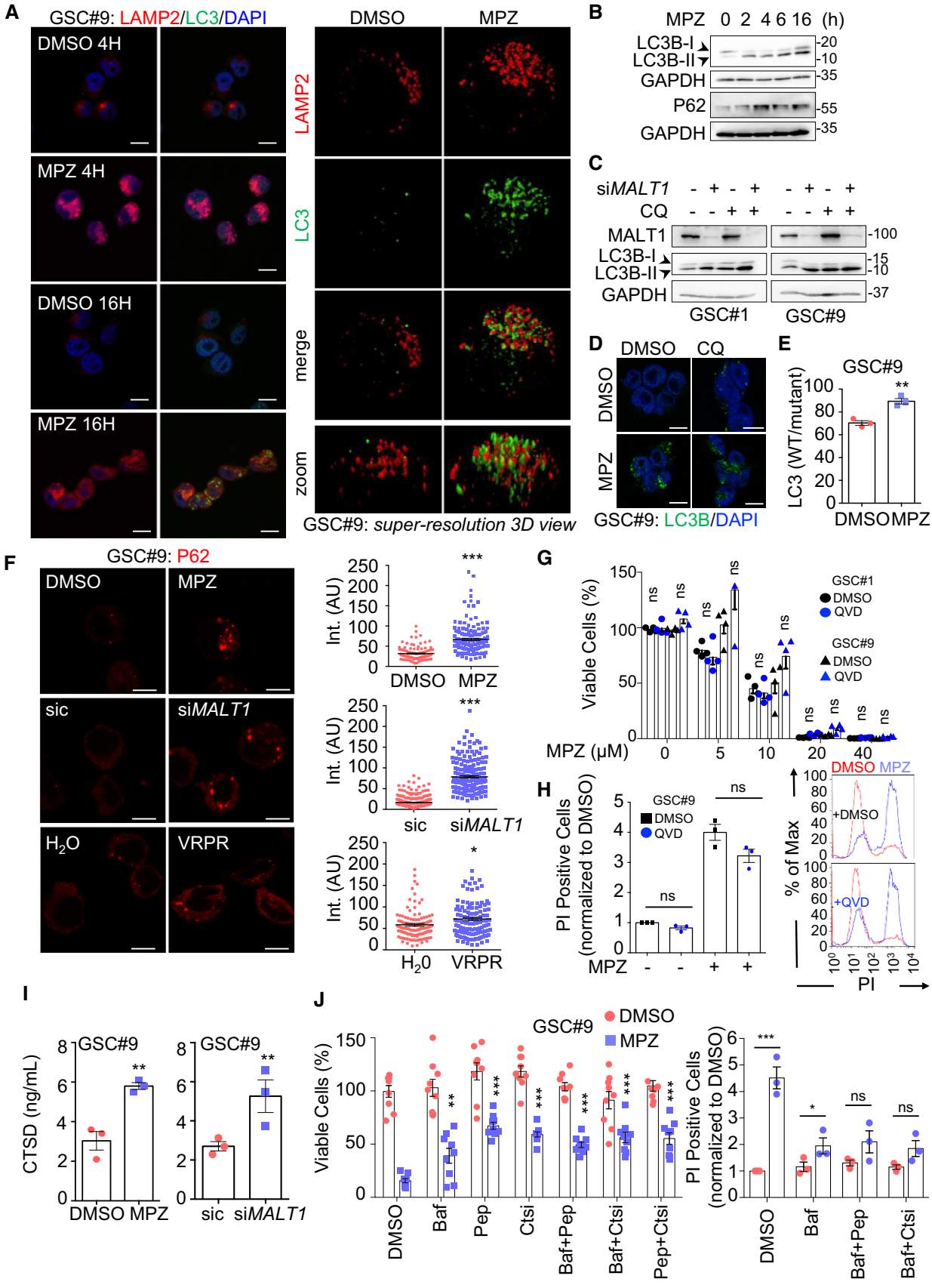

Figure 5.

Figure 5. MALT1 inhibition induces autophagic features in GSCs.

A (Left) Confocal analysis of LAMP2 (red) and LC3B (green) in GSC#9 treated for 4 and 16 h with vehicle (DMSO) and MPZ (20 μM). Nuclei (DAPI) are shown in blue. Scale bars: 10 μm. (Right) Super-resolution imaging (SIM, Structured Illumination Microscopy) of LAMP2 (red) and LC3B (green) staining in GSC#9 treated for 16 h with vehicle (DMSO) or MPZ (20 μM).

B Western blot analysis of LC3B and P62 in total protein lysates from GSC#9 at 0, 2, 4, 6, and 16 h post-MPZ treatment (20 μM). GAPDH served as a loading control.

C Western blot analysis of LC3B in total protein lysates from GSCs #1 and #9 at 72 h post-transfection with sic or si*MALT1* and subsequently treated 4 h with vehicle (DMSO) or chloroquine (CQ, 20 μM). Knockdown was verified by MALT1 blotting and GAPDH served as a loading control.

D Confocal analysis of LC3B (green) in GSC#9 treated for 16 h with vehicle (DMSO) and MPZ (20 μM) with or without chloroquine (CQ, 20 μM). Nuclei (DAPI) are shown in blue. Scale bars: 10 μm.

E GSC#9 were transfected with LC3B reporters (wild-type WT or G120A mutant, which cannot be lipidated), treated 24 h later with vehicle (DMSO) or MPZ (20 μM) for 6 more hours. Ratios of WT/mutant luciferase signals are presented as the mean ± SEM of three independent experiments.

F Confocal analysis of P62 staining (red) in GSC#9 treated for 16 h with vehicle (DMSO) or MPZ (20 μM). Alternatively, GSC#9 was either transfected with sic or si*MALT1* (middle) or treated for 16 h with H_2O or Z-VRPR-FMK (75 μM) (bottom). Quantification of P62 staining pixel intensity on GSC#9 treated for 16 h with vehicle (DMSO or H_2O), MPZ (20 μM) or Z-VRPR-FMK (75 μM) or sic and si*MALT1*. Data are presented as the mean ± SEM on three independent experiments. Each dot represents one cell. $n > 30$.

G Cell viability was measuring using Cell TiterGlo in GSCs #1 and #9 pre-treated for 1 h with vehicle (DMSO) or QVD (20 μM) and treated for 72 h more with the indicated doses of MPZ. Data were normalized to the vehicle-treated controls and are presented as the mean ± SEM of 4 independent experiments.

H FACS analysis of propidium iodide (PI) incorporation in GSC#9 treated for 48 h with vehicle (DMSO) or MPZ (15 μM) in combination with QVD (20 μM). (Left) Percentage of PI-positive cells, normalized to vehicle-treated controls are presented as the mean ± SEM on three independent experiments. (Right) Histogram plots for representative experiment (DMSO in red and MPZ in blue).

I CTSD ELISA was performed on culture media from GSC#9 treated for 8 h with vehicle (DMSO) or MPZ (20 μM). Alternatively, cells were transfected with sic or si*MALT1* and analyzed 72 h later. Data are presented as the mean ± SEM of three independent experiments.

J (Left) Cell viability was measured using Cell TiterGlo luminescent assay in GSC#9 treated for 48 h with vehicle (DMSO) or MPZ (10 μM), following a 30-min pre-treatment with the following drugs: Bafilomycin A1 (Baf, 100 nM), pepstatin A (Pep, 1 μg/ml), or CTS inhibitor 1 (Ctsi, 1 μM). Data were normalized to the vehicle-treated controls and are presented as the mean ± SEM of three independent experiments in triplicate, stars refer to comparison to vehicle + MPZ group (blue squares). (Right) FACS analysis of propidium iodide (PI) incorporation in GSC#9 treated for 48 h with vehicle (DMSO) or MPZ (15 μM) in combination with Baf, Pep, and Ctsi. Percentage of PI-positive cells normalized to vehicle-treated controls are presented as the mean ± SEM on three independent experiments.

Data Information: All data are representative of $n = 3$, unless specified. Statistics were performed using a two-tailed *t*-test with a 95% confidence interval for all experiments with *P*-values stated, except panel (G, H, J), which used a two-way ANOVA with Bonferroni post-test at 95% confidence interval. $*P < 0.05$, $**P < 0.01$, $***P < 0.001$.

Source data are available online for this figure.

and BCL10 silencing, as well as the expression of catalytically dead MALT1, clearly support a role for MALT1 in maintaining the endo-lysosomal homeostasis in GSCs. Although pharmacological inhibitors largely recapitulated the phenotype obtained with molecular interference, nonselective action of drugs remains of concern when it comes to clinics. Indeed, because some of the less potent MALT1 inhibitors, such as promethazine (Nagel *et al*, 2012; Schlauderer *et al*, 2013), also provoke changes LAMP2 and LC3B-II increase, we cannot exclude that some of the lysosomal effects of phenothiazine derivatives result from potential off-target accumulation in the lysosome. Likewise, it has been shown that Z-VRPR-FMK can efficiently inhibit cathepsin B (Eitelhuber *et al*, 2015). Nevertheless, since these drugs efficiently cross the blood–brain barrier in humans (Korth *et al*, 2001) and since they are currently used in the clinic, they represent an exciting opportunity for drug repurposing.

The disruption of endo-lysosomal homeostasis appears to be the main cause of death upon MALT1 inhibition in GSCs. This is aligned with recent findings that define lysosomes as an Achilles' heel of GBM cells (Shingu *et al*, 2016; Le Joncour *et al*, 2019). As CTSD release is accelerated upon MALT1 blockade, and as inhibitors of lysosomal cathepsins (cathepsin inhibitor 1 and pepstatin A), but not pan-caspase blockade (QVD), can partially rescue cell viability, we hypothesize that cells may be dying from a form of caspase-independent lysosomal cell death (LCD) (Aits & Jaattela, 2013). During this form of death, which may also be initiated by cathepsins, lysosomal membrane permeabilization (LMP) allows cathepsins to act as downstream mediators of cell death upon leakage into the cytosol (Aits & Jaattela, 2013). Additional studies will determine how exactly MALT1 inhibition drives lysosomal death in GSCs. Nevertheless, we found that inhibition of cathepsins provides only partial protection to cells treated with MPZ (Fig 4K). Autophagic features may also play a part in cell death. Induction of autophagy likely occurs due to reduced inhibition of ULK1 (Fig 6G) as a consequence of mTOR dispersion from endo-lysosomes (Yu *et al*, 2010; Settembre *et al*, 2012) (Fig 6K). Whether inducing or blocking autophagy is preferable therapeutic strategy in treating GBM remains up for debate, with some groups reporting beneficial effects of blocking autophagy, and others preferring its activation as a therapeutic strategy (Shchors *et al*, 2015; Rahim *et al*, 2017). Here, we show that the observed increased autophagic features are associated with reduced autophagic flux. Impairment in autophagic flux reduces a cell's ability for bulk degradation (Loos *et al*, 2014). Others have shown that lysosomal dysfunction, such as LMP, can impede upon autophagic flux and eventually lead to cell death (Elrick & Lieberman, 2013; Wang *et al*, 2018b). Because of this, we infer that reduced autophagic flux is a downstream consequence of LMP and ultimately contributes to LCD in our cells.

MALT1 has previously been linked to mTOR activity (Hamilton *et al*, 2014; Nakaya *et al*, 2014). For instance, MALT1 was reported to be necessary for glutamine uptake and mTOR activation after T-cell receptor engagement (Nakaya *et al*, 2014). Subsequently, the inhibition of MALT1 with Z-VRPR-FMK causes a reduction in the phosphorylation of S6 and p70S6K (Hamilton *et al*, 2014). Our data now extend these findings to GSCs, although the exact mechanism by which mTORC1 inhibition occurs remains to be explored in both cellular backgrounds. Immunofluorescence analysis of mTOR positioning after MPZ treatment suggests that inhibition of mTOR is linked to its dispersion from the endo-lysosomes, concurrent with

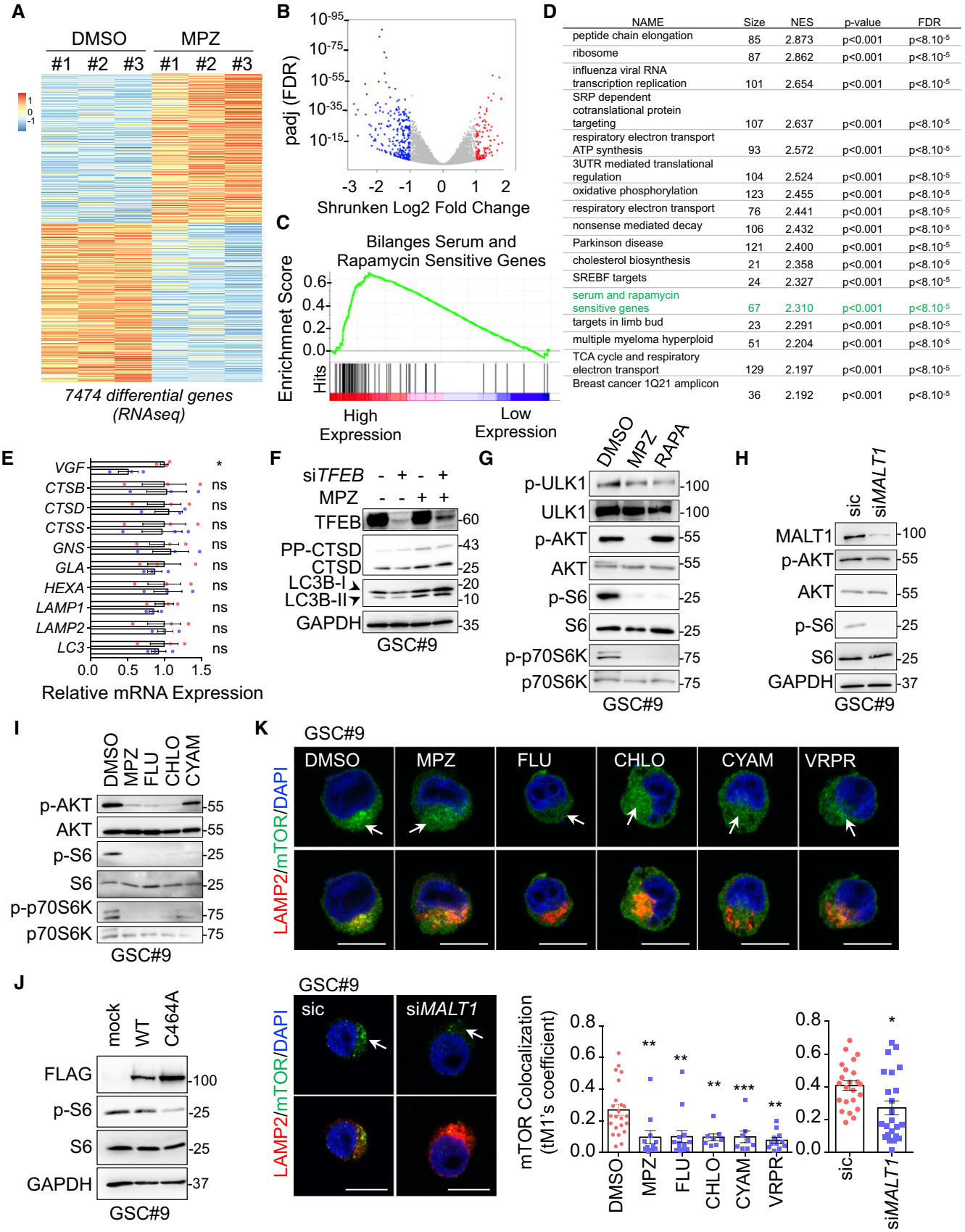

Figure 6.

Figure 6. MALT1 modulates the lysosomal mTOR signaling pathway.

A Heatmap of differentially expressed genes obtained from RNAseq analysis of GSC#9 treated for 4 h with vehicle (DMSO) or MPZ (20 μM), from three biological replicates.

B Volcano plot of differentially expressed genes in RNAseq analysis of GSC#9, expressed as fold changes between vehicle (DMSO) and MPZ-treated cells.

C GSEA (gene set enrichment analysis) plot showing enrichment of "Bilanges serum and rapamycin sensitive genes" signature in vehicle (DMSO) versus MPZ-treated triplicates.

D Table of top differential pathways in DMSO versus MPZ-treated triplicates. Size of each pathway, normalized enrichment scores (NES), *P*-value, and false discovery rate q value (FDR) were indicated.

E qRT–PCR was performed on total RNA from GSC#9 treated for 4 h with vehicle (DMSO) or MPZ (20 μM). Histograms showed changes in RNA expression of indicated targets. Data were normalized to two housekeeping genes (*ACTB*, *HPRT1*) and are presented as the mean ± SEM of technical triplicates.

F Western blot analysis of LC3B, CTSD, and TFEB in total protein lysates from GSC#9 transfected with non-silencing duplexes (sic) or siRNA duplexes targeting *TFEB* (si*TFEB*) and treated with vehicle (DMSO) or MPZ (20 μM) for 16 h. GAPDH served as a loading control.

G Western blot analysis of p-ULK1, p-AKT, p-S6, and p-p70S6K in GSC#9 treated for 1 h with MPZ (20 μM) or rapamycin (RAPA, 50 nM). Total ULK, AKT, S6, and p70S6K served as loading controls. DMSO was used as a vehicle.

H Western blot analysis of MALT1, p-AKT, and p-S6 in total protein lysates from GSC#9 transfected with non-silencing duplexes (sic) or *MALT1* targeting siRNA duplexes (si*MALT1*). Total AKT and S6, as well as GAPDH served as loading controls.

I Western blot analysis of p-AKT, p-S6, and p-p70S6K in total protein lysates from GSC#9 treated for 1 h with vehicle (DMSO) or 20 μM of phenothiazine compounds (MPZ, FLU, CHLO, and CYAM). Total AKT, total S6, and total p70S6K served as loading controls.

J Western blot analysis of p-S6 and FLAG in GSC#9 expressing WT or C464A MALT-FLAG. Total S6 and GAPDH served as loading controls.

K Confocal analysis of LAMP2 (red) and mTOR (green) staining in GSC#9 treated with vehicle (DMSO) or MPZ (20 μM), Z-VRPR-FMK (75 μM), FLU (20 μM), CHLO (20 μM), and CYAM (20 μM). Alternatively, cells were transfected with sic or si*MALT1*. Nuclei (DAPI) are shown in blue. Arrows point to LAMP2-positive area. Scale bars: 10 μm. Quantification of mTOR colocalization score with LAMP2 is shown. The Coloc2 plug-in from ImageJ was used to measure Mander's tM1 correlation factor in LAMP2-positive ROI, using Costes threshold regression. Data are presented as the mean ± SEM on three independent experiments. Each dot represents one cell. $n > 10$.

Data information: All data are representative of $n = 3$, unless specified. Statistics were performed using a two-tailed *t*-test with a 95% confidence interval for all experiments with *P*-values stated. $*P < 0.05$, $**P < 0.01$, $***P < 0.001$.

Source data are available online for this figure.

Figure 7. MALT1 is negatively linked to the endo-lysosomal regulator QKI.

A (Left) Kaplan–Meier curve of the probability of survival for 155 GBM patients with low or high *QKI* RNA level, using median cutoff, based on the TCGA RNAseq dataset. (Right) Differential expression analysis related to either *MALT1* or *QKI* expression highlighted a lysosomal lumen GO function. Venn diagram of overlapping lysosomal enriched protein encoding genes from this comparison showed 7 shared genes, together with 9 and 10 specific genes for *MALT1* and *QKI* expression, respectively. (Bottom) Correlation between *MALT1* and *QKI* expression was analyzed using The Cancer Genome Atlas (TCGA, HG-U133A dataset) on the GlioVis platform (Bowman *et al*, 2007). Pearson correlation factor = −0.21, *P*-value = 0.03.

B GSCs #1 and #9 protein lysates (input) were processed for immunoprecipitation (IP) using control immunoglobulins (Ig), anti-QKI, or anti-BCL10 antibodies. Input and IP fractions were separated on SDS–PAGE and Western blots for MALT1, QKI, and BCL10 antibodies were performed as specified.

C Total protein lysates (input) from GSC#9 treated with vehicle (-, DMSO) or MPZ (+, 20 μM, 1 h) or with vehicle (-, H_2O) or Z-VRPR-FMK (+, 75 μM, 4 h), were processed for control immunoglobulins (Ig) or anti-QKI antibodies immunoprecipitation (IP). Western blots were performed with indicated antibodies. Western blots were performed with indicated antibodies.

D Confocal analysis of Lysotracker (green) or FLAG (red) in GSC#9 overexpressing either empty vector (mock) or FLAG-QKI. Scale bars: 10 μm. Nuclei (DAPI) are shown in blue.

E Confocal analysis of LAMP2 (green) or FLAG (red) in GSC#9 transfected with either empty vector (mock) or FLAG-QKI. Scale bars: 10 μm. Nuclei (DAPI) are shown in blue. Quantification of LAMP2 staining pixel intensity on GSC#9 transfected with mock and FLAG-QKI. Data are presented as the mean ± SEM on three independent experiments. Each dot represents one cell. $n > 15$.

F Western blot analysis of QKI, LAMP2, and LC3B in GSC#9 overexpressing either empty vector (mock) or FLAG-QKI. GAPDH served as a loading control.

G Confocal analysis of mTOR (green) or FLAG (red) in GSC#9 transfected with either empty vector (mock) or Flag-QKI. Nuclei (DAPI) are shown in blue. Scale bars: 10 μm.

H GSC#1 were transfected with either empty vector (mock) or FLAG-QKI. Total protein lysates were processed for Western blots against p-S6 and FLAG. Total S6 served as a loading control.

I Fraction of surviving cells over time in GSCs #1 and #9, transduced with empty vector (mock) or FLAG-QKI bi-cistronic GFP plasmids. Data are plotted as the percentage of GFP-positive cells at the day of the analysis (Dx), normalized to the starting point (Day 4 post-infection, D4). Data are representative of $n = 3$.

J GSC#9 transfected with non-silencing RNA duplexes (sic) or *QKI* targeting siRNA duplexes (si*QKI*) were treated for 16 h with vehicle (DMSO) or MPZ (10 μM). Total protein lysates were processed for Western blots against LAMP2, CTSD, QKI, and LC3B expression, as indicated. GAPDH served as a loading control.

K Confocal analysis of mTOR (green) and LAMP2 (red) in GSC#9 transfected with sic or si*QKI* and treated for 16 h with vehicle (DMSO) or MPZ (20 μM). Nuclei (DAPI) are shown in blue. Scale bars: 10 μm. Quantification of mTOR colocalization score with LAMP2 is shown. The Coloc2 plug-in from ImageJ was used to measure Mander's tM1 correlation factor in LAMP2-positive ROI, using Costes threshold regression. Data are presented as the mean ± SEM on three independent experiments. Each dot represents one cell. $n > 10$.

L GSC#9 transfected with non-silencing RNA duplexes (sic) or *QKI* targeting siRNA duplexes (si*QKI*) were treated for 1 h with vehicle (DMSO) or MPZ (20 μM). Total protein lysates were processed for Western blots against QKI and p-S6. TUBULIN and total S6 served as loading controls.

M FACS analysis of EdU staining was performed on GSC#9 cells transfected with non-silencing RNA duplexes (sic, pink), *QKI* targeting siRNA duplexes (si*QKI*, light purple), *MALT1* targeting siRNA duplexes (si*MALT1*, blue), or double-transfected with si*QKI* and si*MALT1* (purple).

N FACS analysis of propidium iodide (PI) incorporation in GSC#9 transfected with non-silencing RNA duplexes (sic), *QKI* targeting siRNA duplexes (si*QKI*), *MALT1* targeting siRNA duplexes (si*MALT1*) or double-transfected with si*QKI* and si*MALT1* and analyzed 72 h later. Percentage of PI-positive cells normalized to vehicle-treated controls are presented as the mean ± SEM on three independent experiments.

Data information: All data are representative of $n = 3$, unless specified. Statistics were performed using a two-tailed *t*-test with a 95% confidence interval for all experiments with *P*-values stated. $*P < 0.05$.

Source data are available online for this figure.

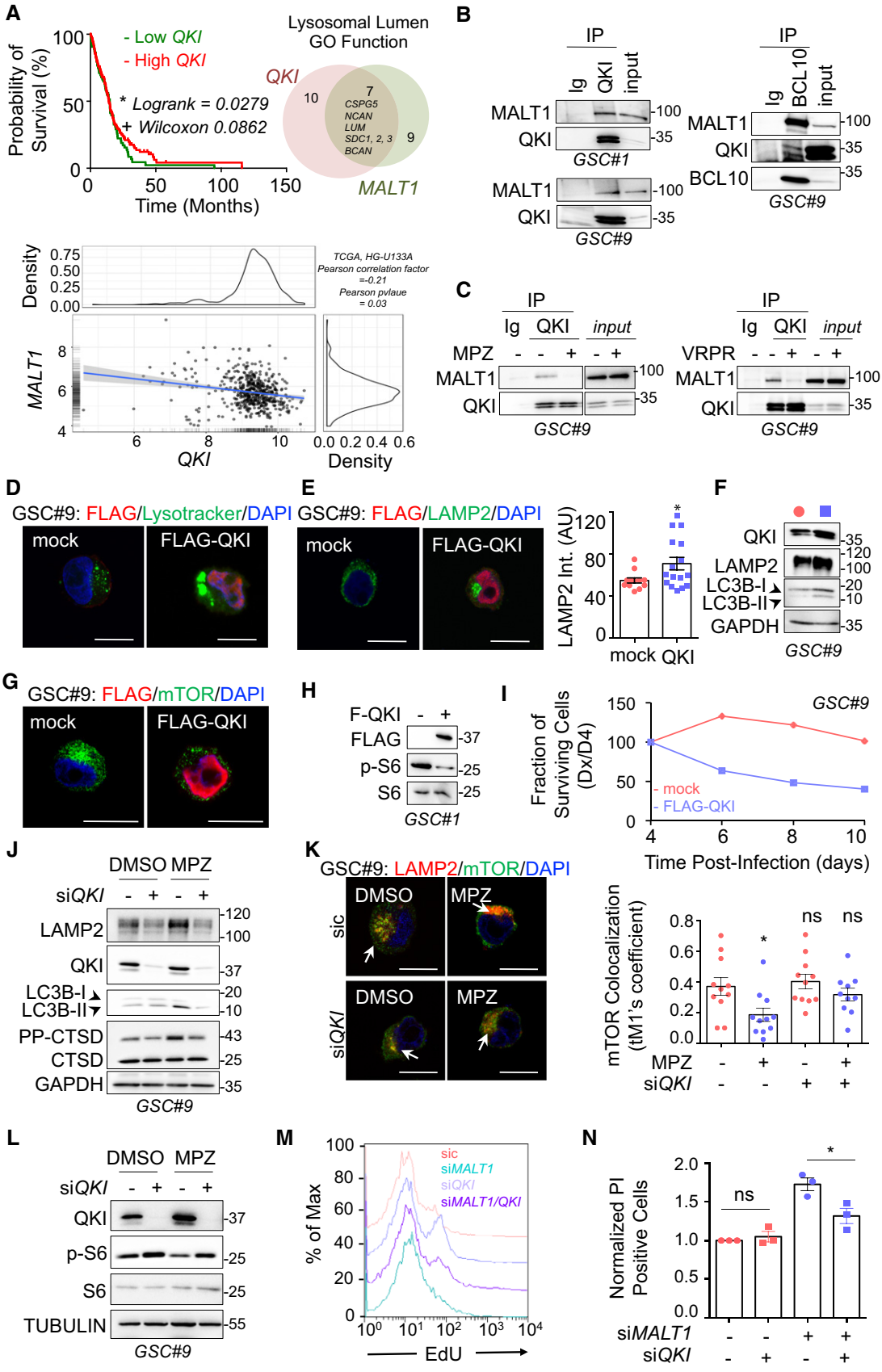

Figure 7.

lysosomal increase. In addition to a reduction in mTORC1 signaling, AKT phosphorylation was also impaired upon MALT1 inhibition in GSCs. It is thus possible that perturbed lysosome positioning might also influence specific pools of mTORC2 and AKT, as recently demonstrated (Jia & Bonifacino, 2019). Accordingly, AKT activity modulated the lysosomal membrane dynamics during autophagy (Arias *et al*, 2015). We and others speculate that there may exist unidentified substrates of MALT1, which link its protease activity directly to mTOR activation (Juilland & Thome, 2018; Thys *et al*, 2018). This may also rationalize the need for constitutive MALT1 activity in GSCs, as mTOR is constantly functioning in these cells (Galan-Moya *et al*, 2011). Moreover, it was suggested that down-regulation of lysosomes reduces recycling of receptors, including EGFR, which allows signaling to continue even in unfavorable niche where GSCs often reside and/or travel (Shingu *et al*, 2016). Less turnover of EGFR may also explain increased mTOR activation despite lysosomal down-regulation (Li *et al*, 2016). In addition, AKT can be central to balance between proliferation and apoptosis, by integrating multiple signaling networks besides mTOR in GBM. One hypothesis is that mTOR inhibition and/or dissociation from endo-lysosomes originate from lack of processing of unknown MALT1 substrates and is then exacerbated once homeostasis is disrupted.

How is QKI involved? Based on our data, we hypothesize that MALT1 sequesters QKI to prevent it from carrying out its RNA-binding function. Interestingly, MALT1 is already known to regulate other RNA-binding proteins Regnase-1/ZC3H12A, Roquin-1/RC3H1, and Roquin-2/RC3H2 (Uehata *et al*, 2013; Jeltsch *et al*, 2014). We propose that upon MALT1 inhibition QKI is released and free to bind its RNA-binding partners. QKI has already been shown to bind directly to lysosomal RNAs in progenitor cells (Shingu *et al*, 2016). It is thus tempting to speculate that QKI-dependent stabilization of lysosomal RNAs would preference the system toward more translation of these genes upon MALT1 inhibition, leading in turn to dysregulated endo-lysosomal protein expression and LMP. Indeed, our RNA-sequencing data suggest changes in translation and RNA biology upon MPZ treatment; however, further study is needed to validate whether there is increased QKI binding to lysosomal RNAs upon MALT1 inhibition. Notably, QKI-dependent lysosomal increase appears to be a post-transcriptional effect, independent of TFEB. As such, we propose a method of dual lysosomal control in GSCs whereby transcriptional biogenesis is tightly checked by known mTOR/TFEB pathway, and MALT1 acts on post-transcriptional regulation by isolating QKI from RNAs.

These findings place MALT1 as a new druggable target operating in non-immune cancer cells and involved in endo-lysosome homeostasis. Lysosomal homeostasis appears vital for glioblastoma cell survival and thus presents an intriguing axis for new therapeutic strategies in GBM.

Materials and Methods

Ethics statement

Informed consent was obtained from all patients prior to sample collection for diagnostic purposes. This study was reviewed and approved by the institutional review boards of Sainte Anne Hospital, Paris, France, and Laennec Hospital, Nantes, France, and performed in accordance with the Helsinki Protocol. Animal procedures were conducted as outlined by the European Convention for the Protection of Vertebrate Animals used for Experimental and other Scientific Purposes (ETS 123) and approved by the French Government (APAFIS#2016-2015092917067009).

The Cancer Genome Atlas (TCGA) analysis

The Cancer Genome Atlas (TCGA) was explored via the Gliovis platform (http://gliovis.bioinfo.cnio.es/) (Bowman *et al*, 2007). RNAseq databases (155 patients) were used to interrogate data related to *MALT1* and *QKI* expression (levels of RNA, probability of survival, correlation with *QKI* expression). Optimal cutoffs were set. All subtypes were included and histology was the only selective criteria.

Cell culture, siRNA and DNA transfection, and lentiviral transduction

GBM patient-derived cells with stem-like properties (GSCs) were isolated as previously described (Treps *et al*, 2016; Harford-Wright *et al*, 2017). GSC#1 (mesenchymal, 68-year-old male), GSC#4 (mesenchymal, 76-year-old female), GSC#9 (classical, 68-year-old female), and GSC#12 (neural, 59-year-old male) were cultured as spheroids in NS34 medium (DMEM-F12, with N2, G5, and B27 supplements, glutamax, and antibiotics). In order to induce differentiation, GSCs were grown in DMEM with 10% fetal bovine serum (FBS), glutamax, and antibiotics, for at least 2 weeks. Differentiation of sister cells (DGC) was monitored through their morphology and NESTIN and/or SOX2 loss of expression. Human brain microvascular endothelial cells (hCMEC/D3, a gift from PO Couraud, Institut Cochin, Paris, France) and HEK-293T cells (ATCC) were cultured as previously described (Treps *et al*, 2016). Human fetal astrocytes SVG-p12 (ATCC) and human neuronal-like cells SK-N-SH (ATCC) were cultured in MEM with 10% fetal bovine serum (FBS), and antibiotics.

Stealth non-silencing control duplexes (low-GC 12935200, Life Technologies), and small interfering RNA duplexes (Stealth RNAi, Life Technologies) were transfected using RNAiMAX lipofectamine (Life Technologies). The following duplexes targeting the respective human genes were as follows: CAGCAUUCUGGAUUGGCAAAUGG AA (*MALT1*), CCTTGAGTATCCTATTGAACCTAGT (*QKI*), UCAGAU GAGAGUAAUUUCUCUGAAA and GGGCUCCUCCUUUGCCACCAGA UCU (*BCL10*), CCCUUUGCGUGAAAGCCCAAGAGAU, ACAUCAC AGGGAGUGUGACACUUAA, and GACAAGGGACCAGAUGGACUG UCGU (*CARD10*), AGACGAAGGUUCAACAUCA (*TFEB*), CCACTCT GTGAGGAATGCACAGATA (*BECN1*).

pFRT/FLAG/HA-DEST QKI was purchased from Addgene and was subsequently cloned into a pCDH1-MSCV-EF1α-GreenPuro vector (SBI). pMSCV-MALT1A-WT and pMSCV-MALT1A-E397A were a gift from Daniel Krappmann (German Research Center for Environmental Health, Neuherberg, Germany). pMSCV-MALT1A-WT was subsequently mutated to C464A. Lentiviral GFP-expressing GIPZ sh*MALT1* (V2LHS_84221 TATAATAACCCATATACTC and V3LHS378343 TCTTCTGCAACTTCATCCA) or non-silencing short hairpin control (shc) was purchased from Open Biosystems. Lentiviral particles were obtained from psPAX2 and pVSVg co-transfected HEK-293T cells and infected as previously described (Dubois *et al*, 2014). pFRT/FLAG/HA-DEST QKI was a gift from Thomas Tuschl

(Landthaler *et al*, 2008); pRluc-LC3wt and pRluc-LC3BG120A were a gift from Marja Jaattela (Farkas & Jaattela, 2017). They were introduced in GSCs using Neon electroporation system according to manufacturer's instructions (Life technologies).

Antibodies and reagents

Cathepsin inhibitor 1 was purchased from SelleckChem, rapamycin from Tocris Bioscience, and mepazine from Chembridge. Bafilomycin A1, cycloheximide, chloroquine, phorbol myristate acetate (PMA), pepstatin A, fluphenazine, cyamemazine, chlorpromazine, pipotiazine, alimemazine, promethazine, and doxylamine were all from Sigma-Aldrich. Z-VRPR-FMK was purchased from Enzo Life Sciences. Q-VD-OPh and tumor necrosis factor-alpha (TNFα) were obtained from R&D Systems. Ionomycin was purchased from Calbiochem. The following primary antibodies were used: NESTIN (Millipore MAB5326), SOX2 (Millipore AB5603), GAPDH (Santa Cruz SC-25778 and SC-32233), TUBULIN (Santa Cruz SC-8035), MALT1 (Santa Cruz SC-46677), LAMP2 (Santa Cruz SC-18822), BCL10 (Santa Cruz SC-13153), BCL10 (Santa Cruz SC-5273), CYLD (Santa Cruz SC-137139), HOIL1 (Santa Cruz SC-393754), QKI (Santa Cruz SC-517305), PARP (Santa Cruz SC-8007), IκBα (CST 9242), p-S32/S36-IκBα (CST 9246), P62 (CST 5114), P62 (CST 88588), mTOR (CST 2983), p-S473-AKT (CST 4060), AKT (CST 9272), p-S235/S236-S6 (CST 2211), p-T183/Y185-JNK (CST 9255), JNK (CST 9258), p-S757-ULK1 (CST 6888), LC3B (CST 3868), p-T37/T46-4E-BP1 (CST 2855), p-T70-4E-BP1 (CST 9455), p-S65-4E-BP1 (CST 9451), 4E-BP1 (CST 9644), eIF4E (CST 2067), TOM20 (CST 42406), p-T421/S424-p70S6K (CST 9204), p70S6K (CST 14130), EEA1 (BD Bioscience 610456), CTSD (BD Bioscience 610800), PEX1 (BD Bioscience 611719), PECAM (BD Bioscience 557355), TFEB (Bethyl A303-673A), PDI (Abcam ab2792), GM130 (Abcam ab52649), QKI (Atlas HPA019123), CTSD (Atlas HPA063001), ULK1 (Sigma A7481), and FLAG (Sigma F1804). HRP-conjugated secondary antibodies (anti-rabbit, mouse Ig, mouse IgG1, mouse IgG2a, and mouse IgG2b) were purchased from Southern Biotech. Alexa-conjugated secondary antibodies were from Life Technologies.

Tumorsphere formation

To analyze tumorsphere formation, GSCs (100/μl) were seeded in triplicate in NS34 media as previously described (Harford-Wright *et al*, 2017). Cells were dissociated manually each day to reduce aggregation influence and maintained at 37°C 5% CO_2 until day 5 (day 4 for siRNA). Tumorspheres per field of view (fov) were calculated by counting the total number of tumorspheres in 5 random fov for each well. The mean of each condition was obtained from the triplicates of three independent experiments.

Limiting dilution assays

In order to evaluate the self-renewal of GSCs, limited dilution assays (LDA) were performed as previously described (Tropepe *et al*, 1999). GSCs were plated in a 96-well plate using serial dilution ranging from 2,000 to 1 cell/well with 8 replicates per dilution and treated as indicated. After 14 days, each well was binarily evaluated for tumorsphere formation. Stemness frequency was then calculated using ELDA software (Hu & Smyth, 2009). The mean stemness frequency for each treatment was calculated by averaging across two independent experiments.

Cell viability

Cell viability was measured using Cell TiterGlo luminescent cell viability assay, according to the manufacturers' protocol. Briefly, cells were seeded at 5,000 cells per well in triplicate per indicated treatment. Two days later, 100 μl of Cell TiterGlo reagent was added to each condition, cells were shaken vigorously, using an orbital shaker, to aid in their lysis, and then, luminescence was measured on a FluStar Optima plate reader (BMG).

ELISA

10×10^6 GSCs were cultured with 20 μM MPZ or DMSO and culture media was collected at 8 h, centrifuged, and filtered. Alternatively, cells were transfected with sic or si*MALT1* and supernatants were collected on day 3 post-transfection, centrifuged, and filtered. Human CTSD ELISA (Sigma) was performed on the culture media according to the manufacturer's instructions.

Animal procedures

Tumor inoculation was performed on female Balb/C nude mice aged 6–7 weeks, as described previously (Harford-Wright *et al*, 2017). Animals were randomly assigned to each group and group-housed in specific pathogen-free (SPF) conditions at 24°C on a 12-h day–night cycle. At all times, animals were allowed access to standard rodent pellets and water *ad libitum*. Mice were subcutaneously injected in each flank with 10^6 GSC#9 in 100 μl of PBS and growth factor-free Matrigel. Once tumors were palpable, mice were injected intraperitoneally daily with MPZ (8 mg/kg) or vehicle (DMSO) for two consecutive weeks, based on previous reports (Nagel *et al*, 2012; McGuire *et al*, 2014). Tumor size was measured daily during treatment and for 1 week following treatment withdrawal, with calipers and tumor volume calculated using the following equation $(\text{width}^2 \times \text{length})/2$.

Luciferase assays

Rluc-LC3B luciferase assay was performed as previously described (Farkas & Jaattela, 2017). Briefly, GSC#9 was transfected with 1 μg plasmid using a Neon Transfection System. 24 h later, cells were treated for 4 h with DMSO or MPZ and then assayed using Dual-Glo Luciferase assay system according to the manufacturers' guidelines. Luminescence was measured on a FluStarOptima plate reader.

Flow cytometry

For EdU analysis, cells we incubated with EdU (10 μM) for 2 h followed by fixation and Click-it reaction according to the manufacturers' protocol. For propidium iodide (PI) staining, cells were incubated for 15 min at room temperature with PI (100 μg/ml) following treatment according to manufacturer's protocol. Flow cytometry analyses were performed on FACSCalibur (BD Biosciences, Cytocell, SFR Francois Bonamy, Nantes, France) and processed using FlowJo software.

Immunostaining

After treatment, cells were seeded onto poly-lysine slides, fixed for 10 min with 4% PFA diluted in PBS, permeabilized in 0.04% Triton X-100, and blocked with PBS–BSA 4% prior to 1 h primary antibody incubation. After PBS washes, cells were incubated with AlexaFluor-conjugated secondary antibodies for 30 min. Next, cells were incubated with DAPI for 10 min and mounted with prolong gold anti-fade mounting medium. For Lysotracker Red DND-99 staining, cells were incubated with 50 nM Lysotracker during the last 30 min of treatment, and cells were fixed for 10 min in 4% PFA. To monitor changes in lysosomal enzyme activity, DQ-ovalbumin assay was performed, as previously described (Ebner *et al*, 2018). Cells were incubated with 10 μg/ml DQ-ovalbumin for 1 h at the end of treatment. Cells were then fixed for 10 min in 4% PFA. For transferrin uptake assay, following treatment, cells were washed in medium and incubated with Alexa596-conjugated transferrin (25 μg/ml) for 30 min at 37°C. Cells were then acid-washed for 40 s and fixed for 10 min in 4% PFA. Mouse tissue sections, 7 μm thickness, were obtained after cryosectioning of xenograft tumor embedded in OCT (Leica cryostat, SC3M facility, SFR Francois Bonamy, Nantes, France). Mouse tissue sections and human GBM samples from patients (IRCNA tumor library IRCNA, CHU Nantes, Integrated Center for Oncology, ICO, St. Herblain, France) were stained as followed. Sections were fixed 20 min in 4% PFA, permeabilized 10 min with PBS–Triton 0.2%, and blocked with 4% PBS–BSA 2 h prior to staining. Primary antibodies were incubated overnight at 4°C. All images were acquired on confocal Nikon A1 Rsi, using a 60× oil-immersion lens (Nikon Excellence Center, MicroPicell, SFR Francois Bonamy, Nantes, France). Structure illumination microscopy (SIM) images were acquired with a Nikon N-SIM microscope. Z-stacks of 0.12 μm were performed using a 100× oil-immersion lens with a 1.49 aperture and reconstructed in 3D using the NIS-Element Software. All images were analyzed and quantified using the ImageJ software.

Immunoblotting and immunoprecipitation

Cells were harvested with cold PBS followed by cellular lysis in TNT lysis buffer (50 mM Tris pH 7.4, 150 mM NaCl, 1% Triton X-100, 1% Igepal, 2 mM EDTA, supplemented with protease inhibitor) for 30 min on ice. Samples were centrifuged at 8,000 *g* to remove insoluble fraction. Tissue samples were lysed in RIPA lysis buffer for 2 h under agitation, following homogenization with mortar and pestle. Lysates were cleared in centrifuge at max speed for 30 min. Cytosol and nuclei separation were performed as previously described (Dubois *et al*, 2014). Briefly, cells were lysed in Buffer A (HEPES 10 mM, KCl 10 mM, EDTA 0.1 mM, EGTA 0.1 mM, DTT 1 mM, Na_3VO_4 1 mM, plus protease inhibitor) on ice for 5 min and then Buffer A + 10% Igepal was added for 5 min. Samples were centrifuged at 1,000 *g* for 3 min. Soluble fraction was cleared at 8,000 *g*. Immunoprecipitation was performed as previously described (Dubois *et al*, 2014). Briefly, cells were lysed in TNT lysis buffer for 30 min and cleared by centrifugation at 8,000 *g*. Samples were precleared by a 30-min incubation with Protein G agarose and then incubated for 2 h at 4°C with Protein G agarose and 5 μg of indicated antibodies. Protein concentrations were determined by BCA. Equal amount of 5–10 μg proteins were resolved by SDS–PAGE and transferred to nitrocellulose membranes. Membranes were revealed using a chemiluminescent HRP substrate and visualized using the Fusion imaging system.

Electron microscopy

After treatment, 1 volume of warm 2.5% glutaraldehyde (0.1M PB buffer, pH 7.2, 37°C) was added to 1 volume of cell suspension for 5 min, RT. Fixative was removed by centrifugation, and cells were treated 2.5% glutaraldehyde for 2 h, RT. Samples were then stored at 4°C in 1% paraformaldehyde until processed. After washes (10 min × 3), cells are post-fixed by 1% OsO_4/1.5% $K_3[Fe(CN)_6]$ for 30 min following washed by ddH_2O 10 min × 3, then dehydrated by 50, 70, 80, 90, 100% ethanol, 100% ethanol/100% acetone (1:1) for 5 min, 100% acetone for 3 min. Cells were infiltrated by 100% acetone/pure resin 1:1, 1:2, 1:3 for 1 h, pure resin overnight, pure resin for 1 h, then cells were embedded in the pure resin and polymerized at 60°C for 48 h. 70-nm sections were stained by uranyl acetate and lead citrate then observed under TEM at 80 kV (Technology Center for Protein Sciences, School of Life Sciences, Tsinghua University, Beijing, China).

RNAseq analysis

5×10^6 GSC#9 were treated with vehicle (DMSO) and MPZ (20 μM) for 4 h, in three biological replicates and snap-frozen on dry ice. RNA extraction (all RIN > 9.0), library preparation, RNAseq, and bioinformatics analysis were performed at Active Motif (Carlsbad, California, USA). Briefly, 2 μg of total RNA was isolated using the Qiagen RNeasy Mini Kit and further processed in Illumina's TruSeq Stranded mRNA Library kit. Libraries are sequenced on Illumina NextSeq 500 as paired-end 42-nt reads. Sequence reads are analyzed with the STAR alignment—DESeq2 software pipeline described in the Data Explanation document. The list of differentially expressed genes from DESeq2 output was selected based on 10% adjusted *P*-value level and FDR of 0.1 (please see Fig 6A and D, Table EV1). Gene ontology and KEGG pathway enrichment analysis were done using DAVID bioinformatics resources portal.

qPCR

3×10^6 GSC#9 were treated with vehicle (DMSO) and MPZ (20 μM) for 4 h, in three biological replicates and were snap-frozen. RNA extraction was done using Qiagen RNeasy kit. Equal amounts of RNA were reverse-transcribed using the Maxima Reverse Transcriptase kit, and 30 ng of the resulting cDNA was amplified by qPCR using PerfeCTa SYBR Green SuperMix Low ROX. Data were analyzed using the 2-ΔΔCt methods and normalized by the housekeeping genes ACTB and HPRT1.

The following primers were used: VGF forward GACCCTCCTCTC CACCTCTC, VGF reverse ACCGGCTCTTTATGCTCAGA, GNS forward CCCATTTTGAGAGGTGCCAGT, GNS reverse TGACGT TACGGCCTTCTCCTT, HEXA forward CAACCAACACATTCTTCTC CA, HEXA reverse CGCTATCGTGACCTGCTTTT, GLA forward AGCCAGATTCCTGCATCAGTG, GLA reverse ATAACCTGCATCCTT CCAGCC, CTSD forward CAACAGCGACAAGTCCAGC, CTSD reverse CTGAATCAGCGGCACGGC, LAMP2 forward CGTTCTGGTCTGCC TAGTC, LAMP2 reverse CAGTGCCATGGTCTGAAATG, LAMP1

forward ACCTGTCGAGTGGCAACTTCA, LAMP1 reverse GGGCA CAAGTGGTGGTGAG, CSTB forward AGTGGAGAATGGCACACC CTA, CSTB reverse AAGAAGCCATTGTCACCCCA, CTSS forward GCCTGATTCTGTGGACTGG, CTSS reverse GATGTACTGGAAAGCC GTTG, LC3B forward GCTCATCAAGATAATTAGAAGGCG, LC3B reverse CTGGGAGGCATAGACCATGT, ACTB forward GGACTTC GAGCAAGAGATGG, ACTB reverse AGCACTGTGTTGGCGTACAG, HPRT1 forward TGACACTGGCAAAACAA TGCA, HPRT1 reverse GGTCCTTTTCACCAGCAAGCT, CAV1 forward CGTAGACTCG GAGGGACATC, CAV1 reverse GCCTTCCAAATGCCGTCAAA, CTGF forward CATCTTCGGTGGTACGGTGT, CTGF reverse TTCCAGT CGGTAAGCCGC, EGR3 forward GTGCTATGACCGGCAAACTC, EGR3 reverse TGTCCATTACATTCTCTGTAGCCA, GLIPR1 forward TACACTCAGGTTGTTTGGGCA, GLIPR1 reverse ACGTTTGAC TTGGTCTCGCT, IL7R forward ACGATGTAGCTTACCGCCAG, IL7R reverse TAGGATCCATCTCCCCTGAGC, CXCL10 forward TGGCATT CAAGGAGTACCTCTC, CXCL10 reverse TGATGGCCTTCGATT CTGGA, DRP2 forward CCGTGTGAGTGGCTATCGTA, DRP2 reverse AGCTCTAACCTGAGGGTGGG, ITGAM forward CGATATCAG CACATCGGCCT, ITGAM reverse AGCCCTCTGCCCCCTG, MSLN forward ACTCCCGTCTGCTGTGACG, MSLN reverse AAGAGCAGG AACAGGAGGCT, CARD10 forward GGACCTGAGCCTCACAACTC, CARD10 reverse CCACCCTTTGCTCTCTTGGT.

Statistics

Data are representative of at least three independent experiments, unless otherwise stated. Statistical analysis was performed with GraphPad Prism5 using one-way analysis of variance (ANOVA), two-way ANOVA, or an unpaired two-tailed *t*-test (Student's *t*-test). For each statistical test, *P*-value of < 0.05 was considered significant.

Data availability

The datasets produced in this study are available in the following databases:

RNA-seq data: Gene Expression Omnibus GSE139018 (https://www.ncbi.nlm.nih.gov/geo/query/acc.cgi?acc=GSE139018).

Expanded View for this article is available online.

Acknowledgements

We thank SOAP team members (Nantes, France). We thank Steven Nedellec from MicroPicell, as well as Cytocell, and UTE facilities (SFR Santé François Bonamy, Nantes, France). We are also grateful to Daniel Krappmann (German Research Center for Environmental Health, Neuherberg, Germany), Rudi Beyaert (VIB, Ghent, Belgium), and Li Yu (Tsinghua University, Beijing, China) for reagents and helpful discussion. This research was funded by Fondation pour la Recherche Medicale (Equipe labellisée DEQ20180339184), Fondation ARC contre le Cancer (JG PJA20171206146), Ligue nationale contre le cancer comités de Loire-Atlantique, Maine et Loire, Vendée, Ille-et-Vilaine (JG, NB), Région Pays de la Loire et Nantes Métropole under Connect Talent Grant (JG), and SIRIC ILIAD INCa-DGOS-Inserm_12558. KAJ received PhD fellowships from Nantes Métropole and Fondation ARC; TD received PhD fellowship from Nantes Métropole; GAG and AT hold postdoctoral fellowships from Fondation de France and Fondation ARC, respectively.

Author contributions

KAJ, JG, NB: conception and design, acquisition of data, analysis and interpretation of data, drafting or revising the article; GA-G, CM, AT, YL, EH-W, KT, TD, CAN: acquisition of data, analysis and interpretation of data; J-SF: conception and interpretation of data. All authors approved the manuscript. All data needed to evaluate the conclusions in the paper are present in the paper and/or the Supplementary Materials. Additional data related to this paper may be requested from the authors.

Conflict of interest

The authors declare that they have no conflict of interest.

References

Aits S, Jaattela M (2013) Lysosomal cell death at a glance. *J Cell Sci* 126: 1905 – 1912

Arias E, Koga H, Diaz A, Mocholi E, Patel B, Cuervo AM (2015) Lysosomal mTORC2/PHLPP1/Akt regulate chaperone-mediated autophagy. *Mol Cell* 59: 270 – 284

Bao S, Wu Q, McLendon RE, Hao Y, Shi Q, Hjelmeland AB, Dewhirst MW, Bigner DD, Rich JN (2006) Glioma stem cells promote radioresistance by preferential activation of the DNA damage response. *Nature* 444: 756 – 760

Bargou RC, Leng C, Krappmann D, Emmerich F, Mapara MY, Bommert K, Royer HD, Scheidereit C, Dörken B (1996) High-level nuclear NF-kappa B and Oct-2 is a common feature of cultured Hodgkin/Reed-Sternberg cells. *Blood* 87: 4340 – 4347

Bowman RL, Wang Q, Carro A, Verhaak RGW, Squatrito M (2007) GlioVis data portal for visualization and analysis of brain tumor expression datasets. *Neuro Oncol* 19: 139 – 141

Brown CE, Alizadeh D, Starr R, Weng L, Wagner JR, Naranjo A, Ostberg JR, Blanchard MS, Kilpatrick J, Simpson J *et al* (2016) Regression of glioblastoma after chimeric antigen receptor T-cell therapy. *N Engl J Med* 375: 2561 – 2569

Calabrese C, Poppleton H, Kocak M, Hogg TL, Fuller C, Hamner B, Oh EY, Gaber MW, Finklestein D, Allen M *et al* (2007) A perivascular niche for brain tumor stem cells. *Cancer Cell* 11: 69 – 82

Chen J, Li Y, Yu TS, McKay RM, Burns DK, Kernie SG, Parada LF (2012) A restricted cell population propagates glioblastoma growth after chemotherapy. *Nature* 488: 522 – 526

Chinot OL, Wick W, Mason W, Henriksson R, Saran F, Nishikawa R, Carpentier AF, Hoang-Xuan K, Kavan P, Cernea D *et al* (2014) Bevacizumab plus radiotherapy-temozolomide for newly diagnosed glioblastoma. *N Engl J Med* 370: 709 – 722

Davis RE, Brown KD, Siebenlist U, Staudt LM (2001) Constitutive nuclear factor kappaB activity is required for survival of activated B cell-like diffuse large B cell lymphoma cells. *J Exp Med* 194: 1861 – 1874

Di Pilato M, Kim EY, Cadilha BL, Prüßmann JN, Nasrallah MN, Seruggia D, Usmani SM, Misale S, Zappulli V, Carrizosa E *et al* (2019) Targeting the CBM complex causes Treg cells to prime tumours for immune checkpoint therapy. *Nature* 570: 112 – 116

Douanne T, Gavard J, Bidere N (2016) The paracaspase MALT1 cleaves the LUBAC subunit HOIL1 during antigen receptor signaling. *J Cell Sci* 129: 1775 – 1780

Dubois SM, Alexia C, Wu Y, Leclair HM, Leveau C, Schol E, Fest T, Tarte K, Chen ZJ, Gavard J *et al* (2014) A catalytic-independent role for the LUBAC in NF-kappaB activation upon antigen receptor engagement and in lymphoma cells. *Blood* 123: 2199 – 2203

Ebner P, Poetsch I, Deszcz L, Hoffman T, Zuber J, Fumiyo I (2018) The IAP family member BRUCE regulates autophagosome-lysosome fusion. *Nat Commun* 9: 599

Eitelhuber AC, Vosyka O, Nagel D, Bognar M, Lenze D, Lammens K, Schlauderer F, Hlahla D, Hopfner KP, Lenz G *et al* (2015) Activity-based probes for detection of active MALT1 paracaspase in immune cells and lymphomas. *Chem Biol* 22: 129 – 138

Elrick MJ, Lieberman AP (2013) Autophagic dysfunction in a lysosomal storage disorder due to impaired proteolysis. *Autophagy* 9: 234 – 235

Farkas T, Jaattela M (2017) Chapter one - renilla luciferase-LC3B based reporter assay for measuring autophagic flux. *Methods Enzymol* 588: 1 – 13

Fennelly C, Amaravadi RK (2017) Lysosomal biology in cancer. *Methods Mol Biol* 1594: 293 – 308

Galan-Moya EM, Le Guelte A, Lima Fernandes E, Thirant C, Dwyer J, Bidere N, Couraud PO, Scott MG, Junier MP, Chneiweiss H *et al* (2011) Secreted factors from brain endothelial cells maintain glioblastoma stem-like cell expansion through the mTOR pathway. *EMBO Rep* 12: 470 – 476

Gingras AC, Kennedy SG, O'Leary MA, Sonenberg N, Hay N (1998) 4EBP1, a repressor of mRNA translation, is phosphorylated and inactivated by the AKT (PKB) signaling pathway. *Genes Dev* 12: 502 – 513

Hamilton KS, Phong B, Corey C, Cheng J, Gorentla B, Zhong X, Shiva S, Kane LP (2014) T cell receptor-dependent activation of mTOR signaling in T cells is mediated by Carma1 and MALT1, but not Bcl10. *Sci Signal* 7: ra55

Hailfinger S, Lenz G, Ngo V, Posvitz-Fejfar A, Rebeaud F, Guzzardi M, Penas EMM, Dierlamm J, Chan WC, Staudt LM *et al* (2009) Essential role of MALT1 protease activity in activated B cell-like diffuse large B-cell lymphoma. *Proc Natl Acad Sci USA* 106: 19946 – 19951

Harford-Wright E, Andre-Gregoire G, Jacobs KA, Treps L, Le Gonidec S, Leclair HM, Gonzalez-Diest S, Roux Q, Guillonneau F, Loussouarn D *et al* (2017) Pharmacological targeting of apelin impairs glioblastoma growth. *Brain* 140: 2939 – 2954

Hu Y, Smyth GK (2009) ELDA: extreme limiting dilution analysis for comparing depleted and enriched populations in stem cell and other assays. *J Immunol Methods* 347: 70 – 78

Jacobs KA, Harford-Wright E, Gavard J (2017) Neutralizing gp130 interferes with endothelial-mediated effects on glioblastoma stem-like cells. *Cell Death Differ* 24: 384

Jeltsch KM, Hu D, Brenner S, Zöller J, Heinz GA, Nagel D, Vogel KU, Rehage N, Warth SC, Edelmann SL *et al* (2014) Cleavage of roquin and regnase-1 by the paracaspase MALT1 releases their cooperatively repressed targets to promote TH17 differentiation. *Nat Immunol* 15: 1079 – 1089

Jia R, Bonifacino JS (2019) Lysosome positioning influences mTORC2 and AKT signaling. *Mol Cell* 75: 26 – 38

Jin X, Kim LJY, Wu Q, Wallace LC, Prager BC, Sanvoranart T, Gimple RC, Wang X, Mack SC, Miller TE *et al* (2017) Targeting glioma stem cells through combined BMI1 and EZH2 inhibition. *Nat Med* 23: 1352 – 1361

Juilland M, Thome M (2018) Holding all the CARDs: how MALT1 controls CARMA/CARD-dependent signaling. *Front Immunol* 9: 1927

Karin M, Greten FR (2005) NF-kappaB: linking inflammation and immunity to cancer development and progression. *Nat Rev Immunol* 5: 749 – 759

Kip E, Staal J, Verstrepen L, Tima HG, Terryn S, Romano M, Lemeire K, Suin V, Hamouda A, Kalai M *et al* (2018) MALT1 controls attenuated rabies virus by inducing early inflammation and T cell activation in the brain. *J Virol* 92: e02029 – 17

Korolchuk VI, Saiki S, Lichtenberg M, Siddiqi FH, Roberts EA, Imarisio S, Jahreiss L, Sarkar S, Futter M, Menzies FM *et al* (2011) Lysosomal positioning coordinates cellular nutrient responses. *Nat Cell Biol* 13: 453 – 460

Korth C, May BC, Cohen FE, Prusiner SB (2001) Acridine and phenothiazine derivatives as pharmacotherapeutics for prion disease. *Proc Natl Acad Sci USA* 98: 9836 – 9841

Landthaler M, Gaidatzis D, Rothballer A, Chen PY, Soll SJ, Dinic L, Ojo T, Hafner M, Zavolan M, Tuschl T (2008) Molecular characterization of human Argonaute-containing ribonucleoprotein complexes and their bound target mRNAs. *RNA* 14: 2580 – 2596

Lathia JD, Mack SC, Mulkearns-Hubert EE, Valentim CL, Rich JN (2015) Cancer stem cells in glioblastoma. *Genes Dev* 29: 1203 – 1217

Le Joncour V, Filppu P, Hyvonen M, Holopainen M, Turunen SP, Sihto H, Burghardt I, Joensuu H, Tynninen O, Jaaskelainen J *et al* (2019) Vulnerability of invasive glioblastoma cells to lysosomal membrane destabilization. *EMBO Mol Med* 11: e9034

Li J, Jia H, Xie L, Wang X, Wang X, He H, Lin Y, Hu L (2009) Association of constitutive nuclear factor-kappaB activation with aggressive aspects and poor prognosis in cervical cancer. *Int J Gynecol Cancer* 19: 1421 – 1426

Li W, Wu C, Chen N, Gu H, Yen A, Cao L, Wang E, Wang L (2016) PI3K/Akt/mTOR signaling pathway and targeted therapy for glioblastoma. *Oncotarget* 7: 33440 – 33450

Lomas JL (1957) Treatment of schizophrenia. *Br Med J* 2: 78 – 80

Loos B, du Toit A, Hofmeyr JHS (2014) Defining and measuring autophagosome flux-concept and reality. *Autophagy* 10: 2087 – 2096

Luo J, Solimini NL, Elledge SJ (2009) Principles of cancer therapy: oncogene and non-oncogene addiction. *Cell* 138: 807

Mai TT, Hamai A, Hienzsch A, Caneque T, Müller S, Wicinski J, Cabaud O, Leroy C, David A, Acevedo V *et al* (2017) Salinomycin kills cancer stem cells by sequestering iron in lysosomes. *Nat Chem* 10: 1025 – 1033

Man J, Yu X, Huang H, Zhou W, Xiang C, Huang H, Miele L, Liu Z, Bebek G, Bao S *et al* (2017) Hypoxic induction of vasorin regulates Notch1 turnover to maintain glioma stem-like cells. *Cell Stem Cell* 22: 104 – 118

McAuley JR, Bailey KM, Ekambaram P, Klei LR, Kang H, Hu D, Freeman TJ, Concel VJ, Hubel NE, Lee JL *et al* (2019) MALT1 is a critical mediator of PAR1-driven NF-κB activation and metastasis in multiple tumor types. *Oncogene* 38: 7384 – 7398

McGuire C, Elton L, Wieghofer P, Staal J, Voet S, Demeyer A, Nagel D, Krappmann D, Prinz M, Beyaert R *et al* (2014) Pharmacological inhibition of MALT1 protease activity protects mice in a mouse model of multiple sclerosis. *J Neuroinflammation* 11: 124

Meloni L, Verstrepen L, Kreike M, Staal J, Driege Y, Afonina IS, Beyaert R (2018) Mepazine inhibits RANK-induced osteoclastogenesis independent of its MALT1 inhibitory function. *Molecules* 23: 3144

Nagel D, Spranger S, Vincendeau M, Grau M, Raffegerst S, Kloo B, Hlahla D, Neuenschwander M, Peter von Kries J, Hadian K *et al* (2012) Pharmacologic inhibition of MALT1 protease by phenothiazines as a therapeutic approach for the treatment of aggressive ABC-DLBCL. *Cancer Cell* 22: 825 – 837

Nakaya M, Xiao Y, Zhou X, Chang JH, Chang M, Cheng X, Blonska M, Lin X, Sun SC (2014) Inflammatory T cell responses rely on amino acid transporter ASCT2 facilitation of glutamine uptake and mTORC1 kinase activation. *Immunity* 40: 692 – 705

Ngo VN, Davis RE, Lamy L, Yu X, Zhao H, Lenz G, Lam LT, Dave S, Yang L, Powell J *et al* (2006) A loss-of-function RNA interference screen for molecular targets in cancer. *Nature* 441: 106 – 110

Oliva CR, Zhang W, Langford C, Suto MJ, Griguer CE (2017) Repositioning chlorpromazine for treating chemoresistant glioma through the inhibition of cytochrome c oxidase bearing the COX4-1 regulatory subunit. *Oncotarget* 8: 37568 – 37583

Pietras A, Katz AM, Ekström EJ, Wee B, Halliday JJ, Pitter KL, Werbeck JL, Amankulor NM, Huse JT, Holland EC (2014) Osteopontin-CD44 signaling in the glioma perivascular niche enhances cancer stem cell phenotypes and promotes aggressive tumor growth. *Cell Stem Cell* 14: 357 – 369

Qin X, Jiang B, Zhang Y (2016) 4E-BP1, a multifactor regulated multifunctional protein. *Cell Cycle* 15: 781 – 786

Rahim SAA, Dirkse A, Oudin A, Schuster A, Bohler J, Barthelemy V, Muller A, Vallar L, Janji B, Golebiewska A *et al* (2017) Regulation of hypoxia – induced autophagy in glioblastoma involves ATG9A. *Br J Cancer* 117: 813 – 825

Rebeaud F, Hailfinger S, Posevitz-Fejfar A, Tapernoux M, Moser R, Rueda D, Gaide O, Guzzardi M, Lancu EM, Rufer N *et al* (2008) The proteolytic activity of the paracaspase MALT1 is key in T cell activation. *Nat Immunol* 9: 272 – 281

Rosenbaum M, Gewies A, Pechloff K, Heuser C, Engleitner T, Gehring T, Hartjes L, Krebs S, Krappmann D, Kriegsmann M *et al* (2019) Bcl10-controlled Malt1 paracaspase activity is key for the immune suppressive function of regulatory T cells. *Nat Commun* 10: 2352

Sardiello M, Palmieri M, di Ronza A, Medina DL, Valenza M, Gennarino VA, Di Malta C, Donaudy F, Embrione V, Polishchuk RS *et al* (2009) A gene network regulating lysosomal biogenesis and function. *Science* 325: 473 – 477

Schlauderer F, Lammens K, Nagel D, Vincendeau M, Eitelhuber AC, Verhelst SH, Kling D, Chrusciel A, Ruland J, Krappman D *et al* (2013) Structural analysis of phenothiazine derivatives as allosteric inhibitors of the MALT1 paracaspase. *Angew Chem Int Ed Engl* 52: 10384 – 10387

Settembre C, Zoncu R, Medina DL, Vetrini F, Erdin S, Erdin S, Huynh T, Ferron M, Karsenty G, Vellard MC *et al* (2012) A lysosome-to-nucleus signalling mechanism senses and regulates the lysosome via mTOR and TFEB. *EMBO J* 31: 1095 – 1108

Shchors K, Massaras A, Hanahan D (2015) Dual targeting of autophagic regulatory circuitry in gliomas with repurposed drugs elicits cell-lethal autophagy and therapeutic benefit. *Cancer Cell* 28: 456 – 471

Shingu T, Ho AL, Yuan L, Zhou X, Dai C, Zheng S, Wang Q, Zhong Y, Chang Q, Horner JW *et al* (2016) Qki deficiency maintains stemness of glioma stem cells in suboptimal environment by downregulating endolysosomal degradation. *Nat Genet* 49: 75 – 86

Singh SK, Hawkins C, Clarke ID, Squire JA, Bayani J, Hide T, Henkelman RM, Cusimano MD, Dirks PB (2004) Identification of human brain tumour initiating cells. *Nature* 432: 396 – 401

Staal J, Driege Y, Bekaert T, Demeyer A, Muyllaert D, Van Damme P, Gevaert K, Beyaert R (2011) T-cell receptor-induced JNK activation requires proteolytic inactivation of CYLD by MALT1: CYLD is cleaved by MALT1. *EMBO J* 30: 1742 – 1752

Staudt LM (2010) Oncogenic activation of NF-kappaB. *Cold Spring Harb Perspect Biol* 2: a000109

Stupp R, Hegi ME, Mason WP, van den Bent MJ, Taphoorn MJ, Janzer RC, Ludwin SK, Allgeier A, Fisher B, Belanger K *et al* (2009) Effects of radiotherapy with concomitant and adjuvant temozolomide versus radiotherapy alone on survival in glioblastoma in a randomised phase III study: 5-year analysis of the EORTC-NCIC trial. *Lancet Oncol* 10: 459 – 466

Stupp R, Taillibert S, Kanner AA, Kesari S, Steinberg DM, Toms SA, Taylor LP, Lieberman F, Silvani A, Fink KL *et al* (2015) Maintenance therapy with tumor-treating fields plus temozolomide vs temozolomide alone for glioblastoma: a randomized clinical trial. *JAMA* 314: 2535 – 2543

Tan SK, Jermakowicz A, Mookhtiar Adnan K, Nemeroff CB, Schurer SC, Ayad NG (2018) Drug repositioning in glioblastoma: a pathway perspective. *Front Pharmacol* 9: 218

Thys A, Douanne T, Bidere N (2018) Post-translational modifications of the CARMA1-BCL10-MALT1 complex in lymphocytes and activated B-cell like subtype of diffuse large B-cell lymphoma. *Front Oncol* 8: 498

Treps L, Edmond S, Harford-Wright E, Galan-Moya EM, Schmitt A, Azzi S, Citerne A, Bidere N, Ricard D, Gavard J (2016) Extracellular vesicle-transported Semaphorin3A promotes vascular permeability in glioblastoma. *Oncogene* 35: 2615 – 2623

Tropepe V, Sibilia M, Ciruna BG, Rossant J, Wagner EF, van der Kooy D (1999) Distinct neural stem cells proliferate in response to EGF and FGF in the developing mouse telencephalon. *Dev Biol* 208: 166 – 188

Uehata T, Iwasaki H, Vandenbon A, Matsushita K, Hernandez-Cuellar E, Kuniyoshi K, Satoh T, Mino T, Suzuki Y, Standley DM *et al* (2013) Malt1-induced cleavage of Regnase-1 in $CD4^+$ helper T cells regulates immune activation. *Cell* 153: 1036 – 1049

Wang F, Salvati A, Boya P (2018a) Lysosome-dependent cell death and deregulated autophagy induced by amine-modified polystyrene nanoparticles. *Open Biol* 8: 170271

Wang X, Prager BC, Wu Q, Kim LJY, Gimple RC, Shi Y, Yang K, Morton AR, Zhou W, Zhu Z *et al* (2018b) Reciprocal signaling between glioblastoma stem cells and differentiated tumor cells promotes malignant progression. *Cell Stem Cell* 22: 514 – 528

Weyerhäuser P, Kantelhardt SR, Kim EL (2018) Re-purposing chloroquine for glioblastoma: potential merits and confounding variables. *Front Oncol* 8: 335

Wu J, Zhou L, Tonissen K, Tee R, Artzt K (1999) The quaking 1-5 protein (QKI-5) has a novel nuclear localization signal and shuttles between the nucleus and the cytoplasm. *J Biol Chem* 274: 29202 – 29210

Yan K, Yang K, Rich JN (2013) The evolving landscape of glioblastoma stem cells. *Curr Opin Neurol* 26: 701 – 707

Yu L, McPhee CK, Zheng L, Mardones GA, Rong Y, Peng J, Mi N, Zhao Y, Liu Z, Wan F *et al* (2010) Termination of autophagy and reformation of lysosomes regulated by mTOR. *Nature* 465: 942 – 946

Zielke S, Meyer N, Mari M, Abou-El-Ardat K, Reggiori F, van Wijk SJL, Kögel D, Fulda S (2018) Loperamide, pimozide, and STF-62247 trigger autophagy-dependent cell death in glioblastoma cells. *Cell Death Dis* 9: 994

Expanded View Figures

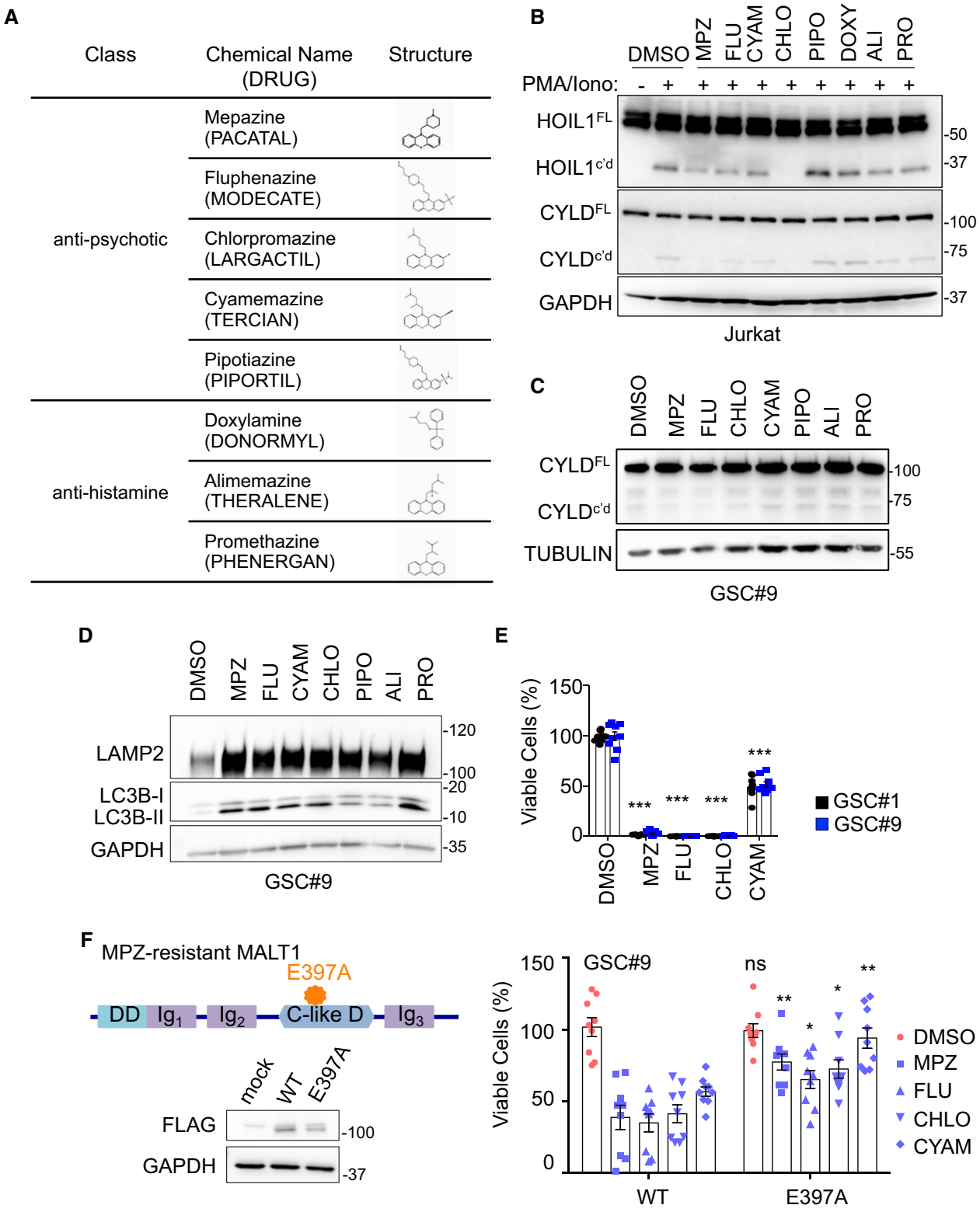

Figure EV1.

Figure EV1. Impact of phenothiazines on MALT1 protease activity and lysosomes.

A Table summarizing eight phenothiazines used in clinics as either anti-psychotic or anti-histaminic, along with their generic and brand names (cap letters), and chemical structures.

B Western blot analysis of two MALT1 substrates, HOIL1 and CYLD, either full length (FL) or cleaved (c'd) in Jurkat T cells treated with vehicle (DMSO) or phenothiazines, as follows: 20 μM CYAM (cyamemazine), CHLO (chlorpromazine), PIPO (pipotiazine), DOXY (doxylamine), ALI (alimemazine), and PRO (promethazine), and 10 μM MPZ (mepazine) and FLU (fluphenazine) for 30 min and stimulated for 30 min more with PMA (20 ng/ml) and Ionomycin (Iono, 300 ng/ml). TUBULIN served as a loading control.

C Western blot analysis of CYLD processing in GSC#9 treated with vehicle (DMSO) or phenothiazines (20 μM CYAM, CHLO, PIPO, DOXY, ALI, and PRO, 10 μM MPZ and FLU) for 60 min. GAPDH served as a loading control.

D Western blot analysis of LAMP2 and LC3B in equal amount of total protein lysates from GSC#9 treated for 6 h with vehicle (DMSO) or 20 μM phenothiazines (MPZ, FLU, CYAM, CHLO, ALI, PRO). GAPDH served as a loading control.

E Cell viability of GSC#1 and GSC#9 using 20 μM of MPZ, FLU, CHLO, and CYAM, using Cell TiterGlo assays. Data were normalized to their respective DMSO-treated controls and are presented as the mean ± SEM of three independent experiments in triplicate.

F Schematic drawing of MALT1 structures highlighting the E397A substitution in the mepazine-resistant version. DD: death domain, C-like D: caspase-like domain, Ig: immunoglobulin domain. Western blot analysis of FLAG in equal amount of total protein lysates from HEK-293T cells transfected with empty vector (mock), MALT-WT, or MALT1-E397A. GAPDH serves as a loading control. GSC#9 were transduced with MALT-WT or MALT1-E397A and treated with phenothiazines (10 μM of MPZ, FLU, CYAM, CHLO) for 24 h. Cell Viability was analyzed using Cell TiterGlo assay. Data were normalized to their respective DMSO-treated controls and are presented as the mean ± SEM of three independent experiments in triplicate.

Data information: All data were repeated in three independent experiments. Statistics were performed using a one-way ANOVA with a 95% confidence interval for all experiments with *P*-values stated. $*P < 0.05$, $**P < 0.01$, $***P < 0.001$.

Source data are available online for this figure.

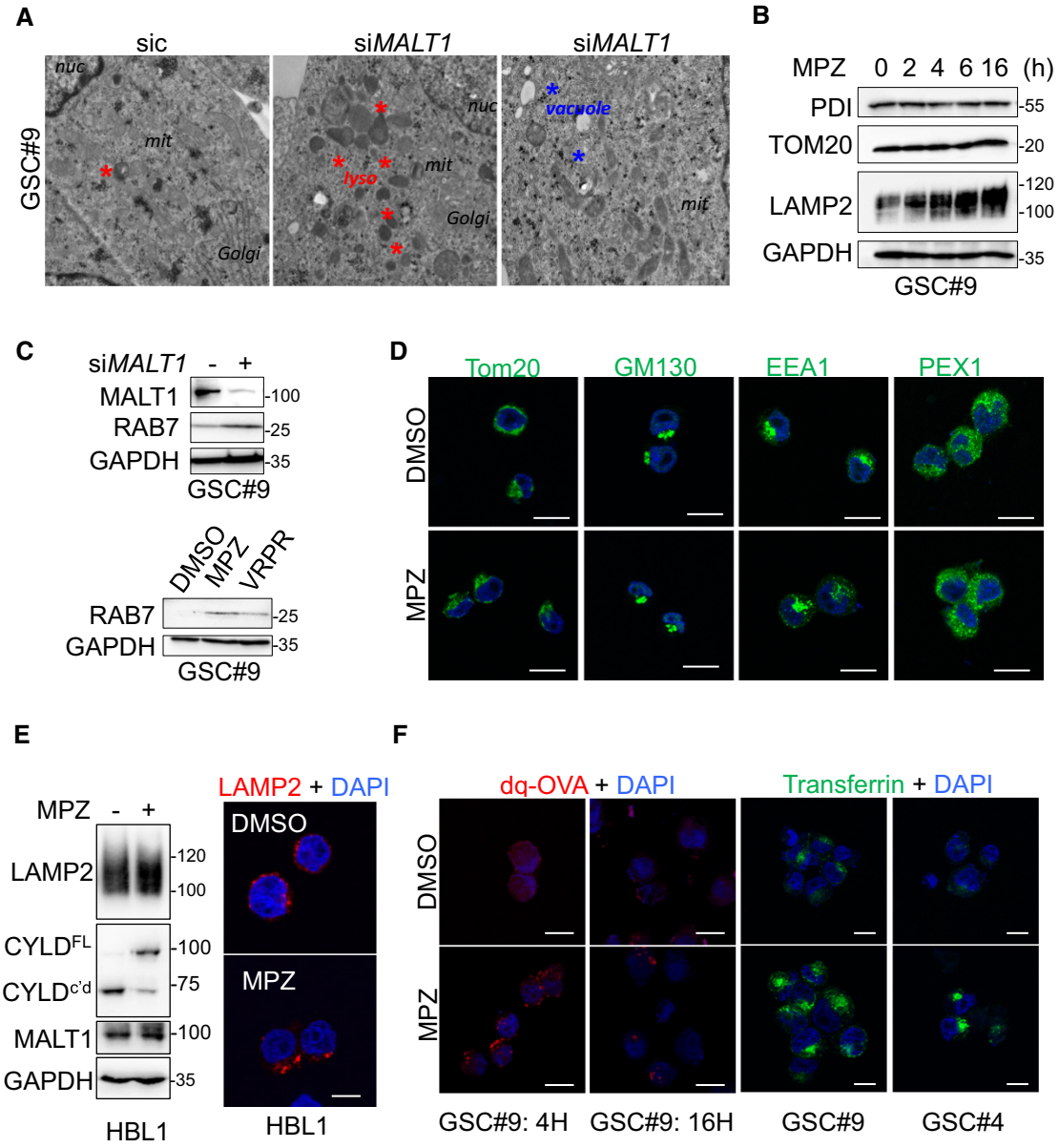

Figure EV2. Impact of MALT1 inhibition on intracellular organelles.

A Transmission electron microscopy images from GSC#9 transfected with non-silencing duplexes (sic) or siRNA duplexes targeting *MALT1* (si*MALT1*). Multiple images and sections from one experiment were analyzed. Red stars denote lysosomes; blue stars vacuoles.

B Western blot analysis of PDI, TOM20, and LAMP2 in total protein lysates from GSC#9 treated vehicle (DMSO) or MPZ (20 μM) for the indicated times. GAPDH serves as a loading control.

C Western blot analysis of RAB7 and MALT1 in GSC#9 in total protein lysates from GSC#9 transfected with non-silencing duplexes (sic) or siRNA duplexes targeting *MALT1* (si*MALT1*). Alternatively, GSC#9 received Z-VRPR-FMK (VRPR, 75 μM, 16 h) and mepazine (MPZ, 20 μM, 16 h). GAPDH serves as a loading control.

D Confocal analysis of TOM20, GM130, EEA1, and PEX1 immunostaining (green) in GSC#9 treated with vehicle (DMSO) or MPZ (20 μM) for 4 h. Nuclei (DAPI) are shown in blue. Scale bars: 10 μm.

E ABC DLBCL lymphoma cells HBL1 treated with vehicle (DMSO) or MPZ (20 μM) for 4 h. (Left) Western blot analysis of LAMP2 and CYLD (full length, FL, or cleaved, c'd) in total protein lysates. MALT1 and GAPDH serve as loading controls. (Right) Confocal analysis of LAMP2 (red). Nuclei (DAPI) are shown in blue. Scale bars: 10 μm.

F Confocal analysis of dq-ovalbumin (dq-OVA, red) in GSC#9 treated with vehicle (DMSO) or MPZ (20 μM) for 4 or 16 h. Nuclei (DAPI) are shown in blue. Alternatively, confocal analysis of transferrin uptake (green) in GSC#9 and GSC#4 treated with vehicle (DMSO) or MPZ (20 μM) for 4 h. Nuclei (DAPI) are shown in blue. Scale bars: 10 μm.

Data information: All data were repeated in three independent experiments, unless specified.

Source data are available online for this figure.

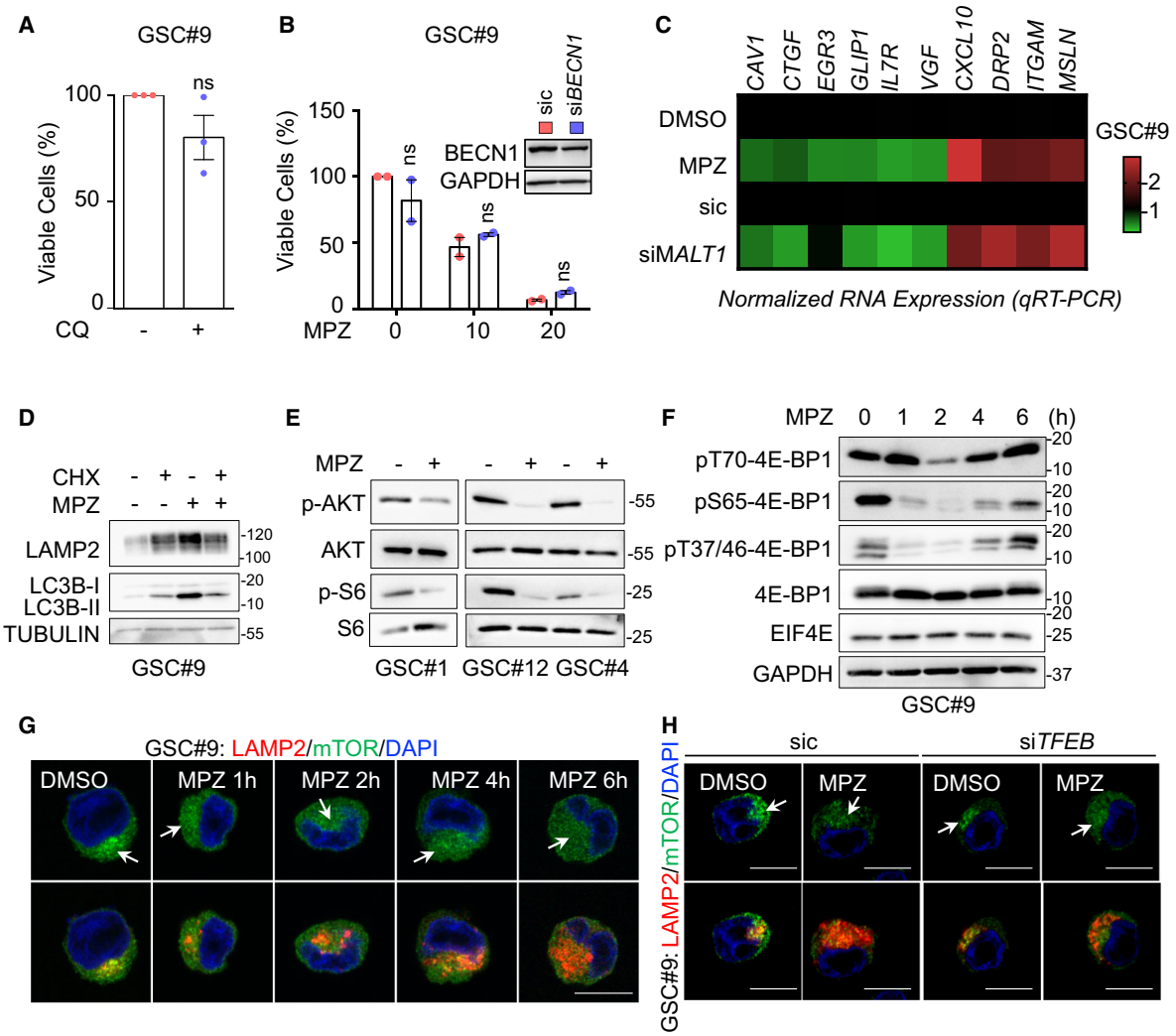

Figure EV3. Impact of MALT1 inhibition on cell death and mTOR signaling.

A Cell viability was measured using Cell TiterGlo luminescent assay in GSC#9 treated for 72 h with vehicle (DMSO) or chloroquine (CQ, 20 μM). Data were normalized to the vehicle-treated controls and are presented as the mean ± SEM of three independent experiments in triplicate.

B Cell viability was measured using Cell TiterGlo luminescent assay in GSC#9 transfected with non-silencing duplexes (sic, red) or siRNA duplexes targeting *BECLIN1* (si*BECN1*, blue) and further treated with vehicle (DMSO) and MPZ (10 and 20 μM) for 72 h. Data were normalized to the vehicle-treated controls and are presented as the mean ± SEM of two independent experiments in triplicate. Knockdown efficiency was checked at the end point by Western blot. GAPDH serves as a loading control.

C GSC#9 were treated with vehicle (DMSO) and mepazine (MPZ, 20 μM) for 16 h. Alternatively, GSC#9 were transfected with non-silencing duplexes (sic) or siRNA duplexes targeting *MALT1* (si*MALT1*). RNAs were processed for qRT–PCR on 10 gene candidates from RNAseq data (Table EV1). Data are represented as heatmap representation of RNA expression, normalized to two housekeeping genes (*HPRT1* and *ACTB*).

D Western blot analysis of LAMP2 and LC3B in total protein lysates from GSC#9 treated with vehicle (DMSO) and mepazine (MPZ, 20 μM) in the presence of cycloheximide (CHX, 50 μg/ml) for 16 h. TUBULIN served as a loading control.

E Western blot analysis of indicated antibodies in total protein lysates from GSC#1, GSC#12, and GSC#4 that received vehicle (DMSO, –) or mepazine (MPZ, 20 μM, 1 h).

F Western blot analysis of indicated antibodies in total protein lysates from GSC#9 treated vehicle (DMSO) or mepazine (MPZ, 20 μM) for the indicated times. GAPDH serves as a loading control.

G Confocal analysis of LAMP2 (red) and mTOR (green) staining in GSC#9 treated vehicle (DMSO) or MPZ (20 μM) for the indicated times. Arrows point to LAMP2-positive area. Nuclei (DAPI) are shown in blue. Scale bars: 10 μm.

H GSC#9 were transfected with sic or si*TFEB* and treated with vehicle (DMSO) or MPZ (20 μM) for 16 h. Samples were analyzed as described in (G). Arrows point to LAMP2-positive area. Nuclei (DAPI) are shown in blue. Scale bars: 10 μm.

Data information: All data were repeated in three independent experiments, unless specified.

Source data are available online for this figure.

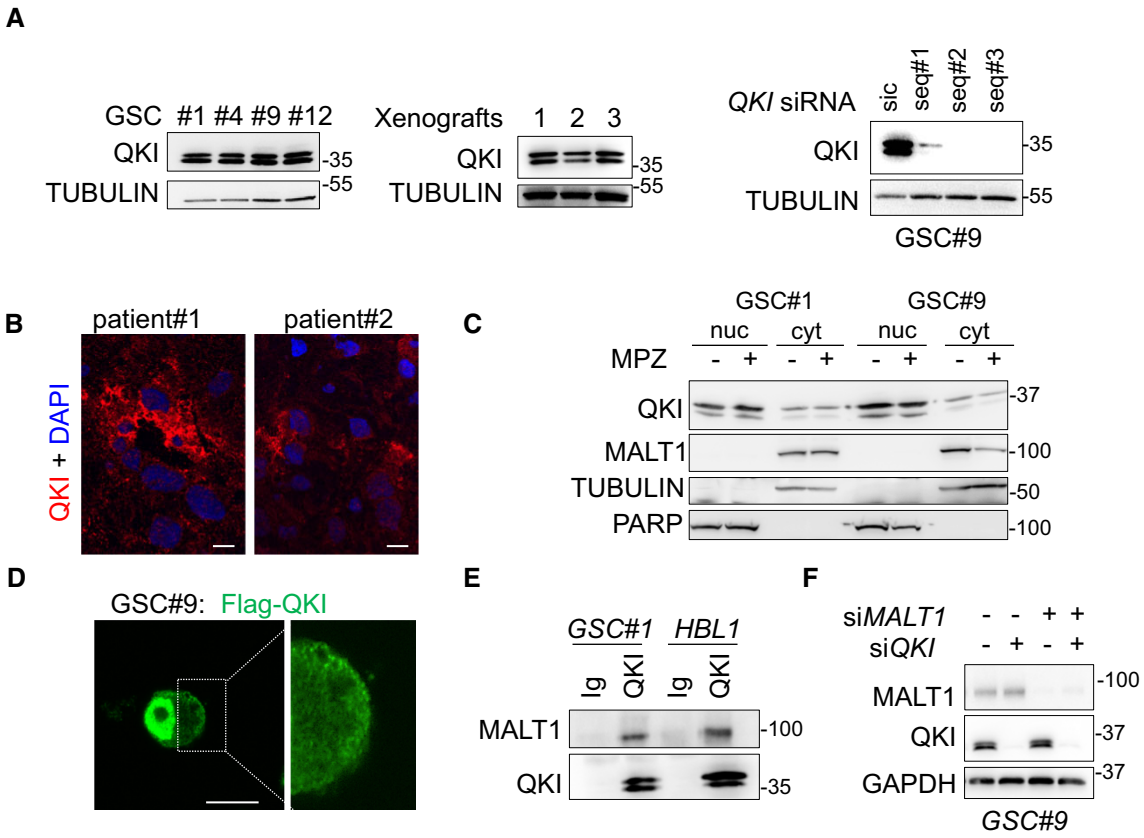

Figure EV4. Characterization of the RNA-binding protein QKI in glioblastoma cells.

A Western blot analysis of QKI in total protein lysates from GSC #1, #4, #9, #12, and from GSC-xenografted tumors. Alternatively, GSC#9 were transfected with sic or si*QKI* using three different duplexes. TUBULIN served as a loading control.

B Confocal analysis of QKI immunostaining (red) in glioblastoma tissue sections from two patients. Nuclei (DAPI) are shown in blue. Scale bars: 10 μm.

C Western blot analysis of QKI in cytosolic (cyt.) and nuclear (nuc.) cell fractionation from GSC#1 and GSC#9, treated with vehicle (–) and mepazine (MPZ, 20 mM, 1 h). TUBULIN and PARP served as loading controls for each fraction. Each panel was replicated at least twice.

D Confocal analysis of FLAG-QKI (green) localization in transfected GSC#9. Scale bars: 10 μm.

E GSC#1 and HBL1 protein lysates were processed for immunoprecipitation using control immunoglobulins (Ig) and anti-QKI antibodies. Western blots were performed using anti-MALT1 and anti-QKI, as specified.

F GSC#9 were transfected with non-silencing RNA duplexes (sic), *QKI* targeting siRNA duplexes (si*QKI*), *MALT1* targeting siRNA duplexes (si*MALT1*), or double-transfected with si*QKI* and si*MALT1* and analyzed 72 h later. Knockdown efficiency was checked by Western blot analysis using the indicated antibodies.

Source data are available online for this figure.

2) Maghe C et al., The paracaspase MALT1 controls cholesterol homeostasis in glioblastoma stem-like cells through lysosome proteome shaping. Cell Reports, in revision, 2023.

I participated in the conception and design of the study. I acquired, analyzed, and interpreted the generated data. I also contributed to the redaction of the article.

In this study, I pursued the description of the functions of MALT1 on endo-lysosomes homeostasis and GSCs cell fitness. By reanalyzing previously published RNAseq data and coupling it to proteomic description of MALT1-inhibited GSCs, I uncovered that GSCs rely on a tightly balanced cholesterol homeostasis for their survival. By establishing the LysoIP technique in our cellular model, I demonstrated that MALT1 modulates the abundance of essential cholesterol transporters at the surface of lysosomes, further regulating GSCs homeostasis.

By combining the proteomic definition of GSCs and of the purified lysosomal compartment upon genetic and pharmacologic inhibition of MALT1, we uncovered the lysosomal-cholesterol transport machinery as central in GSCs survival. Notably, the Niemann-Pick type C1 (NPC1) protein, major lysosomal cholesterol exporter, was dispersed from the degradative organelle. Using microscopy techniques coupled to biochemical assays, we demonstrated the sequestration of cholesterol in lysosomes of MALT1-inhibited GSCs. Autophagy blockade, transcriptional upregulation of the cholesterol synthesis pathway as well as cell death induced by loss of NPC1 lysosomal localization were rescued by addition of exogenous cholesterol, placing this lipid at the intersection between lysosomal homeostasis and GSCs fate. Consecutively, the direct inhibition of NPC1 activity resulted in the specific elimination of GSCs, emphasizing the functions of the lysosomal cholesterol handling machinery in GSCs' life and death decisions.

Together, our results identify the role of MALT1 on lysosomal cholesterol handling and its implications on GSCs survival.

The paracaspase MALT1 controls cholesterol homeostasis in glioblastoma stem-like cells through lysosome proteome shaping

Clément Maghe[1,2], Kilian Trillet[1,2], Gwennan André-Grégoire[1,2,3], Mathilde Kerhervé[1,2], Laura Merlet[1,2], Kathryn A Jacobs[1,2], Kristine Schauer[4], Nicolas Bidère[1,2], Julie Gavard[1,2,3,5,*]

[1] Team SOAP, CRCI[2]NA, Nantes Université, Inserm, CNRS, Université d'Angers, Nantes, 44000, France

[2] Equipe Labellisée Ligue Nationale Contre le Cancer, Paris, 75013, France

[3] Institut de Cancérologie de l'Ouest (ICO), Saint-Herblain, 44800, France

[4] Institut Gustave Roussy, Université Paris-Saclay, Inserm, CNRS, Villejuif, 94800, France

[5] Lead Contact, CRCI[2]NA, 8 quai Moncousu, Nantes, 44000, France

* Corresponding Author, julie.gavard@inserm.fr

SUMMARY

Glioblastoma stem-like cells (GSCs) compose a tumor-initiating and -propagating population, remarkably vulnerable to variation in the stability and integrity of the lysosomal compartment. Previous work showed that the expression and activity of the paracaspase MALT1 control GSC viability via lysosome abundance. However, the underlying mechanisms remain elusive. By combining RNAseq with proteome-wide label-free quantification, we now report that MALT1 repression in patient-derived GSCs alters the homeostasis of cholesterol, which accumulates in late endosomes (LE)-lysosomes. This failure in cholesterol supply culminates in cell death and autophagy defects, which can be partially reverted by providing exogenous membrane-permeable cholesterol to GSCs. From a molecular standpoint, a targeted lysosome proteome analysis unraveled that Niemann-Pick type C (NPC) lysosomal cholesterol transporters are diluted when MALT1 is impaired. Accordingly, we found that NPC1/2 inhibition and silencing partially mirror MALT1 loss-of-function phenotypes. This supports the notion that GSC fitness relies on lysosomal cholesterol homeostasis.

INTRODUCTION

Glioblastoma (GB) is the most common and aggressive primary brain tumor in adults, with a median survival rate of around 15 months[1,2]. This aggressiveness can be ascribed to the tumor-initiating and -propagating potential of a subpopulation of cells harboring stem properties, referred to as glioblastoma stem-like cells (GSCs)[3,4]. A growing body of literature now suggests that an intrinsic and tight regulation of the lysosomes is required for sustaining GSC stemness capacities and viability[5–7]. Accordingly, breaking the lysosomal homeostasis has proven efficient in halting GSC growth and triggering GB decline[5,6].

Lysosomes play crucial roles in nutrient and lipid sensing[8–11], as they contribute to the spreading of lipids and cholesterol in intracellular membranes[12,13]. Mutations in the lysosomal cholesterol transporters Niemann-Pick type C, NPC1 and NPC2, provoke abnormal accumulation of cholesterol in the lumen and the limiting membrane of lysosomes, which may ultimately impair neuronal functionalities and culminate in mild-to-severe neurological defects in NPC diseases[14,15]. However, the putative roles of NPC1/2 in brain cancer were not examined.

Cholesterol bioavailability is tightly regulated by actionable checkpoints[16], among which the sterol regulatory element-binding protein-2 (SREBP2) transcription factor. For instance, SREBP2 governs the expression of proteins and enzymes involved in *de novo* cholesterol synthesis and uptake to counteract cellular cholesterol deficits[16,17]. Counterbalancing mechanisms, such as the down-regulation of the ABC family exporters via the inhibition of LXR and RXR transcription factors[16,18], concomitantly occur. Despite these intricate regulatory pathways being explored in other cancers[19], their implications in GB have mostly been limited to *in silico* analysis and expression patterns[20–22]. Nonetheless, lowering intracellular cholesterol concentration by LXR activation was reported lethal to GB cell[23]. However, further description is needed to clarify the dependency of GSCs on cholesterol availability.

Recently, we demonstrated that the paracaspase MALT1, an arginine-protease previously linked with lymphocyte activation and signaling downstream of G-Protein Coupled Receptors and Receptor Tyrosine Kinases[24], regulates GSC viability by maintaining lysosome abundance[5]. However, how precisely MALT1 operates on the

lysosome compartment remains unknown. By combining RNAseq and quantitative proteomic analysis, we now report that the repression of MALT1 activity provokes the dearth in the lysosome loading of cholesterol transporters. Disrupting intracellular cholesterol trafficking by modifying the lysosome compartment might therefore represent a promising opportunity for GSC eradication.

RESULTS

The inhibition of MALT1 triggers the SREBP2 transcriptional program in GSCs.

To investigate the molecular basis for MALT1 influence on the late-endosome (LE)-lysosome fitness[5,25], a dual approach of RNAseq and proteome-wide label-free quantification (LFQ) analysis was conducted in patient-derived GSCs treated with the MALT1 inhibitor mepazine[26] (Figures 1A, S1A-B). The terms "cholesterol biosynthesis", "regulation of cholesterol biosynthesis by SREBP", and "metabolism of steroids" emerged as the top up-regulated pathways identified within the previously published RNAseq dataset[5] (Figure 1B, GSE139018). This enrichment of mRNA akin to cholesterol-related genes was confirmed through gene set enrichment analysis, underscoring cholesterol-associated signatures (Figure 1B). Accordingly, the proteomic analysis highlighted an over-representation of proteins related to "lipid" node, in addition to “spindle”, “actin”, and “RNA” associated networks (Figure 1C, Tables S1-2, ProteomeXchange identifier PXD040862). Given that *de novo* cholesterol synthesis occurs primarily through the mevalonate pathway[27], we next compared the level of transcripts and proteins involved in this metabolic arm (Figure 1D). Remarkably, most of the enzymes identified with this dual-omic approach were increased when MALT1 was inhibited (Figure 1D). This effect was further validated at the RNA level for 8 out of 10 enzymes, upon MALT1 pharmacological inhibition with two compounds (mepazine and MLT748)[26,28] (Figure 1E). of note, mepazine treatment did not alter the expression of MALT1 in patient-derived GSCs (Figure S1C). MALT1 silencing by RNA interference with two independent duplexes yielded similar responses (Figures 1E, S1D). We also validated these results on the HSD17B7 target in two additional patient-derived GSCs (Figure 1F).

Most of these enzymes are under the control of the SREBP2 transcription factor, which shuttles from the ER to nucleus upon processing and activation (Figure S2A)[29,30]. Interestingly, we found that MALT1 inhibition caused a two-fold increase in the SREBP2 promoter activity (Figure 1G). Furthermore, datamining in the TCGA database uncovered correlation between SREBP2 expression level and probability of survival in GB patients. In fact, SREBP2, but not SREBP1, appeared significantly less expressed in GB samples (Figures S1E-F). Western-blot analysis revealed SREBP2 processing upon mepazine treatment in three patient-derived GSCs, albeit with variable intensities (Figures 1H, S2B). Moreover, the pharmacological inhibition of MALT1 or its silencing led to an increased expression, both at the mRNA and protein levels, of LDLR, the primary entry road for extracellular cholesterol, and a canonical SREBP2 target[12] (Figures 1H-I, S2B). Additionally, CHIP-qPCR of mepazine-challenged GSCs confirmed the activation of endogenous SREBP2 transcription factor (Figure S2C). Both drugs and siRNA had minimal-to-no effects on the levels of SREBP1 canonical targets, including DGAT1, SCD1, and ACLY, in contrast to the enhanced expression of FASN (Figure S2D), suggesting that there may be distinct responses in lipid metabolism-related genes to MALT1 modulation. Taken together, these results indicate that targeting MALT1 preferentially activates the SREBP2 transcriptional program in GSCs, culminating in the expression of the enzymes involved in the synthesis and uptake of cholesterol.

We next examined whether MALT1 inhibition/silencing provoked alterations in intracellular cholesterol concentration and/or its handling in GSCs (Figure S2E). First, we observed that MALT1 silencing resulted in elevated cholesterol concentration in cell lysates (Figure S2F). Likewise, staining with the fluorescent cholesterol probe filipin-III was increased in response to MALT1 inhibition and silencing as assessed by flow cytometry and confocal microscopy (Figures S2G-H), suggesting an overall rise in cholesterol content. We also found that MALT1-silenced GSCs significantly accumulated more LDL, one mechanism for transferring cholesterol (Figure S2I). The same was true with mepazine and MLT748. In contrast, MALT1 inhibition strongly reduced the expression of the cholesterol exporters ABCA1 and ABCG1[16] (Figure S2J). Hence, suppressing MALT1 caused GSCs to deploy an arsenal of strategies to increase total cholesterol concentration via synthesis and uptake, while reducing its export.

Bioavailable cholesterol partially counteracts MALT1 inhibition-induced loss of cell viability

We next explored whether cell death resulting from MALT1 inhibition[5] could be attributed to SREBP2 activation. As anticipated, SREBP2 silencing precluded the mepazine-associated increase in LDLR abundance (Figure S3A). However, the loss of cell viability caused by mepazine was further augmented upon SREBP2 silencing (Figure S3B). Similar results were obtained with cerivastatin-induced inhibition of HMGCR, the rate-limiting enzyme in the cholesterol biosynthetic pathway[31] (Figure S3C). Autophagy obstruction, as illustrated by the accumulation of P62 and LC3B lipidation, was also exacerbated when MALT1 and SREBP2 were inhibited and silenced, respectively (Figures S3D-E). Conversely, SREBP2 siRNA alone was not sufficient to drive loss of cell viability and autophagy defects in GSCs (Figures S3B, S3D-E).

Given that SREBP2 silencing aggravated the MALT1-based drop in cell viability, we postulated that GSCs encountered a defective distribution of intracellular cholesterol, despite its apparent global accumulation. To challenge this hypothesis, cell viability was estimated in mepazine-treated GSCs, upon cholesterol feeding with free or membrane-permeable MβCD-coupled cholesterol[17]. As expected, the depletion of cellular cholesterol with MβCD alone killed GSCs (Figure 2A). MβCD-coupled cholesterol significantly rescued mepazine-treated GSCs, while free cholesterol did not, across three patient-derived GSCs (Figure 2A). By contrast, astrocytes and brain endothelial cells remained unaffected to mepazine and cholesterol treatments (Figure S3F). Moreover, cholesterol similarly restored GSC viability when cultured in serum-free, complete serum, and delipidated serum containing medium (Figure S3F). However, neither free nor complexed cholesterol protected GSCs from cell loss driven by lysosomal-destabilizing drugs (LLOMe and clemastine[6]) and mitochondrial-mediated intrinsic apoptosis activator (raptinal[32])(Figure 2B), suggesting that cholesterol supplementation selectively counteract MALT1 inhibition. Flow cytometry analysis of propidium iodide incorporation further demonstrated that cholesterol feeding robustly rescued GSCs from mepazine-induced death (Figure 2C). Functionally, the levels of SREBP2 cleavage and of its downstream target LDLR were restored upon cholesterol

feeding in MALT1-inhibited GSCs (Figures 2D, S3G). Taken together, these data demonstrated that bioavailable cholesterol rescued cells exposed to MALT1 inhibition.

We then explored how cholesterol supplementation may operate, given that MALT1 inhibition caused an aberrant organization in the LE-lysosome compartment[5] (Figure S3H). First, we found that MALT1 remained outside of the LE-lysosome-enriched fractions in control and mepazine-treated GSCs (Figures S3I-J). Moreover, MALT1 remained inhibited by mepazine and MLT748 in the presence of exogenous cholesterol, as visualized by the cleavage of its substrate HOIL1[33] (Figure S3G), suggesting that cholesterol did not directly alter neither MALT1 activity nor its pharmacological inhibition.

Next, while the abundance of the lysosomal proteins LAMP2 and TMEM192, and the lysotracker signal intensities were not normalized upon cholesterol addition, it did alleviate autophagic defects (Figures 2E-F, S3K). Hence, P62 accumulation and, to a lesser extent, LC3B lipidation, were reduced upon cholesterol addition in the context of MALT1 inhibition (Figures 2F, S3L). This suggests that an exogenous source of permeable cholesterol might circumvent lysosome-based defects but not the upstream deregulation of the LE-lysosomes. The importance of MALT1 in tumor cell expansion was investigated in patient-derived GSC#9 xenografts. Similar to mepazine challenge[5], MLT748 significantly reduced tumor burden (Figure 2G).

MALT1 inhibition edits the lysosomal proteome and affects the lysosomal cholesterol export machinery

Because exogenous cholesterol retrieved several phenotypes resulting from MALT1 blockade, we next investigated whether lysosomes correctly convey cholesterol[9,34–36] when MALT1 activity and expression were repressed. To this end, lysosomes were immunopurified (LysoIP[37]) from GSCs stably expressing HA- and FLAG-tagged lysosomal protein TMEM192 (referred to as HA-lyso and Flag-lyso, respectively, Figures 3A-C). Flag-lyso cells served as control cells for anti-HA LysoIP. LysoIP resulted in the enrichment of the lysosomal compartment, as confirmed by the presence of the lysosomal membrane proteins LAMP2 and NPC1, while proteins typical of other organelles were absent (Figure 3D). A portion of the Golgi protein GM130 was, however, trapped in these fractions.

The lysosomal proteomes from vehicle- and mepazine-treated GSCs were then inspected by LFQ (Figure 3A, ProteomeXchange identifier PXD040855). This unveiled a strong enrichment in lysosomal proteins with few confounding proteins (Table S3). Unlike proteins resident of other organelles, lysosomal proteins were significantly increased in LysoIP samples compared to whole cell lysates (Figures 3E-F, S4A-B). The proteome analysis highlighted autophagy defects in mepazine-treated GSCs, with a substantial accumulation of the classical autophagic receptors TAX1BP1 and P62 (Figures S4C-D). This initial examination of the lysosome proteome supports the notion that MALT1 inhibition leads to a defect in their degradative capacity. A closer exploration into the differentially expressed proteins identified a modest reduction in the levels of most proteins related to cholesterol in lysosomes, like NPC1, NPC2, and SCARB2 transporters, while this was not observed in total lysates (Figures 3G, S4D). The mRNA level of NPC1 and NPC2 were left unchanged in response to MALT1 inhibition and silencing (Figure S4E), indicating a potential shift in the relative repartition of these lysosomal resident proteins, rather than a drop in their expression. This reduced presence of NPC1 in lysosomes was independently validated in cells challenged with MALT1 inhibitors and siRNA (Figure 3H). Indeed, NPC1 was less closely associated with lysosomes, based on confocal analysis and proximity ligation assay (PLA) (Figures 3I, S4F), suggesting a reduction in the number of NPC1-positive lysosomes.

We next explored the role of Quaking (QKI), a KH domain containing RNA binding protein, reported to interact with MALT1[5] and SREBP2[38,39] and to downregulate LE-lysosomes[5,25], in MALT1-induced phenotypes. QKI silencing negated the effects of MALT1 inhibition on the upregulation of LDLR and HSD17B7 (Figures S5A-B). A similar but partial effect of QKI repression was noted on the expression of the cholesterol efflux transporter ABCA1 (Figure S5A). Staining with filipin-III revealed that cholesterol accumulation in mepazine-treated GSCs was attenuated following QKI silencing (Figure S5C). Moreover, LysoIP and PLA assays indicated that the level of NPC1 protein was restored in TMEM192-positive organelles when MALT1 inhibition was combined with QKI silencing (Figures S5D-E). Thus, QKI is required for the impaired association of cholesterol transporters with lysosomes, engendered by MALT1 targeting.

NPC1 blockade partially recapitulates MALT1-repressed phenotypes in GSCs

In silico analysis of the TGCA showed that low NPC1 RNA expression correlated with a significantly higher probability of survival in GB patients (Figure S6A). This was however not significant for NPC2 (Figure S6B). Patient clustering based on RNA expression levels of both NPC1 and NPC2 highlighted an improved probability of survival for patients with low NPC1/2 RNA expression (Figures 4A, S6C). Moreover, patients with low NPC1/2 expression exhibited higher SREBP2 RNA expression, linked to a higher probability of survival (Figure S6D).

We next explored whether the change in NPC1/lysosome ratio could execute MALT1-related cell death in GSCs. As expected, U18666A, a classical NPC1 inhibitor[40], promoted substantial SREBP2 processing and LDLR expression[40] (Figure 4B). Likewise, reporter assays indicated that SREBP2 was activated upon NPC1 blockade (Figure 4C). Thus, MALT1 inhibition paralleled both effects of NPC1 inhibition on SREBP2 and LDLR, albeit to a lesser extent. Moreover, cholesterol, as assessed by bioluminescent assay and staining with filipin-III, was globally increased in NPC1-silenced GSCs (Figures 4D-F). Interestingly, filipin-III-stained cholesterol accumulated in TMEM192-positive lysosomes upon NPC1 inhibition and silencing, similarly to cells exposed to MALT1 targeting drugs and siRNA (Figure 4F). The levels of the lipid lysobisphosphatidic acid (LBPA), which significantly accumulates in NPC1-inhibited cells[41], also augmented with the repression of MALT1 (Figure 4G). This indicates shared responses to MALT1 and NPC1 suppression in GSCs, although with varying amplitude. However, hindering NPC1 and NPC2 did not recapitulate the lysosomal increase observed when MALT1 activity/expression was abrogated (Figures 4H, S6E). The accumulation of the autophagic receptor P62 was nonetheless phenocopied by the use of U18666A (Figure 4H), suggesting that lysosomes from MALT1 and NPC1-inhibited GSCs may feature similar degradative defects. Likewise, U18666A treatment and the silencing of NPC1 and NPC2 significantly reduced GSC viability (Figures 4I-J, S6F). Of note, blocking MALT1 proved more effective at driving cell death than targeting NPC transporters, suggesting possible, additional mediators, such as the number of lysosomes themselves and/or their permeability extent. U18666A was not as toxic in astrocytes and brain endothelial cells (Figures S6F-G), recapitulating the neutral impact

of mepazine[5]. In line with this, Jurkat and BJAB lymphocytes without intrinsic MALT1 activity were left intact, unlike the MALT1-dependent OCI-Ly3 lymphoma cells[42,43] (Figure S6G), raising the possibility of a causal link between MALT1 activity and sensitivity to U18666A. To evaluate the potential of targeting NPC1 in GB, xenograft model was revisited with U18666A administration, which significantly reduced plasmatic cholesterol concentration (Figures 4K-L). Similar to mepazine[5] and MLT748, tumor growth was lessened, underscoring the importance of lysosomal cholesterol transport for GB growth.

DISCUSSION

Taken together, our results lend support to an underestimated role of MALT1 in the regulation of intracellular cholesterol equilibrium. Indeed, suppressing MALT1 activity/expression causes a profound remodeling of the LE-lysosomal compartment, accompanied by the retention of cholesterol and subsequent failure in its intracellular delivery. These defects ultimately culminate in GSC's demise. Concomitantly to an accumulation of intracellular cholesterol, MALT1-repressed cells deploy a myriad of strategies to cope with cholesterol demands[16,30]. Our results suggest that MALT1-inhibited GSCs launch a compensatory program to counteract cholesterol retention. In a MALT1-suppressed context, hampering SREBP2-mediated cholesterol synthesis with RNA interference or cerivastatin[31], aggravates both autophagy defects and cell death in GSCs. This highlights the strong dependency of these cells on finely-tuned cholesterol homeostasis. As U18666A and MLT748 proved efficacy in reducing tumor growth in xenografted mice, combining the targeting of MALT1 and cholesterol supply may therefore represent a valid strategy for GSC eradication. However, one caveat with the canonical use of statins resides in the reported adverse effects on non-tumor cells, like astrocytes[23,44]. Hence, more selective cholesterol-lowering agents may be valuable[23].

Our data identify that MALT1-inhibited cells experience a deficiency in cholesterol handling, likely due to the reduced levels of cholesterol transporters within lysosomes. We provide evidence that NPC1 abundance is reduced within these organelles while cellular expression remains steady, suggesting that MALT1 inhibition may cause the paucity of cholesterol transporters in lysosomes. Paralleling the situation in NPC-

patients with mutations affecting protein folding or ability to anchor in lipid-rich membranes[45], it is plausible that NPC1 is retained in the ER. Although we cannot rule out its rerouting to different cellular membranes, NPC1 might alternatively become diluted in the pool of newly generated lysosomes. Notably, QKI silencing, which attenuates MALT1-associated lysosomal defects, also mitigates the dispersal of NPC1 from lysosomes. In keeping with this notion, MALT1 silencing might create NPC1-exhausted lysosomes, making the as-produced lysosome population less prone to export cholesterol[13,35,36]. Arguing in favor of the apparition of a pool of dysfunctional NPC1-defective lysosomes, targeted proteomic highlights an autophagy signature. This aligns with previous studies that demonstrate the pronounced autophagic defects in NPC1-null models[9,46]. Overall, the increased abundance of abnormal lysosomes results in a widespread accumulation and sequestration of cholesterol, which subsequently contribute to most of the MALT1-dependent phenotypes.

How exactly the cholesterol inflation in lysosomes leads to cell death remains to be elucidated. Paralleling lysosomal storage diseases, where cholesterol is trapped in lysosomes[9,36], MALT1 suppression reiterates traits seen in NPC diseases, including the accumulation of cholesterol in lysosomes, lysosomal membrane fragility, and compromised proteolysis capacities[9,46,47]. The resulting cholesterol depletion in other intracellular compartments, the potential disorganization in cellular membranes, and the disassembly of essential signaling pathways could globally weaken cell fitness[16,21].

Taken together, our data substantiate the notion that the viability of MALT1-active GSCs hinges on effective cholesterol distribution. These cells are ultimately vulnerable to failure in the cholesterol dispatch, as blocking the NPC1 transporter and/or increasing the number of lysosomes as storage sites prove to be lethal.

LIMITATIONS OF THE STUDY

This study did not establish the exact mechanistic link between MALT1 and cholesterol regulation, albeit several mediator hints were identified (QKI, SREBP2, NPC1). Detailed studies of the lysosomal compartment could help define the precise role of NPC1, notably its influence on ER-lysosome cholesterol transfer as an alternate source besides LDLR uptake. Non-GSC models, such as astrocytes and endothelial cells, were used

only with parsimony to control for the effects of MALT1. It will be of paramount importance to next evaluate the role of MALT1 on cholesterol distribution in non-cancer contexts, notably upon MALT1 physiological activation. Ultimately, further research is essential to explore the *in vivo* translation of our discoveries, with a particular focus on understanding the contribution of cholesterol supply and overall homeostasis.

Acknowledgements. We are grateful to SOAP team members (CRCI2NA, Nantes, France), especially Agniezska Barbach and Lucas Ottero. We also thank Cédric Broussard, Johanna Bruce, Philippe Chafey, and François Guillonneau, from Proteom'IC facility, Université Paris Cité, CNRS, INSERM, Institut Cochin, F-75014 PARIS, France (supported by the DIM Thérapie Génique Paris Ile-de-France Région, IBiSA, and the Labex GR-Ex) for performing sample preparation, acquisition, and analysis. We are also grateful to Cédric Le May, Xavier Prieur, and Thibaud Sotin (L'Institut du Thorax, Nantes, France) for technical advices, as well as Laetitia Durand and François Paris ($CRCI^2NA$, Nantes, France). We would like to acknowledge the core-facilities from UMS Biocore, Nantes, France (MicroPICell ANR-10-INBS-04 and Cytocell).

Financial support. This work was supported by Fondation ARC contre le Cancer, INCa PLBIO (2019-151, 2019-291, 2023-044, INCa PAIR-CEREB INCa_16285), Ligue Nationale Contre le Cancer (EL2022) and Comités Ligue 35, 44, 49, 72, 85, and Region Pays de la Loire. CM, MK, and LM received a fellowship from Ligue Contre le Cancer, KAJ from Fondation ARC. The team is part of the SIRIC ILIAD (INCa-DGOS-Inserm_12558).

Author contribution. C.M., conception and design, acquisition and visualization of data, analysis and interpretation of data, draft of the article. K.T., G.A.G., M.K., L.M., K.A.J., acquisition of data, analysis and interpretation of data. K.S. provided essential reagents and interpretation of data. N.B., conception and design, analysis and interpretation of data, draft the article. J.G., conception and design, analysis and interpretation of data, write the article. All authors approved the manuscript.

Declaration of interests. The authors declare no competing interests.

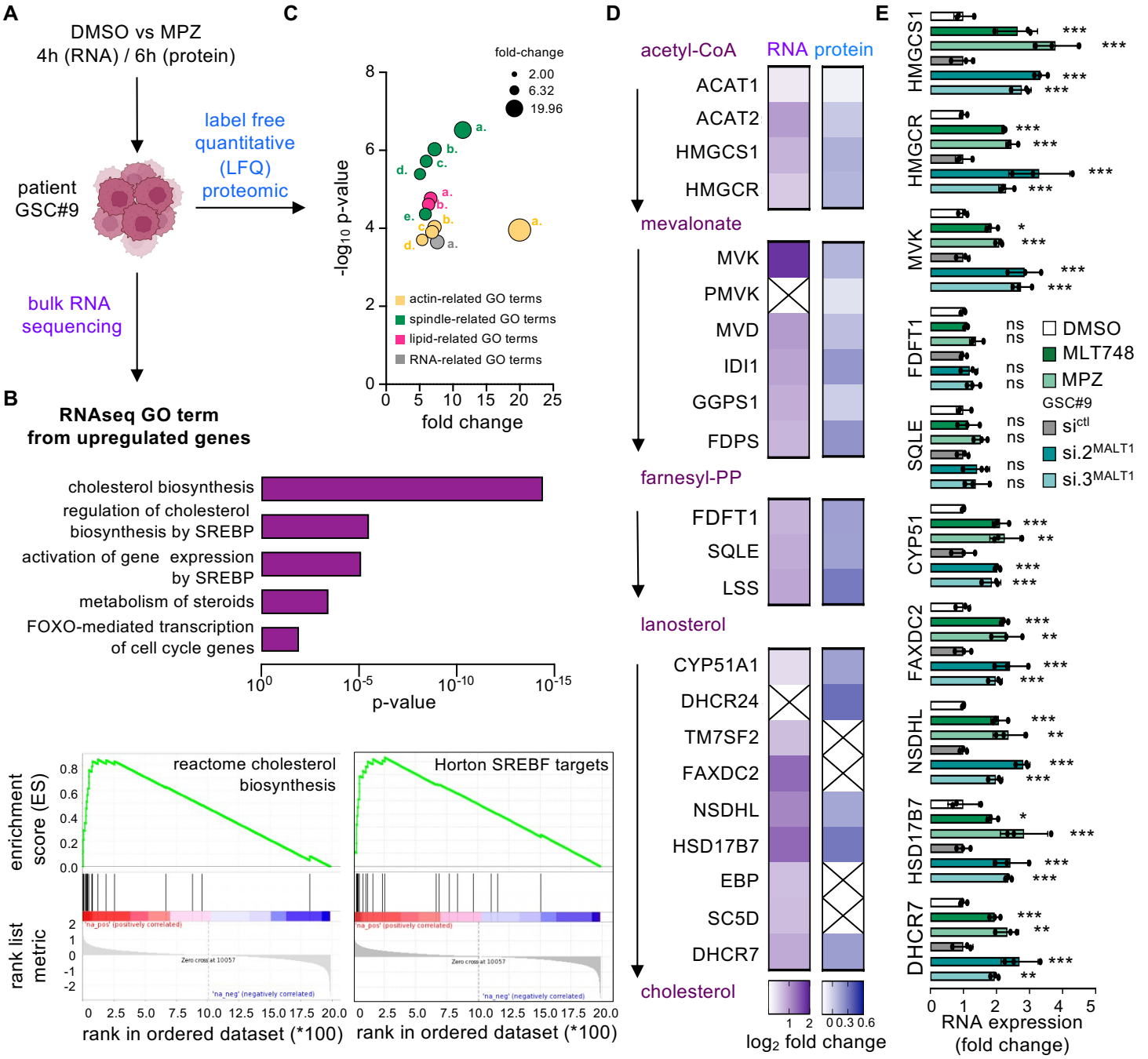
A
DMSO vs MPZ
4h (RNA) / 6h (protein)
patient GSC#9
label free quantitative (LFQ) proteomic
bulk RNA sequencing
B
RNAseq GO term from upregulated genes
cholesterol biosynthesis
regulation of cholesterol biosynthesis by SREBP
activation of gene expression by SREBP
metabolism of steroids
FOXO-mediated transcription of cell cycle genes
p-value
reactome cholesterol biosynthesis
Horton SREBF targets
enrichment score (ES)
rank list metric
rank in ordered dataset (*100)
C
fold-change
2.00
6.32
19.96
-log10 p-value
fold change
actin-related GO terms
spindle-related GO terms
lipid-related GO terms
RNA-related GO terms
D
acetyl-CoA
RNA protein
ACAT1
ACAT2
HMGCS1
HMGCR
mevalonate
MVK
PMVK
MVD
IDI1
GGPS1
FDPS
farnesyl-PP
FDFT1
SQLE
LSS
lanosterol
CYP51A1
DHCR24
TM7SF2
FAXDC2
NSDHL
HSD17B7
EBP
SC5D
DHCR7
cholesterol
log2 fold change
E
HMGCS1
HMGCR
MVK
FDFT1
SQLE
CYP51
FAXDC2
NSDHL
HSD17B7
DHCR7
DMSO
MLT748
MPZ
GSC#9
sictl
si.2MALT1
si.3MALT1
RNA expression (fold change)
F
DMSO
MPZ
HSD17B7 RNA expression (fold change)
GSC#4
GSC#6
G
DMSO
MLT748
MPZ
SREWT/SREMut
ns (0.051)
GSC#9
H
DMSO
MPZ
FL
SREBP2
cleaved
GAPDH
LDLR
GAPDH
GSC#4
GSC#6
GSC#9
I
DMSO
MLT748
MPZ
sictl
si.2MALT1
si.3MALT1
LDLR RNA expression (fold change)
GSC#9
GSC#4
GSC#6

Figure 1

Figure 1. The inhibition of MALT1 triggers the SREBP2 transcriptional program in GSCs

(A-D) Patient-derived glioblastoma stem-like cells GSC#9 received vehicle (DMSO) or MALT1 inhibitor (MPZ, 20μM). (A) Workflow of the dual RNAseq transcriptomic (n=3) and LFQ proteomic (n=4) approach. (B, top) REAC enrichment analysis of the top upregulated pathways from RNAseq. (B, bottom) Upregulated genes (fold-change > 1.5) analyzed for gene set enrichment analysis (GSEA). (C) Differentially upregulated proteins analyzed with Pantherdb[48]. GO terms are in Table S1. (D) Heatmap of cholesterol synthesis pathway genes and proteins expression. Cross: non-identified hits.

(E) RT-qPCR analysis of the indicated targets in GSC#9 treated for 4h with DMSO, MPZ (20μM), and MLT748 (5μM). Alternatively, cells received non-silencing (si^{ctl}) and 2 duplexes targeting MALT1 (si^{MALT1}) for 3 days. Data were normalized to housekeeping genes (HPRT1, ACTB).

(F) RT-qPCR analysis of HSD17B7 in the indicated GSCs treated as in (E).

(G) SREBP2 reporter activity was evaluated in GSC#9 treated for 16h with DMSO, MPZ (20μM), and MLT748 (5μM).

(H) Western-blot analysis of SREBP2 and LDLR in the indicated GSCs treated for 3h and 24h, respectively, with DMSO and MPZ (20μM). Green and red arrowheads: FL (full length) and cleaved SREBP2, respectively.

(I) RT-qPCR analysis of LDLR in the indicated GSCs treated as in (E).

All panels are representative of n=3, unless otherwise specified. t-test and ANOVA, *p<0.05, **p<0.01, ***p<0.001.

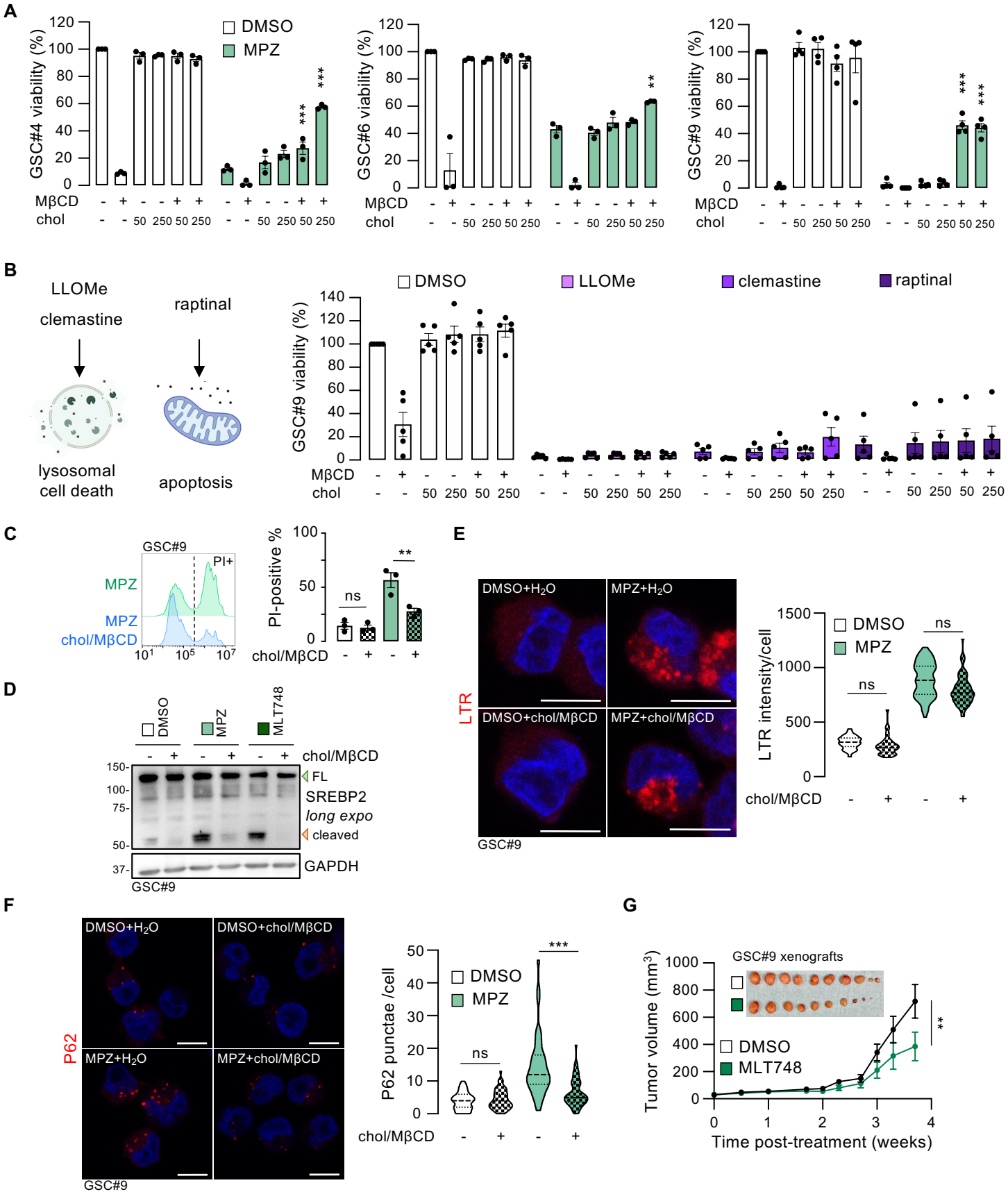
A
GSC#4 viability (%)
GSC#6 viability (%)
GSC#9 viability (%)
DMSO
MPZ
MβCD
chol
B
LLOMe
clemastine
raptinal
lysosomal cell death
apoptosis
C
GSC#9
PI+
MPZ
chol/MβCD
PI-positive %
ns
D
MLT748
chol/MβCD
FL
SREBP2
long expo
cleaved
GAPDH
E
DMSO+H2O
MPZ+H2O
DMSO+chol/MβCD
MPZ+chol/MβCD
LTR
LTR intensity/cell
F
P62
P62 punctae /cell
G
GSC#9 xenografts
Tumor volume (mm3)
Time post-treatment (weeks)

Figure 2

Figure 2. Bioavailable cholesterol partially counteracts MALT1 inhibition-induced cell death

(A) Cell viability in the indicated GSCs pretreated with DMSO and MPZ (20μM, 1h), and challenged for 48h with vehicle (H_2O), MβCD (0.1%), and either cholesterol alone (50 and 250μM) or in complex with MβCD (chol/MβCD) (n≥3).

(B) Schematic representation of the lysosomal-destabilizing (LLOMe, 1μM, 1h and clemastine, 20μM, 1h) and pro-apoptotic (raptinal, 2μM, 1h) drugs used. Cell viability as in (A) (n=5).

(C) Propidium iodide (PI) incorporation by flow cytometry in GSC#9 as in (A).

(D) Western-blot analysis of SREBP2 in GSC#9 pretreated for 1h with DMSO, MPZ (20μM), and MLT748 (5μM), and challenged for 3h with H_2O and chol/MβCD (250μM). Green and red arrowheads: FL (full length) and cleaved SREBP2, respectively.

(E-F) Confocal analysis of LysoTracker (LTR, E) and P62 (F) staining in GSC#9 pretreated for 1h with DMSO and MPZ (20μM), and challenged for 16h with H_2O and chol/MβCD (250μM). Scale bar: 10μm. Violin representations: quantification of LTR intensity/cell (n>71) and P62 punctae/cell (n>39).

(G) Nude mice were implanted with GSC#9 and treated with DMSO or MLT748 (4mg/kg) daily, once tumors were palpable. Tumor volume was measured twice a week. Inset: end-point tumors (n=5 mice/group).

All panels are representative of n=3, unless otherwise specified. t-test and ANOVA, *p<0.05, **p<0.01, ***p<0.001.

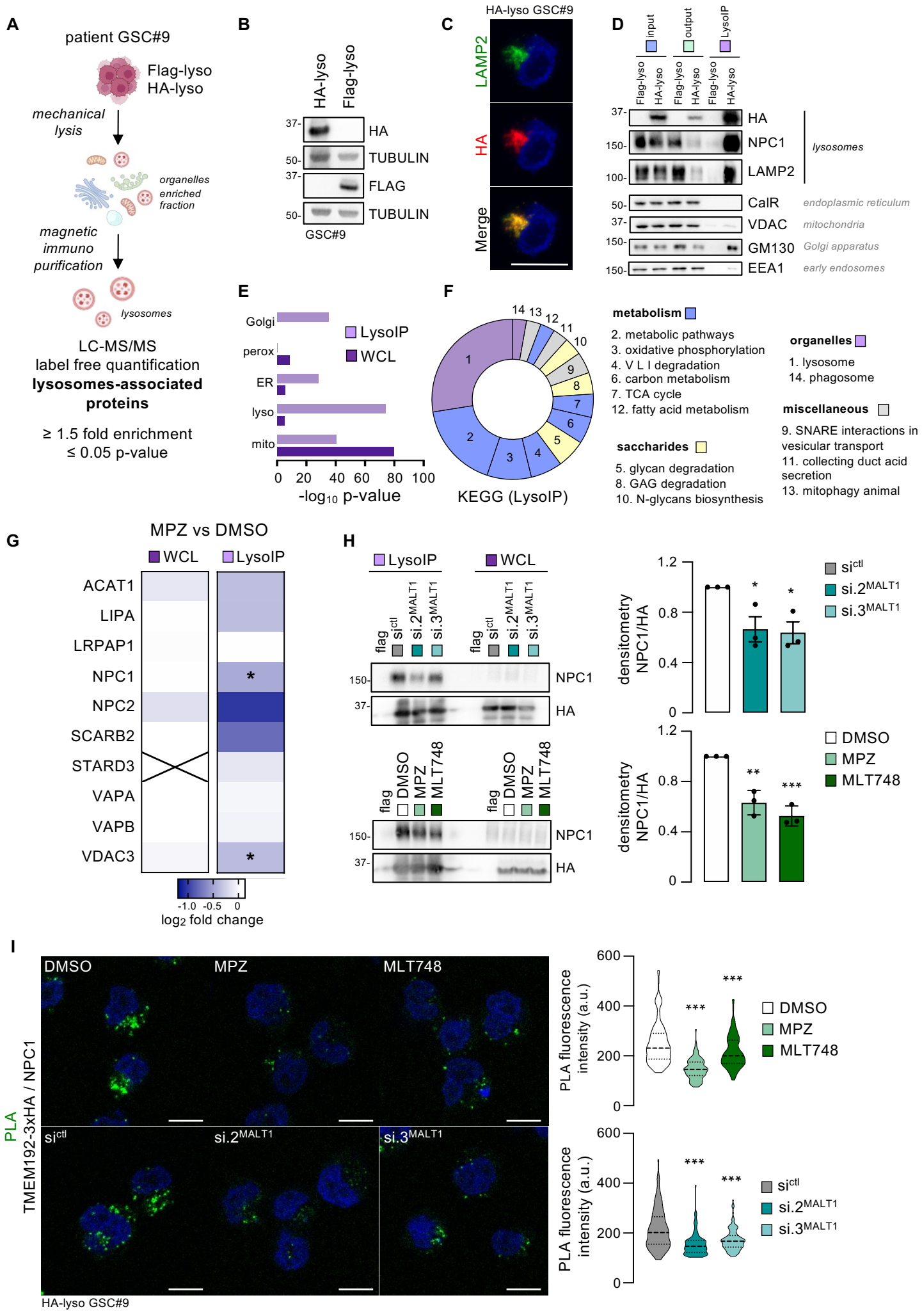
A
patient GSC#9
Flag-lyso
HA-lyso
mechanical lysis
organelles enriched fraction
magnetic immuno purification
lysosomes
LC-MS/MS
label free quantification
lysosomes-associated proteins
≥ 1.5 fold enrichment
≤ 0.05 p-value
B
HA-lyso
Flag-lyso
HA
TUBULIN
FLAG
TUBULIN
GSC#9
C
HA-lyso GSC#9
LAMP2
HA
Merge
D
input
output
LysoIP
Flag-lyso
HA-lyso
HA
NPC1
LAMP2
lysosomes
CalR
endoplasmic reticulum
VDAC
mitochondria
GM130
Golgi apparatus
EEA1
early endosomes
E
Golgi
perox
ER
lyso
mito
LysoIP
WCL
-log10 p-value
F
KEGG (LysoIP)
metabolism
2. metabolic pathways
3. oxidative phosphorylation
4. V L I degradation
6. carbon metabolism
7. TCA cycle
12. fatty acid metabolism
saccharides
5. glycan degradation
8. GAG degradation
10. N-glycans biosynthesis
organelles
1. lysosome
14. phagosome
miscellaneous
9. SNARE interactions in vesicular transport
11. collecting duct acid secretion
13. mitophagy animal
G
MPZ vs DMSO
WCL
LysoIP
ACAT1
LIPA
LRPAP1
NPC1
NPC2
SCARB2
STARD3
VAPA
VAPB
VDAC3
log2 fold change
H
LysoIP
WCL
flag
sictl
si.2MALT1
si.3MALT1
NPC1
HA
DMSO
MPZ
MLT748
densitometry NPC1/HA
I
DMSO
MPZ
MLT748
PLA
TMEM192-3xHA / NPC1
sictl
si.2MALT1
si.3MALT1
HA-lyso GSC#9
PLA fluorescence intensity (a.u.)

Figure 3

Figure 3. MALT1 edits the lysosomal proteome and affects the lysosomal cholesterol export machinery

(A) LFQ proteomic after anti-HA immunopurification (LysoIP) in GSC#9 stably expressing the lysosomal protein TMEM192 (HA- or Flag-lyso); fold-changes on HA/Flag ratio (n=4).

(B-C) Western-blot (B) and confocal (C) analysis as indicated in Flag-lyso and HA-lyso GSC#9. Scale bar: 10µm.

(D) Western-blot analysis as indicated in Flag-lyso or HA-lyso GSC#9 inputs, outputs, and LysoIP.

(E) GO:CC enrichment analysis from the whole cell lysate (WCL) and LysoIP proteomics analysis.

(F) KEGG enrichment analysis of lysosome-associated proteins (fold-change >1.5 and p-value ≤0.05, in HA/Flag ratio).

(G) Heatmap of KEGG: Cholesterol Metabolism hits from WCL and LysoIP in HA-lyso GSC#9 treated with DMSO and MPZ (20µM, 6h). Cross: not-identified candidates.

(H) Western-blot analysis of NPC1 from Flag-lyso and HA-lyso GSC#9 LysoIP and WCL. Top: cells transfected with non-silencing (si^{ctl}) and 2 duplexes targeting MALT1 (si^{MALT1}) for 3 days. Bottom: cells treated for 6h with DMSO, MPZ (20µM), and MLT748 (5µM). Densitometric analysis of NPC1 level normalized to TMEM192-3xHA (HA).

(I) Confocal analysis of Proximity Ligation Assay (PLA) between TMEM192-3xHA and NPC1. HA-lyso GSC#9 were treated as described in (H). Scale bar: 10µm. Violin representations: quantification of PLA signal intensity/cell (n>108).

All panels are representative of n=3, unless otherwise specified. ANOVA, *p<0.05, **p<0.01, ***p<0.001.

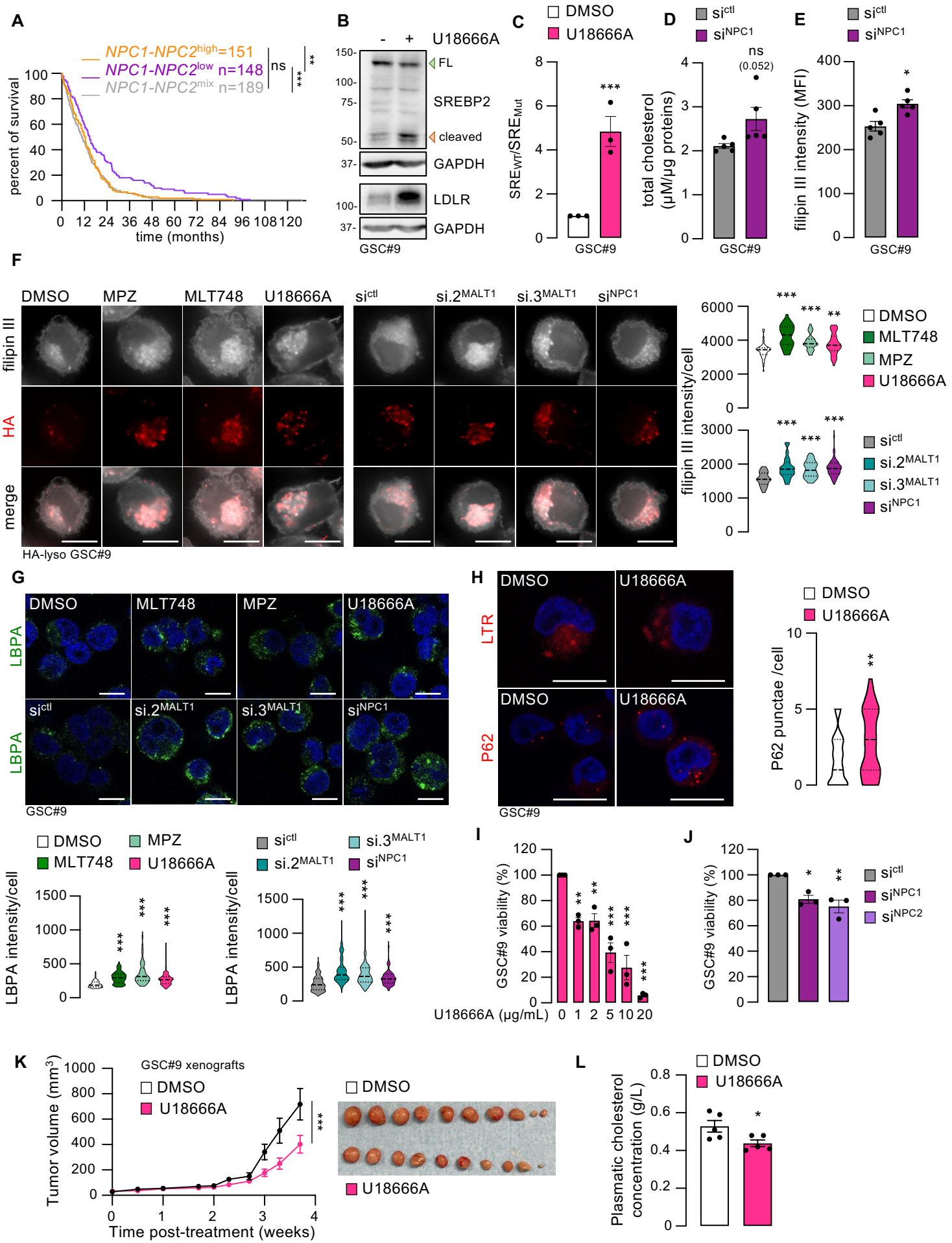
A
NPC1-NPC2high=151
NPC1-NPC2low n=148
NPC1-NPC2mix n=189
ns
***
**
percent of survival
time (months)
B
U18666A
FL
SREBP2
cleaved
GAPDH
LDLR
GAPDH
GSC#9
C
DMSO
U18666A
SREWT/SREMut
GSC#9
D
sictl
siNPC1
ns
(0.052)
total cholesterol (µM/µg proteins)
GSC#9
E
sictl
siNPC1
filipin III intensity (MFI)
GSC#9
F
DMSO
MPZ
MLT748
U18666A
sictl
si.2MALT1
si.3MALT1
siNPC1
filipin III
HA
merge
HA-lyso GSC#9
filipin III intensity/cell
G
LBPA
GSC#9
LBPA intensity/cell
H
LTR
P62
GSC#9
P62 punctae /cell
I
GSC#9 viability (%)
U18666A (µg/mL)
J
GSC#9 viability (%)
siNPC2
K
GSC#9 xenografts
Tumor volume (mm3)
Time post-treatment (weeks)
L
Plasmatic cholesterol concentration (g/L)

Figure 4

Figure 4. NPC1 blockade partially recapitulated MALT1-repressed phenotypes in GSCs

(A) Kaplan-Meier curve for 488 GB patients (TCGA Agilent-4502A dataset), grouped based on *NPC1* and *NPC2* mRNA levels low (purple), high (orange), or mixed (grey). Log-rank p-values are indicated.

(B) Western-blot analysis of SREBP2 and LDLR in GSC#9 treated 3h and 24h, respectively, with DMSO and U18666A (2µg/mL). Green and red arrowheads: FL (full length) and cleaved SREBP2, respectively.

(C) SREBP2 reporter activity in GSC#9 treated as in (B) for 16h.

(D-E) Total cholesterol level in GSC#9 transfected with non-silencing (si^{ctl}) and NPC1 targeting duplexes (si^{NPC1}) for 3 days, measured by bioluminescent assay (ratio cholesterol/proteins, µM/µg, n=5, D), and estimated with filipin-III flow cytometry (mean fluorescence intensity, n=5, E).

(F) Confocal analysis of filipin-III and TMEM192-3xHA (HA) staining in HA-lyso GSC#9 treated for 16h with DMSO, MPZ (20µM), MLT748 (5µM), and U18666A (2µg/mL). Alternatively, cells received si^{ctl}, si^{NPC1}, and si^{MALT1} for 3 days. Scale bar: 10µm. Violin representations: quantification of filipin-III signal intensity/cell (n>38).

(G-H) Confocal analysis of lysobisphosphatidic acid (LBPA) (G), LysoTracker (LTR) (H, Top), and P62 (H, Bottom) in GSC#9 treated as in (F) for 24h. Scale bar: 10µm. Violin representations: quantification of LBPA signal intensity/cell (G, n>112) and P62 punctae/cell (H, n=41).

(I-J) Cell viability was measured in GSC#9 treated for 48h with DMSO and U18666A at the indicated doses (I). Alternatively, cells were transfected for 3 days with si^{ctl}, si^{NPC1}, and si^{NPC2} (J).

(K-L) Nude mice were implanted with GSC#9 in each flank and treated with either DMSO or U18666A (4mg/kg) daily, once tumors were palpable. Tumor volume was measured twice a week (K left). End-point tumors (K right), and plasmatic cholesterol at end-point (L) (n=5 mice/group).

All panels are representative of n=3, unless otherwise specified. t-test and ANOVA, *p<0.05, **p<0.01, ***p<0.001.

Key resources table

REAGENT or RESOURCE	SOURCE	IDENTIFIER
Antibodies		
CALRETICULIN	Cell Signaling Technology	Cat#12238; RRID:AB_2688013
CATHEPSIN D	BD Biosciences	Cat#610800; RRID:AB_398119
EEA1	BD Biosciences	Cat#610456; RRID:AB_397829
FLAG	Cell Signaling Technology	Cat#F1804; RRID:AB_262044
GAPDH	Santa Cruz Biotechnology	Cat#sc-32233; RRID:AB_627679
GM130	Abcam	Cat#ab52649; RRID:AB_880266
HA	Merck Millipore	Cat#H3663; RRID:AB_262051
HA	Cell Signaling Technology	Cat#3724; RRID:AB_1549585
HOIL1	Santa Cruz Biotechnology	Cat#sc-393754
LAMP2	Santa Cruz Biotechnology	Cat#sc-18822; RRID:AB_626858
LBPA	Merck Millipore	Cat#MABT837
LC3B	Cell Signaling Technology	Cat#3868; RRID:AB_2137707
LDLR	Proteintech	Cat#10785-1-AP; RRID:AB_2281164
NPC1	Abcam	Cat#ab134113; RRID:AB_2734695
NPC2	ABclonal	Cat#A5413; RRID:AB_2766221
P62	Cell Signaling Technology	Cat#88588; RRID:AB_2800125
QKI	Santa Cruz Biotechnology	Cat#sc-517305; RRID:AB_2941818
SREBP2	R&D Systems	Cat#MAB7119
SREBP2	Cayman Chemical	Cat#10007663; RRID:AB_2615896
VDAC	Cell Signaling Technology	Cat#4661; RRID:AB_10557420
α-TUBULIN	Proteintech	Cat#66031-1-Ig; RRID:AB_11042766
α-TUBULIN	Santa Cruz Biotechnology	Cat#sc-8035; RRID:AB_628408
Goat Anti-Mouse Ig, Human ads-HRP	Southern Biotech	Cat#1010-05
Goat Anti-Mouse IgG1, Human ads-HRP	Southern Biotech	Cat#1070-05
Goat Anti-Mouse IgG2a, Human ads-HRP	Southern Biotech	Cat#1080-05
Goat Anti-Mouse IgG2b, Human ads-HRP	Southern Biotech	Cat#1090-05
Goat Anti-Rabbit IgG(H+L), Mouse/Human ads-HRP	Southern Biotech	Cat#4050-05
Goat anti-Mouse IgG1 Cross-Adsorbed Secondary Antibody, Alexa Fluor 546	Life Technologies	Cat#A-21123
Goat anti-Rabbit IgG (H+L) Highly Cross-Adsorbed Secondary Antibody, Alexa Fluor 546	Life Technologies	Cat#A-11035
Goat anti-Mouse IgG1 Cross-Adsorbed Secondary Antibody, Alexa Fluor 488	Life Technologies	Cat#A-21121
Goat anti-Rabbit IgG (H+L) Highly Cross-Adsorbed Secondary Antibody, Alexa Fluor 488	Life Technologies	Cat#A-11034
Bacterial and virus strains		
One Shot Stbl3 Chemically Competent E. coli	Life Technologies	Cat#C7373-03
Biological samples		

Patient-derived glioblastoma stem-like cells GSC#1, GSC#4, GSC#6, GSC#9	Harford-Wright E. et al. (2017)	N/A
GSC#9 3xHA	This paper	N/A
GSC#9 2xFLAG	This paper	N/A
Luciferase-GFP-expressing GSC#9	André-Grégoire G. et al. (2022)	N/A
Chemicals, peptides, and recombinant proteins		
Mepazine	ChemBridge	Cat#5216177; CAS: 738596-90-2
MLT-748	Selleck Chemicals	Cat#S8898; CAS: 1832578-30-9
U18666A	Selleck Chemicals	Cat#S9669; CAS: 3039-71-2
Cerivastatin	Merck Millipore	Cat#SML0005; CAS: 143201-11-0
LLOMe	Merck Millipore	Cat#L7393; CAS: 16689-14-8
Clemastine	Selleck Chemicals	Cat#S1847; CAS: 14976-57-9
Raptinal	Merck Millipore	Cat#SML-1745; CAS: 1176-09-6
Cholesterol	Merck Millipore	Cat#C3045; CAS: 57-88-5
Methyl-β-cyclodextrin (MβCD)	Merck Millipore	Cat#C4555; CAS: 128446-36-6
Ponceau S Solution	Santa Cruz Biotechnology	Cat#sc-301558; CAS: 6226-79-5
Paraformaldehyde (PFA)	Electron Microscopy Sciences	Cat#15710; CAS: 30525-89-4
Triton X-100	Merck Millipore	Cat#T9284; CAS: 9036-19-5
Bovine Serum Albumin (BSA)	Merck Millipore	Cat#A2153; CAS: 9048-46-8
DAPI Solution	Life Technologies	Cat#62248; CAS: 28718-90-3
Glycin	Eurobio Scientific	Cat#GEPGLY00-66; CAS: 56-40-6
Filipin Complex from *Streptomyces filipinensis*	Merck Millipore	Cat#F9765; CAS: 11078-21-0
Fibronectin	Merck Millipore	Cat#F1056; CAS: 86088-83-7
Matrigel	Corning	Cat#356237
Critical commercial assays		
BC assay: protein assay kit	Interchim	Cat#FT-40840A
CellTiter-Glo 2.0 Cell Viability Assay	Promega	Cat#G9243
Duolink In Situ Detection Reagents Far Red	Merck Millipore	Cat#DUO92013
Duolink In Situ PLA Probe Anti-Mouse PLUS	Merck Millipore	Cat#DUO92001
Duolink In Situ PLA Probe Anti-Rabbit MINUS	Merck Millipore	Cat#DUO92005
Dual-Luciferase Reporter Assay System	Promega	Cat#E1910
Cholesterol/Cholesterol Ester-Glo Assay	Promega	Cat#J3190
Blood cholesterol measurement kit	Sobioda	Cat#W1306139
Pierce™ Magnetic ChIP Kit	Life Technologies	Cat#26157
Propidium iodide	Life Technologies	Cat#V13245
Deposited data		
Label-free quantification proteomic analysis of total cell lysates from vehicle versus mepazine-treated GSC#9	This paper	PXD040862
Label-free quantification proteomic analysis of immunopurified lysosomes (LysoIP) from vehicle versus mepazine-treated GSC#9	This paper	PXD040855

RNAseq analysis of vehicle versus mepazine-treated GSC#9	Jacobs et al. (2019)	GSE139018
Experimental models: Cell lines		
HEK293T embryonic kidney cells	ATCC	Cat#CRL-3216; RRID:CVCL_0063
Jurkat T-cells E6-1	ATCC	Cat#TIB-152; RRID:CVCL_0367
BJAB Burkitt lymphoma cells	DSMZ	Cat#ACC 757; RRID:CVCL_5711
OCI-LY3 B-lymphoma cells	DSMZ	Cat#ACC 761
hCMEC/D3 brain endothelial cells	Gift from Couraud P.O.	N/A
SVG p12 astrocytes	ATCC	Cat#CRL-8621; RRID:CVCL_3797
Experimental models: Organisms/strains		
Mouse: BALB/CAnN.Cg-Foxn1 nu/nu	Charles River	N/A
Oligonucleotides		
Stealth non-silencing low-GC RNA duplexes CGACAAUUGUGAGGUCUAAACUAUU	Life Technologies	Cat#12935111
siRNA targeting human MALT1 (si.2MALT1) CAGCAUUCUGGAUUGGCAAAUGGAA	This paper	N/A
siRNA targeting human MALT1 (si.3MALT1) CCUGUGAAAUAGUACUGCACUUACA	Life Technologies	Cat#10620312
siRNA targeting human NPC1 (siNPC1) ACCAATTGTGATAGCAATATT	This paper	N/A
siRNA targeting human NPC2 (siNPC2) GGAUGGAGUUAUAAAGGAA	This paper	N/A
siRNA targeting human SREBP2 (siSREBP2) GCGCUCUCAUUUUACCAAATT	This paper	N/A
siRNA targeting human QKI (siQKI) CCTTGAGTATCCTATTGAACCTAGT	Life Technologies	Cat#1299001
Primers for qPCR and ChIP-qPCR, see Table S4	This paper	N/A
Recombinant DNA		
pLJC5-Tmem192-3xHA	Addgene	Cat#102930; RRID:Addgene_102930
pLJC5-Tmem192-2xFLAG	Addgene	Cat#102929; RRID:Addgene_102929
pSynSRE-T-Luc	Addgene	Cat#60444; RRID:Addgene_60444
pSynSRE-Mut-T-Luc	Addgene	Cat#60490; RRID:Addgene_60490
pRL-TK-Renilla-Luc	Promega	Cat#E2241
psPAX2	Addgene	Cat#12260
pCMV-VSV-G	Addgene	Cat#8454
Mixture of pLNT-LucF/pFG12-eGFP	André-Grégoire G. et al. (2022)	N/A
Software and algorithms		
Gliovis Platform	Bowman R. et al. (2017)	Version: 0.20
ImageJ/FIJI	NIH	Version: 2.3.0/1.53q
g:Profiler	Raudvere, U. et al. (2019)	Version: e107_eg54_p17_bf42210

Panther Classification System	Thomas P.D. et al. (2022)	Version: 17.0
Prism 9.3.0.463	GraphPad	Serial number: GPS-2575813-L###-####
FlowJo X	BD Biosciences	Version: 10.0.7r2
NIS-Elements	Nikon	Version: 5.30.03
Other		
N-2 Supplement	LifeTechnologies	Cat#17502048
G-5 Supplement	LifeTechnologies	Cat# 17503012
B-27 Supplement	LifeTechnologies	Cat#17504044
GeneJuice Transfection Reagent	Merck Millipore	Cat#70967
Lipofectamine RNAiMAX Transfection Reagent	LifeTechnologies	Cat#13778150
HALT Protease Inhibitor Cocktail	LifeTechnologies	Cat#78429
Substrat HRP Immobilon Western	Merck Millipore	Cat# WBKLS0500
FUSION FX Imaging System	Vilber	Cat#FUSION-FX7-826.WL / SuperBright
Protran Nitrocellulose Western Blotting Membranes	Amersham	Cat#GE10600002
Dil Labeled Native LDL	Kalen Biomedical, LLC	Cat#NC9839048
ProLong Gold Antifade Mountant	Life Technologies	Cat#P36934
NucleoSpin RNA, Mini Kit for RNA Purification	Macherey-Nagel	Cat#740955
Maxima First Strand cDNA Synthesis Kit for RT-qPCR	Life Technologies	Cat#K1642
PerfeCTa SYBR Green FastMix Low ROX	QuantaBio	Cat#95074-05K
FLUOstar Optima Plate Reader	BMG Labtech	Serial number: 413-3408
Pierce Anti-HA Magnetic Beads	Life Technologies	Cat#88837
LysoTracker™ Red DND-99	Life Technologies	Cat#L7528
Charcoal Stipped Fetal Bovine Serum, Delipidated	Life Technologies	Cat#A3382101
Polybrene	Santa Cruz Biotechnology	Cat#sc-134220

STAR METHODS

Resource Availability

Lead Aontact

Further information and requests for resources and reagents should be directed to and will be fulfilled by the lead contact, Julie Gavard (julie.gavard@inserm.fr).

Materials Availability

This study did not generate new unique reagents.

Data and Code Availability

This paper analyzed existing, publicly available RNAseq data deposited in Gene Expression Omnibus (GEO) under the accession numbers GEO: GSE139018

Raw and processed proteomic data have been deposited at ProteomeXchange with identifiers PXD040862 for whole cell lysate analysis, and PXD040855 for immunopurified lysosomes-targeted proteomic, and are publicly available as of the date of publication

This paper does not report original code.

Any additional information required to reanalyze the data reported in this paper is available from the lead contact upon request.

Experimental model and study participant details

Animals

Animal experiments were approved by the French Government (Ministry of Higher Education and Research, APAFIS#24400-2020022713064016 v2) and conducted in agreement with the European Convention for the Protection of Vertebrate Animals used for Experimental and other Scientific Purposes (ETS 123). Animals had continuous access to food and water, in a specific pathogen-free (SPF) environment with regulated temperature and hygrometry, following a 12h day-night cycle. Xenografts were conducted on six-to-seven-weeks-old female Balb/c Nude mice (BALB/CAnN.Cg-Foxn1 nu/nu, Janvier Labs).

Cell culture

All cells were cultured according to the French Ministry of Higher Education and Research rules under the #DUO10524 authorization. GB patient-derived stem-like cells (GSCs) were dissociated from primary glioblastoma tissue (MACS Dissociator, Miltenyi). All subjects have given their informed consent. This study was approved by the institutional review boards of Sainte-Anne Hospital, Paris, France, and Laennec Hospital, Nantes, France, and performed in accordance with the Declaration of Helsinki Protocol. They were characterized for their self-renewal capabilities, cell surface antigens, expression of stemness markers, their ability to differentiate, and to initiate tumor formation[49]. GSC#1 (mesenchymal, 68-year-old male), GSC#4 (mesenchymal, 76-year-old female), GSC#6 (mesenchymal, 68-year-old male), and GSC#9 (classical, 68-year-old female) were routinely cultured in sphere-forming conditions in serum-free NS34 medium (DMEM-F12, Glutamax, and antibiotics, further supplemented with N2, G5, and B27). HEK293T human embryonic kidney cells, Jurkat E6.1 T lymphocyte cells, SVG-p12 human astrocyte, OCI-Ly3 B-lymphoma cells and BJAB Burkitt lymphoma cells were cultured as per the manufacturer's instructions. Human brain endothelial cells (hCMEC/D3) were a gift from P.O. Couraud (Institut Cochin, Paris, France) and cultured accordingly[50].

Method details

Mice xenograft models

Six-to-seven-weeks-old female Balb/c nude mice (Janvier Labs) were subcutaneously injected in each flank with GFP-Luciferase-expressing $0.5.10^5$ GSC#9[51]. Tumorspheres were dissociated prior to injection to ensure implantation of a single cell suspension in PBS:matrigel (1:1).

Ten days after grafts, mice were treated intraperitoneally 5 times per week with vehicle (10% DMSO in PBS), MLT-748 (4mg/kg), or U18666A (4mg/kg), until a critical point was reached (tumor volume >1000 mm^3). Tumor size was measured twice a week with calipers and tumor volume calculated using the following equation ($width^2$ × length)/2. At euthanasia, tumors were dissected and fixed in PFA. Total blood was collected by intracardiac puncture on EDTA tubes and centrifugated (1000xg, 15min, 4°C) before freezing at −80°C. Blood cholesterol measurement was performed following company instruction (Sobioda).

siRNA transfection

RNA duplexes targeting the respective human genes were transfected using RNAiMAX Lipofectamine. Stealth non-silencing Low-GC RNA duplexes (si^{ctl}) were used as non-silencing control.

Plasmid transfection and lentiviral transduction

SRE-T-Luc, SRE-Mut-T-Luc, and renilla plasmid transfection was performed using the GeneJuice transfection reagent following the manufacturer's instructions. For stable expression of TMEM192-3xHA and TMEM192-2xFLAG, lentiviral particles were produced in HEK-293T cells, according to established procedures[52]. Briefly, cells were transfected with pPAX2 and pVSVg and supernatants were collected after 2 days. Particles were applied on GSC#9 during a 1,000g centrifugation for 90 min in the presence of 8 µg/mL polybrene. For selection, cells were cultured with 1µg/mL puromycin.

TCGA analysis

The Cancer Genome Atlas (TCGA) was interrogated using the Gliovis Platform (http://gliovis.bioinfo.cnio.es)[53]. RNAseq (155 patients) and Agilent 4502A (488 patients) databases were used to investigate data related to SREBP1/2 and NPC1/2, respectively (RNA expression, probability of survival, and number at risks). All subtypes of Grade IV, Glioblastoma were included. Low/High expression groups were set at median expression for each individual gene. They were further classified into 3 groups of High/High, Mixed, and Low/Low NPC1 and NPC2 expression. Again, RNA expression, probability of survival, and number at risks were analyzed.

Cholesterol/MβCD complexes preparation

Cholesterol was dissolved to a final concentration of 5 mM in a solution of 0.1% MβCD prepared in sterile H_2O. The solution was vigorously vortexed, heated at 37°C for 2h, and stored at 4°C.

Cell lysis and western-blots

Cells were harvested on ice, washed in cold PBS, pelleted (500xg, 3 min, 4°C) and lysed in RIPA buffer (25 mM Tris-HCl pH 7.4, 150 mM NaCl, 0.1% SDS, 0.5% Na-Deoxycholate, 1% NP-40, 1 mM EDTA) supplemented with Halt protease inhibitor cocktail for 30 min on ice. Lysates were cleared by centrifugation (10,000xg, 10 min, 4°C) to pellet insoluble debris and nuclei. Protein concentrations in supernatants were determined using a micro-BCA assay kit. An equal amount of proteins (10 µg) was resolved by SDS-PAGE and transferred onto nitrocellulose membranes. Proteins were fixed to the membranes using a Ponceau S solution, and nonspecific protein binding sites were saturated with 5% milk in PBS-Tween 0.05%. Primary (1/1,000 dilution except LAMP2 at 1/5,000, GAPDH at 1/20,000) and secondary (1/5,000 dilution) antibodies were incubated with membranes in a similar blocking solution.

Revelation was performed using Immobilon western chemiluminescent HRP substrate and the Fusion imaging system.

Cellular fractionation

15.10^6 GSC#9 were treated as indicated, washed in PBS, and resuspended in a hypotonic buffer (20 mM HEPES, 1.5 mM $MgCl_2$, 60 mM KCl, in H_2O) containing anti-proteases. Some cells were collected before lysis for whole cell lysate input. Cells were lysed with 15 strokes of a 29-gauge syringe at 4°C. Nuclei were pelleted with a 1,000xg centrifugation for 5 min at 4°C and discarded. The supernantant was centrifuged at 100,000xg for 1h at 4°C (S100). The pellet was washed once with hypotonic buffer at 100,000xg for 1h at 4°C and lysed with RIPA lysis buffer (P100). S100 and P100 fractions were then processed for western blot analysis.

Cell viability and cell death assays

Cell viability was measured using CellTiter-Glo luminescent cell viability assay following the manufacturer's protocol. Experiments were performed in 96-well plates in 100 µL final volume of media. Briefly, GSCs were seeded at 10,000 cells per well in triplicate for 2 days with the indicated drugs and vehicle. Alternatively, GSCs were seeded at 8,000 cells per well in triplicate for each condition and further challenged with siRNA transfection. Viability was read after 3 more days. Experiments were harvested by the addition of 100 µL of the CellTiter-Glo reagent and luminescence was read using a FLUOstar Optima plate reader. For propidium iodide (PI) staining, cells were treated as mentioned and PI (100 µg/mL) was added for 10 min at room temperature according to the manufacturer's protocol. Flow cytometry analyses were performed on FACSCanto II (Cytocell core facility, UMS Biocore, Inserm US16, UAR CNRS 3556, Nantes Université, Nantes, France). All data were analyzed on FlowJo. For cell viability assays using HEK293T human embryonic kidney cells, Jurkat E6.1 T lymphocyte cells, SVG-p12 human astrocytes, hCMEC/D3 human brain endothelial cells, OCI-Ly3 B-lymphoma cells and BJAB Burkitt lymphoma cells, cells were cultured in their routine culture medium containing FBS and processed as GSCs. For each cell line, data were normalized to their respective control DMSO treatment.

Immunofluorescence staining

3.10^5 cells were seeded onto glass slides and fixed for 12 min at room temperature with a solution of 4% paraformaldehyde (PFA) diluted in PBS. Cells were permeabilized using a solution of Triton-X100 (0.2%) diluted in PBS, for 5 min at room temperature. Blocking solution (4% BSA in PBS) was added for 30 min prior to incubation 1h at room temperature with primary antibodies (1/200 dilution in the blocking solution). Secondary antibodies (1/400 dilution in the blocking solution) were applied, and samples were further processed for confocal analysis. For LysoTracker staining, cells were incubated with 100 nM of the probe for 30 min at 37°C before PFA fixation (4%, 12min, room temperature), and further processed for confocal analysis. For dil-LDL uptake, 3.10^5 cells were treated as indicated (16h for drug treatments, 3 days for siRNA transfection), followed by incubation with dil-LDL (5 µg/mL) for 2h at 37°C. Cells were then seeded onto glass slides and fixed for 12 min at room temperature with 4% PFA and further processed for confocal analysis.

Micropatterning

Ring-shaped micropatterned coverslips were prepared using the photolithography method and provided by K. Schauer (Institut Gustave Roussy, Villejuif, France)[54]. For use with GSCs, micropatterned were first coated with 50 µg/mL of fibronectin for 1h at room temperature. Then, 60,000 cells were seeded in NS34 in the presence of 10% FBS. Following 1 hour of incubation at 37°C, coverslips were washed 5 times with culture media to remove non-attached cells. Cells were then incubated overnight at 37°C before fixation

with 4% PFA. Immunofluorescent staining was performed as described and processed for confocal analysis.

Proximity ligation assay (PLA)

PLA was performed using the Duolink *in situ* detection reagents far-red kit, PLA-probe anti-mouse PLUS, and PLA-probe anti-rabbit MINUS, according to the manufacturer's protocol. Briefly, GSCs were treated as indicated (3 days siRNA transfection or 6h drug treatment) and seeded onto glass slides before PFA fixation and Triton-X100 permeabilization. Primary antibodies (anti-HA, 1/1,000 and anti-NPC1, 1/200) were incubated at 4°C for 16h in a humid chamber before processing according to the manufacturer's protocol. Samples were processed for confocal analysis.

Confocal analysis

Except when mentioned, nuclei were stained with DAPI (1/5,000) and slides were mounted with prolong gold anti-fade mounting medium before imaging. Images were acquired on confocal Nikon A1 Rsi, using a 60x oil-immersion lens (IBISA MicroPICell facility, UMS Biocore, Inserm US16, UAR CNRS 3556, Nantes Université, Nantes, France). Unless otherwise specified in figures legends, images were visualized as single confocal plans. All images were analyzed and quantified using the ImageJ software.

Filipin-III staining for imaging and flow cytometry

Cells were seeded onto glass slides and fixed for 12 min at room temperature with a solution of 4% PFA diluted in PBS. PFA was quenched for 10 min at room temperature using a glycine/PBS solution (1.5 mg/mL). The filipin-III stock solution (25 mg/mL in DMSO) was diluted to 0.5 mg/mL in a 4% bovine serum albumin (BSA) solution and added to the cells for 2h at room temperature. Finally, cells were mounted with prolong gold anti-fade mounting medium. Alternatively, cells were incubated with the filipin-III/BSA solution for 30 min prior to antibody incubation. Primary antibodies were diluted in the filipin-III/BSA solution and added for 1h, followed by 30 min with secondary antibodies also diluted in the solution of filipin-III/BSA. No DAPI counterstaining was performed because the excitation wavelength is the same as filipin-III. Slides were imaged on a Zeiss AXIO Observer.Z1. For enhanced resolution, images were further deconvoluted using the Nikon Imaging System (NIS-Elements) software. For FACS analysis, GSCs were similarly processed in 96-V-well plates and using a filipin-III concentration of 0.125 mg/mL diluted in PBS. Fluorescence intensity was measured using the UV 379/28 laser (BD FACSymphony A5, Cytocell core facility, UMS Biocore, Inserm US16, UAR CNRS 3556, Nantes Université, Nantes, France). All data were analyzed with FlowJo.

qPCR analysis

RNA was extracted from 1.10^6 GSCs using the NucleoSpin RNA Plus purification kit. Equal amounts of RNA were reverse-transcribed using the Maxima First Strand cDNA Synthesis kit, and 30 ng of the resulting cDNA was amplified by qPCR using PerfeCTa SYBR Green SuperMix Low ROX. Data were analyzed using the 2-ΔΔCt methods and normalized by the housekeeping genes ACTB and HPRT1. All primers used are listed in Table S4.

ChIP-qPCR

The ChIPq-PCR assay was performed using the Pierce Magnetic ChIP Kit according to the manufacturer's protocol. Briefly, GSC#9 cells were treated with vehicle or MPZ (20 µM) for 6h and samples were crosslinked in a PBS/PFA solution (1%) for 10 min. Glycine was added to quench PFA before PBS washes. Cell pellets were lysed with 100 µL of IP buffer containing anti-proteases before MNase digestion of DNA for 15 min at 37°C. Fragmented DNA was released from cells by sonication using a Bioruptor plus

(Diagenode) device, and parameters were as follows: HIGH setting, 6 cycles of 30 sec ON/30 sec OFF. Supernantants containing fragmented DNA were collected after a 5 min, 9,000xg centrifugation. 10 µL of the DNA-containing supernatant was saved as 10% input control. The remaining 90 µL were incubated with primary antibodies solutions (anti-RNA Pol II, Normal Rabbit IgG, anti-SREBP2, 5 mg/mL) for 16h at 4°C with rotation. 20 µL of magnetic beads were added to each IP reaction and incubated for 2h at 4°C with rotation. A magnetic stand was used to wash the beads. Immunopurified DNA fragments were eluted at 65°C for 40 min and by vortexing every 10 min. Proteins from IP samples and inputs were removed by incubation with proteinase K for 1h30 at 65°C. DNA was recovered using the columns and buffers furnished in the kit. qPCR was performed according to the manufacturer's recommendations. All primers used are listed in Table S4.

RNAseq analysis

5.10^6 GSC#9 cells were treated for 4h with a vehicle (DMSO) or MPZ (20 µM) and snap-frozen on dry ice. Samples and data were processed at Active Motif (Carlsbad, California, USA). Briefly, 2 µg of total RNA was isolated using the Qiagen RNeasy Mini Kit and further processed in Illumina's TruSeq Stranded mRNA Library kit. Libraries are sequenced on Illumina NextSeq 500 as paired-end 42-nt reads. Sequence reads are analyzed with the STAR alignment—DESeq2 software pipeline[5]. The RNAseq data have been deposited to the Gene Expression Omnibus (GEO) platform and are available with the dataset identifier GSE139018.

Luciferase SREBP2 reporter assay

2.10^6 cells were transfected with 2 µg of either pSynSRE-T-Luc (SRE wild-type) or pSynSRE-Mut-T-Luc (SRE-mut), to which SREBP2 cannot bind, in combination with 0.1 µg pRL-TK-Renilla using the GeneJuice transfection reagent. After 24h, cells were seeded in a 96-well plate in triplicate per condition and cultured for further 16h in the presence of the indicated drugs. At the end of the experiment, cells were pelleted and lysed with 30 µL of lysis buffer. 20 µL of the lysate was revealed using the Dual-Glo luciferase assay system following the manufacturer's protocol. Luminescence was measured using a FLUOstar Optima plate reader. Luminescence values were calculated as the ratio SRE_{WT}/SRE_{Mut}, and further normalized to Renilla intensities.

Cholesterol dosage

Cellular cholesterol was measured using the Cholesterol/Cholesterol Ester-Glo Assay Kit following manufacturer's instructions. Briefly, 1.10^5 GSCs were lysed for 30 min at 37°C. A volume of 25 µL of the lysate was used for cholesterol quantification. Cholesterol level was determined by reading luminescence after 1h incubation with cholesterol reductase and cholesterol esterase reagents at room temperature. Cholesterol concentration was extrapolated from a standard curve prepared for each experiment and normalized to protein concentration.

Lysosome immunoprecipitation (LysoIP)

15.10^6 GSCs expressing TMEM192-3xHA were used per condition. TMEM192-2xFLAG expressing cells were used as a control. Each step was conducted at 4°C. After the indicated treatments, cells were washed in cold PBS and centrifuged at 1,000xg for 2 min. Pelleted cells were resuspended in 500 µL cold PBS + anti-proteases and 100 µL were saved for whole cell lysate control. The remaining 400 µL were mechanically lysed with 10 strokes of a 29-gauge syringe and centrifuged at 1,000xg for 2 min. Supernatants containing organelles were incubated with 75 µL of Pierce anti-HA magnetic beads for 15 min under rotation. Beads were then washed 3 times with cold PBS + anti-proteases. For further analysis, beads were eluted twice with 50 µL of elution buffer (50 mM Tris/HCl pH 8.5 with 2% SDS) and boiled at 95°C for 5 min. Eluates were further processed for western blot and proteomic analyses. Alternatively, samples were stored at -80°C.

Label-free quantification (LFQ) proteomic processing and analysis of whole cell lysates

For sample preparation, pelleted cells were solubilized in lysis buffer (2% SDS, 200 mM TEAB, pH 8.5) and heated for 5 min at 95°C. The protein concentration of the supernatants was estimated with a BCA assay. Proteins were then reduced and alkylated with 10 mM TCEP and 50 mM chloroacetamide. Bottom-up experiments' tryptic peptides were obtained by S-Trap Micro Spin Column according to the manufacturer's protocol (Protifi, NY, USA). Briefly, 30 µg of proteins were digested during 14h at 37°C with 1 µg Trypsin sequencing grade (Promega). The S-Trap Micro Spin Column was used according to the manufacturer's protocol. After speed-vacuum drying, eluted peptides were solubilized in 2% trifluoroacetic acid (TFA) and fractionated by strong cationic exchange (SCX) Stage-Tips[55].

Liquid Chromatography-coupled Mass spectrometry analysis (LC-MS) analyses were performed on a Dionex U3000 RSLC nano-LC- system (Thermo Fisher scientific, Les Ulis, France) coupled to a TIMS-TOF Pro mass spectrometer (Bruker Daltonik GmbH, Bremen, Germany). After drying, peptides from SCX Stage-Tip, the 5 fractions were solubilized in 10 µL of 0.1% TFA containing 10% acetonitrile (ACN). 1 µL was loaded, concentrated, and washed for 3 min on a C_{18} reverse phase precolumn (3 µm particle size, 100 Å pore size, 75 µm inner diameter, 2 cm length, from Thermo Fisher Scientific). Peptides were separated on an Aurora C_{18} reverse phase resin (1.6 µm particle size, 100Å pore size, 75 µm inner diameter, 25 cm length mounted to the Captive nanoSpray Ionisation module, IonOpticks, Middle Camberwell Australia) with a 120-minutes overall run time with a gradient ranging from 99% of solvent A containing 0.1% formic acid in milliQ-grade H_2O to 40% of solvent B containing 80% acetonitrile, 0.085% formic acid in mQH_2O. The mass spectrometer acquired data throughout the elution process and operated in DDA PASEF mode with a 1.1 second/cycle, with Timed Ion Mobility Spectrometry (TIMS) mode enabled and a data-dependent scheme with full MS scans in Parallel Accumulation and Serial Fragmentation (PASEF) mode. This enabled a recurrent loop analysis of a maximum of the 120 most intense nLC-eluting peptides which were CID-fragmented between each full scan every 1.1sec. Ion accumulation and ramp time in the dual TIMS analyzer were set to 166 msec each and the ion mobility range was set from 1/K0 = 0.6 Vs cm^{-2} to 1.6 Vs cm^{-2}. Precursor ions for MS/MS analysis were isolated in positive mode with the PASEF mode set to « on » in the 100-1.700 m/z range by synchronizing quadrupole switching events with the precursor elution profile from the TIMS device. Singly charged precursor ions were excluded from the TIMS stage by tuning the TIMS using the otof control software, (Bruker Daltonik GmbH). Precursors for MS/MS were picked from an intensity threshold of 1000 arbitrary units (a.u.) and resequenced until reaching a 'target value' of 20.000 a.u. taking into account a dynamic exclusion of 0.40 s elution gap.

Regarding protein quantification and comparison, mass spectrometry data were analyzed using Maxquant version 1.6.6.0[56]. The database used was a *Human* sequence from the Uniprot databases (release March 2020). The enzyme specificity was that for trypsin. The cleavage specificity was trypsin's with maximum 2 missed cleavages. Carbamidomethylation of cysteines was set as constant modification, whereas acetylation of the protein N terminus and oxidation of methionines were set as variable modifications. The false discovery rate was kept below 1% on both peptides and proteins. Label-free protein quantification (LFQ) was performed using both unique and razor peptides. At least two such peptides were required for LFQ. The "match between runs" (MBR) option was allowed with a match time window of 0.7min and an alignment time window of 20min. For differential analysis, LFQ results from MaxQuant, were imported into Perseus software version 1.6.14.0 (Max-Planck Institute of Biochemistry). Reverse and contaminant proteins were excluded from the bioinformatic analysis. LFQ data were transformed into log_2. A t-test (p-value<0,05) was carried out on proteins and proteins with at least 3 valid values in at least one group. Moreover, PCA (principal component analysis) was performed on all proteins with imputation.

Label-free quantification (LFQ) proteomic processing and analysis of LysoIP

For sample preparation, IP samples were solubilized in lysis buffer (2% SDS, 200 mM Tris-HCl, pH 8.5, 10 mM TCEP, 50 mM chloroacetamide). Bottom-up experiments' tryptic peptides were obtained by S-Trap

Micro Spin Column according to the manufacturer's protocol (Protifi, NY, USA). Briefly: Proteins were digested during 14h at 37°C with 1 µg Trypsin sequencing grade (Promega). The S-Trap Micro Spin Column was used according to the manufacturer's protocol. After speed-vacuum drying, eluted peptides were solubilized in 10 µL of 10% acetonitrile and 0.1% trifluoroacetic acid (TFA).
Liquid Chromatography-coupled Mass spectrometry analysis (LC-MS) analysis was done with similar parameters to the LFQ analysis of the WCL (see previous section), except the peptide separation run time was 60 min, ion accumulation and ramp time were 100ms, and precursors picking for MS/MS: 2,500 arbitrary units (a.u.).
The parameters for protein quantification and comparison were the same as for the LFQ analysis of the WCL, excepted for the MBR option that was not run (see previous section), and for the statistical test used (paired T-test). The mass spectrometry proteomics data have been deposited to the ProteomeXchange Consortium via the PRIDE partner repository with the dataset identifiers PXD040862 (WCL) and PXD040855 (LysoIP).

Proteomic and RNAseq enrichment analysis
Enrichment analysis of the proteomic and RNAseq experiments were performed using g:Profiler[57] (version e107_eg54_p17_bf42210) applying a significance threshold of 0.05. The Panther classification system[48] was also used to identify the main GO:function enriched in the proteomic analysis.

Quantification and statistical analysis
Densitometry and imaging quantifications were performed using the ImageJ software. All graphs were mounted and statistically tested using Prism 9. Unless otherwise specified, error bars on graphs are shown as mean $\pm$ s.e.m. of at least three independent biological replicates. A p-value of <0.05 was considered significant. The RNAseq experiment was performed on three independent biological replicates. All proteomics experiments were performed on four independent biological replicates. Viability assays were performed on three independent experiments, each in triplicate.

Supplementary Tables Legends
Table S1. List of upregulated GO term signatures in the WCL proteomic analysis of MALT1-inhibited GSCs. Related to Figure 1.
Differentially up-regulated proteins from DMSO versus MPZ-treated GSC#9 were analyzed with the Pantherdb[48] pathway browser. Four main GO term signatures were identified as follows: 1. actin (1.a: actin filament network formation, 1.b: actin filament bundle assembly, 1.c: actin filament bundle organization, 1.d: positive regulation of actin filament polymerization), 2. spindle (2.a mitotic spindle organization, 2.b: mitotic spindle organization, 2.c: microtubule cytoskeleton organization involved in mitosis, 2.d: spindle assembly, 2.e: spindle organization), 3. lipid (3.a fatty acid oxidation, 3.b lipid oxidation), and, 4. RNA (4.a transcription elongation from RNA polymerase II promoter).

Table S2. Proteome-wide label-free quantification in control versus mepazine-treated GSCs. Related to Figures 1 and 3.
Statistical and fold-change analysis, as well as Principal Component Analysis (PCA) and heatmaps were done with Perseus software (1.6.14.0) to compare DMSO and mepazine (MPZ)-treated groups. Each group was performed in quadruplicates.

Table S3. Immunopurified lysosomes proteome label-free quantification in control versus mepazine-treated GSCs. Related to Figure 3.
Statistical and fold change analysis, as well as Principal Component Analysis (PCA) and heatmaps were done with Perseus software (1.6.14.0) to compare the following groups: HA_DMSO vs Flag_DMSO,

HA_MPZ vs Flag_MPZ, Flag_MPZ vs Flag_DMSO and HA_MPZ vs HA_DMSO. Statistical and fold-change analysis were done with LFQ values (without imputation) and paired t-test p-value. Each group was performed in quadruplicates.

Table S4. List of qPCR primers used in this study. Related to STAR Methods.

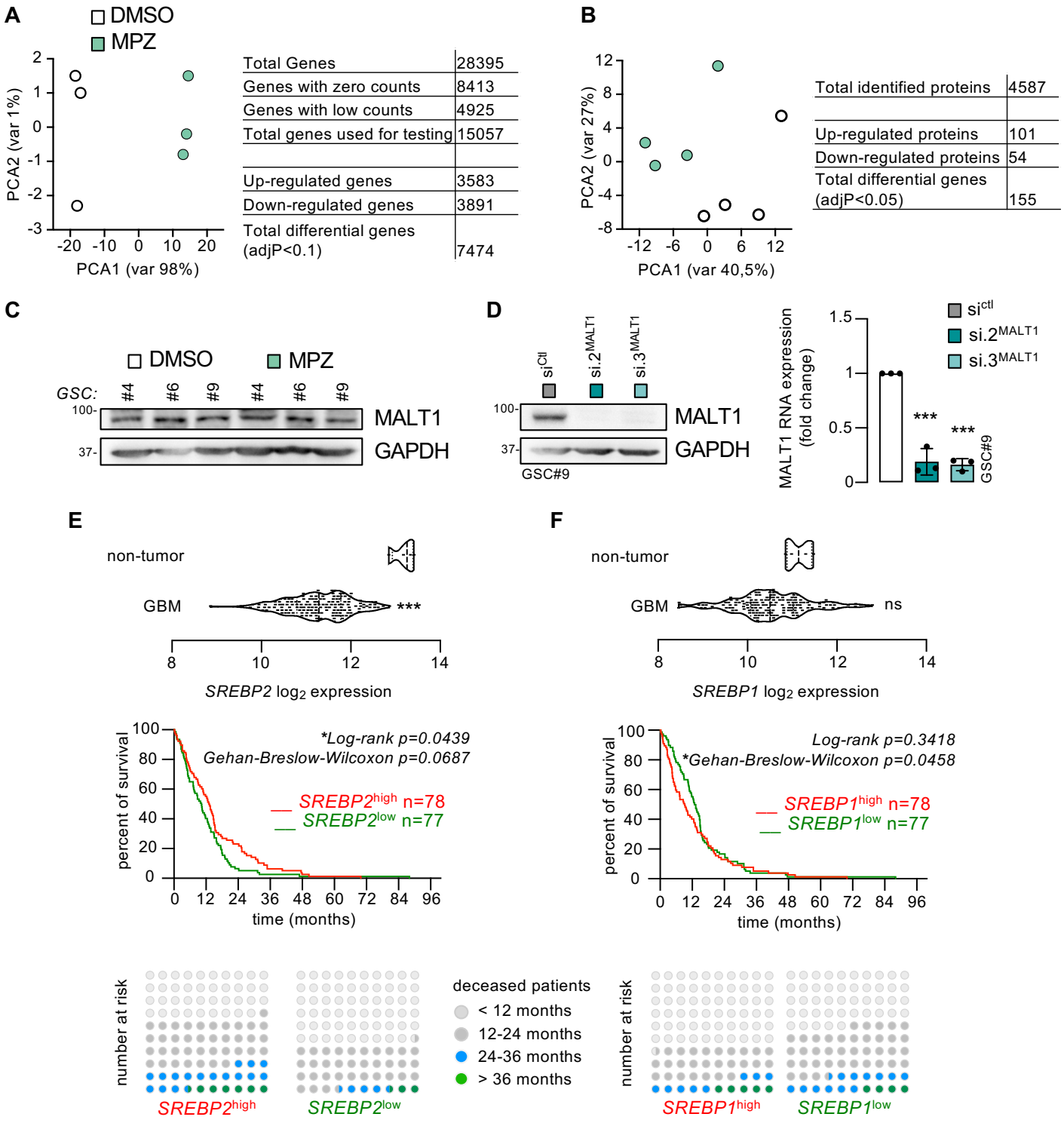
A
DMSO
MPZ
PCA2 (var 1%)
PCA1 (var 98%)
Total Genes 28395
Genes with zero counts 8413
Genes with low counts 4925
Total genes used for testing 15057
Up-regulated genes 3583
Down-regulated genes 3891
Total differential genes (adjP<0.1) 7474
B
PCA2 (var 27%)
PCA1 (var 40,5%)
Total identified proteins 4587
Up-regulated proteins 101
Down-regulated proteins 54
Total differential genes (adjP<0.05) 155
C
DMSO
MPZ
GSC: #4 #6 #9 #4 #6 #9
100-
37-
MALT1
GAPDH
D
siCtl
si.2MALT1
si.3MALT1
GSC#9
MALT1 RNA expression (fold change)
***
E
non-tumor
GBM
***
SREBP2 log2 expression
*Log-rank p=0.0439
Gehan-Breslow-Wilcoxon p=0.0687
SREBP2high n=78
SREBP2low n=77
percent of survival
time (months)
number at risk
deceased patients
< 12 months
12-24 months
24-36 months
> 36 months
F
non-tumor
GBM
ns
SREBP1 log2 expression
Log-rank p=0.3418
*Gehan-Breslow-Wilcoxon p=0.0458
SREBP1high n=78
SREBP1low n=77

Figure S1

Figure S1. Quality controls related to -omic analysis, MALT1 levels of expression, and TCGA analysis. Related to Figures 1 and 3.

(A) Principal Component Analysis (PCA) for the RNAseq samples, as prepared in Figure 1A. DESeq2 report on count data is presented in the table.

(B) Principal Component Analysis (PCA) for the proteomics samples, as prepared in Figure 1A. DEqMS report on count data is presented in the table. n=4

(C) Western-blot analysis of MALT1 in the indicated GSCs, treated for 16h with DMSO and MPZ (20µM).

(D) Western-blot (Left) and qPCR (Right) analysis of MALT1 in GSC#9 transfected with non-silencing (si^{ctl}) and 2 duplexes targeting MALT1 (si^{MALT1}) for 3 days. qPCR data were normalized to 2 housekeeping genes (HPRT1, ACTB).

(E-F) Violin plots of SREBP2 (E) and SREBP1 (F) mRNA expression in non-tumor and GB samples (TCGA RNAseq dataset). Each dot represents one clinical sample. Kaplan-Meier curve for 155 GB patients (TCGA RNAseq dataset) with low (green) or high (red) SREBP2 (E) and SREBP1 (F) mRNA level. Parts of whole dot plot for patients with low and high levels of SREBP2 (E) and SREBP1 (F), representing number of patients at risk, at the indicated elapsed time post-diagnosis.

All panels are representative of at least n=3, unless otherwise specified. t-test and ANOVA, *p<0.05, **p<0.01, ***p<0.001.

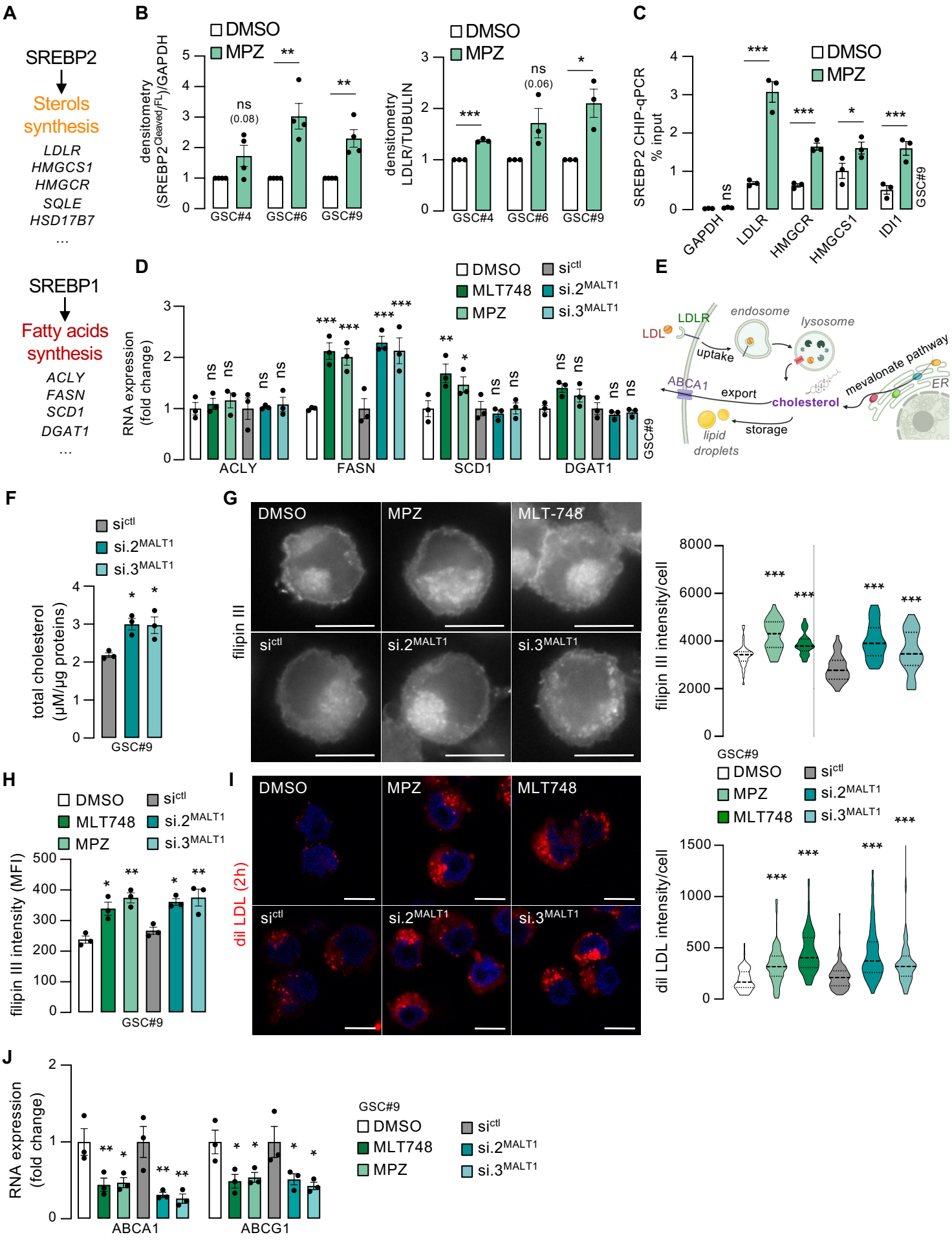
A
SREBP2
Sterols synthesis
LDLR
HMGCS1
HMGCR
SQLE
HSD17B7
...
SREBP1
Fatty acids synthesis
ACLY
FASN
SCD1
DGAT1
...
B
DMSO
MPZ
densitometry (SREBP2Cleaved/FL)/GAPDH
densitometry LDLR/TUBULIN
GSC#4
GSC#6
GSC#9
ns
(0.08)
(0.06)
C
SREBP2 CHIP-qPCR % input
GAPDH
LDLR
HMGCR
HMGCS1
IDI1
GSC#9
D
DMSO
MLT748
MPZ
sictl
si.2MALT1
si.3MALT1
RNA expression (fold change)
ACLY
FASN
SCD1
DGAT1
E
LDL
LDLR
endosome
lysosome
uptake
ABCA1
export
cholesterol
mevalonate pathway
ER
lipid droplets
storage
F
total cholesterol (µM/µg proteins)
G
filipin III
DMSO
MPZ
MLT-748
filipin III intensity/cell
H
filipin III intensity (MFI)
I
dil LDL (2h)
MLT748
dil LDL intensity/cell
J
RNA expression (fold change)
ABCA1
ABCG1

Figure S2

Figure S2. SREBP2 is preferentially activated in response to MALT1 inhibition. Related to Figures 1 and 2.

(A) Schematic representation of the different canonical targets under the control of SREBP2 and SREBP1 transcription factors, which regulate sterols and fatty acids synthesis, respectively.

(B) Densitometric analysis of the cleaved fragment of SREBP2 normalized to the full-length, as performed in Figure 1H. Values were normalized to GAPDH. Densitometric analysis of LDLR normalized to TUBULIN, as performed in Figure 1H.

(C) ChIP-qPCR analysis of SREBP2 binding to the indicated targets in GSC#9 treated for 4h with DMSO and MPZ (20μM). Data were normalized to the GAPDH housekeeping gene and to the input level of the indicated genes.

(D) RT-qPCR of the indicated targets in GSC#9 treated as in (C). Alternatively, cells received non-silencing (si^{ctl}) and 2 duplexes targeting MALT1 (si^{MALT1}) for 3 days. Data were normalized to housekeeping genes (HPRT1, ACTB).

(E) Schematic representation of the different pathways which control the intracellular level of cholesterol: i) capture of cholesterol-filled LDL upon binding to the LDLR and trafficking through the endocytic/endosomal pathway, ii) *de novo* cholesterol synthesis into the mevalonate pathway, iii) handling the pool of free cholesterol via storage into lipid droplets, and, iv) export through different transporters.

(F) Bioluminescent evaluation of total cholesterol level (cholesterol/protein ratio, μM/μg) in GSC#9 transfected with non-silencing (si^{ctl}) and 2 duplexes targeting MALT1 (si^{MALT1}) for 3 days.

(G-H) Filipin-III staining analyzed by confocal (G) and flow cytometry (H) in GSC#9 treated with DMSO, MPZ (20μM), and MLT748 (5μM) for 24h, or transfected with si^{ctl}, $si.2^{MALT1}$, and $si.3^{MALT1}$ for 3 days. Scale bar: 10μm. Violin representation: quantification of filipin-III signal (intensity/cell, G, n=38, and, mean fluorescence intensity, H).

(I) Confocal analysis of dil-LDL uptake (5μg/mL, 2h) in GSC#9 treated as in (G) for 16h. Scale bar: 10μm. Violin representation: quantification of dil-LDL signal intensity/cell (n>70).

(J) RT-qPCR of ABCA1 and ABCG1 in GSC#9 treated for 4h with DMSO, MPZ, (20μM), and MLT748 (5μM). Alternatively, cells received si^{ctl}, $si.2^{MALT1}$, and $si.3^{MALT1}$, for 3 days. Data were normalized to housekeeping genes (HPRT1, ACTB).

All panels are representative of at least n=3, unless otherwise specified. t-test and ANOVA, *p<0.05, **p<0.01, ***p<0.001.

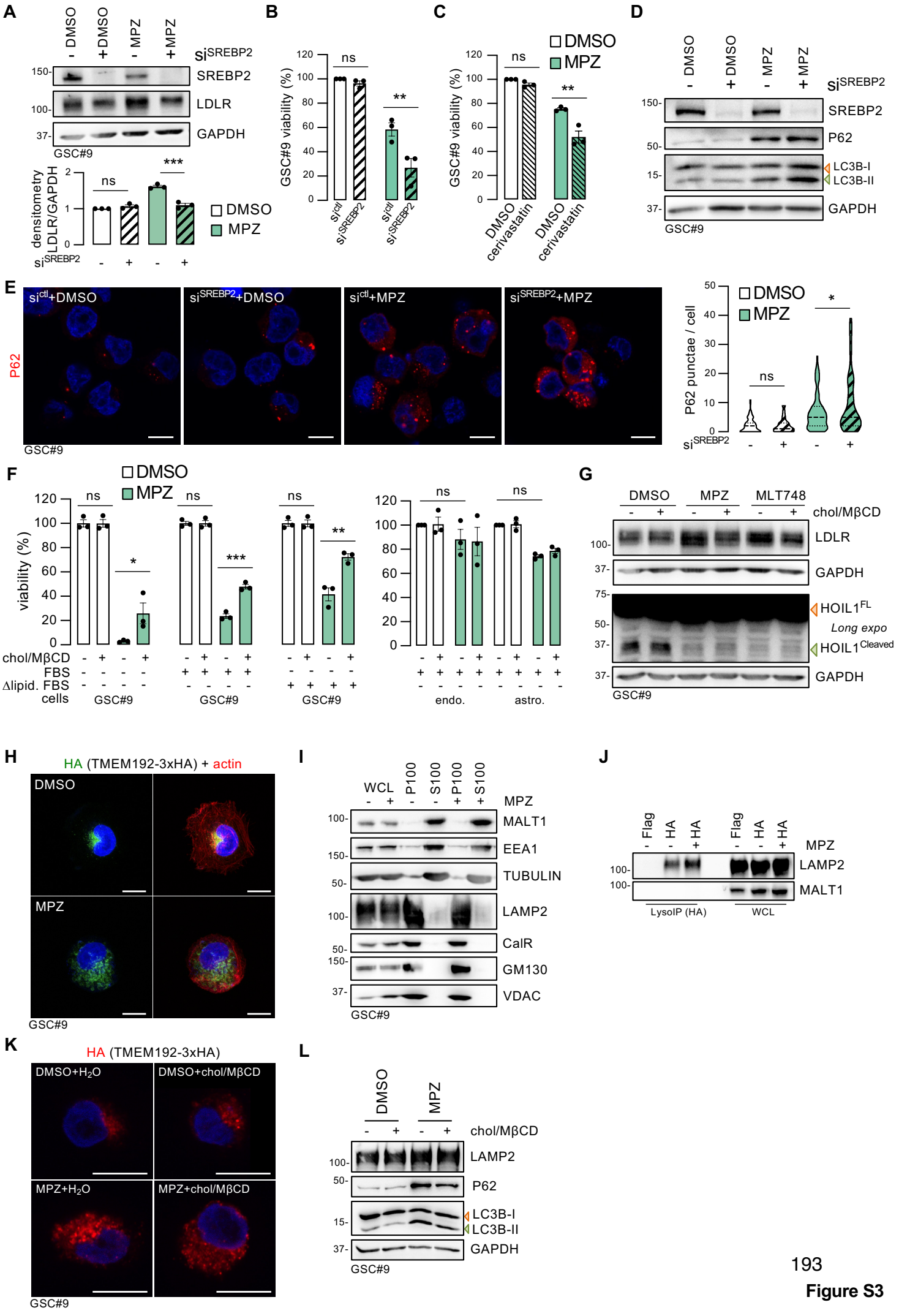
A
- DMSO
+ DMSO
- MPZ
+ MPZ
siSREBP2
SREBP2
LDLR
GAPDH
GSC#9
densitometry LDLR/GAPDH
ns
***
DMSO
MPZ
B
GSC#9 viability (%)
ns
**
sictl
siSREBP2
C
DMSO
MPZ
GSC#9 viability (%)
ns
**
DMSO
cerivastatin
D
P62
LC3B-I
LC3B-II
E
sictl+DMSO
siSREBP2+DMSO
sictl+MPZ
siSREBP2+MPZ
P62
GSC#9
P62 punctae / cell
F
viability (%)
chol/MβCD
FBS
Δlipid. FBS
cells
endo.
astro.
G
DMSO
MPZ
MLT748
chol/MβCD
LDLR
GAPDH
HOIL1FL
Long expo
HOIL1Cleaved
H
HA (TMEM192-3xHA) + actin
DMSO
MPZ
I
WCL
P100
S100
MPZ
MALT1
EEA1
TUBULIN
LAMP2
CalR
GM130
VDAC
J
Flag
HA
MPZ
LAMP2
MALT1
LysoIP (HA)
WCL
K
HA (TMEM192-3xHA)
DMSO+H2O
DMSO+chol/MβCD
MPZ+H2O
MPZ+chol/MβCD
L
DMSO
MPZ
chol/MβCD
LAMP2
P62
LC3B-I
LC3B-II
GAPDH

Figure S3

Figure S3. SREBP2 blockade exacerbates MALT1-inhibition induced phenotypes, while partially rescued with cholesterol supplementation. Related to Figure 2.

(A-B) GSC#9 transfected for 2 days with non-silencing (si^{ctl}) and SREBP2 targeting (si^{SREBP2}) duplexes, and treated for 24h with DMSO and MPZ (20μM). Western-blot analysis of SREBP2 and LDLR and densitometric analysis of LDLR normalized to GAPDH (A). Cell viability at 48h.

(C) Cell viability in GSC#9 pretreated for 1h with DMSO and cerivastatin (10nM), and challenged for 48h with DMSO and MPZ (20μM).

(D) Western-blot analysis as indicated in GSC#9 treated as described in (A). Green and red arrowheads: unlipidated (LC3B-I) and lipidated (LC3B-II), respectively.

(E) Confocal analysis of P62 staining in GSC#9 treated as described in (A). Scale bar: 10μm. Violin representation: number of P62 punctae/cell (n>69).

(F) Cell viability in GSC#9 cultured in complete medium (NS34) supplemented with either FBS (10%) or delipidated FBS (Δlipid. FBS, 10%), and in human brain endothelial cells (hCMEC/D3) and human astrocytes (SVG-p12), cultured in FBS containing medium (10%). Cells were pretreated for 1h with DMSO and MPZ (20μM), and challenged for 48h with H_2O or with MβCD-complexed cholesterol (chol/MβCD, 250μM).

(G) Western-blot analysis of LDLR at 24h and HOIL1 at 6h in GSC#9 pretreated for 1h with DMSO, MPZ (20μM), and MLT748 (5μM), and challenged with H_2O or chol/MβCD (250μM). Green and red arrowheads: FL (full length) and cleaved HOIL1, respectively.

(H) Confocal analysis of TMEM192-3xHA (HA) and actin (phalloidin) staining in HA-lyso GSC#9 seeded on ring-shaped micropatterns and treated for 16h with DMSO and MPZ (20μM). z-stack maximum projection. Scale bar: 10μm.

(I) Western-blot analysis as indicated in GSC#9 whole cell lysate (WCL), P100 fraction (organelles), and S100 fraction (cytosol). GSC#9 were treated with DMSO and MPZ (20μM) for 2h.

(J) Western-blot analysis as indicated in Flag-lyso and HA-lyso GSC#9 immunopurified lysosomes (LysoIP) and WCL. Flag-lyso and HA-lyso GSC#9 were treated with DMSO and MPZ (20μM) for 6h.

(K) Confocal analysis of TMEM192-3xHA (HA) staining in HA-lyso GSC#9 pre-treated for 1h with DMSO and MPZ (20μM), and challenged for 24h with H_2O or with chol/MβCD (250μM). Scale bar: 10μm.

(L) Western-blot analysis as indicated in GSC#9 treated as described in (F). Green and red arrowheads: unlipidated (LC3B-I) and lipidated (LC3B-II) LC3B, respectively.

All panels are representative of at least n=3, unless otherwise specified. ANOVA, *p<0.05, **p<0.01, ***p<0.001.

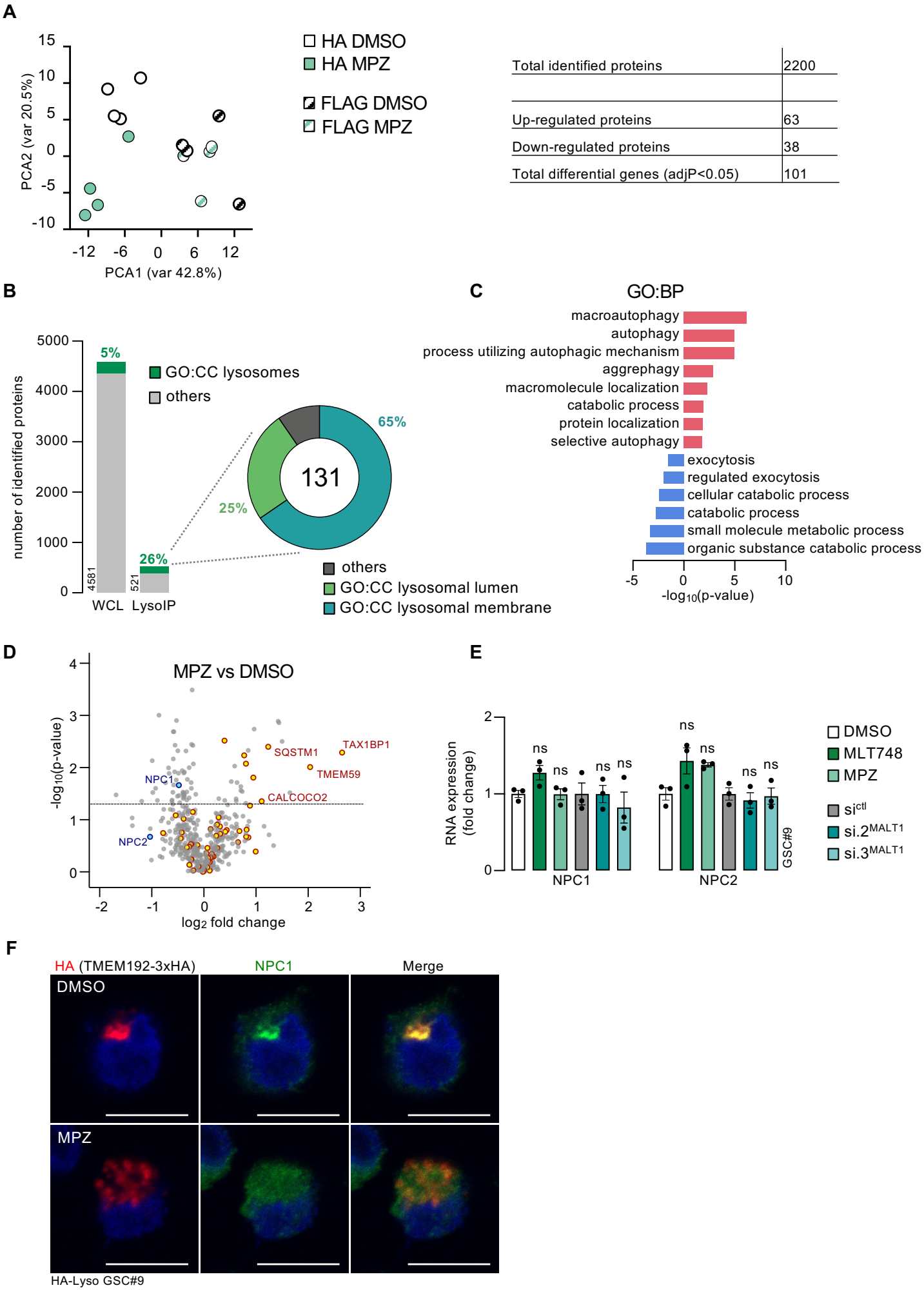
A
HA DMSO
HA MPZ
FLAG DMSO
FLAG MPZ
PCA2 (var 20.5%)
PCA1 (var 42.8%)
Total identified proteins 2200
Up-regulated proteins 63
Down-regulated proteins 38
Total differential genes (adjP<0.05) 101
B
number of identified proteins
5%
26%
4581
521
WCL
LysoIP
GO:CC lysosomes
others
65%
25%
131
others
GO:CC lysosomal lumen
GO:CC lysosomal membrane
C
GO:BP
macroautophagy
autophagy
process utilizing autophagic mechanism
aggrephagy
macromolecule localization
catabolic process
protein localization
selective autophagy
exocytosis
regulated exocytosis
cellular catabolic process
catabolic process
small molecule metabolic process
organic substance catabolic process
-log10(p-value)
D
MPZ vs DMSO
-log10(p-value)
log2 fold change
NPC1
NPC2
SQSTM1
TAX1BP1
TMEM59
CALCOCO2
E
RNA expression (fold change)
ns
NPC1
NPC2
DMSO
MLT748
MPZ
sictl
si.2MALT1
si.3MALT1
GSC#9
F
HA (TMEM192-3xHA)
NPC1
Merge
DMSO
MPZ
HA-Lyso GSC#9

Figure S4

Figure S4. Lysosomes from MALT1-inhibited GSCs accumulate autophagic cargo and lose cholesterol transporters. Related to Figure 3.

(A) Principal Component Analysis (PCA) for the LysoIP proteomic samples, as prepared in Figure 4A. DEqMS report on count data is presented in the table. n=4

(B) Graph represents the number of proteins identified in the whole cell lysate (WCL) and the immunopurified lysosome fractions (LysoIP, grey bar graphs) of HA-lyso GSC#9, as depicted in Figure 3A. The percentage of GO:CC lysosomes proteins is indicated in green. Donut graph represents the percentage of membranous (blue), and luminal (green) lysosomal proteins identified in the LysoIP proteomic analysis. The percentage of other type of proteins is shown in grey. For each graph, the number of proteins is reported.

(C) GO:BP enrichment analysis of proteins differentially expressed with fold change >1.5, either positively (red) or negatively (blue), in LysoIP as in B.

(D) Volcano plot analysis of differentially expressed proteins from the LysoIP proteomic analysis. Yellow dots: GO:BP autophagy associated proteins, blue dots: NPC1 and NPC2. Dashed line represents the significant threshold ($p<0.05$).

(E) RT-qPCR of NPC1 and NPC2 in GSC#9 treated for 6h with DMSO, MPZ (20μM), and MLT748 (5μM). Alternatively, cells received non-silencing (si^{ctl}) and MALT1 targeting (si^{MALT1}) duplexes for 3 days. Data were normalized to housekeeping genes (HPRT1, ACTB).

(F) Confocal analysis of TMEM192-3xHA (HA) and NPC1 staining in HA-lyso GSC#9 treated for 6h with DMSO and MPZ (20μM). Scale bar: 10μm.

All panels are representative of at least n=3, unless otherwise specified. ANOVA, *$p<0.05$, **$p<0.01$, ***$p<0.001$.

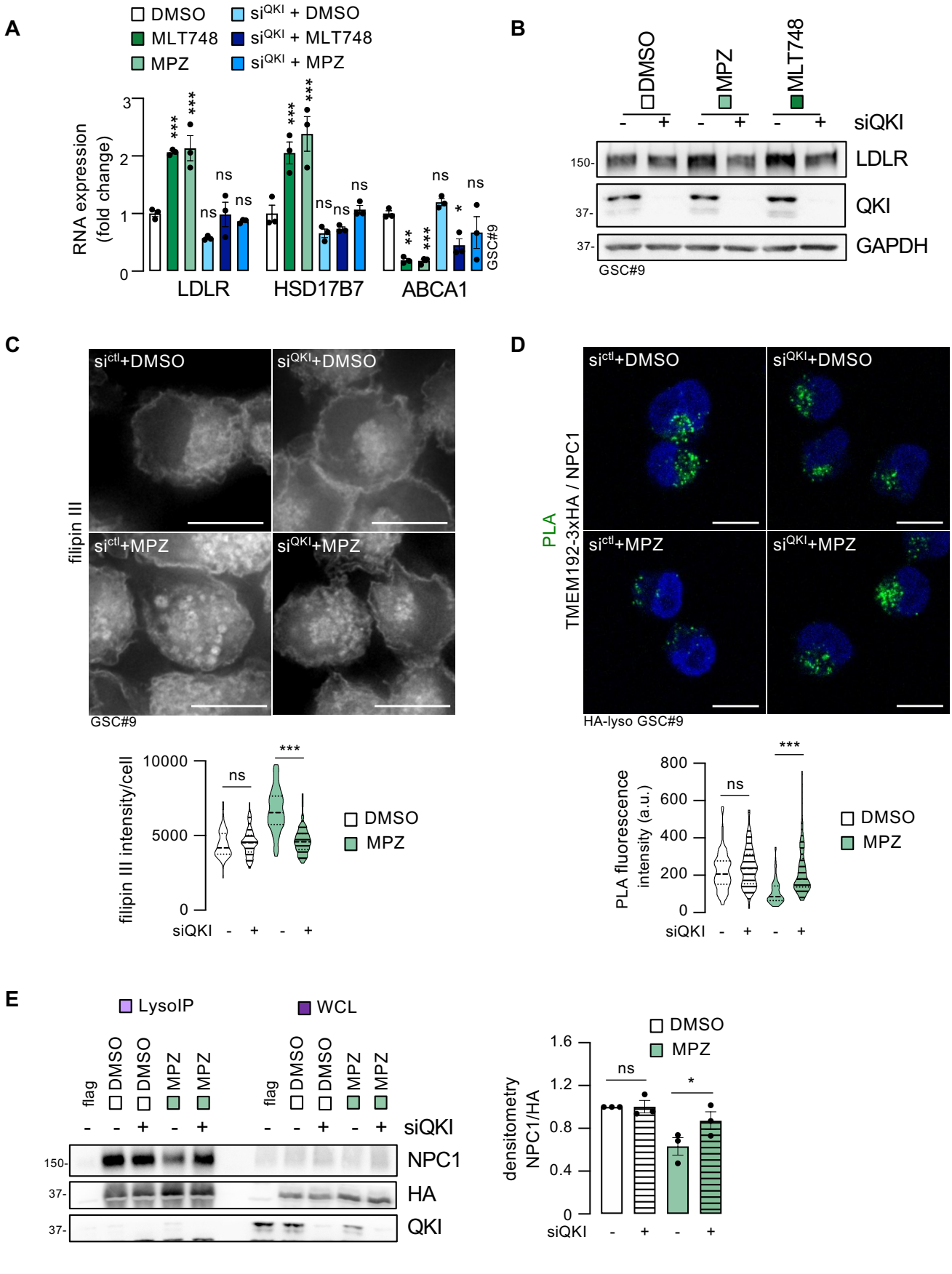
A
DMSO
MLT748
MPZ
siQKI + DMSO
siQKI + MLT748
siQKI + MPZ
RNA expression (fold change)
LDLR
HSD17B7
ABCA1
GSC#9
B
DMSO
MPZ
MLT748
siQKI
LDLR
QKI
GAPDH
GSC#9
C
filipin III
sictl+DMSO
siQKI+DMSO
sictl+MPZ
siQKI+MPZ
GSC#9
filipin III intensity/cell
DMSO
MPZ
siQKI
D
PLA
TMEM192-3xHA / NPC1
HA-lyso GSC#9
PLA fluorescence intensity (a.u.)
E
LysoIP
WCL
flag
siQKI
NPC1
HA
densitometry NPC1/HA
ns

Figure S5

Figure S5. QKI silencing counterbalances the effects of MALT1 targeting on cholesterol deregulation. Related to Figure 3.

(A) RT-qPCR analysis as indicated in GSC#9 transfected with non-silencing duplexes (si^{ctl}) and QKI targeting (si^{QKI}) duplexes for 3 days, and treated for 4h with DMSO, MPZ (20μM), and MLT748 (5μM). Data were normalized to housekeeping genes (HPRT1, ACTB).

(B-C) GSC#9 transfected for 2 days with non-silencing (si^{ctl}) and QKI targeting (si^{QKI}) duplexes, and treated for 24h with DMSO, MPZ (20μM), and MLT748 (5μM). Western-blot as indicated (B) and confocal analysis of filipin-III (C). Scale bar: 10μm. Violin representation: quantification of filipin-III signal intensity/cell (n>35).

(D) Confocal analysis of Proximity Ligation Assay (PLA) between TMEM192-3xHA and NPC1. HA-lyso GSC#9 were treated as described in (B) for 6h. Fluorescent signal reflects a <40nm proximity. Scale bar: 10μm. Violin representation: quantification of PLA signal intensity/cell (n=74).

(E) Western-blot analysis of NPC1 from Flag-lyso and HA-lyso GSC#9 LysoIP and WCL. Flag-lyso and HA-lyso GSC#9 were treated as described in (D). Densitometric analysis of NPC1 level normalized to TMEM192-3xHA (HA).

All panels are representative of at least n=3, unless otherwise specified. ANOVA, *p<0.05, **p<0.01, ***p<0.001.

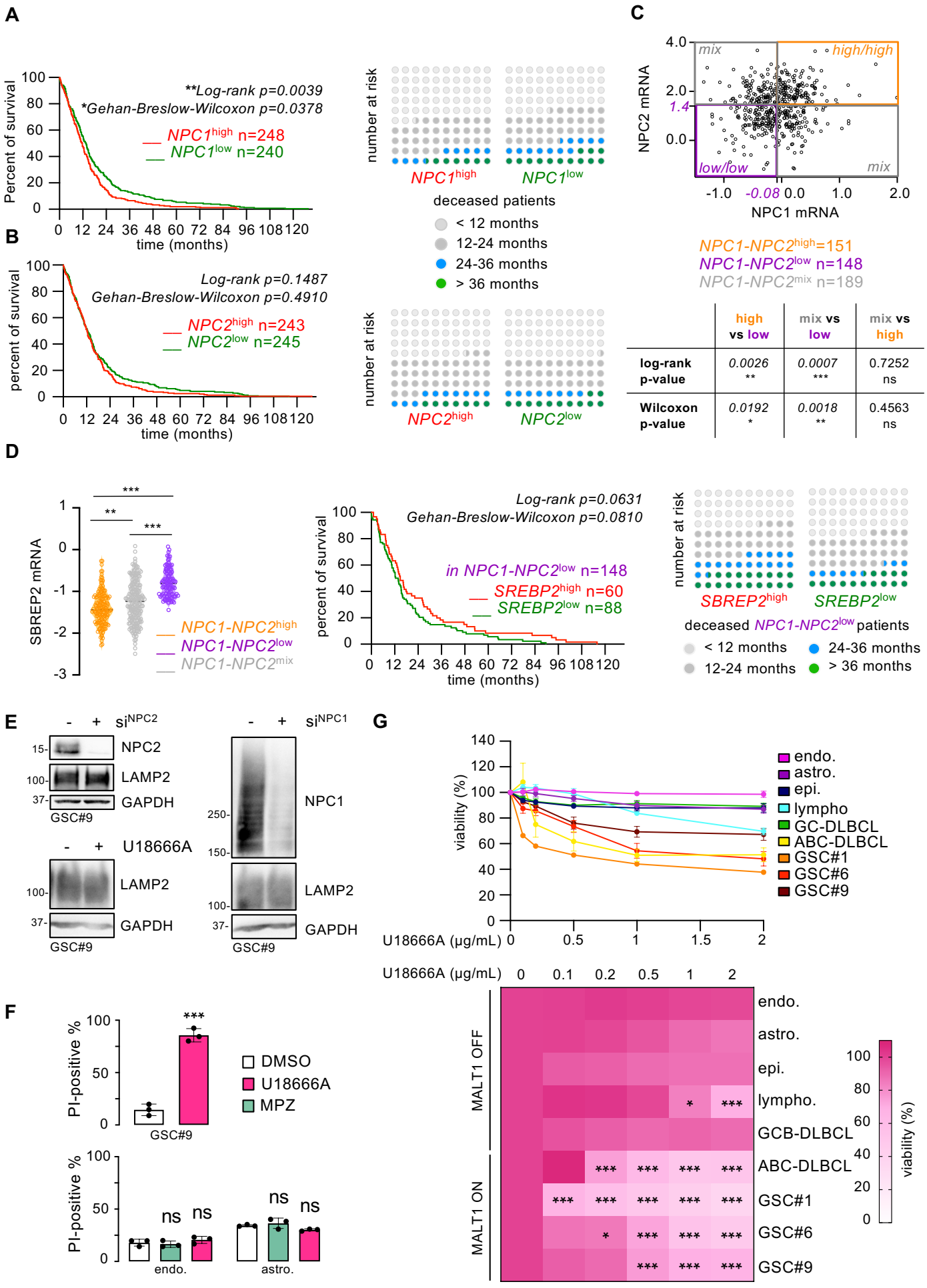
A
Percent of survival
**Log-rank p=0.0039
*Gehan-Breslow-Wilcoxon p=0.0378
NPC1high n=248
NPC1low n=240
time (months)
number at risk
NPC1high
NPC1low
deceased patients
< 12 months
12-24 months
24-36 months
> 36 months
B
percent of survival
Log-rank p=0.1487
Gehan-Breslow-Wilcoxon p=0.4910
NPC2high n=243
NPC2low n=245
time (months)
number at risk
NPC2high
NPC2low
C
NPC2 mRNA
NPC1 mRNA
mix
high/high
low/low
mix
NPC1-NPC2high=151
NPC1-NPC2low n=148
NPC1-NPC2mix n=189
high vs low
mix vs low
mix vs high
log-rank p-value
0.0026 **
0.0007 ***
0.7252 ns
Wilcoxon p-value
0.0192 *
0.0018 **
0.4563 ns
D
SBREP2 mRNA
NPC1-NPC2high
NPC1-NPC2low
NPC1-NPC2mix
percent of survival
Log-rank p=0.0631
Gehan-Breslow-Wilcoxon p=0.0810
in NPC1-NPC2low n=148
SREBP2high n=60
SREBP2low n=88
time (months)
number at risk
SBREP2high
SREBP2low
deceased NPC1-NPC2low patients
< 12 months
12-24 months
24-36 months
> 36 months
E
siNPC2
NPC2
LAMP2
GAPDH
GSC#9
U18666A
siNPC1
NPC1
LAMP2
GAPDH
GSC#9
G
viability (%)
endo.
astro.
epi.
lympho
GC-DLBCL
ABC-DLBCL
GSC#1
GSC#6
GSC#9
U18666A (µg/mL)
U18666A (µg/mL)
MALT1 OFF
MALT1 ON
endo.
astro.
epi.
lympho.
GCB-DLBCL
ABC-DLBCL
GSC#1
GSC#6
GSC#9
viability (%)
F
PI-positive %
DMSO
U18666A
MPZ
GSC#9
endo.
astro.
ns

Figure S6

Figure S6. NPC1 inhibition abrogates GSC survival. Related to Figure 4.

(A-B) Kaplan-Meier curve for 488 GB patients (TCGA Agilent-4502A dataset), grouped based on low (green) or high (red) *NPC1* (A) and *NPC2* (B) mRNA levels. Parts of whole dot plot for patients with low and high levels of NPC1 (A) and NPC2 (B), representing number of patients at risk, at the indicated elapsed time post-diagnosis.

(C) Correlation plot between *NPC1* and *NPC2* mRNA levels in 488 GB patients (TCGA Agilent-4502A dataset). Patients were clustered in three groups: $NPC1^{low}/NPC2^{low}$ (purple); $NPC1^{high}/NPC2^{high}$ (orange) and $NPC1^{mix}/NPC2^{mix}$ (grey). log-rank and Wilcoxon p-values are indicated for the Kaplan-Meier curve presented in Figure 4A.

(D) Violin plot of SREBP2 mRNA expression in GB patients, clustered as in (C). Kaplan-Meier curve for 148 GB patients (TCGA Agilent-4502A dataset) with low (green) and high (red) *SREBP2* mRNA level in $NPC1^{low}/NPC2^{low}$ patients. Parts of whole dot plot for patients with low and high levels of SREBP2 in the $NPC1^{low}/NPC2^{low}$ group, representing number of patients at risk, at the indicated elapsed time post-diagnosis.

(E) Western-blot analysis as indicated in GSC#9, transfected with non-silencing (si^{ctl}), NPC1 targeting (si^{NPC1}) and NPC2 targeting (si^{NPC2}) duplexes for 3 days, or treated for 16h with DMSO and U18666A (2µg/mL).

(F) Propidium iodide (PI) incorporation by flow cytometry in GSC#9, human brain endothelial cells (endo., hCMEC/D3) and human astrocytes (astro., SVG-p12), treated for 48h with DMSO, MPZ (20µM), and U18666A (2 µg/mL).

(G) Cell viability in each cell line treated for 48h with DMSO and U18666A at the indicated doses. All cell lines, except GSCs in their mitogen-defined medium, were maintained in FBS containing medium for the duration of the tests. Endo.: brain endothelial cells hCMEC/D3, astro.: astrocyte SVGp12, epi.: epithelial cells HEK293T, lympho.: lymphocyte Jurkat E6.1, GC-DLBCL: germinal center B-cell like diffuse large B-cell lymphoma BJAB, ABC-DLBCL: activated B-cell-like diffuse large B-cell lymphoma OCI-Ly3. Heatmap of the cell viability.

All panels are representative of at least n=3, unless otherwise specified. t-test and ANOVA, *p<0.05, **p<0.01, ***p<0.001.

References

1. Ohgaki, H., and Kleihues, P. (2005). Population-Based Studies on Incidence, Survival Rates, and Genetic Alterations in Astrocytic and Oligodendroglial Gliomas. J. Neuropathol. Exp. Neurol. *64*, 479–489. 10.1093/jnen/64.6.479.

2. Stupp, R., Hegi, M.E., Mason, W.P., van den Bent, M.J., Taphoorn, M.J.B., Janzer, R.C., Ludwin, S.K., Allgeier, A., Fisher, B., Belanger, K., et al. (2009). Effects of radiotherapy with concomitant and adjuvant temozolomide versus radiotherapy alone on survival in glioblastoma in a randomised phase III study: 5-year analysis of the EORTC-NCIC trial. Lancet Oncol. *10*, 459–466. 10.1016/S1470-2045(09)70025-7.

3. Lathia, J.D., Mack, S.C., Mulkearns-Hubert, E.E., Valentim, C.L.L., and Rich, J.N. (2015). Cancer stem cells in glioblastoma. Genes Dev. *29*, 1203–1217. 10.1101/gad.261982.115.

4. Singh, S.K., Hawkins, C., Clarke, I.D., Squire, J.A., Bayani, J., Hide, T., Henkelman, R.M., Cusimano, M.D., and Dirks, P.B. (2004). Identification of human brain tumour initiating cells. Nature *432*, 396–401. 10.1038/nature03128.

5. Jacobs, K.A., André-Grégoire, G., Maghe, C., Thys, A., Li, Y., Harford-Wright, E., Trillet, K., Douanne, T., Alves Nicolau, C., Frénel, J.-S., et al. (2020). Paracaspase MALT1 regulates glioma cell survival by controlling endo-lysosome homeostasis. EMBO J. *39*, e102030. 10.15252/embj.2019102030.

6. Le Joncour, V., Filppu, P., Hyvönen, M., Holopainen, M., Turunen, S.P., Sihto, H., Burghardt, I., Joensuu, H., Tynninen, O., Jääskeläinen, J., et al. (2019). Vulnerability of invasive glioblastoma cells to lysosomal membrane destabilization. EMBO Mol. Med. *11*. 10.15252/emmm.201809034.

7. Zhou, W., Guo, Y., Zhang, X., and Jiang, Z. (2020). Lys05 induces lysosomal membrane permeabilization and increases radiosensitivity in glioblastoma. J. Cell. Biochem. *121*, 2027–2037. 10.1002/jcb.29437.

8. Castellano, B.M., Thelen, A.M., Moldavski, O., Feltes, M., van der Welle, R.E.N., Mydock-McGrane, L., Jiang, X., van Eijkeren, R.J., Davis, O.B., Louie, S.M., et al. (2017). Lysosomal cholesterol activates mTORC1 via an SLC38A9–Niemann-Pick C1 signaling complex. Science *355*, 1306–1311. 10.1126/science.aag1417.

9. Davis, O.B., Shin, H.R., Lim, C.-Y., Wu, E.Y., Kukurugya, M., Maher, C.F., Perera, R.M., Ordonez, M.P., and Zoncu, R. (2021). NPC1-mTORC1 Signaling Couples Cholesterol Sensing to Organelle Homeostasis and Is a Targetable Pathway in Niemann-Pick Type C. Dev. Cell *56*, 260-276.e7. 10.1016/j.devcel.2020.11.016.

10. Shin, H.R., Citron, Y.R., Wang, L., Tribouillard, L., Goul, C.S., Stipp, R., Sugasawa, Y., Jain, A., Samson, N., Lim, C.-Y., et al. (2022). Lysosomal GPCR-like protein LYCHOS signals cholesterol sufficiency to mTORC1. Science *377*, 1290–1298. 10.1126/science.abg6621.

11. Lawrence, R.E., and Zoncu, R. (2019). The lysosome as a cellular centre for signalling, metabolism and quality control. Nat. Cell Biol. *21*, 133–142. 10.1038/s41556-018-0244-7.

12. Trinh, M.N., Brown, M.S., Goldstein, J.L., Han, J., Vale, G., McDonald, J.G., Seemann, J., Mendell, J.T., and Lu, F. (2020). Last step in the path of LDL cholesterol from lysosome to plasma membrane to ER is governed by phosphatidylserine. Proc. Natl. Acad. Sci. *117*, 18521–18529. 10.1073/pnas.2010682117.

13. Meng, Y., Heybrock, S., Neculai, D., and Saftig, P. (2020). Cholesterol Handling in Lysosomes and Beyond. Trends Cell Biol. *30*, 452–466. 10.1016/j.tcb.2020.02.007.

14. Winkler, M.B.L., Kidmose, R.T., Szomek, M., Thaysen, K., Rawson, S., Muench, S.P., Wüstner, D., and Pedersen, B.P. (2019). Structural Insight into Eukaryotic Sterol Transport through Niemann-Pick Type C Proteins. Cell *179*, 485-497.e18. 10.1016/j.cell.2019.08.038.

15. Cariati, I., Masuelli, L., Bei, R., Tancredi, V., Frank, C., and D'Arcangelo, G. (2021). Neurodegeneration in Niemann–Pick Type C Disease: An Updated Review on Pharmacological and Non-Pharmacological Approaches to Counteract Brain and Cognitive Impairment. Int. J. Mol. Sci. *22*, 6600. 10.3390/ijms22126600.

16. Luo, J., Yang, H., and Song, B.-L. (2020). Mechanisms and regulation of cholesterol homeostasis.

Nat. Rev. Mol. Cell Biol. *21*, 225–245. 10.1038/s41580-019-0190-7.
17. Radhakrishnan, A., Goldstein, J.L., McDonald, J.G., and Brown, M.S. (2008). Switch-like Control of SREBP-2 Transport Triggered by Small Changes in ER Cholesterol: A Delicate Balance. Cell Metab. *8*, 512–521. 10.1016/j.cmet.2008.10.008.
18. Lee, M.-S., and Bensinger, S.J. (2022). Reprogramming cholesterol metabolism in macrophages and its role in host defense against cholesterol-dependent cytolysins. Cell. Mol. Immunol. *19*, 327–336. 10.1038/s41423-021-00827-0.
19. Beckwitt, C.H., Brufsky, A., Oltvai, Z.N., and Wells, A. (2018). Statin drugs to reduce breast cancer recurrence and mortality. Breast Cancer Res. *20*, 144. 10.1186/s13058-018-1066-z.
20. Li, D., Li, S., Xue, A.Z., Smith Callahan, L.A., and Liu, Y. (2020). Expression of SREBP2 and cholesterol metabolism related genes in TCGA glioma cohorts. Medicine (Baltimore) *99*, e18815. 10.1097/MD.0000000000018815.
21. Huang, B., Song, B., and Xu, C. (2020). Cholesterol metabolism in cancer: mechanisms and therapeutic opportunities. Nat. Metab. *2*, 132–141. 10.1038/s42255-020-0174-0.
22. Lewis, C.A., Brault, C., Peck, B., Bensaad, K., Griffiths, B., Mitter, R., Chakravarty, P., East, P., Dankworth, B., Alibhai, D., et al. (2015). SREBP maintains lipid biosynthesis and viability of cancer cells under lipid- and oxygen-deprived conditions and defines a gene signature associated with poor survival in glioblastoma multiforme. Oncogene *34*, 5128–5140. 10.1038/onc.2014.439.
23. Villa, G.R., Hulce, J.J., Zanca, C., Bi, J., Ikegami, S., Cahill, G.L., Gu, Y., Lum, K.M., Masui, K., Yang, H., et al. (2016). An LXR-Cholesterol Axis Creates a Metabolic Co-Dependency for Brain Cancers. Cancer Cell *30*, 683–693. 10.1016/j.ccell.2016.09.008.
24. Jaworski, M., and Thome, M. (2016). The paracaspase MALT1: biological function and potential for therapeutic inhibition. Cell. Mol. Life Sci. *73*, 459–473. 10.1007/s00018-015-2059-z.
25. Shingu, T., Ho, A.L., Yuan, L., Zhou, X., Dai, C., Zheng, S., Wang, Q., Zhong, Y., Chang, Q., Horner, J.W., et al. (2016). Qki deficiency maintains stemness of glioma stem cells in suboptimal environment by downregulating endolysosomal degradation. Nat. Genet. *49*, 75. 10.1038/ng.3711.
26. Schlauderer, F., Lammens, K., Nagel, D., Vincendeau, M., Eitelhuber, A.C., Verhelst, S.H.L., Kling, D., Chrusciel, A., Ruland, J., Krappmann, D., et al. (2013). Structural Analysis of Phenothiazine Derivatives as Allosteric Inhibitors of the MALT1 Paracaspase. Angew. Chem. Int. Ed. *52*, 10384–10387. 10.1002/anie.201304290.
27. Mazein, A., Watterson, S., Hsieh, W.-Y., Griffiths, W.J., and Ghazal, P. (2013). A comprehensive machine-readable view of the mammalian cholesterol biosynthesis pathway. Biochem. Pharmacol. *86*, 56–66. 10.1016/j.bcp.2013.03.021.
28. Quancard, J., Klein, T., Fung, S.-Y., Renatus, M., Hughes, N., Israël, L., Priatel, J.J., Kang, S., Blank, M.A., Viner, R.I., et al. (2019). An allosteric MALT1 inhibitor is a molecular corrector rescuing function in an immunodeficient patient. Nat. Chem. Biol. *15*, 304–313. 10.1038/s41589-018-0222-1.
29. Horton, J.D., Shah, N.A., Warrington, J.A., Anderson, N.N., Park, S.W., Brown, M.S., and Goldstein, J.L. (2003). Combined analysis of oligonucleotide microarray data from transgenic and knockout mice identifies direct SREBP target genes. Proc. Natl. Acad. Sci. *100*, 12027–12032. 10.1073/pnas.1534923100.
30. Horton, J.D., Goldstein, J.L., and Brown, M.S. (2002). SREBPs: activators of the complete program of cholesterol and fatty acid synthesis in the liver. J. Clin. Invest. *109*, 1125–1131. 10.1172/JCI0215593.
31. Kuhlmann, J., Mück, W., Bischoff, H., Keutz, E., and Llewellyn, M. (1998). Cerivastatin (BAY w 6228): A Novel HMG-CoA Reductase Inhibitor. Cardiovasc. Drug Rev. *16*, 236–263. 10.1111/j.1527-3466.1998.tb00357.x.
32. Palchaudhuri, R., Lambrecht, M.J., Botham, R.C., Partlow, K.C., van Ham, T.J., Putt, K.S., Nguyen, L.T., Kim, S.-H., Peterson, R.T., Fan, T.M., et al. (2015). A Small Molecule that Induces Intrinsic Pathway Apoptosis with Unparalleled Speed. Cell Rep. *13*, 2027–2036. 10.1016/j.celrep.2015.10.042.
33. Douanne, T., Gavard, J., and Bidère, N. (2016). The paracaspase MALT1 cleaves the LUBAC

subunit HOIL1 during antigen receptor signaling. J. Cell Sci. 10.1242/jcs.185025.
34. Chu, B.-B., Liao, Y.-C., Qi, W., Xie, C., Du, X., Wang, J., Yang, H., Miao, H.-H., Li, B.-L., and Song, B.-L. (2015). Cholesterol transport through lysosome-peroxisome membrane contacts. Cell *161*, 291–306. 10.1016/j.cell.2015.02.019.
35. Lange, Y., Ye, J., and Steck, T.L. (1998). Circulation of Cholesterol between Lysosomes and the Plasma Membrane. J. Biol. Chem. *273*, 18915–18922. 10.1074/jbc.273.30.18915.
36. Lim, C.-Y., Davis, O.B., Shin, H.R., Zhang, J., Berdan, C.A., Jiang, X., Counihan, J.L., Ory, D.S., Nomura, D.K., and Zoncu, R. (2019). ER–lysosome contacts enable cholesterol sensing by mTORC1 and drive aberrant growth signalling in Niemann–Pick type C. Nat. Cell Biol. *21*, 1206–1218. 10.1038/s41556-019-0391-5.
37. Abu-Remaileh, M., Wyant, G.A., Kim, C., Laqtom, N.N., Abbasi, M., Chan, S.H., Freinkman, E., and Sabatini, D.M. (2017). Lysosomal metabolomics reveals V-ATPase and mTOR-dependent regulation of amino acid efflux from lysosomes. Science *358*, 807–813. 10.1126/science.aan6298.
38. Shin, S., Zhou, H., He, C., Wei, Y., Wang, Y., Shingu, T., Zeng, A., Wang, S., Zhou, X., Li, H., et al. (2021). Qki activates Srebp2-mediated cholesterol biosynthesis for maintenance of eye lens transparency. Nat. Commun. *12*, 3005. 10.1038/s41467-021-22782-0.
39. Zhou, X., Shin, S., He, C., Zhang, Q., Rasband, M.N., Ren, J., Dai, C., Zorrilla-Veloz, R.I., Shingu, T., Yuan, L., et al. (2021). Qki regulates myelinogenesis through Srebp2-dependent cholesterol biosynthesis. eLife *10*, e60467. 10.7554/eLife.60467.
40. Lu, F., Liang, Q., Abi-Mosleh, L., Das, A., De Brabander, J.K., Goldstein, J.L., and Brown, M.S. (2015). Identification of NPC1 as the target of U18666A, an inhibitor of lysosomal cholesterol export and Ebola infection. eLife *4*, e12177. 10.7554/eLife.12177.
41. Ilnytska, O., Lai, K., Gorshkov, K., Schultz, M.L., Tran, B.N., Jeziorek, M., Kunkel, T.J., Azaria, R.D., McLoughlin, H.S., Waghalter, M., et al. (2021). Enrichment of NPC1-deficient cells with the lipid LBPA stimulates autophagy, improves lysosomal function, and reduces cholesterol storage. J. Biol. Chem. *297*, 100813. 10.1016/j.jbc.2021.100813.
42. Hailfinger, S., Lenz, G., Ngo, V., Posvitz-Fejfar, A., Rebeaud, F., Guzzardi, M., Penas, E.-M.M., Dierlamm, J., Chan, W.C., Staudt, L.M., et al. (2009). Essential role of MALT1 protease activity in activated B cell-like diffuse large B-cell lymphoma. Proc. Natl. Acad. Sci. U. S. A. *106*, 19946–19951. 10.1073/pnas.0907511106.
43. Ferch, U., Kloo, B., Gewies, A., Pfänder, V., Düwel, M., Peschel, C., Krappmann, D., and Ruland, J. (2009). Inhibition of MALT1 protease activity is selectively toxic for activated B cell-like diffuse large B cell lymphoma cells. J. Exp. Med. *206*, 2313–2320. 10.1084/jem.20091167.
44. März, P., Otten, U., and Miserez, A.R. (2007). Statins induce differentiation and cell death in neurons and astroglia. Glia *55*, 1–12. 10.1002/glia.20422.
45. Shammas, H., Kuech, E.-M., Rizk, S., Das, A.M., and Naim, H.Y. (2019). Different Niemann-Pick C1 Genotypes Generate Protein Phenotypes that Vary in their Intracellular Processing, Trafficking and Localization. Sci. Rep. *9*, 5292. 10.1038/s41598-019-41707-y.
46. Sarkar, S., Carroll, B., Buganim, Y., Maetzel, D., Ng, A.H.M., Cassady, J.P., Cohen, M.A., Chakraborty, S., Wang, H., Spooner, E., et al. (2013). Impaired Autophagy in the Lipid-Storage Disorder Niemann-Pick Type C1 Disease. Cell Rep. *5*, 1302–1315. 10.1016/j.celrep.2013.10.042.
47. Moreau, D., Vacca, F., Vossio, S., Scott, C., Colaco, A., Paz Montoya, J., Ferguson, C., Damme, M., Moniatte, M., Parton, R.G., et al. (2019). Drug-induced increase in lysobisphosphatidic acid reduces the cholesterol overload in Niemann–Pick type C cells and mice. EMBO Rep. *20*. 10.15252/embr.201847055.
48. Mi, H., Muruganujan, A., Huang, X., Ebert, D., Mills, C., Guo, X., and Thomas, P.D. (2019). Protocol Update for large-scale genome and gene function analysis with the PANTHER classification system (v.14.0). Nat. Protoc. *14*, 703–721. 10.1038/s41596-019-0128-8.
49. Harford-Wright, E., Andre-Gregoire, G., Jacobs, K.A., Treps, L., Le Gonidec, S., Leclair, H.M., Gonzalez-Diest, S., Roux, Q., Guillonneau, F., Loussouarn, D., et al. (2017). Pharmacological targeting of

apelin impairs glioblastoma growth. Brain J. Neurol. *140*, 2939–2954. 10.1093/brain/awx253.
50. Le Guelte, A., Galan-Moya, E.-M., Dwyer, J., Treps, L., Kettler, G., Hebda, J.K., Dubois, S., Auffray, C., Chneiweiss, H., Bidere, N., et al. (2012). Semaphorin 3A elevates endothelial cell permeability through PP2A inactivation. J. Cell Sci., jcs.108282. 10.1242/jcs.108282.
51. André-Grégoire, G., Maghe, C., Douanne, T., Rosińska, S., Spinelli, F., Thys, A., Trillet, K., Jacobs, K.A., Ballu, C., Dupont, A., et al. (2022). Inhibition of the pseudokinase MLKL alters extracellular vesicle release and reduces tumor growth in glioblastoma. iScience *25*, 105118. 10.1016/j.isci.2022.105118.
52. Trillet, K., Jacobs, K.A., André-Grégoire, G., Thys, A., Maghe, C., Cruard, J., Minvielle, S., Diest, S.G., Montagnac, G., Bidère, N., et al. (2021). The glycoprotein GP130 governs the surface presentation of the G protein–coupled receptor APLNR. J. Cell Biol. *220*, e202004114. 10.1083/jcb.202004114.
53. Bowman, R.L., Wang, Q., Carro, A., Verhaak, R.G.W., and Squatrito, M. (2017). GlioVis data portal for visualization and analysis of brain tumor expression datasets. Neuro-Oncol. *19*, 139–141. 10.1093/neuonc/now247.
54. Lachuer, H., Le, L., Lévêque-Fort, S., Goud, B., and Schauer, K. (2023). Spatial organization of lysosomal exocytosis relies on membrane tension gradients. Proc. Natl. Acad. Sci. *120*, e2207425120. 10.1073/pnas.2207425120.
55. Kulak, N.A., Pichler, G., Paron, I., Nagaraj, N., and Mann, M. (2014). Minimal, encapsulated proteomic-sample processing applied to copy-number estimation in eukaryotic cells. Nat. Methods *11*, 319–324. 10.1038/nmeth.2834.
56. Tyanova, S., Temu, T., Carlson, A., Sinitcyn, P., Mann, M., and Cox, J. (2015). Visualization of LC-MS/MS proteomics data in MaxQuant. PROTEOMICS *15*, 1453–1456. 10.1002/pmic.201400449.
57. Raudvere, U., Kolberg, L., Kuzmin, I., Arak, T., Adler, P., Peterson, H., and Vilo, J. (2019). g:Profiler: a web server for functional enrichment analysis and conversions of gene lists (2019 update). Nucleic Acids Res. *47*, W191–W198. 10.1093/nar/gkz369.

Discussion

I- Defining the MALT1-NPC1-cholesterol axis

I-1- Functions of the MALT1 paracaspase activity

The paracaspase MALT1 is a central modulator of NF-κB activity downstream of antigen receptors. Of interest, MALT1 acts as a scaffold within the CBM complex, and as an arginine protease able to cleave fourteen known substrates involved in several cellular processes such as regulation of the NF-κB pathway or mRNA stability[734]. However, the complete extent of MALT1 substrates and their biological functions are still currently being discovered.

Potential substrates and interactors of MALT1 involved in lysosomal modulation, regulation of cholesterol homeostasis, and mTORC1 signaling, will be discussed.

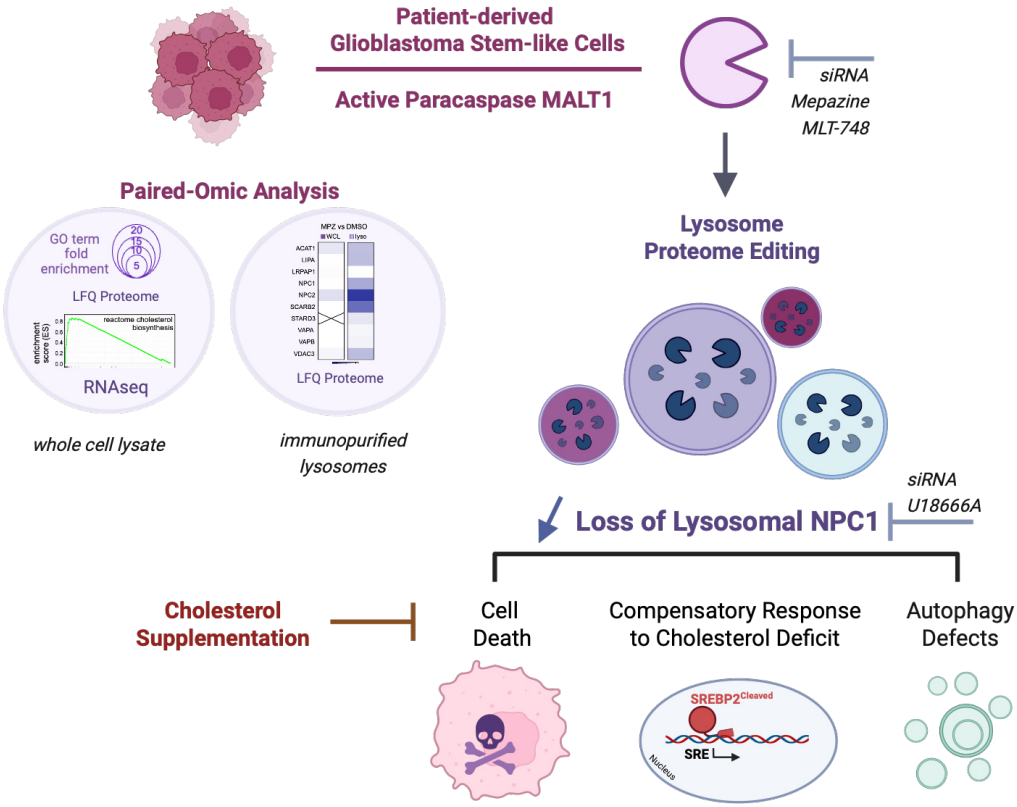

Figure 32: Graphical abstract. A paired-omic analysis of glioblastoma stem-like cells unravels the primordial function of the active paracaspase MALT1 in the maintenance of the lysosomal and cholesterol homeostasis. The use of MALT1 inhibitors as well as its siRNA-based silencing highlight that the lysosomal proteome is reshaped in response to the blockade of the paracaspase. Notably, the lysosomal cholesterol transporter NPC1 is found less abundant in the degradative compartment, resulting in cholesterol sequestration. This further leads to autophagy defects, activation of a compensatory response to cholesterol deficit, and ultimately, cell death. This places the MALT1-NPC1-cholesterol axis as a targetable pathway in GSCs.

I-1-A- In cholesterol homeostasis

Our work uncovered a strong modification of the cholesterol homeostatic pathways in response to MALT1 inhibition. Notably, the use of mepazine and MLT-748, two allosteric inhibitors of the paracaspase proteolytic function[691,696], allowed us to highlight the paucity of lysosomal NPC1 and the subsequent lysosomal cholesterol retention, partially responsible for GSCs cell death. In parallel, we identified QKI, known partner of MALT1, as responsible for the previously enunciated phenotypes. Therefore, we confirmed MALT1 as a regulator of lysosomal homeostasis and GSCs fate and implemented a novel function on lysosomal cholesterol transport. However, how exactly MALT1 protease function controls these biological outputs remains mysterious, as no substrates have been identified in this pathway.

By analyzing a recent *in silico* study[542], it appears that direct modulators of lysosomal homeostasis and cholesterol trafficking are not represented among the top potential MALT1 substrates. NPC1 and NPC2, for example, are ranked over 10,000 in the list of potential MALT1 substrates. However, this classification takes into account the function of the protein for its ranking, therefore minimizing the score of these proteins, as MALT1 has never been associated with cholesterol homeostasis before. Refining this *in silico* study may help predicting new MALT1 substrates involved in lysosomal and cholesterol homeostasis.

In parallel, we used the SitePrediction web tool[735], assessing the similarities between the known cleavage sites of a protease, here MALT1, and the sequence of a protein of interest. This analysis did not highlight complete overlap between NPC1 sequence and the known cleavage sites of the paracaspase, but one potential cleavage site emerged with an important frequency and similarity score. This potential hit was however located at the arginine 96 of NPC1, in the N-terminal cholesterol binding domain, oriented in the lumen of lysosomes, where MALT1 cannot access (Fig. 33). Therefore, NPC1 appears not to be a direct substrate of MALT1, but rather indirectly regulated.

A

B

rank	position	site	N fragment	C fragment	frequency score	similarity maxscore	similarity maxsite
1	93 to 99	FLSR.CPS	10.7 kD	131.5 kD	0.635	72.973	LVSRCPA
2	408 to 414	LIIR.APL	45.9 kD	96.2 kD	0.010	43.243	LVSRCPA
3	1103 to 1109	GVSL.GAI	123.3 kD	18.9 kD	0.004	35.484	LVSRGAA
4	799 to 805	CCVR.GAE	89.6 kD	52.6 kD	0.001	52.500	CLSRGAH
5	149 to 155	GQSF.ANA	17.1 kD	125.0 kD	0.002	29.412	GASRGEA

C

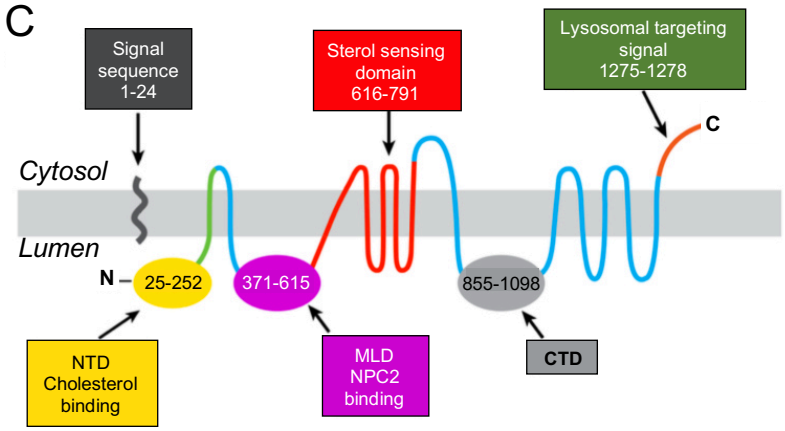

Figure 33: Cleavage pattern of MALT1 paracaspase. A) Cleavage pattern of MALT1 paracaspase. The size of each amino acid is correlated with its representation in all known substrates. B) Top hits of potential MALT1 cleavage sites in the NPC1 protein sequence. The frequency score denotes the score based on the occurrence of each amino acid at each position in the original (known) sites. C) Predicted topology of the human NPC1 protein.
NPC: Niemann-Pick type C, NTD: N-terminal domain, MLD: Middle lumenal domain, CTD: D-terminal domain, TM: Transmembrane, SSD: Sterol sensing domain

Another hypothesis could come from the role of the protein LIMA1 in the cellular addressing of NPC1L1[736]. LIMA1 being a substrate of the API2-MALT1 fusion protein[737], and NPC1L1 sharing important similarities with NPC1 (51% similarity, 42% identity)[738], an indirect function of MALT1 proteolytic activity on cholesterol trafficking is therefore conceivable. A recent study indeed characterized the role of LIMA1 in NPC1L1 addressing to the plasma membrane in intestinal cells. By bridging the cholesterol transporter to the actin cytoskeleton through Myosin Vb interaction, LIMA1 allows NPC1L1 to transit toward its site of action. The effect of LIMA1 cleavage by MALT1 on this phenotype however remains to be determined. Even

though the conclusions of this study are concordant with our model positioning MALT1 as a modulator of NPC1 lysosomal localization, several points need to be taken into account: 1) GSCs do not express the API2-MALT1 fusion protein, 2) LIMA1 is not cleaved in GSCs, and 3) no such control of NPC1 transport have been described in the literature. LIMA1 may then not be responsible for NPC1 mislocalization in MALT1 inhibited GSCs, but the parallel with our model remains intriguing and will need further exploration.

To fully ascribe a function for the proteolytic activity of MALT1 on cholesterol homeostasis in GSCs, the results generated will also need confirmation using the MALT1-protease dead (MALT1-PD; C464A) construct. If such a regulation exists, the expression of MALT1-PD should phenocopy the results obtained by pharmacological and genetic targeting of the paracaspase, such as NPC1 dispersion from the lysosomal compartment, lysosomal cholesterol accumulation, and SREBP2 activation.

I-1-B- In mTOR signaling

MALT1 protease activity is a reported regulator of the mTOR pathway. Two independent studies demonstrated that activation of the paracaspase upon TCR engagement in lymphocytes leads to mTORC1 stimulation, and that the abrogation of the protease activity of MALT1 using z-VRPR-fmk can effectively block mTOR activity[686,687]. Moreover, our group confirmed this in the context of GSCs using pharmacologic inhibitors as well as the MALT1-PD mutant[497]. Despite these results, the potential implication of a substrate is still only hypothesized.

MALT1 positively controls mTORC1, and as such, the candidate substrates are most likely negative regulators of the pathway. This information notably helped in the setup of an *in silico* screening for regulators of mTORC1 cleaved by the paracaspase. Using the SitePrediction web tool (see section I-1-A), most of the known negative regulators of mTORC1 were screened. Among the best candidates was DEPTOR (DEP domain-containing mTOR-interacting protein), direct interactor of mTOR, and potent inhibitor of its activity[739]. Of interest, DEPTOR is expressed in the brain and was linked to the development of neurodegenerative diseases such as Alzheimer[740]. Moreover, DEPTOR protein level was linked to the activity of CK1α[741], known interactor of the CBM complex[615,616]. Therefore, DEPTOR potential processing was assessed by western blot in GSCs. Although not showing cleavage bands

reminiscent of the potential processing of the protein in untreated conditions, MALT1 inhibition resulted in an increase of the full-length form of the protein. The use of other antibodies targeting different epitopes of DEPTOR might help visualizing a potential cleavage band. Accordingly, DEPTOR processing by MALT1 represents a plausible hypothesis, but will obviously need further investigation. Moreover, as the level of DEPTOR is tightly regulated by proteasomal degradation as well as at the transcriptional level in response to numerous inputs such as glucose concentration, hypoxia, or DNA damage[742,743], the increase observed in DEPTOR protein level upon MALT1 inhibition may be the consequence of such a regulatory mechanism, that could be assessed by RT-qPCR analysis.

Another layer of regulation of mTORC1 by MALT1 could come from our demonstration of cholesterol homeostasis modulation by lysosomal dispersion of NPC1. NPC1 has recently been associated with mTORC1, a lower activity of the lysosomal cholesterol transporter correlating with increased mTORC1 substrates phosphorylation[744–746]. Appearing counterintuitive, this result however raises several hypotheses regarding the modulation of mTORC1 in our model. LYCHOS, the lysosomal cholesterol sensor responsible for mTORC1 recruitment and activation at the surface of lysosomes have been shown to be transcriptionally regulated by the feeding state of cells[747]. MALT1 inhibited GSCs deploy a response for intracellular cholesterol replenishment, resembling the one identified in starved cells (increased cholesterol uptake and synthesis, decreased cholesterol export)[748]. As such, investigation of LYCHOS transcript and protein levels in MALT1 inhibited GSCs could help the description of how mTORC1 is regulated upon MALT1 blockade.

In parallel, NPC1 loss was associated with a higher propensity for lysosomal membrane rupture[744]. As lysosomal stability is crucial in mTORC1 recruitment and activation[749,750], the dispersion of NPC1 coupled to the important remodeling of the lysosomal compartment upon MALT1 inhibition may synergize to promote lysosomal membrane instability, therefore responsible for mTORC1 dysfunction. Lysosomal membrane permeabilization should therefore be investigated in the context of MALT1 inhibition, in parallel of cholesterol manipulation and NPC1 blockade, and the subsequent mTORC1 activity assessed by biochemical assays.

I-1-C- On QKI functions

In GSCs, the Quaking (QKI) STAR RNA-binding protein is held in check by the constitutive activity of MALT1, therefore repressing the lysosomal compartment[497]. The precise mechanism by which MALT1 activity represses QKI functions however remains to be elucidated. The inhibitory interaction mediated by MALT1 protease may rely on the activity of an intermediate yet unidentified substrate, as the expression of the MALT1-PD mutant unleashes QKI activity and promotes lysosomal biogenesis[497]. Moreover, the specific subset of mRNA encoding lysosomal proteins translated with the help of QKI in MALT1-inhibited conditions is still unknown. The use of photoactivatable-ribonucleoside-enhanced cross-linking and immunoprecipitation (PAR-CLIP)-coupled RNA–seq analysis[496] of RNA linked to QKI after MALT1 inhibition could answer this question.

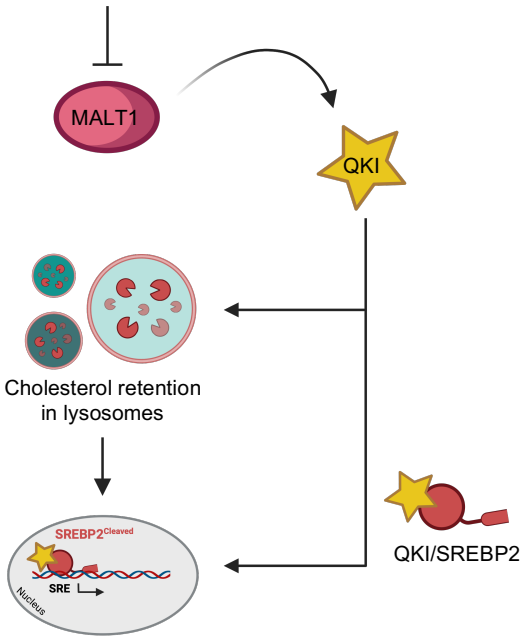

Figure 34: QKI activity on SREBP2. MALT1 inhibition releases QKI, unleashing its activity toward lysosomes modulation. Cholesterol becomes trapped in the aberrant lysosomal compartment, reducing its concentration in other cellular compartments, resulting in the activation of the SREBP2 transcription factor. In parallel, QKI is thought to directly mediate SREBP2 transcriptional activity, increasing cholesterol uptake and synthesis.

In parallel, our work demonstrated the activation of the SREBP2 transcription factor and the subsequent increase in the cholesterol biosynthetic pathway in response to MALT1 inhibition as visualized by ChIP-qPCR, RNAseq, as well as biochemical assays. Interestingly, the Jian Hu laboratory recently published two papers coupling QKI activity to SREBP2 mediated regulation of the cholesterol biosynthetic pathway[751,752]. Notably, QKI was shown to be a direct interactor of SREBP2, its knock-out resulting in myelogenesis deficits and cataract development as a consequence of impaired cholesterol biosynthesis. Our work corroborates the involvement of QKI in SREBP2-mediated cholesterol level increase in GSCs inhibited

for MALT1. However, whether QKI is directly involved in this phenotype, or indirectly though the dispersion of NPC1 and lysosomal cholesterol sequestration requires attention. QKI silencing resulted in the rescue of NPC1 level in the lysosomal compartment of MALT1-inhibited GSCs, pointing toward the indirect modulation of SREBP2 by QKI, but the binding of the RNA-binding protein to the SREBP2 transcription factor should be assessed by co-immunoprecipitation experiments.

II- Clarifying the implications of MALT1 in GSCs' cell death

MALT1 activity have been linked to the survival of GSCs, its pharmacologic and genetic inhibition eradicating this cell subpopulation[497]. Our previous work highlighted lysosomal proteases release as partially involved in GSCs cell death induction, with the use of cathepsins inhibitors significantly reducing this phenotype[497]. Even though significant, cell death was only partially rescued, implementing other mechanisms alongside lysosomal membrane permeabilization (LMP) in MALT1 inhibition-induced cell death.

The implication of MALT1 inhibition-mediated lysosomal cholesterol sequestration, mTORC1 inhibition, and autophagy defects, will be discussed in regard of the loss of lysosomal homeostasis and consecutive cell death.

II-1- Lysosomal cell death

The description of the mechanisms by which cells sense and cope with lysosomal membrane destabilization have recently attracted a lot of effort. Upon lysosomal membrane rupture, galectins bind to accessible intra-lysosomal β-galactosides, therefore offering a tool for LMP visualization[753,754]. From a molecular standpoint, galectins recruitment to damaged lysosomes have also been ascribed important molecular functions, such as recruitment of the ESCRT complexes for lysosomal repair, or mTORC1 inhibition for autophagic removal[749,750,755]. In our system, LMP remains however hardly detectable, as we cannot visualize galectins agglomeration on lysosomes upon MALT1 inhibition. Other tools should be used to examine the implication of this pathway for lysosomal repair. We could also hypothesize the low expression of this machinery in GSCs as compared to healthy cells, therefore explaining the important sensibility of GSCs toward lysosomal destabilization[121–127].

In parallel, the ‘’rapid lysosomal repair machinery’’ setup by cells to overcome lysosomes damage[756,757] should be assessed in our model. Notably, the establishment of a pool of phosphoinositide 4-phosphate (PI(4)P) on damaged lysosomes for the consecutive ER-to-lysosome transfer of cholesterol for membrane repair would be an important parameter to follow in response to MALT1 inhibition. The use of recently developed probes specifically staining phosphoinositides[756,757], as well as lipidomic analysis of the immunopurified lysosomal compartment could improve our understanding of the mechanisms responsible for the lysosomal susceptibility.

Finally, lysosomal cholesterol accumulation is an important phenotype to consider in the onset of LMP. However, divergent studies ascribed opposite functions of this lipid in lysosomal sensibility to damage. Three independent groups defined lysosomal cholesterol sequestration as a protective event[757–760], whereas one demonstrated the contrary, with the use of the NPC1 inhibitor U18666A increasing the sensibility of lysosomes to LLOMe-induced damage[744]. As the abovementioned studies all employed different cell types, this raised the hypothesis of a cell type dependent mechanism. In this context, GSCs appear sensitive to lysosomal cholesterol sequestration, as the sole use of the NPC1 inhibitor U18666A can effectively reduce GSCs survival, and as MALT1 inhibition induces the combination of lysosomal cholesterol retention followed by LMP. A pretreatment of GSCs with U18666A followed by LLOMe administration and assessment of LMP by dosage of cathepsins release could complete our knowledge about the precise function of lysosomal cholesterol retention on lysosomal stability.

II-2- mTOR/autophagy

The serine/threonine kinase mTOR acts at the surface of lysosomes to control catabolism and anabolism. As such, the activation of mTOR is linked to proliferation, growth, and survival[761]. In the context of GB, several commonly observed mutations were linked to increased activity of the mTOR pathway, notably EGFR amplification and PTEN loss[762,763]. Therefore, inhibiting mTOR was highlighted as an attractive therapeutic option for GB. However, clinical trials failed to prove efficacy, probably as the inefficiency of previously used inhibitors to jointly block all the aspects regulated by mTOR, such as autophagy or protein translation[764–766]. *In vitro*, mTOR blockage

demonstrated partial reduction in GSCs viability via apoptosis induction[767,768]. As such, defining the extent of mTOR implication in GSCs survival and GB development, as well as its upstream regulators, is of particular interest.

As already discussed, MALT1 activity participates in mTOR signaling (see section I-1-B)[686,687]. In GSCs, the constitutive activity of the paracaspase supports the binding of mTOR to lysosomes and its subsequent downstream signaling[497]. Therefore, MALT1 inhibition results in mTOR dispersion from its lysosomal hub and shutdown of the pathway as visualized with the decrease in phosphorylation of its known substrates[497]. In this context, mTOR inhibition might participate in the mechanisms involved in GSCs death. The use of mTOR activators, such as MHY1485[769], to counteract the effect of MALT1 inhibition on mTOR, could help understand its implication on the phenotypes described in our model, notably cell death.

In parallel, mTOR dampens the autophagic pathway via phosphorylation of TFEB, ULK, and ATGs[761]. Autophagy implication in GSCs survival is still importantly debated. Indeed, via degradation of damaged organelles and unwanted material, the autophagic pathway may sustain GSCs homeostasis, but other studies suggested a detrimental effect of autophagy inhibition, placing autophagy inhibitors as therapeutical opportunities for GB treatment[770,771]. In our hands, the autophagy defects observed upon MALT1 inhibition correlate with the extent of cell death. Indeed, the addition of cholesterol-methyl-β-cyclodextrin (Chol/MβCD) complexes, shown to significantly rescue cell death, also counteracted LC3B and P62 accumulation. While appearing as a consequence of lysosomal dysfunctions, autophagy blockade may participate in the cell death mechanism engaged by GSCs upon MALT1 inhibition.

Altogether, the lysosomal defects, the inhibition of mTOR, and the autophagic flux blockade observed in our model, may synergize to induce GSCs death.

II-3- Cholesterol

Cholesterol is a major building block for cellular membrane composition and contributes to signaling events. Of interest, twenty percent of all body cholesterol is located in the brain, and deregulation of its homeostasis have been linked to the development of neurodegenerative diseases such as Alzheimer and Parkinson[150]. In line with this, mutations in NPC1 or NPC2 engender Niemann-Pick disease, a rare

metabolic lysosomal storage disease characterized by cholesterol retention in lysosomes[772]. Our data support the fact that NPC1 is dispersed from the lysosomal compartment upon MALT1 inhibition, therefore recapitulating the phenotypes identified in NPC1 deficient cells. Of note, GSCs were demonstrated as sensitive to NPC1 inhibition. Moreover, SREBP2-dependent cholesterol synthesis was shown to protect GSCs from MALT1-induced cell death, and the use of the cholesterol depleting agent methyl-β-cyclodextrin efficiently abrogated GSCs survival. All these phenotypes strongly suggest a protective role of cholesterol in this setup.

This is in line with the study of Genaro Villa that highlighted the dependency of GB cells to a finely regulated cholesterol homeostasis. It was notably showed that GB cells rely on exogenous cholesterol uptake to survive, as their cholesterol synthesis machinery is downregulated when compared to healthy brain cells. Afterward, by using LXR agonists (reduced cholesterol synthesis and uptake, increased cholesterol secretion), the group was able to specifically eradicate GB cells *in vitro* and *in vivo*. Overall, this corroborates our findings and places cholesterol as a pro-survival lipid in glioblastoma. The combination of LXR agonists and MALT1 inhibitors might increase the specificity and the efficiency of both treatments.

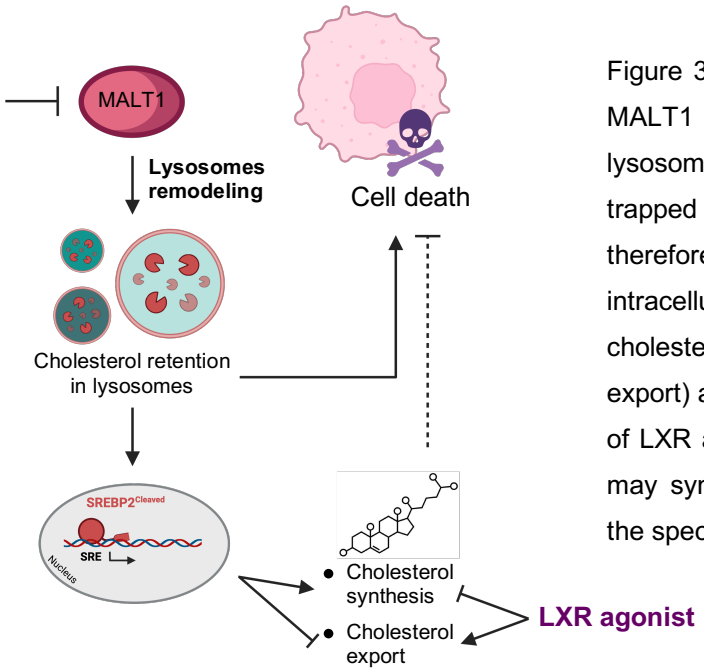

Figure 35: Use of LXR agonists in GB. In GSCs, MALT1 inhibition results in the remodeling of the lysosomal compartment. Cholesterol becomes trapped in the degradative organelle. GSCs therefore deploy an arsenal to replenish intracellular cholesterol level (increased cholesterol synthesis and uptake, decreased export) and to try to counteract cell death. The use of LXR agonists, activating the opposite pathway, may synergize with MALT1 inhibition to promote the specific cell death of GSCs.

III- Hypothesizing the use of lysosome storage diseases' inducers as a therapy for glioblastoma

Lysosomal storage diseases (LSDs) are a group of more than seventy inherited disorders impairing lysosomal functions. While individually rare, LSDs are collectively affecting nearly one in five thousand births. Clinically, LSD patients mostly develop neurodegenerative symptoms, although other organs can be affected. Notably, the incapacity of lysosomes to complete their degradative functions, as well as the intra-lysosomal accumulation of undigested material (mostly lipids and proteins), is harmful for the cells[451].

III-1- Niemann-Pick disease type C

Niemann–Pick disease types C1 and C2 (NPC) develop in patients harboring mutations in the cholesterol transport proteins NPC1 and NPC2 respectively. NPC2 is a lysosomal lumenal protein able to capture the lysosomal pool of free cholesterol and works in concert with the lysosomal membranous protein NPC1[773]. By contacting NPC1, NPC2 increases the rate of lysosomal cholesterol export[774]. Indeed, NPC1 acts as a lysosomal cholesterol exporter[468,775] in parallel to the discrete function of other lysosomal membrane proteins such as LAMP2 or LIMP2[776,777]. Therefore, loss-of-function mutations in NPC1 and NPC2 induce lysosomal cholesterol retention, altering their catabolic functions, ending up in the development of neurologic symptoms[463].

Our work unraveled that MALT1 inhibition remodels the lysosomal proteome of GSCs, notably by reducing the level of cholesterol-related proteins in the degradative compartment. NPC2, and mostly NPC1, were shown to be less abundant in the lysosomes of MALT1 inhibited GSCs. Consecutively, we could observe classical NPC phenotypes, such as lysosomal cholesterol and LBPA accumulation, reduced autophagic flux, and activation of the SREBP2 pathway. This culminated in the specific cell death of GSCs, as healthy astrocytes and brain endothelial cells were resistant to MALT1 inhibition. This could be explained by the increased sensitivity of GSCs to lysosomal destabilization[121–127], as well as their vulnerability to cholesterol homeostasis deregulation[151,153]. Similarly, directly inhibiting the function of NPC1 by a pharmacological approach (U18666A[778]), or by siRNA-based silencing, significantly affected GSCs viability as compared to healthy brain cells. This result is concordant

with *in silico* analysis of the TCGA demonstrating the increased probability of survival of GB patients presenting low expression of NPC1 and NPC2. Moreover, the *in vivo* data generated in xenograft mice models suggests the effectiveness of inhibiting MALT1 or NPC1 to counteract GB growth. As previously stated, GSCs, the main reservoir for GB initiation and recurrence, are especially sensitive to lysosome destabilization and cholesterol homeostasis modulation. As such, the induction of LSD phenotypes appears of interest for the targeting of this cell subpopulation, especially because the viability of healthy astrocytes and brain endothelial cells was not overtly affected by NPC1 and MALT1 inhibition. However, while viability is not affected, whether their functions are impaired is still unknown and will need further investigations before stating that NPC1 is a targetable protein in the context of GB.

The targeting of MALT1 represents another option for GB treatment. Mepazine as well as MLT748, two allosteric inhibitors of the paracaspase[691,696], efficiently reduced the growth of xenotransplanted GSCs[121]. As compared to NPC1 inhibition, MALT1 targeting may prove specificity for GSCs targeting. Indeed, MALT1 has been found active in this subset of cells as compared to healthy brain cells. Its pharmacological targeting as well as its genetic inhibition results in GSCs' elimination by mean of LSD phenotypes induction. However, and as for NPC1 inhibition, while not killed by MALT1 inhibition, healthy brain cells still need to be characterized in response to mepazine or MLT748 treatments, to discard potential off-target effects of the compounds.

Moreover, the precise mechanism by which MALT1 controls NPC1 lysosomal localization is still uncertain. Two main hypotheses can be raised.

1) Retention

As demonstrated by performing proteomic analysis of total GSC lysate combined to the one performed in immunopurified lysosomes, MALT1 inhibition results in the reduction of NPC1 level specifically in the lysosomes, without modification of its total cellular concentration. As some mutations identified in the NPC1 gene and responsible for the development of the NPC disease were linked to retention of the protein in the ER[779–781], MALT1 inhibition may therefore modify the localization and transport of the protein to its site of action.

2) Dilution

MALT1 inhibition have been linked to the release and activation of QKI, positively correlating with the abundance of lysosomes[121]. The number of lysosomes

importantly increasing after blockage of the paracaspase, meanwhile NPC1 transcript and protein level not being modified, NPC1 may therefore be diluted among the pool of newly formed and aberrant lysosomes.

Several experiments could be considered to investigate these two hypotheses. Firstly, immunofluorescent staining of NPC1 combined with the revelation of specific organelle markers could help identify whether NPC1 is relocalized to another compartment in response to MALT1 inhibition. Coupling this to the use of micropatterned microscopic slides to ensure the spreading of GSCs and the enlargement of their cytosolic compartment could be useful to precisely determine NPC1 localization. Secondly, the use of density gradient to separate cellular organelles may highlight a potential repositioning of NPC1. Notably, this technique may allow the characterization of a potential lysosomal heterogeneity upon MALT1 inhibition, with the cholesterol-filled lysosomes being separated from the pool of NPC1-positive lysosomes.

Altogether, targeting NPC1, either directly or via the use of MALT1 inhibitors, appears as a promising opportunity for GSCs eradication and GB treatment. This is however dampened by the effect of such targeting on non-cancerous cells. While their viability is not overtly affected, a deeper phenotypic characterization will warrant the safety of these approaches for the treatment of GB.

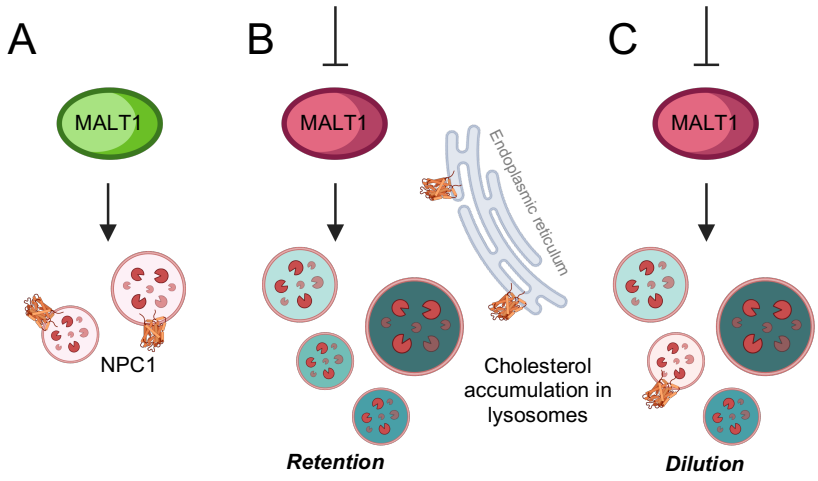

Figure 36: NPC1 localization in MALT1-inhibited GSCs. A) In basal conditions, MALT1 is found constitutively active in GSCs. This represses the lysosomal compartment. B) Upon MALT1 inhibition, NPC1 may relocalize in other cellular compartments such as the ER. C) Newly generated lysosomes are aberrant, NPC1 is therefore diluted, leading to lysosomal cholesterol accumulation.

III-2- GSCs specificity

Genes defined as non-oncogene addictions (NOA) support the propagation of cancers, without showing mutations or impact in tumorigenesis[733]. Paralleling what can be observed in the ABC subtype of DLBCL, MALT1 and its constitutive activity have been defined as a non-oncogene addiction for GSCs, its targeting being deleterious for the growth and survival of this cell subpopulation[121,782]. How is MALT1 constitutively active in this context is still mysterious, but upstream modulators of the CBM assembly and further MALT1 activation such as the EGFR are often found mutated in GB[734,762], potentially opening new effective and broader therapeutic opportunities.

The inhibition of MALT1 and the subsequent lysosomal editing and cholesterol homeostasis modulation are particularly effective for the elimination of GSCs (see section II) [122,153]. But whether the same regulation of lysosomal stability and cholesterol homeostasis is operated by MALT1 in other cell types is still unknown. Visualization of the lysosomal compartment and cholesterol traffic upon MALT1 inhibition in the ABC subtype of DLBCL would be of interest.

Finally, pharmacological inhibition of NPC1 using U18666A repressed GSCs viability. Importantly, this treatment did not significantly decrease the viability of healthy astrocytes and brain endothelial cells, suggesting a specificity toward GSCs. However, and interestingly, ABC-DLBCL, relying on MALT1 constitutive activity for their survival were almost as sensitive as the GSCs to the U18666A treatment. Rather than only appearing as a specificity in GSCs, NPC1 inhibition seems deleterious for MALT1-active cells. As only tested in one ABC-DLBCL cell line, this result obviously needs confirmation, but opens an interesting hypothesis concerning a broader function of MALT1 in lysosome editing.

Conclusion and Perspectives

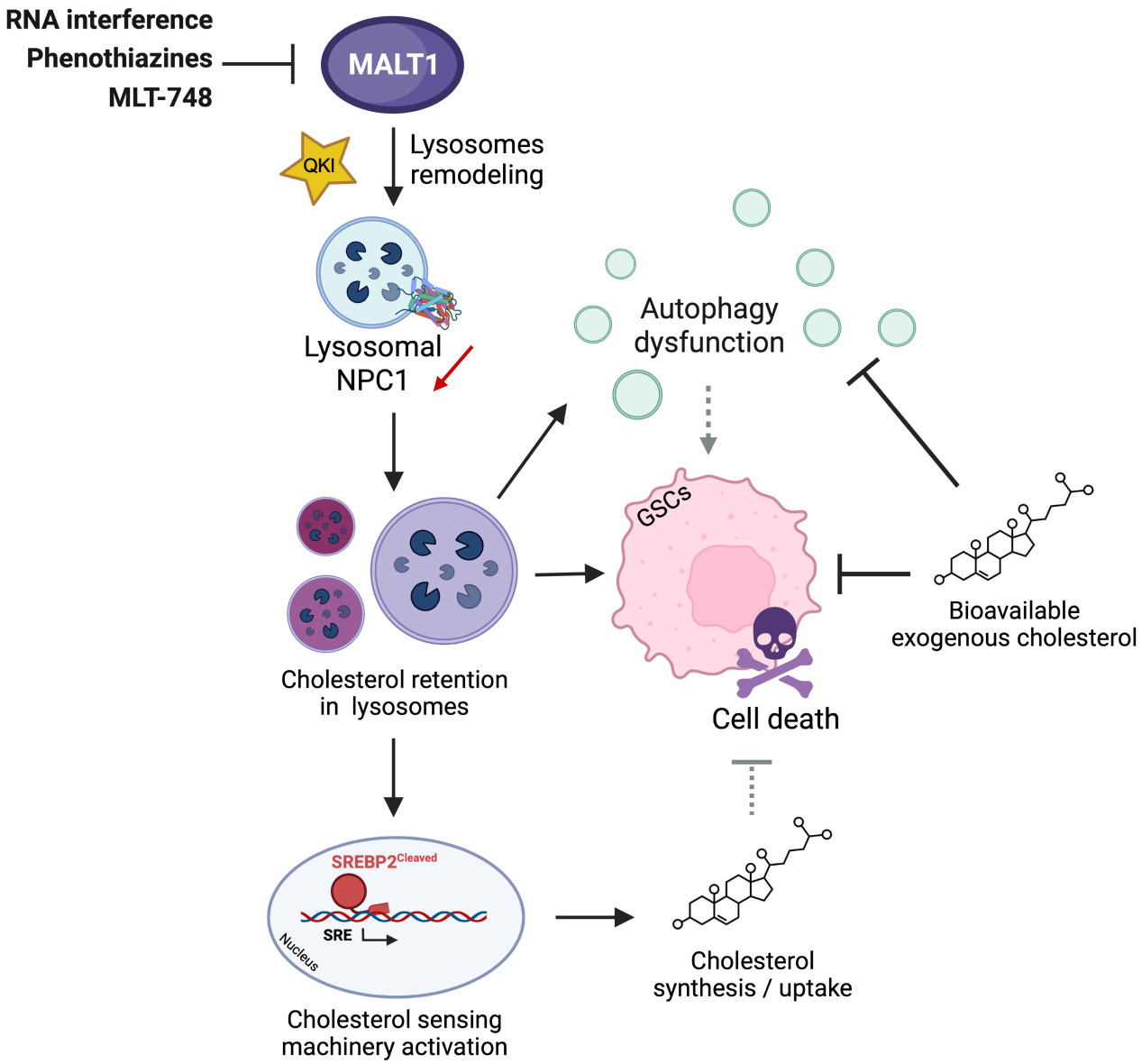

Figure 37: MALT1 modulates lysosomal NPC1 and cholesterol homeostasis. In GSCs, inhibiting the constitutive activity of MALT1 remodels the lysosomal proteome and notably reduces NPC1 level in this organelle. The subsequent lysosomal cholesterol sequestration induces autophagy disfunction, the activation of the cholesterol replenishment machinery, and finally, cell death. Feeding MALT1 inhibited GSCs with cholesterol partially counteracts all the above-mentioned phenotypes, placing lysosomal cholesterol handling as a targetable mechanism in GSCs.

To explore the roles of MALT1 and NPC1 in GSCs, we employed a combination of RNA silencing and pharmacological agents. While these approaches yielded similar responses (SREBP2 activation, cholesterol accumulation, autophagy, and cell viability), they may induce divergent responses in terms of amplitude and kinetics. This will warrant further investigation at a multiscale resolution. Moreover, non-GSC models such as astrocytes and endothelial cells, were used with parsimony to control for the effects of MALT1. It will be of paramount importance to next evaluate the role of MALT1 on cholesterol distribution in non-cancer contexts, notably upon MALT1 physiological activation (e.g. lymphocyte activation). Ultimately, further research is essential to fully explore the in vivo translation of our discoveries, with a particular focus on understanding the contribution of cholesterol supply and overall homeostasis.

- Matched-omic approach reveals that the paracaspase MALT1 adjusts cholesterol level
- MALT1 blockage causes cholesterol sequestration in supernumerary lysosomes
- MALT1 prevents cholesterol transporters exhaustion and lysosomal proteome editing
- The targeting of NPC1 abrogates glioblastoma cell viability

Annexes

Annex 1 – Review - Glioblastome multiforme - Les fleurs du MALT1

Annex 2 – Review - Lysosomes in glioblastoma: pump up the volume

Annex 3 – Scientific publications

Annex 4 – Scientific communications

Annex 1 – Glioblastome multiforme - Les fleurs du MALT1

Glioblastome multiforme

Les fleurs du MALT1

Clément Maghe[1], Kathryn A. Jacobs[1], Nicolas Bidère[1], Julie Gavard[1,2]

[1]Équipe SOAP (Signalisation en oncogenèse, angiogenèse et perméabilité), CRCINA (centre de recherche en cancérologie et immunologie Nantes Angers), Inserm, CNRS, Université de Nantes, Université d'Angers, IRSUN (Institut de recherche en santé de l'université de Nantes), 8 quai Moncousu, 44000 Nantes, France.
[2]Institut de cancérologie de l'Ouest (ICO), Saint-Herblain, France.
julie.gavard@inserm.fr

Le glioblastome multiforme, un cancer incurable

L'Organisation mondiale de la santé (OMS) a défini le glioblastome multiforme comme un cancer astrocytaire de grade IV. La survie médiane de cette tumeur cérébrale est d'environ 15 mois, malgré un traitement combinant chirurgie intracrânienne et séances concomitantes de radiothérapie et de chimiothérapie [205]. Les rechutes à proximité de la tumeur initiale, quasi inéluctables, évoluent rapidement et inexorablement jusqu'au décès du patient. Cet échec thérapeutique peut s'expliquer non seulement par les résistances intrinsèques des cellules tumorales, mais aussi par la présence d'un groupe minoritaire de cellules tumorales aux caractéristiques de cellules souches (*glioblastoma stem-like cells,* GSC). Les résultats de plusieurs travaux convergent vers l'idée que les GSC contrôlent l'initiation, la progression et la rechute de ces tumeurs [205], bien que les mécanismes en jeu restent mal compris. Ces cellules partagent de nombreuses caractéristiques avec les cellules souches neurales adultes, notamment la capacité d'autorenouvellement et de différenciation dans le lignage neural [205]. Éradiquer cette fraction de cellules tumorales apparaît donc comme une stratégie thérapeutique pertinente.

MALT1 et la gliomagenèse

Afin d'identifier des facteurs de vulnérabilité contrôlant l'expansion des GSC, les données transcriptomiques du TCGA (*the cancer genome atlas*) concernant plus de 400 patients atteints d'un glioblastome ont été interrogées. En se concentrant sur les gènes impliqués dans l'activation du facteur de transcription NF-κB (*nuclear factor-kappa B*), une voie essentielle dans la prolifération et la survie cellulaires dans de nombreux cancers [205, 206], la paracaspase MALT1 (*mucosa-associated lymphoid tissue lymphoma translocation protein 1*) a émergé comme un nouvel acteur potentiel de la gliomagenèse [205]. L'expression de cette enzyme apparaît en effet corrélée à la fois au grade des tumeurs cérébrales et à la survie des patients atteints d'un glioblastome. Les fonctions cellulaires de MALT1 sont doubles. D'une part, elle agit en tant que protéine adaptatrice au sein du complexe de protéines impliqué dans la mise en place de la voie de signalisation NF-κB [205, 206], et, d'autre part, elle exerce une activité protéolytique à un site consensus de la séquence de ses protéines cibles, après un résidu arginine. Le nombre de substrats avérés de MALT1 se limite à une dizaine, mais leur champ d'action s'étend du contrôle des voies NF-κB et JNK (*jun N-terminal kinase*), à l'adhérence cellulaire et à la stabilité des ARN [205] (*Figure 1*). La protéase MALT1, normalement maintenue dans une conformation inactive, est activée dans les cellules immunitaires pour contrôler la signalisation antigénique [205]. C'est aussi le cas dans les cellules non-immunitaires en réponse à l'activation de certains récepteurs membranaires (*Figure 1*). Pourtant, une étude biochimique du répertoire connu des substrats de MALT1 montre qu'une fraction de cette protéase est constitutivement active dans les GSC [205]. En accord avec ce résultat, l'expression d'une version de MALT1 dépourvue d'activité catalytique permet de réduire la protéolyse de ses substrats dans les cellules de patients atteints d'un glioblastome. Nos résultats sont en faveur de l'idée que MALT1 serait « piratée » dans le glioblastome, comme c'est le cas dans certains lymphomes [203–205].

MALT1 contribue à la survie des GSC

Par analogie avec les travaux démontrant l'addiction de cellules de lymphomes à l'activité de MALT1 [205, 206], nous avons exploré l'impact de l'expression et de l'activité de cette protéase sur le maintien du réservoir de GSC et avons montré que la réduction de l'expression de MALT1 dans des GSC induit une diminution de leur prolifération, de leur survie, et de l'expression de marqueurs de ces cellules [205]. Ces résultats ont été reproduits en utilisant des inhibiteurs de MALT1, tels que l'antagoniste peptidique compétitif z-VRPR-fmk, et des médicaments de la famille des phénothiazines, comme la molécule anti-psychotique mépazine, un inhibiteur allostérique de MALT1 [205] (*Figure 2*). Ces agents pharmacologiques ont une toxicité sélective pour les GSC, et n'affectent pas la viabilité de cellules saines du cerveau (astrocytes, neurones, et cellules endothéliales) [205]. Finalement, l'administration journalière de mépazine permet de réduire de façon significative la croissance tumorale dans un modèle de souris greffées avec des GSC humaines [205]. Ces résultats montrent que la protéase MALT1 est nécessaire au maintien des GSC et contribue à l'expansion tumorale.

https://doi.org/10.1051/medsci/20203605073

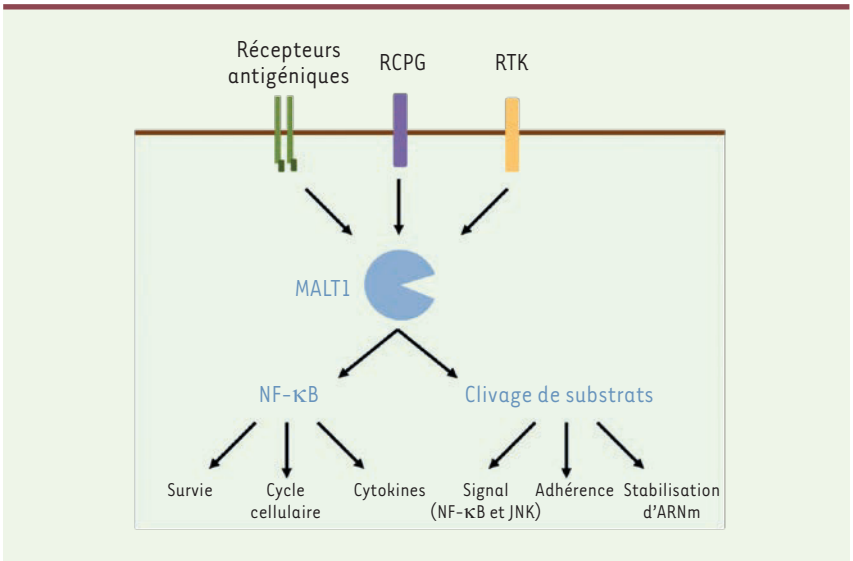

Figure 1. ***MALT1 est un acteur essentiel de la voie de signalisation NF-κB.*** La protéine MALT1 est activée par la stimulation des récepteurs antigéniques dans les cellules immunitaires, ainsi que par l'activation des récepteurs à activité tyrosine kinase (RTK) ou couplés aux protéines G (RCPG) dans les cellules non-immunitaires. Par sa fonction de protéine adaptatrice, MALT1 contribue à l'élaboration d'un complexe de signalisation en charge d'activer le facteur de transcription NF-κB. Cette cascade de signalisation libère également l'activité enzymatique de la paracaspase MALT1. La protéolyse des substrats de MALT1 module des mécanismes d'adhérence cellulaire, de stabilité des ARN messagers (ARNm), et de la régulation des voies NF-κB et JNK.

Rôle de MALT1 dans l'homéostasie des lysosomes

Fonctionnellement, nos résultats indiquent que la mort des GSC induite par la mépazine n'implique pas un processus de mort cellulaire programmée par apoptose ou nécroptose [205]. En revanche, le blocage des enzymes du lysosome, telles que les cathepsines, contrecarre en partie l'effet de la mépazine sur la viabilité des GSC. En outre, l'inhibition de MALT1 est associée au relargage de protéases du lysosome dans le cytoplasme, suggérant donc un phénomène de perméabilisation de la membrane lysosomale [205], fatal aux GSC. Par ailleurs, des analyses du compartiment endo-lysosomal des GSC par imagerie cellulaire ont montré une augmentation de l'abondance de ce compartiment en cas d'inhibition de MALT1 ou de réduction de son expression [205]. Ces résultats font écho aux données récentes indiquant que le nombre de lysosomes est finement régulé dans les cellules souches neurales normales, et que ce nombre contrôle la survie des GSC [205-205]. MALT1 agirait donc comme un rempart contre une augmentation de la quantité de lysosomes, nocive pour les GSC, dévoilant ainsi un facteur de vulnérabilité de ces cellules *(Figure 2)*.

Dans le but de comprendre le lien entre MALT1 et les lysosomes, nous avons mené une analyse transcriptomique par séquençage de l'ARN dans les GSC traitées ou non à la mépazine [205]. Étonnamment, l'expression des gènes impliqués dans l'homéostasie et la biogenèse endo-lysosomales n'est pas modifiée en réponse à l'inhibition de MALT1. En revanche, l'analyse *in silico* des données transcriptomiques prédit la modification d'une signature de gènes correspondant à la voie de signalisation mTOR (*mammalian/mechanistic target of rapamycin*). Ces résultats nous ont conduits à étudier plus en détail la voie de signalisation mTOR, dont une partie des protéines est ancrée aux lysosomes. Nous avons montré que l'inhibition de MALT1 déconnecte mTOR des lysosomes et atténue la voie de signalisation mTOR tumorale [205], essentielle au maintien des GSC [205]. Ainsi, l'inactivation de MALT1 entraîne une augmentation incontrôlée de la biosynthèse des lysosomes qui, en plus, semblent dysfonctionnels. En effet, nos résultats suggèrent que les lysosomes nouvellement formés ont une plus grande perméabilité de leur membrane, ce qui permet à des enzymes protéolytiques, normalement confinées à l'intérieur des lysosomes, d'exercer leur activité dans le cytosol. En outre, une analyse en imagerie confocale montre que les lysosomes nouvellement formés sont déconnectés de la voie de signalisation mTOR. Nos recherches s'attachent désormais à mieux caractériser les défauts de ces lysosomes.

Comment MALT1 peut-elle moduler la quantité de lysosomes ? L'action déterminante de *quaking* (QKI), une protéine qui se lie à l'ARN messager (ARNm), dans le maintien des GSC a récemment été rapportée [205]. Cette protéine permet en effet de stabiliser des ARNm codant des protéines endo-lysosomales. Nous avons montré que MALT1 et QKI interagissent dans les GSC [205]. La surexpression de QKI, qui modifie la stœchiométrie du complexe MALT1/QKI, suffit à reproduire les effets de l'inhibition de MALT1 dans les GSC. Inversement, la réduction de l'expression de QKI permet de contrer l'effet de l'inhibition de MALT1 dans ces cellules [205]. Ainsi, il existe une interaction réciproque antagoniste entre ces deux protéines.

Perspectives

Nos travaux attribuent donc un nouveau rôle à la protéase MALT1 dans l'homéostasie des lysosomes. Par la rétention de QKI, MALT1 restreint la genèse du compartiment endo-lysosomal. Nous montrons également que l'activité de MALT1 permet la signalisation mTOR, essentielle à l'expansion des GSC, renforçant l'idée que MALT1 participe au contrôle de cette voie métabolique. En révélant

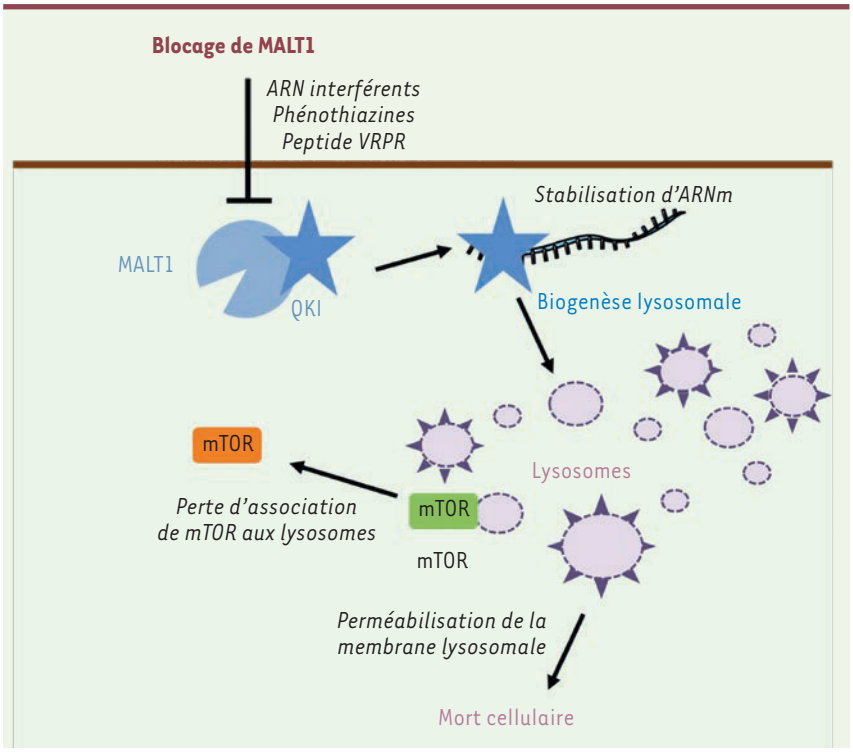

Figure 2. ***MALT1 est un agent essentiel de l'homéostasie des lysosomes dans les GSC.*** Dans les cellules de type « cellule souche » du glioblastome (GSC, *glioblastoma stem-like cells*), MALT1 interagit avec la protéine *quaking* (QKI), une protéine de liaison à l'ARN. L'inhibition de l'activité enzymatique de MALT1 par les phénothiazines ou par le peptide compétitif VRPR, ainsi que la réduction de son expression par des ARN interférents libère QKI, qui exerce alors son activité de protéine de liaison à l'ARN, et autorise la traduction d'ARN messagers (ARNm) codant des protéines du lysosome. Il en résulte une abondance anormale des lysosomes. Les lysosomes nouvellement formés ont une membrane plus perméable aux protéases et sont déconnectés de la voie de signalisation mTOR. La perte d'intégrité de la membrane de ces lysosomes induit un déversement de leurs enzymes dégradatives dans le cytosol, conduisant à la mort des GSC.

le rôle de la protéase MALT1 dans le contrôle de la quantité et de l'activité des lysosomes qui, lorsqu'ils sont en excès, empêchent l'expansion des GSC, nos résultats ouvrent une perspective thérapeutique originale dans le combat contre le glioblastome multiforme. ◊

MALT1 in glioblastoma: the Flowers of Evil

REMERCIEMENTS

Nous tenons à remercier les membres présents et passés du laboratoire « Signalisation en oncogenèse, angiogenèse et perméabilité », Centre de recherche en cancérologie-immunologie de Nantes Angers, Inserm, CNRS, université de Nantes. Les projets de l'équipe sont soutenus par la fondation pour la recherche médicale, la fondation ARC, la Ligue contre le cancer, la Fondation de France, et l'Institut national du cancer.

LIENS D'INTÉRÊT

Les auteurs déclarent n'avoir aucun lien d'intérêt concernant les données publiées dans cet article.

RÉFÉRENCES

1. Stupp R, Mason WP, Van den Bent MJ, *et al.* Radiotherapy plus concomitant and adjuvant temozolomide for glioblastoma. *N Engl J Med* 2005 ; 352 : 987-96.
2. Lathia JD, Mack SC, Mulkearns-Hubert EE, *et al.* Cancer stem cells in glioblastoma. *Genes Dev* 2015 ; 29 : 1203-17.
3. Thys A, Douanne T, Bidere N. Post-translational modifications of the CARMA1-BCL10-MALT1 complex in lymphocytes and activated B-cell-like subtype of diffuse large B-cell lymphoma. *Front Oncol* 2018 ; 8 : 498.
4. Nagel D, Spranger S, Vincendeau M, *et al.* Pharmacologic inhibition of MALT1 protease by phenothiazines as a therapeutic approach for the treatment of aggressive ABC-DLBCL. *Cancer Cell* 2012 ; 22 : 825-37.
5. Jacobs KA, André-Grégoire G, Maghe C, *et al.* Paracaspase MALT1 regulates glioma cell survival by controlling endo-lysosome homeostasis. *EMBO J* 2020 ; 39 : e102030.
6. Aits S, Jäättelä M. Lysosomal cell death at a glance. *J Cell Sci* 2013 ; 126 : 1905-12.
7. Shingu T, Ho A L, Yuan L, *et al.* Qki deficiency maintains stemness of glioma stem cells in suboptimal environment by downregulating endolysosomal degradation. *Nat Genet* 2017 ; 49 : 75-86.
8. Leeman DS, Hebestreit K, Ruetz T, *et al.* Lysosome activation clears aggregates and enhances quiescent neural stem cell activation during aging. *Science* 2018 ; 359 : 1277-83.
9. Le Joncour V, Filppu P, Hyvönen M, *et al.* Vulnerability of invasive glioblastoma cells to lysosomal membrane destabilization. *EMBO Mol Med* 2019 ; 11 : e9034.
10. Galan-Moya EM, Le Guelte A, Lima Fernandes E, *et al.* Secreted factors from brain endothelial cells maintain glioblastoma stem-like cell expansion through the mTOR pathway. *EMBO Rep* 2011 ; 12 : 470-6.

Annex 2 – Lysosomes in glioblastoma: pump up the volume

CELL CYCLE
2020, VOL. 19, NO. 17, 2094–2104
https://doi.org/10.1080/15384101.2020.1796016

Taylor & Francis
Taylor & Francis Group

REVIEW

Lysosomes in glioblastoma: pump up the volume

Kathryn A Jacobs[a], Clément Maghe[a], and Julie Gavard[a,b]

[a]Team SOAP, CRCINA, Inserm, CNRS, Université De Nantes, Université d'Angers, Nantes, France; [b]Integrated Center for Oncology, ICO, St. Herblain, France

ABSTRACT

Lysosomes are acidic, dynamic organelles that supervise catabolism, integrate signaling cascades, and tune cellular trafficking. Moreover, the loss of their integrity may jeopardize cell viability. In cancer cells, lysosomes are qualitatively and quantitatively modified for the tumor's own benefit. For all these reasons, these organelles emerge as appealing intracellular targets to manipulate non-oncogene addiction. This is of particular interest for brain diseases, including neurodegenerative disorders and cancer, in which stem cells are exhausted and transformed, respectively. Recent publications had demonstrated that stem cells displayed disarmed lysosomes in terms of number and functions during aging and oncogenic progression. Likewise, our laboratory identified that the arginine protease MALT1, normally dedicated to the assembly of proper NF-kB activation and processing a number of substrates, arbitrates lysosome biogenesis and mTOR signaling in glioblastoma stem-like cells. Indeed, blocking either the expression or the activity of this enzyme leads to an aberrant increase of lysosomes, alongside of the down-regulation of the mTOR signaling. This surge of lysosomes eradicates glioblastoma stem-like cells. Targeting lysosomes might thus inspire the design of new strategies to face this devastating human cancer. Here, we provide an overview of the functions of the lysosome as well as its role as a cell death initiator, to highlight the potential of lysosomal drugs for glioblastoma therapy.

ARTICLE HISTORY
Received 25 March 2020
Revised 29 June 2020
Accepted 30 June 2020

KEYWORDS
Lysosome; glioma; stem cells; membrane permeabilization; mTOR; MALT1

Glioblastoma Multiforme (GBM) is a deadly brain tumor in adults, for which treatments remain unsatisfactory. Not only do therapies need to reach the brain and selectively destroy the tumor within this privileged, protected tissue, but also the anticancer arsenal has to deal with high molecular and high cellular heterogeneity and plasticity. Thus, median survival plateaus at 15 months, and 5-years survival does not exceed 5% [1–3]. It is now well admitted that GBM arises from a pool of transformed initiating cells, termed as glioblastoma stem-like cells (GSCs) [1,4–6]. This subpopulation of tumor cells is capable of tumor initiation, expansion and relapse. Targeting GSCs is thus of paramount potential. Boosted by the advances in targeting intracellular homeostasis, such as metabolism and proteostasis, organelles and their functions had received increasing attention in the field of cancer research. In this perspective, we presented recent findings highlighting how lysosomes are paralyzed in glioblastoma stem-like cells [7–9].

1. Lysosomes: an overview

Lysosomes are acidic organelles, with an intraluminal pH ranging between 4.5 and 5.5, that were discovered by Christian de Duve's group in 1955 [10]. These intracellular entities pilot degradation and metabolic signaling. Lysosomes are composed of two main classes of proteins: hydrolases and membrane proteins. Hydrolases reside in the acidic lysosomal lumen, where each enzyme acts on a particular subset of cargos in order to fulfill their varied functions, including catabolism, antigen and pro-protein processing, extracellular matrix degradation, or apoptosis initiation [11]. Lysosomal membrane proteins, by contrast, are heavily glycosylated and occupy the limiting membrane of the lysosome; their roles echelon to acidification, membrane fusion, and protein import and export [12–14].

1.1. Biogenesis and assembly

Seminal work from Andrea Ballabio's group identified that many lysosomal genes contain in their

CONTACT Julie Gavard julie.gavard@inserm.fr

promoter a consensus sequence, GTCACGTGAC, termed the CLEAR element (coordinated lysosomal expression and regulation). The basic helix-loop-helix leucine zipper transcription factors from the MITF (melanocyte inducing transcription factor) family, among which is TFEB (the transcription factor EB), bind to this site and regulate lysosomal biogenesis. In fact, TFEB overexpression promotes lysosomal gene transcription in HeLa cells [15]. Subsequently, the same group uncovered that the CLEAR element is also located in the promoter of many autophagy-related genes, underlining an intermingled regulation between lysosomal biogenesis and autophagosome formation [16]. TFEB is regulated via inactivating phosphorylation at multiple sites, which promotes its cytosolic retention. Upon dismantlement of lysosome functions or cellular starvation, TFEB is dephosphorylated and subsequently shuttled to the nucleus, promoting the transcription of its target genes [17]. Both ERK2 and the mechanistic target of rapamycin complex (mTORC1) have been implicated in TFEB phosphorylation under nutrient-rich conditions [18,19]. As mTORC1 counteracts autophagy induction, this emphasizes the interplay between lysosomal biogenesis, autophagy, and mTORC1 signaling. Furthermore, recent work by Kevin Ryan's laboratory demonstrated that bromodomain-containing protein 4 (BRD4) functions as a transcriptional repressor of the CLEAR network, independent of TFEB. Indeed, the knockdown or inhibition of BRD4 induced CLEAR network gene transcription even upon co-silencing of TFEB [20]. Therefore, there may be alternate, yet unknown, mechanisms regulating lysosomal gene transcription.

Newly synthesized hydrolases traffic to the lysosome, from the trans-golgi network (TGN), via the mannose-6-phosphate receptor (M6PR) transport system. Clathrin-coated vesicles, containing M6PR and hydrolases, leave the TGN and travel to early endosomes. Upon endosome maturation, pH changes cause hydrolases to dissociate from M6PR, which can in turn recycle back to the TGN. Of note, M6PR also localizes at the cell surface to shuttle extracellular content to the lysosome via the endocytosis pathway [21–24]. Hence, lysosomes can acquire integral components via two routes, *i.e. de novo* synthesis and endocytic uptake.

1.2. Fusion of lysosomes to cellular membranes

Functionally, lysosomes act as a delivery receptacle for multiple degradative processes, including autophagy and endocytosis. Moreover, lysosomes can fuse with the plasma membrane and undergo exocytosis to expel certain contents. These varied functions converge on the fusion of lysosomes with different cellular membranes including autophagosomes, endosomes, and the plasma membrane (Figure 1).

In addition to degrading internalized cargos, a key role of the lysosome in endocytosis resides in ligand/receptor recycling. Upon endocytosis, the acidic conditions drive low-density lipoprotein ligands to dissociate from receptors and to be consequently chopped by hydrolases. Transmembrane receptors can then travel back to the cell surface for further signaling [25]. In this way, the lysosome can alter the duration of signaling cascades in the cell. Additionally, endocytosis serves to remodel the plasma membrane by removing transporters and adhesion molecules [26].

Autophagy is a cellular process for bulk degradation in reaction to certain stimuli including stress, starvation, and hypoxia. Upon initiation, autophagy-related proteins (ATG) converge at punctate structures, termed as the phagophore assembly site (PAS). The phagophore isolates designated cargos or organelles, sealing off into double-membrane vesicles (autophagosomes). Autophagosomes then fuse with the lysosome to degrade their freight [27]. Autophagy is tightly regulated by a variety of cues including at the transcriptional level (*e.g.* TFEB). Activated TFEB promotes the transcription of genes involved in the initiation of autophagy [28]. Additionally, mTOR hinders autophagy via inhibitory phosphorylation of multiple pathway components, such as the Unc-51 like autophagy activating kinase ULK1 and ATG13 [29–32].

Finally, lysosomal exocytosis is a calcium-dependent process exploited by cells for plasma membrane repair, as well as pathogen removal

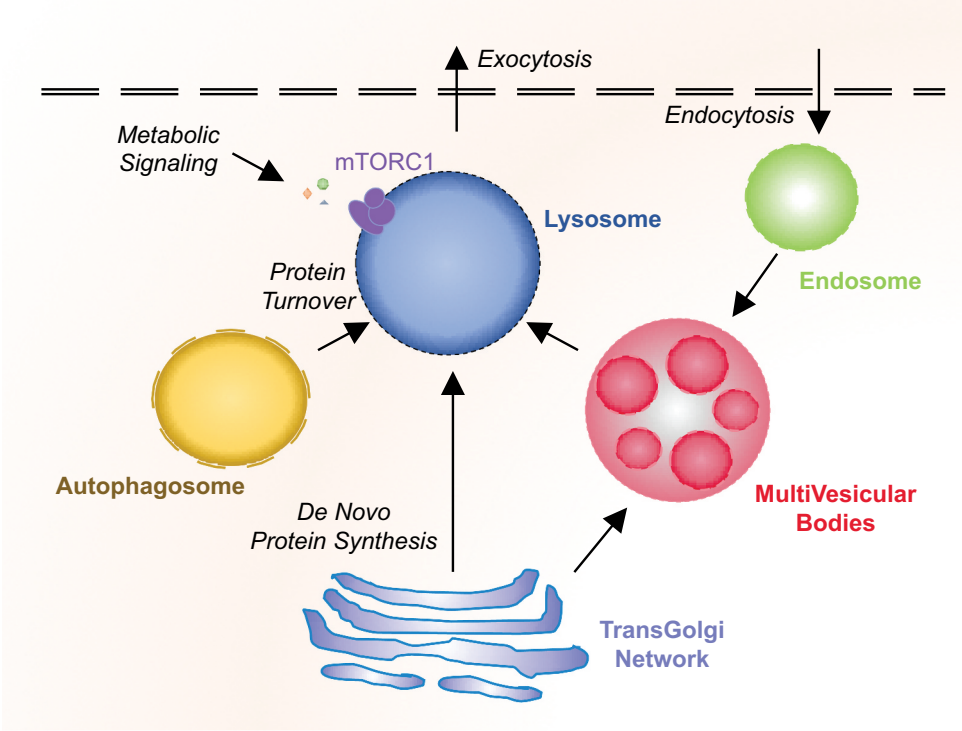

Figure 1. Overview of lysosomal functions.

Lysosomes assemble from both neo-synthetized and endocytosed materials. Their cargos are delivered through the transgolgi network (TGN) or the multivesicular bodies (MVB). MVB themselves emanate from endosomes and/or TGN. Lysosomes exerted varied cellular functions, including: metabolic signaling via mammalian/mechanistic Target Of Rapamycin Complex 1 (mTORC1) docking on their surface, protein turnover via the degradation of cellular contents following fusion with autophagosomes (autophagy) or endosomes, and exocytosis via fusion with the plasma membrane.

[33–35]. In cancer cells, increasing evidence suggests that this pathway is also co-opted to digest the extracellular matrix of surrounding cells during invasion [36].

Thus, lysosomes sit at the crossroad of multiple organizational and functional intracellular commands.

1.3. mTORC1 metabolic signaling

Lysosomes play a key role in metabolic signaling, since they act as docking sites for active mTORC1. Upon growth factor or amino acid stimulation, cytosolic mTORC1 migrates to the surface of the lysosome, where its kinase activity operates to stimulate mRNA translation and metabolism (via nucleotide, lipid, and glucose synthesis), while inhibiting protein turnover (via inhibition of autophagy and lysosomal biogenesis) [37]. Besides controlling cell size, mTOR signaling orchestrates metabolism, proliferation and survival, as such, this pathway can be pirated to the cancer cell's benefits. In fact, approximately 30% of human tumors experience hyperactivation of the cascade [37]. Therefore, targeting mTOR signaling may be important for effective anti-cancer therapy.

2. Lysosome-induced cell death

The idea of lysosomes as initiators of cell death was suggested early on following their discovery. However, this capacity was not fully explored until recently, likely owing to the fact that their ultrastructure appeared unaltered during cellular demise [38,39]. Damage to lysosomes comprises alteration in hydrolase expression, as well as changes in their size, number, pH and cellular positioning [40]. They also show deficiencies in autophagic flux.

Lysosomes work at acidic pH. Inhibition of the proton pump vacuolar-ATPase, *e.g.* with bafilomycin A1 increases intraluminal pH and thus reduces their catabolic capacity. This results in lysosomal dysfunction and defect in fusion with the

autophagosome [41,42]. Similarly, the autophagic inhibitor chloroquine also suppresses the lysosomal mission. Rather than blocking acidification, this weak base accumulates in lysosomes, increasing *de facto* the pH. This also limits autophagosome-lysosome fusion and thus, clearance of cargos [43] (Figure 2). Inhibitors of mTOR can too alter lysosomal function in a cell. As already mentioned, there is a reciprocal interplay between mTOR inhibition and autophagy induction. Therefore, mTOR inhibitors can increase autophagic degradation, and thus switch on the lysosomal activity [44].

Furthermore, lysosomal membrane integrity is crucial to circumscribe degradative enzymes and to maintain confined acidic pH. Conversely, lysosomal membrane permeabilization (LMP) results in an exodus of the lysosome cargos toward the cytosol. This LMP term encompasses varying degrees of membrane alterations, from selective cathepsin release, instigating death via tunable signaling cascades, to total lysosomal lysis, which lowers cellular pH and prompts necrosis [40,45,46]. LMP can be induced by a variety of methods. For instance, lysosomotropic agents are weak bases, which passively cross the lysosomal membrane and accumulate into the lumen. Amines with hydrophobic side-chains such as morphomine, cisprofloxacin, sphingosine, imidazole, and siramesine are all classified as lysosomotropic detergents [39,47–49]. Furthermore, microtubule poisons, such as vincristine and paclitaxel also modify the stability of lysosomes [50,51].

One major method of altering the stability of lysosomal membranes, and thus inciting LMP, is arbitrated by the modification of sphingolipids. Acid sphingomyelinase (ASM) binds to both HSP70 and its docking lipid BMP (bis monoacylglycerophosphate), to foster membrane stability [52,53]. Drugs that target ASM displace it from BMP to promote its degradation, resulting in sphingomyelin accumulation. These drugs, ranging from antihistamines to antidepressants, are collectively known as cationic amphiphilic drugs

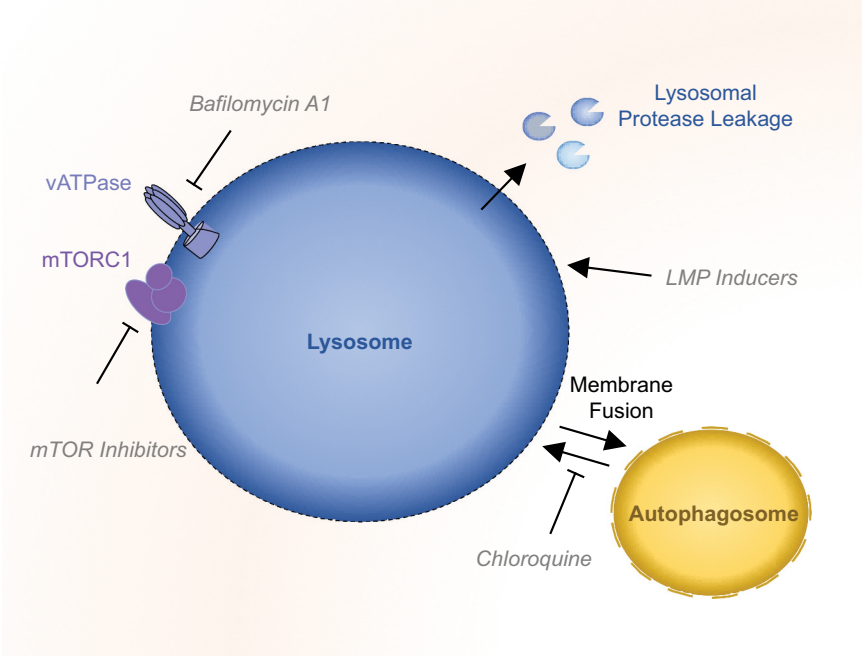

Figure 2. Therapeutic targeting of the lysosome.

Numerous pharmacological compounds are reported to alter lysosomal functions and stability. mammalian/mechanistic Target Of Rapamycin (mTOR) inhibitors prevent metabolic signaling from occurring and induce initiation of autophagy. Bafilomycin A1 blocks the lysosomal proton pump (vATPase), elevating pH and therefore limiting catabolic actions. Chloroquine increases lysosomal pH, reducing degradative capacity and fusion with autophagosomes. Lysosomal Membrane Permeabilization (LMP) inducing drugs destabilize the organelle membrane, allowing for the leakage of lysosomal proteases into the cytosol and ultimately resulting in cell death.

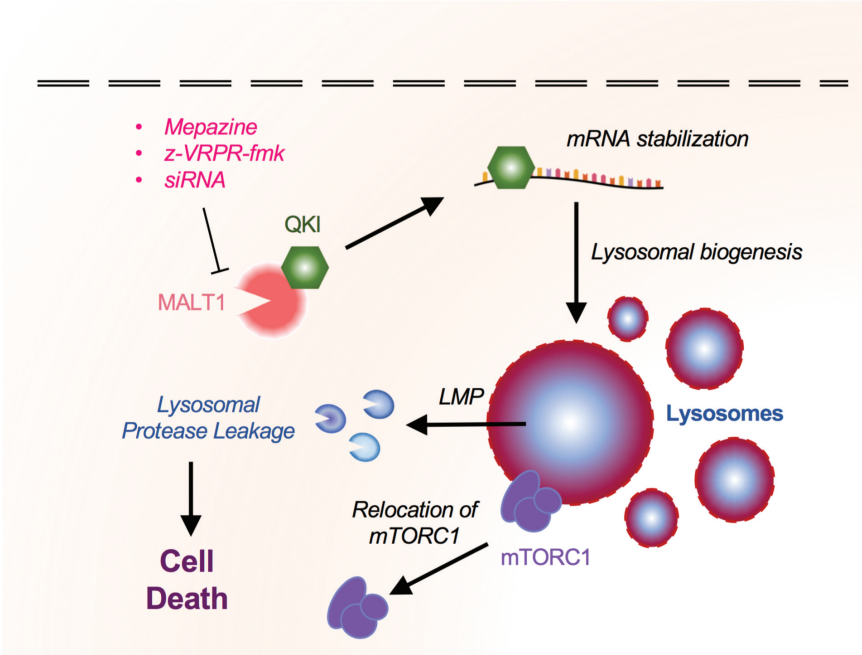

Figure 3. MALT1 interacts with QKI and regulates lysosomal homeostasis in Glioblastoma Stem-like Cells.

Mucosa-Associated Lymphoid Tissue lymphoma translocation protein 1 (MALT1) interacts with QKI in Glioblastoma Stem-like Cells (GSCs), thus restraining QKI activity. Upon MALT1 inhibition, QKI is released and possibly free to bind to lysosome-coding mRNAs, leading to lysosomal biogenesis. This lysosomal exaggeration ruptures its integrity, culminating in mTOR (mammalian/mechanistic Target Of Rapamycin Complex 1) dispersion, and lysosomal membrane permeabilization (LMP). As a result, lysosomal proteases induce GSC death, thus restraining GBM development.

(CAD), as they have hydrophilic amine groups and hydrophobic ring structures [54,55]. Marja Jäättelä's group has done extensive research on CADs, including siramesine. They demonstrated that siramesine is a lysosomal detergent, which disrupts autophagy [49]. Moreover, this compound shows selectivity toward cancer cells, and can help resensitizing them to chemotherapy [51,55]. Additionally, inhibitors of HSP70 also halt ASM stability and trigger LMP [53,56,57]. Hence, drugs that revise lysosomal sphingolipids have an exciting anti-cancer potential.

When LMP is induced, cells engage several damage response mechanisms to avoid death. For instance, inactivation of mTORC1 prompts TFEB-dependent lysosomal biogenesis [58,59]. In this vein, TFEB nuclearization enhances with the addition of lysosomotropic agents [60]. Moreover, minor perturbation in lysosomal membrane integrity stimulates the recruitment of the ESCRT (endosomal sorting complexes required for transport) machinery to heal membrane flaws. Indeed, knockdown of ESCRT components increased lysosomal damage-induced cell death [61]. Concurrently, Phyllis Hanson's laboratory demonstrated that ESCRT knockdown reduced lysosomal repair, using the cathepsin probe Magic Red [62]. In contrast, numerous studies have demonstrated that more severe LMP leads to the recruitment of galectins 3, 8, and 9, as sensors that bind β-galactosides on the injured organelles to recruit the autophagic machinery for selective clearance (termed as lysophagy) [63–67]. Additionally, lysosomes can undergo exocytosis in response to anti-cancer agents [68]. For instance, recent work demonstrated a calcium-dependent fusion of lysosomes with the plasma membrane following ionizing radiation [69].

Lysosomal disorder efficiently induces cell death, providing an opportunity to exploit this process for novel anti-cancer therapies.

3. Targeting lysosomes in glioblastoma stem-like cells

Lysosomes not only engage in recycling and signaling but also supervise stem cell fate alongside development and aging. Recent work by Villegas et al.

identified TFE3, a MITF family transcription factor, known to promote the transcription of lysosomal genes, as a major regulator of Embryonic Stem Cell (ESC) differentiation. Genome-wide CRISPR/Cas9 screen, performed in mouse ESCs, indeed illustrated that the self-renewal state is controlled by the activity of TFE3, thus linking stem cell fate to the lysosomes [70]. Anne Brunet's group provided additional evidence for a role of lysosomes in the maintenance of stem cell properties in brain. It is noteworthy that quiescent Neural Stem Cells (qNSCs) have more numerous and larger lysosomes than their activated counterparts (aNSCs). qNSCs are further involved in maintaining brain function and repair after injury [71]. However, the lysosomal compartment is exhausted in older NSCs (19–22 months), as compared to young NSCs (3–4 months), together with the accumulation of protein aggregates [71]. The weakening of differentiation potential in older qNSCs accompanied the decline of the lysosomal compartment, suggesting that the impact of aging on lysosomes alters stemness [71]. Therefore, lysosomal homeostasis may be of great importance in the process of aging, culminating with neurodegenerative pathologies, such as Alzheimer's and Parkinson's diseases. This might further be the case in GBM development, as this cancer occurs more frequently in older patients [72].

As briefly mentioned, GBM contains a subset of cells with stem properties, namely Glioblastoma Stem-like Cells (GSCs), which may arise from mutations in NSCs [6,73,74], and consequently may show similar lysosomal vulnerability. As these cells may govern initiation, resistance to treatments, and relapse, how the lysosomal compartment contributes to their fate is of high interest. Pivotal findings by Shingu et al. identified QKI, an RNA binding protein highly expressed in the brain, as a regulator of lysosomes in NSCs and GSCs [9]. Gene deletion of *Qki* in transformed NSCs leads to the maintenance of stemness properties, even outside the favorable environment of the NSC niche, while recapitulating GBM development in mice brains. QKI can bind specifically to and stabilize lysosomal RNAs in these cells [9]. Correspondingly, QKI silencing restricts the endo-lysosomal compartment, resulting in reduced receptor recycling. This prolongs, in turn, self-renewal signaling emanating from receptors, and therefore culminates in maintaining their survival even in harsh environments [9]. Conversely, one can envision that reversing lysosomal shutdown might be deleterious for GSCs. In keeping with this idea, several groups tried to take advantage of this putative frailty in GSCs to improve therapeutic targets in GBM (Table 1).

From this view, lysosomotropic drugs penetrate cells, accumulate in the lysosomal lumen, and therefore may be interesting compounds to disrupt lysosomes in GBM [68,75]. For instance, betulinic acid derivative B10 kills glioblastoma cell lines *in vitro*, as well as patient-derived cell cultures, when combined with the PI3 K inhibitor GDC-0941 [76]. From a molecular standpoint, PI3K inhibition activates TFEB-dependent accumulation of lysosomes, destabilized in turn by B10. This was hindered by Ca-074Me, a known cathepsin B inhibitor, arguing in favor of a lysosomal-mediated death [76]. Lys05, another lysosomotropic molecule, also showed promising results for the treatment of GBM [77]. This drug was reported to impair lysosomal function in glioma cell lines, as assessed by Lysotracker and acridine orange staining, two acid-activated fluorophores. Lys05 accumulation in lysosomes executes LMP, as evaluated by Galectin3 puncta formation [77]. Viability was further rescued upon Ca-074Me administration. Lys05 radio-sensitizes glioma cell lines *in vitro*, suggesting the potential of combining lysosomal destabilization with standard-of-care therapies. Similar experiments were conducted with the previously described CAD, siramesine, in glioma cell lines and patient-derived cells *in vitro* [78]. However, the administration of siramesine failed to curb proliferation and survival of GBM cells in organotypic spheroid-brain slice culture and in xenograft mouse models [78]. Thus, lysosomotropic drugs showed promising results mainly in *in vitro* studies, poisoning a large proportion of cancerous cells without any major effects on normal neural cells, but may require further evaluation to determine their *in vivo* efficacy.

In addition to lysosome destabilization, targeting lipid homeostasis emerged as a potential strategy to

Table 1. Compounds reported to induce lysosome membrane permeabilization in glioblastoma.

Chemical Drug (Name)	Family	Structure	Molecular/ Functional Targets	Reference
GDC-0941 (PICTILISIB)	anti-neoplasic	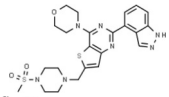	Phosphatidyl Inositol 3 Kinase [PI3 K)	[76]
Lys05	polyamine	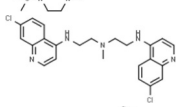	Cationic Amphiphilic Drug [CAD]	[77]
Lu-28-179 (SIRAMESINE]	anti-depressant	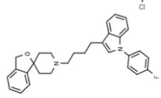	Cationic Amphiphilic Drug [CAD)	78
SapC-DOPS [BXQ-350]	nanovesicle	n.a	Lysosomal Sphingolipid Metabolism	[81]
TLI	combination	n.a	Lysosomal Sphingolipid Metabolism	[82]
Clemastine (TAVIST]	anti-histamine	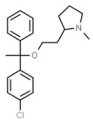	Cationic Amphiphilic Drug [CAD)	[8]
Mepazine [PACATAL]	anti-psychotic	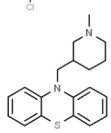	MALT1 Paracaspase	[7]
SKI-II	sphingosine kinase-2 inhibitor	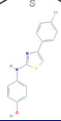	Sphingosine Kinase	[82]

This table summarizes reported drugs with poisoning capability on glioblastoma cells *in vitro*. Chemical and brand names are recapitulated, alongside family of each compound, structure, and reference. TLI: TNFα, Lipopolysaccharide, Interferonγ; n.a: not available.

eradicate tumor cells in GBM. Indeed, lysosomal integrity relies on the lipid membrane composition and organization, while these organelles play several roles in lipid catabolism and transfer [79,80]. Thus, any rupture in this fine-tuned process might prove to efficiently induce LMP and subsequent lysosomal cell death in GBM. An original treatment, developed by the group of Balveen Kaur, uses nanovesicles formed by the coupling of saposin C, an activator of sphingosine production, to dioleoylphosphatidylserine (DOPS). These engineered nanovesicles foster ceramide followed by sphingosine production, culminating in LMP-dependent cell death of GBM cells *in vitro* and *in vivo* [81]. Furthermore, glioma cell lines were eliminated upon treatment with a combination of tumor necrosis factor alpha TNFα, lipopolysaccharide LPS, and interferon gamma IFNγ (TLI). TLI provokes ceramide accumulation in the lysosomes, causing the destabilization of the lysosomal membrane and subsequent LMP. The inhibition of the sphingosine kinase (SK), an enzyme required for lipid recycling outside of lysosomes was also proposed to induce LMP specifically in glioma cells [82]. More recently, Le Joncour et al. discovered MDGI (Mammary-Derived Growth Inhibitor) as an important regulator of lysosomal membrane composition. In fact, its down-regulation impairs fatty acid transport in patient-derived GBM cells, abetting dramatic changes in lysosomal membrane composition. MDGI deficiency prompts LMP and subsequent death of GBM cells. In this vein, the CAD compound, clemastine, engendered lysosomal cell death *in vitro* and reduced tumor growth *in vivo*, in agreement with the susceptibility of GBM cells to lysosomal dysfuntions [8].

While investigating intrinsic mechanisms for autonomous survival of GSCs, our group unmasked another previously unknown mechanism by which GSCs regulate lysosomal biogenesis, and described a family of drugs directing lysosomal-dependent cell death in patient-derived cells *in vitro*, as well as to tumor growth reduction in xenograft mouse models [7]. The expression of the paracaspase MALT1, an arginine protease, involved in antigen-signaling in immune cells, NF-kB signaling, and development of certain forms of aggressive lymphoma [83–87] was negatively correlated with the probability of survival

in GBM patients. MALT1 was found basally active in GSCs [7]. Pharmacological inhibition of MALT1 using phenothiazines such as mepazine (MPZ) [85,88], previously used in clinics in order to treat psychic disorders, specifically exterminates patient-derived cells, while sparing neural resident cell types [7]. This effect was recapitulated with the competitive peptide MALT1 antagonist z-VRPR-fmk, MALT1 silencing with RNA interference, and the expression of a protease-dead version of MALT1. Altogether, several means deployed to halt MALT1 in GSCs converge on increased cell death, reduction of proliferation, and loss of stemness markers [7]. Further, transmission electron microscopy (TEM) unveiled an accumulation of vacuoles and lysosomes in MALT1-inhibited cells. The intensification of the Lysotracker and LAMP2 staining confirmed an increased abundance of lysosomes. While MALT1 inhibition provokes cathepsin release, blocking these lysosomal enzymes rescued GSCs, at least partially, from MPZ-dependent cell death. Given the previously described role of QKI in regulating lysosome biogenesis [9], the functional interaction between QKI and MALT1 was explored in-depth. In fact, QKI binds to MALT1 in proliferating GSCs and was released upon MALT1 inhibition [7]. Thus, the inhibition of MALT1 frees QKI, which is then permitted to dictate the translation of lysosomal genes, independently of TFEB. Conversely, the knockdown of QKI opposes MPZ-induced cell death in GSCs, underlying the major roles of MALT1 and QKI in the regulation of lysosomal homeostasis in GSCs.

In addition to the roles of MALT1 and QKI, our recent work also linked mTOR to the maintenance of a low lysosome load in GSCs [7]. In MALT1-inhibited cells, the constitutive mTOR activity was dampened and the kinase was dispersed from lysosome foci [7,89]. This might also contribute to diminished GSC expansion. Because mTOR activity is intimately linked to lysosomal stability [20,21], inhibiting mTOR, by destabilizing lysosomes, might prove beneficial to downsize cancer cell reservoir. Our work thus identified an unexpected mechanism by which GSC control lysosomal homeostasis, and defined phenothiazines as potential therapeutic options against GBM, inducing LMP-dependent cell death.

GBM is a deadly cancer, characterized by massive infiltration and heterogeneity [92,93]. Finding new weapons to fight this disease is a real challenge, because of the delicate environment and the blood-brain barrier acting as a shield to many therapeutic molecules. Numerous recent studies point toward lysosomes as an Achille's heel for GBM, and many tested molecules show impressive results *in vitro*, despite poor outcome for *in vivo* studies. Translation to clinics will require an efficient molecule to target GSCs, while safely penetrating the brain.

Acknowledgments

We thank SOAP team members (Nantes, France).

Disclosure statement

No potential conflict of interest was reported by the authors.

Funding

This research was funded by Fondation pour la Recherche Medicale [Equipe labellisée DEQ20180339184], Fondation ARC contre le Cancer [JG PJA20171206146], Ligue nationale contre le cancer comités de Loire-Atlantique, Maine et Loire, Vendée, Ille-et-Vilaine (JG) and Région Pays de la Loire et Nantes Métropole under Connect Talent Grant (JG). KAJ received PhD fellowships from Nantes Métropole and Fondation ARC; CM received PhD fellowship from Ligue nationale contre le cancer comité de Loire-Atlantique. The team is part of the SIRIC ILIAD (INCA-DGOS-Inserm _12558).

ORCID

Kathryn A Jacobs http://orcid.org/0000-0003-3632-6400
Clément Maghe http://orcid.org/0000-0002-3454-3869
Julie Gavard http://orcid.org/0000-0002-7985-9007

References

[1] Lathia JD, Mack SC, Mulkearns-Hubert EE, et al. Cancer stem cells in glioblastoma. Genes Dev. 2015;29:1203–1217.
[2] Stupp R, Mason WP, van den Bent MJ, et al. Radiotherapy plus concomitant and adjuvant temozolomide for glioblastoma. N Engl J Med. 2005;352:987–996.

[3] Stupp R, Hegi ME, Mason WP, et al. Effects of radiotherapy with concomitant and adjuvant temozolomide versus radiotherapy alone on survival in glioblastoma in a randomised phase III study: 5-year analysis of the EORTC-NCIC trial. Lancet Oncol. 2009;10:459–466.
[4] Bao S, Wu Q, McLendon RE, et al. Glioma stem cells promote radioresistance by preferential activation of the DNA damage response. Nature. 2006;444:756–760.
[5] Chen J, Li Y, Yu T-S, et al. a restricted cell population propagates glioblastoma growth after chemotherapy. Nature. 2012;488:522–526.
[6] Singh SK, Hawkins C, Clarke ID, et al. Identification of human brain tumour initiating cells. Nature. 2004;432:396–401.
[7] Jacobs KA, André-Grégoire G, Maghe C, et al. Paracaspase MALT1 regulates glioma cell survival by controlling endo-lysosome homeostasis. Embo J. 2020;39:e102030.
[8] Le Joncour V, Filppu P, Hyvönen M, et al. Vulnerability of invasive glioblastoma cells to lysosomal membrane destabilization. EMBO Mol Med. 2019;11:e9034.
[9] Shingu T, Ho AL, Yuan L, et al. Qki deficiency maintains stemness of glioma stem cells in suboptimal environment by downregulating endolysosomal degradation. Nat Genet. 2017;49:75–86.
[10] de Duve C, Pressman BC, Gianetto R, et al. Tissue fractionation studies. 6. Intracellular distribution patterns of enzymes in rat-liver tissue. Biochem J. 1955;60:604–617.
[11] Conus S, Simon H-U. Cathepsins: key modulators of cell death and inflammatory responses. Biochem Pharmacol. 2008;76:1374–1382.
[12] Eskelinen E-L, Tanaka Y, Saftig P. At the acidic edge: emerging functions for lysosomal membrane proteins. Trends Cell Biol. 2003;13:137–145.
[13] Kornfeld S, Mellman I. The biogenesis of lysosomes. Annu Rev Cell Biol. 1989;5:483–525.
[14] Saftig P, Klumperman J. Lysosome biogenesis and lysosomal membrane proteins: trafficking meets function. Nat Rev Mol Cell Biol. 2009;10:623–635.
[15] Sardiello M, Palmieri M, Di Ronza a, et al. a gene network regulating lysosomal biogenesis and function. Science. 2009;325:473–477.
[16] Settembre C, Ballabio a. TFEB regulates autophagy: an integrated coordination of cellular degradation and recycling processes. Autophagy. 2011;7:1379–1381.
[17] Napolitano G, Ballabio a. TFEB at a glance. J Cell Sci. 2016;129:2475–2481.
[18] Martina JA, Chen Y, Gucek M, et al. MTORC1 functions as a transcriptional regulator of autophagy by preventing nuclear transport of TFEB. Autophagy. 2012;8:903–914.
[19] Roczniak-Ferguson a, Petit CS, Froehlich F, et al. The transcription factor TFEB links mTORC1 signaling to transcriptional control of lysosome homeostasis. Sci Signal. 2012;5:ra42–ra42.
[20] Sakamaki J, Wilkinson S, Hahn M, et al. Bromodomain protein BRD4 is a transcriptional repressor of autophagy and lysosomal function. Mol Cell. 2017;66:517–532.e9.
[21] Dahms NM. Insulin-like growth factor II/cation-independent mannose 6-phosphate receptor and lysosomal enzyme recognition. Biochem Soc Trans. 1996;24:136–141.
[22] Gary-Bobo M, Nirdé P, Jeanjean a, et al. Mannose 6-phosphate receptor targeting and its applications in human diseases. Curr Med Chem. 2007;14:2945–2953.
[23] Kornfeld S. Structure and function of the mannose 6-phosphate/insulinlike growth factor II receptors. Annu Rev Biochem. 1992;61:307–330.
[24] Munier-Lehmann H, Mauxion F, Hoflack B. Function of the two mannose 6-phosphate receptors in lysosomal enzyme transport. Biochem Soc Trans. 1996;24:133–136.
[25] Kirchhausen T, Owen D, Harrison SC. Molecular structure, function, and dynamics of clathrin-mediated membrane traffic. Cold Spring Harb Perspect Biol. 2014;6:a016725.
[26] Ross E, Ata R, Thavarajah T, et al. AMP-activated protein kinase regulates the cell surface proteome and integrin membrane traffic. Plos One. 2015;10:e0128013.
[27] Dikic I, Elazar Z. Mechanism and medical implications of mammalian autophagy. Nat Rev Mol Cell Biol. 2018;19:349–364.
[28] Settembre C, Fraldi a, Medina DL, et al. Signals from the lysosome: a control centre for cellular clearance and energy metabolism. Nat Rev Mol Cell Biol. 2013;14:283–296.
[29] Ganley IG, Lam DH, Wang J, et al. ULK1·ATG13·FIP200 complex mediates mTOR signaling and is essential for autophagy. J Biol Chem. 2009;284:12297–12305.
[30] Hosokawa N, Hara T, Kaizuka T, et al. Nutrient-dependent mTORC1 association with the ULK1–Atg13–FIP200 complex required for autophagy. Mol Biol Cell. 2009;20:1981–1991.
[31] Jung CH, Jun CB, Ro S-H, et al. ULK-Atg13-FIP200 complexes mediate mTOR signaling to the autophagy machinery. Mol Biol Cell. 2009;20:1992–2003.
[32] Puente C, Hendrickson RC, Jiang X. Nutrient-regulated phosphorylation of ATG13 inhibits starvation-induced autophagy. J Biol Chem. 2016;291:6026–6035.
[33] Huynh C, Roth D, Ward DM, et al. Defective lysosomal exocytosis and plasma membrane repair in Chediak-Higashi/beige cells. Proc Natl Acad Sci U S A. 2004;101:16795–16800.

[34] Jaiswal JK, Andrews NW, Simon SM. Membrane proximal lysosomes are the major vesicles responsible for calcium-dependent exocytosis in nonsecretory cells. J Cell Biol. 2002;159:625–635.
[35] Reddy a, Caler EV, Andrews NW. Plasma membrane repair is mediated by Ca(2+)-regulated exocytosis of lysosomes. Cell. 2001;106:157–169.
[36] Machado E, White-Gilbertson S, Vlekkert D, et al. Regulated lysosomal exocytosis mediates cancer progression. Sci Adv. 2015;1:e1500603.
[37] Saxton RA, Sabatini DM. mTOR signaling in growth, metabolism, and disease. Cell. 2017;168:960–976.
[38] Brunk UT, Ericsson JL. Cytochemical evidence for the leakage of acid phosphatase through ultrastructurally intact lysosomal membranes. Histochem J. 1972;4:479–491.
[39] Firestone RA, Pisano JM, Bonney RJ. Lysosomotropic agents. 1. Synthesis and cytotoxic action of lysosomotropic detergents. J Med Chem. 1979;22:1130–1133.
[40] Aits S, Jäättelä M. Lysosomal cell death at a glance. J Cell Sci. 2013;126:1905–1912.
[41] Mauvezin C, Neufeld TP. Bafilomycin A1 disrupts autophagic flux by inhibiting both V-ATPase-dependent acidification and Ca-P60A/SERCA-dependent autophagosome-lysosome fusion. Autophagy. 2015;11:1437–1438.
[42] Nakashima S, Hiraku Y, Tada-Oikawa S, et al. Vacuolar H+-ATPase inhibitor induces apoptosis via lysosomal dysfunction in the human gastric cancer cell line MKN-1. J Biochem (Tokyo). 2003;134:359–364.
[43] Mauthe M, Orhon I, Rocchi C, et al. Chloroquine inhibits autophagic flux by decreasing autophagosome-lysosome fusion. Autophagy. 2018;14:1435–1455.
[44] Zhou J, Tan S-H, Nicolas V, et al. Activation of lysosomal function in the course of autophagy via mTORC1 suppression and autophagosome-lysosome fusion. Cell Res. 2013;23:508–523.
[45] Loison F, Zhu H, Karatepe K, et al. Proteinase 3–dependent caspase-3 cleavage modulates neutrophil death and inflammation. J Clin Invest. 2014;124:4445–4458.
[46] Zhao K, Zhao X, Tu Y, et al. Lysosomal chymotrypsin B potentiates apoptosis via cleavage of Bid. Cell Mol Life Sci. 2010;67:2665–2678.
[47] Boya P, Andreau K, Poncet D, et al. Lysosomal membrane permeabilization induces cell death in a mitochondrion-dependent fashion. J Exp Med. 2003;197:1323–1334.
[48] Kågedal K, Zhao M, Svensson I, et al. Sphingosine-induced apoptosis is dependent on lysosomal proteases. Biochem J. 2001;359:335–343.
[49] Ostenfeld MS, Høyer-Hansen M, Bastholm L, et al. Anti-cancer agent siramesine is a lysosomotropic detergent that induces cytoprotective autophagosome accumulation. Autophagy. 2008;4:487–499.
[50] Castino R, Peracchio C, Salini a, et al. Chemotherapy drug response in ovarian cancer cells strictly depends on a cathepsin D-Bax activation loop. J Cell Mol Med. 2009;13:1096–1109.
[51] Groth-Pedersen L, Ostenfeld MS, Høyer-Hansen M, et al. Vincristine induces dramatic lysosomal changes and sensitizes cancer cells to lysosome-destabilizing siramesine. Cancer Res. 2007;67:2217–2225.
[52] Gabandé-Rodríguez E, Boya P, Labrador V, et al. High sphingomyelin levels induce lysosomal damage and autophagy dysfunction in Niemann Pick disease type a. Cell Death Differ. 2014;21:864–875.
[53] Kirkegaard T, Roth AG, Petersen NHT, et al. Hsp70 stabilizes lysosomes and reverts Niemann-Pick disease-associated lysosomal pathology. Nature. 2010;463:549–553.
[54] Gulbins E, Kolesnick RN. It takes a CAD to kill a tumor cell with a LMP. Cancer Cell. 2003;24:279–281.
[55] Petersen NHT, Olsen OD, Groth-Pedersen L, et al. Transformation-associated changes in sphingolipid metabolism sensitize cells to lysosomal cell death induced by inhibitors of acid sphingomyelinase. Cancer Cell. 2013;24:379–393.
[56] Granato M, Lacconi V, Peddis M, et al. HSP70 inhibition by 2-phenylethynesulfonamide induces lysosomal cathepsin D release and immunogenic cell death in primary effusion lymphoma. Cell Death Dis. 2013;4:e730.
[57] Nylandsted J, Wick W, Hirt UA, et al. Eradication of glioblastoma, and breast and colon carcinoma xenografts by Hsp70 depletion. Cancer Res. 2002;62:7139–7142.
[58] Papadopoulos C, Meyer H. Detection and clearance of damaged lysosomes by the endo-lysosomal damage response and lysophagy. Curr Biol CB. 2017;27:R1330–R1341.
[59] Raben N, Puertollano R. TFEB and TFE3: linking lysosomes to cellular adaptation to stress. Annu Rev Cell Dev Biol. 2016;32:255–278.
[60] Lu S, Sung T, Lin N, et al. Lysosomal adaptation: how cells respond to lysosomotropic compounds. Plos One. 2017;12:e0173771.
[61] Radulovic M, Schink KO, Wenzel EM, et al. ESCRT-mediated lysosome repair precedes lysophagy and promotes cell survival. Embo J. 2018;37:e99753.
[62] Skowyra ML, Schlesinger PH, Naismith TV, et al. Triggered recruitment of ESCRT machinery promotes endolysosomal repair. Science. 2018;360:eaar5078.
[63] Chauhan S, Kumar S, Jain a, et al. TRIMs and galectins globally cooperate and TRIM16 and Galectin-3 Co-direct autophagy in endomembrane damage homeostasis. Dev Cell. 2016;39:13–27.

[64] Jia J, Abudu YP, Claude-Taupin a, et al. Galectins control MTOR and AMPK in response to lysosomal damage to induce autophagy. Autophagy. 2019;15:169–171.
[65] Jia J, Bissa B, Brecht L, et al. AMPK, a regulator of metabolism and autophagy, is activated by lysosomal damage via a novel galectin-directed ubiquitin signal transduction system. Mol Cell. 2020a;77:951–969.e9.
[66] Jia J, Claude-Taupin a, Gu Y, et al. Galectin-3 coordinates a cellular system for lysosomal repair and removal. Dev Cell. 2020b;52:69–87.e8.
[67] Thurston TLM, Wandel MP, von Muhlinen N, et al. Galectin 8 targets damaged vesicles for autophagy to defend cells against bacterial invasion. Nature. 2012;482:414–418.
[68] Zhitomirsky B, Assaraf YG. Lysosomal accumulation of anticancer drugs triggers lysosomal exocytosis. Oncotarget. 2017;8:45117–45132.
[69] Ferranti CS, Cheng J, Thompson C, et al. Fusion of lysosomes to plasma membrane initiates radiation-induced apoptosis. J Cell Biol. 2020;219:e201903176.
[70] Villegas F, Lehalle D, Mayer D, et al. Lysosomal signaling licenses embryonic stem cell differentiation via inactivation of Tfe3. Cell Stem Cell. 2019;24:257–270.e8.
[71] Leeman DS, Hebestreit K, Ruetz T, et al. Lysosome activation clears aggregates and enhances quiescent neural stem cell activation during aging. Science. 2018;359:1277–1283.
[72] Young JS, Chmura SJ, Wainwright DA, et al. Management of glioblastoma in elderly patients. J Neurol Sci. 2017;380:250–255.
[73] Lee JH, Lee JE, Kahng JY, et al. Human glioblastoma arises from subventricular zone cells with low-level driver mutations. Nature. 2018;560:243–247.
[74] Singh SK, Clarke ID, Terasaki M, et al. Identification of a cancer stem cell in human brain tumors. Cancer Res. 2003;63:5821–5828.
[75] Kaufmann AM, Krise JP. Lysosomal sequestration of amine-containing drugs: analysis and therapeutic implications. J Pharm Sci. 2007;96:729–746.
[76] Enzenmüller S, Gonzalez P, Karpel-Massler G, et al. GDC-0941 enhances the lysosomal compartment via TFEB and primes glioblastoma cells to lysosomal membrane permeabilization and cell death. Cancer Lett. 2013;329:27–36.
[77] Zhou W, Guo Y, Zhang X, et al. Lys05 induces lysosomal membrane permeabilization and increases radiosensitivity in glioblastoma. J Cell Biochem. 2020;121:2027–2037.
[78] Jensen SS, Petterson SA, Halle B, et al. Effects of the lysosomal destabilizing drug siramesine on glioblastoma in vitro and in vivo. BMC Cancer. 2017;17:178.
[79] Jaishy B, Abel ED. Lipids, lysosomes, and autophagy. J Lipid Res. 2016;57:1619–1635.
[80] Lawrence RE, Zoncu R. The lysosome as a cellular centre for signalling, metabolism and quality control. Nat Cell Biol. 2019;21:133–142.
[81] Wojton J, Meisen WH, Jacob NK, et al. SapC-DOPS-induced lysosomal cell death synergizes with TMZ in glioblastoma. Oncotarget. 2014;5:9703–9709.
[82] Mora R, Dokic I, Kees T, et al. Sphingolipid rheostat alterations related to transformation can be exploited for specific induction of lysosomal cell death in murine and human glioma: sphingosine kinase and lysosomal cell death. Glia. 2010;58:1364–1383.
[83] Hailfinger S, Lenz G, Ngo V, et al. Essential role of MALT1 protease activity in activated B cell-like diffuse large B-cell lymphoma. Proc Natl Acad Sci. 2009;106:19946–19951.
[84] Jaworski M, Thome M. The paracaspase MALT1: biological function and potential for therapeutic inhibition. Cell Mol Life Sci. 2016;73:459–473.
[85] Nagel D, Spranger S, Vincendeau M, et al. Pharmacologic Inhibition of MALT1 protease by phenothiazines as a therapeutic approach for the treatment of aggressive ABC-DLBCL. Cancer Cell. 2012;22:825–837.
[86] Thys a, Douanne T, Bidère N. Post-translational Modifications of the CARMA1-BCL10-MALT1 Complex in Lymphocytes and Activated B-Cell Like Subtype of Diffuse Large B-Cell Lymphoma. Front Oncol. 2018;8:498.
[87] Weil R, Israel a. Deciphering the pathway from the TCR to NF-kB. Cell Death Differ. 2006;13:826–833.
[88] Schlauderer F, Lammens K, Nagel D, et al. Structural analysis of phenothiazine derivatives as allosteric inhibitors of the MALT1 paracaspase. Angew Chem Int Ed. 2013;52:10384–10387.
[89] Galan-Moya EM, Le Guelte a, Lima-Fernandes E, et al. Secreted factors from brain endothelial cells maintain glioblastoma stem-like cell expansion through the mTOR pathway. EMBO Rep. 2011;12:470–476.
[90] Puertollano R. mTOR and lysosome regulation. F1000Prime Rep. 2014;6:52.
[91] Zhitomirsky B, Yunaev a, Kreiserman R, et al. Lysosomotropic drugs activate TFEB via lysosomal membrane fluidization and consequent inhibition of mTORC1 activity. Cell Death Dis. 2018;9:1191.
[92] Cuddapah VA, Robel S, Watkins S, et al. a neurocentric perspective on glioma invasion. Nat Rev Neurosci. 2014;15:455–465.
[93] Patel AP, Tirosh I, Trombetta JJ, et al. Single-cell RNA-seq highlights intratumoral heterogeneity in primary glioblastoma. Science. 2014;344:1396–1401.

Annex 3 – Scientific publications

Annex 4 – Scientific communications

2020

- **November 23-25**

Oral Presentation - 5th congress of GDR 3697 MICRONIT ''Microenvironnement des Niches Tumorales''

Paracaspase MALT1 regulates glioma cell survival by controlling endo-lysosome homeostasis

2021

- **January 14-26**

Supervision of practical courses on Immunology at Nantes University (License 2 SV - SVT)

- **March 4**

Chairman - CRCINA PhD Students Scientific Days

- **April 13**

Oral Presentation – 3rd Edition of ''Nos Doctorants ont la Parole'' of NET Network

Paracaspase MALT1 regulates glioma cell survival by controlling endo-lysosome homeostasis

*Best Oral Presentation

- **October 13-15**

Oral Presentation - 9th Proteasome & Autophagy Congress, Clermont-Ferrand

Paracaspase MALT1 regulates glioma cell survival by controlling endo-lysosome homeostasis

*Best Oral Presentation

- **December 10**

Poster - 4th Edition of "The Scientific Days" of the Doctoral School EDBS

Paracaspase MALT1 regulates glioma cell survival by controlling endo-lysosome homeostasis

2022

- **May 5-6**

Poster - LYSOFOR2625 Symposium, Berlin

Paracaspase MALT1 regulates glioma cell survival by controlling endo-lysosome homeostasis

- **June 9**

Chairman, Round table, and Discussion - Unit seminar, Prof. Pirjo Laakkonen

Involvement of lysosomal-cholesterol transport in the survival of glioblastoma stem-like cells

- **November 27**

Oral Presentation – 3rd FiBTRA Virtual Symposium

Purification and description of lysosomes from glioblastoma stem-like cells

2023

- **March 17**

Oral Presentation – Week of the Brain, Nantes University

Le glioblastome, un cancer dans un organe pas comme les autres

- **March 21**

Chairman, Round table, and Discussion - Unit seminar, Dr. Kristine Schauer

MALT1 paracaspase controls cholesterol homeostasis in glioblastoma stem-like cells through lysosome proteome shaping

- **April 20**

Round table, and Discussion - Unit seminar, Dr. Olivier Ayrault

MALT1 paracaspase controls cholesterol homeostasis in glioblastoma stem-like cells through lysosome proteome shaping

Bibliography

1. Louis, D. N. *et al.* The 2021 WHO Classification of Tumors of the Central Nervous System: a summary. *Neuro-Oncol.* **23**, 1231–1251 (2021).
2. Stoyanov, G. S. *et al.* Reclassification of Glioblastoma Multiforme According to the 2021 World Health Organization Classification of Central Nervous System Tumors: A Single Institution Report and Practical Significance. *Cureus* (2022) doi:10.7759/cureus.21822.
3. Louis, D. N. *et al.* The 2016 World Health Organization Classification of Tumors of the Central Nervous System: a summary. *Acta Neuropathol. (Berl.)* **131**, 803–820 (2016).
4. Ostrom, Q. T. *et al.* CBTRUS Statistical Report: Primary Brain and Other Central Nervous System Tumors Diagnosed in the United States in 2015–2019. *Neuro-Oncol.* **24**, v1–v95 (2022).
5. Nakada, M. *et al.* Aberrant Signaling Pathways in Glioma. *Cancers* **3**, 3242–3278 (2011).
6. Prasad, G. & Haas-Kogan, D. Radiation-induced gliomas. *ExpertRevNeurother* **9**, (2009).
7. Wrensch, M., Minn, Y., Chew, T., Bondy, M. & Berger, M. S. Epidemiology of primary brain tumors: Current concepts and review of the literature. (2002).
8. Salvati, M. *et al.* Radiation-induced gliomas. *Surg. Neurol.* **60**, 60–67 (2003).
9. Hanif, F., Muzaffar, K., Perveen, kahkashan, Malhi, S. & Simjee, S. Glioblastoma Multiforme: A Review of its Epidemiology and Pathogenesis through Clinical Presentation and Treatment. *Asian Pac. J. Cancer Prev.* **18**, (2017).
10. Shukla, G. *et al.* Advanced magnetic resonance imaging in glioblastoma: a review. *Chin. Clin. Oncol.* **6**, 40–40 (2017).
11. Brown, T. J. *et al.* Association of the Extent of Resection With Survival in Glioblastoma: A Systematic Review and Meta-analysis. *JAMA Oncol.* **2**, 1460 (2016).
12. Stummer, W. *et al.* Fluorescence-guided surgery with 5-aminolevulinic acid for resection of malignant glioma: a randomised controlled multicentre phase III trial. *Lancet Oncol.* **7**, 392–401 (2006).
13. Stupp, R. *et al.* Radiotherapy plus Concomitant and Adjuvant Temozolomide for Glioblastoma. *N. Engl. J. Med.* (2005).
14. Stupp, R., Hegi, M. E. & Mason, W. P. Effects of radiotherapy with concomitant and adjuvant temozolomide versus radiotherapy alone on survival in glioblastoma in a randomised phase III study: 5-year analysis of the EORTC-NCIC trial. **10**, (2009).
15. Stupp, R. *et al.* Maintenance Therapy With Tumor-Treating Fields Plus Temozolomide vs Temozolomide Alone for Glioblastoma: A Randomized Clinical Trial. *JAMA* **314**, 2535 (2015).
16. Binabaj, M. M. *et al.* The prognostic value of MGMT promoter methylation in glioblastoma: A meta-analysis of clinical trials. *J. Cell. Physiol.* **233**, 378–386 (2018).
17. Agarwala, S. S. & Kirkwood, J. M. Temozolomide, a Novel Alkylating Agent with Activity in the Central Nervous System, May Improve the Treatment of Advanced Metastatic Melanoma. *The Oncologist* **5**, 144–151 (2000).
18. Schulte, J. D., Aghi, M. K. & Taylor, J. W. Anti-angiogenic therapies in the management of glioblastoma. *Chin. Clin. Oncol.* **10**, 37–37 (2021).
19. Cohen, M. H., Shen, Y. L., Keegan, P. & Pazdur, R. FDA Drug Approval Summary: Bevacizumab (Avastin®) as Treatment of Recurrent Glioblastoma Multiforme. *The Oncologist* **14**, 1131–1138 (2009).
20. Bao, S. *et al.* Stem Cell–like Glioma Cells Promote Tumor Angiogenesis through Vascular Endothelial Growth Factor. *Cancer Res.* **66**, 7843–7848 (2006).

21. Calabrese, C. *et al.* A Perivascular Niche for Brain Tumor Stem Cells. *Cancer Cell* **11**, 69–82 (2007).
22. Wick, W. *et al.* Lomustine and Bevacizumab in Progressive Glioblastoma. *N. Engl. J. Med.* **377**, 1954–1963 (2017).
23. Chinot, O. L. *et al.* Bevacizumab plus Radiotherapy–Temozolomide for Newly Diagnosed Glioblastoma. *N. Engl. J. Med.* **370**, 709–722 (2014).
24. Gilbert, M. R. *et al.* A Randomized Trial of Bevacizumab for Newly Diagnosed Glioblastoma. *N. Engl. J. Med.* **370**, 699–708 (2014).
25. Nagpal, S., Harsh, G. & Recht, L. Bevacizumab Improves Quality of Life in Patients with Recurrent Glioblastoma. *Chemother. Res. Pract.* **2011**, 1–6 (2011).
26. Gómez-Oliva, R. *et al.* Evolution of Experimental Models in the Study of Glioblastoma: Toward Finding Efficient Treatments. *Front. Oncol.* **10**, 614295 (2021).
27. Hong, X., Chedid, K. & Kalkanis, S. N. Glioblastoma cell line-derived spheres in serum-containing medium versus serum-free medium: A comparison of cancer stem cell properties. *Int. J. Oncol.* **41**, 1693–1700 (2012).
28. Lee, J. *et al.* Tumor stem cells derived from glioblastomas cultured in bFGF and EGF more closely mirror the phenotype and genotype of primary tumors than do serum-cultured cell lines. *Cancer Cell* **9**, 391–403 (2006).
29. Allen, M., Bjerke, M., Edlund, H., Nelander, S. & Westermark, B. Origin of the U87MG glioma cell line: Good news and bad news. *Sci. Transl. Med.* **8**, (2016).
30. Brewer, G. J., Torricelli, J. R., Evege, E. K. & Price, P. J. Optimized survival of hippocampal neurons in B27-supplemented neurobasal?, a new serum-free medium combination. *J. Neurosci. Res.* **35**, 567–576 (1993).
31. Reynolds, B. A. & Weiss, S. Generation of Neurons and Astrocytes from Isolated Cells of the Adult Mammalian Central Nervous System. *Science* **255**, 1707–1710 (1992).
32. Galli, R. *et al.* Isolation and Characterization of Tumorigenic, Stem-like Neural Precursors from Human Glioblastoma. *Cancer Res.* **64**, 7011–7021 (2004).
33. Singh, S. K. *et al.* Identification of human brain tumour initiating cells. *Nature* **432**, 396–401 (2004).
34. Singh, S. K. *et al.* Identification of a Cancer Stem Cell in Human Brain Tumors. *Cancer Res.* **63**, 5821–5828 (2003).
35. Robertson, F. L., Marqués-Torrejón, M.-A., Morrison, G. M. & Pollard, S. M. Experimental models and tools to tackle glioblastoma. *Dis. Model. Mech.* **12**, dmm040386 (2019).
36. Baskaran, S. *et al.* Primary glioblastoma cells for precision medicine: a quantitative portrait of genomic (in)stability during the first 30 passages. *Neuro-Oncol.* **20**, 1080–1091 (2018).
37. Xiao, W., Sohrabi, A. & Seidlits, S. K. Integrating the glioblastoma microenvironment into engineered experimental models. *Future Sci. OA* **3**, FSO189 (2017).
38. Kerhervé, M. *et al.* Neuropilin-1 modulates the 3D invasive properties of glioblastoma stem-like cells. *Front. Cell Dev. Biol.* **10**, 981583 (2022).
39. Marques-Torrejon, M. A., Gangoso, E. & Pollard, S. M. Modelling glioblastoma tumour-host cell interactions using adult brain organotypic slice co-culture. *Dis. Model. Mech.* dmm.031435 (2017) doi:10.1242/dmm.031435.
40. Lancaster, M. A. *et al.* Cerebral organoids model human brain development and microcephaly. *Nature* **501**, 373–379 (2013).
41. Hubert, C. G. *et al.* A Three-Dimensional Organoid Culture System Derived from Human Glioblastomas Recapitulates the Hypoxic Gradients and Cancer Stem

Cell Heterogeneity of Tumors Found *In Vivo*. *Cancer Res.* **76**, 2465–2477 (2016).
42. Ogawa, J., Pao, G. M., Shokhirev, M. N. & Verma, I. M. Glioblastoma Model Using Human Cerebral Organoids. *Cell Rep.* **23**, 1220–1229 (2018).
43. Jacob, F. *et al.* A Patient-Derived Glioblastoma Organoid Model and Biobank Recapitulates Inter- and Intra-tumoral Heterogeneity. *Cell* **180**, 188-204.e22 (2020).
44. Linkous, A. *et al.* Modeling Patient-Derived Glioblastoma with Cerebral Organoids. *Cell Rep.* **26**, 3203-3211.e5 (2019).
45. Read, R. D. *Drosophila melanogaster* as a model system for human brain cancers. *Glia* **59**, 1364–1376 (2011).
46. Reimunde, P. *et al.* Cellular and Molecular Mechanisms Underlying Glioblastoma and Zebrafish Models for the Discovery of New Treatments. *Cancers* **13**, 1087 (2021).
47. Herranz, C. *et al.* Spontaneously Arising Canine Glioma as a Potential Model for Human Glioma. *J. Comp. Pathol.* **154**, 169–179 (2016).
48. Fernández, F. *et al.* Presence of neural progenitors in spontaneous canine gliomas: A histopathological and immunohistochemical study of 20 cases. *Vet. J.* **209**, 125–132 (2016).
49. Stoica, G. *et al.* Identification of Cancer Stem Cells in Dog Glioblastoma. *Vet. Pathol.* **46**, 391–406 (2009).
50. Szatmari, T. *et al.* Detailed characterization of the mouse glioma 261 tumor model for experimental glioblastoma therapy. *Cancer Sci.* **97**, 546–553 (2006).
51. Wei, Q. *et al.* High-Grade Glioma Formation Results from Postnatal Pten Loss or Mutant Epidermal Growth Factor Receptor Expression in a Transgenic Mouse Glioma Model. *Cancer Res.* **66**, 7429–7437 (2006).
52. Weissenberger, J. *et al.* Development and malignant progression of astrocytomas in GFAP-v-src transgenic mice. *Oncogene* **14**, 2005–2013 (1997).
53. Ding, H., Roncari, L. & Shannon, P. Astrocyte-specific Expression of Activated p21-ras Results in Malignant Astrocytoma Formation in a Transgenic Mouse Model of Human Gliomas.
54. Bardella, C. *et al.* Expression of Idh1R132H in the Murine Subventricular Zone Stem Cell Niche Recapitulates Features of Early Gliomagenesis. *Cancer Cell* **30**, 578–594 (2016).
55. Zhu, Y. *et al.* Early inactivation of p53 tumor suppressor gene cooperating with NF1 loss induces malignant astrocytoma. *Cancer Cell* **8**, 119–130 (2005).
56. Jensen, N. A. *et al.* Astroglial c-Myc Overexpression Predisposes Mice to Primary Malignant Gliomas. *J. Biol. Chem.* **278**, 8300–8308 (2003).
57. Lassman, A. B., Dai, C., Fuller, G. N., Vickers, A. J. & Holland, E. C. Overexpression of c-MYC promotes an undifferentiated phenotype in cultured astrocytes and allows elevated Ras and Akt signaling to induce gliomas from GFAP-expressing cells in mice. *Neuron Glia Biol.* **1**, 157–163 (2004).
58. Garcia-Diaz, C. *et al.* Glioblastoma cell fate is differentially regulated by the microenvironments of the tumor bulk and infiltrative margin. *Cell Rep.* **42**, 112472 (2023).
59. Shingu, T. *et al.* Qki deficiency maintains stemness of glioma stem cells in suboptimal environment by downregulating endolysosomal degradation. *Nat. Genet.* **49**, 75 (2016).
60. Rahme, G. J. *et al.* Modeling epigenetic lesions that cause gliomas. *Cell* S0092867423007298 (2023) doi:10.1016/j.cell.2023.06.022.
61. Lapidot, T. *et al.* A cell initiating human acute myeloid leukaemia after transplantation into SCID mice. *Nature* **367**, 645–648 (1994).

62. Bonnet, D. & Dick, J. E. Human acute myeloid leukemia is organized as a hierarchy that originates from a primitive hematopoietic cell. *Nat. Med.* **3**, 730–737 (1997).
63. Pardal, R., Clarke, M. F. & Morrison, S. J. Applying the principles of stem-cell biology to cancer. *Nat. Rev. Cancer* **3**, 895–902 (2003).
64. Reya, T., Morrison, S. J., Clarke, M. F. & Weissman, I. L. Stem cells, cancer, and cancer stem cells. *Nature* **414**, 105–111 (2001).
65. Batlle, E. & Clevers, H. Cancer stem cells revisited. *Nat. Med.* **23**, 1124–1134 (2017).
66. Suh, H. *et al.* In Vivo Fate Analysis Reveals the Multipotent and Self-Renewal Capacities of Sox2+ Neural Stem Cells in the Adult Hippocampus. *Cell Stem Cell* **1**, 515–528 (2007).
67. Lois, C. & Alvarez-Buylla, A. Proliferating subventricular zone cells in the adult mammalian forebrain can differentiate into neurons and glia. *Proc. Natl. Acad. Sci.* **90**, 2074–2077 (1993).
68. Lathia, J. D., Mack, S. C., Mulkearns-Hubert, E. E., Valentim, C. L. L. & Rich, J. N. Cancer stem cells in glioblastoma. *GENES Dev.* **29**, 1203–1217 (2015).
69. Beier, D. *et al.* CD133+ and CD133− Glioblastoma-Derived Cancer Stem Cells Show Differential Growth Characteristics and Molecular Profiles. *Cancer Res.* **67**, 4010–4015 (2007).
70. Hemmati, H. D. *et al.* Cancerous stem cells can arise from pediatric brain tumors. *Proc. Natl. Acad. Sci.* **100**, 15178–15183 (2003).
71. Trépant, A.-L. *et al.* Identification of OLIG2 as the most specific glioblastoma stem cell marker starting from comparative analysis of data from similar DNA chip microarray platforms. *Tumor Biol.* **36**, 1943–1953 (2015).
72. Zbinden, M. *et al.* NANOG regulates glioma stem cells and is essential in vivo acting in a cross-functional network with GLI1 and p53. *EMBO J.* **29**, 2659–2674 (2010).
73. Jin, X., Jin, X., Jung, J.-E., Beck, S. & Kim, H. Cell surface Nestin is a biomarker for glioma stem cells. *Biochem. Biophys. Res. Commun.* **433**, 496–501 (2013).
74. Chen, J., McKay, R. M. & Parada, L. F. Malignant Glioma: Lessons from Genomics, Mouse Models, and Stem Cells. *Cell* **149**, 36–47 (2012).
75. Lee, J. H. *et al.* Human glioblastoma arises from subventricular zone cells with low-level driver mutations. *Nature* **560**, 243–247 (2018).
76. Wang, R. *et al.* Glioblastoma stem-like cells give rise to tumour endothelium. *Nature* **468**, 829–833 (2010).
77. Ricci-Vitiani, L. *et al.* Tumour vascularization via endothelial differentiation of glioblastoma stem-like cells. *Nature* **468**, 824–828 (2010).
78. El Hallani, S. *et al.* A new alternative mechanism in glioblastoma vascularization: tubular vasculogenic mimicry. *Brain* **133**, 973–982 (2010).
79. Cheng, L. *et al.* Glioblastoma Stem Cells Generate Vascular Pericytes to Support Vessel Function and Tumor Growth. *Cell* **153**, 139–152 (2013).
80. Guichet, P.-O. *et al.* Notch1 Stimulation Induces a Vascularization Switch With Pericyte-Like Cell Differentiation of Glioblastoma Stem Cells. *Stem Cells* **33**, 21–34 (2015).
81. Sampetrean, O. *et al.* Invasion Precedes Tumor Mass Formation in a Malignant Brain Tumor Model of Genetically Modified Neural Stem Cells. *Neoplasia* **13**, 784-IN3 (2011).
82. Winkler, F. *et al.* Imaging glioma cell invasion *in vivo* reveals mechanisms of

dissemination and peritumoral angiogenesis. *Glia* **57**, 1306–1315 (2009).
83. Volovetz, J. *et al.* Identifying conserved molecular targets required for cell migration of glioblastoma cancer stem cells. *Cell Death Dis.* **11**, 152 (2020).
84. Annabi, B., Lachambre, M.-P., Plouffe, K., Sartelet, H. & Béliveau, R. Modulation of invasive properties of CD133(+) glioblastoma stem cells: A role for MT1-MMP in bioactive lysophospholipid signaling. *Mol. Carcinog.* **48**, 910–919 (2009).
85. Takahashi. Cancer stem-like cells of glioblastoma characteristically express MMP-13 and display highly invasive activity. *Int. J. Oncol.* **37**, (2010).
86. Liu, G. *et al.* Analysis of gene expression and chemoresistance of CD133+ cancer stem cells in glioblastoma. *Mol. Cancer* **5**, 67 (2006).
87. Hegi, M. E. *et al.* MGMT Gene Silencing and Benefit from Temozolomide in Glioblastoma. *N. Engl. J. Med.* (2005).
88. Chen, J. *et al.* A restricted cell population propagates glioblastoma growth after chemotherapy. *Nature* **488**, 522–526 (2012).
89. Deleyrolle, L. P. *et al.* Evidence for label-retaining tumour-initiating cells in human glioblastoma. *Brain* **134**, 1331–1343 (2011).
90. Xie, X. P. *et al.* Quiescent human glioblastoma cancer stem cells drive tumor initiation, expansion, and recurrence following chemotherapy. *Dev. Cell* **57**, 32-46.e8 (2022).
91. Bao, S. *et al.* Glioma stem cells promote radioresistance by preferential activation of the DNA damage response. *Nature* **444**, 756–760 (2006).
92. Hambardzumyan, D. & Bergers, G. Glioblastoma: Defining Tumor Niches. *Trends Cancer* **1**, 252–265 (2015).
93. Rosińska, S. & Gavard, J. Tumor Vessels Fuel the Fire in Glioblastoma. *Int. J. Mol. Sci.* **22**, 6514 (2021).
94. Hambardzumyan, D. *et al.* PI3K pathway regulates survival of cancer stem cells residing in the perivascular niche following radiation in medulloblastoma in vivo. *Genes Dev.* **22**, 436–448 (2008).
95. Galan-Moya, E. M. *et al.* Secreted factors from brain endothelial cells maintain glioblastoma stem-like cell expansion through the mTOR pathway. *EMBO Rep.* **12**, 470–476 (2011).
96. Harford-Wright, E. *et al.* Pharmacological targeting of apelin impairs glioblastoma growth. *Brain* **140**, 2939–2954 (2017).
97. Frisch, A. *et al.* Apelin Controls Angiogenesis-Dependent Glioblastoma Growth. *Int. J. Mol. Sci.* **21**, 4179 (2020).
98. Jacobs, K. A., Harford-Wright, E. & Gavard, J. Neutralizing gp130 interferes with endothelial-mediated effects on glioblastoma stem-like cells. *Cell Death Differ.* **24**, 384–384 (2017).
99. Trillet, K. *et al.* The glycoprotein GP130 governs the surface presentation of the G protein–coupled receptor APLNR. *J. Cell Biol.* **220**, e202004114 (2021).
100. Filppu, P. *et al.* CD109-GP130 interaction drives glioblastoma stem cell plasticity and chemoresistance through STAT3 activity. *JCI Insight* **6**, e141486 (2021).
101. Rong, Y., Durden, D. L., Meir, E. G. V. & Brat, D. J. FPseudopalisading` Necrosis in Glioblastoma: A Familiar Morphologic Feature That Links Vascular Pathology, Hypoxia, and Angiogenesis. *J Neuropathol Exp Neurol* **65**, (2006).
102. Seidel, S. *et al.* A hypoxic niche regulates glioblastoma stem cells through hypoxia inducible factor 2α. *Brain* **133**, 983–995 (2010).
103. Soeda, A. *et al.* Hypoxia promotes expansion of the CD133-positive glioma

stem cells through activation of HIF-1α. *Oncogene* **28**, 3949–3959 (2009).
104. Bar, E. E., Lin, A., Mahairaki, V., Matsui, W. & Eberhart, C. G. Hypoxia Increases the Expression of Stem-Cell Markers and Promotes Clonogenicity in Glioblastoma Neurospheres. *Am. J. Pathol.* **177**, 1491–1502 (2010).
105. Cuddapah, V. A., Robel, S., Watkins, S. & Sontheimer, H. A neurocentric perspective on glioma invasion. *Nat. Rev. Neurosci.* **15**, 455–465 (2014).
106. Watkins, S. *et al.* Disruption of astrocyte–vascular coupling and the blood–brain barrier by invading glioma cells. *Nat. Commun.* **5**, 4196 (2014).
107. Verhaak, R. G. W. *et al.* Integrated Genomic Analysis Identifies Clinically Relevant Subtypes of Glioblastoma Characterized by Abnormalities in PDGFRA, IDH1, EGFR, and NF1. *Cancer Cell* **17**, 98–110 (2010).
108. Wang, Q. *et al.* Tumor Evolution of Glioma-Intrinsic Gene Expression Subtypes Associates with Immunological Changes in the Microenvironment. *Cancer Cell* **32**, 42-56.e6 (2017).
109. Patel, A. P. *et al.* Single-cell RNA-seq highlights intratumoral heterogeneity in primary glioblastoma. *Science* **344**, 1396–1401 (2014).
110. Gill, B. J. *et al.* MRI-localized biopsies reveal subtype-specific differences in molecular and cellular composition at the margins of glioblastoma. *Proc. Natl. Acad. Sci.* **111**, 12550–12555 (2014).
111. Bastola, S. *et al.* Glioma-initiating cells at tumor edge gain signals from tumor core cells to promote their malignancy. *Nat. Commun.* **11**, 4660 (2020).
112. Bowman, R. L., Wang, Q., Carro, A., Verhaak, R. G. W. & Squatrito, M. GlioVis data portal for visualization and analysis of brain tumor expression datasets. *Neuro-Oncol.* **19**, 139–141 (2017).
113. Puchalski, R. B. *et al.* An anatomic transcriptional atlas of human glioblastoma. *Science* **360**, 660–663 (2018).
114. Yuan, S., Norgard, R. J. & Stanger, B. Z. Cellular Plasticity in Cancer. *Cancer Discov.* **9**, 837–851 (2019).
115. Yabo, Y. A., Niclou, S. P. & Golebiewska, A. Cancer cell heterogeneity and plasticity: A paradigm shift in glioblastoma. *Neuro-Oncol.* **24**, 669–682 (2022).
116. Neftel, C. *et al.* An Integrative Model of Cellular States, Plasticity, and Genetics for Glioblastoma. *Cell* **178**, 835-849.e21 (2019).
117. Castellan, M. *et al.* Single-cell analyses reveal YAP/TAZ as regulators of stemness and cell plasticity in glioblastoma. *Nat. Cancer* **2**, 174–188 (2020).
118. Minata, M. *et al.* Phenotypic Plasticity of Invasive Edge Glioma Stem-like Cells in Response to Ionizing Radiation. *Cell Rep.* **26**, 1893-1905.e7 (2019).
119. Wang, J. *et al.* Clonal evolution of glioblastoma under therapy. *Nat. Genet.* **48**, 768–776 (2016).
120. Ballabio, A. & Bonifacino, J. S. Lysosomes as dynamic regulators of cell and organismal homeostasis. *Nat. Rev. Mol. Cell Biol.* **21**, 101–118 (2020).
121. Jacobs, K. A. *et al.* Paracaspase MALT1 regulates glioma cell survival by controlling endo-lysosome homeostasis. *EMBO J.* **39**, e102030 (2020).
122. Le Joncour, V. *et al.* Vulnerability of invasive glioblastoma cells to lysosomal membrane destabilization. *EMBO Mol. Med.* **11**, (2019).
123. Jensen, S. S., Petterson, S. A., Halle, B., Aaberg-Jessen, C. & Kristensen, B. W. Effects of the lysosomal destabilizing drug siramesine on glioblastoma in vitro and in vivo. *BMC Cancer* **17**, 178 (2017).
124. Zhou, W., Guo, Y., Zhang, X. & Jiang, Z. Lys05 induces lysosomal membrane permeabilization and increases radiosensitivity in glioblastoma. *J. Cell. Biochem.* **121**, 2027–2037 (2020).

125. Wojton, J. *et al.* SapC-DOPS-induced lysosomal cell death synergizes with TMZ in glioblastoma. *Oncotarget* **5**, (2014).
126. Mora, R. *et al.* Sphingolipid rheostat alterations related to transformation can be exploited for specific induction of lysosomal cell death in murine and human glioma. *Glia* **58**, 1364–1383 (2010).
127. Enzenmüller, S., Gonzalez, P., Karpel-Massler, G., Debatin, K.-M. & Fulda, S. GDC-0941 enhances the lysosomal compartment via TFEB and primes glioblastoma cells to lysosomal membrane permeabilization and cell death. *Cancer Lett.* **329**, 27–36 (2013).
128. Saxton, R. A. & Sabatini, D. M. mTOR Signaling in Growth, Metabolism, and Disease. *Cell* **168**, 960–976 (2017).
129. Chakravarti, A. *et al.* The Prognostic Significance of Phosphatidylinositol 3-Kinase Pathway Activation in Human Gliomas. *J. Clin. Oncol.* **22**, 1926–1933 (2004).
130. Galanis, E. *et al.* Phase II Trial of Temsirolimus (CCI-779) in Recurrent Glioblastoma Multiforme: A North Central Cancer Treatment Group Study. *J. Clin. Oncol.* **23**, 5294–5304 (2005).
131. Cloughesy, T. F. *et al.* Antitumor Activity of Rapamycin in a Phase I Trial for Patients with Recurrent PTEN-Deficient Glioblastoma. *PLoS Med.* **5**, e8 (2008).
132. Chinnaiyan, P. *et al.* A randomized phase II study of everolimus in combination with chemoradiation in newly diagnosed glioblastoma: results of NRG Oncology RTOG 0913. *Neuro-Oncol.* **20**, 666–673 (2018).
133. Kreisl, T. N. *et al.* A pilot study of everolimus and gefitinib in the treatment of recurrent glioblastoma (GBM). *J. Neurooncol.* **92**, 99–105 (2009).
134. Sarbassov, D. D. *et al.* Prolonged rapamycin treatment inhibits mTORC2 assembly and Akt/PKB. *Mol. Cell* **22**, 159–168 (2006).
135. Thoreen, C. C. *et al.* An ATP-competitive Mammalian Target of Rapamycin Inhibitor Reveals Rapamycin-resistant Functions of mTORC1. *J. Biol. Chem.* **284**, 8023–8032 (2009).
136. Papavassiliou, K. A. & Papavassiliou, A. G. The Bumpy Road towards mTOR Inhibition in Glioblastoma: Quo Vadis? *Biomedicines* **9**, 1809 (2021).
137. Galan-Moya, E. M. *et al.* Endothelial Secreted Factors Suppress Mitogen Deprivation-Induced Autophagy and Apoptosis in Glioblastoma Stem-Like Cells. *PLOS ONE* **9**, e93505 (2014).
138. Kahn, J. *et al.* The mTORC1/mTORC2 inhibitor AZD2014 enhances the radiosensitivity of glioblastoma stem-like cells. *Neuro-Oncol.* **16**, 29–37 (2014).
139. Ryskalin, L. *et al.* The Autophagy Status of Cancer Stem Cells in Gliobastoma Multiforme: From Cancer Promotion to Therapeutic Strategies. *Int. J. Mol. Sci.* **20**, 3824 (2019).
140. Natsumeda, M. *et al.* Targeting Notch Signaling and Autophagy Increases Cytotoxicity in Glioblastoma Neurospheres: Targeting Notch and Autophagy in GBM. *Brain Pathol.* **26**, 713–723 (2016).
141. Ferrucci, M. *et al.* Rapamycin promotes differentiation increasing βIII-tubulin, NeuN, and NeuroD while suppressing nestin expression in glioblastoma cells. *Oncotarget* **8**, 29574–29599 (2017).
142. Catalano, M. *et al.* Autophagy induction impairs migration and invasion by reversing EMT in glioblastoma cells. *Mol. Oncol.* **9**, 1612–1625 (2015).
143. Zhuang, W. *et al.* Curcumin promotes differentiation of glioma-initiating cells by inducing autophagy. *Cancer Sci.* **103**, 684–690 (2012).
144. Zhuang, W. *et al.* Induction of autophagy promotes differentiation of glioma-initiating cells and their radiosensitivity. *Int. J. Cancer* **129**, 2720–2731 (2011).

145. Tao, Z. *et al.* Autophagy suppresses self-renewal ability and tumorigenicity of glioma-initiating cells and promotes Notch1 degradation. *Cell Death Dis.* **9**, 1063 (2018).
146. Shakya, S. *et al.* Altered lipid metabolism marks glioblastoma stem and non-stem cells in separate tumor niches. *Acta Neuropathol. Commun.* **9**, 101 (2021).
147. Cheng, X. *et al.* Targeting DGAT1 Ameliorates Glioblastoma by Increasing Fat Catabolism and Oxidative Stress. *Cell Metab.* **32**, 229-242.e8 (2020).
148. Wu, X. *et al.* Lipid Droplets Maintain Energy Homeostasis and Glioblastoma Growth via Autophagic Release of Stored Fatty Acids. *iScience* **23**, 101569 (2020).
149. Le Joncour, V. *et al.* Vulnerability of invasive glioblastoma cells to lysosomal membrane destabilization. *EMBO Mol. Med.* **11**, (2019).
150. Dietschy, J. M. Central nervous system: cholesterol turnover, brain development and neurodegeneration. *bchm* **390**, 287–293 (2009).
151. Han, M. *et al.* Therapeutic implications of altered cholesterol homeostasis mediated by loss of CYP46A1 in human glioblastoma. *EMBO Mol. Med.* **12**, e10924 (2020).
152. Guo, D. *et al.* An LXR Agonist Promotes Glioblastoma Cell Death through Inhibition of an EGFR/AKT/SREBP-1/LDLR–Dependent Pathway. *Cancer Discov.* **1**, 442–456 (2011).
153. Villa, G. R. *et al.* An LXR-Cholesterol Axis Creates a Metabolic Co-Dependency for Brain Cancers. *Cancer Cell* **30**, 683–693 (2016).
154. Eberlé, D., Hegarty, B., Bossard, P., Ferré, P. & Foufelle, F. SREBP transcription factors: master regulators of lipid homeostasis. *Biochimie* **86**, 839–848 (2004).
155. Lewis, C. A. *et al.* SREBP maintains lipid biosynthesis and viability of cancer cells under lipid- and oxygen-deprived conditions and defines a gene signature associated with poor survival in glioblastoma multiforme. *Oncogene* **34**, 5128–5140 (2015).
156. Li, D., Li, S., Xue, A. Z., Smith Callahan, L. A. & Liu, Y. Expression of SREBP2 and cholesterol metabolism related genes in TCGA glioma cohorts. *Medicine (Baltimore)* **99**, e18815 (2020).
157. de Duve, C., Berthet, J., Hers, H. & Dupret, L. Le système hexose-phosphatasique. Existence d'une glucose-6-phosphatase spécifique dans le foie. *Bull. Société Chim. Biol.* **31**, 1242–1253 (1949).
158. Berthet, J. & De Duve, C. Tissue fractionation studies. 1. The existence of a mitochondria-linked, enzymically inactive form of acid phosphatase in rat-liver tissue. *Biochem. J.* **50**, 174-181. (1951).
159. Berthet, J., Berthet, L., Appelmans, F. & De Duve, C. Tissue fractionation studies. 2. The nature of the linkage between acid phosphatase and mitochondria in rat-liver tissue. *Biochem. J.* **50**, 182–189 (1951).
160. Appelmans, F. & De Duve, C. Tissue fractionation studies. 3. Further observations on the binding of acid phosphatase by rat-liver particles. *Biochem. J.* **59**, 426–433 (1955).
161. Appelmans, F., Wattiaux, R. & De Duve, C. Tissue fractionation studies. 5. The association of acid phosphatase with a special class of cytoplasmic granules in rat liver. *Biochem. J.* **59**, 438–445 (1955).
162. Gianetto, R. & Duve, C. D. Tissue fractionation studies. 4. Comparative study of the binding of acid phosphatase, β-glucuronidase and cathepsin by rat-liver particles. *Biochem. J.* **59**, 433–438 (1955).
163. de Duve, C., Pressman, B. C., Gianetto, R., Wattiaux, R. & Appelmans, F.

Tissue fractionation studies. 6. Intracellular distribution patterns of enzymes in rat-liver tissue. *Biochem. J.* **60**, 604–617 (1955).
164. Novikoff, A. B., Beaufay, H. & de Duve, C. ELECTRON MICROSCOPY OF LYSOSOME-RICH FRACTIONS FROM RAT LIVER. *J. Biophys. Biochem. Cytol.* **2**, 179–184 (1956).
165. Baudhuin, P., Beaufay, H. & de Duve, C. Combined biochemical and morphological study of particulate fractions from rat liver. Analysis of preparations enriched in lysosomes or in particles containing urate oxidase, D-amino acid oxidase, and catalase. *J. Cell Biol.* **26**, 219–243 (1965).
166. De Duve, C. Exploring Cells with a Centrifuge. *Science* **189**, 186–194 (1975).
167. Shin, H. R. & Zoncu, R. The Lysosome at the Intersection of Cellular Growth and Destruction. *Dev. Cell* **54**, 226–238 (2020).
168. Huotari, J. & Helenius, A. Endosome maturation. *EMBO J.* **30**, 3481–3500 (2011).
169. Trivedi, P. C., Bartlett, J. J. & Pulinilkunnil, T. Lysosomal Biology and Function: Modern View of Cellular Debris Bin. *Cells* **9**, 1131 (2020).
170. Saftig, P. & Klumperman, J. Lysosome biogenesis and lysosomal membrane proteins: trafficking meets function. *Nat. Rev. Mol. Cell Biol.* **10**, 623–635 (2009).
171. Rennick, J. J., Johnston, A. P. R. & Parton, R. G. Key principles and methods for studying the endocytosis of biological and nanoparticle therapeutics. *Nat. Nanotechnol.* **16**, 266–276 (2021).
172. Cullen, P. J. & Steinberg, F. To degrade or not to degrade: mechanisms and significance of endocytic recycling. *Nat. Rev. Mol. Cell Biol.* **19**, 679–696 (2018).
173. Wallroth, A. & Haucke, V. Phosphoinositide conversion in endocytosis and the endolysosomal system. *J. Biol. Chem.* **293**, 1526–1535 (2018).
174. Poteryaev, D., Datta, S., Ackema, K., Zerial, M. & Spang, A. Identification of the Switch in Early-to-Late Endosome Transition. *Cell* **141**, 497–508 (2010).
175. Gruenberg, J. Life in the lumen: The multivesicular endosome. *Traffic* **21**, 76–93 (2020).
176. Rink, J., Ghigo, E., Kalaidzidis, Y. & Zerial, M. Rab Conversion as a Mechanism of Progression from Early to Late Endosomes. *Cell* **122**, 735–749 (2005).
177. Bissig, C., Hurbain, I., Raposo, G. & van Niel, G. PIKfyve activity regulates reformation of terminal storage lysosomes from endolysosomes. *Traffic Cph. Den.* **18**, 747–757 (2017).
178. McGuire, C. M. & Forgac, M. Glucose starvation increases V-ATPase assembly and activity in mammalian cells through AMP kinase and phosphatidylinositide 3-kinase/Akt signaling. *J. Biol. Chem.* **293**, 9113–9123 (2018).
179. Xu, M. *et al.* The biogenesis and secretion of exosomes and multivesicular bodies (MVBs): Intercellular shuttles and implications in human diseases. *Genes Dis.* S2352304222000976 (2022) doi:10.1016/j.gendis.2022.03.021.
180. Casey, J. R., Grinstein, S. & Orlowski, J. Sensors and regulators of intracellular pH. *Nat. Rev. Mol. Cell Biol.* **11**, 50–61 (2010).
181. Forgac, M. Vacuolar ATPases: rotary proton pumps in physiology and pathophysiology. *Nat. Rev. Mol. Cell Biol.* **8**, 917–929 (2007).
182. Stransky, L. A. & Forgac, M. Amino Acid Availability Modulates Vacuolar H⁺-ATPase Assembly. **290**, (2015).
183. Ratto, E. *et al.* Direct control of lysosomal catabolic activity by mTORC1 through regulation of V-ATPase assembly. *Nat. Commun.* **13**, 4848 (2022).
184. Xu, Y. *et al.* Epidermal Growth Factor-induced Vacuolar (H+)-ATPase Assembly. *J. Biol. Chem.* **287**, 26409–26422 (2012).

185. Banerjee, S. & Kane, P. M. Regulation of V-ATPase Activity and Organelle pH by Phosphatidylinositol Phosphate Lipids. *Front. Cell Dev. Biol.* **8**, 510 (2020).
186. Osei-Owusu, J. *et al.* Proton-activated chloride channel PAC regulates endosomal acidification and transferrin receptor-mediated endocytosis. *Cell Rep.* **34**, 108683 (2021).
187. Perera, R. M. & Zoncu, R. The Lysosome as a Regulatory Hub. *Annu. Rev. Cell Dev. Biol.* **32**, 223–253 (2016).
188. Bright, N. A., Davis, L. J. & Luzio, J. P. Endolysosomes Are the Principal Intracellular Sites of Acid Hydrolase Activity. *Curr. Biol. CB* **26**, 2233–2245 (2016).
189. Lawrence, R. E. & Zoncu, R. The lysosome as a cellular centre for signalling, metabolism and quality control. *Nat. Cell Biol.* **21**, 133–142 (2019).
190. Balderhaar, H. J. K. & Ungermann, C. CORVET and HOPS tethering complexes – coordinators of endosome and lysosome fusion. *J. Cell Sci.* **126**, 1307–1316 (2013).
191. Nickerson, D. P., Brett, C. L. & Merz, A. J. Vps-C complexes: gatekeepers of endolysosomal traffic. *Curr. Opin. Cell Biol.* **21**, 543–551 (2009).
192. Balderhaar, H. J. K. *et al.* The CORVET complex promotes tethering and fusion of Rab5/Vps21-positive membranes. *Proc. Natl. Acad. Sci.* **110**, 3823–3828 (2013).
193. Peplowska, K., Markgraf, D. F., Ostrowicz, C. W., Bange, G. & Ungermann, C. The CORVET Tethering Complex Interacts with the Yeast Rab5 Homolog Vps21 and Is Involved in Endo-Lysosomal Biogenesis. *Dev. Cell* **12**, 739–750 (2007).
194. Price, A., Seals, D., Wickner, W. & Ungermann, C. The Docking Stage of Yeast Vacuole Fusion Requires the Transfer of Proteins from a Cis-Snare Complex to a Rab/Ypt Protein. *J. Cell Biol.* **148**, 1231–1238 (2000).
195. Shelke, G. V., Williamson, C. D., Jarnik, M. & Bonifacino, J. S. Inhibition of endolysosome fusion increases exosome secretion. *J. Cell Biol.* **222**, e202209084 (2023).
196. Aman, Y. *et al.* Autophagy in healthy aging and disease. *Nat. Aging* **1**, 634–650 (2021).
197. Yim, W. W.-Y. & Mizushima, N. Lysosome biology in autophagy. *Cell Discov.* **6**, 6 (2020).
198. Ganesan, D. & Cai, Q. Understanding amphisomes. *Biochem. J.* **478**, 1959–1976 (2021).
199. Chen, Y. & Yu, L. Recent progress in autophagic lysosome reformation. *Traffic* **18**, 358–361 (2017).
200. Yu, L. *et al.* Termination of autophagy and reformation of lysosomes regulated by mTOR. *Nature* **465**, 942–946 (2010).
201. Du, W. *et al.* Kinesin 1 Drives Autolysosome Tubulation. *Dev. Cell* **37**, 326–336 (2016).
202. Bhattacharya, A. *et al.* A lysosome membrane regeneration pathway depends on TBC1D15 and autophagic lysosomal reformation proteins. *Nat. Cell Biol.* **25**, 685–698 (2023).
203. Ni, X. & Morales, C. R. The lysosomal trafficking of acid sphingomyelinase is mediated by sortilin and mannose 6-phosphate receptor. *Traffic Cph. Den.* **7**, 889–902 (2006).
204. Canuel, M., Korkidakis, A., Konnyu, K. & Morales, C. R. Sortilin mediates the lysosomal targeting of cathepsins D and H. *Biochem. Biophys. Res. Commun.* **373**, 292–297 (2008).
205. Reczek, D. *et al.* LIMP-2 is a receptor for lysosomal mannose-6-phosphate-

independent targeting of beta-glucocerebrosidase. *Cell* **131**, 770–783 (2007).
206. Coutinho, M. F., Prata, M. J. & Alves, S. Mannose-6-phosphate pathway: A review on its role in lysosomal function and dysfunction. *Mol. Genet. Metab.* **105**, 542–550 (2012).
207. Munier-Lehmann, H., Mauxion, F. & Hoflack, B. Function of the two mannose 6-phosphate receptors in lysosomal enzyme transport. *Biochem. Soc. Trans.* **24**, 133–136 (1996).
208. Janvier, K. & Bonifacino, J. S. Role of the Endocytic Machinery in the Sorting of Lysosome-associated Membrane Proteins. *Mol. Biol. Cell* **16**, 4231–4242 (2005).
209. Lefrancois, S. The lysosomal trafficking of sphingolipid activator proteins (SAPs) is mediated by sortilin. *EMBO J.* **22**, 6430–6437 (2003).
210. Braulke, T. & Bonifacino, J. S. Sorting of lysosomal proteins. *Biochim. Biophys. Acta BBA - Mol. Cell Res.* **1793**, 605–614 (2009).
211. Pechincha, C. *et al.* Lysosomal enzyme trafficking factor LYSET enables nutritional usage of extracellular proteins. *Science* **378**, eabn5637 (2022).
212. Richards, C. M. *et al.* The human disease gene LYSET is essential for lysosomal enzyme transport and viral infection. *Science* **378**, eabn5648 (2022).
213. Munier-Lehmann, H., Mauxion, F., Bauer, U., Lobel, P. & Hoflack, B. Re-expression of the Mannose 6-Phosphate Receptors in Receptor-deficient Fibroblasts. *J. Biol. Chem.* **271**, 15166–15174 (1996).
214. Paton, L. *et al.* A Novel Mouse Model of a Patient Mucolipidosis II Mutation Recapitulates Disease Pathology. *J. Biol. Chem.* **289**, 26709–26721 (2014).
215. Dittmer, F. Alternative mechanisms for trafficking of lysosomal enzymes in mannose 6- phosphate receptor-deficient mice are cell type-specific. *J. Cell Sci.* **112**, 1591–1597 (1999).
216. Bonifacino, J. S. & Traub, L. M. Signals for Sorting of Transmembrane Proteins to Endosomes and Lysosomes. *Annu. Rev. Biochem.* **72**, 395–447 (2003).
217. Sardiello, M. *et al.* A gene network regulating lysosomal biogenesis and function. *Science* **325**, 473–477 (2009).
218. Raben, N. & Puertollano, R. TFEB and TFE3: Linking Lysosomes to Cellular Adaptation to Stress. *Annu. Rev. Cell Dev. Biol.* **32**, 255–278 (2016).
219. Settembre, C. *et al.* TFEB Links Autophagy to Lysosomal Biogenesis. *Science* **332**, 1429–1433 (2011).
220. Napolitano, G. *et al.* mTOR-dependent phosphorylation controls TFEB nuclear export. *Nat. Commun.* **9**, 3312 (2018).
221. Settembre, C. *et al.* A lysosome-to-nucleus signalling mechanism senses and regulates the lysosome via mTOR and TFEB. *EMBO J.* **31**, 1095–1108 (2012).
222. Martina, J. A., Chen, Y., Gucek, M. & Puertollano, R. MTORC1 functions as a transcriptional regulator of autophagy by preventing nuclear transport of TFEB. *Autophagy* **8**, 903–914 (2012).
223. Roczniak-Ferguson, A. *et al.* The Transcription Factor TFEB Links mTORC1 Signaling to Transcriptional Control of Lysosome Homeostasis. *Sci. Signal.* **5**, ra42–ra42 (2012).
224. Puertollano, R., Ferguson, S. M., Brugarolas, J. & Ballabio, A. The complex relationship between TFEB transcription factor phosphorylation and subcellular localization. *EMBO J.* **37**, (2018).
225. Medina, D. L. *et al.* Lysosomal calcium signalling regulates autophagy through calcineurin and TFEB. *Nat. Cell Biol.* **17**, 288–299 (2015).
226. Napolitano, G. & Ballabio, A. TFEB at a glance. *J. Cell Sci.* **129**, 2475–2481 (2016).

227. Shin, H.-J. R. *et al.* AMPK–SKP2–CARM1 signalling cascade in transcriptional regulation of autophagy. *Nature* **534**, 553–557 (2016).
228. Shi, J. & Vakoc, C. R. The Mechanisms behind the Therapeutic Activity of BET Bromodomain Inhibition. *Mol. Cell* **54**, 728–736 (2014).
229. Sakamaki, J. *et al.* Bromodomain Protein BRD4 Is a Transcriptional Repressor of Autophagy and Lysosomal Function. *Mol. Cell* **66**, 517-532.e9 (2017).
230. Shingu, T. *et al.* Qki deficiency maintains stemness of glioma stem cells in suboptimal environment by downregulating endolysosomal degradation. *Nat. Genet.* **49**, 75–86 (2017).
231. Araujo, M. E. G., Liebscher, G., Hess, M. W. & Huber, L. A. Lysosomal size matters. *Traffic* **21**, 60–75 (2020).
232. Winchester, B. G. Lysosomal membrane proteins. *Eur. J. Paediatr. Neurol.* **5**, 11–19 (2001).
233. Möbius, W. *et al.* Recycling Compartments and the Internal Vesicles of Multivesicular Bodies Harbor Most of the Cholesterol Found in the Endocytic Pathway: **Cholesterol in the Endocytic Pathway**. *Traffic* **4**, 222–231 (2003).
234. Kaushik, S., Massey, A. C. & Cuervo, A. M. Lysosome membrane lipid microdomains: novel regulators of chaperone-mediated autophagy. *EMBO J.* **25**, 3921–3933 (2006).
235. Roh, K. *et al.* Lysosomal control of senescence and inflammation through cholesterol partitioning. *Nat. Metab.* (2023) doi:10.1038/s42255-023-00747-5.
236. Barriocanal, J. G., Bonifacino, J. S., Yuan, L. & Sandoval, I. V. Biosynthesis, glycosylation, movement through the Golgi system, and transport to lysosomes by an N-linked carbohydrate-independent mechanism of three lysosomal integral membrane proteins. *J. Biol. Chem.* **261**, 16755–16763 (1986).
237. Kundra, R. & Kornfeld, S. Asparagine-linked Oligosaccharides Protect Lamp-1 and Lamp-2 from Intracellular Proteolysis. *J. Biol. Chem.* **274**, 31039–31046 (1999).
238. Nishino, I. *et al.* Primary LAMP-2 deficiency causes X-linked vacuolar cardiomyopathy and myopathy (Danon disease). *Nature* **406**, 906–910 (2000).
239. Tanaka, Y. *et al.* Accumulation of autophagic vacuoles and cardiomyopathy in LAMP-2-deficient mice. *Nature* **406**, 902–906 (2000).
240. Eskelinen, E.-L. *et al.* Disturbed Cholesterol Traffic but Normal Proteolytic Function in LAMP-1/LAMP-2 Double-deficient Fibroblasts□D. *Mol. Biol. Cell* **15**, (2004).
241. Andrejewski, N. *et al.* Normal Lysosomal Morphology and Function in LAMP-1-deficient Mice. *J. Biol. Chem.* **274**, 12692–12701 (1999).
242. Heybrock, S. *et al.* Lysosomal integral membrane protein-2 (LIMP-2/SCARB2) is involved in lysosomal cholesterol export. *Nat. Commun.* **10**, 3521 (2019).
243. Lübke, T., Lobel, P. & Sleat, D. E. Proteomics of the lysosome. *Biochim. Biophys. Acta BBA - Mol. Cell Res.* **1793**, 625–635 (2009).
244. Schröder, B. *et al.* Integral and Associated Lysosomal Membrane Proteins. *Traffic* **8**, 1676–1686 (2007).
245. Zhang, H. *et al.* Lysosomal Membranes from Beige Mice Contain Higher Than Normal Levels of Endoplasmic Reticulum Proteins. *J. Proteome Res.* **6**, 240–249 (2007).
246. Bagshaw, R. D., Mahuran, D. J. & Callahan, J. W. A Proteomic Analysis of Lysosomal Integral Membrane Proteins Reveals the Diverse Composition of the Organelle. *Mol. Cell. Proteomics* **4**, 133–143 (2005).
247. Menon, S. *et al.* Spatial control of the TSC complex integrates insulin and nutrient regulation of mTORC1 at the lysosome. *Cell* **156**, 771–785 (2014).

248. Wolfson, R. L. *et al.* KICSTOR recruits GATOR1 to the lysosome and is necessary for nutrients to regulate mTORC1. *Nature* **543**, 438–442 (2017).
249. Shin, H. R. *et al.* Lysosomal GPCR-like protein LYCHOS signals cholesterol sufficiency to mTORC1. *Science* **377**, 1290–1298 (2022).
250. Akter, F. *et al.* Multi–Cell Line Analysis of Lysosomal Proteomes Reveals Unique Features and Novel Lysosomal Proteins. *Mol. Cell. Proteomics* **22**, 100509 (2023).
251. Yadati, T., Houben, T., Bitorina, A. & Shiri-Sverdlov, R. The Ins and Outs of Cathepsins: Physiological Function and Role in Disease Management. *Cells* **9**, 1679 (2020).
252. Johnson, D. E., Ostrowski, P., Jaumouillé, V. & Grinstein, S. The position of lysosomes within the cell determines their luminal pH. *J. Cell Biol.* **212**, 677–692 (2016).
253. Wu, J. Z. *et al.* ClC-7 drives intraphagosomal chloride accumulation to support hydrolase activity and phagosome resolution. *J. Cell Biol.* **222**, e202208155 (2023).
254. Zhang, Q., Li, Y., Jian, Y., Li, M. & Wang, X. Lysosomal chloride transporter CLH-6 protects lysosome membrane integrity via cathepsin activation. *J. Cell Biol.* **222**, e202210063 (2023).
255. Christensen, K. A., Myers, J. T. & Swanson, J. A. pH-dependent regulation of lysosomal calcium in macrophages. *J. Cell Sci.* **115**, 599–607 (2002).
256. Cao, Q. *et al.* Calcium release through P2X4 activates calmodulin to promote endolysosomal membrane fusion. *J. Cell Biol.* **209**, 879–894 (2015).
257. Bargal, R. *et al.* Identification of the gene causing mucolipidosis type IV. *Nat. Genet.* **26**, 118–122 (2000).
258. Sun, M. Mucolipidosis type IV is caused by mutations in a gene encoding a novel transient receptor potential channel. *Hum. Mol. Genet.* **9**, 2471–2478 (2000).
259. Vergarajauregui, S., Connelly, P. S., Daniels, M. P. & Puertollano, R. Autophagic dysfunction in mucolipidosis type IV patients. *Hum. Mol. Genet.* **17**, 2723–2737 (2008).
260. LaPlante, J. M. *et al.* Lysosomal exocytosis is impaired in mucolipidosis type IV. *Mol. Genet. Metab.* **89**, 339–348 (2006).
261. Scotto Rosato, A. *et al.* TPC2 rescues lysosomal storage in mucolipidosis type IV , NIEMANN–PICK type C1, and Batten disease. *EMBO Mol. Med.* **14**, e15377 (2022).
262. Abu-Remaileh, M. *et al.* Lysosomal metabolomics reveals V-ATPase and mTOR-dependent regulation of amino acid efflux from lysosomes. *Science* **358**, 807–813 (2017).
263. Wyant, G. A. *et al.* mTORC1 Activator SLC38A9 Is Required to Efflux Essential Amino Acids from Lysosomes and Use Protein as a Nutrient. *Cell* **171**, 642-654.e12 (2017).
264. Jung, J., Genau, H. M. & Behrends, C. Amino Acid-Dependent mTORC1 Regulation by the Lysosomal Membrane Protein SLC38A9. *Mol. Cell. Biol.* **35**, 2479–2494 (2015).
265. Rebsamen, M. *et al.* SLC38A9 is a component of the lysosomal amino acid sensing machinery that controls mTORC1. *Nature* **519**, 477–481 (2015).
266. Wang, S. *et al.* Lysosomal amino acid transporter SLC38A9 signals arginine sufficiency to mTORC1. *Science* **347**, 188–194 (2015).
267. Wyant, G. A. *et al.* NUFIP1 is a ribosome receptor for starvation-induced ribophagy. *Science* **360**, 751–758 (2018).
268. Zhang, S. *et al.* The regulation, function, and role of lipophagy, a form of

selective autophagy, in metabolic disorders. *Cell Death Dis.* **13**, 132 (2022).
269. Meng, Y., Heybrock, S., Neculai, D. & Saftig, P. Cholesterol Handling in Lysosomes and Beyond. *Trends Cell Biol.* **30**, 452–466 (2020).
270. Gomaraschi, M., Bonacina, F. & Norata, G. D. Lysosomal Acid Lipase: From Cellular Lipid Handler to Immunometabolic Target. *Trends Pharmacol. Sci.* **40**, 104–115 (2019).
271. Settembre, C. & Ballabio, A. Lysosome: regulator of lipid degradation pathways. *Trends Cell Biol.* **24**, 743–750 (2014).
272. Anderson, R. A., Byrum, R. S., Coates, P. M. & Sando, G. N. Mutations at the lysosomal acid cholesteryl ester hydrolase gene locus in Wolman disease. *Proc. Natl. Acad. Sci.* **91**, 2718–2722 (1994).
273. Marques, AndréR. A. *et al.* Glucosylated cholesterol in mammalian cells and tissues: formation and degradation by multiple cellular β-glucosidases. *J. Lipid Res.* **57**, 451–463 (2016).
274. Qian, H. *et al.* Structural Basis of Low-pH-Dependent Lysosomal Cholesterol Egress by NPC1 and NPC2. *Cell* **182**, 98-111.e18 (2020).
275. Schneede, A. *et al.* Role for LAMP-2 in endosomal cholesterol transport. *J. Cell. Mol. Med.* **15**, 280–295 (2011).
276. Cariati, I. *et al.* Neurodegeneration in Niemann–Pick Type C Disease: An Updated Review on Pharmacological and Non-Pharmacological Approaches to Counteract Brain and Cognitive Impairment. *Int. J. Mol. Sci.* **22**, 6600 (2021).
277. Davis, O. B. *et al.* NPC1-mTORC1 Signaling Couples Cholesterol Sensing to Organelle Homeostasis and Is a Targetable Pathway in Niemann-Pick Type C. *Dev. Cell* **56**, 260-276.e7 (2021).
278. Castellano, B. M. *et al.* Lysosomal cholesterol activates mTORC1 via an SLC38A9–Niemann-Pick C1 signaling complex. *Science* **355**, 1306–1311 (2017).
279. Hosios, A. M. *et al.* mTORC1 regulates a lysosome-dependent adaptive shift in intracellular lipid species. *Nat. Metab.* **4**, 1792–1811 (2022).
280. Wang, L., Klionsky, D. J. & Shen, H.-M. The emerging mechanisms and functions of microautophagy. *Nat. Rev. Mol. Cell Biol.* **24**, 186–203 (2023).
281. Lee, C., Lamech, L., Johns, E. & Overholtzer, M. Selective Lysosome Membrane Turnover Is Induced by Nutrient Starvation. *Dev. Cell* **55**, 289-297.e4 (2020).
282. Deng, Z. *et al.* Autophagy Receptors and Neurodegenerative Diseases. *Trends Cell Biol.* **27**, 491–504 (2017).
283. Papadopoulos, C., Kravic, B. & Meyer, H. Repair or Lysophagy: Dealing with Damaged Lysosomes. *J. Mol. Biol.* **432**, 231–239 (2020).
284. Gubas, A. & Dikic, I. A guide to the regulation of selective autophagy receptors. *FEBS J.* **289**, 75–89 (2022).
285. Wild, P., McEwan, D. G. & Dikic, I. The LC3 interactome at a glance. *J. Cell Sci.* jcs.140426 (2014) doi:10.1242/jcs.140426.
286. Hung, Y.-H., Chen, L. M.-W., Yang, J.-Y. & Yang, W. Y. Spatiotemporally controlled induction of autophagy-mediated lysosome turnover. *Nat. Commun.* **4**, 2111 (2013).
287. Yoshida, Y. *et al.* Ubiquitination of exposed glycoproteins by SCF ^{FBXO27} directs damaged lysosomes for autophagy. *Proc. Natl. Acad. Sci.* **114**, 8574–8579 (2017).
288. Eapen, V. V., Swarup, S., Hoyer, M. J., Paulo, J. A. & Harper, J. W. Quantitative proteomics reveals the selectivity of ubiquitin-binding autophagy receptors in the turnover of damaged lysosomes by lysophagy. *eLife* **10**, e72328

(2021).
289. Koerver, L. *et al.* The ubiquitin-conjugating enzyme UBE 2 QL 1 coordinates lysophagy in response to endolysosomal damage. *EMBO Rep.* **20**, e48014 (2019).
290. Thurston, T. L. M., Wandel, M. P., von Muhlinen, N., Foeglein, A. & Randow, F. Galectin 8 targets damaged vesicles for autophagy to defend cells against bacterial invasion. *Nature* **482**, 414–418 (2012).
291. Chauhan, S. *et al.* TRIMs and Galectins Globally Cooperate and TRIM16 and Galectin-3 Co-direct Autophagy in Endomembrane Damage Homeostasis. *Dev. Cell* **39**, 13–27 (2016).
292. Jia, J. *et al.* Galectins Control mTOR in Response to Endomembrane Damage. *Mol. Cell* **70**, 120-135.e8 (2018).
293. Jia, J. *et al.* Galectin-3 Coordinates a Cellular System for Lysosomal Repair and Removal. *Dev. Cell* **52**, 69-87.e8 (2020).
294. Melia, T. J., Lystad, A. H. & Simonsen, A. Autophagosome biogenesis: From membrane growth to closure. *J. Cell Biol.* **219**, e202002085 (2020).
295. Kim, J., Kundu, M., Viollet, B. & Guan, K.-L. AMPK and mTOR regulate autophagy through direct phosphorylation of Ulk1. *Nat. Cell Biol.* **13**, 132–141 (2011).
296. Karanasios, E. *et al.* Dynamic association of the ULK1 complex with omegasomes during autophagy induction. *J. Cell Sci.* **126**, 5224–5238 (2013).
297. Axe, E. L. *et al.* Autophagosome formation from membrane compartments enriched in phosphatidylinositol 3-phosphate and dynamically connected to the endoplasmic reticulum. *J. Cell Biol.* **182**, 685–701 (2008).
298. Yamamoto, H. *et al.* Atg9 vesicles are an important membrane source during early steps of autophagosome formation. *J. Cell Biol.* **198**, 219–233 (2012).
299. Orsi, A. *et al.* Dynamic and transient interactions of Atg9 with autophagosomes, but not membrane integration, are required for autophagy. *Mol. Biol. Cell* **23**, 1860–1873 (2012).
300. Nguyen, A. *et al.* Metamorphic proteins at the basis of human autophagy initiation and lipid transfer. *Mol. Cell* S1097276523003210 (2023) doi:10.1016/j.molcel.2023.04.026.
301. Ichimura, Y. *et al.* A ubiquitin-like system mediates protein lipidation. *Nature* **408**, 488–492 (2000).
302. Fujita, N. *et al.* An Atg4B Mutant Hampers the Lipidation of LC3 Paralogues and Causes Defects in Autophagosome Closure. *Mol. Biol. Cell* **19**, 4651–4659 (2008).
303. Weidberg, H. *et al.* LC3 and GATE-16 N Termini Mediate Membrane Fusion Processes Required for Autophagosome Biogenesis. *Dev. Cell* **20**, 444–454 (2011).
304. Takahashi, Y. *et al.* An autophagy assay reveals the ESCRT-III component CHMP2A as a regulator of phagophore closure. *Nat. Commun.* **9**, 2855 (2018).
305. Vietri, M., Radulovic, M. & Stenmark, H. The many functions of ESCRTs. *Nat. Rev. Mol. Cell Biol.* **21**, 25–42 (2020).
306. Ravenhill, B. J. *et al.* The Cargo Receptor NDP52 Initiates Selective Autophagy by Recruiting the ULK Complex to Cytosol-Invading Bacteria. *Mol. Cell* **74**, 320-329.e6 (2019).
307. Vargas, J. N. S. *et al.* Spatiotemporal Control of ULK1 Activation by NDP52 and TBK1 during Selective Autophagy. *Mol. Cell* **74**, 347-362.e6 (2019).
308. Nguyen, T. N. *et al.* Unconventional initiation of PINK1/Parkin mitophagy by Optineurin. *Mol. Cell* **83**, 1693-1709.e9 (2023).
309. Itakura, E., Kishi-Itakura, C. & Mizushima, N. The Hairpin-type Tail-Anchored SNARE Syntaxin 17 Targets to Autophagosomes for Fusion with

Endosomes/Lysosomes. *Cell* **151**, 1256–1269 (2012).
310. Balderhaar, H. J. K. & Ungermann, C. CORVET and HOPS tethering complexes **–** coordinators of endosome and lysosome fusion. *J. Cell Sci.* **126**, 1307–1316 (2013).
311. Jiang, P. *et al.* The HOPS complex mediates autophagosome–lysosome fusion through interaction with syntaxin 17. *Mol. Biol. Cell* **25**, 1327–1337 (2014).
312. McEwan, D. G. *et al.* PLEKHM1 regulates autophagosome-lysosome fusion through HOPS complex and LC3/GABARAP proteins. *Mol. Cell* **57**, 39–54 (2015).
313. Pankiv, S. *et al.* FYCO1 is a Rab7 effector that binds to LC3 and PI3P to mediate microtubule plus end–directed vesicle transport. *J. Cell Biol.* **188**, 253–269 (2010).
314. Cantalupo, G. Rab-interacting lysosomal protein (RILP): the Rab7 effector required for transport to lysosomes. *EMBO J.* **20**, 683–693 (2001).
315. Brunger, A. T. *et al.* The pre-synaptic fusion machinery. *Curr. Opin. Struct. Biol.* **54**, 179–188 (2019).
316. Antonin, W., Fasshauer, D., Becker, S., Jahn, R. & Schneider, T. R. Crystal structure of the endosomal SNARE complex reveals common structural principles of all SNAREs. *Nat. Struct. Biol.* **9**, 107–111 (2002).
317. Shvarev, D. *et al.* Structure of the HOPS tethering complex, a lysosomal membrane fusion machinery. *eLife* **11**, e80901 (2022).
318. Reggiori, F. *et al.* Glycans in autophagy, endocytosis and lysosomal functions. *Glycoconj. J.* **38**, 625–647 (2021).
319. Zhao, L., Zhao, J., Zhong, K., Tong, A. & Jia, D. Targeted protein degradation: mechanisms, strategies and application. *Signal Transduct. Target. Ther.* **7**, 113 (2022).
320. Sakamoto, K. M. *et al.* Protacs: Chimeric molecules that target proteins to the Skp1–Cullin–F box complex for ubiquitination and degradation. *Proc. Natl. Acad. Sci.* **98**, 8554–8559 (2001).
321. Cuervo, A. M. & Wong, E. Chaperone-mediated autophagy: roles in disease and aging. *Cell Res.* **24**, 92–104 (2014).
322. Fan, X., Jin, W. Y., Lu, J., Wang, J. & Wang, Y. T. Rapid and reversible knockdown of endogenous proteins by peptide-directed lysosomal degradation. *Nat. Neurosci.* **17**, 471–480 (2014).
323. Takahashi, D. *et al.* AUTACs: Cargo-Specific Degraders Using Selective Autophagy. *Mol. Cell* **76**, 797-810.e10 (2019).
324. Li, Z., Zhu, C., Ding, Y., Fei, Y. & Lu, B. ATTEC: a potential new approach to target proteinopathies. *Autophagy* **16**, 185–187 (2020).
325. Ji, C. H. *et al.* The AUTOTAC chemical biology platform for targeted protein degradation via the autophagy-lysosome system. *Nat. Commun.* **13**, 904 (2022).
326. Cotton, A. D., Nguyen, D. P., Gramespacher, J. A., Seiple, I. B. & Wells, J. A. Development of Antibody-Based PROTACs for the Degradation of the Cell-Surface Immune Checkpoint Protein PD-L1. *J. Am. Chem. Soc.* **143**, 593–598 (2021).
327. Banik, S. M. *et al.* Lysosome-targeting chimaeras for degradation of extracellular proteins. *Nature* **584**, 291–297 (2020).
328. Cabukusta, B. & Neefjes, J. Mechanisms of lysosomal positioning and movement. *Traffic* **19**, 761–769 (2018).
329. Raiborg, C. How Nutrients Orchestrate Lysosome Positioning. *Contact* **1**, 251525641875611 (2018).
330. Jordens, I. *et al.* The Rab7 effector protein RILP controls lysosomal transport by inducing the recruitment of dynein-dynactin motors. *Curr. Biol.* **11**, 1680–1685

(2001).
331. Johansson, M. *et al.* Activation of endosomal dynein motors by stepwise assembly of Rab7–RILP–p150Glued, ORP1L, and the receptor βIII spectrin. *J. Cell Biol.* **176**, 459–471 (2007).
332. Rocha, N. *et al.* Cholesterol sensor ORP1L contacts the ER protein VAP to control Rab7-RILP-p150 Glued and late endosome positioning. *J. Cell Biol.* **185**, 1209–1225 (2009).
333. Kesisova, I. A., Robinson, B. P. & Spiliotis, E. T. A septin GTPase scaffold of dynein–dynactin motors triggers retrograde lysosome transport. *J. Cell Biol.* **220**, e202005219 (2021).
334. Dong, X. *et al.* PI(3,5)P2 controls membrane trafficking by direct activation of mucolipin Ca2+ release channels in the endolysosome. *Nat. Commun.* **1**, 38 (2010).
335. Li, X. *et al.* A Molecular Mechanism to Regulate Lysosome Motility for Lysosome Positioning and Tubulation. *Nat. Cell Biol.* **18**, 404–417 (2016).
336. Wang, W. *et al.* Up-regulation of lysosomal TRPML1 channels is essential for lysosomal adaptation to nutrient starvation. *Proc. Natl. Acad. Sci.* **112**, (2015).
337. Willett, R. *et al.* TFEB regulates lysosomal positioning by modulating TMEM55B expression and JIP4 recruitment to lysosomes. *Nat. Commun.* **8**, 1580 (2017).
338. Sasazawa, Y. *et al.* Oxidative stress-induced phosphorylation of JIP4 regulates lysosomal positioning in coordination with TRPML1 and ALG2. *EMBO J.* **41**, e111476 (2022).
339. Raiborg, C. *et al.* Repeated ER-endosome contacts promote endosome translocation and neurite outgrowth. *Nature* **520**, 234–238 (2015).
340. Guardia, C. M., Farías, G. G., Jia, R., Pu, J. & Bonifacino, J. S. BORC Functions Upstream of Kinesins 1 and 3 to Coordinate Regional Movement of Lysosomes along Different Microtubule Tracks. *Cell Rep.* **17**, 1950–1961 (2016).
341. Rosa-Ferreira, C. & Munro, S. Arl8 and SKIP Act Together to Link Lysosomes to Kinesin-1. *Dev. Cell* **21**, 1171–1178 (2011).
342. Pu, J. *et al.* BORC, a multisubunit complex that regulates lysosome positioning. *Dev. Cell* **33**, 176–188 (2015).
343. Starling, G. P. *et al.* Folliculin directs the formation of a Rab34– RILP complex to control the nutrient-dependent dynamic distribution of lysosomes. *EMBO Rep.* **17**, 823–841 (2016).
344. Filipek, P. A. *et al.* LAMTOR/Ragulator is a negative regulator of Arl8b- and BORC-dependent late endosomal positioning. *J. Cell Biol.* **216**, 4199–4215 (2017).
345. Pu, J., Keren-Kaplan, T. & Bonifacino, J. S. A Ragulator–BORC interaction controls lysosome positioning in response to amino acid availability. *J. Cell Biol.* **216**, 4183–4197 (2017).
346. Korolchuk, V. I. *et al.* Lysosomal positioning coordinates cellular nutrient responses. *Nat. Cell Biol.* **13**, 453–460 (2011).
347. Heuser, J. Changes in lysosome shape and distribution correlated with changes in cytoplasmic pH. *J. Cell Biol.* **108**, 855–864 (1989).
348. Hong, Z. *et al.* PtdIns3P controls mTORC1 signaling through lysosomal positioning. *J. Cell Biol.* **216**, 4217–4233 (2017).
349. Pu, J., Guardia, C. M., Keren-Kaplan, T. & Bonifacino, J. S. Mechanisms and functions of lysosome positioning. *J. Cell Sci.* **129**, 4329–4339 (2016).
350. Kimura, S., Noda, T. & Yoshimori, T. Dynein-dependent Movement of Autophagosomes Mediates Efficient Encounters with Lysosomes. *Cell Struct. Funct.* **33**, 109–122 (2008).

351. Tancini, B. *et al.* Lysosomal Exocytosis: The Extracellular Role of an Intracellular Organelle. *Membranes* **10**, 406 (2020).
352. Reddy, A., Caler, E. V. & Andrews, N. W. Plasma membrane repair is mediated by Ca(2+)-regulated exocytosis of lysosomes. *Cell* **106**, 157–169 (2001).
353. Castro-Gomes, T., Corrotte, M., Tam, C. & Andrews, N. W. Plasma Membrane Repair Is Regulated Extracellularly by Proteases Released from Lysosomes. *PLOS ONE* **11**, e0152583 (2016).
354. Chen, C.-C. *et al.* A small molecule restores function to TRPML1 mutant isoforms responsible for mucolipidosis type IV. *Nat. Commun.* **5**, 4681 (2014).
355. Medina, D. L. *et al.* Transcriptional Activation of Lysosomal Exocytosis Promotes Cellular Clearance. *Dev. Cell* **21**, 421–430 (2011).
356. Shen, D. *et al.* Lipid storage disorders block lysosomal trafficking by inhibiting a TRP channel and lysosomal calcium release. *Nat. Commun.* **3**, 731 (2012).
357. Zhong, X. Z. *et al.* BK channel agonist represents a potential therapeutic approach for lysosomal storage diseases. *Sci. Rep.* **6**, 33684 (2016).
358. Ghosh, S. *et al.* β-Coronaviruses Use Lysosomes for Egress Instead of the Biosynthetic Secretory Pathway. *Cell* **183**, 1520-1535.e14 (2020).
359. Chen, D. *et al.* ORF3a of SARS-CoV-2 promotes lysosomal exocytosis-mediated viral egress. *Dev. Cell* **56**, 3250-3263.e5 (2021).
360. Kim, D.-H. *et al.* GbetaL, a positive regulator of the rapamycin-sensitive pathway required for the nutrient-sensitive interaction between raptor and mTOR. *Mol. Cell* **11**, 895–904 (2003).
361. Kim, D.-H. *et al.* mTOR interacts with raptor to form a nutrient-sensitive complex that signals to the cell growth machinery. *Cell* **110**, 163–175 (2002).
362. Hara, K. *et al.* Raptor, a binding partner of target of rapamycin (TOR), mediates TOR action. *Cell* **110**, 177–189 (2002).
363. Nojima, H. *et al.* The mammalian target of rapamycin (mTOR) partner, raptor, binds the mTOR substrates p70 S6 kinase and 4E-BP1 through their TOR signaling (TOS) motif. *J. Biol. Chem.* **278**, 15461–15464 (2003).
364. Schalm, S. S., Fingar, D. C., Sabatini, D. M. & Blenis, J. TOS motif-mediated raptor binding regulates 4E-BP1 multisite phosphorylation and function. *Curr. Biol. CB* **13**, 797–806 (2003).
365. Peterson, T. R. *et al.* DEPTOR is an mTOR inhibitor frequently overexpressed in multiple myeloma cells and required for their survival. *Cell* **137**, 873–886 (2009).
366. Haar, E. V., Lee, S., Bandhakavi, S., Griffin, T. J. & Kim, D.-H. Insulin signalling to mTOR mediated by the Akt/PKB substrate PRAS40. *Nat. Cell Biol.* **9**, 316–323 (2007).
367. Sancak, Y. *et al.* PRAS40 is an insulin-regulated inhibitor of the mTORC1 protein kinase. *Mol. Cell* **25**, 903–915 (2007).
368. Wang, L., Harris, T. E., Roth, R. A. & Lawrence, J. C. PRAS40 regulates mTORC1 kinase activity by functioning as a direct inhibitor of substrate binding. *J. Biol. Chem.* **282**, 20036–20044 (2007).
369. Albers, M. W. *et al.* A mammalian protein targeted by Gl-arresting rapamycin-receptor complex. (1994).
370. Sabatini, D. M., Erdjument-Bromage, H., Lui, M., Tempst, P. & Snyder, S. H. RAFT1: a mammalian protein that binds to FKBP12 in a rapamycin-dependent fashion and is homologous to yeast TORs. *Cell* **78**, 35–43 (1994).
371. Choi, J., Chen, J., Schreiber, S. L. & Clardy, J. Structure of the FKBP12-Rapamycin Complex Interacting with Binding Domain of Human FRAP. *Science* **273**, 239–242 (1996).

372. Chung, J., Kuo, C. J., Crabtree, G. R. & Blenis, J. Rapamycin-FKBP specifically blocks growth-dependent activation of and signaling by the 70 kd S6 protein kinases. *Cell* **69**, 1227–1236 (1992).
373. Laplante, M. & Sabatini, D. M. mTOR signaling at a glance. *J. Cell Sci.* **122**, 3589–3594 (2009).
374. Winter, J. N., Jefferson, L. S. & Kimball, S. R. ERK and Akt signaling pathways function through parallel mechanisms to promote mTORC1 signaling. *Am. J. Physiol.-Cell Physiol.* **300**, C1172–C1180 (2011).
375. Garami, A. *et al.* Insulin Activation of Rheb, a Mediator of mTOR/S6K/4E-BP Signaling, Is Inhibited by TSC1 and 2. *Mol. Cell* **11**, 1457–1466 (2003).
376. Inoki, K., Li, Y., Xu, T. & Guan, K.-L. Rheb GTPase is a direct target of TSC2 GAP activity and regulates mTOR signaling. *Genes Dev.* **17**, 1829–1834 (2003).
377. Yang, H. *et al.* Mechanisms of mTORC1 activation by RHEB and inhibition by PRAS40. *Nature* **552**, 368–373 (2017).
378. Prentzell, M. T. *et al.* G3BPs tether the TSC complex to lysosomes and suppress mTORC1 signaling. *Cell* **184**, 655-674.e27 (2021).
379. Tee, A. R., Manning, B. D., Roux, P. P., Cantley, L. C. & Blenis, J. Tuberous sclerosis complex gene products, Tuberin and Hamartin, control mTOR signaling by acting as a GTPase-activating protein complex toward Rheb. *Curr. Biol. CB* **13**, 1259–1268 (2003).
380. Mihaylova, M. M. & Shaw, R. J. The AMPK signalling pathway coordinates cell growth, autophagy and metabolism. *Nat. Cell Biol.* **13**, 1016–1023 (2011).
381. Inoki, K. *et al.* TSC2 Integrates Wnt and Energy Signals via a Coordinated Phosphorylation by AMPK and GSK3 to Regulate Cell Growth. *Cell* **126**, 955–968 (2006).
382. Brugarolas, J. *et al.* Regulation of mTOR function in response to hypoxia by REDD1 and the TSC1/TSC2 tumor suppressor complex. *Genes Dev.* **18**, 2893–2904 (2004).
383. Gwinn, D. M. *et al.* AMPK Phosphorylation of Raptor Mediates a Metabolic Checkpoint. *Mol. Cell* **30**, 214–226 (2008).
384. Jia, J. *et al.* Galectin-3 Coordinates a Cellular System for Lysosomal Repair and Removal. *Dev. Cell* **52**, 69-87.e8 (2020).
385. Feng, Z. *et al.* The regulation of AMPK β1, TSC2, and PTEN expression by p53: Stress, cell and tissue specificity, and the role of these gene products in modulating the IGF-1-AKT-mTOR pathways. *Cancer Res.* **67**, 3043–3053 (2007).
386. Bar-Peled, L. *et al.* A Tumor suppressor complex with GAP activity for the Rag GTPases that signal amino acid sufficiency to mTORC1. *Science* **340**, 1100–1106 (2013).
387. Peng, M., Yin, N. & Li, M. O. SZT2 dictates GATOR control of mTORC1 signalling. *Nature* **543**, 433–437 (2017).
388. Sancak, Y. *et al.* Ragulator-Rag Complex Targets mTORC1 to the Lysosomal Surface and Is Necessary for Its Activation by Amino Acids. *Cell* **141**, 290–303 (2010).
389. Bar-Peled, L., Schweitzer, L. D., Zoncu, R. & Sabatini, D. M. Ragulator Is a GEF for the Rag GTPases that Signal Amino Acid Levels to mTORC1. *Cell* **150**, 1196–1208 (2012).
390. Petit, C. S., Roczniak-Ferguson, A. & Ferguson, S. M. Recruitment of folliculin to lysosomes supports the amino acid–dependent activation of Rag GTPases. *J. Cell Biol.* **202**, 1107–1122 (2013).
391. Tsun, Z.-Y. *et al.* The Folliculin Tumor Suppressor Is a GAP for the RagC/D

GTPases That Signal Amino Acid Levels to mTORC1. *Mol. Cell* **52**, 495–505 (2013).
392. Lawrence, R. E. *et al.* Structural mechanism of a Rag GTPase activation checkpoint by the lysosomal folliculin complex. *Science* **366**, 971–977 (2019).
393. Shen, K. *et al.* Cryo-EM Structure of the Human FLCN-FNIP2-Rag-Ragulator Complex. *Cell* **179**, 1319-1329.e8 (2019).
394. Gollwitzer, P., Grützmacher, N., Wilhelm, S., Kümmel, D. & Demetriades, C. A Rag GTPase dimer code defines the regulation of mTORC1 by amino acids. *Nat. Cell Biol.* **24**, 1394–1406 (2022).
395. Gu, X. *et al.* SAMTOR is an S-adenosylmethionine sensor for the mTORC1 pathway. *Science* **358**, 813–818 (2017).
396. Chantranupong, L. *et al.* The CASTOR Proteins Are Arginine Sensors for the mTORC1 Pathway. *Cell* **165**, 153–164 (2016).
397. Saxton, R. A., Chantranupong, L., Knockenhauer, K. E., Schwartz, T. U. & Sabatini, D. M. Mechanism of arginine sensing by CASTOR1 upstream of mTORC1. *Nature* **536**, 229–233 (2016).
398. Chantranupong, L. *et al.* The Sestrins Interact with GATOR2 to Negatively Regulate the Amino-Acid-Sensing Pathway Upstream of mTORC1. *Cell Rep.* **9**, 1–8 (2014).
399. Parmigiani, A. *et al.* Sestrins Inhibit mTORC1 Kinase Activation through the GATOR Complex. *Cell Rep.* **9**, 1281–1291 (2014).
400. Wolfson, R. L. *et al.* Sestrin2 is a leucine sensor for the mTORC1 pathway. *Science* **351**, 43–48 (2016).
401. Chen, J. *et al.* SAR1B senses leucine levels to regulate mTORC1 signalling. *Nature* **596**, 281–284 (2021).
402. Zoncu, R. *et al.* mTORC1 senses lysosomal amino acids through an inside-out mechanism that requires the Vacuolar H+-ATPase. *Science* **334**, 678–683 (2011).
403. Khamzina, L., Veilleux, A., Bergeron, S. & Marette, A. Increased Activation of the Mammalian Target of Rapamycin Pathway in Liver and Skeletal Muscle of Obese Rats: Possible Involvement in Obesity-Linked Insulin Resistance. *Endocrinology* **146**, 1473–1481 (2005).
404. Lim, C.-Y. *et al.* ER–lysosome contacts enable cholesterol sensing by mTORC1 and drive aberrant growth signalling in Niemann–Pick type C. *Nat. Cell Biol.* **21**, 1206–1218 (2019).
405. Holz, M. K., Ballif, B. A., Gygi, S. P. & Blenis, J. mTOR and S6K1 mediate assembly of the translation preinitiation complex through dynamic protein interchange and ordered phosphorylation events. *Cell* **123**, 569–580 (2005).
406. Brunn, G. J. *et al.* Phosphorylation of the translational repressor PHAS-I by the mammalian target of rapamycin. *Science* **277**, 99–101 (1997).
407. Gingras, A.-C. *et al.* Regulation of 4E-BP1 phosphorylation: a novel two-step mechanism. *Genes Dev.* **13**, 1422–1437 (1999).
408. Ben-Sahra, I., Howell, J. J., Asara, J. M. & Manning, B. D. Stimulation of de novo pyrimidine synthesis by growth signaling through mTOR and S6K1. *Science* **339**, 1323–1328 (2013).
409. Düvel, K. *et al.* Activation of a Metabolic Gene Regulatory Network Downstream of mTOR Complex 1. *Mol. Cell* **39**, 171–183 (2010).
410. Robitaille, A. M. *et al.* Quantitative Phosphoproteomics Reveal mTORC1 Activates de Novo Pyrimidine Synthesis. *Science* **339**, 1320–1323 (2013).
411. Ben-Sahra, I., Hoxhaj, G., Ricoult, S. J. H., Asara, J. M. & Manning, B. D. mTORC1 induces purine synthesis through control of the mitochondrial tetrahydrofolate cycle. *Science* **351**, 728–733 (2016).

412. Peterson, T. R. *et al.* mTOR complex 1 regulates lipin 1 localization to control the SREBP pathway. *Cell* **146**, 408–420 (2011).
413. Eberlé, D., Hegarty, B., Bossard, P., Ferré, P. & Foufelle, F. SREBP transcription factors: master regulators of lipid homeostasis. *Biochimie* **86**, 839–848 (2004).
414. Dodd, K. M., Yang, J., Shen, M. H., Sampson, J. R. & Tee, A. R. mTORC1 drives HIF-1α and VEGF-A signalling via multiple mechanisms involving 4E-BP1, S6K1 and STAT3. *Oncogene* **34**, 2239–2250 (2015).
415. Yuan, H.-X., Russell, R. C. & Guan, K.-L. Regulation of PIK3C3/VPS34 complexes by MTOR in nutrient stress-induced autophagy. *Autophagy* **9**, 1983–1995 (2013).
416. Kim, Y.-M. *et al.* mTORC1 Phosphorylates UVRAG to Negatively Regulate Autophagosome and Endosome Maturation. *Mol. Cell* **57**, 207–218 (2015).
417. Rousseau, A. & Bertolotti, A. An evolutionarily conserved pathway controls proteasome homeostasis. *Nature* **536**, 184–189 (2016).
418. Zhao, J., Zhai, B., Gygi, S. P. & Goldberg, A. L. mTOR inhibition activates overall protein degradation by the ubiquitin proteasome system as well as by autophagy. *Proc. Natl. Acad. Sci. U. S. A.* **112**, 15790–15797 (2015).
419. Napolitano, G. *et al.* A substrate-specific mTORC1 pathway underlies Birt–Hogg–Dubé syndrome. *Nature* **585**, 597–602 (2020).
420. Aits, S. & Jäättelä, M. Lysosomal cell death at a glance. *J. Cell Sci.* **126**, 1905–1912 (2013).
421. Boya, P. & Kroemer, G. Lysosomal membrane permeabilization in cell death. *Oncogene* **27**, 6434–6451 (2008).
422. Brunk, U. T. & Ericsson, J. L. Cytochemical evidence for the leakage of acid phosphatase through ultrastructurally intact lysosomal membranes. *Histochem. J.* **4**, 479–491 (1972).
423. Kågedal, K., Zhao, M., Svensson, I. & Brunk, U. T. Sphingosine-induced apoptosis is dependent on lysosomal proteases. *Biochem. J.* **359**, 335–343 (2001).
424. Bivik, C. A., Larsson, P. K., Kågedal, K. M., Rosdahl, I. K. & Öllinger, K. M. UVA/B-Induced Apoptosis in Human Melanocytes Involves Translocation of Cathepsins and Bcl-2 Family Members. *J. Invest. Dermatol.* **126**, 1119–1127 (2006).
425. Roberg, K., Kågedal, K. & Öllinger, K. Microinjection of Cathepsin D Induces Caspase-Dependent Apoptosis in Fibroblasts. *Am. J. Pathol.* **161**, 89–96 (2002).
426. Gyrd-Hansen, M. *et al.* Apoptosome-Independent Activation of the Lysosomal Cell Death Pathway by Caspase-9. *Mol. Cell. Biol.* **26**, 7880–7891 (2006).
427. Werneburg, N., Guicciardi, M. E., Yin, X.-M. & Gores, G. J. TNF-α-mediated lysosomal permeabilization is FAN and caspase 8/Bid dependent. *Am. J. Physiol.-Gastrointest. Liver Physiol.* **287**, G436–G443 (2004).
428. Ségui, B. *et al.* Involvement of FAN in TNF-induced apoptosis. *J. Clin. Invest.* **108**, 143–151 (2001).
429. Werneburg, N. W., Guicciardi, M. E., Bronk, S. F. & Gores, G. J. Tumor necrosis factor-␣-associated lysosomal permeabilization is cathepsin B dependent. **283**, (2002).
430. Taha, T. A. *et al.* Tumor necrosis factor induces the loss of sphingosine kinase-1 by a cathepsin B-dependent mechanism. *J. Biol. Chem.* **280**, 17196–17202 (2005).
431. Rizzollo, F., More, S., Vangheluwe, P. & Agostinis, P. The lysosome as a master regulator of iron metabolism. *Trends Biochem. Sci.* **46**, 960–975 (2021).
432. Terman, A., Kurz, T., Gustafsson, B. & Brunk, U. Lysosomal labilization.

IUBMB Life Int. Union Biochem. Mol. Biol. Life **58**, 531–539 (2006).
433. Mai, T. T. *et al.* Salinomycin kills cancer stem cells by sequestering iron in lysosomes. *Nat. Chem.* **9**, 1025–1033 (2017).
434. Groth-Pedersen, L., Ostenfeld, M. S., Høyer-Hansen, M., Nylandsted, J. & Jäättelä, M. Vincristine Induces Dramatic Lysosomal Changes and Sensitizes Cancer Cells to Lysosome-Destabilizing Siramesine. *Cancer Res.* **67**, 2217–2225 (2007).
435. Ostenfeld, M. S. *et al.* Effective Tumor Cell Death by σ-2 Receptor Ligand Siramesine Involves Lysosomal Leakage and Oxidative Stress. *Cancer Res.* **65**, 8975–8983 (2005).
436. Ostenfeld, M. S. *et al.* Anti-cancer agent siramesine is a lysosomotropic detergent that induces cytoprotective autophagosome accumulation. *Autophagy* **4**, 487–499 (2008).
437. Appelqvist, H. *et al.* Attenuation of the Lysosomal Death Pathway by Lysosomal Cholesterol Accumulation. *Am. J. Pathol.* **178**, 629–639 (2011).
438. Appelqvist, H. *et al.* Sensitivity to Lysosome-Dependent Cell Death Is Directly Regulated by Lysosomal Cholesterol Content. *PLoS ONE* **7**, e50262 (2012).
439. Reiners, J. J., Kleinman, M., Kessel, D., Mathieu, P. A. & Caruso, J. A. Nonesterified cholesterol content of lysosomes modulates susceptibility to oxidant-induced permeabilization. *Free Radic. Biol. Med.* **50**, 281–294 (2011).
440. Aits, S. *et al.* Sensitive detection of lysosomal membrane permeabilization by lysosomal galectin puncta assay. *Autophagy* **11**, 1408–1424 (2015).
441. Radulovic, M. *et al.* ESCRT-mediated lysosome repair precedes lysophagy and promotes cell survival. *EMBO J.* **37**, (2018).
442. Skowyra, M. L., Schlesinger, P. H., Naismith, T. V. & Hanson, P. I. Triggered recruitment of ESCRT machinery promotes endolysosomal repair. *Science* **360**, (2018).
443. Shukla, S., Larsen, K. P., Ou, C., Rose, K. & Hurley, J. H. In vitro reconstitution of calcium-dependent recruitment of the human ESCRT machinery in lysosomal membrane repair. *Proc. Natl. Acad. Sci.* **119**, e2205590119 (2022).
444. Tan, J. X. & Finkel, T. A phosphoinositide signalling pathway mediates rapid lysosomal repair. *Nature* **609**, 815–821 (2022).
445. Radulovic, M. *et al.* Cholesterol transfer via endoplasmic reticulum contacts mediates lysosome damage repair. *EMBO J.* **41**, e112677 (2022).
446. Chin, S. J. & Fuller, M. Prevalence of lysosomal storage disorders in Australia from 2009 to 2020. *Lancet Reg. Health - West. Pac.* **19**, 100344 (2022).
447. Platt, F. M., d'Azzo, A., Davidson, B. L., Neufeld, E. F. & Tifft, C. J. Lysosomal storage diseases. *Nat. Rev. Dis. Primer* **4**, 27 (2018).
448. Waldek, S., Patel, M. R., Banikazemi, M., Lemay, R. & Lee, P. Life expectancy and cause of death in males and females with Fabry disease: Findings from the Fabry Registry. *Genet. Med.* **11**, 790–796 (2009).
449. Hahn, A. & Schänzer, A. Long-term outcome and unmet needs in infantile-onset Pompe disease. *Ann. Transl. Med.* **7**, 283–283 (2019).
450. Mokhtariye, A., Hagh-Nazari, L., Varasteh, A.-R. & Keyfi, F. Diagnostic methods for Lysosomal Storage Disease.
451. Platt, F. M., d'Azzo, A., Davidson, B. L., Neufeld, E. F. & Tifft, C. J. Lysosomal storage diseases. *Nat. Rev. Dis. Primer* **4**, 27 (2018).
452. Beck, M. Treatment strategies for lysosomal storage disorders. *Dev. Med. Child Neurol.* **60**, 13–18 (2018).
453. Curelaru, S. Favorable outcomes following early onset oral miglustat in early infantile Niemann Pick Type C. *Mol. Genet. Metab. Rep.* (2021).

454. Patterson, C *et al.* Stable or improved neurological manifestations during miglustat therapy in patients from the international disease registry for Niemann-Pick disease type C: an observational cohort study. *Orphanet J. Rare Dis.* **10**, 65 (2015).
455. Kirkegaard, T. *et al.* Hsp70 stabilizes lysosomes and reverts Niemann-Pick disease-associated lysosomal pathology. *Nature* **463**, 549–553 (2010).
456. Nylandsted, J. *et al.* Heat Shock Protein 70 Promotes Cell Survival by Inhibiting Lysosomal Membrane Permeabilization. *J. Exp. Med.* **200**, 425–435 (2004).
457. Kirkegaard, T. *et al.* Heat shock protein–based therapy as a potential candidate for treating the sphingolipidoses. *Sci. Transl. Med.* **8**, (2016).
458. Kilsdonk, E. P. C. *et al.* Cellular Cholesterol Efflux Mediated by Cyclodextrins. *J. Biol. Chem.* **270**, 17250–17256 (1995).
459. Dai, S. *et al.* Methyl-β-cyclodextrin restores impaired autophagy flux in Niemann-Pick C1-deficient cells through activation of AMPK. *Autophagy* **13**, 1435–1451 (2017).
460. Vance, J. E. & Karten, B. Niemann-Pick C disease and mobilization of lysosomal cholesterol by cyclodextrin. *J. Lipid Res.* **55**, 1609–1621 (2014).
461. Singhal, A., Krystofiak, E. S., Jerome, W. G. & Song, B. 2-Hydroxypropyl-gamma-cyclodextrin overcomes NPC1 deficiency by enhancing lysosome-ER association and autophagy. *Sci. Rep.* **10**, 8663 (2020).
462. Brown, A. PEG-lipid micelles enable cholesterol efflux in Niemann-Pick Type C1 disease-based lysosomal storage disorder. *Sci. Rep.*
463. Vanier, M. T. Niemann-Pick disease type C. *Orphanet J. Rare Dis.* **5**, 16 (2010).
464. Gabandé-Rodríguez, E., Boya, P., Labrador, V., Dotti, C. G. & Ledesma, M. D. High sphingomyelin levels induce lysosomal damage and autophagy dysfunction in Niemann Pick disease type A. *Cell Death Differ.* **21**, 864–875 (2014).
465. Schuchman, E. H. & Desnick, R. J. Types A and B Niemann-Pick disease. *Mol. Genet. Metab.* **120**, 27–33 (2017).
466. Qian, H. *et al.* Structural Basis of Low-pH-Dependent Lysosomal Cholesterol Egress by NPC1 and NPC2. *Cell* **182**, 98-111.e18 (2020).
467. Labrecque, M., Touma, L., Bhérer, C., Duquette, A. & Tétreault, M. Estimated prevalence of Niemann–Pick type C disease in Quebec. *Sci. Rep.* **11**, 22621 (2021).
468. Li, X., Saha, P., Li, J., Blobel, G. & Pfeffer, S. R. Clues to the mechanism of cholesterol transfer from the structure of NPC1 middle lumenal domain bound to NPC2. *Proc. Natl. Acad. Sci.* **113**, 10079–10084 (2016).
469. Kwon, H. J. *et al.* Structure of N-Terminal Domain of NPC1 Reveals Distinct Subdomains for Binding and Transfer of Cholesterol. *Cell* **137**, 1213–1224 (2009).
470. Shammas, H., Kuech, E.-M., Rizk, S., Das, A. M. & Naim, H. Y. Different Niemann-Pick C1 Genotypes Generate Protein Phenotypes that Vary in their Intracellular Processing, Trafficking and Localization. *Sci. Rep.* **9**, 5292 (2019).
471. Zhang, M. *et al.* Astrocyte-only Npc1 reduces neuronal cholesterol and triples life span of *Npc1* $^{-/-}$ mice. *J. Neurosci. Res.* **86**, 2848–2856 (2008).
472. Takikita, S., Fukuda, T., Mohri, I., Yagi, T. & Suzuki, K. Perturbed Myelination Process of Premyelinating Oligodendrocyte in Niemann-PickType C Mouse. *J. Neuropathol. Exp. Neurol.* **63**, 660–673 (2004).
473. Yu, T. & Lieberman, A. P. Npc1 Acting in Neurons and Glia Is Essential for the Formation and Maintenance of CNS Myelin. *PLoS Genet.* **9**, e1003462 (2013).
474. Lopez, M. E., Klein, A. D., Dimbil, U. J. & Scott, M. P. Anatomically Defined Neuron-Based Rescue of Neurodegenerative Niemann–Pick Type C Disorder. *J. Neurosci.* **31**, 4367–4378 (2011).

475. Mitroi, D. N. *et al.* NPC 1 enables cholesterol mobilization during long-term potentiation that can be restored in Niemann–Pick disease type C by CYP 46A1 activation. *EMBO Rep.* **20**, e48143 (2019).
476. Aman, Y. *et al.* Autophagy in healthy aging and disease. *Nat. Aging* **1**, 634–650 (2021).
477. Liu, G. Y. & Sabatini, D. M. mTOR at the nexus of nutrition, growth, ageing and disease. *Nat. Rev. Mol. Cell Biol.* **21**, 183–203 (2020).
478. Gonçalves, J. T., Schafer, S. T. & Gage, F. H. Adult Neurogenesis in the Hippocampus: From Stem Cells to Behavior. *Cell* **167**, 897–914 (2016).
479. Villegas, F. *et al.* Lysosomal Signaling Licenses Embryonic Stem Cell Differentiation via Inactivation of Tfe3. *Cell Stem Cell* **24**, 257-270.e8 (2019).
480. Leeman, D. S. *et al.* Lysosome activation clears aggregates and enhances quiescent neural stem cell activation during aging. *Science* **359**, 1277–1283 (2018).
481. Giachino, C. *et al.* Molecular Diversity Subdivides the Adult Forebrain Neural Stem Cell Population. *Stem Cells* **32**, 70–84 (2014).
482. Nixon, R. A. *et al.* Extensive Involvement of Autophagy in Alzheimer Disease: An Immuno-Electron Microscopy Study. *J Neuropathol Exp Neurol* **64**, (2005).
483. An, W.-L. *et al.* Up-Regulation of Phosphorylated/Activated p70 S6 Kinase and Its Relationship to Neurofibrillary Pathology in Alzheimer's Disease. *Am. J. Pathol.* **163**, 591–607 (2003).
484. Hara, T. *et al.* Suppression of basal autophagy in neural cells causes neurodegenerative disease in mice. *Nature* **441**, 885–889 (2006).
485. Harrison, D. E. *et al.* Rapamycin fed late in life extends lifespan in genetically heterogeneous mice. *Nature* **460**, 392–395 (2009).
486. Powers, R. W., Kaeberlein, M., Caldwell, S. D., Kennedy, B. K. & Fields, S. Extension of chronological life span in yeast by decreased TOR pathway signaling. *Genes Dev.* **20**, 174–184 (2006).
487. Jia, K., Chen, D. & Riddle, D. L. The TOR pathway interacts with the insulin signaling pathway to regulate *C. elegans* larval development, metabolism and life span. *Development* **131**, 3897–3906 (2004).
488. Selman, C. *et al.* Ribosomal Protein S6 Kinase 1 Signaling Regulates Mammalian Life Span. *Science* **326**, 140–144 (2009).
489. Lang, U. E. *et al.* Immunosuppression Using the Mammalian Target of Rapamycin (mTOR) Inhibitor Everolimus: Pilot Study Shows Significant Cognitive and Affective Improvement. *Transplant. Proc.* **41**, 4285–4288 (2009).
490. European Alzheimer's Disease Initiative (EADI) *et al.* Meta-analysis of 74,046 individuals identifies 11 new susceptibility loci for Alzheimer's disease. *Nat. Genet.* **45**, 1452–1458 (2013).
491. Corder, E. H. *et al.* Gene Dose of Apolipoprotein E Type 4 Allele and the Risk of Alzheimer's Disease in Late Onset Families. *Science* **261**, 921–923 (1993).
492. Blanchard, J. W. *et al.* APOE4 impairs myelination via cholesterol dysregulation in oligodendrocytes. *Nature* **611**, 769–779 (2022).
493. Lin, Y.-T. *et al.* APOE4 Causes Widespread Molecular and Cellular Alterations Associated with Alzheimer's Disease Phenotypes in Human iPSC-Derived Brain Cell Types. *Neuron* **98**, 1141-1154.e7 (2018).
494. Sienski, G. *et al. APOE4* disrupts intracellular lipid homeostasis in human iPSC-derived glia. *Sci. Transl. Med.* **13**, eaaz4564 (2021).
495. Jacobs, K. A., Maghe, C. & Gavard, J. Lysosomes in glioblastoma: pump up the volume. *Cell Cycle* **19**, 2094–2104 (2020).
496. Shingu, T. *et al.* Qki deficiency maintains stemness of glioma stem cells in

suboptimal environment by downregulating endolysosomal degradation. *Nat. Genet.* **49**, 75–86 (2017).
497. Jacobs, K. A. *et al.* Paracaspase MALT1 regulates glioma cell survival by controlling endo-lysosome homeostasis. *EMBO J.* **39**, e102030 (2020).
498. Davidson, S. M. & Vander Heiden, M. G. Critical Functions of the Lysosome in Cancer Biology. *Annu. Rev. Pharmacol. Toxicol.* **57**, 481–507 (2017).
499. Zhitomirsky, B. & Assaraf, Y. G. Lysosomes as mediators of drug resistance in cancer. *Drug Resist. Updat.* **24**, 23–33 (2016).
500. Goldman, S. D., Funk, R. S., Rajewski, R. A. & Krise, J. P. Mechanisms of amine accumulation in, and egress from, lysosomes. *Bioanalysis* **1**, 1445–1459 (2009).
501. Zhitomirsky, B. & Assaraf, Y. G. Lysosomal sequestration of hydrophobic weak base chemotherapeutics triggers lysosomal biogenesis and lysosome-dependent cancer multidrug resistance. *Oncotarget* **6**, 1143–1156 (2014).
502. Gotink, K. J. *et al.* Cross-resistance to clinically used tyrosine kinase inhibitors sunitinib, sorafenib and pazopanib. *Cell. Oncol.* **38**, 119–129 (2015).
503. Zhitomirsky, B. *et al.* Lysosomotropic drugs activate TFEB via lysosomal membrane fluidization and consequent inhibition of mTORC1 activity. *Cell Death Dis.* **9**, 1191 (2018).
504. Martínez Sempere, J. F. *et al.* Study of the expression of cathepsins in histological material from pancreatic lesions. *Rev. Esp. Enfermedades Dig.* **108**, (2016).
505. Chauhan, S. S., Goldstein, L. J. & Gottesman, M. M. Expression of Cathepsin L in Human Tumors. (1991).
506. Grimm, J. *et al.* Use of gene expression profiling to direct *in vivo* molecular imaging of lung cancer. *Proc. Natl. Acad. Sci.* **102**, 14404–14409 (2005).
507. Spyratos, F. *et al.* CATHEPSIN D: AN INDEPENDENT PROGNOSTIC FACTOR FOR METASTASIS OF BREAST CANCER. *The Lancet* **334**, 1115–1118 (1989).
508. Garcia, M. *et al.* Biological and Clinical Significance of Cathepsin D in Breast Cancer Metastasis. *STEM CELLS* **14**, 642–650 (1996).
509. Seo, S. U. *et al.* Cathepsin D as a potential therapeutic target to enhance anticancer drug-induced apoptosis via RNF183-mediated destabilization of Bcl-xL in cancer cells. *Cell Death Dis.* **13**, 115 (2022).
510. Tancini, B. *et al.* Lysosomal Exocytosis: The Extracellular Role of an Intracellular Organelle. *Membranes* **10**, 406 (2020).
511. Machado, E. *et al.* Regulated lysosomal exocytosis mediates cancer progression. *Sci. Adv.* **1**, e1500603 (2015).
512. Damaghi, M. *et al.* Chronic acidosis in the tumour microenvironment selects for overexpression of LAMP2 in the plasma membrane. *Nat. Commun.* **6**, 8752 (2015).
513. Kallunki, T., Olsen, O. D. & Jäättelä, M. Cancer-associated lysosomal changes: friends or foes? *Oncogene* **32**, 1995–2004 (2013).
514. Fehrenbacher, N. *et al.* Sensitization to the lysosomal cell death pathway by oncogene-induced down-regulation of lysosome-associated membrane proteins 1 and 2. *Cancer Res.* **68**, 6623–6633 (2008).
515. Fehrenbacher, N. *et al.* Sensitization to the lysosomal cell death pathway upon immortalization and transformation. *Cancer Res.* **64**, 5301–5310 (2004).
516. Dumitru, C. A. & Gulbins, E. TRAIL activates acid sphingomyelinase via a redox mechanism and releases ceramide to trigger apoptosis. *Oncogene* **25**, 5612–

5625 (2006).
517. Gupta, S. *et al.* Lysosomal retargeting of Myoferlin mitigates membrane stress to enable pancreatic cancer growth. *Nat. Cell Biol.* **23**, 232–242 (2021).
518. Chen, A.-J. *et al.* STAR RNA-binding protein Quaking suppresses cancer via stabilization of specific miRNA. *Genes Dev.* **26**, 1459–1472 (2012).
519. Jacobs, K. A. *et al.* Paracaspase MALT1 regulates glioma cell survival by controlling endo-lysosome homeostasis. *EMBO J.* **39**, (2020).
520. Jensen, S. S., Petterson, S. A., Halle, B., Aaberg-Jessen, C. & Kristensen, B. W. Effects of the lysosomal destabilizing drug siramesine on glioblastoma in vitro and in vivo. *BMC Cancer* **17**, (2017).
521. Zhou, W., Guo, Y., Zhang, X. & Jiang, Z. Lys05 induces lysosomal membrane permeabilization and increases radiosensitivity in glioblastoma. *J. Cell. Biochem.* **121**, 2027–2037 (2020).
522. Wojton, J. *et al.* SapC-DOPS-induced lysosomal cell death synergizes with TMZ in glioblastoma. *Oncotarget* **5**, 9703–9709 (2014).
523. Mora, R. *et al.* Sphingolipid rheostat alterations related to transformation can be exploited for specific induction of lysosomal cell death in murine and human glioma. *Glia* **58**, 1364–1383 (2010).
524. Enzenmüller, S., Gonzalez, P., Karpel-Massler, G., Debatin, K.-M. & Fulda, S. GDC-0941 enhances the lysosomal compartment via TFEB and primes glioblastoma cells to lysosomal membrane permeabilization and cell death. *Cancer Lett.* **329**, 27–36 (2013).
525. Brandtzaeg, P., Kiyono, H., Pabst, R. & Russell, M. W. Terminology: nomenclature of mucosa-associated lymphoid tissue. *Mucosal Immunol.* **1**, 31–37 (2008).
526. Isaacson, P. & Wright, D. H. Malignant lymphoma of mucosa-associated lymphoid tissue. A distinctive type of B-cell lymphoma. *Cancer* **52**, 1410–1416 (1983).
527. Troppan, K., Wenzl, K., Neumeister, P. & Deutsch, A. Molecular Pathogenesis of MALT Lymphoma. *Gastroenterol. Res. Pract.* **2015**, 1–10 (2015).
528. Isaacson, P. & Du, M.-Q. MALT lymphoma: from morphology to molecules. *Nature Reviews Cancer* 644–653 (2004).
529. Kiesewetter, B. *et al.* Transformed mucosa-associated lymphoid tissue lymphomas: A single institution retrospective study including polymerase chain reaction-based clonality analysis. *Br. J. Haematol.* **186**, 448–459 (2019).
530. Maeshima, A. M. *et al.* Clinicopathological features of histological transformation from extranodal marginal zone B-cell lymphoma of mucosa-associated lymphoid tissue to diffuse large B-cell lymphoma: an analysis of 467 patients. *Br. J. Haematol.* **174**, 923–931 (2016).
531. Dierlamm, J. *et al.* The Apoptosis Inhibitor Gene API2 and a Novel 18q Gene,MLT, Are Recurrently Rearranged in the t(11;18)(q21;q21) Associated With Mucosa-Associated Lymphoid Tissue Lymphomas. *Blood* **93**, 3601–3609 (1999).
532. Akagi, T. *et al.* A novel gene, MALT1 at 18q21, is involved in t(11;18) (q21;q21) found in low-grade B-cell lymphoma of mucosa-associated lymphoid tissue. *Oncogene* **18**, 5785–5794 (1999).
533. Uren, A. G. *et al.* Identification of paracaspases and metacaspases: two ancient families of caspase-like proteins, one of which plays a key role in MALT lymphoma. *Mol. Cell* **6**, 961–967 (2000).
534. Streubel, B. *et al.* Variable frequencies of MALT lymphoma-associated genetic aberrations in MALT lymphomas of different sites. *Leukemia* **18**, 1722–1726 (2004).

535. Che, T. *et al.* MALT1/Paracaspase Is a Signaling Component Downstream of CARMA1 and Mediates T Cell Receptor-induced NF-κB Activation. *J. Biol. Chem.* **279**, 15870–15876 (2004).
536. Ruland, J., Duncan, G. S., Wakeham, A. & Mak, T. W. Differential Requirement for Malt1 in T and B Cell Antigen Receptor Signaling. *Immunity* **19**, 749–758 (2003).
537. Ruefli-Brasse, A. A., French, D. M. & Dixit, V. M. Regulation of NF-kappaB-dependent lymphocyte activation and development by paracaspase. *Science* **302**, 1581–1584 (2003).
538. McAllister-Lucas, L. M. & Lucas, P. C. Finally, MALT1 is a protease! *Nat. Immunol.* **9**, 231–233 (2008).
539. Rebeaud, F. *et al.* The proteolytic activity of the paracaspase MALT1 is key in T cell activation. *Nat. Immunol.* **9**, 272–281 (2008).
540. Coornaert, B. *et al.* T cell antigen receptor stimulation induces MALT1 paracaspase-mediated cleavage of the NF-kappaB inhibitor A20. *Nat. Immunol.* **9**, 263–271 (2008).
541. Ruland, J. & Hartjes, L. CARD-BCL-10-MALT1 signalling in protective and pathological immunity. *Nat. Rev. Immunol.* **19**, 118–134 (2019).
542. Bell, P. A. *et al.* Integrating knowledge of protein sequence with protein function for the prediction and validation of new MALT1 substrates. *Comput. Struct. Biotechnol. J.* **20**, 4717–4732 (2022).
543. Ferch, U. *et al.* Inhibition of MALT1 protease activity is selectively toxic for activated B cell-like diffuse large B cell lymphoma cells. *J. Exp. Med.* **206**, 2313–2320 (2009).
544. Hailfinger, S. *et al.* Essential role of MALT1 protease activity in activated B cell-like diffuse large B-cell lymphoma. *Proc. Natl. Acad. Sci. U. S. A.* **106**, 19946–19951 (2009).
545. Wiesmann, C. *et al.* Structural determinants of MALT1 protease activity. *J. Mol. Biol.* **419**, 4–21 (2012).
546. Yu, J. W., Jeffrey, P. D., Ha, J. Y., Yang, X. & Shi, Y. Crystal structure of the mucosa-associated lymphoid tissue lymphoma translocation 1 (MALT1) paracaspase region. *Proc. Natl. Acad. Sci.* **108**, 21004–21009 (2011).
547. Qiao, Q. *et al.* Structural architecture of the CARMA1/Bcl10/MALT1 signalosome: nucleation-induced filamentous assembly. *Mol. Cell* **51**, 766–779 (2013).
548. Schlauderer, F. *et al.* Molecular architecture and regulation of BCL10-MALT1 filaments. *Nat. Commun.* **9**, 4041 (2018).
549. David, L. *et al.* Assembly mechanism of the CARMA1–BCL10–MALT1–TRAF6 signalosome. *Proc. Natl. Acad. Sci.* **115**, 1499–1504 (2018).
550. Festjens, N., Cornelis, S., Lamkanfi, M. & Vandenabeele, P. Caspase-containing complexes in the regulation of cell death and inflammation. *Biol. Chem.* **387**, (2006).
551. Bertin, J. *et al.* CARD9 Is a Novel Caspase Recruitment Domain-containing Protein That Interacts With BCL10/CLAP and Activates NF-κB. *J. Biol. Chem.* **275**, 41082–41086 (2000).
552. Bertin, J. *et al.* CARD11 and CARD14 Are Novel Caspase Recruitment Domain (CARD)/Membrane-associated Guanylate Kinase (MAGUK) Family Members that Interact with BCL10 and Activate NF-κB. *J. Biol. Chem.* **276**, 11877–11882 (2001).
553. Gaide, O. *et al.* Carma1, a CARD-containing binding partner of Bcl10, induces

Bcl10 phosphorylation and NF-κB activation [1]. *FEBS Lett.* **496**, 121–127 (2001).
554. Juilland, M. & Thome, M. Holding All the CARDs: How MALT1 Controls CARMA/CARD-Dependent Signaling. *Front. Immunol.* **9**, 1927 (2018).
555. Rosebeck, S., Rehman, A. O., Lucas, P. C. & McAllister-Lucas, L. M. From MALT lymphoma to the CBM signalosome: Three decades of discovery. *Cell Cycle* **10**, 2485–2496 (2011).
556. Jiang, C. & Lin, X. Regulation of NF-κB by the CARD proteins: CARD protein and NF-κB. *Immunol. Rev.* **246**, 141–153 (2012).
557. Gross, O. *et al.* Card9 controls a non-TLR signalling pathway for innate anti-fungal immunity. *Nature* **442**, 651–656 (2006).
558. Hara, H. *et al.* The MAGUK Family Protein CARD11 Is Essential for Lymphocyte Activation. *Immunity* **18**, 763–775 (2003).
559. Harden, J. L. *et al.* CARD14 Expression in Dermal Endothelial Cells in Psoriasis. *PLoS ONE* **9**, e111255 (2014).
560. Jordan, C. T. *et al.* Rare and Common Variants in CARD14, Encoding an Epidermal Regulator of NF-kappaB, in Psoriasis. *Am. J. Hum. Genet.* **90**, 796–808 (2012).
561. Van Nuffel, E. *et al.* MALT 1 targeting suppresses CARD 14-induced psoriatic dermatitis in mice. *EMBO Rep.* **21**, e49237 (2020).
562. Ekambaram, P. *et al.* The CARMA3-Bcl10-MALT1 Signalosome Drives NFκB Activation and Promotes Aggressiveness in Angiotensin II Receptor-Positive Breast Cancer. *Cancer Res.* **78**, 1225–1240 (2018).
563. Jiang, T. *et al.* CARMA3 is Crucial for EGFR-Induced Activation of NF-κB and Tumor Progression. *Cancer Res.* **71**, 2183–2192 (2011).
564. Grabiner, B. C. *et al.* CARMA3 deficiency abrogates G protein-coupled receptor-induced NF-κB activation. *Genes Dev.* **21**, 984–996 (2007).
565. Martin, D., Galisteo, R. & Gutkind, J. S. CXCL8/IL8 Stimulates Vascular Endothelial Growth Factor (VEGF) Expression and the Autocrine Activation of VEGFR2 in Endothelial Cells by Activating NFκB through the CBM (Carma3/Bcl10/Malt1) Complex. *J. Biol. Chem.* **284**, 6038–6042 (2009).
566. McAllister-Lucas, L. M., Kohrt, D. & Mak, T. W. CARMA3Bcl10MALT1-dependent NF- B activation mediates angiotensin II-responsive inflammatory signaling in nonimmune cells. *PNAS* **104**, 139–144 (2007).
567. Matsumoto, R. *et al.* Phosphorylation of CARMA1 Plays a Critical Role in T Cell Receptor-Mediated NF-κB Activation. *Immunity* **23**, 575–585 (2005).
568. Sommer, K. *et al.* Phosphorylation of the CARMA1 Linker Controls NF-κB Activation. *Immunity* **23**, 561–574 (2005).
569. McAllister-Lucas, L. M. *et al.* Bimp1, a MAGUK Family Member Linking Protein Kinase C Activation to Bcl10-mediated NF-κB Induction. *J. Biol. Chem.* **276**, 30589–30597 (2001).
570. Schmitt, A. *et al.* MALT1 Protease Activity Controls the Expression of Inflammatory Genes in Keratinocytes upon Zymosan Stimulation. *J. Invest. Dermatol.* **136**, 788–797 (2016).
571. Strasser, D. *et al.* Syk Kinase-Coupled C-type Lectin Receptors Engage Protein Kinase C-δ to Elicit Card9 Adaptor-Mediated Innate Immunity. *Immunity* **36**, 32–42 (2012).
572. Eitelhuber, A. C. *et al.* Dephosphorylation of Carma1 by PP2A negatively regulates T-cell activation: Dephosphorylation of Carma1 by PP2A. *EMBO J.* **30**, 594–605 (2011).
573. Shah, K., Al-Haidari, A., Sun, J. & Kazi, J. U. T cell receptor (TCR) signaling in

health and disease. *Signal Transduct. Target. Ther.* **6**, 412 (2021).
574. Reth, M. Antigen receptor tail clue. *Nature* **338**, 383–384 (1989).
575. Getahun, A. & Cambier, J. C. Of ITIMs, ITAMs, and ITAMis: revisiting immunoglobulin Fc receptor signaling. *Immunol. Rev.* **268**, 66–73 (2015).
576. Veillette, A., Bookman, M. A., Horak, E. M. & Bolen, J. B. The CD4 and CD8 T Cell Surface Antigens Are Associated with the Internal Membrane Tyrasine-Protein Kinase p56LCK. *Cell* **55**, 301–308 (1988).
577. Elder, M. E. *et al.* Human Severe Combined Immunodeficiency Due to a Defect in ZAP-70, a T Cell Tyrosine Kinase. *Science* **264**, 1596–1599 (1994).
578. Zhang, W., Sloan-Lancaster, J., Kitchen, J., Trible, R. P. & Samelson, L. E. LAT: The ZAP-70 Tyrosine Kinase Substrate that Links T Cell Receptor to Cellular Activation. *Cell* **92**, 83–92 (1998).
579. Carpenter, G. & Ji, Q. Phospholipase C-gamma as a Signal-Transducing Element. *Exp. Cell Res.* 15–24 (1999).
580. Fu, G. *et al.* Phospholipase Cγ1 is essential for T cell development, activation, and tolerance. *J. Exp. Med.* **207**, 309–318 (2010).
581. Shaw, J.-P. *et al.* Identification of a Putative Regulator of Early T Cell Activation Genes. *Science* **241**, 202–205 (1988).
582. Macian, F. NFAT proteins: key regulators of T-cell development and function. *Nat. Rev. Immunol.* **5**, 472–484 (2005).
583. Roose, J. P., Mollenauer, M., Gupta, V. A., Stone, J. & Weiss, A. A Diacylglycerol-Protein Kinase C-RasGRP1 Pathway Directs Ras Activation upon Antigen Receptor Stimulation of T Cells. *Mol. Cell. Biol.* **25**, 4426–4441 (2005).
584. Nishizuka, Y. Intracellular Signaling by Hydrolysis of Phospholipids and Activation of Protein Kinase C. *Science* **258**, 607–614 (1992).
585. Meininger, I. *et al.* Alternative splicing of MALT1 controls signalling and activation of CD4+ T cells. *Nat. Commun.* **7**, 11292 (2016).
586. Ma, X. *et al.* Cryo-EM structures of two human B cell receptor isotypes. (2022).
587. Burger, J. A. & Wiestner, A. Targeting B cell receptor signalling in cancer: preclinical and clinical advances. *Nat. Rev. Cancer* **18**, 148–167 (2018).
588. Hashimoto, A. *et al.* Cutting Edge: Essential Role of Phospholipase C-γ2 in B Cell Development and Function. *J Immunol* **165**, 1738–1742 (2000).
589. Gross, O. *et al.* Multiple ITAM-coupled NK-cell receptors engage the Bcl10/Malt1 complex via Carma1 for NF-κB and MAPK activation to selectively control cytokine production. *Blood* **112**, 2421–2428 (2008).
590. Hara, H. *et al.* Cell Type-Specific Regulation of ITAM-Mediated NF-κB Activation by the Adaptors, CARMA1 and CARD9. *J. Immunol.* **181**, 918–930 (2008).
591. Klemm, S. *et al.* The Bcl10–Malt1 complex segregates FcεRI-mediated nuclear factor κB activation and cytokine production from mast cell degranulation. *J. Exp. Med.* **203**, 337–347 (2006).
592. Yu, J. W. *et al.* MALT1 Protease Activity Is Required for Innate and Adaptive Immune Responses. *PloS One* **10**, e0127083 (2015).
593. Hara, H. *et al.* The adaptor protein CARD9 is essential for the activation of myeloid cells through ITAM-associated and Toll-like receptors. *Nat. Immunol.* **8**, 619–629 (2007).
594. Shenderov, K. *et al.* Cord Factor and Peptidoglycan Recapitulate the Th17-Promoting Adjuvant Activity of Mycobacteria through Mincle/CARD9 Signaling and the Inflammasome. *J. Immunol.* **190**, 5722–5730 (2013).
595. Zhao, X.-Q. *et al.* C-type Lectin Receptor Dectin-3 Mediates Trehalose 6,6′-Dimycolate (TDM)-induced Mincle Expression through CARD9/Bcl10/MALT1-

dependent Nuclear Factor (NF)-κB Activation. *J. Biol. Chem.* **289**, 30052–30062 (2014).
596. Delekta, P. C. *et al.* Thrombin-dependent NF-κB Activation and Monocyte/Endothelial Adhesion Are Mediated by the CARMA3·Bcl10·MALT1 Signalosome. *J. Biol. Chem.* **285**, 41432–41442 (2010).
597. Rehman, A. O. & Wang, C. CXCL12/SDF-1α Activates NF-κB and Promotes Oral Cancer Invasion through the Carma3/Bcl10/Malt1 Complex. *Int. J. Oral Sci.* **1**, 105–118 (2009).
598. McAllister-Lucas, L. M. *et al.* The CARMA3-Bcl10-MALT1 Signalosome Promotes Angiotensin II-dependent Vascular Inflammation and Atherogenesis. *J. Biol. Chem.* **285**, 25880–25884 (2010).
599. Deng, P. & Xin, L. Epithelial growth factor receptor-activated nuclear factor kappaB signaling and its role in epithelial growth factor receptor-associated tumors. *Cancer J.* **19**, 461–467 (2013).
600. Pan, D. *et al.* MALT1 is required for EGFR-induced NF-κB activation and contributes to EGFR-driven lung cancer progression. *Oncogene* **35**, 919–928 (2016).
601. Okkenhaug, K. & Vanhaesebroeck, B. PI3K in lymphocyte development, differentiation and activation. *Nat. Rev. Immunol.* **3**, 317–330 (2003).
602. Cheng, J., Hamilton, K. S. & Kane, L. P. Phosphorylation of Carma1, but not Bcl10, by Akt regulates TCR/CD28-mediated NF-κB induction and cytokine production. *Mol. Immunol.* **59**, 110–116 (2014).
603. Cabalzar, K. *et al.* Monoubiquitination and Activity of the Paracaspase MALT1 Requires Glutamate 549 in the Dimerization Interface. *PLoS ONE* **8**, e72051 (2013).
604. Pelzer, C. *et al.* The protease activity of the paracaspase MALT1 is controlled by monoubiquitination. *Nat. Immunol.* **14**, 337–345 (2013).
605. Schairer, R. *et al.* Allosteric activation of MALT1 by its ubiquitin-binding Ig3 domain. *Proc. Natl. Acad. Sci.* **117**, 3093–3102 (2020).
606. Sun, L., Deng, L., Ea, C.-K., Xia, Z.-P. & Chen, Z. J. The TRAF6 Ubiquitin Ligase and TAK1 Kinase Mediate IKK Activation by BCL10 and MALT1 in T Lymphocytes. *Mol. Cell* **14**, 289–301 (2004).
607. Oeckinghaus, A. *et al.* Malt1 ubiquitination triggers NF-κB signaling upon T-cell activation. *EMBO J.* **26**, 4634–4645 (2007).
608. Bardet, M. *et al.* MALT1 activation by TRAF6 needs neither BCL10 nor CARD11. *Biochem. Biophys. Res. Commun.* **506**, 48–52 (2018).
609. O'Neill, T. J. *et al.* TRAF6 prevents fatal inflammation by homeostatic suppression of MALT1 protease. *Sci. Immunol.* **6**, eabh2095 (2021).
610. Li, Y. *et al.* The HECTD3 E3 Ubiquitin Ligase Suppresses Cisplatin-Induced Apoptosis via Stabilizing MALT1. *Neoplasia* **15**, 39-IN15 (2013).
611. Cho, J. J. *et al.* Hectd3 promotes pathogenic Th17 lineage through Stat3 activation and Malt1 signaling in neuroinflammation. *Nat. Commun.* **10**, 701 (2019).
612. Stilo, R., Varricchio, E., Liguoro, D., Leonardi, A. & Vito, P. A20 is a negative regulator of BCL10- and CARMA3-mediated activation of NF-κB. *J. Cell Sci.* **121**, 1165–1171 (2008).
613. Düwel, M. *et al.* A20 Negatively Regulates T Cell Receptor Signaling to NF-κB by Cleaving Malt1 Ubiquitin Chains. *J. Immunol.* **182**, 7718–7728 (2009).
614. Nicolau, C. A., Gavard, J. & Bidère, N. TAK1 lessens the activity of the paracaspase MALT1 during T cell receptor signaling. *Cell. Immunol.* **353**, 104115 (2020).
615. Gehring, T. *et al.* MALT1 Phosphorylation Controls Activation of T Lymphocytes and Survival of ABC-DLBCL Tumor Cells. *Cell Rep.* **29**, 873-888.e10

(2019).
616. Bidère, N. *et al.* Casein kinase 1α governs antigen-receptor-induced NF-κB activation and human lymphoma cell survival. *Nature* **458**, 92 (2008).
617. Thys, A., Douanne, T. & Bidère, N. Post-translational Modifications of the CARMA1-BCL10-MALT1 Complex in Lymphocytes and Activated B-Cell Like Subtype of Diffuse Large B-Cell Lymphoma. *Front. Oncol.* **8**, 498 (2018).
618. Ishiguro, K. *et al.* Ca $^{2+}$ /Calmodulin-Dependent Protein Kinase II Is a Modulator of CARMA1-Mediated NF-κB Activation. *Mol. Cell. Biol.* **26**, 5497–5508 (2006).
619. Shinohara, H., Maeda, S., Watarai, H. & Kurosaki, T. IκB kinase β–induced phosphorylation of CARMA1 contributes to CARMA1–Bcl10–MALT1 complex formation in B cells. *J. Exp. Med.* **204**, 3285–3293 (2007).
620. Brenner, D. *et al.* Phosphorylation of CARMA1 by HPK1 is critical for NF- B activation in T cells.
621. Moreno-García, M. E. *et al.* MAGUK-Controlled Ubiquitination of CARMA1 Modulates Lymphocyte NF-κB Activity. *Mol. Cell. Biol.* **30**, 922–934 (2010).
622. Welteke, V. *et al.* COP9 signalosome controls the Carma1–Bcl10–Malt1 complex upon T-cell stimulation. *EMBO Rep.* **10**, 642–648 (2009).
623. Pedersen, S. M., Chan, W., Jattani, R. P., Mackie, deMauri S. & Pomerantz, J. L. Negative Regulation of CARD11 Signaling and Lymphoma Cell Survival by the E3 Ubiquitin Ligase RNF181. *Mol. Cell. Biol.* **36**, 794–808 (2016).
624. Hu, S. cIAP2 is a ubiquitin protein ligase for BCL10 and is dysregulated in mucosa-associated lymphoid tissue lymphomas. *J. Clin. Invest.* **116**, 174–181 (2005).
625. Yang, Y. *et al.* Targeting Non-proteolytic Protein Ubiquitination for the Treatment of Diffuse Large B Cell Lymphoma. *Cancer Cell* **29**, 494–507 (2016).
626. Lobry, C. & Lopez, T. Negative feedback loop in T cell activation through I B kinase-induced phosphorylation and degradation of Bcl10. *PNAS* **104**, 908–913 (2006).
627. Scharschmidt, E., Wegener, E., Heissmeyer, V., Rao, A. & Krappmann, D. Degradation of Bcl10 Induced by T-Cell Activation Negatively Regulates NF- B Signaling. *MOL CELL BIOL* **24**, (2004).
628. Wu, C.-J. & Ashwell, J. D. NEMO recognition of ubiquitinated Bcl10 is required for T cell receptor-mediated NF- B activation. *PNAS* **105**, 3023–3028 (2008).
629. Alexia, C. *et al.* The Endoplasmic Reticulum Acts as a Platform for Ubiquitylated Components of Nuclear Factor kB Signaling. *Sci. Signal.* **6**, (2013).
630. Douanne, T., Chapelier, S., Rottapel, R., Gavard, J. & Bidère, N. The LUBAC participates in lysophosphatidic acid-induced NF-κB activation. *Cell. Immunol.* **353**, 104133 (2020).
631. Dubois, S. M. *et al.* A catalytic-independent role for the LUBAC in NF-κB activation upon antigen receptor engagement and in lymphoma cells. *Blood* **123**, 2199–2203 (2014).
632. Yang, Y.-K. *et al.* Molecular Determinants of Scaffold-induced Linear Ubiquitinylation of B Cell Lymphoma/Leukemia 10 (Bcl10) during T Cell Receptor and Oncogenic Caspase Recruitment Domain-containing Protein 11 (CARD11) Signaling. *J. Biol. Chem.* **291**, 25921–25936 (2016).
633. Satpathy, S. *et al.* Systems-wide analysis of BCR signalosomes and downstream phosphorylation and ubiquitylation. *Mol. Syst. Biol.* **11**, 810 (2015).
634. Park, Y., Jin, H. & Liu, Y.-C. Regulation of T cell function by the ubiquitin-specific protease USP9X via modulating the Carma1-Bcl10-Malt1 complex. *Proc.*

Natl. Acad. Sci. **110**, 9433–9438 (2013).
635. Ishiguro, K., Ando, T., Goto, H. & Xavier, R. Bcl10 is phosphorylated on Ser138 by Ca2+/calmodulin-dependent protein kinase II. *Mol. Immunol.* **44**, 2095–2100 (2007).
636. Zeng, H. *et al.* Phosphorylation of Bcl10 Negatively Regulates T-Cell Receptor-Mediated NF-κB Activation. *Mol. Cell. Biol.* **27**, 5235–5245 (2007).
637. Oruganti, S. R., Edin, S., Grundström, C. & Grundström, T. CaMKII targets Bcl10 in T-cell receptor induced activation of NF-κB. *Mol. Immunol.* **48**, 1448–1460 (2011).
638. Wegener, E. *et al.* Essential Role for IκB Kinase β in Remodeling Carma1-Bcl10-Malt1 Complexes upon T Cell Activation. *Mol. Cell* **23**, 13–23 (2006).
639. Bognar, M. K. *et al.* Oncogenic CARMA1 couples NF-κB and β-catenin signaling in diffuse large B-cell lymphomas. *Oncogene* **35**, 4269–4281 (2016).
640. Abd-Ellah, A., Voogdt, C., Krappmann, D., Möller, P. & Marienfeld B., R. GSK3β modulates NF-κB activation and RelB degradation through site-specific phosphorylation of BCL10. *Scientific Reports* vol. 8 (2018).
641. Frischbutter, S., Gabriel, C., Bendfeldt, H., Radbruch, A. & Baumgrass, R. Dephosphorylation of Bcl-10 by calcineurin is essential for canonical NF-κB activation in Th cells. *Eur. J. Immunol.* **41**, 2349–2357 (2011).
642. Palkowitsch, L. *et al.* The Ca2+-dependent Phosphatase Calcineurin Controls the Formation of the Carma1-Bcl10-Malt1 Complex during T Cell Receptor-induced NF-κB Activation. *J. Biol. Chem.* **286**, 7522–7534 (2011).
643. Yu, H., Lin, L., Zhang, Z., Zhang, H. & Hu, H. Targeting NF-κB pathway for the therapy of diseases: mechanism and clinical study. *Signal Transduct. Target. Ther.* **5**, 209 (2020).
644. Kanayama, A. *et al.* TAB2 and TAB3 Activate the NF- B Pathway through Binding to Polyubiquitin Chains. *Mol. Cell* **15**, 535–548 (2004).
645. Wang, C. *et al.* TAK1 is a ubiquitin-dependent kinase of MKK and IKK. *Nature* **412**, 346–351 (2001).
646. Takaesu, G. *et al.* TAB2, a Novel Adaptor Protein, Mediates Activation of TAK1 MAPKKK by Linking TAK1 to TRAF6 in the IL-1 Signal Transduction Pathway. *Mol. Cell* **5**, 649–658 (2000).
647. Besse, A. *et al.* TAK1-dependent Signaling Requires Functional Interaction with TAB2/TAB3. *J. Biol. Chem.* **282**, 3918–3928 (2007).
648. Cheung, P. C. F., Nebreda, A. R. & Cohen, P. TAB3, a new binding partner of the protein kinase TAK1. *Biochem. J.* **378**, 27–34 (2004).
649. Hayden, M. S. & Ghosh, S. Shared Principles in NF-κB Signaling. *Cell* **132**, 344–362 (2008).
650. Adhikari, A., Xu, M. & Chen, Z. J. Ubiquitin-mediated activation of TAK1 and IKK. *Oncogene* **26**, 3214–3226 (2007).
651. Viatour, P., Merville, M.-P., Bours, V. & Chariot, A. Phosphorylation of NF-κB and IκB proteins: implications in cancer and inflammation. *Trends Biochem. Sci.* **30**, 43–52 (2005).
652. Pahl, H. L. Activators and target genes of Rel/NF-kB transcription factors. *Oncogene* **18**, 6853 ± 6866 (1999).
653. Jaworski, M. *et al.* Malt1 protease inactivation efficiently dampens immune responses but causes spontaneous autoimmunity. *EMBO J.* **33**, 2765–2781 (2014).
654. Bornancin, F. *et al.* Deficiency of MALT1 paracaspase activity results in unbalanced regulatory and effector T and B cell responses leading to multiorgan inflammation. *J. Immunol. Baltim. Md 1950* **194**, 3723–3734 (2015).

655. Gewies, A. *et al.* Uncoupling Malt1 threshold function from paracaspase activity results in destructive autoimmune inflammation. *Cell Rep.* **9**, 1292–1305 (2014).
656. Brüstle, A. *et al.* The NF-κB regulator MALT1 determines the encephalitogenic potential of Th17 cells. *J. Clin. Invest.* **122**, 4698–4709 (2012).
657. Punwani, D. *et al.* Combined Immunodeficiency Due to MALT1 Mutations, Treated by Hematopoietic Cell Transplantation. *J. Clin. Immunol.* **35**, 135–146 (2015).
658. McKinnon, M. L. *et al.* Combined immunodeficiency associated with homozygous MALT1 mutations. *J. Allergy Clin. Immunol.* **133**, 1458-1462.e7 (2014).
659. Jabara, H. H. *et al.* A homozygous mucosa-associated lymphoid tissue 1 (MALT1) mutation in a family with combined immunodeficiency. *J. Allergy Clin. Immunol.* **132**, 151–158 (2013).
660. Boone, D. L. *et al.* The ubiquitin-modifying enzyme A20 is required for termination of Toll-like receptor responses. *Nat. Immunol.* **5**, 1052–1060 (2004).
661. Mauro, C. *et al.* ABIN-1 Binds to NEMO/IKKγ and Co-operates with A20 in Inhibiting NF-κB. *J. Biol. Chem.* **281**, 18482–18488 (2006).
662. Shembade, N., Ma, A. & Harhaj, E. W. Inhibition of NF-κB Signaling by A20 Through Disruption of Ubiquitin Enzyme Complexes. *Science* **327**, 1135–1139 (2010).
663. Yin, H. *et al.* A20 and ABIN-1 cooperate in balancing CBM complex-triggered NF-κB signaling in activated T cells. *Cell. Mol. Life Sci.* **79**, 112 (2022).
664. Mc Guire, C. *et al.* Paracaspase MALT1 Deciency Protects Mice from Autoimmune-Mediated Demyelination. *J. Immunol.* **192**, 129.6-129.6 (2013).
665. Kovalenko, A., Chable-Bessia, C. & Cantarella, G. The tumour suppressor CYLD negatively regulates NF-kB signalling by deubiquitination. **424**, (2003).
666. Staal, J. *et al.* T-cell receptor-induced JNK activation requires proteolytic inactivation of CYLD by MALT1. *EMBO J.* **30**, 1742–1752 (2011).
667. Hailfinger, S. *et al.* Malt1-dependent RelB cleavage promotes canonical NF-kappaB activation in lymphocytes and lymphoma cell lines. *Proc. Natl. Acad. Sci. U. S. A.* **108**, 14596–14601 (2011).
668. Baens, M. *et al.* MALT1 auto-proteolysis is essential for NF-κB-dependent gene transcription in activated lymphocytes. *PloS One* **9**, e103774 (2014).
669. Baens, M. *et al.* Malt1 self-cleavage is critical for regulatory T cell homeostasis and anti-tumor immunity in mice. *Eur. J. Immunol.* **48**, 1728–1738 (2018).
670. Ginster, S. *et al.* Two Antagonistic MALT1 Auto-Cleavage Mechanisms Reveal a Role for TRAF6 to Unleash MALT1 Activation. *PLOS ONE* **12**, e0169026 (2017).
671. Elton, L. *et al.* MALT1 cleaves the E3 ubiquitin ligase HOIL-1 in activated T cells, generating a dominant negative inhibitor of LUBAC-induced NF-κB signaling. *FEBS J.* **283**, 403–412 (2016).
672. Klein, T. *et al.* The paracaspase MALT1 cleaves HOIL1 reducing linear ubiquitination by LUBAC to dampen lymphocyte NF-κB signalling. *Nat. Commun.* **6**, (2015).
673. Douanne, T., Gavard, J. & Bidère, N. The paracaspase MALT1 cleaves the LUBAC subunit HOIL1 during antigen receptor signaling. *J. Cell Sci.* jcs.185025 (2016) doi:10.1242/jcs.185025.
674. Uehata, T. *et al.* Malt1-induced cleavage of regnase-1 in CD4(+) helper T cells regulates immune activation. *Cell* **153**, 1036–1049 (2013).
675. Jeltsch, K. M. *et al.* Cleavage of roquin and regnase-1 by the paracaspase MALT1 releases their cooperatively repressed targets to promote T(H)17

differentiation. *Nat. Immunol.* **15**, 1079–1089 (2014).
676. Matsushita, K. *et al.* Zc3h12a is an RNase essential for controlling immune responses by regulating mRNA decay. *Nature* **458**, 1185–1190 (2009).
677. Yamasoba, D. *et al.* N4BP1 restricts HIV-1 and its inactivation by MALT1 promotes viral reactivation. *Nat. Microbiol.* **4**, 1532–1544 (2019).
678. Lucas, P. *et al.* A dual role for the API2 moiety in API2-MALT1-dependent NF-jB activation: heterotypic oligomerization and TRAF2 recruitment. *Oncogene* **26**, 5643–5654 (2007).
679. Rosebeck, S. *et al.* Cleavage of NIK by the API2-MALT1 fusion oncoprotein leads to noncanonical NF-kappaB activation. *Science* **331**, 468–472 (2011).
680. Sun, S.-C. Non-canonical NF-κB signaling pathway. *Cell Res.* **21**, 71–85 (2011).
681. Nie, Z. *et al.* Conversion of the LIMA1 tumour suppressor into an oncogenic LMO-like protein by API2-MALT1 in MALT lymphoma. *Nat. Commun.* **6**, 5908 (2015).
682. Juilland, M. *et al. Malt1-dependent cleavage of Tensin-3 controls B-cell adhesion and lymphomagenesis*. http://biorxiv.org/lookup/doi/10.1101/2022.09.29.510036 (2022) doi:10.1101/2022.09.29.510036.
683. Wan, Y. Y., Chi, H., Xie, M., Schneider, M. D. & Flavell, R. A. The kinase TAK1 integrates antigen and cytokine receptor signaling for T cell development, survival and function. *Nat. Immunol.* **7**, 851–858 (2006).
684. Blonska, M. *et al.* The CARMA1-Bcl10 Signaling Complex Selectively Regulates JNK2 Kinase in the T Cell Receptor-Signaling Pathway. *Immunity* **26**, 55–66 (2007).
685. Sinclair, L. V. *et al.* Phosphatidylinositol-3-OH kinase and nutrient-sensing mTOR pathways control T lymphocyte trafficking. *Nat. Immunol.* **9**, 513–521 (2008).
686. Hamilton, K. S. *et al.* T cell receptor-dependent activation of mTOR signaling in T cells is mediated by Carma1 and MALT1, but not Bcl10. *Sci. Signal.* **7**, ra55 (2014).
687. Nakaya, M. *et al.* Inflammatory T cell responses rely on amino acid transporter ASCT2 facilitation of glutamine uptake and mTORC1 kinase activation. *Immunity* **40**, 692–705 (2014).
688. Eichhold, T. H., Hookfin, E. B., Taiwo, Y. O., De, B. & Wehmeyer, K. R. Isolation and quantification of fluoroacetate in rat tissues, following dosing of Z-Phe-Ala-CH2-F, a peptidyl fluoromethyl ketone protease inhibitor. *J. Pharm. Biomed. Anal.* **16**, 459–467 (1997).
689. Fontan, L. *et al.* MALT1 small molecule inhibitors specifically suppress ABC-DLBCL in vitro and in vivo. *Cancer Cell* **22**, 812–824 (2012).
690. Nagel, D. *et al.* Pharmacologic Inhibition of MALT1 Protease by Phenothiazines as a Therapeutic Approach for the Treatment of Aggressive ABC-DLBCL. *Cancer Cell* **22**, 825–837 (2012).
691. Schlauderer, F. *et al.* Structural Analysis of Phenothiazine Derivatives as Allosteric Inhibitors of the MALT1 Paracaspase. *Angew. Chem. Int. Ed.* **52**, 10384–10387 (2013).
692. LOMAS, J. L. Treatment of schizophrenia pacatal and chlorpromazine compared. *Br. Med. J.* **2**, 78–80 (1957).
693. Sarwer-Foner, G. J. & Koranyi, E. K. THE CLINICAL INVESTIGATION OF PACATAL IN OPEN PSYCHIATRIC SETTINGS. **77**, (1957).
694. Whittier, J. R., Klein, D. F., Levine, G. & Weiss, D. Mepazine (pacatal): Clinical trial with placebo control and psychological study. *Psychopharmacologia* **1**, 280–287

(1960).
695. Di Pilato, M. *et al.* Translational Studies Using the MALT1 Inhibitor (*S*)-Mepazine to Induce Treg Fragility and Potentiate Immune Checkpoint Therapy in Cancer. *J. Immunother. Precis. Oncol.* **6**, 61–73 (2023).
696. Quancard, J. *et al.* An allosteric MALT1 inhibitor is a molecular corrector rescuing function in an immunodeficient patient. *Nat. Chem. Biol.* **15**, 304–313 (2019).
697. Lu, T. *et al.* Discovery and optimization of a series of small-molecule allosteric inhibitors of MALT1 protease. *Bioorg. Med. Chem. Lett.* **29**, 126743 (2019).
698. Schmitz, R. *et al.* Genetics and Pathogenesis of Diffuse Large B-Cell Lymphoma. *N. Engl. J. Med.* **378**, 1396–1407 (2018).
699. Liang, X. *et al.* MALT1 as a promising target to treat lymphoma and other diseases related to MALT1 anomalies. *Med. Res. Rev.* **41**, 2388–2422 (2021).
700. Davis, R. E. *et al.* Chronic active B-cell-receptor signalling in diffuse large B-cell lymphoma. *Nature* **463**, 88–92 (2010).
701. Lenz, G. *et al.* Oncogenic *CARD11* Mutations in Human Diffuse Large B Cell Lymphoma. *Science* **319**, 1676–1679 (2008).
702. Knies, N. *et al.* Lymphomagenic CARD11/BCL10/MALT1 signaling drives malignant B-cell proliferation via cooperative NF-κB and JNK activation. *Proc. Natl. Acad. Sci.* **112**, (2015).
703. Compagno, M. *et al.* Mutations of multiple genes cause deregulation of NF-κB in diffuse large B-cell lymphoma. *Nature* **459**, 717–721 (2009).
704. Honma, K. *et al.* TNFAIP3 is the target gene of chromosome band 6q23.3-q24.1 loss in ocular adnexal marginal zone B cell lymphoma. *Genes. Chromosomes Cancer* **47**, 1–7 (2008).
705. Honma, K. *et al.* TNFAIP3/A20 functions as a novel tumor suppressor gene in several subtypes of non-Hodgkin lymphomas. *Blood* **114**, 2467–2475 (2009).
706. Rahal, R. *et al.* Pharmacological and genomic profiling identifies NF-κB–targeted treatment strategies for mantle cell lymphoma. *Nat. Med.* **20**, 87–92 (2014).
707. Yang, Y. *et al.* Essential Role of the Linear Ubiquitin Chain Assembly Complex in Lymphoma Revealed by Rare Germline Polymorphisms. *Cancer Discov.* **4**, 480–493 (2014).
708. Sun, S.-C., Chang, J.-H. & Jin, J. Regulation of nuclear factor-κB in autoimmunity. *Trends Immunol.* **34**, 282–289 (2013).
709. Goldenberg, M. M. Multiple Sclerosis Review. *P&T* **37**, 175–184 (2012).
710. Steinman, L. & Zamvil, S. S. Virtues and pitfalls of EAE for the development of therapies for multiple sclerosis. *Trends Immunol.* **26**, 565–571 (2005).
711. Mc Guire, C. *et al.* Pharmacological inhibition of MALT1 protease activity protects mice in a mouse model of multiple sclerosis. *J. Neuroinflammation* **11**, 124 (2014).
712. Medoff, B. D. *et al.* CARMA1 is critical for the development of allergic airway inflammation in a murine model of asthma. *J Immunol* vol. 176 7272–7277 (2006).
713. Ramadas, R. A. *et al.* CARMA1 Is Necessary for Optimal T Cell Responses in a Murine Model of Allergic Asthma. *J. Immunol.* **187**, 6197–6207 (2011).
714. Causton, B. *et al.* CARMA3 Is Critical for the Initiation of Allergic Airway Inflammation. *J. Immunol.* **195**, 683–694 (2015).
715. Lowes, M. A., Bowcock, A. M. & Krueger, J. G. Pathogenesis and therapy of psoriasis. *Nature* **445**, 866–873 (2007).
716. Jordan, C. T. *et al.* PSORS2 Is Due to Mutations in CARD14. *Am. J. Hum. Genet.* **90**, 784–795 (2012).

717. Bardet, M. *et al.* The T-cell fingerprint of MALT 1 paracaspase revealed by selective inhibition. *Immunol. Cell Biol.* **96**, 81–99 (2018).
718. Afonina, I. S. *et al.* The paracaspase MALT 1 mediates CARD 14-induced signaling in keratinocytes. *EMBO Rep.* **17**, 914–927 (2016).
719. Nunettsu Asaba, K. *et al.* Discovery of orally bioavailable inhibitors of MALT1 with in vivo activity for psoriasis. *Bioorg. Med. Chem. Lett.* **82**, 129155 (2023).
720. Quancard, J. *et al.* Optimization of the *In Vivo* Potency of Pyrazolopyrimidine MALT1 Protease Inhibitors by Reducing Metabolism and Increasing Potency in Whole Blood. *J. Med. Chem.* **63**, 14594–14608 (2020).
721. Schlapbach, A. *et al.* N-aryl-piperidine-4-carboxamides as a novel class of potent inhibitors of MALT1 proteolytic activity. *Bioorg. Med. Chem. Lett.* **28**, 2153–2158 (2018).
722. Togashi, Y., Shitara, K. & Nishikawa, H. Regulatory T cells in cancer immunosuppression — implications for anticancer therapy. *Nat. Rev. Clin. Oncol.* **16**, 356–371 (2019).
723. Rosenbaum, M. *et al.* Bcl10-controlled Malt1 paracaspase activity is key for the immune suppressive function of regulatory T cells. *Nat. Commun.* **10**, (2019).
724. Di Pilato, M. *et al.* Targeting the CBM complex causes Treg cells to prime tumours for immune checkpoint therapy. *Nature* **570**, 112–116 (2019).
725. Pan, D. *et al.* The CBM Complex Underwrites NF-κB Activation to Promote HER2-Associated Tumor Malignancy. *Mol. Cancer Res.* **14**, 93–102 (2016).
726. Lee, J.-Y. L. *et al.* MALT1 Is a Targetable Driver of Epithelial-to-Mesenchymal Transition in Claudin-Low, Triple-Negative Breast Cancer. *Mol. Cancer Res.* **20**, 373–386 (2022).
727. McAuley, J. R. *et al.* MALT1 is a critical mediator of PAR1-driven NF-κB activation and metastasis in multiple tumor types. *Oncogene* 1–15 (2019) doi:10.1038/s41388-019-0958-4.
728. Mahanivong, C. *et al.* Protein kinase Ca-CARMA3 signaling axis links Ras to NF-jB for lysophosphatidic acid-induced urokinase plasminogen activator expression in ovarian cancer cells. *Oncogene* **27**, 1273–1280 (2008).
729. Israël, L. *et al.* CARD10 cleavage by MALT1 restricts lung carcinoma growth in vivo. *Oncogenesis* **10**, 32 (2021).
730. Konczalla, L. *et al.* Biperiden and mepazine effectively inhibit MALT1 activity and tumor growth in pancreatic cancer. *Int. J. Cancer* **0**, (2019).
731. Kurden-Pekmezci, A. *et al.* MALT1 paracaspase is overexpressed in hepatocellular carcinoma and promotes cancer cell survival and growth. *Life Sci.* **323**, 121690 (2023).
732. Liu, X. *et al.* MALT1 is a potential therapeutic target in glioblastoma and plays a crucial role in EGFR-induced NF-κB activation. *J. Cell. Mol. Med.* **24**, 7550–7562 (2020).
733. Luo, J., Solimini, N. L. & Elledge, S. J. Principles of cancer therapy: oncogene and non-oncogene addiction. *Cell* **136**, 823–837 (2009).
734. Jaworski, M. & Thome, M. The paracaspase MALT1: biological function and potential for therapeutic inhibition. *Cell. Mol. Life Sci.* **73**, 459–473 (2016).
735. Verspurten, J., Gevaert, K., Declercq, W. & Vandenabeele, P. SitePredicting the cleavage of proteinase substrates. *Trends Biochem. Sci.* **34**, 319–323 (2009).
736. Zhang, Y.-Y. *et al.* A LIMA1 variant promotes low plasma LDL cholesterol and decreases intestinal cholesterol absorption. (2018).
737. Nie, Z. *et al.* Conversion of the LIMA1 tumour suppressor into an oncogenic LMO-like protein by API2–MALT1 in MALT lymphoma. *Nat. Commun.* **6**, 5908

(2015).
738. Jia, L., Betters, J. L. & Yu, L. Niemann-Pick C1-Like 1 (NPC1L1) Protein in Intestinal and Hepatic Cholesterol Transport. *Annu. Rev. Physiol.* **73**, 239–259 (2011).
739. Peterson, T. R. *et al.* DEPTOR is an mTOR inhibitor frequently overexpressed in multiple myeloma cells and required for their survival. *Cell* **137**, 873–886 (2009).
740. Davies, J., Zachariades, E., Rogers-Broadway, K.-R. & Karteris, E. Elucidating the role of DEPTOR in Alzheimer's disease. *Int. J. Mol. Med.* **34**, 1195–1200 (2014).
741. Duan, S. *et al.* mTOR Generates an Auto-Amplification Loop by Triggering the βTrCP- and CK1α-Dependent Degradation of DEPTOR. *Mol. Cell* **44**, 317–324 (2011).
742. Caron, A., Briscoe, D. M., Richard, D. & Laplante, M. DEPTOR at the Nexus of Cancer, Metabolism, and Immunity. *Physiol. Rev.* **98**, 1765–1803 (2018).
743. Zhao, Y., Xiong, X. & Sun, Y. DEPTOR, an mTOR Inhibitor, Is a Physiological Substrate of SCFβTrCP E3 Ubiquitin Ligase and Regulates Survival and Autophagy. *Mol. Cell* **44**, 304–316 (2011).
744. Davis, O. B. *et al.* NPC1-mTORC1 Signaling Couples Cholesterol Sensing to Organelle Homeostasis and Is a Targetable Pathway in Niemann-Pick Type C. *Dev. Cell* **56**, 260-276.e7 (2021).
745. Castellano, B. M. *et al.* Lysosomal cholesterol activates mTORC1 via an SLC38A9–Niemann-Pick C1 signaling complex. *Science* **355**, 1306–1311 (2017).
746. Lim, C.-Y. *et al.* ER–lysosome contacts enable cholesterol sensing by mTORC1 and drive aberrant growth signalling in Niemann–Pick type C. *Nat. Cell Biol.* **21**, 1206–1218 (2019).
747. Shin, H. R. *et al.* Lysosomal GPCR-like protein LYCHOS signals cholesterol sufficiency to mTORC1. *Science* **377**, 1290–1298 (2022).
748. Huang, B., Song, B. & Xu, C. Cholesterol metabolism in cancer: mechanisms and therapeutic opportunities. *Nat. Metab.* **2**, 132–141 (2020).
749. Jia, J. *et al.* Galectins Control mTOR in Response to Endomembrane Damage. *Mol. Cell* **70**, 120-135.e8 (2018).
750. Jia, J. *et al.* Galectin-3 Coordinates a Cellular System for Lysosomal Repair and Removal. *Dev. Cell* **52**, 69-87.e8 (2020).
751. Shin, S. *et al.* Qki activates Srebp2-mediated cholesterol biosynthesis for maintenance of eye lens transparency. *Nat. Commun.* **12**, 3005 (2021).
752. Zhou, X. *et al.* Qki regulates myelinogenesis through Srebp2-dependent cholesterol biosynthesis. *eLife* **10**, e60467 (2021).
753. Thurston, T. L. M., Wandel, M. P., von Muhlinen, N., Foeglein, A. & Randow, F. Galectin 8 targets damaged vesicles for autophagy to defend cells against bacterial invasion. *Nature* **482**, 414–418 (2012).
754. Aits, S. *et al.* Sensitive detection of lysosomal membrane permeabilization by lysosomal galectin puncta assay. *Autophagy* **11**, 1408–1424 (2015).
755. Chauhan, S. *et al.* TRIMs and Galectins Globally Cooperate and TRIM16 and Galectin-3 Co-direct Autophagy in Endomembrane Damage Homeostasis. *Dev. Cell* **39**, 13–27 (2016).
756. Tan, J. X. & Finkel, T. A phosphoinositide signalling pathway mediates rapid lysosomal repair. *Nature* **609**, 815–821 (2022).
757. Radulovic, M. *et al.* Cholesterol transfer via endoplasmic reticulum contacts mediates lysosome damage repair. *EMBO J.* **41**, e112677 (2022).
758. Appelqvist, H. *et al.* Attenuation of the Lysosomal Death Pathway by Lysosomal Cholesterol Accumulation. *Am. J. Pathol.* **178**, 629–639 (2011).

759. Appelqvist, H. *et al.* Sensitivity to Lysosome-Dependent Cell Death Is Directly Regulated by Lysosomal Cholesterol Content. *PLoS ONE* **7**, e50262 (2012).
760. Reiners, J. J., Kleinman, M., Kessel, D., Mathieu, P. A. & Caruso, J. A. Nonesterified cholesterol content of lysosomes modulates susceptibility to oxidant-induced permeabilization. *Free Radic. Biol. Med.* **50**, 281–294 (2011).
761. Saxton, R. A. & Sabatini, D. M. mTOR Signaling in Growth, Metabolism, and Disease. *Cell* **168**, 960–976 (2017).
762. Verhaak, R. G. W. *et al.* Integrated genomic analysis identifies clinically relevant subtypes of glioblastoma characterized by abnormalities in PDGFRA, IDH1, EGFR, and NF1. *Cancer Cell* **17**, 98–110 (2010).
763. Chakravarti, A. *et al.* The Prognostic Significance of Phosphatidylinositol 3-Kinase Pathway Activation in Human Gliomas. *J. Clin. Oncol.* **22**, 1926–1933 (2004).
764. Thoreen, C. C. *et al.* An ATP-competitive Mammalian Target of Rapamycin Inhibitor Reveals Rapamycin-resistant Functions of mTORC1. *J. Biol. Chem.* **284**, 8023–8032 (2009).
765. Galanis, E. *et al.* Phase II Trial of Temsirolimus (CCI-779) in Recurrent Glioblastoma Multiforme: A North Central Cancer Treatment Group Study. *J. Clin. Oncol.* **23**, 5294–5304 (2005).
766. Cloughesy, T. F. *et al.* Antitumor Activity of Rapamycin in a Phase I Trial for Patients with Recurrent PTEN-Deficient Glioblastoma. *PLoS Med.* **5**, e8 (2008).
767. Galan-Moya, E. M. *et al.* Secreted factors from brain endothelial cells maintain glioblastoma stem-like cell expansion through the mTOR pathway. *EMBO Rep.* **12**, 470–476 (2011).
768. Galan-Moya, E. M. *et al.* Endothelial Secreted Factors Suppress Mitogen Deprivation-Induced Autophagy and Apoptosis in Glioblastoma Stem-Like Cells. *PLoS ONE* **9**, e93505 (2014).
769. Choi, Y. J. *et al.* Inhibitory Effect of mTOR Activator MHY1485 on Autophagy: Suppression of Lysosomal Fusion. *PLoS ONE* **7**, e43418 (2012).
770. Shchors, K., Massaras, A. & Hanahan, D. Dual Targeting of the Autophagic Regulatory Circuitry in Gliomas with Repurposed Drugs Elicits Cell-Lethal Autophagy and Therapeutic Benefit. *Cancer Cell* **28**, 456–471 (2015).
771. Abdul Rahim, S. A. *et al.* Regulation of hypoxia-induced autophagy in glioblastoma involves ATG9A. *Br. J. Cancer* **117**, 813–825 (2017).
772. Cariati, I. *et al.* Neurodegeneration in Niemann–Pick Type C Disease: An Updated Review on Pharmacological and Non-Pharmacological Approaches to Counteract Brain and Cognitive Impairment. *Int. J. Mol. Sci.* **22**, 6600 (2021).
773. Vanier, M. T. & Millat, G. Structure and function of the NPC2 protein. *Biochim. Biophys. Acta BBA - Mol. Cell Biol. Lipids* **1685**, 14–21 (2004).
774. Infante, R. E. *et al.* NPC2 facilitates bidirectional transfer of cholesterol between NPC1 and lipid bilayers, a step in cholesterol egress from lysosomes. *Proc. Natl. Acad. Sci.* **105**, 15287–15292 (2008).
775. Scott, C. & Ioannou, Y. A. The NPC1 protein: structure implies function. *Biochim. Biophys. Acta BBA - Mol. Cell Biol. Lipids* **1685**, 8–13 (2004).
776. Heybrock, S. *et al.* Lysosomal integral membrane protein-2 (LIMP-2/SCARB2) is involved in lysosomal cholesterol export. *Nat. Commun.* **10**, 3521 (2019).
777. Schneede, A. *et al.* Role for LAMP-2 in endosomal cholesterol transport. *J. Cell. Mol. Med.* **15**, 280–295 (2011).
778. Lu, F. *et al.* Identification of NPC1 as the target of U18666A, an inhibitor of lysosomal cholesterol export and Ebola infection. *eLife* **4**, e12177 (2015).
779. Blom, T. S. *et al.* Defective endocytic trafficking of NPC1 and NPC2 underlying

infantile Niemann–Pick type C disease. *Hum. Mol. Genet.* **12**, 257–272 (2003).
780. Scott, C., Higgins, M. E., Davies, J. P. & Ioannou, Y. A. Targeting of NPC1 to Late Endosomes Involves Multiple Signals, Including One Residing within the Putative Sterol-sensing Domain *. *J. Biol. Chem.* **279**, 48214–48223 (2004).
781. Watari, H. *et al.* Niemann-Pick C1 protein: Obligatory roles for N-terminal domains and lysosomal targeting in cholesterol mobilization. *Proc. Natl. Acad. Sci. U. S. A.* **96**, 805–810 (1999).
782. Staudt, L. M. Oncogenic activation of NF-kappaB. *Cold Spring Harb. Perspect. Biol.* **2**, a000109 (2010).

COLLEGE ED BIOLOGIE
DOCTORAL SANTE
PAYS DE LA LOIRE

Nantes Université

Titre : Élucider la Vulnérabilité des Cellules Souches de Glioblastome aux Dysfonctions Lysosomales

Mots clés : Glioblastome, Cellules Souches Cancéreuses, Lysosomes, Maladies Lysosomales, MALT1 paracaspase

Résumé : Le glioblastome (GB) est le cancer du système nerveux central de l'adulte le plus commun et le plus meurtrier. Malgré un traitement invasif de résection chirurgicale suivi de séances de radio- et de chimiothérapies, la survie des patients atteints difficilement les 15 mois. Cette agressivité est considérée comme liée notamment à la présence de cellules souches cancéreuses appelées cellules de type souche de glioblastome, ou GSCs. Ces cellules, impliquées dans l'initiation, la croissance, et la récurrence du GB, sont considérées comme des cibles préférentielles.
Les lysosomes jouent un rôle critique dans le maintien de l'homéostasie des GSCs. Ces organelles, agissant à la croisée des mécanismes d'anabolisme et de catabolisme, permettent la survie des GSCs hors de leur niche protectrice. Dans les GSCs, leur déstabilisation culmine en une mort spécifique, définissant ainsi les lysosomes comme un point de contrôle des décisions vie-et-mort dans ce contexte cellulaire.
La paracaspase MALT1 a récemment été définie comme un médiateur crucial de l'homéostasie des lysosomes dans les GSCs. Cette protéase, initialement décrite comme impliquée dans les réponses immunitaires, restreint le compartiment lysosomal, son inhibition aboutissant en une mort lysosome-dépendante des GSCs, via un mécanisme impliquant la protéine de liaison à l'ARNm Quaking. Cependant, les événements engendrant la déstabilisation lysosomale ainsi que la mort des GSCs restaient incertains.
Ainsi, mon travail de thèse a permis la cartographie des événements au niveau cellulaire et des organelles, participant à la déstabilisation lysosomale suivant le ciblage moléculaire et pharmacologique de la paracaspase MALT1.

Title : Elucidating the Vulnerability of Glioblastoma Stem-like Cells to Lysosomal Dysfunctions

Keywords : Glioblastoma, Cancer Stem Cells, Lysosomes, Lysosomal Storage Diseases, MALT1 paracaspase

Abstract : Glioblastoma (GB) is the deadliest and most prevalent primary tumor of the central nervous system (CNS) in adults. Despite invasive treatments of surgical resection followed by radio- and chemotherapy, the median survival of patients hardly reaches 15 months. This aggressiveness is thought to be in part linked to the presence of a subset of cancer stem cells termed glioblastoma stem-like cells (GSCs) within the tumor mass. Involved in the initiation, growth, and recurrence of GB tumors, these cells therefore represent a promising target.
In this context, lysosomes are critical for the maintenance of GSCs homeostasis. These organelles, standing at the crossroad between anabolism and catabolism, permit the survival of GSCs in unfavorable conditions.
Their destabilization culminates in the specific cell death of GSCs, defining lysosomes as a checkpoint for life-and-death decisions in this cellular context.
The MALT1 paracaspase was recently defined as a crucial mediator of lysosomal homeostasis in GSCs. This protease, initially involved in immune responses, restrains the lysosomal compartment, its inhibition resulting in lysosomal-dependent cell death of GSCs through a mechanism involving the RNA binding protein Quaking. However, the events resulting in the lysosomal destabilization and cell death of GSCs remained unclear.
In this context, my thesis work allowed the cartography of cellular and organellar events leading to GSC cell death upon MALT1 inhibition and silencing.